



**FRONTIERS AT THE  
INTERFACE OF  
HOMOGENEOUS AND  
HETEROGENEOUS  
CATALYSIS, II**

**Meeting of the Catalysis Science Program  
Chemical Sciences, Geosciences and Biosciences Division  
Office of Basic Energy Sciences  
U.S. Department of Energy**

**Westin Annapolis  
Annapolis, Maryland  
July 20–23, 2014**

This document was produced under contract number DE-AC05-06OR23100 between the U.S. Department of Energy and Oak Ridge Associated Universities.

## FOREWORD

The 2014 Catalysis Science Program Meeting is sponsored by the Division of Chemical Sciences, Geosciences and Biosciences, Office of Basic Energy Sciences (BES), U.S. Department of Energy. It is being held on July 20–23, 2014, at the Westin Annapolis Hotel, Annapolis, Maryland. The purposes of this meeting are to discuss the recent advances in the chemical, physical, and biological bases of catalysis science, to foster exchange of ideas and cooperation among participants, and to discuss the new challenges and opportunities recently emerging in energy technologies.

Catalysis activities within BES emphasize fundamental research aimed at understanding mechanisms and ultimately controlling the chemical conversion of natural and artificial feedstocks. The long-term goal of this research is to discover fundamental principles and produce insightful approaches to predict structure-reactivity behavior. Such knowledge, integrated with advances in chemical and materials synthesis, *in situ* and *operando* analytical instrumentation, and chemical kinetics and quantum chemistry methods, will allow the control of chemical reactions along desired pathways. This new knowledge will impact the efficiency of conversion of natural resources into fuels, chemicals, materials, or other forms of energy, while minimizing the impact to the environment.

This year's meeting pursues the same goal as the 2013 meeting of highlighting the potential advances in catalysis science to be made at the interface between homogeneous and heterogeneous systems. These advances entail creating new catalysts structures as well as different approaches to control the pathways of catalytic transformations of reactions relevant to DOE's missions: C-H activation in general, selective oxidation, biomass-related conversions, polymer synthesis, energy generation and storage, etc. Methods classical in organic and organometallic chemistry can be combined with solid state and surface chemistry to study reaction mechanisms and structures of catalytic sites, and eventually produce innovative approaches and new catalysts.

Special thanks go to the program investigators and their students, postdocs, and collaborators for their dedication to the continuous success and visibility of the BES Catalysis Science Program, and to the session moderators for their invaluable help. We also thank Diane Marceau<sup>3</sup> and the Oak Ridge Institute for Science and Education staff for the logistical and web support and the compilation of this volume.

Geoffrey Coates<sup>1</sup>, Jens Norskov<sup>2</sup> and Raul Miranda<sup>3</sup>

<sup>1</sup>Cornell University

<sup>2</sup>Stanford University and SLAC National Accelerator Laboratory

<sup>3</sup>Office of Basic Energy Sciences - U.S. Department of Energy

This page is intentionally blank.

## 2014 Meeting of the Catalysis Science Program

*Catalysis Research PI Meeting  
Frontiers at the Interface between Homogeneous and Heterogeneous Catalysis, II  
Chemical Sciences, Geosciences and Biosciences Division  
Office of Basic Energy Sciences, U.S. Department of Energy  
Westin Annapolis, Annapolis, Maryland  
July 20–23, 2014*

### Sunday, July 20

- 3:00 pm            **Registration opens**
- 6:45 pm            **Welcoming Remarks**
- Biomass Conversion***
- 7:00–7:30 pm     James Dumesic (Wisconsin)
- 7:30–8:00 pm     Robert Waymouth (Stanford)
- 8:00–10:00 pm    **Poster Session I**

### Monday, July 21

- 7:00–8:30 am     **Breakfast**
- Catalysts for Polymer Synthesis***
- 8:30–9:00 am     Richard Schrock (MIT)
- 9:00–9:30 am     Colin Nuckolls (Columbia)
- 9:30–10:00 am    **Coffee Break**
- Catalysis in Energy Applications***
- 10:00–10:30 am   Umit Ozkan (Ohio State)
- 10:30–11:00 am   Thomas Jaramillo (Stanford)
- 11:30–12:00 pm   Steve Overbury (ORNL)
- 12:00–2:00 pm    **Networking Lunch**
- Catalysis Basic Advances***
- 2:00–2:30 pm     John Berry (Wisconsin)
- 2:30–3:00 pm     Franklin Tao (Notre Dame)
- 3:00–3:30 pm     Joshua Figueroa (UC San Diego)
- 3:30–4:00 pm     **Coffee Break**

4:00–4:30 pm Thomas Bligaard (SLAC)  
4:30–5:00 pm Christine Thomas (Brandeis)  
5:30–6:00 pm John Kitchin (Carnegie Mellon)  
  
6:00–7:30 pm **Dinner**  
  
8:00–10:00 pm **Poster Session II**

## **Tuesday, July 22**

7:00–8:30 am **Breakfast**  
  
***Catalysis of C–H Activation***  
8:30–9:00 am William Jones (Rochester)  
9:00–9:30 am John Yates (Virginia)  
9:30–10:00 am **Coffee Break**  
  
***Catalysis of C–H Activation***  
10:00–10:30 am Melanie Sanford (Michigan)  
10:30–11:00 am Horia Metiu (UC Santa Barbara)  
11:30–12:00 pm Daniel Mindiola (U Pennsylvania)  
  
12:00–2:00 pm **Networking Lunch**  
  
***Nanocluster Catalysts***  
2:00–2:30 pm Richard Finke (Colorado State)  
2:30–3:00 pm Charles Campbell (U Washington)  
3:00–3:30 pm Peng Chen (Cornell)  
3:30–4:00 pm **Coffee Break**  
  
4:30–5:30 pm Breakout Session I  
(Energy Conversion, Small-molecule activation, Selective oxidation,  
Tandem and parallel conversions)  
  
5:30–6:30 pm **Dinner**  
  
7:00–8:00 pm Breakout Session II  
(Energy Conversion, Small-molecule activation, Selective oxidation,  
Tandem and parallel conversions)  
  
8:00–10:00 pm **Poster Session III**

## Wednesday, July 23

7:00–8:30 am      **Breakfast**

### ***Breakout Sessions Presentations and Discussion***

8:30–8:45 am      Energy conversion – Tobin Marks (Northwestern)

8:45–9:00 am      Small-molecule activation – Aaron Sadow (Iowa State)

9:00–9:15 am      Selective oxidation – Alex Bell (UC Berkeley)

9:15–9:30 am      Tandem and parallel conversions – Ged Parkin (Columbia)

### ***Oxidation Catalysis***

9:30–10:00 am      David Dixon (Alabama)

10:00–10:30 am      Cynthia Friend (Harvard)

10:30–11:00 am      Shannon Stahl (Wisconsin)

11:30–12:00 pm      Fabio Ribeiro (Purdue)

12:00–12:30 pm      Final Discussion – Bruce Gates (UC Davis)

12:30 pm            **Departure**

This page is intentionally blank.

## Table of Contents

<b>Foreword</b> .....	i
<b>Agenda</b> .....	iii
 <b>Sunday Evening: <i>Biomass Conversion</i></b>	
James A. Dumesic – <i>Liquid-Phase Conversion of Lignocellulosic Biomass to Fuels and Chemicals</i> .....	3
Robert M. Waymouth – <i>Challenges and Opportunities in the Selective Transformation of Biomass to Useful Chemical Intermediates and Materials</i> .....	6
 <b>Monday Morning: <i>Catalysis for Polymer Synthesis</i></b>	
Richard R. Schrock – <i>Synthesis of Stereoregular ROMP Polymers</i> .....	13
Colin P. Nuckolls – <i>Catalytic Growth of Molecular Scale Wiring</i> .....	15
 <b>Monday Morning: <i>Catalysis in Energy Applications</i></b>	
U. S. Ozkan – <i>A Comparison of N-Containing Carbon Nano-Structures (CN<sub>x</sub>) and N-Coordinated Iron-Carbon Catalysts (FeNC) for the Oxygen Reduction Reaction in Acidic Media</i> .....	19
Thomas F. Jaramillo – <i>Engineering Electrocatalysts at the Nano-Scale for the Hydrogen Evolution Reaction (HER) and the Oxygen Reduction Reaction (ORR)</i> ...	24
Steven H. Overbury – <i>Probing Catalytic Chemistry of Oxygenates on Oxide Catalysts using CeO<sub>2</sub> Model Films and Shaped Nanoparticles</i> .....	28
 <b>Monday Afternoon: <i>Catalysis Basic Advances</i></b>	
John Berry – <i>Studies of Metal-Metal Bonded Catalysts for Group Transfer Reactions</i> .....	41
Franklin (Feng) Tao – <i>Energy and Chemical Transformations of Methane on Oxide Catalysts</i> .....	42
Joshua S. Figueroa – <i>Modeling Catalytic and Stoichiometric Intermediates with Transition-Metal Isocyanides</i> .....	48
Thomas Bligaard – <i>Error Estimation in Simulated Catalytic Trend Studies</i> .....	51
Christine M. Thomas – <i>Early-Late Heterobimetallic Complexes Featuring Metal-Metal Bonds: Small Molecule Activation and Catalytic Applications</i> .....	58

John R. Kitchin – <i>Modeling Bulk Composition Dependent H<sub>2</sub> Dissociative Adsorption Energies on Cu<sub>x</sub>Pd<sub>1-x</sub> Alloy (111) Surfaces</i> .....	63
--	----

### **Tuesday Morning, Catalysis of C–H Activation**

William D. Jones – <i>A Systematic Investigation of Ligand Effects on the Energetics of C–H Activation at Rhodium in Tp'Rh(L)(R)H Complexes</i> .....	69
---	----

John T. Yates, Jr. – <i>C–H Bond Activation at Perimeter Sites on Au/TiO<sub>2</sub>—The Oxidative-Dehydrogenation of Alkyl Side Chains in Carboxylic Acids</i> .....	73
---	----

Melanie S. Sanford – <i>Synthesis, Characterization, and Activity of Single Site Catalysts Supported in Metal Organic Frameworks via Ion Exchange</i> .....	76
---	----

Horia Metiu – <i>Investigation of C–H Bond Activation and Doped Metal Oxide Catalysis</i> .....	80
---	----

Daniel J. Mindiola – <i>Synthesis and Exploratory Catalysts of 3d Metals: Group-Transfer, Alkane Activation and Functionalization with Greenhouse Gases</i> .....	84
---	----

### **Tuesday Afternoon, Nanocluster Catalysts**

Richard G. Finke – <i>Nucleation is Bimolecular in Strong Bonding Systems</i> .....	89
---	----

Charles T. Campbell – <i>Supported Metal Nanoparticles: Correlating Structure with Catalytic Function via Metal Atom Energetics</i> .....	93
---	----

Peng Chen – <i>Single-Molecule Nanocatalysis: From Intraparticle Catalytic Communication to Reactivity-Guided Engineering of Single-Particle Photoelectrocatalysts</i> .....	97
--	----

### **Wednesday Morning, Oxidation Catalysis**

David A. Dixon – <i>Catalytic Reactions of Alcohols on Transition Metal Oxide Nanoclusters</i> .....	105
--	-----

Cynthia M. Friend – <i>Closing the Materials and Pressure Gap: Selective Oxidation using Gold</i> .....	106
---	-----

Shannon S. Stahl – <i>Aerobic Oxidation of Organic Molecules with Homogeneous, Nanoparticle and Heterogeneous Pd Catalysts</i> .....	112
--	-----

Fabio H. Ribeiro – <i>Fundamental Studies of Oxidation Reactions on Model Catalysts: Catalytic Sites for Propylene Epoxidation by O<sub>2</sub> and H<sub>2</sub> over Au/Titanium Silicalite-1</i> .....	117
---	-----

## Poster Presentations

1. Frank Abild-Pedersen (SLAC) – *Trends in Nano Particle Catalysis*..... 125
2. Eric I. Altman (Yale Univ.) – *Shape and Phase Transitions of Co Oxide Particles* ..... 133
3. Perla B. Balbuena (Texas A&M Univ.) – *Roles of Catalyst-Substrate and Growing Structure-Catalyst Interactions during Nucleation and Growth of Single-Walled Carbon Nanotubes*..... 137
4. Ludwig Bartels (Univ. of California–Riverside) – *Multiscale Imaging and DFT Analysis of Reactant Interactions on Single-Layer MoS<sub>2</sub> and Related Molybdenum-Sulfur Materials*..... 142
5. Bart M. Bartlett (Univ. of Michigan) – *Bridging Molecules and Surfaces for Energy-Relevant Catalytic Chemical Transformations* ..... 148
6. Alexis T. Bell (LBNL) – *Catalysts for the Selective Oxidation of Hydrocarbons* ..... 153
7. Aditya Bhan (Univ. of Minnesota) – *Catalytic Deoxygenation*..... 157
8. Suzanne A. Blum (Univ. of Calif.–Irvine) – *Single-Molecule Fluorescence Microscopy Tools for Catalysis and Chemistry: Polymerization*..... 159
9. David F. Cox (Virginia Tech) – *Interaction of D<sub>2</sub>O, CO<sub>2</sub> and Na with Manganese Oxide and NaMnO<sub>2</sub>-Like Surfaces*..... 163
10. W. Nicholas Delgass (Purdue Univ.) – *Heterogeneous and Homogeneous Catalyst Design by Discovery Informatics* ..... 167
11. Zdenek Dohnálek (PNNL) – *Water Dynamics on RuO<sub>2</sub>(110)* ..... 171
12. Anatoly I. Frenkel (Yeshiva Univ.) – *Zooming In on Active Species: Correlative, Operando XAS and TEM Studies of Catalytic Mechanisms* ..... 172
13. Andrew J. Gellman (Carnegie Mellon Univ.) – *Competing Forces in Enantioselective Heterogeneous Catalysis and Separations: Enantiospecific Energetics and Auto-Amplification* ..... 178
14. Michael A. Henderson (PNNL) – *Partial Oxidation of Alkenes on TiO<sub>2</sub>(110) through Photochemistry* ..... 187
15. Andreas Heyden (Univ. of South Carolina) – *Theoretical Investigation of Heterogeneous Catalysis at the Solid-Liquid Interface for the Conversion of Lignocellulosic Biomass Model Molecules* ..... 188
16. Christopher W. Jones (Georgia Tech) – *Immobilized Molecular Catalysts in Cooperative Catalysis and Cascade Reactions* ..... 191
17. Alexander Katz (Univ. of Calif.–Berkeley) – *Tuning Catalytic Properties of Molecular Metal Clusters on Supports*..... 197

18. Harold H. Kung (Northwestern Univ.) – <i>Exploring New Chemistry with Molecular Nanocages</i> .....	202
19. Johannes A. Lercher (PNNL) – <i>Multifunctional Solid Catalysts for Lignin to Hydrocarbons: Understanding and Controlling Scalable Catalytic Routes in Aqueous Phase</i> .....	206
20. Ping Liu (BNL) – <i>Water Gas Shift Reactions on Metal-Oxide Catalysts: Mechanistic Understanding and Rational Catalyst Optimization</i> .....	220
21. Tobin J. Marks (Northwestern Univ.) – <i>Supported Organometallic Complexes: Surface Chemistry, Spectroscopy, Catalysis and Homogeneous Models</i> .....	231
22. Liviu M. Mirica (Washington Univ.–St. Louis) – <i>Organometallic Reactivity of Paramagnetic Late Transition Metal Complexes</i> .....	235
23. David R. Mullins (ORNL) – <i>Variations in Reactivity on Different Crystallographic Orientations of Cerium Oxide</i> .....	240
24. C. Buddie Mullins (Univ. of Texas–Austin) – <i>The Effects of Surface Hydroxyl and Oxygen Species on the Partial Oxidation of Allylic Alcohols on Au(111)</i> .....	241
25. SonBinh Nguyen (Northwestern Univ.) – <i>Institute for Catalysis in Energy Processes</i> .....	247
26. Jack R. Norton (Columbia Univ.) – <i>Uptake of Dihydrogen by Paramagnetic Metal Complexes</i> .....	259
27. Justin M. Notestein (Northwestern Univ.) – <i>Quantifying Active Sites in Supported Oxide Catalysts</i> .....	262
28. Gerard Parkin (Columbia Univ.) – <i>Catalysts for the Dehydrogenation of Formic Acid and for the Functionalization of CO<sub>2</sub></i> .....	267
29. Talat S. Rahman (Univ. of Central Florida) – <i>A Combined DFT+KMC Study of Selective Oxidation of NH<sub>3</sub> on Rutile RuO<sub>2</sub>(110) at Ambient Pressures</i> .....	271
30. Ashwin Ramasubramaniam (Univ. of Massachusetts–Amherst) – <i>Ab Initio Studies of CO Adsorption and Oxidation on Graphene–Pt<sub>13</sub> Nanocomposites</i> .....	272
31. John J. Rehr (Univ. of Washington–Seattle) – <i>Understanding Supported Pt Nanoparticles by Combining Theoretical and Experimental Spectroscopy and Ab Initio Molecular Dynamics</i> .....	275
32. Robert M. Rioux (Pennsylvania State Univ.) – <i>Influence of Multi-Valency, Electrostatics and Molecular Recognition on the Adsorption of Transition Metal Complexes on Metal Oxides: A Molecular Approach to Supported Catalyst Synthesis</i> .....	282

33. José A. Rodriguez (BNL) – <i>Catalysis for Advanced Fuels</i> .....	287
34. Aaron D. Sadow (Ames Laboratory) – <i>Solution-Phase and Immobilized Ligands in Catalytic Carbonyl Chemistry</i> .....	295
35. Aditya (Ashi) Savara (ORNL) – <i>Elucidation of Heterogeneous Catalysis Mechanisms with Organic Oxygenates: Aldol Condensation on Cerium Oxide (111) and (100) Crystal Faces, and Benzylic Alcohol Oxidation on Palladium Nanoparticles</i> .....	297
36. William F. Schneider (Univ. of Notre Dame) – <i>Cluster Expansions in Catalysis</i> .....	298
37. Susannah L. Scott (Univ. of California–Santa Barbara) – <i>Intrinsic Heterogeneity in Supported Organometallic Catalysts</i> .....	302
38. Annabella Selloni (Princeton Univ.) – <i>Theoretical Studies of Water Oxidation on Titanium, Cobalt, and Nickel/Iron Oxides</i> .....	306
39. Wendy J. Shaw (PNNL) – <i>Enhancing the Performance of Hydrogenase Mimics with an Enzyme-Inspired Outer Coordination Sphere</i> .....	310
40. Sara E. Skrabalak (Indiana Univ.–Bloomington) – <i>Shaping the Catalytic Performance of Core@Shell Noble Metal Nanocatalysts</i> .....	314
41. Igor I. Slowing (Ames Laboratory) – <i>Hybrid Organic-Inorganic Catalysts for Carbon-Carbon Coupling and Redox Reactions: Characterization, Catalytic Activity and Reaction Mechanisms</i> .....	315
42. Darío J. Stacchiola (BNL) – <i>Nanostructured Oxide Catalysts: Studies from UHV to In Situ Conditions</i> .....	324
43. Albert E. Stiegman (Florida State Univ.) – <i>Elucidation of Active Site Formation in the Phillips Ethylene Polymerization Catalyst</i> .....	325
44. Steven L. Tait (Indiana Univ.) – <i>Redox-Active On-Surface Assembly of Metal-Organic Chains with Single-Site Pt(II)</i> .....	328
45. T. Don Tilley (LBNL) – <i>New Approaches for Activation of Substrates at a Metal Center</i> .....	332
46. YuYe J. Tong (Georgetown Univ.) – <i>In Situ SEIRAS Investigation of MOR on PtRu and FAOR on PtPb at Low Electrode Potential: A Re-visit of CO Poisoning and Bifunctional Mechanisms</i> .....	337
47. David A. Vicic (Lehigh Univ.) – <i>A Five-Coordinate Nickel(II) Fluoroalkyl Complex as a Precursor to a Spectroscopically Detectable Ni(III) Species</i> .....	343
48. John M. Vohs (Univ. of Pennsylvania) – <i>Surface Science Studies of Nano-Crystalline TiO<sub>2</sub></i> .....	349

49. Yong Wang (Washington State Univ.) – <i>Sub-Nanometer-Sized Clusters for Heterogeneous Catalysis</i> .....	353
50. Michael G. White (BNL/Stony Brook Univ.) – <i>Role of Charge Transfer and Stoichiometry in Promoting Water Dissociation on Supported Metal Oxide Clusters</i> .....	360
51. Judith C. Yang (Univ. of Pittsburgh) – <i>Noncrystalline-to-Crystalline Transformations in Pt Nanoparticles</i> .....	368
52. Francisco Zaera (Univ. of California–Riverside) – <i>Au/TiO<sub>2</sub> in Thermal and Photoassisted Catalysis</i> .....	374
<b>Participant List</b> .....	383

**Sunday Evening**

**Biomass Conversion**

This page is intentionally blank.

James A. Dumesic

## **Liquid-phase conversion of lignocellulosic biomass to fuels and chemicals**

James A. Dumesic

Department of Chemical and Biological Engineering  
University of Wisconsin, Madison, WI 53706

We will present strategies for the catalytic conversion of the C<sub>5</sub> and C<sub>6</sub> sugars present in hemi-cellulose and cellulose, respectively, to produce gamma-valerolactone (GVL). We will present a processing approach that uses GVL as a solvent to convert simultaneously the C<sub>5</sub> and C<sub>6</sub> sugars in biomass, thereby simplifying separation steps, because GVL is one of the reaction products. Additionally, GVL solubilizes the degradation products typically formed during biomass deconstruction, and this approach can thus be implemented using continuous flow reactors. We will demonstrate that we can produce soluble carbohydrates from corn stover, hardwood and softwood at high yields (80-90%) in a solvent consisting of biomass-derived GVL, water, and dilute acid (0.005 M). We will show that these carbohydrates can be recovered and concentrated (up to 130 g/L) in an aqueous phase by extraction of GVL using CO<sub>2</sub>. These yields and sugar concentrations are comparable to those obtained using multiple steps and/or high-cost chemicals or bio-catalysts, such as hydrolysis in concentrated mineral acids, pretreatment and enzymatic hydrolysis, or ionic liquid hydrolysis. We will then present results from reaction kinetics studies to quantify the effects of polar aprotic organic solvents on reaction rates and selectivities of acid-catalyzed reactions of relevance for biomass conversion (e.g., xylose dehydration to furfural). We will suggest that the aprotic organic solvent affects the stabilization of the acidic proton relative to the protonated transition states, leading to accelerated reaction rates for these acid-catalyzed biomass conversion reactions.

## **Fundamental Studies of the Reforming of Oxygenated Compounds over Supported Metal Catalysts (DE-FG02-84ER13183)**

James A. Dumesic (PI)

University of Wisconsin – Madison

The main objective of our research is to elucidate the fundamental concepts associated with controlling the activity, selectivity, and stability/recyclability of heterogeneous catalysts for liquid-phase conversion of oxygenated hydrocarbons, such as compounds derived from biomass. In our recent work, we have shown that bimetallic catalysts that combine a highly-reducible metal (e.g., Pt, Rh) with an oxophilic promoter (e.g., Re) are promising materials for conversion of oxygenated hydrocarbons because of their high activity and selectivity for C-O scission reactions. We have synthesized nanoparticles with well-controlled and defined particle size and composition by means of controlled surface reactions. We have studied the active site of these synthesized catalysts by a multi-technique analytical approach employing temperature-programmed reduction (TPR), scanning transmission electron microscopy-energy dispersive spectroscopy (STEM-EDS), Fourier transform infrared spectroscopy (FTIR), X-ray absorption spectroscopy (XAS), and by their performance in selective C-O hydrogenolysis reactions.

An important issue in liquid-phase catalytic processing is catalyst stability and recyclability. It would be desirable to replace precious metals (e.g., Pt) with base metals that are more earth abundant (e.g., Cu); however, base metals are more susceptible to irreversible deactivation through sintering and leaching, especially in the reaction conditions common in the

processing of biomass-derived oxygenates. To address this challenge, we have employed a method to stabilize copper nanoparticles supported on  $\gamma$ -Al<sub>2</sub>O<sub>3</sub> by atomic layer deposition (ALD) of an alumina overcoat. We have extended our work on ALD overcoating of catalysts by utilizing the overcoat to add functionality to the catalyst, such as the addition of niobia to add acidity. This research has employed the use of high resolution STEM studies to map elemental composition and to quantify morphologies and spatial distributions of ALD overlayers on model catalysts consisting of non-porous silica nanospheres as catalyst supports.

The primary focus of our studies is to elucidate the catalytic properties of catalysts for liquid-phase reactions of oxygenated hydrocarbons. We anticipate that the knowledge obtained from these studies will allow us to identify promising directions for new catalysts that show high activity, selectivity, and stability for important reactions in the conversion of biomass-derived oxygenated hydrocarbons to fuels and chemicals.

**Publications with joint funding from DOE (2011 – 2014):**

- Kandoi, S.; Greeley J.; Simonetti, D.; Shabaker, J.; Mavrikakis, M.; Dumesic, J. A., Reaction Kinetics of Ethylene Glycol Reforming over Platinum in the Vapor versus Aqueous Phases. *Journal of Physical Chemistry C*. **2011**, 115, 961.
- Bond, J. Q.; Martin Alonso, D.; Wang, E.; Dumesic, J. A., Activation of Amberlyst-70 for alkene oligomerization in hydrophobic media. *Topics in Catalysis*. **2011**, 54, 447.
- Pagán-Torres, Y. J.; Marcel R. Gallo, J.; Wang, D.; Pham, H. N.; Libera, J. A.; Marshall, C. L.; Elam, J. W.; Datye, A. K.; Dumesic, J. A., Synthesis of highly ordered hydrothermally stable mesoporous niobia catalysts by atomic layer deposition. *ACS Catalysis*. **2011**, 1, 1234.
- Gürbüz, E. I.; Martin Alonso, D.; Bond, J. Q.; Dumesic, J. A., Reactive extraction of levulinate esters and conversion to  $\gamma$ -valerolactone for production of liquid fuels. *Chemistry and Sustainability*. **2011**, 4, 357.
- Serrano-Ruiz, J. C.; Dumesic, J. A., Catalytic routes for the conversion of biomass into liquid hydrocarbon transportation fuels. *Energy and Environmental Science*. **2011**, 4, 83.
- Bond, J. Q.; Wang, D.; Martin Alonso, D.; Dumesic, J. A., Inter-conversion between  $\gamma$ -valerolactone and pentenoic acid combined with decarboxylation to form butene over silica/alumina. *Journal of Catalysis*. **2011**, 281, 290.
- Braden, D. J.; Henao, C. A.; Heltzel, J.; Maravelias, C. T.; Dumesic, J. A., Production of liquid hydrocarbon fuels by catalytic conversion of biomass-derived levulinic acid. *Green Chemistry*. **2011**, 7, 1755.
- Gürbüz, E. I.; Wettstein, S. G.; Dumesic, J. A., Conversion of hemicellulose to furfural and levulinic acid using biphasic reactors with alkylphenol solvents. *Chemistry and Sustainability*. **2012**, 5, 383.
- Wettstein, S. G.; Bond, J. Q.; Alonso, D.; Pham, H. N.; Datye, A. K.; Dumesic, J. A., RuSn bimetallic catalysts for selective hydrogenation of levulinic acid to  $\gamma$ -valerolactone. *Applied Catalysis B: Environmental*. **2012**, 117, 321.
- González Maldonado, G. M.; Assary, R. S.; Curtiss, L. A.; Dumesic, J. A., Experimental and Theoretical Studies of the Acid-Catalyzed Conversion of Furfuryl Alcohol to Levulinic Acid in Aqueous Solution. *Energy and Environmental Science*. **2012**, 5, 6981.
- Brandon O'Neill, B. J.; Gürbüz, E. I.; Dumesic, J. A., Reaction kinetics studies of the conversions of formic acid and butyl formate over carbon-supported palladium in the liquid phase. *Journal of Catalysis*. **2012**, 290, 193.

- González Maldonado, G. M.; Assary, R. S.; Curtiss, L. A.; Dumesic, J. A., Acid-Catalyzed Conversion of Furfuryl Alcohol to Ethyl Levulinate in Liquid Ethanol. *Energy and Environmental Science*. **2012**, 5, 8990.
- Wettstein, S. G.; Martin Alonso, D.; Gurbuz, E. I.; Dumesic, J. A., A roadmap for conversion of lignocellulosic biomass to chemicals and fuels. *Current Opinion in Chemical Engineering*. **2012**, 1, 218.
- Wettstein, S. G.; Martin Alonso, D.; Chong, Y.; Dumesic, J. A., Production of levulinic acid and gamma-valerolactone (GVL) from cellulose using GVL as a solvent in biphasic systems. *Energy and Environmental Science*. **2012**, 5, 8199.
- Martin Alonso, D.; Wettstein, S. G.; Dumesic, J. A., Bimetallic catalysts for upgrading of biomass to fuels and chemicals. *Chemical Society Reviews*. **2012**, 41, 8075.
- Martin Alonso, D.; Wettstein, S. G.; Gurbuz, E. I.; Mellmer, M. A.; Dumesic, J. A., Integrated Conversion of Hemicellulose and Cellulose from Lignocellulosic Biomass. *Energy and Environmental Science*. **2013**, 6, 76.
- Gürbüz, E. I.; Marcel R. Gallo, J.; Martin Alonso, D.; Wettstein, S. G.; Lim, W. Y.; Dumesic, J. A., Conversion of hemicellulose to furfural using solid acid catalysts in  $\gamma$ -valerolactone, a biomass-derived solvent. *Angewandte Chemie International Edition*. **2013**, 52, 1270.
- Wang, D.; Mårup Osmundsen, C.; Taarning, E.; Dumesic, J. A., Selective production of aromatics from alkylfurans over solid acid catalysts. *Heterogeneous, Homogeneous, and Bio-Catalysis (ChemCatChem)*. **2013**, 5, 2044.
- Marcel R. Gallo, J.; Martin Alonso, D.; Mellmer, M. A.; Dumesic, J. A., Production and upgrading of 5-hydroxymethylfurfural using heterogeneous catalysts and biomass-derived solvents. *Green Chemistry*. **2013**, 15, 85.
- Martin Alonso, D.; Marcel R. Gallo, J.; Mellmer, M. A.; Wettstein, S. G.; Dumesic, J. A., Direct conversion of cellulose to levulinic acid and gamma-valerolactone using solid acid catalysts. *Catalysis Science & Technology*. **2013**, 3, 927.
- Martin Alonso, D.; Wettstein, S. G.; Dumesic, J. A., Gamma valerolactone, a sustainable platform molecule derived from lignocellulosic biomass. *Green Chemistry*. **2013**, 15, 584.
- Dietrich, P. J.; Wu, T.; Sumer, A.; Jellinek, J.; Delgass, W. N.; Ribeiro, F. H.; Miller, J. T.; Dumesic, J. A., Aqueous Phase Glycerol Reforming with Pt and PtMo Bimetallic Nanoparticle Catalysts: The Role of the Mo Promoter. *Topics in Catalysis*. **2013**, 56, 1814.
- Marcel R. Gallo, J.; Martin Alonso, D.; Mellmer, M. A.; Yeap, J. H.; Wong, H. C.; Dumesic, J. A., Production of furfural from lignocellulosic biomass using Beta Zeolite and biomass-derived solvent. *Topics in Catalysis*. **2013**, 56, 1775.
- Wang, D.; Hakim, S.; Martin Alonso, D.; Dumesic, J. A., A highly selective route to linear alpha olefins from biomass-derived lactones and unsaturated acids, *Chemical Communications*. **2013**, 49, 7040.
- Chia, M.; O'Neill, B. J.; Alamillo, R.; Dietrich, P. J.; Ribeiro, F. H.; Miller, J. T.; Dumesic, J. A., Bimetallic RhRe/C catalysts for the production of biomass-derived chemicals. *Journal of Catalysis*. **2013**, 308, 226.
- O'Neill, B. J.; Jackson, D. H. K.; Crisci, A. J.; Farberow, C. A.; Shi, F.; Alba-Rubio, A. C.; Lu, J.; Dietrich, P. J.; Gu, X.; Marshall, C. L.; Stair, P. C.; Elam, J. W.; Miller, J. T.; Ribeiro, F. H.; Voyles, P. M.; Greeley, J.; Mavrikakis, M.; Scott, S. L.; Kuech, T. J.; Dumesic, J. A., Stabilization by Atomic Layer Deposition of Cu Catalysts for Liquid-Phase Reactions. *Angewandte Chemie International Edition*. **2013**, 52, 13808.

**Robert M. Waymouth**

## **Challenges and Opportunities in the Selective Transformation of Biomass to Useful Chemical Intermediates and Materials**

Robert M. Waymouth  
*Department of Chemistry, Stanford University,*  
*Stanford CA 94305*  
*waymouth@stanford.edu*

Catalysis is also a foundational pillar for sustainable chemical processes; the discovery of highly active, environmentally benign catalytic processes is a central goal of Green Chemistry. The development of biomass-derived chemical and energy feedstocks is a key element of strategies to identify alternatives to our current petrochemical-based economies.

The dominance of fossil fuels and the environmental impact of petroleum and coal-based economies highlight the need for alternative and more varied sources of energy and chemicals to provide the energy, materials, products and technologies that improve our lives while preserving the environment for future generations. The utilization of renewable biomass requires selective catalysts that can convert highly hydroxylated biomass feedstocks into new chemical intermediates and thermoplastics. New scientific advances in the development of selective catalysts to transform these highly functionalized feedstocks will expand the range of options for transforming biomass into useful and environmentally sustainable products. We have developed new catalytic methods for transforming biomass feedstocks into new monomers and chemical intermediates based on the chemoselective oxidation of polyols. Mechanistic and theoretical investigations have illuminated several of the factors that lead to high chemoselectivities, but many challenges remain for the design of catalysts that are both tolerant and selective for the transformation of highly functionalized feedstocks.

### **DOE DE-SC0005430 - Enabling Catalytic Strategies for Biomass Conversion**

**PI:** Prof. Robert M. Waymouth

**Students:** Timothy Blake, Kevin Chung

### **RECENT PROGRESS**

***Selective Catalytic Oxidation of Biomass-derived Polyols.***<sup>1-3</sup> We discovered the cationic palladium-neocuproine complex **1** as a catalyst precursor that can mediate the selective aerobic oxidation of biomass-derived polyols to  $\alpha$ -hydroxyketones (Fig. 1). The chemoselective oxidation of glycerol yields dihydroxyacetone.<sup>4</sup>

Either air or benzoquinone can be utilized as terminal oxidants; oxidations proceed under mild reaction conditions and can be carried out on a large scale (20 g) in organic solvents or in water. This is an important advance, since glycerol is typically produced as a 12 wt% aqueous solution in bio-refineries.

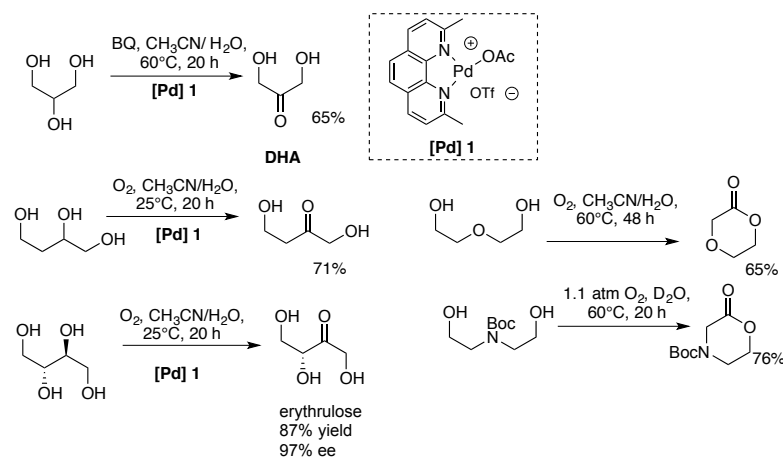


**Figure 2.** Chemoselective oxidation of polyols

with our first generation of catalysts was moderate (e.e. approx. 24% for the oxidation of erythritol to (S)-erythulose), these promising results illustrate the potential for converting unprotected biomass-derived polyols to new families of important chemical intermediates.<sup>2</sup> The selective catalytic oxidation of erythritol to erythulose provides a new strategy to this commodity product used in the cosmetics industry. In addition, the catalytic oxidative lactonization of oxa- or aza-1,5-diols generates the corresponding lactones,<sup>5</sup> which we are investigating as monomers with the organocatalytic polymerization strategies developed in our group.

**Mechanistic insights on Aerobic Pd oxidation catalysis.**<sup>3</sup> Mechanistic studies of the aerobic oxidation of polyols led to the identification of a novel trinuclear palladium oxide  $[(LPd(II))_3(m^3-O)_2]^{2+}$  (L = 2,9-dimethylphenanthroline). This trinuclear Pd compound was independently prepared and shown to be a competent intermediate in these aerobic oxidation reactions, illuminating a new pathway for the oxidation of Pd by O<sub>2</sub> (Fig 3).

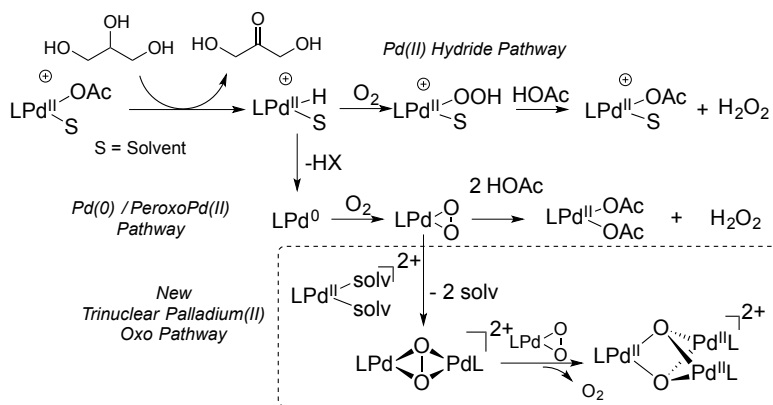


**Figure 3.** Generation of trinuclear  $[(LPd)_3(m^3-O)_2]^{2+}$  in aerobic oxidation reactions.

**Integrated catalytic strategy for the synthesis of high-melting polycarbonates from glycerol.**<sup>6</sup> Our discoveries of a catalytic strategies for the selective oxidation of glycerol to dihydroxyacetone, and the oxidative carbonylation of 1,3-diols to cyclic carbonates

(Fig. 4)<sup>7</sup> enabled us to develop an integrated catalytic strategy for the synthesis of poly(dihydroxyacetone carbonate) p(DHAC) from glycerol.<sup>6</sup> With these results, we have achieved one of the specific objectives for this project - to generate new families of high-performance thermoplastics from a bio-refinery feedstock.

The oxidative carbonylation of 1,3-diols is an important advance, as the standard procedure for generating polymerizable 6-membered carbonates involves phosgenation of 1,3-diols, but the hazards associated with phosgene-derived reagents limit the attractiveness of this approach.<sup>8</sup>

We have utilized our recently developed organic catalysts<sup>9</sup> for the ring-opening polymerization of the dimethyl acetal of dihydroxyacetone carbonate (MeODHAC, Fig. 5). The polymerization of MeODHAC can be carried out in the melt to generate poly(dihydroxyacetone carbonate) p(DHAC), after removal of the dimethyl acetal protecting groups. Investigation of the p(DHAC) homopolymer by differential scanning calorimetry (DSC), thermogravimetric analysis (TGA) and wide-angle X-ray scattering (WAXS) reveals this material to be a semicrystalline thermoplastic with a melting point of 245°C. The similarity of the melting point of p(DHAC) to that of the ethylene/CO alternating copolymer Carilon<sup>TM</sup> ( $T_m = 260^\circ\text{C}$ )<sup>10,11</sup> supports our original hypothesis that the polycarbonate derived from dihydroxyacetone would be a high melting thermoplastic. Co-polymerization of MeODHAC with  $\epsilon$ -caprolactone (CL) in the presence of 2.5-5 mol% TBD at 90-120°C generates random copolymers of caprolactone and dihydroxyacetone carbonate (Figure 5).

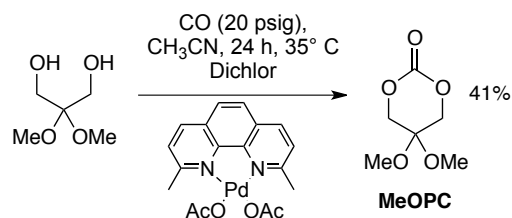


**Figure 4.** Oxidative carbonylation of diols to cyclic carbonates.

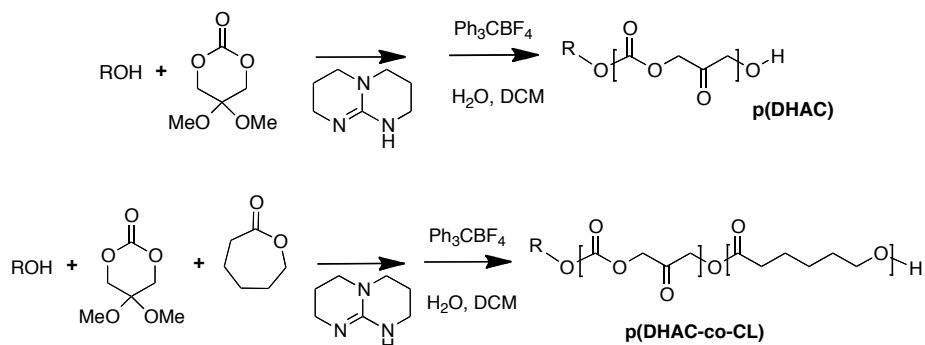


**Figure 5.** Bulk synthesis of p(DHAC) and co-polymers in using TBD as catalyst.

- (1) Chung, Y.-L.; Olsson, J. V.; Li, R. J.; Frank, C. W.; Waymouth, R. M.; Billington, S.; Sattely, E. "Graft polymerization of Lactide onto Lignin and Application in Biobased Composites" *ACS Sustainable Chem. Eng.* **2013**, *1*, 1231-1238.
- (2) De Crisci, A. G.; Chung, K.; Oliver, A. G.; Solis-Ibarra, D.; Waymouth, R. M. "Chemoselective Oxidation of Polyols with Chiral Palladium Catalysts" *Organometallics* **2013**, *32*, 2257-2266.
- (3) Ingram, A. J.; Solis-Ibarra, D.; Zare, R. N.; Waymouth, R. M. "Trinuclear Pd<sub>3</sub>O<sub>2</sub> Intermediate in Aerobic Oxidation Catalysis" *Angewandte Chemie International Edition* **2014**, *53*, 5648-5652.
- (4) Painter, R. M.; Pearson, D. M.; Waymouth, R. M. "Selective Catalytic Oxidation of Glycerol to Dihydroxyacetone" *Angew. Chem., Int. Ed.* **2010**, *49*, 9456-9459.

- (5) Chung, K.; Banik, S. M.; De Crisci, A. G.; Pearson, D. M.; Blake, T. R.; Olsson, J. V.; Ingram, A. J.; Zare, R. N.; Waymouth, R. M. "Chemoselective Pd-Catalyzed Oxidation of Polyols: Synthetic Scope and Mechanistic Studies" *J. Am. Chem. Soc.* **2013**, *135*, 7593-7602.
- (6) Simon, J.; Olsson, J. V.; Kim, H.; Tenney, I. F.; Waymouth, R. M. "Semicrystalline Dihydroxyacetone Copolymers Derived from Glycerol" *Macromolecules* **2012**, *45*, 9275-9281.
- (7) Pearson, D. M.; Conley, N. R.; Waymouth, R. M. "Palladium-Catalyzed Carbonylation of Diols to Cyclic Carbonates" *Adv. Synth. Catal.* **2011**, *353*, 3007-3013.
- (8) Shaikh, A. A. G.; Sivaram, S. "Organic carbonates" *Chem. Rev.* **1996**, *96*, 951-976.
- (9) Kiesewetter, M. K.; Shin, E. J.; Hedrick, J. L.; Waymouth, R. M. "Organocatalysis: Opportunities and Challenges for Polymer Synthesis" *Macromolecules* **2010**, *43*, 2093-2107.
- (10) Govaert, L. E.; de Vries, P. J.; Fennis, P. J.; Nijenhuis, W. F.; Keustermans, J. P. "Influence of strain rate, temperature and humidity on the tensile yield behaviour of aliphatic polyketone" *Polymer* **2000**, *41*, 1959-1962.
- (11) Carilon Thermoplastic Polymers, electronic resource: [www.sri.com/rd/carilon.pdf](http://www.sri.com/rd/carilon.pdf)
- (12) Zelikin, A. N.; Zawaneh, P. N.; Putnam, D. "A functionalizable biomaterial based on dihydroxyacetone, an intermediate of glucose metabolism" *Biomacromolecules* **2006**, *7*, 3239-3244.

#### **Publications Acknowledging this Grant in 2011-2014**

1. Pearson, D. M.; Conley, N. R.; Waymouth, R. M. "Palladium-Catalyzed Carbonylation of Diols to Cyclic Carbonates" *Adv. Synth. Cat.* **2011**, *353*, 3007-3013.
2. Kim, H.; Hedrick, J. L.; Waymouth, R. M. "Facile Synthesis of Functionalized Lactones and Organocatalytic Ring Opening Polymerization" *ACS Macro Letters*, **2012**, *1*, 845-847.
3. Simon, J.; Olsson, J. V.; Kim, H.; Tenney, I. F.; Waymouth, R. M. "Semicrystalline Dihydroxyacetone Copolymers Derived from Glycerol" *Macromolecules*, **2012**, *45*, 9275-9281.
4. De Crisci, A., Chung, K., Oliver, A., Waymouth, R. M. "Chemo- and Stereoselective Alcohol Oxidation with Chiral Palladium Catalysts" *Organometallics*, **2013**, *32*, 2257-2266.
5. Chung, K.; Banik, S. M.; De Crisci, A. G.; Pearson, D. M.; Blake, T.; Olsson, J. V.; Ingram, A. J.; Zare, R. N.; Waymouth, R. M. "Chemoselective Pd-catalyzed Oxidation of Polyols: Synthetic Scope and Mechanistic Studies" *J. Am. Chem. Soc.*, **2013**, *135*, 7593-7602.
6. Chung, Y.-L.; Olsson, J. V.; Li, R.J.; Frank, C. W.; Waymouth, R. M.; Billington, S.; Sattely, E. "Graft polymerization of Lactide onto Lignin and Application in Biobased Composites" *ACS Sustainable Chem. Eng.*, **2013**, *1*, 1231-1238.
7. Ingram, A. J.; Solis-Ibarra, D.; Zare, R. N.; Waymouth, R. M., "Trinuclear Pd<sub>3</sub>O<sub>2</sub> Intermediate in Aerobic Oxidation Catalysis" *Angew. Chem., Int. Ed.*, **2014**, *53*, 5648-5652.

This page is intentionally blank.

**Monday Morning**

**Catalysts for  
Polymer Synthesis**

This page is intentionally blank.

Richard R. Schrock

## Synthesis of Stereoregular ROMP Polymers

Richard R. Schrock  
Massachusetts Institute of Technology

### Presentation Abstract

Some of the most readily available and inexpensive monomers for Ring-Opening-Metathesis Polymerization (ROMP) are norbornenes or substituted norbornadienes. Polymers made from them have tacticities that remain in the polymer backbone after the C=C bonds in the polymer backbone are hydrogenated. Formation of polymers with exclusively one tacticity was rare until approximately twenty years ago when well-defined ROMP catalysts based on molybdenum imido alkylidene complexes that contain a biphenolate or binaphtholate ligand (Mo(NR)(CHR')(Biphen) catalysts) were shown to yield *cis, isotactic* poly(2,3-dicarbomethoxynorbornadiene) and related polymers from other monomers. In the last five years Mo and W MAP (MonoAryloxy Pyrrolide) imido alkylidene initiators, M(NR)(CHR')((Pyrrolide)(OR'''), have been found to produce *cis, syndiotactic* polynorbornenes and substituted norbornadienes through what has been called stereogenic metal control. A syndiotactic structure is formed because the approach of the monomer to the metal is regulated by the chirality at the metal, and that chirality switches with each monomer addition. The mode of forming *cis, syndiotactic* polynorbornenes has allowed the formation of a third regular structure, syndiotactic polymers prepared from *racemic* monomers that contain alternating enantiomers within the main chain, so-called "*cis, syndiotactic, alt*" structures where *alt* refers to the alternating incorporation of enantiomers. Although pure *trans* ROMP polymers prepared from Mo or W catalysts is not yet possible, pure *cis, syndiotactic* and *cis, isotactic* ROMP polymers can be formed with good generality. Therefore, pure *syndiotactic and isotactic hydrogenated polymers* can be formed from them for the first time. ROMP polymerizations of this general type often are also living, so a variety of more elaborated polymers with stereoregular sequences in them should be possible. The talk will focus on the use of recently prepared tungsten oxo alkylidene initiators in ROMP chemistry.

### 6412100: Catalysts for the Living Polymerizations of Olefins

**Postdocs:** William Forrest, Benjamin Autenrieth

**Students:** Hyangsoo Jeong

### Publications Acknowledging this Grant in 2011-2014

1. Flook, M. M.; Ng, V. W. L.; Schrock, R. R. Synthesis of *cis, syndiotactic* ROMP Polymers Containing Alternating Enantiomers. *J. Amer. Chem. Soc.* **2011**, *133*, 1784-1786

2. Schrock, R. R. Synthesis of stereoregular ROMP polymers using molybdenum and tungsten imido alkylidene initiators. *Dalton Trans* **2011**, *40*, 7484-7495.
3. Flook, M. M.; Börner, J.; Kilyanek, S.; Gerber, L. C. H.; Schrock, R. R. Five-Coordinate Rearrangements of Metallacyclobutane Intermediates During Ring-Opening Metathesis Polymerization (ROMP) of 2,3-Dicarboalkoxynorbornenes by Molybdenum and Tungsten Monoalkoxide Pyrrolide (MAP) Initiators. *Organometallics* **2012**, *31*, 6231-6243.
4. Yuan, J.; Schrock, R. R.; Gerber, L. C. H.; Müller, P.; Smith, S. J. Synthesis and ROMP Chemistry of Decafluoroterphenoxide Molybdenum Imido Alkylidene and Ethylene Complexes. *Organometallics* **2013**, *32*, 2983-2992.
5. Jeong, H.; Kozera, D. J.; Schrock, R. R.; Smith, S. J.; Zhang, J.; Ren, N.; Hillmyer, M. A. Z-Selective Ring-Opening Metathesis Polymerization of 3-Substituted Cyclooctenes by Monoaryloxide Pyrrolide Imido Alkylidene (MAP) Catalysts of Molybdenum and Tungsten. *Organometallics* **2013**, *32*, 4843-4850.
6. Forrest, W. P.; Axtell, J. C.; Schrock, R. R. Tungsten Oxo Alkylidene Complexes as Initiators for the Stereoregular Polymerization of 2,3-Dicarbomethoxy-norbornadiene. *Organometallics* **2014**, *33*, 2313-2325.

## **Catalytic Growth of Molecular Scale Wiring**

Prof. Colin Nuckolls  
Columbia University

### **Presentation Abstract**

This presentation will present the catalytic methods for the synthesis of carbon-based nanoelectronic materials. This is a field that is currently limited by the dearth of methods available to cleanly produce atomically defined materials such as carbon nanotubes and graphene ribbons. We utilize ring-opening alkyne metathesis polymerization (ROAMP) as the basis for creating an entire class of new electronic materials. The presentation is comprised of three integrated areas: (1) monomer design, (2) catalyst design, and (3) post-polymerization reactivity. These studies promise state of the art catalysts and monomers to create advanced materials.

### **DE-FG02-01ER15264: Catalytic Growth of Molecular Scale Wiring**

**Postdoc(s):** Brandon Fowler, Bharat Kumar

**Student(s):** Daniel Paley

### **RECENT PROGRESS**

We have developed the first example of a living ROAMP reaction, and further shown that multidentate ligands in the form of salicylimine ligands create more well-behaved living polymerizations. Building from these studies, we recently discovered the first new bench stable catalytic system that is able to effect the ROAMP reactions in protic solvents such as methanol and water. We have also begun a detailed mechanistic study of the ROAMP reaction of a dibenzocyclooctadiyne derivative reaction and have identified a metallotetrahedrane intermediate in the reaction.

## Publications Acknowledging this Grant in 2011-2014

(1) “Photochemical Reactivity of Graphene”, H. Liu, S. Ryu, Z. Chen, M. L. Steigerwald, C. Nuckolls, L. Brus, *J. Am. Chem. Soc.*, **2009**, *131*, 17099-17101. DOI: 10.1021/ja9043906.

(2) “Photovoltaic Universal Joints: Ball-and-Socket Interfaces in Molecular Photovoltaic Cells” N. J. Tremblay, A. A. Gorodetsky, M. Cox, T. Schiros, B. Kim, R. Steiner, Z. Bullard, A. Sattler, W-Y. So, Y. Itoh, M. F. Toney, H. Ogasawara, A. P. Ramirez, I. Kymissis, M. L. Steigerwald, C. Nuckolls, *Chem. Phys. Chem.*, **2010**, *11*, 799-803. DOI: 10.1002/cphc.200900941.

(3) “Design of Living Ring-Opening Alkyne Metathesis”, F. R. Fischer and C. Nuckolls, *Ang. Chem. Int. Ed.*, **2010**, *40*, 7257-7260. DOI: 10.1002/anie.201003549.

(4) “Bending Contorted Hexabenzocoronene into a Bowl”, A. C. Whalley, K. N. Plunkett, C. L. Schenck, A. A. Gorodetsky, C.-Y. Chiu, M. L. Steigerwald, C. Nuckolls, *Chem. Sci.*, **2011**, *2*, 132-135; DOI: 10.1039/C0SC00470G.

(5) “A Single-Molecule Potentiometer”, J. S. Meisner, M. Kamenetska, M. Krikorian, M. L. Steigerwald, L. Venkataraman, C. Nuckolls, *Nano Lett.*, **2011**, *4*, 1575-1579; DOI: 10.1021/nl104411f.

- Highlighted in April 4, 2011 *Chemical and Engineering News*.

(6) “Bidentate Phenoxides as Ideal Activating Ligands for Living Ring Opening Alkyne Metathesis Polymerization” D.F. Sedbrook, D.W. Paley, M. L. Steigerwald, C. Nuckolls and F. R. Fischer. *Macromol.*, **2012**, *45*, (12), 5040-5044. DOI: 10.1021/ma300876q.

(7) “Alcohol-Promoted Ring-Opening Alkyne Metathesis Polymerization” D.W. Paley, D. F. Sedbrook, J. Decatur, F.R. Fischer, M.L. Steigerwald, and C. Nuckolls, *Angew. Chemie. Int. Ed.* **2013**, *52*, 17, 4491-4594. DOI: 10.1002/ange.201300758.

(8) “Multicolor Live-Cell Chemical Imaging by Isotopically Edited Alkyne Vibrational Palette” Z. Chen; D. Paley; L. Wei, A. Weisman, R. Friesner, C. Nuckolls, W. Min. *J. Am. Chem. Soc.* **2014**. DOI: 10.1021/ja502706q.

**Monday Morning**

**Catalysis in  
Energy Applications**

This page is intentionally blank.

**A comparison of N-containing Carbon Nano-structures (CN<sub>x</sub>) and N-coordinated Iron-Carbon Catalysts (FeNC) for the Oxygen Reduction Reaction in Acidic Media**

U. S. Ozkan\*<sup>1</sup>, D. Singh<sup>1</sup>, J. Tian<sup>1</sup>, K. Mamtani<sup>1</sup>, J. King<sup>1</sup>, J. T. Miller<sup>2</sup>

<sup>1</sup> *Department of Chemical and Biomolecular Engineering, The Ohio State University.*

<sup>2</sup> *Chemical Sciences and Engineering Division, Argonne National Laboratory.*

**Presentation Abstract**

Two different classes of non-precious metal oxygen reduction catalysts for Proton Exchange Membrane (PEM) fuel cells, namely nitrogen-containing carbon nanostructures (CN<sub>x</sub>) and iron-nitrogen co-ordinated catalysts supported on carbon (FeNC) were studied. The motivation behind this study was to understand some of the key differences between the two and help resolve the existing active site debate related to these two classes of non-noble metal catalysts. Activity evaluation was performed by voltammetry techniques and fuel cell testing. X-ray Photoelectron Spectroscopy (XPS), Temperature Programmed Oxidation (TPO), X-ray Absorption Near Edge Spectroscopy (XANES), Extended X-ray Absorption Fine Structure spectroscopy (EXAFS), Mössbauer spectroscopy, Transmission Electron Microscopy (TEM), and SQUID magnetometry were used for characterization.

**USDOE DE-FG02-07ER15896**

**Heteroatom-doped carbon materials as oxygen reduction electro-catalysts in acidic and alkaline media**

**Postdocs:** Juan Tian, Anne-Marie Alexander, Doruk Dogu, Department of Chemical and Biomolecular Engineering, The Ohio State University

**Graduate students:** Deepika Singh, Kuldeep Mamtani, Department of Chemical and Biomolecular Engineering, The Ohio State University

**Undergraduate students:** Jesaiah King, Christopher R. Bruening, Kyle Qian, Robert Warburton, Department of Chemical and Biomolecular Engineering, The Ohio State University

**Collaborators:** Dr. Jeffrey Miller, Argonne National Laboratory, Dr. Jean-Marc Millet, CNRS Catalysis Research Institute Lyon-France, Dr. Aravind Ashtagiri, Department of Chemical and Biomolecular Engineering, The Ohio State University.

## RECENT PROGRESS

### *A comparison of N-containing Carbon Nano-structures (CN<sub>x</sub>) and N-coordinated Iron-Carbon Catalysts (FeNC) for the Oxygen Reduction Reaction in Acidic Media*

The primary objective of this study was to evaluate the differences in active sites of CN<sub>x</sub> and FeNC catalysts to help resolve the long-standing active site debate about these NNMCs. The study involved activity tests in a half-cell and fuel cell as well as a number of catalyst characterization techniques.

The Rotating Ring Disk Electrode (RRDE) activity test results showed that, between the two catalysts, FeNC is clearly more active than CN<sub>x</sub>, with an onset potential of 0.87V (unwashed) versus the onset potential of CN<sub>x</sub>, which is 0.78V vs. NHE (washed). The effect of acid washing is markedly different on the two catalysts. While CN<sub>x</sub> shows a dramatic improvement in activity after acid washing, FeNC, on the other hand, shows a noticeable decrease in its activity for the washed catalyst. This trend is an evidence of the inherent differences in the catalytic active sites of the catalysts. Acid washing possibly leaches away some of the Fe from the active Fe-N<sub>x</sub> sites in FeNC, leading to an activity loss, while in the case of CN<sub>x</sub>, the effect of acid washing is to eliminate the inactive iron species from the catalyst surface, along with the oxide support. After acid washing, CN<sub>x</sub>, which does not have exposed iron species, and consists of carbon

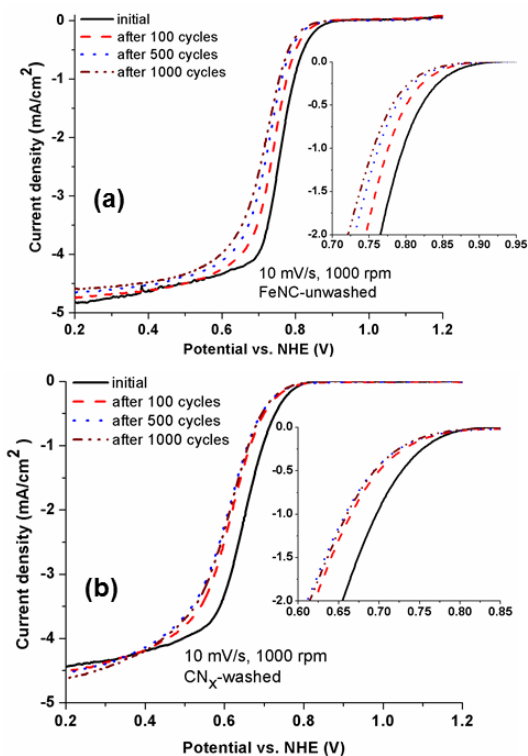


**Figure 1. Accelerated durability tests on the two most active catalysts. (a) FeNC-unwashed and (b) CN<sub>x</sub>-washed**

nanostructures with Fe embedded within the graphitic matrix, exhibits significantly higher ORR activity.

Accelerated durability tests (ADTs) were also conducted on CN<sub>x</sub> and FeNC. Figure 1(a) shows performance losses by ADTs in FeNC-unwashed. We observed that, over FeNC, there was a continued deterioration of performance with repeated cycles. This may be due to dissolution of iron in the acidic medium. In contrast to FeNC, which showed a steady loss of activity with increasing cycles, CN<sub>x</sub> demonstrated the highest activity loss during the first 100 cycles of repeated CVs (Figure 1b). It reached a pseudo-steady state thereafter, as there was no significant activity loss between cycles 100, 500 and 1000. As we reported previously [2], CN<sub>x</sub> materials do not undergo carbon corrosion as severely as some other carbon supports, such as Vulcan carbon, and this could be an additional factor responsible for its prolonged stability.

iR-free polarization curves obtained before and after a 100-hour potential hold at 0.5V are shown in Figure

2(a) for  $\text{CN}_x$ -washed and FeNC-unwashed, the most active forms of the two catalysts. While  $\text{CN}_x$  performed worse than FeNC, it exhibited better retention of initial activity. FeNC, on the other hand, showed a dramatic loss of activity, such that after the 100-h potential hold, the activities for the two catalysts were very similar. It is worth noting that although  $\text{CN}_x$  exhibited lower initial activity than FeNC catalysts, it also showed significantly less degradation over time.

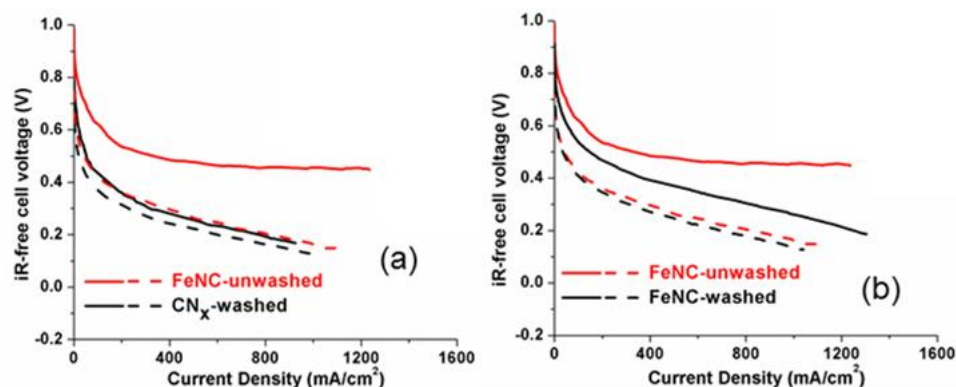


Figure 2. Fuel-cell polarization curves for (a) FeNC-unwashed and  $\text{CN}_x$ -washed, (b) FeNC-unwashed and FeNC-washed before (solid lines) and after (dashed lines) 100h potential hold at 0.5V

We also compared activities of acid-washed and unwashed FeNC catalysts. Figure 2(b) shows polarization curves of FeNC with and without an acid-wash. Although, the unwashed FeNC catalyst possessed a higher initial activity, after the potential hold, it is apparent that both the catalysts deactivated to almost the same level. This observation indicated that the activity loss due to acid washing is similar in magnitude to the activity loss suffered by the catalyst during the potential hold.

In addition to electrochemical performance evaluation, FeNC and  $\text{CN}_x$  catalysts were also characterized using techniques like XPS, TPO, EXAFS, XANES and SQUID magnetometry. The characterization studies showed major differences in surface functional groups, oxidation behavior, magnetization characteristics and oxidation state/coordination environment of Fe in these two groups of catalysts.

### ***Use of $\text{H}_2\text{S}$ to probe the active sites in Fe-N-C catalysts for the Oxygen Reduction Reaction (ORR) in acidic media***

In a previous study conducted by the PI's group,  $\text{H}_2\text{S}$  was used a probe molecule to attempt to exclusively poison any Fe active sites (if present) in  $\text{CN}_x$  catalysts. It was seen that  $\text{CN}_x$  catalysts do not deactivate for ORR with exposure to  $\text{H}_2\text{S}$ , indicating that iron active sites for ORR are absent in these materials. In this study, we have attempted to poison the Fe sites in FeNC catalysts with an initial hypothesis that Fe-based active sites would indeed get poisoned upon exposure to  $\text{H}_2\text{S}$ , thus highlighting the difference in active sites of FeNC and  $\text{CN}_x$  catalysts.

Figure 3 (a) shows the ORR activity for FeNC catalysts, which have already gone through high-temperature Ar and NH<sub>3</sub> exposure steps, before and after H<sub>2</sub>S treatment at 350 °C for 4h. It is evident that H<sub>2</sub>S treatment significantly lowers the activity for FeNC catalysts. To uncouple the heat treatment effect and the reduction effect of H<sub>2</sub>S, the experiments were repeated this time with an inert (Ar) and 5% H<sub>2</sub>/N<sub>2</sub> instead of H<sub>2</sub>S and no drop in the activity was observed. . The effect of H<sub>2</sub>S treatment at two different stages in FeNC synthesis, namely before any heat treatment and after Ar and NH<sub>3</sub> heat treatments was also studied (Figure 3(b)). Onset potential for the catalysts that are exposed to H<sub>2</sub>S are identical, regardless of the stage at which H<sub>2</sub>S was introduced.

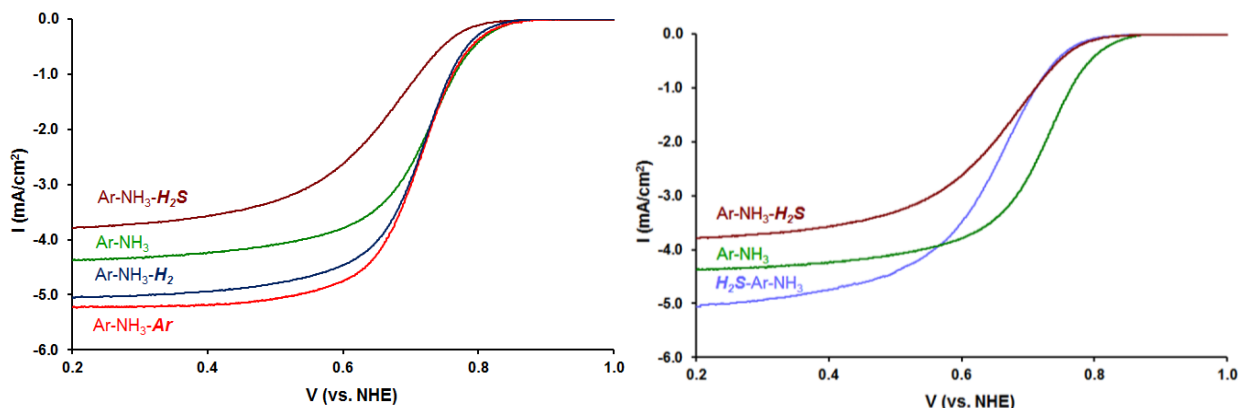


Figure 3. ORR Activity measurements by RDE in 0.5M H<sub>2</sub>SO<sub>4</sub> at 2500rpm (a) Effect of treatment with H<sub>2</sub>S, H<sub>2</sub> or Ar after high-temperature Ar-NH<sub>3</sub> treatment (b) Effect of H<sub>2</sub>S exposure at two different stages (pre-Ar and post-NH<sub>3</sub> treatment)

Characterization studies have also shown Fe coordination with sulfur. Fig. 4 shows a comparison of the FT magnitudes for poisoned and un-poisoned FeNC catalysts. The poisoned catalyst exhibits a very different coordination state from the unpoisoned one, implying that the sulfur treatment brought about a pronounced change in the local bonding environment of iron in FeNC.

These results are significant in highlighting the differences between FeNC and CN<sub>x</sub> catalysts in the terms of the role of iron in their active sites for ORR. In our previous studies, we observed no detrimental effect of H<sub>2</sub>S on CN<sub>x</sub>, while it deactivated platinum/carbon catalyst for ORR quite readily [3]. By demonstrating that H<sub>2</sub>S has a negative effect on ORR activity of FeNC catalysts, we provide concrete evidence that while Fe plays a critical role in catalyzing ORR for FeNC, it does not participate in catalyzing ORR in CN<sub>x</sub>, thereby proving that the two catalysts are indeed different classes of materials with different active sites for oxygen reduction.

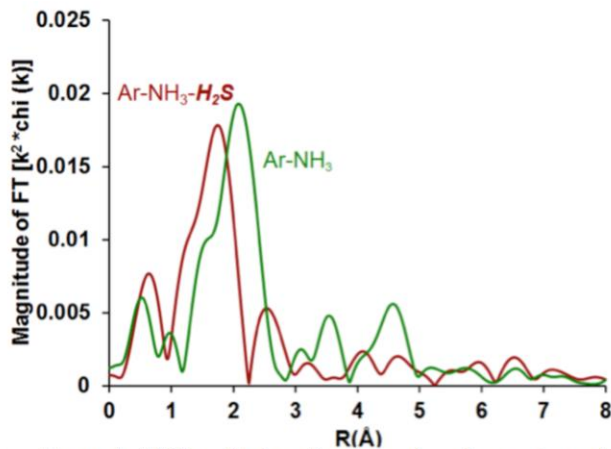


Figure 4. FT Magnitudes of poisoned and un-poisoned FeNC catalysts.

## Publications Acknowledging this Grant in 2011-2014

1. Biddinger, E. J.; von Deak, D.; Singh, D.; Marsh, H.; Tan, B.; Knapke, D. S.; Ozkan, U. S., Examination of catalyst loading effects on the selectivity of CN<sub>x</sub> and Pt/VC ORR catalysts using RRDE. *J. Electrochem. Soc.* **2011**, *158* (4), B402-B409.
2. von Deak, D.; Biddinger, E. J.; Ozkan, U. S., Carbon corrosion characteristics of CN<sub>x</sub> nanostructures in acidic media and implications for ORR performance. *J. Appl. Electrochem.* **2011**, *41* (7), 757-763.
3. von Deak, D.; Singh, D.; Biddinger, E. J.; King, J. C.; Bayram, B.; Miller, J. T.; Ozkan, U. S., Investigation of sulfur poisoning of CN<sub>x</sub> oxygen reduction catalysts for PEM fuel cells. *J. Catal.* **2012**, *285* (1), 145-151.
4. von Deak, D.; Singh, D.; King, J. C.; Ozkan, U. S., Use of carbon monoxide and cyanide to probe the active sites on nitrogen-doped carbon catalysts for oxygen reduction. *Appl. Catal. B-Environ.* **2011**, *113-114*, 126-133.
5. Singh, D.; Soykal, I. I.; Tian, J.; Von Deak, D.; King, J. C.; Miller, J. T.; Ozkan, U. S., In situ characterization of the growth of CN<sub>x</sub> carbon nanostructures as oxygen reduction reaction catalysts. *J. Catal.* **2013**, *304*, 100-111.
6. Bao, X. G.; Nie, X. W.; von Deak, D.; Biddinger, E.; Luo, W. J.; Asthagiri, A.; Ozkan, U.; Hadad, C., A First-Principles Study of the Role of Quaternary-N Doping on the Oxygen Reduction Reaction Activity and Selectivity of Graphene Edge Sites. *Top. Catal.* **2013**, *56* (18-20), 1623-1633.
7. Ozkan, U., Bridging Heterogeneous Catalysis and Electro-catalysis: Catalytic Reactions Involving Oxygen. *Top. Catal.* **2013**, *56* (18-20), 1603-1610.
8. Singh, D.; King, J. C.; Ozkan, U., Modified carbon materials as O<sub>2</sub> reduction reaction electrocatalysts in acid PEM fuel cells. In *Non-Noble Metal Fuel Cell Catalysts*, Wiley-VCH: 2013.
9. Singh, D.; Tian, J.; Mamtani, K.; King, J. C.; Miller, J. T.; Ozkan, U. S., A comparison of N-containing Carbon Nano-structures (CN<sub>x</sub>) and N-coordinated Iron-Carbon Catalysts (FeNC) for the Oxygen Reduction Reaction in Acidic Media. Submitted to *J. Catal.*
10. Singh, D.; Mamtani, K.; Bruening, C. R.; Miller, J. T.; Ozkan, U. S., Use of H<sub>2</sub>S to Probe the Active Sites in FeNC Catalysts for the Oxygen Reduction Reaction (ORR) in Acidic Media. Submitted to *ACS Catalysis*.

**Engineering electrocatalysts at the nano-scale for the hydrogen evolution reaction (HER) and the oxygen reduction reaction (ORR)**

Thomas F. Jaramillo (PI), Ariel Jackson (graduate student), Jakob Kibsgaard (post-doc)  
Department of Chemical Engineering  
381 N-S Axis  
Stanford University  
Stanford, CA 94305-5025  
Phone: (650) 498-6879; Fax: (650) 725-7294  
E-mail: jaramillo@stanford.edu

**Presentation Abstract**

In this project, we are outlining a systematic approach to develop active, selective, and stable catalyst materials for important electrochemical reactions involving energy conversion. Over the past year, we have focused our attention on developing active catalyst materials for the hydrogen evolution reaction (HER) and oxygen reduction reaction (ORR). There is significant room for improvement even for today's state-of-the-art materials. New strategies and approaches are needed to improve HER precious-metal free catalysts and ORR catalysts in order to enable economical hydrogen fuel generation and utilization.

In an effort to develop a scalable HER catalyst with an increased number of active sites we have developed supported thiomolybdate  $[\text{Mo}_3\text{S}_{13}]^{2-}$  nanocluster catalysts in which most sulfur atoms in the structure exhibit a structural motif similar to that observed at  $\text{MoS}_2$  edges. Supported sub-monolayers of  $[\text{Mo}_3\text{S}_{13}]^{2-}$  nanoclusters exhibited excellent HER activity and stability in acid. Imaging at the atomic scale with scanning tunneling microscopy (STM) allowed for direct characterization of these supported catalysts. The  $[\text{Mo}_3\text{S}_{13}]^{2-}$  nanoclusters reported herein demonstrated excellent turnover frequencies; higher than those observed for other non-precious catalysts synthesized by a scalable route. This work was recently published in Nature Chemistry, Vol.6 248-253 (2014).

Regarding catalyst development for the ORR, we have developed a Ru-core, Pt-shell system that exhibits increased specific activity as well as improved mass activity compared to commercial state-of-the-art Pt/C from TKK catalysts. This is an important contribution to the DOE goal of reducing Pt loading since a higher mass activity helps enable low Pt fuel cell electrodes.

**DOE Grant #: DE-SC0008685: Directed surfaces structures and interfaces for enhanced electrocatalyst activity, selectivity, and stability for energy conversion reactions**

**PI:** Lead PI(s) Name(s) (include only if different from above.)

**Postdoc(s):** Jakob Kibsgaard

**Student(s):** Ariel Jackson

## RECENT PROGRESS

### *Hydrogen evolution on thiomolybdate $[\text{Mo}_3\text{S}_{13}]^{2-}$ clusters*

In this project we have developed a new molecular hydrogen evolution reaction (HER) catalyst, thiomolybdate  $[\text{Mo}_3\text{S}_{13}]^{2-}$  nanoclusters that, upon supporting onto carbon electrode surfaces, bridges molecular and solid state electrocatalysis. The  $[\text{Mo}_3\text{S}_{13}]^{2-}$  nanoclusters demonstrated excellent turnover frequencies; higher than those observed for other non-precious catalysts synthesized by a scalable route.

In the modern chemical industry, molecular hydrogen ( $\text{H}_2$ ) is a crucial chemical feedstock with a production rate at the global-scale of approximately 50 billion kg/yr, used primarily in petroleum refining and in the synthesis of  $\text{NH}_3$  for fertilizer. The demand for  $\text{H}_2$  is likely to continue to increase as petroleum feedstocks are getting heavier and as the global population continues to increase. It is widely believed that electrocatalysis can play a key role in next generation sustainable energy conversion technologies and as such significant attention has been devoted to clean hydrogen production through electrocatalytic processes such as photoelectrochemical (PEC) water splitting or electrolysis coupled to renewable energy sources.

The hydrogen evolution reaction (HER,  $2\text{H}^+ + 2\text{e}^- \rightarrow \text{H}_2$ ) constitutes half of the water splitting reaction; active catalysts are required to increase process efficiency by minimizing the overpotential needed to drive the HER. Platinum is currently the best known catalyst for the HER as it requires negligible overpotential even at high reaction rates, but the scarcity and high cost of Pt limits its widespread technological use. Non-noble metal alternatives include nickel and nickel alloy catalysts but their use is typically restricted to alkaline solutions due to corrosion issues in acidic solutions. Recently,  $\text{MoS}_2$  nanoparticles have been identified as promising hydrogen evolution catalysts. However, only the edges of  $\text{MoS}_2$  nanoparticles are active, whereas the (0001) basal planes of  $\text{MoS}_2$  are catalytically inert, and high HER activity thus requires  $\text{MoS}_2$  nanocatalysts with a high number of exposed edge sites.

Thiomolybdate  $[\text{Mo}_3\text{S}_{13}]^{2-}$  nanoclusters contain 3 different types of sulfur ligands, all intrinsically located as edge sulfur atoms, see Figure 1, and can be viewed as molybdenum sulfide with a significant fraction of active sites as nearly all the sulfur atoms have the appropriate atomic structure for effective catalysis.

The catalytic activity of the  $[\text{Mo}_3\text{S}_{13}]^{2-}$  clusters was evaluated for the hydrogen evolution reaction (HER) using a three-electrode electrochemical cell. Figure 2a shows iR-corrected linear sweep voltammograms in the cathodic direction for the bare anodized HOPG surface compared to that with supported  $[\text{Mo}_3\text{S}_{13}]^{2-}$  clusters, normalized to the projected geometric area of the electrode. The bare anodized HOPG surface shows no HER activity in the investigated potential window. The  $[\text{Mo}_3\text{S}_{13}]^{2-}$ /HOPG sample on the other hand shows a sharp, exponential increase in the magnitude of the cathodic current density with increasing overpotential, indicative of HER activity.

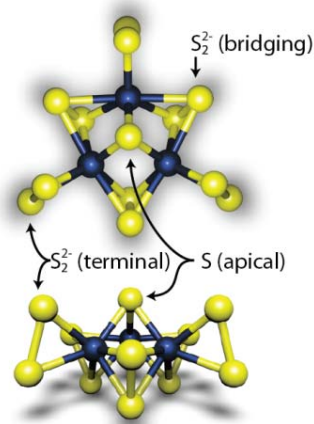


**Figure 1.** Model of a single  $[\text{Mo}_3\text{S}_{13}]^{2-}$  cluster containing 3 different types of sulfur ligands, top and side view.

The HER activity of  $[\text{Mo}_3\text{S}_{13}]^{2-}$  was further evaluated by depositing the clusters onto graphite paper (GP) disks at higher loadings for a more direct comparison to literature data on other molybdenum sulfide HER catalysts. The HER activity of these samples is shown in Figure 2b as iR-corrected cyclic voltammograms. All four samples exhibit excellent catalytic activity for the HER, as evidenced by a very early onset for the reaction at overpotentials of only 0.10 V – 0.12 V, and by reaching a current density of 10 mA/cm<sup>2</sup> at low overpotentials, between 0.18 V – 0.22 V. As expected, we see that higher loadings result in a higher current density at a given potential.

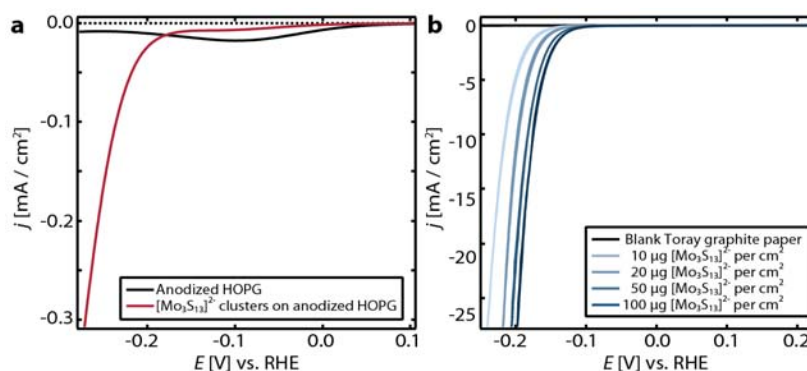


**Figure 2. HER activity of  $[\text{Mo}_3\text{S}_{13}]^{2-}$  clusters.** (a) Polarization curve of sub-monolayer coverage of  $[\text{Mo}_3\text{S}_{13}]^{2-}$  clusters on HOPG. (b). Cyclic voltammograms of  $[\text{Mo}_3\text{S}_{13}]^{2-}$  clusters on Toray graphite paper (GP) with loadings of 10, 20, 50, and 100 µg per cm<sup>2</sup>, respectively.

In this presentation, data will be shown that reveals the excellent stability of the  $[\text{Mo}_3\text{S}_{13}]^{2-}$  catalysts in acid, along with a direct comparison to other high performance HER materials by means of turnover frequency (TOF). These catalysts represent some of the highest TOF catalysts ever developed for the HER, among those that consist of earth-abundant elements with proven stability in acid.

### ***Core–Shell Ru@Pt Electrocatalysts for Oxygen Reduction***

The viability of fuel cell electrochemical systems relies on the identification of active and stable electrocatalysts for the oxygen reduction reaction (ORR). Based on density functional theory (DFT) calculations, ORR activity could be enhanced beyond that of Pt with a suitable weakening of the binding of oxygen intermediates relative to Pt. In the past year we have published on a new catalyst system based on a Ru core and Pt shell (Ru@Pt), which improves the per site activity by a factor of 2.1 over standard nanoparticulate Pt (Pt/C provided by TKK). DFT calculations from our collaborators in Jens Nørskov's group were used to guide the synthesis parameters. The DFT results showed that two opposing effects could be balanced in order to tune the oxygen adsorbate binding energy to the Pt surface ( $\Delta E_{\text{O}}$ ). Undercoordinated sites (such as edges and corners) that are prevalent in nanoparticles slightly strengthen  $\Delta E_{\text{O}}$ , while electronic and strain interactions with the Ru core significantly weaken  $\Delta E_{\text{O}}$ . The careful combination of the two effects allows for the slight overall weakening of  $\Delta E_{\text{O}}$  compared to pure Pt, resulting in the higher ORR activity.

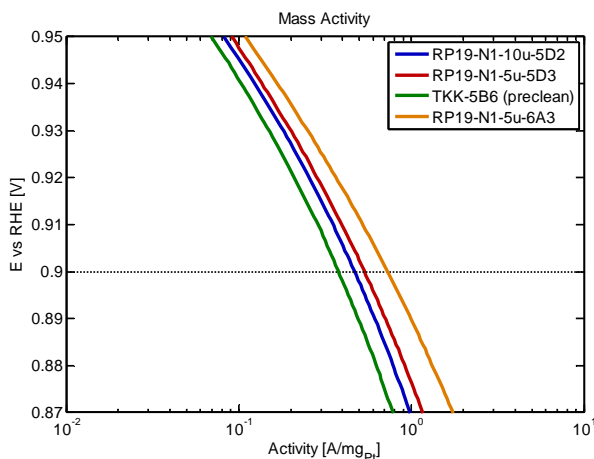
Our recent research has focused on improving the mass activity and quantifying the stability of the Ru@Pt system. A number of approaches have been used to improve the mass activity from a starting point of ~40% of Pt/C. The first step was reducing the amount of Pt, therefore achieving a thinner Pt shell. A thinner Pt shell improves the mass activity in two ways; it decreases the amount of Pt in the subsurface—which is not directly involved in ORR—and increases the prevalence of thin-shell active sites. The second step has been to reduce particle growth due to sintering in post synthesis cleaning and processing. Particle sintering and growth has the same negative effects on mass activity, too much Pt present in the subsurface and a reduction in the availability of thin-shell active sites. The main method to reduce sintering has been to replace a high temperature anneal with a room temperature electrochemical conditioning process.

Figure 3 shows the mass activity for several optimized Ru@Pt samples and a representative Pt/C sample matching the upper end of literature values. The Ru@Pt samples have 125-200% the mass activity of Pt/C at 0.9 V. This represents up to a 5-fold improvement over the initial Ru@Pt mass activity. The value of 0.72 mA mg<sup>-1</sup><sub>Pt</sub> is above the 2017 DOE target of 0.44 mA mg<sup>-1</sup><sub>Pt</sub>.

Finally, we have investigated the stability of the Ru@Pt samples and find that they meet or exceed those of Pt/C. The samples are cycled between 0.6 and 1.0 V vs RHE at 125 mV s<sup>-1</sup> for 30,000 cycles. At the end of 30,000 cycles the Ru@Pt sample maintained 80% of its initial mass activity, while we measured Pt/C as maintaining 75% of its mass activity. This indicates that the Ru@Pt is at least as stable as Pt/C. Additionally, at the end of 30,000 cycles, Ru@Pt has a mass activity of 0.58 mA mg<sup>-1</sup><sub>Pt</sub>, thus even at the end of life (30,000 cycles) the Ru@Pt catalyst is still above the 2017 DOE target for mass activity.

### Publications Acknowledging this Grant in 2011-2014

1. Kibsgaard, J.; Jaramillo, T.F.; Besenbacher, F. Building an appropriate active-site motif into a hydrogen evolution catalyst with thiomolybdate [Mo<sub>3</sub>S<sub>13</sub>]<sup>2-</sup> clusters. *Nature Chemistry* **2014**, *6*, 248-253
2. Jackson, A.; Viswanathan, V.; Forman, A.J.; Larsen, A.H.; Nørskov, J.K.; Jaramillo, T.F. Climbing the Activity Volcano: Core-Shell Ru@Pt Electrocatalysts for Oxygen Reduction. *ChemElectroChem* **2014**, *1*, 67-71.



**Figure 3.** Mass activities of 3 Ru@Pt samples (labeled RP19-xx-xx-xxx) in blue, red, and orange; and a representative Pt/C sample (labeled TKK-6B6) in green. The Ru@Pt samples have 125-200% the mass activity of Pt/C.

**Probing catalytic chemistry of oxygenates on oxide catalysts  
using CeO<sub>2</sub> model films and shaped nanoparticles**

Steven H. Overbury

Chemical Sciences Division, Oak Ridge National Laboratory

**Presentation Abstract**

Within our project, we have been probing the interactions and catalytic reactions of small oxygenates on model CeO<sub>2</sub> surfaces in order to obtain a fundamental understanding of reaction pathways and the relationship between surface structure and catalytic function. To probe this relationship, we have used two types of model catalysts with well-defined structures: highly oriented films of oxidized and reduced CeO<sub>2</sub> with (100) and (111) orientations examined in a UHV environment, and CeO<sub>2</sub> nanoparticles exhibiting {100} and {111} facets and examined within a reactor environment. Using these tools we are able to deduce the role of structure and bridge the gap between these experimental approaches. In this talk I will discuss our results on alcohol and acetaldehyde reactions using this approach.

**FWP: ERKCC96**

**Fundamentals of Catalysis and Chemical Transformations**

**PIs:** S.H. Overbury, Sheng Dai, De-en Jiang, Edward W. Hagaman, Michelle Kidder, Daniel A. Lutterman, David R. Mullins, Aditya (Ashi) Savara, Zili Wu

**Postdoc(s):** Peter Albrecht, J. Christopher Bauer, Florencia Calaza, Tsung-Liang (Alex) Chen, Lance W. Gill, Meijun Li, Amanda K.P. Mann, Zhenan Qiao

**Collaborators:** Larry F. Allard, Ariana Beste, Ye Xu

**Student(s):** Andrew Binder

**Affiliations(s):** Oak Ridge National Laboratory

**RECENT PROGRESS**

*Structure-function relationships in oxide catalysis*

A principal goal of this program is to understand the role that atomic surface structure plays in controlling selectivity in catalysis at oxide surfaces. We have focused upon CeO<sub>2</sub> as a catalytic oxide because of its reducibility that enables redox pathways and the fact that its bulk structure can accommodate high oxygen deficit without large scale change in the bulk structure. We have used two approaches to meet this goal. In the first approach we use highly oriented films with (100) and (111) orientation and explored surface chemistry within a UHV environment. [Mullins,2013a] In the second approach we have used highly oriented nanoparticles, (cubes, rods and octahedra that terminate in specific crystallographic orientations) and explored their catalytic chemistry within a reactor environment. [Qiao,2013] The combination of the

two approaches and comparison of the surface chemistry on the different surfaces led to a new understanding of the structure–function relationships in oxide catalysis.

We have focused on the surface chemistry of alcohols, aldehydes and acids and their interconversions and interactions with the  $\text{CeO}_2$  surface. By probing the species in temperature dependent soft x-ray

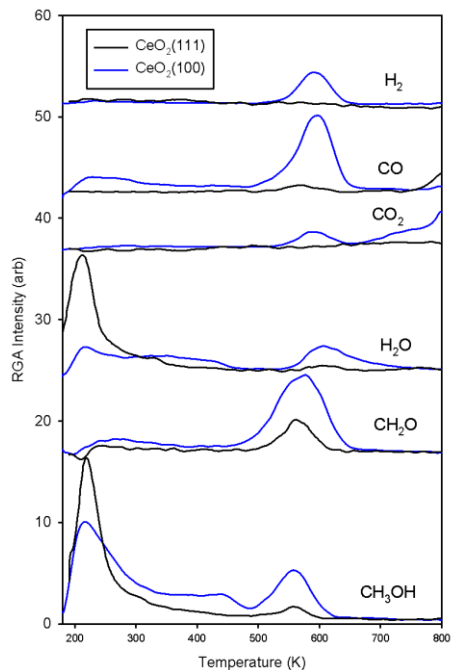


**Figure 2** TPD following methanol adsorption compared on two surfaces of  $\text{CeO}_2$

limited processes that occur in the range of 525 to 550 K for all alcohols.

DFT calculations were performed to clarify the origin of the selectivity differences between the (100) and (111) surfaces for the ethanol selective oxidation. Transition state barriers and structures were computed for the cleavage of the  $\alpha$ - and  $\beta$ -CH bond using the climbing image-nudged elastic band methodology. Transition states are found for both surfaces in which the ethoxy is interacting with the surface through the O and the methyl H, corresponding to pathways for ethylene formation (**Fig 2**). Two-step pathways involving a shallow minimum are also predicted. Heights of the barriers tended to favor acetaldehyde over ethylene for the fully oxidized surfaces for both (111) and (100) although the barriers were lower for the (100). The transition state structures clarify how the ethoxy rotates and shifts in order to activate either the  $\alpha$ - or the  $\beta$ -CH bond on both surfaces (not shown). Interestingly, the (100) surface structure enables the incorporation of the O (from ethylene) or acetaldehyde into the top layer, thereby, stabilizing products and transition states.

The structural dependence found for the oriented films was extended to determine if this factor leads to different selectivity in a catalytic reactor. Structure specific  $\text{CeO}_2$  nanoshapes can be synthesized in the

photoelectron spectroscopy (sXPS), near edge x-ray absorption fine structure (NEXAFS) at the C and O edges, and the desorption products in TPD the trends in reactivity have been mapped out. Adsorption of methanol, ethanol and i-propanol on both the  $\text{CeO}_2(100)$  and  $\text{CeO}_2(111)$  surfaces show differences associated with the variation in structure. [Albrecht,2013; Mullins,2013a] Alcohols bond to both surfaces by deprotonation to form alkoxy on oxidized or partly reduced surface as established by sXPS. However, products during subsequent TPD differ in that the (100) surface generally shows more complete dissociation to  $\text{H}_2$  and CO than the (111) surface (**Fig. 1**), a trend that is observed for all three alcohols.  $\text{CO}_2$  is also observed and is indicative of surface reduction by reactive alcohol adsorption. Selectivity to  $\text{CO}_2$  and the ratio of  $\text{H}_2/\text{H}_2\text{O}$  are consistent with greater ease of reduction of the (100) compared to (111). Dehydrogenation to aldehyde and dehydration to the alkene is observed in comparable amounts for both surfaces, when in the oxidized state, but reduction of the  $\text{CeO}_2$  strongly favors the dehydration pathway. The latter is attributed to the enthalpic tendency of the reduced surface to recover oxygen. Although low T water desorption and recombinative alcohol desorption is observed, most products desorb by reaction

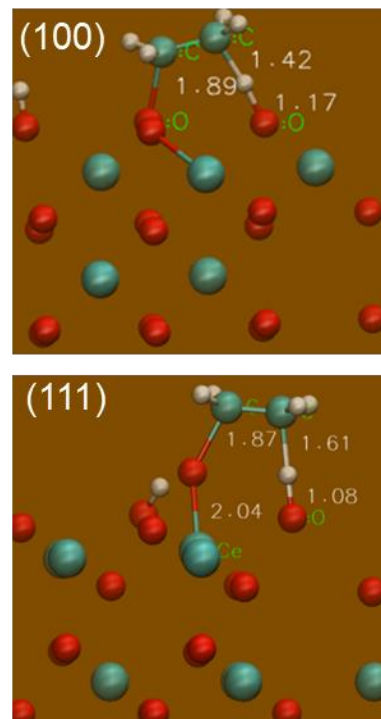


**Figure 1** Side view of transition state structure for ethylene formation on  $\text{CeO}_2(100)$  and (111).

form of cubes that expose primarily {100} facets while octahedra expose primarily {111} oriented surfaces [Lin,2014]. Wires/rods contain high defect levels and a mixture of terminations. Nanosized particles lead to high surface area and so they can be studied directly under catalytically relevant conditions by temperature programmed methods, steady state reaction and DRIFTS surface spectroscopy. This approach was used to probe structure effects in ethanol partial oxidation.[Li,2013] Shape dependent differences are observed in surface adsorbates, their transformation temperatures and the selectivity for dehydration, dehydrogenation and decomposition. Ethoxide and acetate are the primary surface species observed by DRIFTS under both TPD and TPSR conditions for all shapes. Different rates of  $\alpha$ - and  $\beta$ -CH bond scission on the different shapes are responsible for different product selectivity. Structure dependent, reductive vacancy formation and availability of reactant  $O_2$  combine to control surface H which in turn plays a role in controlling product selectivity. For all shapes, the dominant surface species during both TPD and under reaction conditions (TPSR) conditions are ethoxide below 575 K which is eventually reacted away and displaced by acetate and carbonates at higher temperature. Significant differences between TPD in He and TPSR in an ethanol/ $O_2$  reaction mixture are observed including inhibition of ethylene formation under selective oxidation reaction conditions compared to TPD, yielding pronounced differences in acetaldehyde: ethylene:  $CO_2$  selectivity. Factors that may lead to the observed structural differences are the oxygen storage and availability especially as it relates to  $H_2O/H_2$  selectivity, base strength, and mobility of oxygen anions on different surface terminations, variation in acid strength of the Ce cation sites caused by variation in their oxygen coordination, geometry of the adsorption site relative to the molecules and intermediates, and the relative numbers of vacancy or active sites created from oxygen removal during the reaction.

Reactions of acetaldehyde were also examined. On the highly oriented  $CeO_2(100)$  and  $CeO_2(111)$  films, differences were observed in the surface species and product distribution during TPD. Acetaldehyde is weakly adsorbed in an  $\eta^1$ -bonding configuration on  $CeO_2(111)$ , but pre-reduction of the surface leads to stronger adsorption, coupling of the aldehyde on the surface that is observable by RAIRS and the formation of enolates that are stable to above 400 K [Calaza,2012; Chen,2011] Deoxygenation and dehydration also occur, producing ethylene and acetylene at 580 and 620 K, respectively. Crotonaldehyde, a result of an aldol condensation reaction, could be produced by preparation of enolate at 400 K followed by re-adsorption of acetaldehyde at lower temperature. We propose that crotonaldehyde results from coupling of keto-cation and enolate that coexist on the  $CeO_2(111)$ . Acetaldehyde adsorption on  $CeO_2(100)$  is stronger than on the (111) surface and desorption extends through a larger T range from 200 K to above 400 K [Mullins,2013b]. In addition to the parent molecule, decomposition products are observed above 400 K. Total decomposition to CO,  $CO_2$  and  $H_2O$  are the principal pathways with a small amount of dehydration to produce acetylene at 700 K. A small amount of crotonaldehyde is evident at 430 K, a result of the aldol condensation coupling reaction.

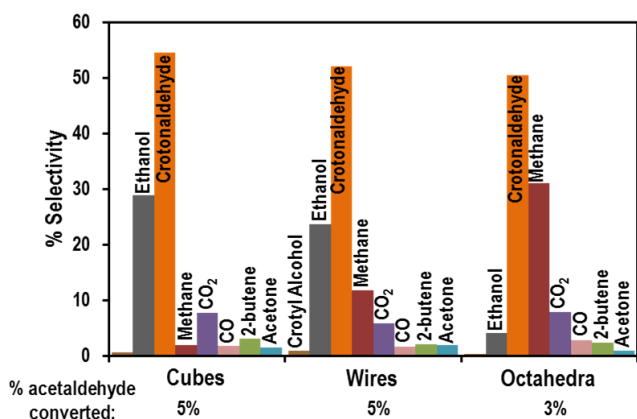


**Figure 3** Product distribution observed in acetaldehyde TPSR over three ceria nanoshapes

The observed coupling reaction was of key interest in reactor based studies of  $CeO_2$  nanoshapes. Rich catalytic chemistry is observed including coupling reactions (to crotonaldehyde, crotyl alcohol, 1,3-butadiene, 2-butene), ketonization (to acetone), Cannizzaro disproportionation (to ethanol and acetate), ring closure (to furan and benzene), and C-C bond cleavage (to methane and  $CO_x$ ). Differences are observed in the reaction selectivity, surface species, and desorption products among the different nanoshapes. (Fig. 3) These differences are attributed to structure-related variation in defect density, surface oxygen coordination, vacancy formation energy, and

acid/base properties. Although rapid deposition of carbonaceous material on the surface occurs, thereby altering the surface chemistry, the following trends in structure-reactivity are observed.

- Reactive coupling of acetaldehyde to produce crotonaldehyde occurs by aldol condensation on all nanoshapes but with higher selectivity on the octahedra at 675 K in TPSR and isothermal reactions.
- Enolate is observed by DRIFTS only on the cubes, but it is believed to be a short-lived intermediate in the aldol condensation to crotonaldehyde observed on all shapes.
- Ethanol is formed by a Cannizzaro disproportionation in TPD and TPSR leaving acetate; wires  $\approx$  cubes  $\gg$  octahedra. Higher base strength of defects and {100} surfaces leads to the activation of acetaldehyde to initiate this reaction.
- Similarly, decreased acetone production from octahedra compared to cubes and wires in TPD, TPSR, and isothermal reaction is attributed to the relative lack of surface acetate caused by the lower base strength predicted for the {111} surfaces compared to {100} and defects.
- C-C bond cleavage to  $\text{CO}_x$  and methane occurs increasingly as T increases on all shapes, with a selectivity at 675 K of wires  $\approx$  cubes  $\gg$  octahedra. This ordering is attributed to easier activation at defects and lower vacancy formation energy of {100} surfaces.
- Desorption of crotonaldehyde from the less reactive {111} facets of octahedra in comparison with the increased activation of adsorbates on defects and active {100} surfaces may explain the lower rates of coking on the octahedra compared to wires and cubes.

The relatively broader distribution of products observed in the reactor compared to TPD from films in UHV is attributed to the increased contacts through repeated adsorption/desorption processes within the reactor and to increased defects and surface hydroxyls groups on the nanoshapes. The variation between the different shapes demonstrates that even in a complex reactor environment the atomic structure of the oxide surface plays a controlling role.

To probe the base sites on  $\text{CeO}_2$  we explored adsorption of carbon dioxide.  $\text{CO}_2$  adsorbs weakly on  $\text{CeO}_2(111)$ , but much more strongly on  $\text{CeO}_2(100)$  surface. For both oxidized  $\text{CeO}_2(100)$  and reduced  $\text{CeO}_{1.7}(100)$ , dosing  $\text{CO}_2$  at 180 K results in carbonate formation and a small amount of physisorbed  $\text{CO}_2$  that desorbed by 250 K. [Albrecht,2014] Both species are distinguished by soft x-ray photoemission. Angle-dependent C k-edge NEXAFS reveals that the carbonate is oriented parallel to the surface in a tridentate configuration. This and other adsorption geometries were tested using DFT PBE+U calculations which confirmed that this most stable configuration (**Fig 4**). The carbonate decomposes in TPD solely as  $\text{CO}_2$  (no CO) even after adsorption on the reduced surface, indicating absence of surface oxidation by  $\text{CO}_2$ . However, carbonate is more stable on the reduced surface than on the oxidized surface.

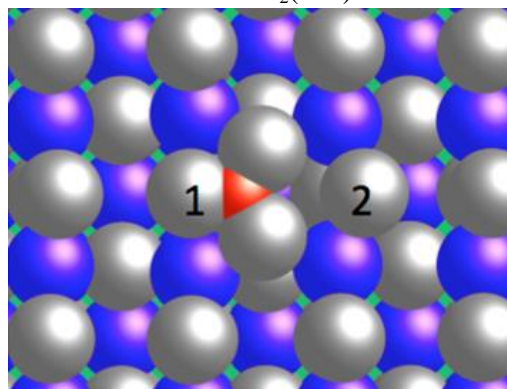


**Figure 4** Carbonate formation on  $\text{CeO}_2(100)$  by DFT. (grey balls O, blue balls Ce, red ball C)

We have examined water interactions on  $\text{CeO}_2$  cubes and octahedra by NMR to elucidate site and dynamic differences that arise from water adsorption. We achieve high resolution proton NMR spectra using ultra-fast magic angle spinning (MAS) and proton dilution using deuterium oxide ( $\text{D}_2\text{O}$ ). Fundamental differences in water behavior are observed. Under ambient conditions, both nanoshapes contain freely exchanging water whose resonance positions depend upon the number of water overlayers and the exchange processes with tightly held water and metal hydroxyl resonances. Also in both shapes, the water resonance exchanges easily with  $\text{D}_2\text{O}$  while the tightly held species exchange slowly. Upon removal of the ‘free’ water, the cubes reveal two broad bands, with multiple resonances apparent within each band. The latter must arise from unique binding sites for both the water and  $\text{CeOH}$  sites. In

contrast, octahedra exhibit two broad resonance bands but without indication of unique sites. The spin-lattice relaxation time,  $T_1$ , monitors the physical coupling of the NMR spin states with lattice motions. In the presence of multiple layers of free water,  $T_1$  of this rapidly exchanging water ( $\sim 10$  ms) dominates the relaxation processes, causing all species on the surface to relax at this rate. Distinct differences for cubes and octahedra become apparent as free water is removed. Reducing the free water to less than monolayer coverage leads to a lengthening of all site-specific resonances on the cubes by an order of magnitude. The octahedra show the same trend but the relaxation times on the octahedral are on the order of seconds. Bimodal relaxation for resonances of both nano-shaped ceria particles is the norm, a direct proof that resonances are heterogeneous with respect to relaxation pathways. A ca. 9 ppm band in the octahedra relaxes with an extraordinarily long  $T_1$  ( $\sim 70$  s) that suggests the protons at this site are isolated from the motion of all other proton species on the surface. We suggest that this is due to subsurface water or hydroxyl.

### *Au catalysts, clusters, bimetallic catalysts and oxides*

Utilization of metal clusters presents a means to prepare uniformly sized metal NPs, and we are combining Au cluster compound with uniformly structured  $\text{CeO}_2$  supports to prepare structurally defined catalysts. Ligands play a key role of stabilizing the Au clusters, but may poison or alter the activity of the Au catalytic sites. Therefore, a key question is how the ligands and the oxide support affect the nature of the Au sites and how they evolve as ligands are removed. Ligand stabilized metal clusters are of interest because it is not known how variation in the metal coordination and the ligands affect the activity of the metal. The effect of thiolate ligands was explored on the catalysis of  $\text{CeO}_2$ -rod supported  $\text{Au}_{25}(\text{SR})_{18}$  ( $\text{SR} = -\text{SCH}_2-\text{CH}_2-\text{Ph}$ ) by using CO oxidation as a probe reaction. Reaction kinetic tests, in situ IR and X-ray absorption spectroscopy, and density functional theory (DFT) were employed to understand how the thiolate ligands affect the nature of active sites, activation of CO and  $\text{O}_2$ , as well as the reaction mechanism and kinetics. The intact  $\text{Au}_{25}(\text{SR})_{18}$  on  $\text{CeO}_2$ -rods is found not able to adsorb CO (Fig. 5). Only when the thiolate ligands are partially removed, starting from the interface between  $\text{Au}_{25}(\text{SR})_{18}$  and  $\text{CeO}_2$  at temperatures of 423 K and above, can the adsorption of CO be observed by IR. DFT calculations suggest that CO adsorbs favorably on the exposed Au atoms. Accordingly, the CO oxidation light-off temperature shifts to lower temperature. Several types of Au sites are probed by IR of CO adsorption during the ligand removal process. The cationic Au sites (charged between 0 and +1) are found to play the major role for low temperature CO oxidation. A similar activation energy and reaction rate are found for CO oxidation on differently treated  $\text{Au}_{25}(\text{SR})_{18}/\text{CeO}_2$ -rod, suggesting a simple site-blocking effect of the thiolate ligands in Au nanoclusters catalysis. Isotopic labelling experiments clearly indicate that CO oxidation on  $\text{Au}_{25}(\text{SR})_{18}/\text{CeO}_2$ -rod proceeds predominantly *via* a redox mechanism where  $\text{CeO}_2$  activates  $\text{O}_2$  while CO is activated on the de-thiolated gold sites.

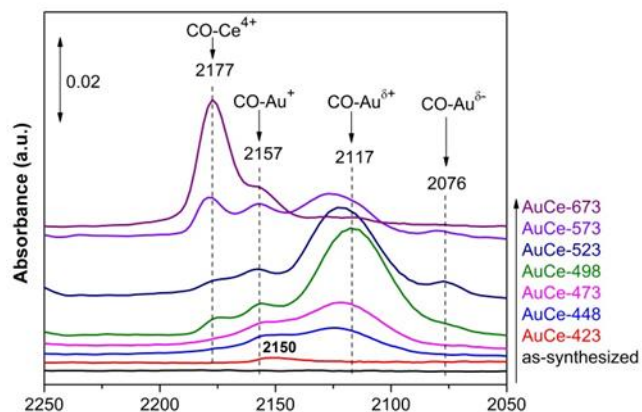


**Figure 5** DRIFTS showing speciation of CO adsorbate as Au cluster catalyst loses its ligands stepwise.

The intact  $\text{Au}_{25}(\text{SR})_{18}$  on  $\text{CeO}_2$ -rods is found not able to adsorb CO (Fig. 5). Only when the thiolate ligands are partially removed, starting from the interface between  $\text{Au}_{25}(\text{SR})_{18}$  and  $\text{CeO}_2$  at temperatures of 423 K and above, can the adsorption of CO be observed by IR. DFT calculations suggest that CO adsorbs favorably on the exposed Au atoms. Accordingly, the CO oxidation light-off temperature shifts to lower temperature. Several types of Au sites are probed by IR of CO adsorption during the ligand removal process. The cationic Au sites (charged between 0 and +1) are found to play the major role for low temperature CO oxidation. A similar activation energy and reaction rate are found for CO oxidation on differently treated  $\text{Au}_{25}(\text{SR})_{18}/\text{CeO}_2$ -rod, suggesting a simple site-blocking effect of the thiolate ligands in Au nanoclusters catalysis. Isotopic labelling experiments clearly indicate that CO oxidation on  $\text{Au}_{25}(\text{SR})_{18}/\text{CeO}_2$ -rod proceeds predominantly *via* a redox mechanism where  $\text{CeO}_2$  activates  $\text{O}_2$  while CO is activated on the de-thiolated gold sites.

A strategy for stabilizing ultra-small gold clusters, derived from thiolated gold clusters ( $\text{Au}_{25}$ ,  $\text{Au}_{144}$ ) was devised. After removal of the protecting thiolate ligands by thermal treatment, the Au clusters can be stabilized onto heterostructured mesoporous supports.[Ma, 2012] The essence of this strategy lies in use of the heterostructured binary oxide supports ( $\text{M}_x\text{O}_y\text{-mSiO}_2$ ) synthesized through a combination of a transition-metal oxide and an ordered mesoporous silica. Monodispersed Au clusters can be readily absorbed into the pores of this heterostructured oxide. The size of the clusters is maintained after

removing the thiolate ligands by thermal treatment in air, making this method superior to *in vacuo* treatment. Small gold clusters supported on these heterostructured mesoporous supports were found to be active for CO oxidation.

Various salts have been explored as supports for Au nanoparticles, including phosphates and sulfates, that may stabilize Au catalysts for gas phase reactions such as CO oxidation. Au catalysts containing BaSO<sub>4</sub> nanocrystals (5–8 nm) were prepared by an *in situ* growth method using an amphiphilic sodium dodecylbenzene sulfonate (SDBS) as the sulfate source, leading to new, highly stable, non-reducible but “active” Au catalyst supports that may be preferable to the typical reducible oxides for low-temperature CO oxidation. [Tian,2013] The results suggest a unique interaction between Au nanoparticles and nanosized BaSO<sub>4</sub> supports. In another approach, heterostructured PbSO<sub>4</sub>-MCF mesoporous material was prepared by an *in situ* growth method using SDBS as a sulfonate precursor and was used as a Au support. [Li,2014] After pretreating at 300 °C this catalyst showed high CO conversion below 100 °C and were found to be highly sinter-resistant.

We have developed a synthetic methodology to create supported, nanoscale AuCuPd ternary alloy nanoparticles through the diffusion of Cu<sup>0</sup> and Pd<sup>0</sup> atoms in an organic solvent using hexadecylamine as a reductant and ligand stabilizer. [Bauer,2013] Subjecting the AuCuPd catalyst to reductive or oxidative pretreatment conditions greatly affected the catalytic activity for the oxidation of CO. *In situ* XRD and EXAFS indicated that oxidizing the catalyst to 300 °C produced a AuPd alloy core that was separated from CuO and a small amount of PdO. Oxidation at 500 °C resulted in the segregation of PdO and CuO to form a decorated Au rich particle. Forming a PdO and CuO rich surface on the AuPd or Au-rich core decreased O<sub>ads</sub> spill over from Cu to Au or Pd sites and hindered access to the Au active sites resulting in decreased catalytic activity. Reducing the catalyst under H<sub>2</sub> formed an AuCuPd alloy with a Cu rich surface and formed the most active catalyst. It is likely that Cu, a base metal, helped to lower the activation energy through the activation O<sub>2</sub> that could migrate to Au or Pd sites. However, AuCu/SiO<sub>2</sub> demonstrated an opposite structure-activity relationship. It showed highest activity following oxidative treatment that formed an oxide-metal heterostructure. The CO oxidation activity of the Au-CuO catalyst was inhibited when C<sub>3</sub>H<sub>6</sub> or NO was introduced into the reaction stream. Interestingly, a physical mixture of Au-CuOx/SiO<sub>2</sub> and Pt/Al<sub>2</sub>O<sub>3</sub> worked in synergy to enhance the oxidation of NO to NO<sub>2</sub> with 90% conversion near 300 °C in the presence of CO. It is postulated that Pt oxidizes NO to prevent the Au-CuOx surface from NO inhibition while Au prevents CO from inhibiting the NO oxidation reaction on the Pt.

Oxides that are highly active in CO oxidation can be synthesized by addition of Cu and Co oxides to CeO<sub>2</sub>. [Liu, 2013] Calcination temperature has a strong effect upon the catalytic activity of ternary CuO<sub>x</sub>-CoO<sub>y</sub>-CeO<sub>2</sub> catalyst synthesized by co-precipitation. Effects of calcination temperature include water desorption, dehydration of hydroxides, mutual interaction among the metal oxide species and decomposition of Co<sub>3</sub>O<sub>4</sub> to CoO. In these steps, mutual interaction between Co<sub>3</sub>O<sub>4</sub> and CeO<sub>2</sub> plays a key role in enhancing the catalytic activity of catalysts and this occurs at temperature equal to or higher than 400 °C. Further, at 600 °C, the enrichment of Cu<sup>+</sup> on the surface of the oxide along with the appearance of oxygen vacancies in CeO<sub>2</sub> lead to highly active (non-precious metal) catalyst that can perform nearly complete conversion of CO in air at 345 K.

### Publications Acknowledging this Grant in 2014-2011

- Albrecht, P. M.; Jiang, D.-e.; Mullins, D. R., CO<sub>2</sub> Adsorption As a Flat-Lying, Tridentate Carbonate on CeO<sub>2</sub>(100), *J. Phys. Chem. C* **2014**, *118* 9042-9050.
- Baggetto, L.; Carroll, K. J.; Hah, H.-Y.; Johnson, C. E.; Mullins, D. R.; Unocic, R. R.; Johnson, J. A.; Meng, Y. S.; Veith, G. M., Probing the Mechanism of Sodium Ion Insertion into Copper Antimony Cu<sub>2</sub>Sb Anodes, *J. Phys. Chem. C* **2014**, *118* 7856-7864.
- Bauer, J. C.; Toops, T. J.; Oyola, Y.; II, J. E. P.; Dai, S.; Overbury, S. H., Catalytic activity and thermal stability of Au-CuO/SiO<sub>2</sub> catalysts for the low temperature oxidation of CO in the presence of propylene and NO, *Catal. Today* **2014**, *231*, 15–21.
- Li, L.; Tian, C. C.; Chai, S. H.; Binder, A.; Brown, S.; Veith, G. M.; Dai, S., Gold nanocatalysts supported on heterostructured PbSO<sub>4</sub>-MCF mesoporous materials for CO oxidation, *Catal. Commun.* **2014**, *46*, 234-237.
- Lin, Y. Y.; Wu, Z. L.; Wen, J. G.; Poepelmeier, K. R.; Marks, L. D., Imaging the Atomic Surface Structures of CeO<sub>2</sub> Nanoparticles, *Nano Letters* **2014**, *14*(1), 191-196.
- Mann, A. K. P.; Wu, Z.; Calaza, F. C.; Overbury, S. H., Adsorption and Reaction of Acetaldehyde on Shape-Controlled CeO<sub>2</sub> Nanocrystals: Elucidation of Structure-function Relationships, *ACS Catal.* **2014**, *submitted*
- Savara, A., Vibrational spectra of CO adsorbed on oxide thin films: A tool to probe the surface defects and phase changes of oxide thin films, *J. Vac. Sci Technol. A* **2014**, *32*, 021505.
- Wu, Z.; Jiang, D.-e.; Mann, A.; Mullins, D. R.; Qiao, Z.; Jr., L. F. A.; Jin, R.; Overbury, S. H., Thiolate ligands: a double-edged sword for CO oxidation on CeO<sub>2</sub>-supported Au<sub>25</sub>(SR)<sub>18</sub> nanoclusters, *J. Am. Chem. Soc* **2014**, *136*, 6111-6122.
- Yu, Y.; Luo, Z.; Chevrier, D. M.; Leong, D. T.; Zhang, P.; Jiang, D.-e.; Xie, J., Identification of a Highly Luminescent Au<sub>22</sub>(SG)<sub>18</sub> Nanocluster, *JACS* **2014**, *136*, 1246-1249.
- Albrecht, P. M.; Mullins, D. R., Adsorption and Reaction of Methanol over CeO<sub>x</sub>(100) Thin Films, *Langmuir* **2013**, *29* 4559–4567.
- Bauer, J. C.; Mullins, D. R.; Oyola, Y.; Overbury, S. H.; Dai, S., Structure Activity Relationships of Silica Supported AuCu and AuCuPd Alloy Catalysts for the Oxidation of CO, *Catal. Lett.* **2013**, *143*(9), 926-935.
- Beste, A.; Buchanan, A. C., III, Computational Investigation of the Pyrolysis Product Selectivity for alpha-Hydroxy Phenethyl Phenyl Ether and Phenethyl Phenyl Ether: Analysis of Substituent Effects and Reactant Conformer Selection, *J. Phys. Chem. A* **2013**, *117*, 3235–3242.
- Binder, A. J.; Qiao, Z. A.; Veith, G. M.; Dai, S., Deposition-Precipitation and Stabilization of a Silica-Supported Au Catalyst by Surface Modification with Carbon Nitride, *Catal. Lett.* **2013**, *143*(12), 1339-1345.
- Galhenage, R. P.; Yan, H.; Tenney, S. A.; Park, N.; Henkelman, G.; Albrecht, P. M.; Mullins, D. R.; Chen, D. A., Understanding the Nucleation and Growth of Metals on TiO<sub>2</sub>: Co compared to Au, Ni and Pt, *J. Phys. Chem. C* **2013**, *117*, 7191-7201.
- Ghidiu, M. J.; Pistner, A. J.; Yap, G. P. A.; Lutterman, D. A.; Rosenthal, J., Thermal versus Photochemical Reductive Elimination of Aryl Chlorides from NHC-Gold Complexes, *Organometallics* **2013**, *32*(18), 5026-5029.
- Jiang, D.-e.; Overbury, S. H.; Dai, S., On the Structure of Au<sub>15</sub>(SR)<sub>13</sub> and its Implication on the Origin of the Nucleus in Thiolated Gold Nanoclusters *JACS* **2013**, *135*, 8786–8789.
- Li, M.; Wu, Z.; Overbury, S. H., Surface structure dependence of selective oxidation of ethanol on faceted CeO<sub>2</sub> nanocrystals, *J. Catal.* **2013**, *306*, 164-176.

- Liu, Z. G.; Chai, S. H.; Binder, A.; Li, Y. Y.; Ji, L. T.; Dai, S., Influence of calcination temperature on the structure and catalytic performance of CuO<sub>x</sub>-CoO<sub>y</sub>-CeO<sub>2</sub> ternary mixed oxide for CO oxidation, *App. Catal., A* **2013**, *451*, 282-288.
- Moses-DeBusk, M.; Yoon, M.; Allard, L. F.; Mullins, D. R.; Wu, Z. L.; Yang, X. F.; Veith, G.; Stocks, G. M.; Narula, C. K., CO Oxidation on Supported Single Pt Atoms: Experimental and ab Initio Density Functional Studies of CO Interaction with Pt Atom on theta-Al<sub>2</sub>O<sub>3</sub>(010) Surface, *JACS* **2013**, *135*(34), 12634-12645.
- Mullins, D. R.; Albrecht, P. M., Acetaldehyde Adsorption and Reaction on CeO<sub>2</sub>(100) Thin Films, *J. Phys. Chem. C* **2013a**, *117*(28), 14692-14700.
- Mullins, D. R.; Albrecht, P. M.; Calaza, F. C., Variations in Reactivity on Different Crystallographic Orientations of Cerium Oxide, *Top. Catal.* **2013b**, *56*, 1345-1362.
- Pistner, A. J.; Lutterman, D. A.; Ghidui, M. J.; Ma, Y.-Z.; Rosenthal, J., Synthesis, Electrochemistry, and Photophysics of a Family of Phlorin Macrocycles That Display Cooperative Fluoride Binding. , *JACS* **2013**, *135*, 6601-6607.
- Pollock, J. B.; Cook, T. R.; Schneider, G. L.; Lutterman, D. A.; Davies, A. S.; Stang, P. J., Photophysical Properties of Endohedral Amine-Functionalized Bis(phosphine) Pt(II) Complexes as Models for Emissive Metallacycles, *Inorg. Chem* **2013**.
- Qiao, Z. A.; Wu, Z. L.; Dai, S., Shape-Controlled Ceria-based Nanostructures for Catalysis Applications, *ChemSusChem* **2013**, *6*(10), 1821-1833.
- Ren, Y.; Ma, Z.; Morris, R. E.; Liu, Z.; Jiao, F.; Dai, S.; Bruce, P. G., A solid with a hierarchical tetramodal micro-meso-macro pore size distribution, *Nat. Commun.* **2013**, *4*.
- Tian, C.; Chai, S.-H.; Mullins, D. R.; Zhu, X.; Binder, A.; Guo, Y.; Dai, S., Heterostructured BaSO<sub>4</sub>-SiO<sub>2</sub> mesoporous materials as new supports for gold nanoparticles in low-temperature CO oxidation, *Chem. Comm.* **2013a**, *49* 3464-3466.
- Tian, C. C.; Oyola, Y.; Nelson, K. M.; Chai, S. H.; Zhu, X.; Bauer, J. C.; Janke, C. J.; Brown, S.; Guo, Y. L.; Dai, S., A renewable HSO<sub>3</sub>/H<sub>2</sub>PO<sub>3</sub>-grafted polyethylene fiber catalyst: an efficient heterogeneous catalyst for the synthesis of 5-hydroxymethylfurfural from fructose in water, *RSC Adv* **2013b**, *3*, 21242-21246.
- Tian, C. C.; Bao, C. H.; Binder, A.; Zhu, Z. Q.; Hu, B.; Guo, Y. L.; Zhao, B.; Dai, S., An efficient and reusable "hairy" particle acid catalyst for the synthesis of 5-hydroxymethylfurfural from dehydration of fructose in water, *Chem. Commun.* **2013c**, *49*, 8668-8670.
- Veith, G. M.; Lupini, A. R.; Baggetto, L.; Browning, J. F.; Keum, J. K.; Villa, A.; Prati, L.; Papandrew, A. B.; Goenaga, G. A.; Mullins, D. R.; Bullock, S. E.; Dudney, N. J., Evidence for the Formation of Nitrogen-Rich Platinum and Palladium Nitride Nanoparticles, *Chem. Mater.* **2013**, *25*(24), 4936-4945.
- Allard, L. F.; Overbury, S. H.; Bigelow, W. C.; Katz, M. B.; Nackashi, D. P.; Damiano, J., Novel MEMS-Based Gas-Cell/Heating Specimen Holder Provides Advanced Imaging Capabilities for In Situ Reaction Studies, *Microsc. Microanal.* **2012**, *18*(4), 656-666.
- Bauer, J. C.; Veith, G. M.; Allard, L. F.; Oyola, Y.; Overbury, S. H.; Dai, S., Silica-Supported Au-CuO<sub>x</sub> Hybrid Nanocrystals as Active and Selective Catalysts for the Formation of Acetaldehyde from the Oxidation of Ethanol, *ACS Catalysis* **2012**, *2*(12), 2537-2546.
- Beste, A.; Buchanan, A. C., III, The Role of Carbon-Carbon Phenyl Migration in the Pyrolysis Mechanism of β-O-4 Lignin Model Compounds: Phenethyl Phenyl Ether and α-Hydroxy Phenethyl Phenyl Ether, *J. Phys. Chem. A* **2012a**, *116*, 12242-12248.
- Beste, A.; Buchanan, A. C., III, Kinetic Simulation of the Thermal Degradation of Phenethyl Phenyl Ether, a Model Compound for the β-O-4 Linkage in Lignin, *Chem. Phys. Lett.* **2012b**, *550*, 19-24.

- Calaza, F. C.; Xu, Y.; Mullins, D. R.; Overbury, S. H., Oxygen Vacancy-Assisted Coupling and Enolization of Acetaldehyde on CeO<sub>2</sub>(111), *JACS* **2012**, *134*(43), 18034-18045.
- Fulvio, P. F.; Mayes, R. T.; Bauer, J. C.; Wang, X. Q.; Mahurin, S. M.; Veith, G. M.; Dai, S., "One-pot" synthesis of phosphorylated mesoporous carbon heterogeneous catalysts with tailored surface acidity, *Catal. Today* **2012**, *186*(1), 12-19.
- Hagaman, E. W.; Chen, B. H.; Jiao, J.; Parsons, W., Solid-state O-17 NMR study of benzoic acid adsorption on metal oxide surfaces, *Solid State Nucl. Magn. Reson* **2012**, *41*, 60-67.
- Jiang, D.-e.; Overbury, S. H.; Dai, S., Structures and Energetics of Pt Clusters on TiO<sub>2</sub>: Interplay between Metal–Metal Bonds and Metal–Oxygen Bonds, *J. Phys. Chem. C* **2012**, *116*(41), 21880-21885.
- Kintzel, E. J. J.; Kidder, M. K.; Buchanan, A. C., III; Britt, P. F.; Mamantov, E.; Zamponi, M.; Herwig, K. W., The Dynamics of 1,3-Diphenylpropane Tethered to the Interior Pore Surfaces of MCM-41, *J. Phys. Chem. C* **2012**, *116*, 923.
- Ma, G. C.; Binder, A.; Chi, M. F.; Liu, C.; Jin, R. C.; Jiang, D. E.; Fan, J.; Dai, S., Stabilizing gold clusters by heterostructured transition-metal oxide-mesoporous silica supports for enhanced catalytic activities for CO oxidation, *Chem. Comm.* **2012**, *48*(93), 11413-11415.
- Mullins, D. R.; Albrecht, P. M.; Chen, T.-L.; Calaza, F.; Biegalski, M. D.; Christen, H. M.; Overbury, S. H., Water Dissociation on CeO<sub>2</sub>(100) and CeO<sub>2</sub>(111) Thin Films, *J. Phys. Chem. C* **2012**, *116*, 19419–19428.
- Qian, H. F.; Jiang, D. E.; Li, G.; Gayathri, C.; Das, A.; Gil, R. R.; Jin, R. C., Monoplatinum Doping of Gold Nanoclusters and Catalytic Application, *JACS* **2012**, *134*(39), 16159-16162.
- Qiao, Z. A.; Huo, Q. S.; Chi, M. F.; Veith, G. M.; Binder, A. J.; Dai, S., A "Ship-In-A-Bottle" Approach to Synthesis of Polymer Dots@Silica or Polymer Dots@Carbon Core-Shell Nanospheres, *Advanced Materials* **2012**, *24*(45), 6017-6021.
- Singh, J. A.; Overbury, S. H.; Dudney, N. J.; Li, M.; Veith, G. M., Gold Nanoparticles Supported on Carbon Nitride: Influence of Surface Hydroxyls on Low Temperature Carbon Monoxide Oxidation, *ACS Catalysis* **2012**, *2*, 1138–1146.
- Tian, C. C.; Chai, S. H.; Zhu, X.; Wu, Z. L.; Binder, A.; Bauer, J. C.; Brown, S.; Chi, M. F.; Veith, G. M.; Guo, Y. L.; Dai, S., In situ growth synthesis of heterostructured LnPO<sub>4</sub>-SiO<sub>2</sub> (Ln = La, Ce, and Eu) mesoporous materials as supports for small gold particles used in catalytic CO oxidation, *J Mater. Chem.* **2012**, *22*(48), 25227-25235.
- Wu, Z.; Li, M.; Overbury, S. H., Raman Spectroscopic Study of the Speciation of Vanadia Supported on Ceria Nanocrystals with Defined Surface Planes, *ChemCatChem* **2012a**, *4*(10), 1653-1661.
- Wu, Z.; Li, M.; Overbury, S. H., On the Structure Dependence of CO Oxidation over CeO<sub>2</sub> Nanocrystals with Well-Defined Surface Planes, *J. Catal.* **2012b**, *285*, 61-73.
- Wu, Z.; Schwartz, V.; Li, M.; Rondinone, A.; Overbury, S. H., Support Shape Effect in Metal Oxide Catalysis: Ceria Nanoshapes Supported Vanadia Catalysts for Oxidative Dehydrogenation of Isobutane, *J. Phys. Chem. C* **2012c**, *3* 1517–1522.
- Wu, Z. L.; Li, M. J.; Mullins, D. R.; Overbury, S. H., Probing the Surface Sites of CeO<sub>2</sub> Nanocrystals with Well-Defined Surface Planes via Methanol Adsorption and Desorption, *ACS Catalysis* **2012d**, *2*(11), 2224-2234.
- Yang, X.; Wu, Z.; Moses-Debusk, M.; Mullins, D. R.; Mahurin, S. M.; Geiger, R. M.; Kidder, M. K.; Narula, C. K., Heterometal Incorporation in M-Exchanged Zeolites Enables Low Temperature Catalytic Activity of NO<sub>x</sub> Reduction, *J. Phys. Chem. C* **2012**, *116*, 23322-23331.
- Yunker, J. M. B., A.; Buchanan, I., A. C., Computational Study of Bond Dissociation Enthalpies for Lignin Model Compounds: β-5 Arylcoumaran, *Chem. Phys. Lett* **2012**, *545*, 100-106.

- Bauer, J. C.; Mullins, D.; Li, M. J.; Wu, Z. L.; Payzant, E. A.; Overbury, S. H.; Dai, S., Synthesis of silica supported AuCu nanoparticle catalysts and the effects of pretreatment conditions for the CO oxidation reaction, *Phys Chem Chem Phys* **2011**, *13*(7), 2571-2581.
- Brooks, J. D.; Chen, T.-L.; Mullins, D. R.; Cox, D. F., Reactions of ethylidene on a model chromia surface: 1,1-dichloroethane on stoichiometric  $\alpha$ -Cr<sub>2</sub>O<sub>3</sub> (10-12), *Surface Science* **2011**, *605*, 1170.
- Calaza, F. C.; Chen, T. L.; Mullins, D. R.; Overbury, S. H., Structure and Reactivity of Alkyl Ethers Adsorbed on CeO<sub>2</sub>(111) Model Catalysts, *Top. Catal.* **2011**, *54*(1-4), 56-69.
- Chen, T.-L.; Mullins, D. R., Ethylene Glycol Adsorption and Reaction over CeO<sub>x</sub>(111) Thin Films, *J. Phys. Chem. C* **2011a**, *115* 13725-13733.
- Chen, T.-L.; Mullins, D. R., Adsorption and Reaction of Acetaldehyde over CeO<sub>x</sub>(111) Thin Films, *J. Phys. Chem. C* **2011b**, *115*, 3385.
- Jiang, D. E.; Dai, S., The Role of Low-coordinate Oxygen on Co<sub>3</sub>O<sub>4</sub>(110) in Catalytic CO Oxidation, *Phys. Chem. Chem. Phys.* **2011a**, *13*, 978.
- Jiang, D. E.; Overbury, S. H.; Dai, S., Interaction of Gold Clusters with a Hydroxylated Surface, *J. Phys. Chem. Lett.* **2011b**, *2*(10), 1211-1215.
- Li, M. J.; Wu, Z. L.; Overbury, S. H., CO oxidation on phosphate-supported Au catalysts: Effect of support reducibility on surface reactions, *J. Catal.* **2011**, *278*(1), 133-142.
- Pei, Y.; Shao, N.; Li, H.; Jiang, D. E.; Zeng, X. C., Hollow Polyhedral Structures in Small Gold-Sulfide Clusters, *ACS Nano* **2011**, *5*, 1441.
- Tenney, S. A.; He, W.; Ratliff, J. S.; Mullins, D. R.; Chen, D. A., Characterization of Pt-Au and Ni-Au Clusters on TiO<sub>2</sub>(110), *Top. Catal.* **2011**, *54*, 42.

This page is intentionally blank.

**Monday Afternoon**

**Catalysis Basic  
Advances**

This page is intentionally blank.

**Studies of Metal-Metal Bonded Catalysts for Group Transfer Reactions**

John F. Berry

Department of Chemistry, University of Wisconsin – Madison, 1101 University Ave., Madison, WI 53706

Metal-metal bonded derivatives of dirhodium tetraacetate are well-known catalysts for carbenoid and nitrenoid transformations of organic compounds. Despite the widespread use of this methodology in synthesis, few mechanistic details of the reactions are known. I will present my research group's efforts to isolate and study reactive intermediates, dirhodium carbene and amido complexes, relevant to these important catalytic transformations, emphasizing the relationship between electronic structure, bonding, and their reactivity. Catalyst stability is a critical issue underlying the quest for designing new catalysts with ultra-high turnover numbers. We will examine how concepts such as the chelate effect and redox stability pertain to catalytic carbenoid and nitrenoid transformations. The use of these concepts toward the development of first-row transition metal catalysts that are cheaper and more sustainable than their precious metal counterparts will also be explored. Related diruthenium nitrido intermediates will also be presented, including their C–H amination reactivity and nitrogen atom transfer reactivity.

## Energy and Chemical Transformations of Methane on Oxide Catalysts

Franklin (Feng) Tao, Shiran Zhang, Junjun-Shan, Luan Nguyen  
Department of Chemistry and Biochemistry, University of Notre Dame

### Presentation Abstract

It is critical to develop a catalyst made of earth-abundant elements highly active for a complete combustion of  $\text{CH}_4$  at a relatively low temperature for transforming the earth-abundant energy resource,  $\text{CH}_4$  to electricity without release of any  $\text{CH}_4$  to ambient environment. The currently available catalysts with high activity consist of precious metal nanoparticles supported on rare earth oxides. The high cost limits the application of these catalysts at industrial scale. Early transition metal oxide-based catalysts,  $\text{Ni}_x\text{Co}_{2-x}\text{O}_4$  and  $\text{NiO}_{1-x}$  only consisting of earth-abundant elements can completely combust  $\text{CH}_4$  at  $350^\circ\text{C}$ - $400^\circ\text{C}$  at a gas hourly space velocity of 1200 ml pure  $\text{CH}_4$  on 1 gram in one hour. The complete combustion of  $\text{CH}_4$  at  $350^\circ\text{C}$  results from an integration of two necessary catalytic sites at atomic scale, in which  $\text{CH}_4$  dissociates on Ni cations at a low temperature and a following oxidation of dissociated species by highly active surface lattice oxygen atoms formed from dissociation of molecular  $\text{O}_2$  on oxygen vacancies.

Contract No. DE-FG02-12ER16353

### Understanding of catalysis on early transition metal oxide-based catalysts through exploration of surface structure and chemistry during catalysis using in-situ approaches

PI: Franklin (Feng) Tao

Postdoc: Junjun Shan

Students: Shiran Zhang and Luan Nguyen

### Recent Progress

#### 1. Catalysis and in-situ studies of combustion of methane on $\text{NiCo}_3\text{O}_4$

Methane ( $\text{CH}_4$ ) is an abundant energy resource. Maturation of hydraulic fracturing technology has dramatically increased the available supply and therefore use of this clean-burning energy source in a safe, reliable manner. ExxonMobil predicted that the global electricity supply from methane will increase from the current level of three thousand terawatt hours to ten thousand terawatt hours in 2040 (1). An efficient chemical or energy transformation of methane has been quite challenging. To efficiently, environmentally-friendly, economically transform the chemical energy

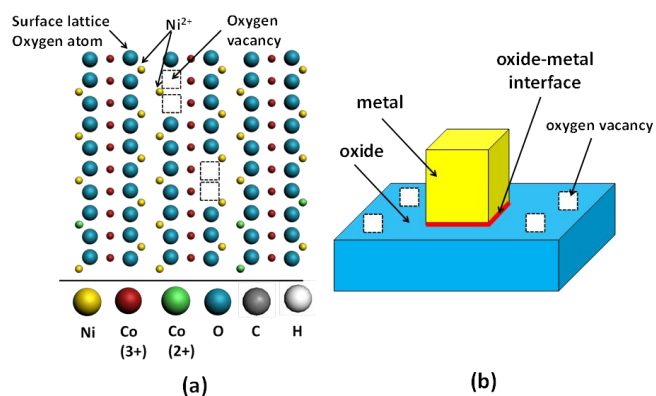


**Figure 1** Schematic showing the difference between (a) a catalyst surface consisting of metal cations (here Ni cation) and surface oxygen atoms integrated at the atomic scale which offers interaction of dissociated species  $\text{CH}_x$  ( $x=0-3$ ) from  $\text{CH}_4$  with immediately neighboring surface lattice oxygen atoms, and (b) a typical bi-functional catalyst consisting of metallic nanoparticles and a reducible oxide. In cases (a) and (b), Ni atoms are at cationic and metallic states, respectively.

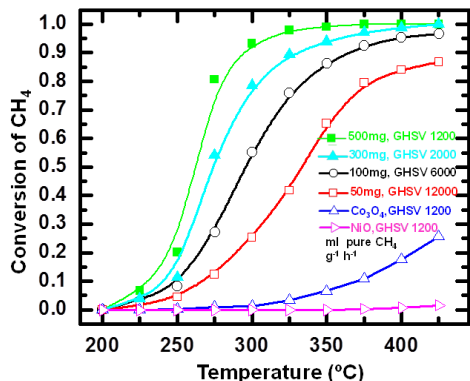


**Figure 2** Conversion of  $\text{CH}_4$  combustion on  $\text{NiCo}_2\text{O}_4$  in the temperature range of 200-425°C at different GSHVs. Conversions of pure commercial  $\text{NiO}$  (no reduction) and pure  $\text{Co}_3\text{O}_4$  were included for comparison. Weights of catalysts are 50-500 mg. The feed gases are 10%  $\text{CH}_4$  balanced with Ar and 100%  $\text{O}_2$ . Molar ratio of  $\text{CH}_4$  to  $\text{O}_2$  in the mixture of the two gases is always 1:5. By using 500 mg  $\text{NiCo}_2\text{O}_4$  catalyst, the GHSV is 12,000 ml 10%  $\text{CH}_4 \text{ g}^{-1} \text{ h}^{-1}$ , which is equivalent to 240,000 ml 0.5%  $\text{CH}_4 \text{ g}^{-1} \text{ h}^{-1}$  or 1,200 pure  $\text{CH}_4 \text{ g}^{-1} \text{ h}^{-1}$ ; at this GHSV, the conversion of  $\text{CH}_4$  at 350°C is 100%.

interfaces, which may be slow and thus reduce the efficiency of the reaction.

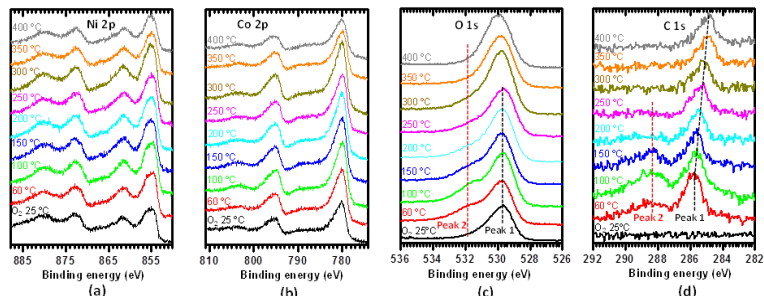
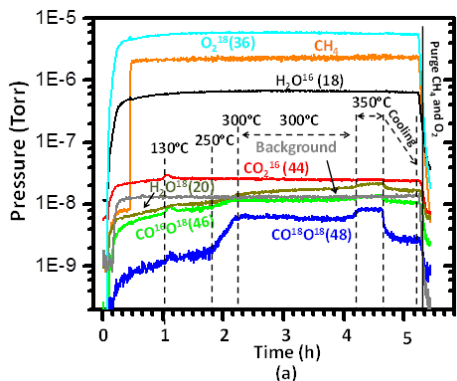


**Figure 3** Photoemission features of Ni 2p, Co 2p, O 1s, and C 1s of  $\text{NiCo}_2\text{O}_4$  at different temperatures during catalysis in  $\text{CH}_4$  and  $\text{O}_2$  with a molar ratio of 1:5 at Torr pressure range.

of  $\text{CH}_4$  to electricity through catalytic combustion to drive gas turbines at industrial scale, it is necessary to design efficient catalysts made of earth-abundant elements which are highly active for *complete* combustion of methane.

Here we proposed to integrate two different catalytic sites to perform the catalytic cycle of  $\text{CH}_4$  combustion. One is a site (A) to dissociate  $\text{CH}_4$ ; the other is a site (B) to dissociate molecular  $\text{O}_2$ . We integrated sites A and B at the atomic scale on the same surface of a catalyst particle to avoid the necessity of spillover across surfaces or/and interfaces, which may be slow and thus reduce the efficiency of the reaction.

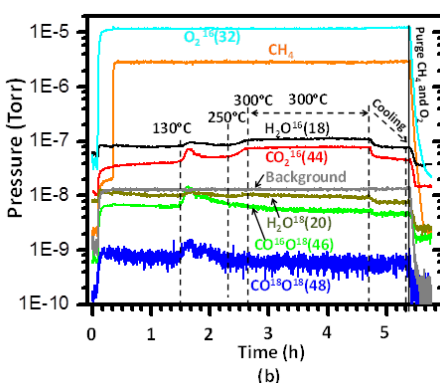


**Figure 4** Track of evolution of products of (a)  $\text{CH}_4$  combustion in  $\text{O}_2^{18}$  on  $\text{NiCo}_2\text{O}_4^{16}$ , and (b)  $\text{CH}_4$  combustion in  $\text{O}_2^{18}$  on isotope-replaced catalyst  $\text{NiCo}_2\text{O}_{4-x}\text{O}_x^{18}$ . To exclude the possibility that gas expansion at high temperature or fast diffusion of molecules from reaction cell of AP-XPS to UHV chamber of mass spectrometer results in an increase of partial pressure of product molecules, Ar gas was introduced as a reference gas (background) to the reaction cell. No any change of the partial pressure of Ar along the increase of reaction temperature (a and b) shows that the increase of partial pressure of  $\text{CO}_2$  and  $\text{H}_2\text{O}$  is not due to thermal expansion of gas or faster thermal diffusion of product molecules at a relatively high temperature.

activity for complete combustion of  $\text{CH}_4$  at a relatively low temperature. Our studies reveal that methane can be completely combusted in  $\text{O}_2$  at 350°C at a gas hourly space velocity (GHSV) of 1200 ml pure  $\text{CH}_4$  per gram per hour on  $\text{NiCo}_2\text{O}_4$  (Figure 2). In-situ AP-XPS studies shows the formation of  $\text{O}_{\text{surface}}\text{-C-O}_{\text{surface}}$  intermediate (peak 2 in Figure 3d) at a low temperature ( $\leq 150^\circ\text{C}$ ). Methane combustion on isotope-labeled catalyst  $\text{NiCo}_2\text{O}_{4-x}\text{O}_x^{18}$  confirms that the participation of surface lattice oxygen atoms and the formation of  $\text{O}_{\text{surface}}^{18}\text{-C-O}_{\text{surface}}^{18}$  intermediate on the

Inspired by the high activity of  $\text{Co}_3\text{O}_4$  in dissociation of molecular oxygen ( $\text{O}_2$ ) (2) to atomic oxygen at a low temperature and the high adsorption energy of  $\text{CH}_4$  on Ni atoms, we incorporated Ni atoms into the spinel  $\text{Co}_3\text{O}_4$  lattice (Figure 1a) and thus developed a new catalyst exhibiting extraordinarily high

surface. These studies show that this integration offers a new catalyst made of earth-abundant elements extraordinarily active for CH<sub>4</sub> combustion at a relatively low temperature of 350°C.

## 2. Catalytic combustion of methane on nonstoichiometric NiO<sub>1-x</sub>

Semi-mesoporous nonstoichiometric nickel oxide was synthesized by preparing Ni(OH)<sub>2</sub> through a hydrothermal method (Figure 5a) and a following calcination in O<sub>2</sub> at 400°C. The synthesized nonstoichiometric nickel oxide (NiO<sub>1-x</sub>) appeared as a hexagonal disk (Figure 5b) consisting of randomly packed nanocrystals as seen in the high resolution TEM image (Figure 5c). The synthesized

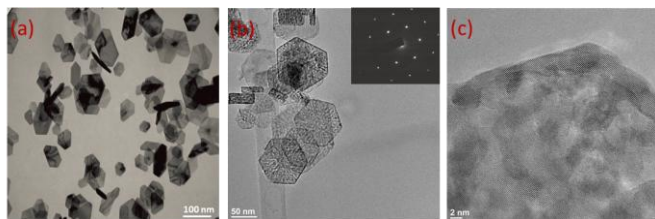


**Figure 5** TEM images of synthesized precursor Ni(OH)<sub>2</sub> (a), synthesized semi-mesoporous NiO<sub>1-x</sub> (b), and high-resolution TEM image of a part of semi-mesoporous NiO<sub>1-x</sub> (c).

nickel oxide is highly active for methane combustion at 400°C with a conversion of 100% at a GHSV (1,200 ml pure CH<sub>4</sub>/min-gram) (Figure 6). In-situ studies by AP-XPS show that the O/Ni ratio of the as-synthesized NiO<sub>1-x</sub> is 0.81 (Figure 7).

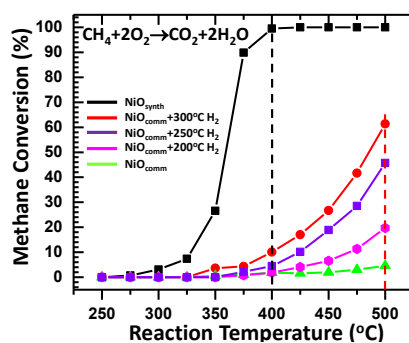


**Figure 6** Catalytic performance of methane combustion on synthesized nonstoichiometric NiO<sub>1-x</sub>, stoichiometric commercial NiO, and reduced commercial NiO<sub>1-x</sub> at different temperatures.

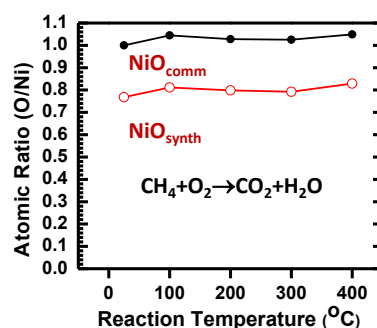


**Figure 7** Atomic ratio (O/Ni) of commercial NiO and synthesized NiO<sub>1-x</sub> during catalysis.

Obviously, there are oxygen vacancies on surface of the synthesized nickel oxide during catalysis. To confirm that the activity of the as-

synthesized catalyst results from the oxygen vacancies, catalytic measurements from methane combustion on commercial NiO without reduction (O/Ni ratio is 1) and with reduction at different temperatures (O/Ni ratio is lower than 1) were performed. As shown in Figure 6, commercial NiO without reduction is nearly not active (only 1% and 2% conversion at 400°C and 450°C, respectively). The commercial NiO reduced at 200°C, 250°C, and 300°C can convert 6%, 18%, 26% of CH<sub>4</sub> at 450°C, respectively (Figure 6). AP-XPS studies showed that the O/Ni ratio of NiO<sub>comm</sub> (without any reduction before catalysis) remains nearly no change (100%) (Figure 7); however the NiO<sub>synth</sub> preserves at ~81% during catalysis in the temperature range of 25°C-400°C (Figure 7). Figures 6 and 7 clearly suggest a correlation of catalytic activity with the oxygen vacancies of nickel oxide. In addition, AP-XPS studies observed the formed intermediate at low temperature and preservation of spectator in the whole temperature range.

## 3. In-situ surface chemistry and catalytic performances of methane partial oxidation for production of syngas on ceria-doped with palladium, platinum, and rhodium

One of the main applications of CH<sub>4</sub> is the chemical transformation of methane to syngas through partial oxidation. Doped CeO<sub>2</sub> is one type of catalysts active for methane partial oxidation (MPO) reported in literature (3). Here we performed a fundamental study of MPO on this type of catalysts through in-situ characterizations of the surface chemistry during catalysis

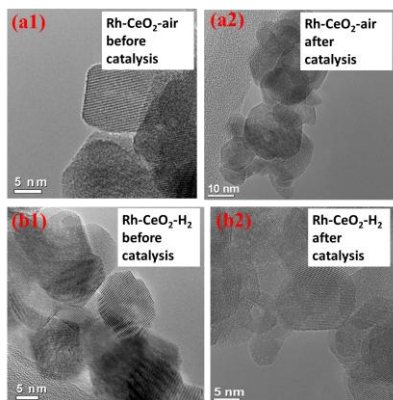


**Figure 8** TEM images of Rh-CeO<sub>2</sub>-H<sub>2</sub> and Rh-CeO<sub>2</sub>-air before and after catalysis.

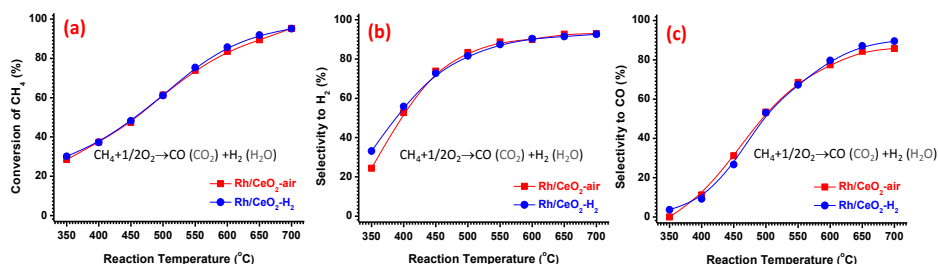


**Figure 9** Catalytic performance of methane partial oxidation on Rh-CeO<sub>2</sub>-air and Rh-CeO<sub>2</sub>-H<sub>2</sub>. (a) Conversion of CH<sub>4</sub> at different reaction temperature. (b) Selectivity for production of H<sub>2</sub> at different temperature. (c) Selectivity for production of CO at different temperature.

## References

- (1) ExxonMobil, The Outlook for Energy: A View to 2040. <http://corporate.exxonmobil.com/en/energy/energy-outlook>, (2013).
- (2) Xie, X. W.; Li, Y.; Liu, Z. Q.; Haruta, M.; Shen, W. J. *Nature* **458**, 746 (Apr, 2009).
- (3) Tang, W.; Hu, Z.; Wang, M.; Stucky, G. D.; Metiu, H.; McFarland, E. W. *J. Catal.* **2010**, *273*, 125–137 (2010).
- (4) Zhu, Y.; Zhang, S. R.; Shan, J. J.; Nguyen, L.; Zhan, S. H.; Gu, X. L.; Tao, F.; *ACS Catalysis* **3**, 2627 (2013).

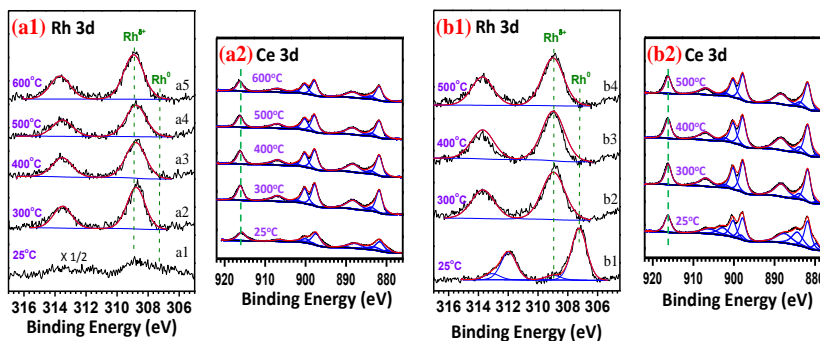


**Figure 10** In-situ studies of surface chemistry of Rh-CeO<sub>2</sub>-air and Rh-CeO<sub>2</sub>-H<sub>2</sub> during catalysis at different temperature. (a1) Rh 3d of Rh-CeO<sub>2</sub>-air; (a2) Ce 3d of Rh-CeO<sub>2</sub>-air; (b1) Rh 3d of Rh-CeO<sub>2</sub>-H<sub>2</sub>; (b2) Ce 3d of Rh-CeO<sub>2</sub>-H<sub>2</sub>.

and measurements of the corresponding catalytic performances (4). CeO<sub>2</sub>-based catalysts prepared with different pretreatments, including Pd-CeO<sub>2</sub>-air, Pd-CeO<sub>2</sub>-H<sub>2</sub>, Pt-CeO<sub>2</sub>-air, Pt-CeO<sub>2</sub>-H<sub>2</sub>, Rh-CeO<sub>2</sub>-air, and Rh-CeO<sub>2</sub>-H<sub>2</sub>, were synthesized through doping noble-metal ions in the synthesis of CeO<sub>2</sub> nanoparticles. The catalytic activity and selectivity in the production of H<sub>2</sub> and CO through MPO on these ceria-based catalysts as well as their surface chemistries during catalysis were investigated (4). Those catalysts exhibit quite different catalytic performances in MPO under an identical catalytic condition.

Correlations between the catalytic performances of these catalysts (Figure 9) and their corresponding surface chemistries

during catalysis (Figure 10) were built. Among these catalysts, Rh-doped CeO<sub>2</sub> (Figure 8) exhibited the highest catalytic activity and selectivity in MPO (Figure 9).

## Publications Acknowledging this Grant in 2012-2014

1. Shan, J.; Huang, W.; Nguyen, L.; Yu, Y.; Zhang, S.; Li, Y.; Frenkel, A.; Tao, F. "Conversion of methane to methanol with a bent mono( $\mu$ -oxo)dinickel anchored on internal surface of micro-pores oxide", *Langmuir*, **2014**, accepted.
2. Zugic, B.; Zhang, S.; Bell, D.; Tao, F.; Flytzani-Stephanopoulos, M. "Understanding the Low-Temperature Water-Gas Shift Activity of Platinum Catalysts Mediated by Pt-Na-OH Stabilization on Carbon Supports", *J. Am. Chem. Soc.* **2014**, *136*, 3238-3245.
3. Zhang, S.; Shan, J.; Zhu, Y.; Frenkel, A.; Patlolla, A.; Huang, W.; Yoon, S.; Wang, L.; Yoshida, H.; Takeda, S.; Tao, F. "WGS Catalysis and In-situ Studies of  $\text{CoO}_{1-x}$ ,  $\text{PtCo}_n/\text{Co}_3\text{O}_4$ , and  $\text{Pt}_m\text{Co}_m/\text{CoO}_{1-x}$  nanorod catalysts", *J. Am. Chem. Soc.* **2013**, *135*, 8283-8293.
4. Sneed, B.; Brodsky, C.; Kuo, C. H.; Lamontagne, L.; Jiang, Y.; Wang, Y.; Tao, F.; Huang, W.; Tsung, C. K.; "Nanoscale-Phase-Separated Pd-Rh Boxes Synthesized via Metal Migration: An Archetype for Studying Lattice Strain Effects in Catalysis", *J. Am. Chem. Soc.* **2013**, *135*, 14691-14700.
5. Zhang, S.; Shan, J.; Zhu, Y.; Tao, F., "Restructuring Transition Metal Oxide Nanorods for 100% Selectivity in Reduction of Nitric Oxide with Carbon Monoxide", *Nano Letters*, **2013**, *13*, 3310-3314.
6. Zhang, S.; Nguyen, L.; Zhu, Y.; Zhan, S.; Tsung, S.; Tao, F. "In-situ Studies of Nanocatalysis", *Acc. Chem. Res.* **2013**, *46*, 1731-1739.
7. Zhu, Y.; Zhang, S.; Shan, J.; Nguyen, L.; Zhan, S.; Gu, X.; Tao, F. "Catalytic performances and in-situ surface chemistries of ceria doped with palladium, platinum and rhodium in methane partial oxidation for production of syngas", *ACS Catalysis*, **2013**, *3*, 2627-2639.
8. Wang, L.; Zhang, S.; Zhu, Y.; Patlolla, A.; Shan, J.; Yoshida, H.; Takeda, S.; Frenkel, A. I.; Tao, F. "Catalysis and In-situ Studies of  $\text{RhCo}_n$  Nanoclusters Supported on  $\text{Co}_3\text{O}_4$  Nanorods", *ACS Catalysis*, **2013**, *3*, 1011-1019.
9. Shan, J. J.; Zhu, Y.; Zhang, S.; Zhu, T.; Rouvimov, S.; Tao, F. "Catalytic Performance and In-situ Surface Chemistry of Pure  $\alpha$ - $\text{MnO}_2$  Nanorods in Selective Reduction of NO and  $\text{N}_2\text{O}$  with CO", *J. Phys. Chem. C.* **2013**, *117*, 8329-8335.
10. Nguyen, L.; Cheng, F.; Zhang, S.; Tao, F. "Visualization of Surfaces in Reactive Environments Using Ambient Pressure Scanning Tunneling Microscopy and Insights on Restructurings of Surfaces of Model Metal Catalysts under Reaction Conditions at Near Ambient Pressure", *J. Phys. Chem. C*, **2013**, *117*, 971-977.
11. Tao, F.; Nguyen, L.; Zhang, S. "Design of A New Reactor-Like High Temperature Near Ambient Pressure Scanning Tunneling Microscope for Catalysis Studies", *Review of Scientific Instruments*, **2013**, *84*, 034101.
12. Nguyen, L. Zhang, S.; Ye, Y.; Zhu, Y.; Wang, L.; Tao, F. "Visualization of Surface Structure of Heterogeneous Catalysts under Reaction Conditions or during Catalysis with High-Pressure Scanning Tunneling Microscopy", in Book "*In-situ Characterization of Heterogeneous Catalysts*" edited by Rodriguez, Hanson, and Chupas, Wiley, ISBN: 978-1-118-00016-8, **2013**.
13. Ma, Z.; Tao, F. "Metal Salt-based Gold Nanocatalysts", in book "*Metal Nanoparticles for Catalysis: Advances and Applications*" edited by Tao, RSC, ISBN: 978-1-78262-033-4, **2014**.
14. Deng, X.; Tao, F. "Application of Soft X-ray Absorption Spectroscopy for In-Situ Studies of Catalysts at Nanoscale", in book entitled "*Heterogeneous Catalysis at Nanoscale and Energy Applications*" edited by Tao, Schneider and Kamat, Wiley, ISBN: 978-0-470-95260-3, **2014**.
15. Ma, Z.; Tao, F.; "Development of new Catalysts for Removing CO from  $\text{H}_2$ ", in book entitled "*Heterogeneous Catalysis at Nanoscale and Energy Applications*" edited by Tao, Schneider and Kamat, Wiley, ISBN: 978-0-470-95260-3, **2014**.
16. Wen, C.; Zhu, Y.; Ye, Y.; Cheng, F.; Wang, P.; Tao, F. "Water-Gas-Shift Reaction on Metal Nanoclusters Encapsulated in Mesoporous Ceria Studied with Ambient Pressure X-ray Photoelectron Spectroscopy", *ACS Nano*, **2012**, *6*, 9305-9313.

17. Pei, Y.; Zhou, G.; Nguyen, L.; Zong, B.; Qiao, M.; Tao, F.; Synthesis and catalysis of chemically reduced metal–metalloid amorphous alloys”, *Chem. Soc. Rev.* **2012**, *41*, 8140-8612.
18. Gu, J.; Zhang, Y.; Tao, F. “Shape Control of Bimetallic Nanocatalysts through Well-designed Colloidal Chemistry Approaches”, *Chem. Soc. Rev.* **2012**, *41*, 8050-8065.
19. Tao, F.; Zhang, S.; Nguyen, L.; Zhang, X. “Action of Bimetallic Nanocatalysts under Reaction Conditions and during Catalysis: Evolution of Chemistry from High Vacuum Conditions to Reaction Conditions”, *Chem. Soc. Rev.* **2012**, *41*, 7980-7993.
20. Zhu, Y.; Zhang, S.; Ye, Y.; Zhang, X.; Wang, L.; Cheng, F.; Tao, F. “Catalytic Conversion of Carbon Dioxide to Methane on Cobalt-ruthenium Bimetallic Nanocatalysts and Correlation between Surface Chemistry of Catalysts under Reaction Conditions and Catalytic Performances”, *ACS Catalysis* **2012**, *2*, 2403-2408.
21. Sun, B.; Xu, K.; Nguyen, L.; Qiao, M. H.; Tao, F.; "Preparation and Catalysis of Carbon-supported Iron Catalysts for Fischer-Tropsch Synthesis", *ChemCatChem*, **2012**, *4*, 1498-1511.

## Modeling Catalytic and Stoichiometric Intermediates with Transition-Metal Isocyanides

Joshua S. Figueroa (PI), Douglas W. Agnew, Alex E. Carpenter and Treffly B. Ditri  
*Department of Chemistry and Biochemistry, University of California, San Diego*

### ABSTRACT

Encumbering *m*-terphenyl isocyanides have been used to kinetically stabilize high-reactive, coordinatively unsaturated transition-metal complexes. In several cases, these unsaturated metal isocyanides serve as direct analogues to the unsaturated binary carbonyls. Importantly, unsaturated binary metal carbonyls have been implicated as catalytic protagonists or intermediates in several transformations mediated by saturated metal-carbonyl precursor complexes. In this presentation, new results relevant to the modeling of homo- and heteroleptic unsaturated metal carbonyl complexes by *m*-terphenyl isocyanides are presented. Specific attention is paid to the isolation and characterization of important catalytic intermediates in electrocatalytic CO<sub>2</sub> reduction by Group 7 metal [XM(CO)<sub>3</sub>L<sub>2</sub>] complexes (M = Mn, Re; X = halide, pseudohalide). In addition, new reactivity patterns of unsaturated metal isocyanide complexes with small-molecule substrates are presented and contextualized to carbonyl analogues where appropriate. For these latter investigations, an expanded library of sterically and electronically diverse *m*-terphenyl isocyanides has been prepared and used to further refine electronic-structure/function properties of this class of complexes.

### DE-SC0008058: Bond-Formation and Catalysis by Base-Metal Unsaturated Isocyanides

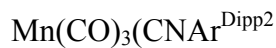
Student(s): Douglas W. Agnew, Alex E. Carpenter and Treffly B. Ditri

### RECENT PROGRESS

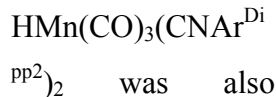
*Specific Goal # 1 – Mn-Based Electrocatalysts:* The major recent results for this award include the detailed characterization, the spectroscopic properties and the reaction chemistry of the Mn-monoradical complex Mn(CO)<sub>3</sub>(CNAr<sup>Dipp2</sup>)<sub>2</sub>. This species is a key intermediate in Group 7 metal electrocatalytic CO<sub>2</sub> reduction sequences and is the first to be isolated and studied in detail by a complement of spectroscopic and synthetic techniques. As described, Mn(CO)<sub>3</sub>(CNAr<sup>Dipp2</sup>)<sub>2</sub> displays an intriguing reaction chemistry with a diverse host of substrates. It is shown that this

species is not competent for CO<sub>2</sub> activation, which is a main finding of the work. The interconversion

between



)<sub>2</sub> and the mono-hydride complex



was also explored in detail

and it is shown that

neither complex is a major contributor to a productive CO<sub>2</sub> reduction sequence. However, the k<sup>1</sup>-formate complex HC(O)O-Mn(CO)<sub>3</sub>(CNAr<sup>Dipp2</sup>)<sub>2</sub> has been prepared by an independent route and is shown to decompose with CO<sub>2</sub> loss HMn(CO)<sub>3</sub>(CNAr<sup>Dipp2</sup>)<sub>2</sub> via a mechanism not previously considered for Group 7 ML<sub>5</sub> electrocatalysts.

Also described are synthetic and spectroscopic efforts leading to an extensive library of electronically

diverse *m*-

terphenyl

isocyanide

ligands. As a

result of this

study, topological

and electronic

criteria have been

established for the

construction of

isocyanide ligands

that present a

significant π-

acidic ligand field akin to carbon monoxide (CO), but that also promote coordinative unsaturation.

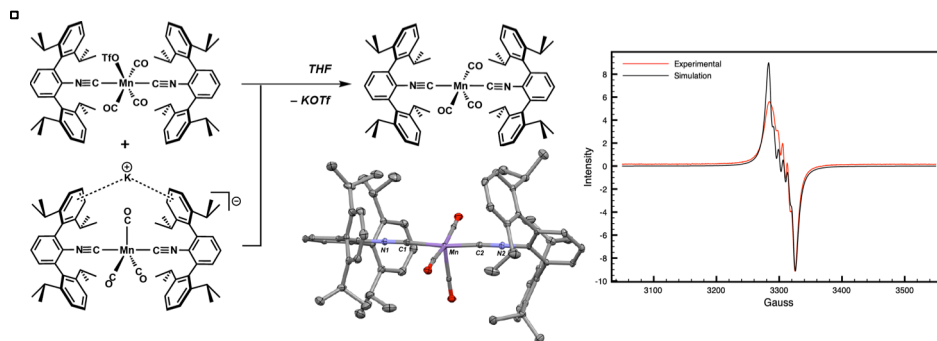


**Figure 1.** Synthesis, solid-state structure and EPR characterization of  $\text{Mn}(\text{CO})_3(\text{CNAr}^{\text{Dipp}2})_2$

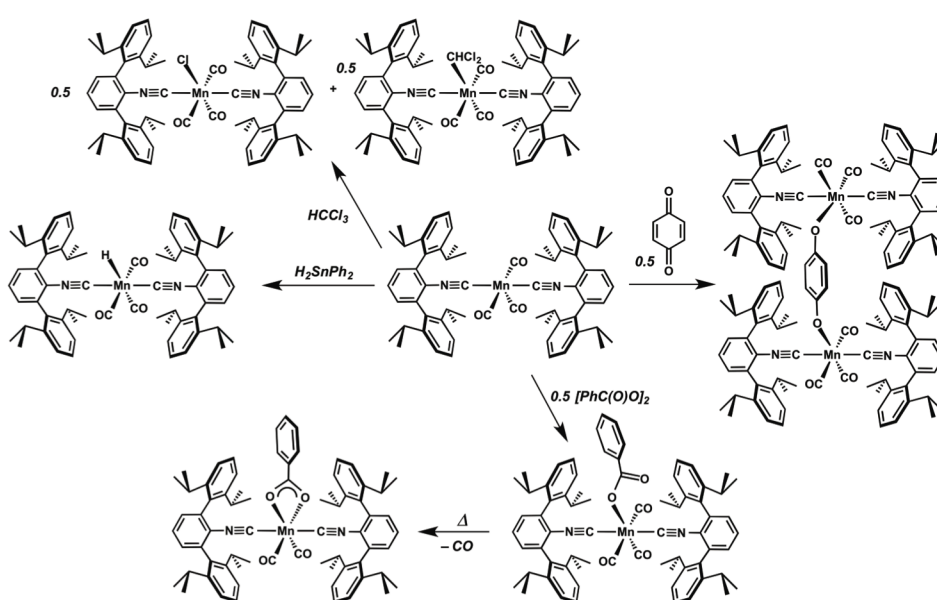


**Figure 2.** One-electron, substrate-reduction reactions accessible to  $\text{Mn}(\text{CO})_3(\text{CNAr}^{\text{Dipp}2})_2$ . All complexes have been structurally characterized.

*Specific Goal # 2 – Co-Based Substrate Activation Reactions:* Synthetic studies and  $pK_a$  measurements have been conducted on the full series of cobalt monohydride complexes  $HCo(CNAr^{Mes2})_{4-n}(CO)_n$ . These studies have sought to establish the relative nucleophilicity of this cobalt system toward exogenous substrates, with  $CO_2$  being the target of interest. The major result of this work is that the relative  $pK_a$  changes as a function of isocyanide ligand have been established. Recent results also demonstrate the reactivity patterns available to the  $HCo(CNAr^{Mes2})_{4-n}(CO)_n$  complexes, as well as the tris-isocyanides  $(\eta^6-PPN)Co(CNAr^{Mes2})_3$  ( $PPN = [Ph_3P=N=PPh_3]^+$ ) and  $Co(SiR_3)(CNAr^{Mes2})_3$  ( $R = Me$  or  $Ph$ ), with  $CO_2$ .

#### **Publications Acknowledging this Grant in 2013 – 2014:**

- 1) “Chloro- and Trifluoromethyl-Substituted Flanking-Ring *m*-Terphenyl Isocyanides:  $\eta^6$ -Arene Binding to Zero-Valent Molybdenum Centers and Comparison to Alkyl-Substituted Derivatives” Ditre, T. B.; Carpenter, A. E.; Ripatti, D. S.; Moore, C. E.; Rheingold, A. L.; Figueroa, J. S. *Inorg. Chem.* **2013**, *52*, 13216–13229.
- 2) “An Isolable Isocyanide Analogue of the Metalloradical  $Mn(CO)_5$ ” Agnew, D. W.; Moore, C. E.; Rheingold, A. L.; Figueroa, J. S. *Submitted*.
- 3) “Variation of Carbonyl Stretching Frequency and Proton-Acceptor Ability of  $[Co(CO)_{4-n}(CNAr)_n]^-$  Anions as a Function of Aryl Isocyanide Ligation” Carpenter, A. E.; Swords, W. B.; Margulieux, G. W.; Moore, C. E.; Rheingold, A. L.; Figueroa, J. S. *In Preparation*.
- 4) “Substituent Effects on the Electronic Influence of *m*-Terphenyl Isocyanides” Carpenter, A. E.; Ripatti, D. S.; Havrylyuk, I.; Kamezawa, R.; Moore, C. E.; Rheingold, A. L.; Figueroa, J. S. *In Preparation*.

## **Error Estimation in Simulated Catalytic Trend Studies**

Jess Wellendorff, Andrew J. Medford, Keld T. Lundgaard, Frank Abild-Pedersen, Felix Studt, Aleksandra Vojvodic, Jens K. Nørskov, and Thomas Bligaard  
SUNCAT Center for Interface Science and Catalysis, Chemical Sciences Division,  
Photon Science Directorate, SLAC National Accelerator Laboratory & Department of  
Chemical Engineering, Stanford University

### **Presentation Abstract**

A fitting methodology for empirical exchange-correlation functionals is presented. The method reproduces catalysis-relevant benchmark materials and chemical properties reasonably, while allowing for a quantitative error estimation ensemble to be constructed. The uncertainties on different but related materials properties are typically correlated, and the error estimation ensemble reproduces to some extent such correlations, while being flexible enough to calculate uncertainties on any property calculate by density functional theory. Often, density functional theory results are used as input to subsequent layers of modeling. The use of density functional theory calculations to parameterize microkinetic models in catalysis is one such use of compounded models. If the uncertainty ensemble reproduces the correlated errors well, it means that uncertainties on conclusions based on a compounded model can be accurately evaluated by establishing compounded models for every functional instance in the error ensemble and evaluating the statistical properties of these compounded models. We utilize this general approach for analyzing the electronic structure uncertainty on catalytic rates over a range of transition metal catalysts. In general the estimated error is significantly reduced due to correlations in the error between various intermediates and surfaces, which highlights the need for systematic methods of error estimation. Uncertainties are shown to be a complex function of reaction condition and catalyst material, and we demonstrate that relative rates between different catalysts are better described than the absolute rates.

### **FWP-10049: SUNCAT Center for Interface Science and Catalysis**

#### **Task 1: Method Development**

**PIs:** Jens K. Nørskov (SUNCAT lead-PI), Thomas Bligaard (Task 1 Lead), Jens Strabo Hummelshøj

**Postdocs:** Jess Wellendorff, Keld T. Lundgaard, Zaoshi Yang, Han-Jung Li

**Students:** Andrew J. Medford, Aidan Klobuchar

### **RECENT PROGRESS**

Over the past couple of decades, electronic structure simulations, especially in the form of density functional theory (DFT), have had a profound impact on the detailed understanding of catalysts, catalytic mechanisms, and catalytic processes. This

impact has relied on the wide availability of highly optimized electronic structure codes with continuously improving exchange-correlation approximations. A fundamental tenet underlying SUNCAT is that theory even has the potential to play a key role in addressing the fundamental challenges associated with the design of catalysts for novel chemical transformations of interest in energy conversion and storage. In order to harvest this potential, further integration between theory and many aspects of catalysis experimentation is needed, and many aspects of theory have to be improved. The Method Development Task at SUNCAT aims to unleash the potential of theory in transition metal surface catalysis by devising efficient and reliable simulation methods and models, create large amounts of high-accuracy simulation data for well-defined model systems, and make the methods and the data available not only to the other SUNCAT theory tasks but to the catalysis community in general. The ambition is to enable faster, more accurate, and more reliable modeling of catalytic systems. This will ultimately enable further integration of modeling and experimentation for the design of catalysts for novel processes. Our approach follows two parallel paths, the development of improved accuracy exchange-correlation functionals with error estimation capabilities, and the development of web-tools to store and analyze massive amounts of simulated catalysis data.

### ***Bayesian Error Estimation Functionals***

We have developed an exchange-correlation (XC) functional that allows for the accurate simultaneous treatment of covalent, metallic, and van der Waals bonding, and which offers quantitative error estimation. Accurate simulations of larger and more realistic systems are computationally intensive, and density functional theory (DFT) currently provides an attractive compromise between accuracy and speed. The accuracy of DFT, however, relies on our ability to find good approximations to complicated quantum mechanical effects through the exchange-correlation functional. Very good functionals have been established for separate materials properties, such as e.g. bulk metals and solids, covalent molecular bonding, adsorption, and van der Waals complexes. Simulations relevant in catalysis studies often involve a number (or all) of these different types of bonding. A functional that simultaneously improves e.g. surface energies, cohesive energies, covalent bonding, and van der Waals bonding is highly desirable. Traditionally, two main avenues of functional development exist, one where exact bounds for simple systems are used to derive functionals that fulfill “reasonable” design criteria, and one where the functional is fitted to accurate databases of small systems. Currently, functional development typically involves some aspects of both approaches.

In order to substantiate the reliability of the scientific conclusions drawn from a catalysis simulation, an understanding of the errors in the underlying calculations is essential, such that these can be combined with a sensitivity analysis to establish confidence in the results. When following a fitting approach, it is possible to use ensemble ideas to establish such a quantitative error model. We have therefore taken a fitting approach to establish the Bayesian Error Estimation Functional with van der Waals interactions (BEEF-vdW). The resulting BEEF-vdW functional is not

extremely good at simulating any specific property, but establishes a “reasonable” compromise between all the represented properties.

We have established a very flexible basis for representing the XC-functional which we optimize using Tikhonov regularization and cross-validation methods from machine learning. We have demonstrated that this yields well-behaved approximations in flexible model spaces, thus avoiding over-fitting. The primary variational freedom in the BEEF-vdW functional is introduced through variations in the exchange enhancement factor.

For complex van der Waals bonded systems, which are difficult for many other functionals does a very reasonable job. Also for more simple reactions, such as hydrogenation of CO and CO<sub>2</sub> to methanol over transition metal surfaces, the BEEF-vdW shows significant quantitative improvements in the descriptions of the reaction energetics.

#### *Improving the Catalysis-Relevant Data*

Fitting improved ensemble exchange correlation functionals to catalysis relevant properties requires three basic ingredients: A functional form that is flexible enough to allow for an accurate fit, good methods for systematically avoiding challenges with over-fitting, and accurate data for a broad palette of catalysis-relevant properties. In our opinion, the currently weakest point of the three key ingredients is the availability of accurate adsorbate-surface interaction data. We thus work with leading experimental experts on establishing databases of reliable experimental and theoretical adsorption energetics. Together with Professor C.T. Campbell we have recently established a set of 25 adsorption processes for which we are making or have high quality single crystal adsorption calorimetry data and computations at various levels.

#### *Improving the Fitting Methodology*

Fitting complex functionals requires careful avoidance of over-fitting. We currently avoid over-fitting by performing Tikhonov regularization with bootstrap cross validation, and by using a “smoothness” norm on the Tikhonov penalty functional, where we define the measure of “smoothness” as an integral of the weighted absolute values of the second derivatives of the exchange enhancement factor. We have recently extended this methodology to define a measure of smoothness for a 2-dimensional exchange enhancement factor. This has been done in a way, which avoids cross validation in more than one dimension. We have utilized this new methodology to design the first Bayesian Error Estimation Functional that includes second derivatives of the electron density (a so-called meta-GGA).

We have then implemented functional fitting with Tikhonov regularization in other norms than the L2 norm. This for example gives access to self-consistently detect outliers in the benchmark data, and to down-weight outliers systematically, thus carrying out more robust fitting. We have tested this methodology systematically, and consistently obtain better fits (with smaller bootstrap-estimated prediction errors). The robust fitting methodology has been applied to the problem of determining a meta-BEEF functional that includes van der Waal’s interactions, and very promising results have been obtained.

### *Catalysis Informatics*

We have designed a stand-alone web applet called CatApp that allows online access to a repository of catalysis-relevant adsorption data from SUNCAT and other catalysis simulation groups.

The CatApp was first designed as a graphical user interface to the CMR, but soon it became a stand-alone web applet with client-side data. This enables facile access to a database of the results of electronic structure calculations of catalysis-relevant properties. It is implemented as a web application in JavaScript, SVG, and HTML, and runs in any modern web browser without any plug-ins. The code and data are downloaded when the application is accessed for the first time, and are kept in the local storage of the browser. This feature allows the user to use the applet even if there is no Internet connection. Very importantly, it also guarantees the user complete privacy, since all queries are performed locally, and not by connecting to our server. On startup, the application will look for any updates to the application code or newly available data, and update itself.

The idea behind the CatApp is that the development of new catalysts could potentially be accelerated significantly if the broader catalysis community had access to systematic data for accurate activation and reaction energies of elementary surface reactions. Such a database would enable the search for new catalyst leads. Ideally, data would come from detailed, systematic experiments, but it is generally not possible to find such data, and electronic structure calculations provide a powerful alternative. We have introduced a set of calculated reaction and activation energies for a large number of elementary surface reactions on a series of metal single-crystal surfaces, including surfaces with defects such as steps. The database includes reaction energies for all surface reactions that involve C-C, C-H, C-O, O-O, O-H, N-N, C-N, O-N, and N-H splitting for molecules with up to three C, N, or O atoms on close-packed face-centered cubic fcc(111), hexagonal close-packed hcp(0001), and body-centered cubic bcc(110) surfaces, as well as stepped fcc and hcp surfaces of Ag, Au, Co, Cu, Fe, Ir, Mo, Ni, Pd, Pt, Re, Rh, Ru, Sc, and V. It also presents C and O adsorption energies on more than thousand transition metal alloys. For reactions for which an activity volcano has been established in terms of the adsorption energies of O and C, this for example makes it possible to get inspiration about which alloys to look at as novel catalyst leads. We have used this feature for example in the search for novel catalysts for anhydrous formaldehyde synthesis from methanol and steam reforming.

The application is not only available to the catalysis community for free, but has also been open for contributions from non-SUNCAT researchers and research groups in form of submission of computational data for surface reactions to the database upon publication. Each piece of data in the CatApp is tied to information about the paper in which it was first published. This gives access to the details about how the calculations were performed, hence turning the CatApp into a search tool for published simulations.

There is ample scope for making the database better and more useful by including more surface structures including nanoparticles, uncertainties in the simulations as established by a Bayesian Error Estimation Ensemble, and by integrating it with other databases of materials properties. CatApp can thus provide the most basic tool

for looking up reaction energies and activation energies over well-defined surface facets, and can serve as a starting point for building more advanced data-mining tools.

The CatApp currently allows access to information about the reaction energies and barriers of a few thousand surface chemical processes, essentially one at a time. This can be useful if one is interested in one particular process. Often, however, we wish to use the data to get an overview of activity or selectivity trends, inspiration for which experiment one should do next, or to figure out whether or not a given catalyst lead is expected to be active and stable under specific reaction conditions. This is the tool that we are currently developing the CatApp into.

#### *Integration of Reaction Cycle Analysis*

The central tool in catalysis studies that DFT helps establish is the potential energy diagram for the reaction cycle. We shall develop an interface for CatApp through which the user can specify a desired catalytic cycle, in terms of elementary reactions. The CatApp will then draw the potential energy diagram for the full reaction cycle based on the elementary reactions currently included in the CatApp. This will give the user a first overview of a given reaction of interest, showing which elementary steps can be problematic due to large barriers or too strong/weak adsorption of intermediates. To take this analysis tool one step further, we shall extend the simulation data available in the CatApp to include the atomic structures, such that the user easily can view the atomic configurations underlying the processes shown in the potential energy diagrams simply by clicking on the appropriate parts of the diagram. The data is also being extended to include vibrational frequencies for adsorbed species and frequencies and gas phase entropies for reactant and product molecules, such that zero-point energy,  $C_p$ -contributions, and entropic contributions can be established, and Gibbs free energy diagrams for the catalytic cycle can be accessed.

We are designing algorithms that can aid the user by automatically decomposing a given gas phase reaction into appropriate catalytic cycles of elementary reaction steps present in the CatApp. Currently, this allows the user to not only obtain the exact set of mechanisms originally specified, but we are working on also having the app obtain a new set of “system-proposed” mechanisms that can be considered further. This type of web-based tool design marks the first significant step toward turning the CatApp into an actual “research tool”. The natural way to make our research available to the community and the public in a transparent fashion is to allow open access not only to data, but also the analysis tools we use. Conversely, the natural way to analyze and access our own research data in a scalable way that allows for intra-group and inter-group collaborations, while ensuring full reproducibility, is exactly through the kind of loosely coupled REST-API structure that CatApp is built upon. A central goal is thus that CatApp becomes not just a graphical interface to our research results, but also the actual research platform for the work performed at SUNCAT.

#### *Integrated Methods for Catalyst Screening and Genomics*

The CatApp is intentionally not limited to specific experimentally observed surfaces or observed surface processes. This relates to our perspective, that if we want the simulations to contribute new knowledge and to enable us to address questions such as: “Which of several different mechanisms is the relevant one?” Then we need to include both the experimentally observed and alternative mechanisms. In addition, the mechanisms may change with the reaction conditions, such that different but similar processes may be relevant under differing circumstances. This naturally raises the question of whether a given surface in the database can exist at all under reaction conditions, and whether the underlying crystalline structure is the experimentally relevant one to be considered. We are thus working on algorithms to identify the most relevant (experimental) structure to help the users of CatApp to obtain not just the data they ask for, but the data “they need”.

### **Publications Acknowledging this Grant in 2011-2014**

1. Wellendorff, J.; Bligaard, T. On the Importance of Gradient-Corrected Correlation for van der Waals Density Functionals. *Top. Catal.* **2011**, *54*, 1143-1150.
2. Møgelhøj, A.; Kelkkanen, A.K.; Wikfeldt, K.T.; Schiøtz, J.; Mortensen, J.J.; Pettersson, L.G.M.; Lundqvist, B.I.; Jacobsen, K.W.; Nilsson, A.; Nørskov, J.K. Ab Initio van der Waals Interactions in Simulations of Water Alter Structure from Mainly Tetrahedral to High-Density-Like. *J. Chem. Phys. B* **2011**, *115*, 14149-14160.
3. Hou, Y.; Abrams, B.L.; Vesborg, P.C.K.; Björketun, M.E.; Herbst, K.; Bech, L.; Setti, A.M.; Damsgaard, C.D.; Pedersen, T.; Hansen, O.; Rossmeisl, J.; Dahl, S.; Nørskov, J.K.; Chorkendorff, I. Bioinspired molecular co-catalysts bonded to a silicon photocathode for solar hydrogen evolution. *Nature Materials* **2011**, *10*, 434-438.
4. Hou, Y.; Abrams, B.L.; Vesborg, P.C.K.; Björketun, M.E.; Herbst, K.; Bech, L.; Seger, B.; Pedersen, T.; Hansen, O.; Rossmeisl, J.; Dahl, S.; Nørskov, J.K.; Chorkendorff, I. Photoelectrocatalysis and electrocatalysis on silicon electrodes decorated with cubane-like clusters. *J. Photonics for Energy* **2012**, *2*, 026001.
5. Wellendorff, J.; Lundgaard, K.T.; Møgelhøj, A.; Petzold, V.; Landis, D.D.; Nørskov, J.K.; Bligaard, T.; Jacobsen, K.W. Density functionals for surface science: Exchange-correlation model development with Bayesian error estimation. *Phys. Rev. B* **2012**, *85*, 235149.
6. Brogaard, R.Y.; Moses, P.G.; Nørskov, J.K. Modeling van der Waals Interactions in Zeolites with Periodic DFT: Physisorption of n-Alkanes in ZSM-22. *Catal. Lett.* **2012**, *142*, 1057-1060.
7. Hummelshøj, J.S.; Abild-Pedersen, F.; Studt, F.; Bligaard, T.; Nørskov, J.K. CatApp: A Web Application for Surface Chemistry and Heterogeneous Catalysis. *Angew. Chem. Int. Ed.* **2012**, *51*, 272-274.

8. Lausche, A.C.; Hummelshøj, J.S.; Abild-Pedersen, F.; Studt, F.; Nørskov, J.K. Application of a new informatics tool in heterogeneous catalysis: Analysis of methanol dehydrogenation on transition metal catalysts for the production of anhydrous formaldehyde. *J. Catal.* **2012**, *291*, 133-137.
9. Landis, D.D.; Hummelshøj, J.S.; Nestorov, S.; Greeley, J.; Dulak, M.; Bligaard, T.; Nørskov, J.K.; Jacobsen, K.W. The Computational Materials Repository. *Comp. Sci. Eng.* **2012**, *14*, 51.
10. Petzold, V.; Bligaard, T.; Jacobsen, K.W. Construction of New Electronic Density Functionals with Error Estimation Through Fitting. *Top. Catal.* **2012**, *55*, 402-417.
11. Nørskov, J.K.; Bligaard, T. The Catalyst Genome. *Angew. Chem. Int. Ed.* **2013**, *52*, 776-777.
12. Xu, Y.; Lausche, A.C.; Wang, S.; Khan, T.S.; Abild-Pedersen, F.; Studt, F.; Nørskov, J.K.; Bligaard, T. In Silico Search for Novel Methane Steam Reforming. *New J. Phys.* **2013**, *15*, 125021.
13. Lysgaard, S.; Landis, D.D.; Bligaard, T.; Vegge, T. Genetic algorithm procreation operators for alloy nanoparticle catalysts. *Top. Catal.* **2014**, *57*, 33.
14. Falsig, H.; Shen, J.; Khan, T.S.; Guo, W.; Jones, G.; Dahl, S.; Bligaard, T. On the structure sensitivity of direct NO decomposition over low-index transition metal facets. *Top. Catal.* **2014**, *57*, 80.
15. Tripkovic, V.; Cerri, I.; Bligaard, T.; Rossmeisl, J. The influence of particle shape and size on the activity of platinum nanoparticles for oxygen reduction reaction: A density functional study, *Catal. Lett.* **2014**, *144*, 380.
16. Vojvodic, A.; Medford, A.J.; Studt, F.; Abild-Pedersen, F.; Khan, T.S.; Bligaard, T.; Nørskov, J.K.: Exploring the limits: A low-pressure, low-temperature Haber-Bosch process, *Chem. Phys. Lett.* **2014**, *598*, 108.
17. Wellendorff, J.; Lundgaard, K.T.; Jacobsen, K.W.; Bligaard, T.: mBEEF: An accurate semi-local Bayesian error estimation functional, *J. Chem. Phys.* **2014**, *140*, 144107.
18. Medford, A.J.; Wellendorff, J.; Vojvodic, A.; Studt, F.; Abild-Pedersen, F.; Jacobsen, K.W.; Bligaard, T.; Nørskov, J.K.: Introducing uncertainty in theoretical predictions of materials properties: Reliability of calculated catalytic ammonia synthesis rates, Submitted, **2014**

Christine M. Thomas

**Early-Late Heterobimetallic Complexes Featuring Metal-Metal Bonds: Small Molecule Activation and Catalytic Applications**

Christine M. Thomas\*, Jeremy P. Krogman, J. Wesley Napoline, Seth L. Marquard, Bing Wu, Wen Zhou, Noam I. Saper, Subramaniam Kuppaswamy, Mark W. Bezpalko, and Bruce M. Foxman  
Brandeis University, Department of Chemistry

**Presentation Abstract**

Our group has been using bridging phosphinoamide ligands to investigate early/late heterobimetallic complexes. The metal-metal interactions in these compounds provide a unique method for tuning redox potentials and promoting  $\sigma$  bond activation processes. In an early example of this phenomenon, a representative tris(phosphinoamide)-supported Zr/Co complex was shown to undergo two-electron reduction at a potential 1 V more positive than a monometallic Co tris(phosphine) analogue. Once reduced by two electrons, the resulting coordinatively unsaturated Zr/Co complexes have been shown to undergo one-, two-, and four-electron transfer processes, activating a wide variety of  $\sigma$  bonds (e.g. O-H, N-H, C-X) and  $\pi$  bonds (e.g. the C=O bond in CO<sub>2</sub>). The reactivity of Zr/Co heterobimetallic complexes has been applied to several catalytic processes, including Kumada cross-coupling and the hydrosilylation of ketones and aldehydes, and it has been demonstrated that both metal centers play a crucial role in catalysis. Computational investigations into the nature of the Zr/Co bonds in tris(phosphinoamide) systems reveals a relatively weak donor/acceptor interaction in Zr<sup>IV</sup>Co<sup>I</sup> complexes, but much stronger metal-metal bonding in reduced Zr<sup>IV</sup>Co<sup>-I</sup> species (oxidation states firmly established using XANES) with both  $\sigma$  and  $\pi$  contributions. Extension of the tris(phosphinoamide) framework to a variety of different metal-metal combinations has been pursued in an effort to expose new reactivity patterns and provide fundamental insight into metal-metal bonding involving first row transition metals. The bonding between early and late first row metals in V/Fe, Cr/Fe, and Cr/Co complexes is much stronger, but this appears to hinder reactivity rather than promote more facile transformations. Ti/Co complexes are under further investigation but appear more promising. We have also investigated homobimetallic complexes in which the two metals are differentiated by their vastly different coordination environments (tris(amide) vs tris(phosphine)) and investigations into cooperative small molecule activation reactivity are underway.

**DE-SC0004019: Early-Late Heterobimetallic Complexes Linked by Phosphinoamide Ligands: Tuning Redox Potentials and Small Molecule Activation**

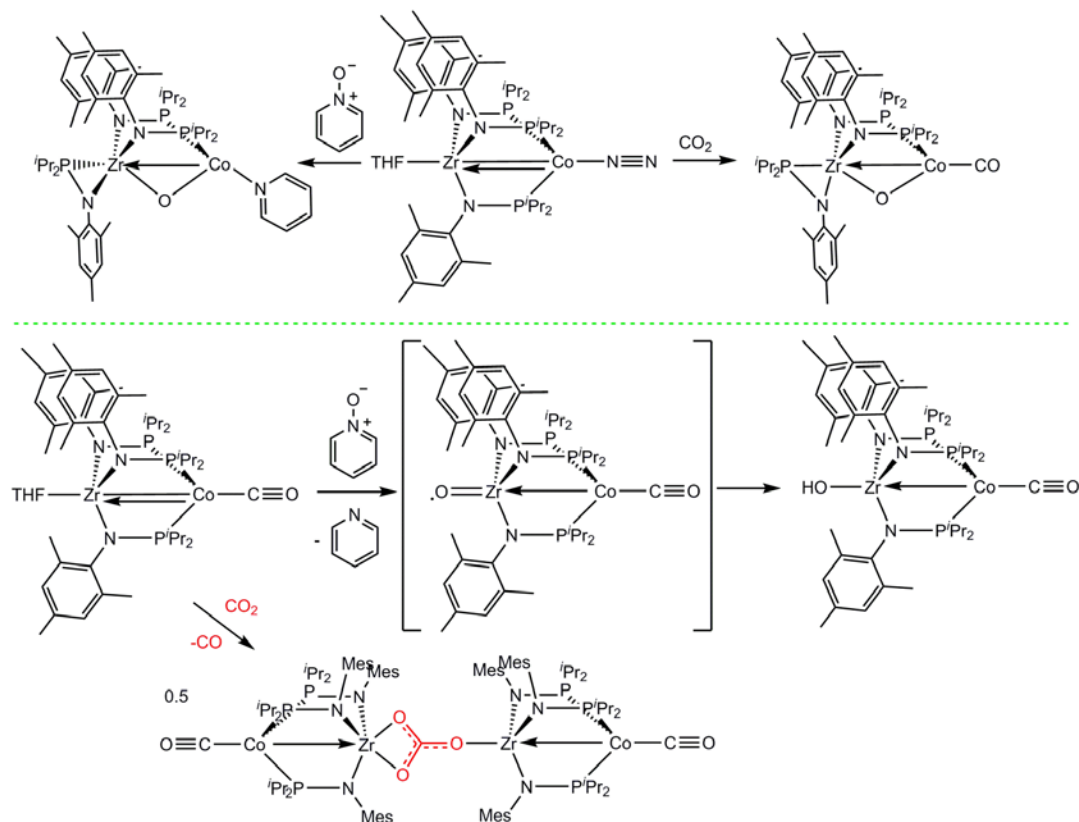
**PI:** Christine M. Thomas

**Postdoc(s):** Subramaniam Kuppaswamy, Seth L. Marquard, Claudia M. Fafard

**Student(s):** Jeremy P. Krogman, J. Wesley Napoline, Bing Wu, Wen Zhou, Ramyaa Mathialagan, Bennett P. Greenwood

## RECENT PROGRESS

**Scheme 1.** Further exploration of CO<sub>2</sub> reactivity with reduced heterobimetallic Zr/Co complexes suggests a mechanism involving initial coordination and one-electron transfer occurring at the Zr site.



**Scheme 2.** The C=O bond of ketones is cleaved across heterobimetallic Zr/Co bonds in a similar fashion to CO<sub>2</sub> via a one-electron-transfer mechanism involving ketyl radical intermediates.

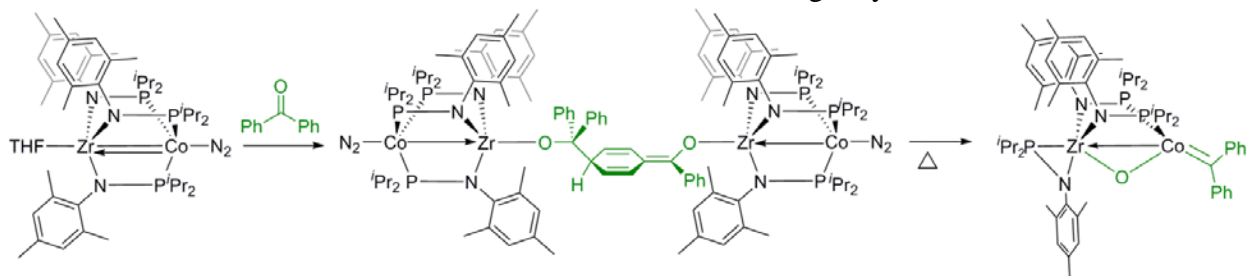


**Figure 1.** A fundamental study involving systematic variation of ligand substituents reveals that the electronic nature and reactivity of the heterobimetallic Zr/Co complexes is remarkably sensitive to variations in aromatic amide substituents.

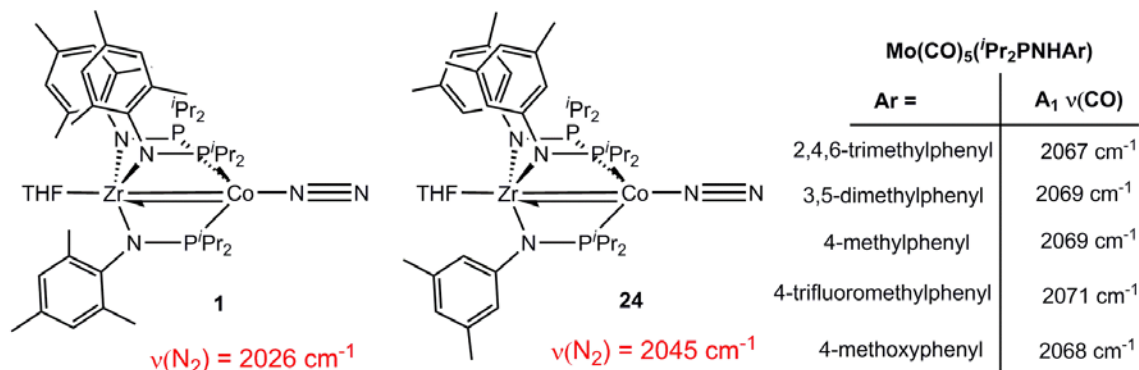
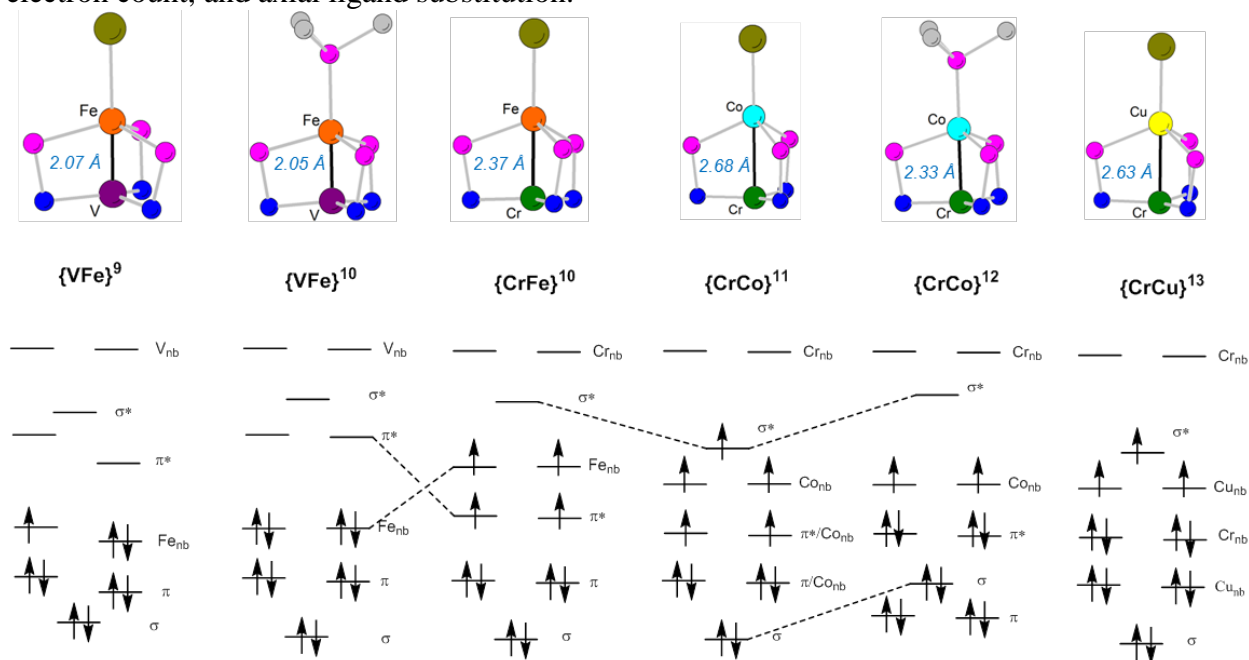
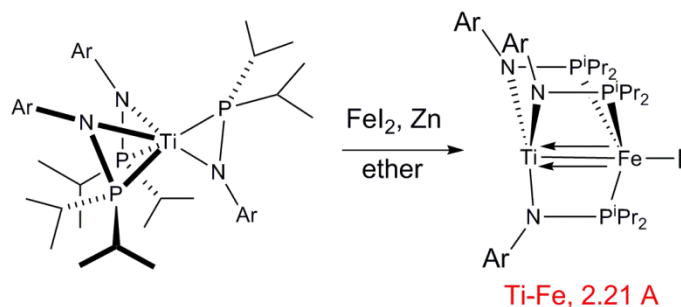


**Figure 2.** Examination of heterobimetallic combinations featuring first row metals reveals more covalent interactions with variations in bond order as a function of metal-metal combination, electron count, and axial ligand substitution.



**Scheme 3.** Heterobimetallic chemistry has been extended to Ti/Fe and Ti/Co, with Ti in both the Ti(IV) and Ti(III) oxidation state.



### Publications Acknowledging this Grant in 2011-2014

1. Kuppuswamy, S.; Powers, T. M.; Johnson, B. M.; Brozek, C. K.; Krogman, J. P.; Bezpalko, M. W.; Berben, L. A.; Keith, J. M.; Foxman, B. M.; Thomas, C. M. One-electron Oxidation Chemistry and Subsequent Reactivity of Diiron Imido Complexes. *Inorg. Chem.* **2014**, DOI: 10.1021/ic403039x.
2. Marquard, S. L.; Bezpalko, M. W.; Foxman, B. M.; Thomas, C. M. Interaction and Activation of Carbon-Heteroatom  $\pi$  Bonds with a Zr/Co Heterobimetallic Complex. *Organometallics* **2014**, *33*, 2071-2079.
3. Kuppuswamy, S.; Bezpalko, M. W.; Powers, T. M.; Wilding, M. J. T.; Brozek, C. K.; Foxman, B. M.; Thomas, C. M. A Series of  $C_3$ -Symmetric Heterobimetallic Cr/M (M = Fe, Co, and Cu) Complexes. *Chem. Sci.* **2014**, *5*, 1617-1626.
4. Zhou, W.; Saper, N. I.; Krogman, J. P.; Foxman, B. M.; Thomas, C. M. Effect of Ligand Modification on the Reactivity of Phosphinoamide-Bridged Heterobimetallic Zr/Co Complexes. *Dalton Trans.* **2014**, *43*, 1984-1989.
5. Napoline, J. W.; Kraft, S. J.; Matson, E. M.; Fanwick, P. E.; Bart, S. C.; Thomas, C. M. Tris(phosphinoamide)-supported Uranium-Cobalt Heterobimetallic Complexes Featuring Co $\rightarrow$ U Dative Interactions. *Inorg. Chem.* **2013**, *52*, 12170-12177.
6. Kuppuswamy, S.; Powers, T. M.; Krogman, J. P.; Bezpalko, M. W.; Foxman, B. M.; Thomas, C. M. Vanadium-Iron Complexes Featuring Metal-Metal Multiple Bonds. *Chem. Sci.* **2013**, *4*, 3557-3565.
7. Marquard, S. L.; Bezpalko, M. W.; Foxman, B. M.; Thomas, C. M. Stoichiometric C=O Bond Oxidative Addition of Benzophenone by a Discrete Radical Intermediate to Form a Cobalt(I) Carbene. *J. Am. Chem. Soc.* **2013**, *135*, 6018-6021.
8. Napoline, J. W.; Krogman, J. P.; Shi, R.; Kuppuswamy, S.; Bezpalko, M. W.; Foxman, B. M.; Thomas, C. M. Activation of E-H and E-E (E = S, O) Bonds by Heterobimetallic Zr/Co Complexes: Evidence for both One- and Two-Electron Processes. *Eur. J. Inorg. Chem.* **2013**, *2013*, 3874-3882.
9. Krogman, J. P.; Bezpalko, M. W.; Foxman, B. M.; Thomas, C. M. Synthesis, Structure, and Reactivity of an Anionic Zr-Oxo Relevant to CO<sub>2</sub> Reduction by a Zr/Co Heterobimetallic Complex. *Inorg. Chem.* **2013**, *52*, 3022-3031.

10. Zhou, W.; Marquard, S. L.; Bezpalko, M. W.; Foxman, B. M.; Thomas, C. M. Catalytic Hydrosilylation of Ketones Using a Co/Zr Heterobimetallic Complex: Evidence for an Unusual Mechanism Involving Ketyl Radicals. *Organometallics* **2013**, *32*, 1766-1772.
11. Mathialagan, R.; Kuppuswamy, S.; De Denko, A. T.; Bezpalko, M. W.; Foxman, B. M.; Thomas, C. M. Metal-Metal Bonding in Low Coordinate Dicobalt Complexes Supported by Phosphinoamide Ligands. *Inorg. Chem.* **2013**, *52*, 701-706.
12. Kuppuswamy, S.; Powers, T. M.; Johnson, B. M.; Bezpalko, M. W.; Brozek, C. K.; Foxman, B. M.; Berben, L. A.; Thomas, C. M. Metal-Metal Interactions in  $C_3$ -Symmetric Diiron Imido Complexes Linked by Phosphinoamide Ligands. *Inorg. Chem.* **2013**, *52*, 4802-4811.
13. Napoline, J. W.; Bezpalko, M. W.; Foxman, B. M.; Thomas, C. M. N-H Activation of Hydrazines by a heterobimetallic Zr-Co Complex: Promotion of One-Electron Chemistry at Zr. *Chem. Commun.* **2013**, *49*, 4388-4390.
14. Kuppuswamy, S.; Bezpalko, M. W.; Powers, T. M.; Turnbull, M. M.; Foxman, B. M.; Thomas, C. M. Utilization of Phosphinoamide Ligands in Homobimetallic Fe and Mn Complexes: The Effect of Disparate Coordination Environments on Metal-Metal Interactions and Magnetic and Redox Properties. *Inorg. Chem.* **2012**, *51*, 8225-8240.
15. Evers, D. A.; Bluestein, A. H.; Foxman, B. M.; Thomas, C. M. Synthesis and investigations of Metal-Metal Interactions in Early/Late Heterobimetallic Complexes Linking Group 5 Imido Fragments to Co(I). *Dalton Trans.* **2012**, *41*, 8111-8115.
16. Kuppuswamy, S.; Cooper, B. G.; Bezpalko, M. W.; Foxman, B. M.; Powers, T. M.; Thomas, C. M. Synthesis and Structural Characterization of High Spin M/Cu (M = Mn, Fe) Heterobimetallic and Fe/Cu<sub>2</sub> Trimetallic Phosphinoamides. *Inorg. Chem.* **2012**, *51*, 1866-1873.
17. Krogman, J. P.; Foxman, B. M.; Thomas, C. M. Activation of CO<sub>2</sub> by a Heterobimetallic Zr/Co Complex. *J. Am. Chem. Soc.* **2011**, *133*, 14582-14585.
18. Setty, V. N.; Zhou, W.; Foxman, B. M.; Thomas, C. M. Subtle Differences Between Zr and Hf in Early/Late Heterobimetallic Complexes with Cobalt. *Inorg. Chem.* **2011**, *50*, 4647-4655.
19. Zhou, W.; Napoline, J. W.; Thomas, C. M. A Catalytic Application of Co/Zr Heterobimetallic Complexes: Kumada Coupling of Unactivated Alkyl Halides with Alkyl Grignard Reagents. *Eur. J. Inorg. Chem.* **2011**, 2029-2033.

## Modeling Bulk Composition Dependent H<sub>2</sub> Dissociative Adsorption Energies on Cu<sub>x</sub>Pd<sub>1-x</sub> Alloy (111) Surfaces

John Kitchin, Jacob Boes, Gamze Guluslu, James Miller, Andrew Gellman

Department of Chemical Engineering, Carnegie Mellon University

### Presentation Abstract

The bulk composition dependent dissociative adsorption energy of hydrogen on CuPd alloys has been measured experimentally and modeled using density functional theory. The hydrogen adsorption energy cannot be simply defined by a single reactive site, nor as a composition weighted average of the pure metal components. Detailed modeling of such systems is difficult due to the distribution of active sites with varying composition, site-dependent, and effects such as segregation. We utilized a composition spread alloy film approach to measure the kinetics of hydrogen dissociation on Cu-Pd alloys as a function of composition. We developed a modeling approach that uses a basis of active sites to estimate the bulk composition dependent adsorption energy, weighted by the site probability distribution for a random alloy. With this method we can explain the composition dependent adsorption energy on Cu-rich alloy surfaces with relatively little computational effort. Deviations from predicted trends in the Pd-rich region can also lend insight into the experimental results at an atomistic level. In Pd-rich alloys a Pd-hydride phase forms which results in deviations from adsorption on the metallic alloy surface.

DESC0004031: Multifunctional Oxygen Evolution Electrocatalyst Design and Synthesis

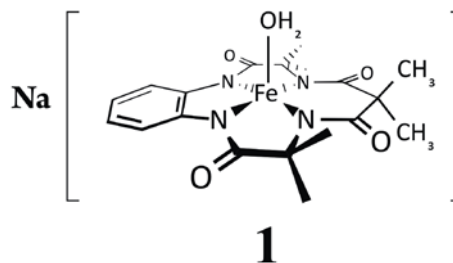
PI: John Kitchin

Students: Qingqi Fan, John Michael

### RECENT PROGRESS

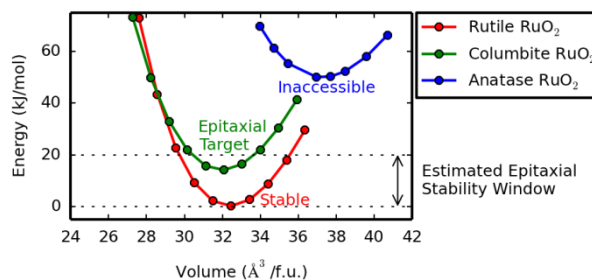
#### *Discovery of a new Fe-based molecular electrocatalyst for oxygen evolution*

We demonstrated that a carbon-black immobilized prototype tetra-amido macrocyclic ligand (TAML) **1** can electrocatalytically oxidize water (Reference 1). The significance of this finding is that the molecular catalyst is based on Fe, a cost-effective, earth abundant element, and the catalyst is oxidatively stable. It is expected that better, more active electrocatalysts may be made by modifying the ligands on **1**.



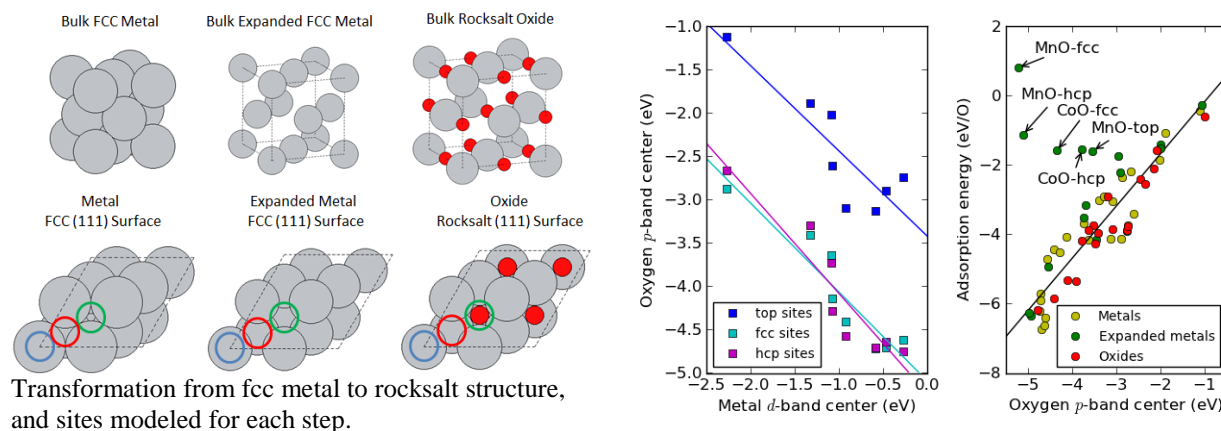
## Prediction of metastable oxide polymorphs

Different polymorphs of oxides can have very different catalytic properties. For example, anatase  $\text{TiO}_2$  is a better photocatalyst than rutile  $\text{TiO}_2$ , and the brookite polymorph is a better photocatalyst than either of those polymorphs. The challenge is how to make these different polymorphs, since they tend to be metastable. Pressure is one way to favor the formation of a low-volume polymorph. Polymorphs may also be stabilized as epitaxial thin films. In Reference 2, we illustrated a methodology to estimate the relative stabilities of  $\text{BO}_2$  oxide polymorphs to identify potential candidates for epitaxial stabilization. A schematic of the methodology is shown below for  $\text{RuO}_2$ . It can be seen that the anatase polymorph is much higher in energy than the known rutile polymorph, and it is probably inaccessible by epitaxial stabilization (and since it is a larger volume phase it cannot be reached by pressure). The columbite polymorph, on the other hand, falls in a window of metastability that we hypothesize makes it a candidate for epitaxial stabilization.



## Relating the electronic structure and reactivity of the 3d transition metal monoxide surfaces

Another goal in this project has been to identify descriptors for oxide surface reactivity. In Reference 3 we describe a successful identification of a descriptor for the 3d metal monoxide surfaces. We recognized a simple structural transformation of an fcc metal to the rocksalt structure. One first expands the metal, and then inserts an fcc lattice of oxygen atoms. We used these steps to identify changes in the adsorption of oxygen on each surface due to the expansion,



and lattice oxidation. The adsorption on the metals was well described by the d-band model, and we examined each step as a perturbation of that model. We found that for this system, the oxygen  $p$ -band and  $d$ -band were moderately coupled, which led to the identification of the

oxygen p-band center as a reasonable descriptor for the adsorption energy of oxygen on all three surfaces, with only a few exceptions.

### ***Reproducible Research Tools***

We have made significant progress in developing tools for documenting and sharing research methods and results. We now document all of our work in a plain text-based format called org-mode. This format enables one to embed source code into documents, run the code and capture the output. Additionally, one can embed images, links, and export the format to a variety of different formats including HTML and PDF. The PI gave a talk on this methodology at the 2013 Scipy conference ([http://www.youtube.com/watch?v=1-dUkyn\\_fZA](http://www.youtube.com/watch?v=1-dUkyn_fZA)) which has been viewed over 12,000 times already. The code we use for this is available at <http://github.com/jkitchin/jmax>.

The power of this new approach is best illustrated by the published papers prepared by us in org-mode (references 2-4 at the end). Notably the supporting information files contain complete records of how the work was done, the actual data, how the data was analyzed, and how the figures were prepared. All future publications are being prepared in this fashion.

### **Publications Acknowledging this Grant in 2011-2014**

1. Ethan L. Demeter , Shayna L. Hilburg , Newell R. Washburn , Terrence J. Collins , and John R. Kitchin, *Electrocatalytic Oxygen Evolution with an Immobilized TAML Activator*, Journal of the American Chemical Society, Accepted March 2014. <http://dx.doi.org/10.1021/ja5015986>
2. Mehta, Prateek; Salvador, Paul; Kitchin, John, *Identifying Potential BO<sub>2</sub> Oxide Polymorphs for Epitaxial Growth Candidates*", ACS Applied Materials and Interfaces, accepted 1/27/2014. <http://pubs.acs.org/doi/full/10.1021/am4059149>.
3. Zhongnan Xu and John R Kitchin, *Relating the Electronic Structure and Reactivity of the 3d Transition Metal Monoxide Surfaces*, Catalysis Communications, Accepted Oct 2013. <http://dx.doi.org/10.1016/j.catcom.2013.10.028>
4. Spencer D. Miller, Vladimir V. Pushkarev, Andrew J. Gellman and John R. Kitchin, *Simulating Temperature Programmed Desorption of Oxygen on Pt(111) Using DFT Derived Coverage Dependent Desorption Barriers*, Topics In Catalysis, 57(1), 106-117 (2013). <http://link.springer.com/article/10.1007%2Fs11244-013-0166-3>
5. Sneha A. Akhade and John R. Kitchin\*, *Effects of strain, d-band filling and oxidation state on the surface electronic structure and reactivity of 3d perovskite surfaces*, J. Chem. Phys. 137, 084703 (2012). <http://dx.doi.org/10.1063/1.4746117>
6. James Landon, Ethan Demeter, Nilay İnođlu, Chris Keturakis, Israel E. Wachs, Relja Vasić, Anatoly I. Frenkel, John R. Kitchin, *Spectroscopic characterization of mixed Fe-Ni oxide*

*electrocatalysts for the oxygen evolution reaction in alkaline electrolytes*, ACS Catalysis, 2, 1793-1801 (2012). <http://dx.doi.org/10.1021/cs3002644> .

7. Sneha A. Akhade and John R. Kitchin\*, *Effects of strain, d-band filling and oxidation state on the bulk electronic structure of cubic 3d perovskites*, J. Chem. Phys. 135, 104702 (2011). <http://dx.doi.org/10.1063/1.3631948>.

**Tuesday Morning**

**Catalysis of C–H  
Activation**

This page is intentionally blank.

## A Systematic Investigation of Ligand Effects on the Energetics of C-H Activation at Rhodium in Tp'Rh(L)(R)H Complexes

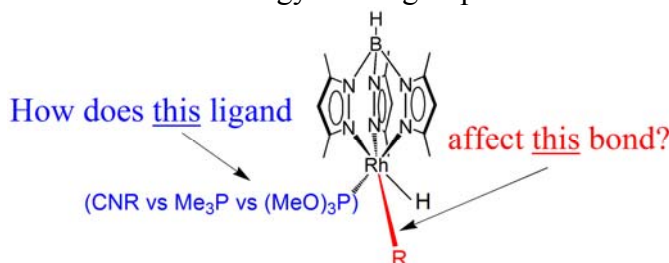
William D. Jones, Meagan E. Evans, James Morris, and Yunzhe Jiao

Department of Chemistry, University of Rochester, Rochester, NY 14627

E-mail: jones@chem.rochester.edu

### Presentation Abstract

A series of kinetic measurements of Tp'Rh(L)(R)H complexes (where L = CNneopentyl, PMe<sub>3</sub>, P(OMe)<sub>3</sub>; R = alkyl, aryl, vinyl, benzyl, allyl, and CH<sub>2</sub>X (X = CN, C≡CMe, CH<sub>2</sub>C(=O)CH<sub>3</sub>, and others; Tp' = tris-(3,5-dimethylpyrazolyl)borate) have been used to determine relative metal-carbon bond energies in these compounds. A thermodynamic analysis allows for the extraction of an increase in bond energy for R groups in which the corresponding anion is resonance stabilized, associated with an increase in the ionic contribution to metal-carbon bonding. Trends will be analyzed in terms of inductive vs. resonance contributions to the bonding. The bond energies will be used to establish factors controlling regioselectivity.




---

### Grant DE-FG02-86ER13569: Transition Metal Activation and Functionalization of Carbon-Hydrogen and Carbon-Carbon Bonds

PI: William D. Jones

Students: Meagan E. Evans, James Morris, and Yunzhe Jiao

#### RECENT PROGRESS

##### Summary

This project has as its overall goal improvement in the intelligent use of our energy resources, specifically petroleum derived products, and is aimed at the development of new routes for the manipulation of C-H and C-C bonds. During this project period, our research is focused on the following general goals: (1) C-H bond activation reactions in functionalized methane substrates (CH<sub>3</sub>X) and fundamental studies of their effects on metal-carbon bond strengths (M-CH<sub>2</sub>X); (2) C-H bond activation in terminal aryl and alkyl alkynes; (3) C-CN cleavage vs. C-H cleavage in nitriles; and (4) DFT studies of the above reactions. These results have been disseminated in the current 3-year grant cycle in the form of 14 publications. Specific accomplishments of this grant period include:

(1) We have measured and quantified experimentally and theoretically the rhodium-carbon bond strengths in 7 terminal alkyne complexes (Rh-C≡CR). This has been done with Tp'Rh(CNR), Tp'Rh(PMe<sub>3</sub>), and Tp'Rh[P(OMe)<sub>3</sub>] substituted systems.<sup>8</sup>

(2) We have made a breakthrough in our understanding of metal-rhodium bond strengths by the examination of the kinetics and thermodynamics of C-H bond activation in several substituted methyl derivatives (Rh-CH<sub>2</sub>X). These derivatives all show a strong effect of substitution at the α-carbon attached to rhodium. The shocking result is that these substitutions usually *weaken* the Rh-C bond, not strengthen it.<sup>2</sup>

(3) We have extended this work to investigate the effect of the spectator ligand on the metal-carbon bond strength in Tp'Rh(PMe<sub>3</sub>) and Tp'Rh[P(OMe)<sub>3</sub>] substituted systems.<sup>3,4,10</sup>

(4) We have answered the question "what makes the [Ni(dippe)] fragment react so differently than the [Tp'Rh(CNR)] fragment with the same substrates?" This was done by

comparing reactivities of  $[\text{Tp}'\text{Rh}(\text{PMe}_3)]$ ,  $[\text{Cp}^*\text{Rh}(\text{PMe}_3)]$ ,  $[\text{Cp}^*\text{Rh}(\text{CNR})]$ ,  $[\text{Rh}(\text{dippe})]$ , and  $[\text{Pt}(\text{dippe})]$ , allowing comparison of  $\text{Tp}'$  vs  $\text{Cp}^*$ ,  $\text{PMe}_3$  vs.  $\text{CNR}$ , and  $d^{10}$  Rh vs.  $d^{10}$  Ni/Pt. The bottom line: it's the isocyanide that is responsible for the unusual change in selectivity.<sup>2,3,4,6</sup>

(5) We determined the complete mechanism of C–CN vs. C–H activation of 2-methyl-3-butene nitrile (2M3BN) by  $[\text{Ni}(\text{dippe})]$  using DFT, which is critical to the DuPont synthesis of Nylon from butadiene. The study includes some 36 intermediates and transition states. These results compare favorably to our earlier experimental investigations of this system, and provide deeper understanding as to what controls selectivity. Solvent effects are incredibly large. Ligand effects on selectivity are also large (e.g., phosphine vs. N-heterocyclic carbene).<sup>1</sup>

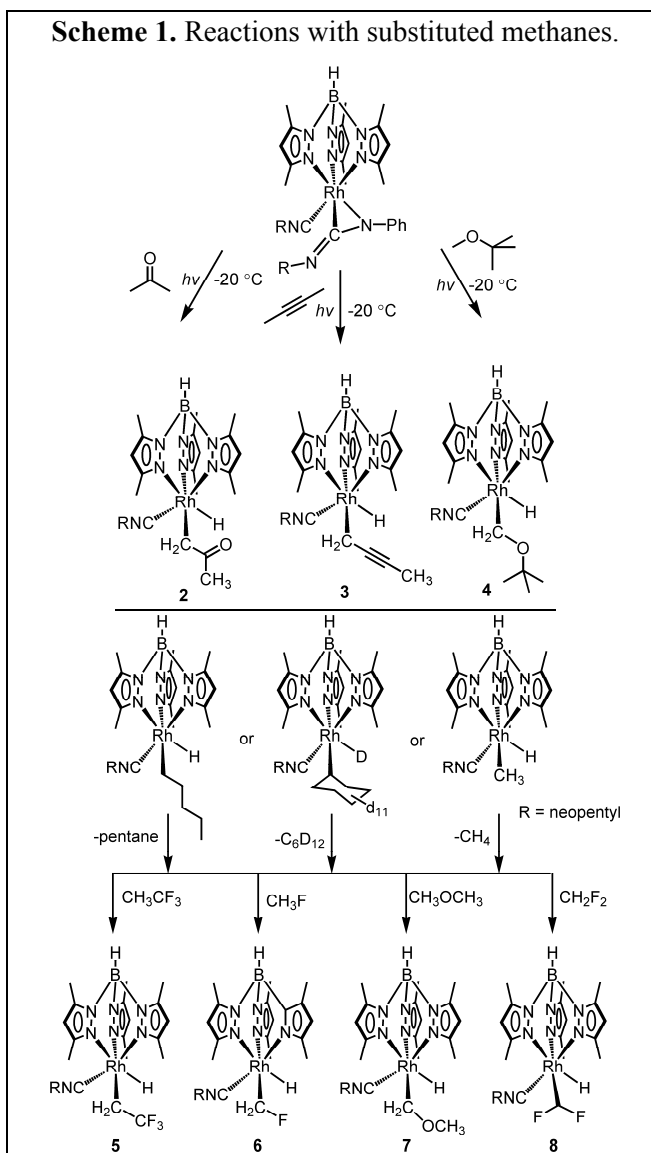
(6) The PI has also participated and published in the *Organometallics* Roundtable,<sup>7</sup> and investigated new nickel PONOP complexes<sup>5</sup> and disulfide additions to  $[\text{Ni}^0(\text{NHC})]$ .<sup>12</sup> A book chapter was written on metal mediated C–C bond activation.<sup>14</sup>

### C–H Activations of Substituted Methyl Derivatives using $\text{Tp}'\text{Rh}(\text{CNR})$ .

The reaction of the fragment  $[\text{Tp}'\text{Rh}(\text{CNR})]$  generated either by irradiation of the carbodimide or by loss of RH from  $\text{Tp}'\text{Rh}(\text{CNR})(\text{R})\text{H}$  with a variety of substituted methanes ( $\text{CH}_3\text{X}$  and  $\text{CH}_2\text{F}_2$ ) were examined and found to give cleanly single products (Scheme 1). Each of these products was then examined for the barrier to reductive elimination in benzene to obtain  $\Delta G^\ddagger$  for the elimination. Competition experiments were examined in benzene to give  $\Delta\Delta G^\ddagger$  values. As above, these values were used to then obtain relative rhodium-carbon bond strengths for these substituted derivatives. A full account appeared in *JACS* recently.<sup>2</sup>

Figure 1 shows a plot of the metal-carbon bond strengths of the *substituted* methanes vs. the C–H bond strengths. Remarkably, a linear correlation is seen that is displaced by  $\sim 7$  kcal mol<sup>-1</sup> above the line for the parent hydrocarbons. Several things are noteworthy. First, for most of the substituents (not F, Cl), the effect of substitution of X for H on a methyl group *weakens* the Rh–C bond strength. Most organometallic chemists would have thought that substitution by an electronegative group at an  $\alpha$ -carbon would strengthen the metal-carbon bond, but this is clearly not the case. In fact, those  $-\text{CH}_2\text{X}$  substituents in which the carbanion is resonance stabilized all have weaker Rh–C bonds than Rh–Me. This can be attributed to hyper-conjugation or to an increase in the ionic character of the metal-carbon bond. DFT calculated bond strengths are shown in comparison, and as before DFT overestimates the slopes by about 10%.

There are many other important ramifications of these correlations. For example,  $\text{Tp}'\text{Rh}(\text{CNR})(\text{CH}_2\text{CN})\text{H}$  must be heated to 100 °C to induce reductive



elimination ( $\tau = 3$  d), whereas  $\text{Tp}'\text{Rh}(\text{CNR})\text{MeH}$  loses methane at 22 °C with a  $t_{1/2}$  of about 5 h. Why does the molecule with the weaker Rh–C bond appear to be more stable (require heating)? The answer is that when reductive elimination of acetonitrile takes place, a 95 kcal mol<sup>-1</sup> bond is formed in the transition state, whereas with reductive elimination of methane, a 105 kcal mol<sup>-1</sup> bond is formed in the transition state, which lowers the barrier to methane elimination compared to acetonitrile elimination.

Another important result is that these bond strengths explain the regioselectivity of olefin insertions in a way that has not been previously recognized. As shown in equation 1, primary alkyl derivatives are thermodynamically favored over secondary alkyl derivatives.

However, introduction of an electron withdrawing group can reverse the selectivity, favoring the branched isomer (eq 2). Most organometallic chemists have taken this as an indication that the electron withdrawing group strengthens the metal-carbon bond, using electronics to overcome the unfavorable sterics in the branched isomers. *Not true, however, as our bond-strength studies show. The metal carbon bonds in the branched isomers are actually weaker.* The real reason for the reversal in selectivity is indicated in equations 3 and 4. It is the C–H bond *that is not even shown* that controls the regiochemistry. In the branched isomer a strong methyl C–H bond is formed (100 kcal mol<sup>-1</sup>) whereas in the linear isomer a weak secondary  $\alpha$ -cyano/benzylic C–H bond is formed! This result suggests that olefin insertion selectivities need to be re-evaluated throughout the literature.

#### C–H Activations of Hydrocarbons using $\text{Tp}'\text{Rh}(\text{L})$ ; $\text{L} = \text{PMe}_3, \text{P}(\text{OMe})_3$ .

Similar investigations of terminal alkyne activations and C–H activations of  $sp^2$  and  $sp^3$  C–H bonds were made with  $[\text{Tp}'\text{Rh}(\text{PMe}_3)]$  (generated by photolysis of  $\text{Tp}'\text{Rh}(\text{PMe}_3)_2$  or methane loss from  $\text{Tp}'\text{Rh}(\text{PMe}_3)(\text{Me})\text{H}$ ) and  $[\text{Tp}'\text{Rh}(\text{P}(\text{OMe})_3)]$  (generated by methane loss from  $\text{Tp}'\text{Rh}[\text{P}(\text{OMe})_3](\text{Me})\text{H}$ ). In both cases, C–H activation products are obtained. As before, reductive elimination barriers in benzene give  $\Delta G^\ddagger$  values, and competition experiments with benzene give  $\Delta\Delta G^\ddagger$  barriers. For each of these metal fragments, a series of rhodium–carbon bond strengths can be determined. These are plotted in Figure 2a for  $[\text{Tp}'\text{Rh}(\text{PMe}_3)]$  and Figure 2b for  $[\text{Tp}'\text{Rh}(\text{P}(\text{OMe})_3)]$ . As before, two trendlines are observed, one for the parent hydrocarbons and one for the substituted methyl derivatives. The difference to be noted is

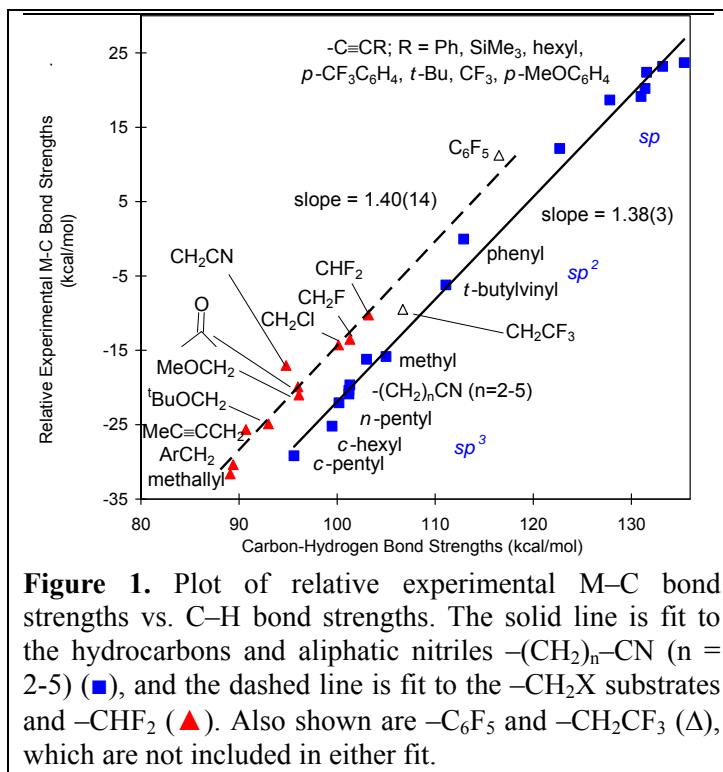
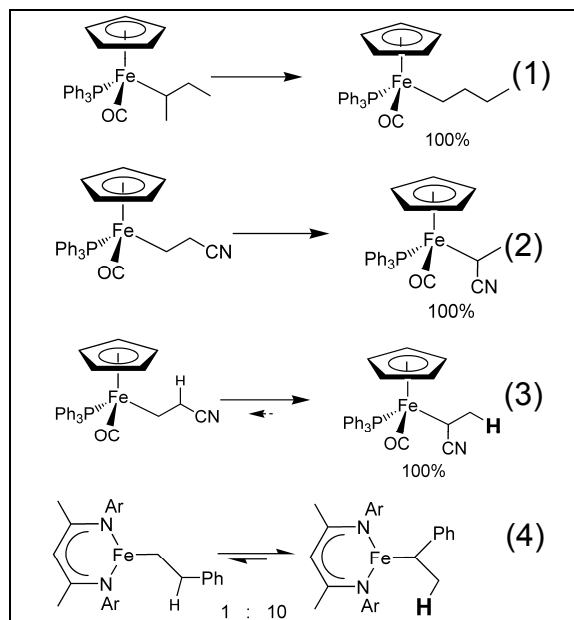


**Figure 1.** Plot of relative experimental M–C bond strengths vs. C–H bond strengths. The solid line is fit to the hydrocarbons and aliphatic nitriles  $-(\text{CH}_2)_n\text{CN}$  ( $n = 2-5$ ) (■), and the dashed line is fit to the  $-\text{CH}_2\text{X}$  substrates and  $-\text{CHF}_2$  (▲). Also shown are  $-\text{C}_6\text{F}_5$  and  $-\text{CH}_2\text{CF}_3$  (Δ), which are not included in either fit.



that with  $\text{PMe}_3$  as spectator ligand, the slopes increase to 1.54 and 1.71, respectively. The effect of substitution of a  $\pi$ -acceptor CNR by a  $\sigma$ -donor  $\text{PMe}_3$  is to spread out the range of rhodium-carbon bond energies. Examination of the slopes for the  $[\text{Tp}'\text{Rh}(\text{P}(\text{OMe})_3)]$  show that they lie in between those for the CNR and  $\text{PMe}_3$  derivatives (1.55 and 1.45), as expected for a ligand with more modest  $\sigma$ -donating ability. These systems were also examined by DFT, and as before, showed an overestimation of the slopes by  $\sim 10\%$ . These results were published recently in *JACS*<sup>11</sup> and *Chemical Science*.<sup>13</sup>

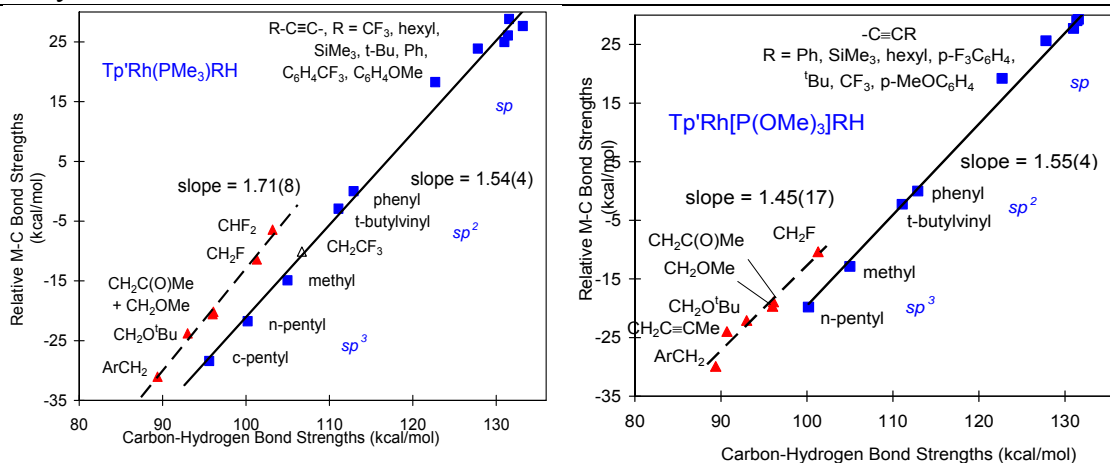


**Fig 2.** Plot of  $D_{rel}(\text{M}-\text{C})$  vs.  $D(\text{C}-\text{H})$  for  $\text{Tp}'\text{Rh}(\text{L})\text{RH}$  (a)  $\text{L} = \text{PMe}_3$  and (b)  $\text{L} = \text{P}(\text{OMe})_3$ ,  $\text{kcal mol}^{-1}$

## References - Pubs from the current grant cycle acknowledging DOE support 2011–14:

1. "DFT Calculations of the Isomerization of 2-Methyl-3-butenitrile by  $[\text{Ni}(\text{bisphosphine})]$  in Relation to the DuPont Adiponitrile Process," Ting Li and William D. Jones, *Organometallics*, **2011**, *30*, 547-555..
2. "C-H and C-CN Bond Activation of Acetonitrile and Succinonitrile by  $[\text{Tp}'\text{Rh}(\text{PR}_3)]$ ," Taro Tanabe, Meagan E. Evans, William W. Brennessel, and William D. Jones, *Organometallics*, **2011**, *30*, 834-843.
3. "C-CN vs. C-H Cleavage of Benzonitrile using  $[(\text{dippe})\text{PtH}]_2$ ," Brett D. Swartz, William W. Brennessel, and William D. Jones, *Organometallics*, **2011**, *30*, 1523-1529.
4. "Controlling the Selectivity for C-H and C-CN Bond Activation at Rhodium: A DFT Examination of Ligand Effects," Meagan E. Evans and William D. Jones, *Organometallics* **2011**, *30*, 3371-3377.
5. "Synthesis and Reactivity of New Ni, Pd and Pt PONOP Pincer Complexes," Sabuj Kundu, William W. Brennessel, and William D. Jones, *Inorg. Chem.*, **2011**, *50*, 9443-9453.
6. "C-CN Bond Activation of Benzonitrile with  $(\text{dippe})\text{Rh}(-1)$ ," Matthew R. Grochowski, William W. Brennessel, and William D. Jones, *Organometallics* **2011**, *30*, 5604-5610.
7. "Organometallics Roundtable 2011", Gladysz, J. A.; Ball, Z. T.; Bertrand, G.; Blum, S. A.; Dong, V. M.; Dorta, R.; Hahn, F. E.; Humphrey, M. G.; Jones, W. D.; Klosin, J.; Manners, I.; Marks, T. J.; Mayer, J. M.; Rieger, B.; Ritter, J.; Sattelberger, A. P.; Schomaker, J. M.; Yam, V. W. W. *Organometallics* **2012**, *31*, 1-18.
8. "C-H Activation of Terminal Alkynes by tris-(3,5-dimethylpyrazolyl)boraterhodium-neopentylisocyanide: New Metal-Carbon Bond Strengths," Gyeongshin Choi, James Morris, William W. Brennessel, and William D. Jones, *J. Am. Chem. Soc.* **2012**, *134*, 9276-9284.
9. "Rhodium-Carbon Bond Energies in  $\text{Tp}'\text{Rh}(\text{CNneopentyl})(\text{CH}_2\text{X})\text{H}$ : Quantifying Stabilization Effects in M-C Bonds," Yunzhe Jiao, Meagan E. Evans, James Morris, William W. Brennessel, and William D. Jones. *J. Am. Chem. Soc.* **2013**, *135*, 6994-7004.
10. "A Trispyrazolylboraterhodium Phosphite Complex that Undergoes an Arbusov-Like Rearrangement," Yunzhe Jiao, William W. Brennessel, and William D. Jones, *Acta Cryst. C*, **2013**, *C69*, 939-942.
11. "Kinetic and Thermodynamic Selectivity of Intermolecular C-H Activation at  $[\text{Tp}'\text{Rh}(\text{PMe}_3)]$ . How Does the Ancillary Ligand Affect the Metal-Carbon Bond Strength?" Yunzhe Jiao, James Morris, William W. Brennessel, and William D. Jones, *J. Am. Chem. Soc.* **2013**, *135*, 16198-16212.
12. "Nickel(0) Addition to a Disulfide Bond," Juanjuan Li, James Morris, William W. Brennessel, William D. Jones, *J. Chem. Cryst.* **2013**, *44*, 15-19.
13. "Synthesis and energetics of  $\text{Tp}'\text{Rh}[\text{P}(\text{OMe})_3](\text{R})\text{H}$ : A systematic investigation of ligand effects on C-H activation at rhodium," Yunzhe Jiao, William W. Brennessel, and William D. Jones, *Chem. Sci.* **2013**, *4*, 804-812. DOI: 10.1039/c3sc52748d
14. *Topics in Current Chemistry, C-C Bond Activation*, Guangbin Dong, Ed., "Mechanistic Studies of Transition Metal-Mediated C-C Bond Activation," W. D. Jones, Springer-Verlag: Berlin, Heidelberg, 2013, in press.

**John T. Yates, Jr.**

**C-H Bond Activation at Perimeter Sites on Au/TiO<sub>2</sub>- The Oxidative-Dehydrogenation of Alkyl Side Chains in Carboxylic Acids**

John T. Yates, Jr.

Department of Chemistry

University of Virginia

Charlottesville, VA 22904

Biomass can be converted into chemicals, energy and fuel in order to replace nonrenewable fossil fuel resources. The activation ( $0.5 \text{ eV} = E_a$ ) of molecular oxygen occurs at the dual perimeter sites surrounding  $\sim 3 \text{ nm}$  diameter Au particles on TiO<sub>2</sub> via a peroxy type intermediate. The oxidative-dehydrogenation of three carboxylate species (acetate, propionate and butyrate) has been investigated by transmission IR spectroscopy and density functional theory on Au/TiO<sub>2</sub> catalysts. The partial oxidation of the three acids proceeds by the scission of the C-H bonds adjacent to the carboxylate group. In the case of the two higher carboxylates, C=C bond formation is observed followed by C-C bond scission. A common intermediate, Au<sub>2</sub>=C=C=O, gold ketenylidene, is observed for all three acids which is a precursor to final oxidation to CO<sub>2</sub>. The IR observation of the rate of formation of Au<sub>2</sub>=C=C=O provides a convenient anchor point for kinetic intercomparisons. Kinetics measurements show that site blocking by alkyl groups reduces the rate of reaction of the carboxylate groups in a monotonic manner scaling with the alkyl group size. Studies of the deuterium kinetic isotope effect have been informative about the role of C-H bond activation on the transition state for partial oxidation of each of the acids.

**DE-SC0002365 “ Observing Carbon-Hydrogen Bond Activation in Chemisorbed Species Using New Highly Sensitive Optical Method”**

**PI:** John T. Yates, Jr. and Matthew Newrock

**Postdocs:** Zhen Zhang; W. Tang

**Students:** Monica McEntee; Isabel Green

## Publications:

1. I. Green, W. Tang, M. Neurock and J. T. Yates, Jr. "Low Temperature Catalytic H<sub>2</sub> Oxidation over Nanoparticle Au/TiO<sub>2</sub> – Dual Perimeter Sites at Work," *Angewandte Chemie*, 50, 1 (2011).
2. I. Green, W. Tang, M. Neurock and J. T. Yates, Jr., "Spectroscopic Observations of Dual Catalytic Sites at Work: Oxidation of CO on a Au/TiO<sub>2</sub> Catalyst," *Science* 333, 736-739, (2011).
3. D. Panayotov, S. P. Burrows, J. T. Yates, Jr., and J. R. Morris , " Mechanistic Studies of Hydrogen Dissociation and Spillover on Au/TiO<sub>2</sub>: IR Spectroscopy of Co-adsorbed CO and H-donated Electrons," *J. Phys. Chem. C* 115, 22400-22408 (2011).
4. J. T. Yates, Jr., "The Search for the Active Site on Catalysts," *Jefferson Journal of Science and Culture*, 2, 35 (2011).
5. Z. Zhang, W. Tang, M. Neurock, and J.T. Yates, Jr., "Electric Charge of Single Au Atoms Adsorbed on TiO<sub>2</sub>(110) and Associated Band Bending," *J. Phys. Chem. C* 115, 23848 – 23853 (2011).
6. I. X. Green, W. Tang, M. McEntee, M. Neurock and J. T. Yates, Jr., "Inhibition at Perimeter Sites of Au/TiO<sub>2</sub> Oxidation Catalyst by Reactant Oxygen," *J. Amer. Chem. Soc.*, 134, 12717-12723 (2012).
7. Z. Zhang and J. T. Yates, Jr., "Band Bending in Semiconductors: Chemical and Physical Consequences at Surfaces and Interfaces," *Chemical Reviews*, 112, 5520-5551 (2012).
8. I. X. Green, W. Tang, M. Neurock and J. T. Yates, Jr., "Localized Partial Oxidation of Acetic Acid at the Dual Perimeter Sites of the Au/TiO<sub>2</sub> Catalyst- Formation of Gold Ketenylidene," *J. Amer. Chem. Soc.*, 134,13569-13572 (2012).
9. I. Green, W. Tang, M. Neurock and J.T. Yates, Jr., "Mechanistic Insights into the Partial Oxidation of Acetic Acid by O<sub>2</sub> at the Dual Perimeter Sites of a Au/TiO<sub>2</sub> Catalyst," *Faraday Discuss.*, 162, 247-265 (2013).
10. Z. Zhang, K.Cao, and J.T. Yates, Jr., "Defect-Electron Spreading on the TiO<sub>2</sub>(110) Semiconductor Surface by Water Adsorption," *J. Phys. Chem. Lett.* ,4, 674-679 (2013).
11. I. Green, M. McEntee, W. Tang, M. Neurock and J.T. Yates, Jr., "Direct Formation of Acetate from Partial Oxidation of Ethylene on a Au/TiO<sub>2</sub> Catalyst," *Top. Catal.*, 56,1512-1524 (2013).
12. I. Green, W. Tang, M. Neurock and J.T. Yates, Jr., "Insights into Catalytic Oxidation at the Au/TiO<sub>2</sub> Dual Perimeter Sites," *Acc. Chem. Res.*, 47, 805-8015 (2013).

13. M. McEntee, W. Tang, M. Newrock and J. T. Yates, Jr., “ Selective Catalytic Oxidation-Dehydrogenation of Carboxylic Acids- Acrylate and Crotonate Formation at the Au/TiO<sub>2</sub> Interface, *J. Amer. Chem. Soc.*, 136, 5116-5120 (2014).

**Synthesis, Characterization, and Activity of Single Site Catalysts Supported in Metal Organic Frameworks via Ion Exchange**

Melanie S. Sanford, Douglas Genna, Signe Korsager, Antek G. Wong-Foy, Adam J. Matzger  
University of Michigan, Department of Chemistry

**Presentation Abstract**

This presentation will discuss our efforts to use the well-defined porous structures of metal organic frameworks (MOFs) as heterogeneous supports for single site alkene hydrogenation and C–H functionalization catalysts. An ion exchange approach to supporting cationic catalysts in anionic frameworks has been developed. The characterization of these supported catalysts and the influence of MOF structure on catalyst performance will be described in detail.

**Grant Number/Title: DE-FG02-08ER15997: Catalyst Control of Site Selectivity in Catalytic C–H Arylation and Alkylation Reactions**

**Lead PI:** Prof. Melanie Sanford; co-PI: Prof. Adam Matzger

**Research Scientist:** Dr Antek Wong-Foy

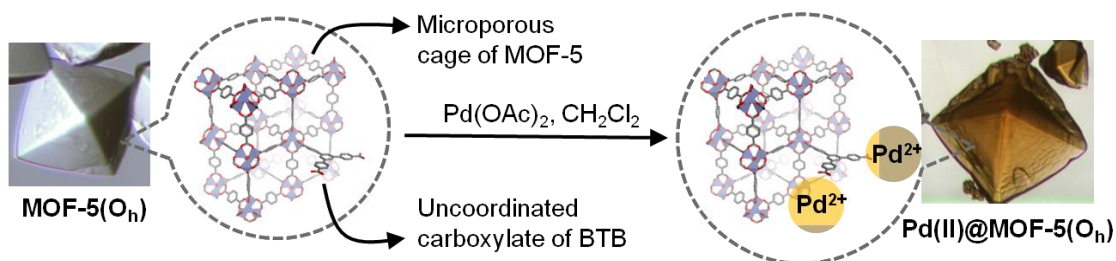
**Post-doc:** Dr. Douglas Genna

**Students:** Signe Korsager, Bryant James

**RECENT PROGRESS**

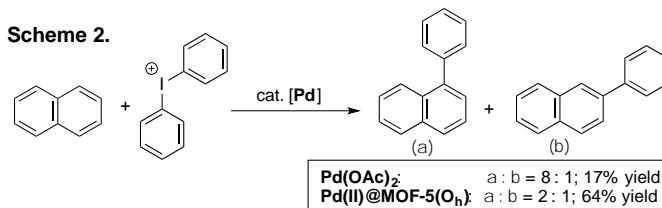
Over the past several years, metal organic frameworks (MOFs) have been widely targeted as supports for catalysts. We aimed to exploit the well defined and highly tunable pore structures of these materials to modulate the stability, reactivity, and selectivity of Pd-derived C–H functionalization catalysts. In collaboration with Professor Adam Matzger (University of Michigan), we tethered Pd(OAc)<sub>2</sub> to a Zn-derived metal organic framework, MOF-5(O<sub>h</sub>), to generate the supported catalyst Pd(II)@MOF-5(O<sub>h</sub>). MOF-5(O<sub>h</sub>) is believed to have the microporous cage structure of MOF-5, which contains terephthalic acid organic linkers joined by Zn<sub>4</sub>O(CO<sub>2</sub>)<sub>6</sub> nodes (CO<sub>2</sub> = carboxylate from

Scheme 1.



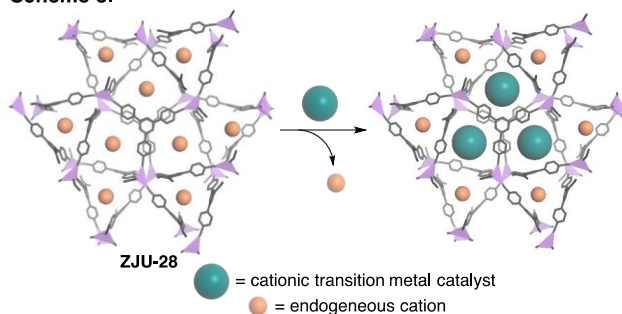
the linker). However, the addition of small amounts of 1,3,5-tri(4-carboxyphenyl)benzene (BTB) during the MOF-5 synthesis results in defect sites that contain dangling carboxylates. As shown in cartoon form in Scheme 1, the Pd(II) of Pd(II)@MOF-5(O<sub>h</sub>) is believed to be covalently attached to the MOF through these defect sites.

We first compared Pd(II)@MOF-5(O<sub>h</sub>) to Pd(OAc)<sub>2</sub> as a catalyst for the C–H arylation of naphthalene. Under otherwise identical conditions, the MOF-supported catalyst provided a significant enhancement in reaction yield (64% versus 17%). The enhanced yield appears to result from slower decomposition of the MOF-supported catalyst. The site selectivity (ratio of α : β-products) also changed significantly from 8 : 1 with Pd(OAc)<sub>2</sub> to 2 : 1 with Pd(II)@MOF-5(O<sub>h</sub>) (Scheme 2). Based on these results in combination with a number of control reactions, we conclude that the MOF support is having a significant influence on catalyst activity and selectivity in this C–H functionalization reaction. However, this system remains limited by the poorly defined (and difficult to characterize) tether sites between the MOF and the Pd catalyst as well as by the modest stability of Pd(II)@MOF-5(O<sub>h</sub>) under the C–H functionalization reaction conditions.



On the basis of these initial findings, we turned our attention to identifying better ways of supporting homogeneous catalysts in MOFs. We aimed to develop an approach that: (1) provides a well-defined mode of catalyst immobilization, (2) avoids the need to covalently tether the catalyst to the MOF (which often requires multistep synthesis and can often adversely impact catalyst activity), (3) has the potential to be applied to diverse catalysts, and (4) generates robust and recyclable supported catalysts. We hypothesized that these objectives could all be accomplished by supporting cationic transition metal catalysts in anionic MOFs via ion exchange (Scheme 3). Importantly, ion exchange has been used previously to introduce diverse cations into MOFs but has not, to our

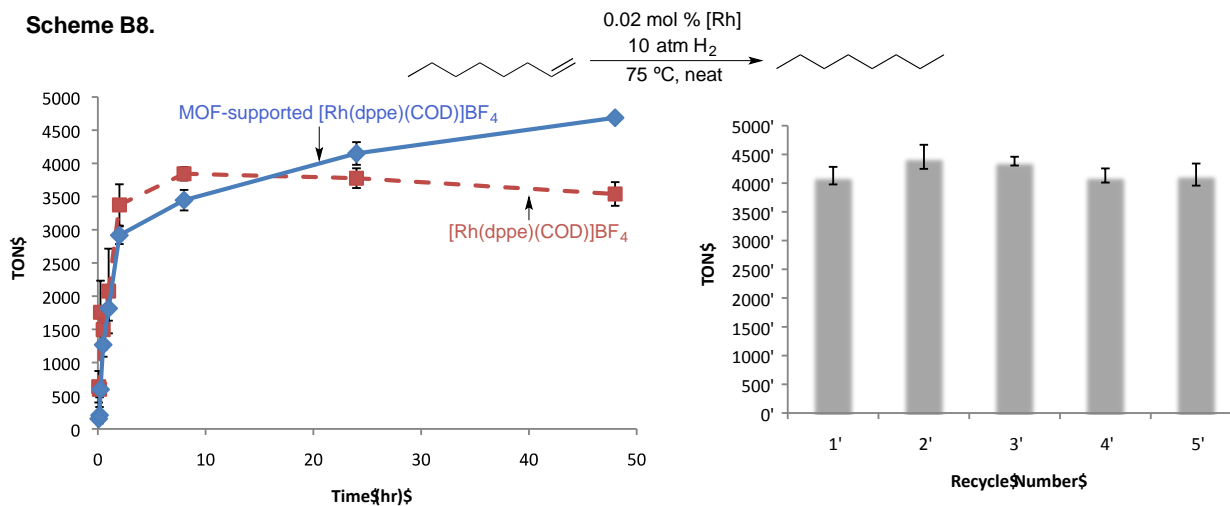
**Scheme 3.**



knowledge, previously been employed in MOF catalysis. This approach would enable well-defined immobilization of cationic catalysts based on a simple balancing of charged sites. It would avoid the requirement for covalent tethering and would enable us to support diverse catalysts without altering their chemical structures.

We selected the anionic MOF ZJU-28 as a support for initial investigations based on its well-known ability to participate in cation exchange as well as its redox inert indium tetracarboxylate metal nodes. The treatment of ZJU-28 with DMF solutions of [FeCp(CO)<sub>2</sub>(thf)]BF<sub>4</sub>, [Pd(CH<sub>3</sub>CN)<sub>4</sub>][BF<sub>4</sub>]<sub>2</sub>, [Ir(PCy<sub>3</sub>)(C<sub>5</sub>H<sub>5</sub>N)(COD)]PF<sub>6</sub>, [Rh(dppe)(COD)]BF<sub>4</sub>, or [Ru(Cp\*)(CH<sub>3</sub>CN)<sub>3</sub>]OTf for 3 days resulted in exchange of the endogenous cation, H<sub>2</sub>NMe<sub>2</sub><sup>+</sup>, for the requisite metal complex. We examined MOF-supported Rh(dppe)(COD)<sup>+</sup> as a catalyst for the hydrogenation of 1-octene to *n*-octane. As shown in Scheme 4, the activity of this supported catalyst compares favorably to its

homogeneous counterpart; furthermore, it could be recycled at least four times without an appreciable decrease in catalyst TON.



Overall, this work provides a new and general approach for supporting catalysts in MOFs. It also sets the stage for us to use metal organic frameworks to tune catalyst stability and selectivity in both alkene hydrogenation and C–H functionalization reactions, both of which we are currently pursuing.

#### Publications Acknowledging this Grant (2011-2014)

- (1) Lyons, T. W.; Hull, K. L.; Sanford M. S. “Controlling Site Selectivity in Palladium-Catalyzed C–H Oxidative Cross-Coupling,” *J. Am. Chem. Soc.* **2011**, *133*, 4455-4464.
- (2) Wagner, A. M.; Sanford, M. S. “Palladium-Catalyzed C–H Arylation of 2,5-Disubstituted Pyrroles,” *Org. Lett.* **2011**, *13*, 288-291.
- (3) Loy, R. N.; Sanford, M. S. “Palladium-Catalyzed C–H Perfluoroalkylation of Arenes,” *Org. Lett.* **2011**, *13*, 2548-2551.
- (4) Hickman, A. J.; Sanford, M. S. “Catalyst Control of Site Selectivity in the Pd<sup>II/IV</sup>-Catalyzed Direct Arylation of Naphthalene,” *ACS Catal.* **2011**, *1*, 170-174. (Featured on cover)
- (5) Park, T.-H.; Hickman, A. J.; Koh, K.; Martin, S.; Wong-Foy, A. G.; Sanford, M. S.; Matzger, A. J. “Highly Dispersed Palladium(II) in a Defective MOF: Application to C–H Activation and Functionalization,” *J. Am. Chem. Soc.* **2011**, *133*, 20138-20141.
- (6) Hickman, A. J.; Cismesia, M. A.; Sanford, M. S. “Structure-Activity Relationship Study of Diimine Pt<sup>II</sup> Catalysts for H/D Exchange,” *Organometallics* **2012**, *31*, 1761-1766.
- (7) Neufeldt, S. R.; Sanford, M. S. “Controlling Site Selectivity in Palladium-Catalyzed C–H Bond Functionalization,” *Acc. Chem. Res.* **2012**, *45*, 936-946.

- (8) Genna, D. T.; Wong-Foy, A. G.; Matzger, A. J.; Sanford, M. S. "Heterogenization of Homogeneous Catalysts in Metal Organic Frameworks via Cation Exchange," *J. Am. Chem. Soc.* **2013**, *135*, 10586-10589.
- (9) Sanhueza, I. A.; Wagner, A. M.; Sanford, M. S.; Schoenebeck, F. "On the Role of Anionic Ligands in the Site Selectivity of Oxidative C–H Functionalization Reactions of Arenes," *Chem. Sci.* **2013**, *4*, 2767-2775.
- (10) Wagner, A. M.; Hickman, A. J.; Sanford, M. S. "Platinum Catalyzed C–H Arylation of Simple Arenes," *J. Am. Chem. Soc.* **2013**, *135*, 15710-15713.
- (11) Wagner, A. M.; Sanford, M. S. "Transition Metal Free Synthesis of Aryl Sulfides from Thiols or Thioethers," *J. Org. Chem.* **2014**, *79*, 2263-2267.

## Investigation of C-H bond Activation and Doped Metal Oxide Catalysis

Eric W. McFarland, Michael J. Gordon, and Horia Metiu

Departments of Chemical Engineering and Chemistry & Biochemistry, University of California,  
Santa Barbara

The activity and synthesis of doped oxide catalysts whereby some of the cations in the oxide are replaced with a different cation has been investigated. From our theoretical work we anticipated and demonstrated several effects of the dopants: 1. Some of the dopants will weaken the bond of the oxygen atoms to the surface, making the doped oxide a better oxidant. 2. Some dopants will be undercoordinated and will adsorb oxygen molecules and activate them. These activated adsorbed  $O_2$  will react with alkanes. Such systems could be used for partial oxidation. 3. Some dopants will make it easier to reduce the oxide and the reduced surface catalyzes reduction reactions (e.g.  $CO_2 + 4 H_2 \rightarrow CH_4 + 2 H_2O$  or  $H_2O + \text{reduced oxide} \rightarrow H_2 + \text{oxide}$ ). By combining all oxides with all possible dopants one obtains a very rich class of potential catalysts. We use theory to help us choose the most promising dopant-oxide pairs and then we synthesize the promising systems by a variety of methods, characterize them, and test their catalytic activity for alkanes or  $CO_2$  activation. Recently we have extended our investigations into halogen mediated oxidative dehydrogenation (ODH) of alkanes. Experiments are performed in which the halogen is  $I_2$  which is either introduced as a gas in the feed, or is obtained in situ by oxidizing molten LiI. Iodine mediated ODH of propane has an excellent propylene yield and theoretical and experimental work is under way for optimizing the process and understanding the mechanism.

### Department of Energy DE-FG03-89ER14048: Investigation of C-H bond Activation and Doped Metal Oxide Catalysis

**Postdoc(s):** Henrik Kristoffersen

**Student(s):** Alan Derk, Ches Upham

#### RECENT PROGRESS

- The activity of the irreducible metal oxide,  $La_2O_3$ , was modified by substitution of higher valence and lower valence dopants for La(III). A beautiful correlation between activity for C-H bond activation and the DFT calculated oxygen vacancy formation energy was discovered.
- Pd-substituted  $CeO_2$  catalysts prepared by ultrasonic spray pyrolysis were found to be active for C-H bond activation only when Pd is in metallic state. Partial oxidation of  $CH_4$  over  $Ce_{0.95}Pd_{0.05}O_{2-\delta}$  yields combustion products along with hydrogen-rich synthesis gas.
- Understanding the impact of specific dopants and the vacancy energetics allowed us to extend the approach used for C-O oxidation to C-H bond activation. The choice of dopant strikes a fine balance between the ability to dissociate the C-H bond on the dopant and

oxidize the reactant, with the ability to form surface oxygen vacancies. Electrophilic Pt atoms were used as atomic dopants in ceria hosts to regulate and utilize the mobile oxygen vacancies. Whereas complete combustion of methane in oxygen occurs preferentially on traditionally supported Pt catalysts, high selectivity for the partial oxidation of methane to CO and H<sub>2</sub> was achieved on Pt-doped CeO<sub>2</sub>. The critical step in facilitating the synthesis gas formation is the decrease in vacancy formation energy caused by the Pt doping of CeO<sub>2</sub>.

- We have investigated “inverse catalysts”, consisting of small oxide clusters supported on a metal surface. We performed density functional calculations for VO<sub>3</sub> and VO<sub>4</sub> supported on Au(111) and Ag(111). Isolated V atoms on Au(111) surface are oxidized when exposed to gas-phase O<sub>2</sub> at a given pressure and temperature and the VO<sub>x</sub> clusters formed this way are capable of breaking the C-H bond in methane with a low activation energy.
- The activity of Ru-substituted CeO<sub>2</sub> catalysts was further investigated and the catalyst shown to be active for dry reforming as well as methanation and water-gas shift. The activity was correlated to the reduced oxide and using pulses of oxygen/hydrogen the activity could be “switched off”/“switched on”. Synchrotron-XRD on doped Ru showed no formation of ruthenium crystallographic phases in the catalyst which confirms that we are making pure doped Ru catalyst. No measurable difference in the catalytic activity for dry reforming of methane between Ru-doped cerium oxide and ruthenium oxide supported on ceria.
- Atomically doping ceria and zirconia with 5% Ru activates both metal oxides for partial oxidation of propane. Low-temperature dry reforming activity for the CeO<sub>2</sub> doped ruthenium may be of interest for syngas production. The catalyst under working conditions is the reduced oxide. We have also found, to our surprise, that there is no difference in reactivity for syngas production between Ru-doped ceria and Ru metallic supported on ceria, even though they differ when physical measurements are used to characterize them.
- Cr-doped SiO<sub>2</sub> catalyst showed the highest yield to propylene with the least coking among all other Cr-doped oxides. Other dopants were also tried. We proved that the doped metal oxide catalyst is more active for propane dehydrogenation than the supported chromium oxide catalyst that has been studied extensively in the literature. Cr-doped SiO<sub>2</sub> was also active for oxidative dehydrogenation of propane with CO<sub>2</sub>. The propylene yield increased with increasing CO<sub>2</sub>:C<sub>3</sub>H<sub>8</sub> feed ratio.
- Ru-doped ceria as a methanation catalyst was studied using *in situ* FTIR. Reduction of CO<sub>2</sub> by hydrogen traditionally follows the Fischer-Tropsch mechanism pathway where CO<sub>2</sub> is reduced to CO via formate ion intermediate. CO thus formed is hydrogenated further to eventually give methane. We found that if Ru is doped (and maintained as ionic) in the CeO<sub>2</sub> matrix (rather than dispersed as nano particles) the mechanism is changed significantly. Ru doped CeO<sub>2</sub> follows the mechanism as CO<sub>2</sub> → CO<sub>3</sub><sup>2-</sup> → CH<sub>4</sub>, rather than CO<sub>2</sub> → HCOOH → HCHO → CH<sub>4</sub>. The structure of the carbonate intermediates was found to be dependent on the degree of reduction of the bulk catalyst.
- We continued to develop and refine consistent methods to synthesize and characterize the doped metal oxides to demonstrate that true “doped oxides” are achieved and not mixed phases. Using synchrotron XRD and Raman, we have increased our confidence that doping has been achieved. Novel reactant-pulse techniques to probe the valence of the active state for dry reforming in ruthenium-doped ceria were also utilized.
- We proposed a set of general rules: doping an oxide with a lower-valence dopant lowers substantially the energy of oxygen-vacancy formation, increases the energy of alkane

dissociative adsorption, and lowers the activation energy for breaking the C-H bond and forming a hydroxide and an alkoxide. An oxide doped with a higher-valence dopant adsorbs gas-phase oxygen and activates it so that it adsorbs alkanes dissociatively.

- We proposed and documented that there is a very strong interaction between a Lewis acid and a Lewis base, when they are coadsorbed on an oxide surface. We showed that the behavior of a very large number of different systems can be explained by this rule: the formation of oxygen vacancies, the difference in behavior between reducible and irreducible oxides, the chemistry of doped oxide surfaces, and the structural changes induced by adsorption of a Lewis acid or a Lewis base.
- We published calculations that show that the activity of dopants, whether having lower and higher valence, is long-ranged. The dopant does not have to be in the top surface layer to influence the catalytic properties of an oxide.
- We found that all alkane dissociation on oxide surfaces (doped, undoped, or having steps) follows the same mechanism. A hydrogen atom from the alkane binds to an oxygen atom in the surface and after that the alkyl group travels along the surface to find another surface-oxygen to bind to. We have also shown that the activation energy for the dissociative adsorption of alkanes on irreducible oxides (doped or not) is close to the activation energy for making a hydroxyl and an alkyl in the gas.

#### **Publications Acknowledging this Grant in 2011-2014**

1. Chrétien, S.; Metiu, H. Electronic Structure of the Partially Reduced Rutile TiO<sub>2</sub>(110) Surface: Where Are the Unpaired Electrons Located? *J. Phys. Chem. C* **2011**, *115*, 4696-4705.
2. García-Mota, M.; Vojvodic, A.; Metiu, H.; Man, I. C.; Su, H.-Y.; Rossmeisl, J.; Nørskov, J. K. Tailoring the Activity for Oxygen Evolution Electrocatalysis on Rutile TiO<sub>2</sub>(110) by Transition-Metal Substitution. *ChemCatChem* **2011**, *3*, 1607-1611.
3. Hu, Z.; Li, B.; Sun, X.; Metiu, H. Chemistry of Doped Oxides: The Activation of Surface Oxygen and the Chemical Compensation Effect. *J. Phys. Chem. C* **2011**, *115*, 3065-3074.
4. Hu, Z.; Metiu, H. Effect of Dopants on the Energy of Oxygen-Vacancy Formation at the Surface of Ceria: Local or Global? *J. Phys. Chem. C* **2011**, *155*, 17898-17909.
5. Hu, Z.; Metiu, H. Halogen Adsorption on CeO<sub>2</sub>: The Role of Lewis Acid-Base Pairing. *J. Phys. Chem. C* **2011**, *116*, 6664-6671.
6. Hu, Z.; Metiu, H. Choice of U for DFT+U Calculations for Titanium Oxides. *J. Phys. Chem. C* **2011**, *115*, 5841-5845.
7. Li, B.; Metiu, H. Dissociation of Methane on La<sub>2</sub>O<sub>3</sub> Surfaces Doped with Cu, Mg, or Zn. *J. Phys. Chem. C* **2011**, *115*, 18239-18246.
8. Li, B.; Metiu, H. Does Halogen Adsorption Activate the Oxygen Atom on an Oxide Surface? I. A Study of Br<sub>2</sub> and HBr Adsorption on La<sub>2</sub>O<sub>3</sub> and La<sub>2</sub>O<sub>3</sub> Doped with Mg or Zr. *J. Phys. Chem. C* **2011**, *116*, 4137-4148.
9. Sharma, S.; Hu, Z. P.; Zhang, P.; McFarland, E. W.; Metiu, H. CO<sub>2</sub> Methanation on Ru-Doped Ceria. *J. Catalysis* **2011**, *278*, 297-309.
10. Chrétien, S.; Metiu, H. DFT Study of the Electronic Properties of LaOCl Surfaces. *J. Phys. Chem. C* **2012**, *116*, 681-691.

11. Ding, K. L.; Derk, A. R.; Zhang, A. H.; Hu, Z. P.; Stoimenov, P.; Stucky, G. D.; Metiu, H.; McFarland, E. W. Hydrodebromination and Oligomerization of Dibromomethane. *ACS Catalysis* **2012**, *2*, 479-486.
12. Metiu, H.; Chrétien, S.; Hu, Z.; Li, B.; Sun, X. Chemistry of Lewis Acid-Base Pairs on Oxide Surfaces. *J. Phys. Chem. C* **2012**, *116*, 10439-10450.
13. Misch, L. M.; Kurzman, J. A.; Derk, A. R.; Kim, Y.-I.; Seshadri, R.; Metiu, H.; McFarland, E. W.; Stucky, G. D. C-H Bond Activation by Pd-Substituted CeO<sub>2</sub>: Substituted Ions versus Reduced Species. *Chemistry of Materials* **2012**, *23*, 5432-5439.
14. Derk, A. R.; Li, B.; Sharma, S.; Moore, G. M.; McFarland, E. W.; Metiu, H. Methane Oxidation by Lanthanum Oxide Doped with Cu, Zn, Mg, Fe, Nb, Ti, Zr, or Ta: The Connection between the Activation Energy and the Energy of Oxygen-Vacancy Formation. *Catalysis Letters* **2013**, *143*, 406-410.
15. Ding, K. L.; Metiu, H.; Stucky, G. D. Interplay between Bromine and Iodine in Oxidative Dehydrogenation. *ChemCatChem* **2013**, *5*, 1906-1910.
16. Ding, K. L.; Metiu, H.; Stucky, G. D. The Selective High-Yield Conversion of Methane Using Iodine-Catalyzed Methane Bromination. *ACS Catalysis* **2013**, *3*, 474-477.
17. Ivanovskaya, A.; Singh, N.; Liu, R.-F.; Kreutzer, H.; Baltrusaitis, J.; Nguyen, T. V.; Metiu, H.; McFarland, E. W. Transition Metal Sulfide Hydrogen Evolution Catalysts for Hydrobromic Acid Electrolysis. *Langmuir* **2013**, *29*, 480-492.
18. McFarland, E. W.; Metiu, H. Catalysis by Doped Oxides. *Chemical Reviews* **2013**, *113*, 4391-4427.
19. Singh, N.; Upham, D. C.; Metiu, H.; McFarland, E. W. Gas-Phase Chemistry to Understand Electrochemical Hydrogen Evolution and Oxidation on Doped Transition Metal Sulfides. *J. Electrochemical Society* **2013**, *160*, A1902-A1906.
20. Sun, X.; Li, B.; Metiu, H. Methane Dissociation on Li-, Na-, K-, and Cu-Doped Flat and Stepped CaO(001). *J. Phys. Chem. C* **2013**, *117*, 7114-7122.
21. Yu, J.; Scheffler, M.; Metiu, H. Oxidative Dehydrogenation of Methane by Isolated Vanadium Oxide Clusters Supported on Au (111) and Ag (111) Surfaces. *J. Phys. Chem. C* **2013**, *117*, 18475-18483.
22. Sun, X.; Li, B.; Metiu, H. Ethane Activation by Nb-Doped NiO. *J. Phys. Chem. C* **2013**, *117*, 23597-23608.
23. Derk, A.; Moore, G. M.; Sharma, S.; McFarland, E. W.; Metiu, H. Catalytic Dry Reforming of Methane on Ruthenium-Doped Ceria and Ruthenium Supported on Ceria. *Topics in Catalysis* **2014**, *57*, 118-124.
24. Singh, N.; Upham, D. C.; Liu, R.; Burk, J.; Economou, N.; Buratto, S.; Metiu, H.; McFarland, E. Investigation of the Active Sites of Rhodium Sulfide for Hydrogen Evolution/Oxidation Using Carbon Monoxide as a Probe, *Langmuir*, Accepted and in Press, May 2014

Other publications are submitted or in preparation.

## Synthesis and Exploratory Catalysis of 3d Metals: Group-Transfer, Alkane Activation and Functionalization with Greenhouse Gases

Rick Thompson, Ba L. Tran, Gang Wu, Jurek Krzystek, Andrew Ozarowski, Joshua Telser, Karsten Meyer, Daniel J. Mindiola\*

*Department of Chemistry, University of Pennsylvania, Philadelphia, PA 19104*

Low-coordinate V(+2) complexes having the skeleton (nacnac)V(X) (nacnac<sup>-</sup> = [ArNC(Me)]<sub>2</sub>CH, Ar = 2,6-<sup>i</sup>Pr<sub>2</sub>C<sub>6</sub>H<sub>3</sub>, X<sup>-</sup> = amide, or alkoxide ligand) have been prepared in our group in multi-gram scales. Our goal is to utilize these systems as templates for small molecule activation, and then take advantage of the V(+3) → V(+5) redox couple to promote H–X bond activation (functionalization of the small molecule) and then promote product release. These highly reduced forms of low-coordinate vanadium are the first of their kind, and are thus highly reactive, given rise to dinitrogen complexes [(nacnac)V(X)]<sub>2</sub>(μ<sub>2</sub>;η<sup>1</sup>,η<sup>1</sup>-N<sub>2</sub>) (upon exposure to N<sub>2</sub> at 25 °C and 1 atm), P<sub>4</sub> activation to form (nacnac)V(X)(cyclo-P<sub>3</sub>), terminal vanadium imides (from organic azides), oxides (from N<sub>2</sub>O or other O-sources) and sulfides (from S<sub>8</sub>), and many other vanadium(+4) complexes bearing cumulene groups. We have also developed a convergent synthetic approach to four-coordinate vanadium complexes bearing a terminal nitride ligand, namely species of the type (nacnac)V(N)(X). We also provide compelling evidence for how these terminal nitrides are formed, in part provided by a series of crossover and synthetic experiments. In addition, reactivity studies surrounding the terminal nitride ligand are reported and in progress (B–H bond activation, Si–H activation, carbonylation, reduction, etc), including catalytic S-atom transfer via a reactive thionitrosyl (nacnac)V(NS)(X) using elemental sulfur. Although the nitride motif has nucleophilic character, this one atom ligand serves as a conduit for electron transfer, thus promoting the reduction of the V(5+) metal ion with concurrent oxidation of the incoming substrate. Lastly, we have expanded our nitride work to titanium and constructed the first well-defined titanium parent imides and nitride salts that serve as a source of mononuclear [LTi≡N]<sup>-</sup>. The nitride motif is superbasic and can engage in heterolytic bond splitting reactions.

### DE-FG02-07ER15893: Synthesis and Exploratory Catalysis of 3d Metals: Group-Transfer, Alkane Activation and Functionalization with Greenhouse Gases

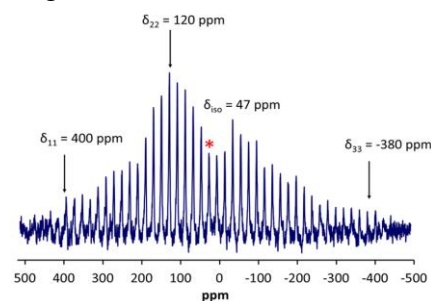
**Postdoc(s):** Marlena Washington, Balazs Pinter, Lindsay Hounjet,

**Student(s):** Rick Thompson, Ba L. Tran, Keith Searles, Debashis Adhikari, Adam J. Nichols (undergrad), and Danielle Henckel (undergrad)

**Affiliation(s):** *Department of Chemistry, Indiana University, Bloomington IN 47405*

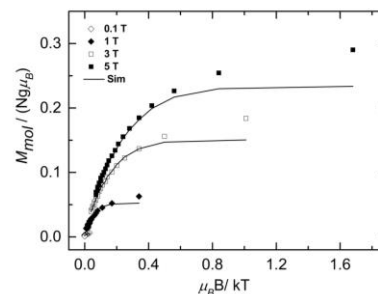
#### RECENT PROGRESS

Redox and Reactivity of Cyclo-P<sub>3</sub> Complexes of Vanadium and the Origin of their P-Chemical Shift. Rick Thompson, Balazs Pinter, Ba L. Tran, Skye Fortier, Gang Wu, Chun-Hsing Chen, Mu-Hyun Baik, and

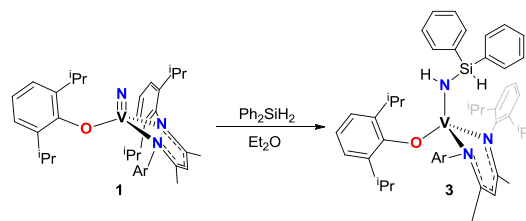


Daniel J. Mindiola, *Manuscript in preparation.*

Reactivity and Electronic Structure of a Mononuclear Ti(II) Complex. Skye Fortier, Timothy A. Jackson, Gayan B. Wijeratne, Chun-Hsing Chen, Patrick J. Carroll, Eva M. Zolnhofer, Karsten Meyer, J. Krzystek, Andrew Ozarowski, Daniel J. Mindiola, and Joshua Telser, *Manuscript in preparation.*



Addition of Si-H and B-H Bonds and Redox Reactivity Involving Low-Coordinate Nitrido Vanadium Complexes. Ba L. Tran, Rick Thompson, Soumya Ghosh, Chung-Hsing Chen, Maren Pink, Xinfeng Gao, Patrick J. Carroll, Mu-Hyun Baik and Daniel J. Mindiola, *Manuscript in preparation.*



### Publications Acknowledging this Grant in 2011-2014

1. Thompson, R.; Wu, G.; Chen, C.-H.; Pink, M.; Mindiola, D. J. A Nitrido Salt Reagent of Titanium. *Manuscript accepted to J. Am. Chem. Soc.*
2. Hounjet, L. J.; Adhikari, D.; Pink, M.; Carroll, P. J.; Mindiola, D. J. Synthesis of an Iron(II) Ethyl Complex Accompanied by Formation of an Unusual Dinitrogen-Ligated Iron(I) Hydride. *Zeitschrift für Anorganische und Allgemeine Chemie (special issue on Reactive Nitrogen-Containing Species: Generation, Characterization and Functionalization)*. *Manuscript accepted for publication.*
3. Franke, S. M.; Tran, B. L.; Heinemann, F. W.; Hieringer, W.; Mindiola, D. J.; Meyer, K. Uranium(III) Complexes with Bulky Aryloxy Ligands Featuring Metal–Arene Interactions and Their Reactivity Towards Nitrous Oxide. *Inorg. Chem.* **2013**, *52*, 10552-10558.
4. Searles, K.; Tran, B. L.; Pink, M.; Chen, C.-H.; Mindiola, D. J. 3d Early Transition Metal Complexes Supported by a New Sterically Demanding Aryloxy Ligand. *Inorg. Chem.* **2013**, *52*, 11126-11135.
5. Tran, B. L.; Krzystek, J.; Ozarowski, A.; Chen, C.-H.; Pink, M.; Karty, J. A.; Telser, J.; Meyer, K.; Mindiola, D. J. Formation and Reactivity of the Terminal Vanadium Nitride Functionality. *Eur. J. Inorg. Chem. (Special issue on small molecule activation)*, **2013**, 3916-3929.
6. Tran, B. L.; Thompson, R.; Ghosh, S.; Gao, X.; Chen, C.-H.; Baik, M.-H.; Mindiola, D. J. A Four-Coordinate Thionitrosyl Complex of Vanadium. *Chem. Commun.* **2013**, *49*, 2768-2770.
7. Searles, K.; Pink, M.; Caulton, K. G.; Mindiola, D. J. An iridium-pyridylpyrrolide complex exhibiting reversible binding of H<sub>2</sub>. *Dalton Trans.* **2012**, *41*, 9619-9622.
8. Telser, J.; Jackson, T.; Wijeratne, G.; Mindiola, D. J.; Wicker, B. F.; Krzystek, J.; Ozarowski, A. Vanadocene de Novo: Spectroscopic and Computational Analysis of Bis(η<sup>5</sup>-cyclopentadienyl)vanadium(II). *Organometallics* **2012**, *31*, 8265–8274.
9. Tran, B. L.; Pinter, B.; Nichols, A. J.; Chen, C.-H.; Krzystek, J.; Ozarowski, A.; Telser, J.; Baik, M.-H.; Meyer, K.; Mindiola, D. J. A Planar Three-Coordinate Vanadium(II) Complex and Terminal

Vanadium Nitrides from N<sub>2</sub>. A Kinetic or Thermodynamic Impediment? *J. Am. Chem. Soc.* **2012**, *134*, 13035-13045.

10. Mossin, S.; Tran, B. L.; Adhikari, D.; Pink, M.; Heinemann, F. W.; Sutter, J.; Szilagy, R. K.; Meyer, K.; Mindiola, D. J. A Mononuclear Fe(III) Single Molecule Magnet with a 3/2 ↔ 5/2 Spin Crossover. *J. Am. Chem. Soc.* **2012**, *134*, 13651-13661.
11. Tran, B. L.; Washington, M.; Henckel, D. A.; Gao, X.; Pink, M.; Mindiola, D. J. A Four Coordinate Parent Imide Via a Titanium Nitridyl. *Chem. Commun.* **2012**, *48*, 1529-1531 (Invited contribution to the "New Talent" special issue).
12. Tran, B. L.; Chen, C.-H.; Mindiola, D. J. Reactivity Studies of a Pseudo Three-Coordinate Vanadium(II) Complex: Synthesis of Terminal Oxo and Sulfido Complexes of Vanadium(IV) and S-S and Se-Se Reductive Bond Cleavage Reactions. *Inorg. Chim. Acta (Special Issue in Honor of Prof. Robert Bergman)*, **2011**, *369*, 215-222.
13. Basuli, F.; Wicker, B.; Huffman, J. C.; Mindiola, D. J. Understanding a Reactive and Easy-to-Prepare Titanium Carboamination Catalyst. *J. Organomet. Chem. Invited Article for the thematic Issue Entitled "Catalytic Addition of E-H Bonds*, **2011**, *696*, 235-243.

# **Tuesday Afternoon**

# **Nanocluster Catalysts**

This page is intentionally blank.

## Nucleation is Bimolecular in Strong Bonding Systems

R. G. Finke and W. W. Laxson  
Colorado State University

### Abstract

Nucleation and growth processes are ubiquitous throughout nature and its phase changes, being central to the formation, size and shape of particles and aggregates such as rain, snow, crystal formation, protein aggregation in all the major neurological diseases, nanoparticle formation, nanoparticle catalyst synthesis, and supported-nanoparticle catalyst formations, to mention just a few among many, many more examples. However, the simplest, most fundamental and therefore most general nucleation, growth and agglomeration mechanism at its (pseudo)elementary step level has proved elusive. Moreover, nucleation rate constants are notoriously hard to measure precisely. The talk will detail our recent DOE-funded work which reveals that nucleation, in the strongly bonded, prototype mechanistic system of Ir(0)<sub>n</sub> nanoparticles stabilized by P<sub>2</sub>W<sub>15</sub>Nb<sub>3</sub>O<sub>62</sub><sup>9-</sup> polyoxoanions, is actually *bimolecular*, not the higher molecularity implied by Classical Nucleation Theory. The significance and anticipated broad application of this fundamental finding to nanoparticle science will be presented and briefly discussed. That discussion will include the 4-step mechanism for supported-nanoparticle catalyst formation and agglomeration in contact with solution discovered through DOE support, also a deliberately minimalistic, Ockham's-razor-obeying, disproof-based and thus expected to be reliable mechanism.

**DE-FG02-03ER15453: Supported-Nanoparticle Catalyst Formation in Contact  
With Solution: Kinetic, Mechanistic and Synthetic Fundamental Studies**

**PI:** Professor Richard G. Finke

**Student:** William W. Laxson

**RECENT PROGRESS**

***Supported-Nanoparticle Catalyst Formation***

Work has continued on the mechanisms of supported-nanoparticle catalyst formation in contact with solution, resulting in four publications [1,3,6,8] including an “editor’s choice” review of surprising poor state of knowledge of the mechanisms of formation of practical, non-UHV supported-nanoparticle heterogeneous catalysts [3]. Importantly, evidence for bimolecular nucleation in the formation of supported-Ir(0)<sub>n</sub> nanoparticles was obtained and published[6]. Related work on the mechanism of Au(0)<sub>m</sub> nanoparticle aggregation was also published via a collaborative effort with Professor W. Buhro and his research group [5]. Some necessary synthetic improvements and characterization work was also published [13], work on the important [(n-C<sub>4</sub>H<sub>9</sub>)<sub>4</sub>N]<sub>9</sub>P<sub>2</sub>W<sub>15</sub>Nb<sub>3</sub>O<sub>62</sub> system and its supported (1,5-COD)Ir(I)<sup>+</sup> organometallic precatalyst, [(n-C<sub>4</sub>H<sub>9</sub>)<sub>4</sub>N]<sub>5</sub>Na<sub>3</sub>[(1,5-COD)Ir•P<sub>2</sub>W<sub>15</sub>Nb<sub>3</sub>O<sub>62</sub>], the precatalyst which underpins the Ir(0)<sub>~300</sub> nanoparticle bimolecular nucleation and growth system and studies.

***The “Who’s The True Catalyst?” and “Is It Homogeneous or Heterogeneous Catalysis?”***

***Problems***

An underlying issue in nearly every catalysis study is the precise nature of the actual, true, catalytically most active site. Identification of the true catalyst, and its distinction from the starting precatalyst, is of enormous significance and general importance to catalysis. This point follows since the rational improvement of any catalyst requires an understanding of the catalyst’s true identity, since all catalytic properties of interest—selectivity, activity, lifetime, poisoning, recovery, regeneration and so on—derive from the catalysts composition, structure and therefore true identity. For this reason, work on the “who’s the true catalyst?” and “is it homogeneous or heterogeneous catalysis?” problems started with prior DOE grants has continued at a lower level,

yet resulted in six publications, including work in the important current area of energy research of water-oxidation catalysis [2,9,10,12]. The first *JACS* communication there has attracted 96 citations already in under 3 years [2]. Fundamental catalyst poisoning studies were also published, catalyst poisoning proving to be one of the most powerful methods of distinguishing homogeneous from nanoparticle heterogeneous catalysts [4]. Catalyst poisoning is also important for counting the number of catalytically active sites [7].

### **Publications Acknowledging this Grant in 2011-2014**

1. Mondloch, J. E.; Finke, R. G. Supported-Nanoparticle Heterogeneous Catalyst Formation in Contact with Solution: Kinetics and Mechanism of the Conversion of Ir(1,5-COD)Cl/ $\gamma$ -Al<sub>2</sub>O<sub>3</sub> to Ir(0)<sub>~900</sub>/ $\gamma$ -Al<sub>2</sub>O<sub>3</sub> *J. Am. Chem. Soc.* **2011**, *133*, 7744-7756.
2. Stracke, J. J.; Finke, R. G. Electrocatalytic water oxidation beginning with the cobalt polyoxometalate [Co<sub>4</sub>(H<sub>2</sub>O)<sub>2</sub>(PW<sub>9</sub>O<sub>34</sub>)<sub>2</sub>]<sup>10-</sup>: Identification of heterogeneous CoO<sub>x</sub> as the dominant catalyst *J. Am. Chem. Soc.* **2011**, *133*, 14872-14875.
3. Mondloch, J. E.; Bayram, E.; Finke, R. G. A Review of the Kinetics and Mechanisms of Formation of Supported-Nanoparticle Heterogeneous Catalysts *J. Mol. Catal. A* **2012**, *355*, 1-38. (“Editor’s Choice” selection).
4. Bayram, E.; Linehan, J. C.; Fulton, J. L.; Roberts, J. A.S.; Szymczak, N. K.; Smurthwaite, T. D.; Özkaz, S.; Balasubramanian, M.; Finke, R. G. Is It Homogeneous or Heterogeneous Catalysis Derived from [RhCp\*Cl<sub>2</sub>]<sub>2</sub>? *In Operando* XAFS, Kinetic and Crucial Kinetic Poisoning Evidence for Subnanometer Rh<sub>4</sub> Cluster-Based Benzene Hydrogenation Catalysis *J. Am. Chem. Soc.* **2011**, *133*, 18889-18902.
5. Shields, S., Buhro, W. E., Finney, E. E.; Finke, R. G. Gold Nanocluster Agglomeration Kinetic Studies: Evidence for Parallel Bimolecular Plus Autocatalytic Agglomeration Pathways as a Mechanistic Alternative to an Avrami-Based Analysis *Chemistry of Materials* **2012**, *24*, 1718-1725.
6. Mondloch, J. E.; Finke, R. G. Kinetic Evidence for Bimolecular Nucleation In Supported-Transition-Metal-Nanoparticle Catalyst Formation In Contact With Solution: The Prototype Ir(1,5-COD)Cl/ $\gamma$ -Al<sub>2</sub>O<sub>3</sub> to Ir(0)<sub>~900</sub>/ $\gamma$ -Al<sub>2</sub>O<sub>3</sub> System *ACS Catalysis* **2012**,

2, 298-305.

7. Bayram, E.; Finke, R. G. Quantitative 1,10-Phenanthroline Catalyst-Poisoning Kinetic Studies of Rh(0)<sub>n</sub> Nanoparticle and Rh<sub>4</sub> Cluster Benzene Hydrogenation Catalysts: Estimates of the Poison  $K_{\text{association}}$  Binding Constants, of the Equivalents of Poison Bound and of the Number of Catalytically Active Sites for Each Catalyst *ACS Catalysis* **2012**, *2*, 1967-1975.

8. Bayram, E.; Lu, J.; Aydin, C.; Uzun, A.; Browning, N. D.; Gates, B. C.; Finke, R. G. Mononuclear Zeolite-Supported Iridium: Kinetic, Spectroscopic, Electron Microscopic, and Size-Selective Poisoning Evidence for an Atomically Dispersed True Catalyst at 22 °C *ACS Catalysis* **2012**, *2*, 1947-1957.

9. Stracke, J. J.; Finke, R. G. Water Oxidation Catalysis Beginning with 2.5 μM [Co<sub>4</sub>(H<sub>2</sub>O)<sub>2</sub>(PW<sub>9</sub>O<sub>34</sub>)<sub>2</sub>]<sup>10-</sup>: Investigation of the True Electrochemically Driven Catalyst at ≥600 mV Overpotential at a Glassy Carbon Electrode *ACS Catalysis* **2013**, *3*, 1209-1219

10. Stracke, J. J.; Finke, R. G. Water Oxidation Catalysis Beginning with Co<sub>4</sub>(H<sub>2</sub>O)<sub>2</sub>(PW<sub>9</sub>O<sub>34</sub>)<sup>10-</sup> when Driven by the Chemical Oxidant Ruthenium(III)tris(2,2'-bipyridine): Stoichiometry, Kinetic, and Mechanistic Studies En Route to Identifying the True Catalyst *ACS Catalysis*, **2014**, *4*, 79-89.

11. Kent, P. D.; Mondloch, J. E.; Finke, R. G. A Four-Step Mechanism for the Formation of Supported-Nanoparticle Heterogeneous Catalysts in Contact with Solution: The Conversion of Ir(1,5-COD)Cl/γ-Al<sub>2</sub>O<sub>3</sub> to Ir(0)<sub>~170</sub>/γ-Al<sub>2</sub>O<sub>3</sub> *J. Am. Chem. Soc.* **2014**, *136*, 1930-1941.

12. Stracke, J. J.; Finke, R. G. Distinguishing Homogeneous from Heterogeneous Water Oxidation Catalysis When Beginning with Polyoxometalates *ACS Catalysis*, **2014**, *4*, 909-933.

13. Laxson, W. W.; Özkar, S.; Finke, R. G. The Tri-Niobium, Wells-Dawson Type Polyoxoanion, [(n-C<sub>4</sub>H<sub>9</sub>)<sub>4</sub>N]<sub>9</sub>P<sub>2</sub>W<sub>15</sub>Nb<sub>3</sub>O<sub>62</sub>: Improvements in the Synthesis, Its Reliability, the Purity of the Product and the Detailed Synthetic Procedure *Inorg. Chem.* **2014**, *53*, 2666-2676.

**Supported Metal Nanoparticles:  
Correlating Structure with Catalytic Function via Metal Atom Energetics**

Charles T. Campbell (PI), Trevor James, Stephanie Hemmingson, James Sharp and Jason Sellers  
University of Washington, Departments of Chemistry and Chemical Engineering

**Presentation Abstract**

Many important catalysts for energy and environmental technologies involve late transition metal nanoparticles dispersed across the surface of some support material. The relationships between the energetic stability of late transition metal particles on oxide supports and their structural, electronic, chemisorption and catalytic properties will be reviewed. Oxide-supported metal catalysts have been studied using well-defined surfaces involving vapor-deposited metals on single-crystal oxide surfaces, where the metal atoms nucleate and grow nanoparticles. The energetic stability of the metal atoms in these nanoparticles has been measured as a detailed function of particle size and support properties using metal atom adsorption calorimetry. The small-molecule chemisorption properties and sintering kinetics of these metal particles have also been measured. Trends in adsorption and metal / oxide adhesion energies will be reviewed. We find correlations amongst the energy of the metal atoms in these nanoparticles (i.e., their chemical potential, which depends on both their particle size and their oxide support) and the strength with which they bond adsorbates, their catalytic kinetics and their sintering rates. This has led to new ideas for sinter-resistant catalysts that were synthesized and proven to sinter more slowly.

Work supported by DOE-OBES under Grant # DE-FG02-96ER14630.

**Grant # DE-FG02-96ER14630: Supported Metal Nanoparticles:  
Correlating Catalytic Kinetics, Energetics and Surface Structure**

**Postdoc:** Yong Yang

**Students:** Trevor James, Stephanie Hemmingson, James Sharp, Jason Sellers, Trent Silbaugh, James Lownsbury

**RECENT PROGRESS**

***Introduction***

This research program combines experiments with theory with the goal of providing the basic understanding needed to develop better catalyst materials for energy and environmental technologies. Our main focus has been on catalysts based on late transition metal nanoparticles anchored to oxide supports. Our results have helped clarify how metal particle size affects catalyst activity and selectivity, and how to maintain catalyst particles at their optimum size for extended periods while running chemical reactions. We have also elucidated several reaction mechanisms. We have done this by studying model catalysts involving well-defined metal nanoparticles on single-crystalline oxide supports, prepared under the clean conditions of ultrahigh vacuum (UHV). The structure of these materials was characterized using a variety of state-of-the-art experimental techniques including surface spectroscopies (XPS, AES, LEIS, TPD) and surface microscopies (STM, AFM). Most importantly, we have used single-crystal adsorption calorimetry (SCAC) to measure the energies of the transition metal atoms in these

catalytic materials and determine how their energy depends upon details of the catalyst structure (particle size and support). We have also measured surface reaction kinetics and catalytic reaction rates, both steady-state and transient (sometimes in UHV and sometimes at higher pressures). We have often interpreted our results using computational results provided by collaborations with theoreticians. Finally, we have also developed some semi-empirical theoretical methods for estimating rate constants in surface reactions.

### ***Metal Adsorption / Adhesion Energies onto Catalyst Supports by Microcalorimetry***

Our metal adsorption calorimetry results are beginning to reveal systematic relationships between the energy of a catalytic surface metal atom and (1) the size of the metal nanoparticle on which it resides, and (2) the support surface to which this metal particle is anchored. We found that the metal atom's energy (or chemical potential) increases strongly with decreasing particle size below ~6 nm but remains nearly constant near the bulk metal value above ~6 nm (see Fig. 1a). For particles below 6 nm, it decreases with increasing metal/support adhesion energy.

**Fig. 1. a.** Calorimetric measurements of the chemical potential of Ag atoms versus particle size on different oxide supports [11]. **b.** Adhesion energies for several metals on clean MgO(100) under UHV [11].

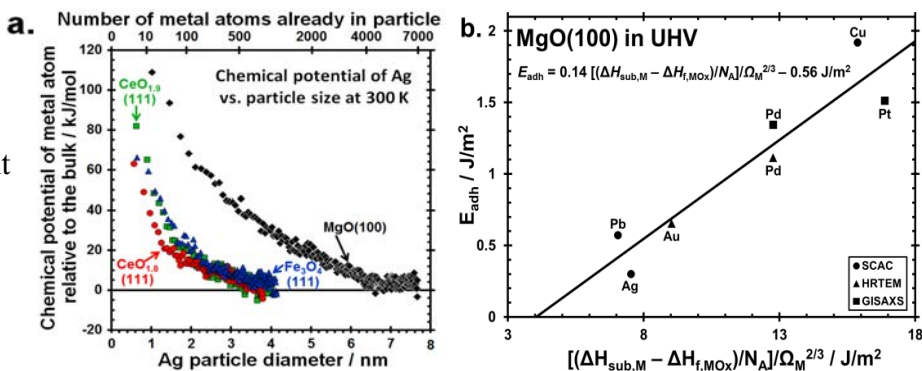


Figure 1b shows that the adhesion energy ( $E_{adh}$ ) of different metals to the same oxide surface grows linearly with the heat of formation of the metal's most stable oxide from metal vapor plus  $O_2(g)$  (i.e.,  $\Delta H_{sub,M} - \Delta H_{f,MOx}$ , where  $\Delta H_{sub,M}$  is the metal's heat of sublimation and  $\Delta H_{f,MOx}$  is the standard heat of formation of the most stable bulk oxide of that metal). This heat reflects the strength of the chemical bonds that metal atom can make to oxygen, consistent with the fact that DFT calculations predict that such metals bind mainly to the oxygen atoms of the oxide's surface. The factor  $N_A \Omega_M^{2/3}$  here converts units from kJ/mol to J/m<sup>2</sup>. Our newest data show that the line for CeO<sub>2</sub>(111) is parallel to this MgO(100) line but lies almost 2 J/m<sup>2</sup> higher.

By going to 100 K, we measured the first heat of adsorption of any late transition metal adsorbed as a monomer on any oxide terrace site: Cu<sub>1</sub> on CeO<sub>2</sub>(111). Such monomer energies have been a long-sought goals, since they are much easier to compare to a DFT calculations than are the energies for metal clusters, and thus serve as key benchmarks for theory. Our newest measurements are of Au adsorption heats, only possible due to calorimeter improvements [17].

Comparing  $E_{adh}$  for the same metals to oxide pairs, we also found the following order of increasing adhesion energy: MgO(100)  $\approx$  TiO<sub>2</sub>(110) <  $\alpha$ -Al<sub>2</sub>O<sub>3</sub>(0001) < CeO<sub>2-x</sub>(111)  $\leq$  Fe<sub>3</sub>O<sub>4</sub>(111) [11]. This is the first reported ranking of clean oxide surfaces with respect their adhesion energies to late transition metals. ( $E_{adh}$  values on clean oxide surface are 2-3 fold larger than old data without verified cleanliness.) We do not yet have a physical explanation for this ranking, but have discussed the factors involved [11]. Qualitatively, it means that metal atoms in the same size nanoparticle on these different supports would have a chemical potential that increases in the opposite order (i.e., with the highest chemical potential when on MgO(100)).

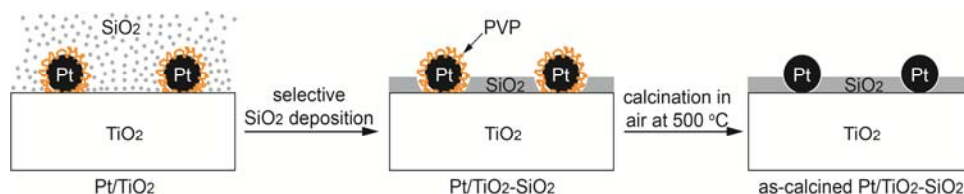
### ***Chemisorption energies of molecules and atoms on well-defined, oxide-supported metal nanoparticles: effects of particle size and support***

We presented a new model for understanding the relationships between metal nanoparticle size and the support material to which it is anchored and the strength with which it chemisorbs small adsorbates, which correlates that strength with the metal's chemical potential [11]. This provides a new way for understanding particle size and support effects in catalysis by transition metals, and even alloy effects. We helped develop a new calorimeter at the Fritz-Haber Institute in Berlin designed for measuring the energies of adsorbed catalytic reaction intermediates as a function of nanoparticle size on clean and well-defined single crystal supports [2], and collaborated in using it to measure how the heat of CO adsorption on size-controlled Pd nanoparticles supported on  $\text{Fe}_3\text{O}_4(111)$  depends on particle size [4].

We also compiled the most comprehensive list of experimental adsorption enthalpies and entropies for atoms and molecular adsorbates on single-crystal oxide surfaces yet reported [12].

We developed a model for sintering kinetics whereby the effects of both particle size and support on sintering rates are calculated based on this same chemical potential of the metal atoms in the nanoparticles that we measure by SCAC [9]. The results led us to a new idea for making more sinter-resistant transition metal catalysts, which we implemented through collaboration with an expert in nanomaterials synthesis, Younan Xia, who developed a wet-chemical method for making this 3-phase material (see Fig. 2) in high-surface-area form [15]. As with the similar structure previously prepared by Atomic Layer Deposition (ALD) by the group at Argonne National Labs (with PC Stair), we found this to sinter much more slowly than Pt on either pure silica or pure titania supports. Our synthesis method would be far easier to implement in making catalysts on an industrial scale than that prior ALD method.

**Fig. 2.** Synthesis of Pt/TiO<sub>2</sub> catalyst where Pt particles are surrounded by a SiO<sub>2</sub> coating [15].



### ***Mechanistic and kinetic studies, education and outreach***

Using sensitive transient kinetics measurements, we elucidated the mechanisms of the methanol synthesis reaction over Cu-based catalysts [8] and the water-gas shift reaction over Pt. Based on a trend in adsorbate entropies we recently discovered, we also developed some new semi-empirical theoretical methods for estimating rate constants in surface reactions [14].

Numerous graduate students, undergraduate students and postdocs have been trained through this highly interdisciplinary research effort. Also, the PI served on numerous national and international advisory boards and review committees, and in major editorial roles.

### **Publications Acknowledging this Grant in 2011-2014**

1. Campbell, C. T.; Sharp, J. C.; Yao, Y. X.; Karp, E. M.; Silbaugh, T. L. Insights into Catalysis by Gold Nanoparticles and their Support Effects through Surface Science Studies of Model Catalysts. *Faraday Discussions* **2011**, 152, 227-239 (invited).
2. Fischer-Wolfarth, J.-H.; Hartmann, J.; Farmer, J. A.; Flores-Camacho, J. M.; Campbell, C. T.; Schauermaier, S.; Freund, H.-J. An improved single-crystal adsorption calorimeter for determining gas adsorption and reaction energies on complex model catalysts, *Review of Scientific Instruments* **2011**, 82, art. No. 024102 (15 pages).

3. Yates, J. T., Jr.; Campbell, C. T. Surface chemistry: Key to control and advance myriad technologies, *Proc. National Academy of Sciences* **2011**, 108, 911-916.
4. Crowe, M. C.; Campbell, C. T. Adsorption Microcalorimetry: Recent Advances in Instrumentation and Application, *Annual Rev. Analytical Chemistry*, **2011**, Vol. 4, 41-58.
5. Flores-Camacho, J. M.; Fischer-Wolfarth, J.-H.; Peter, M.; Campbell, C. T.; Schauermann, S.; Freund, H.-J. Adsorption energetics of CO on supported Pd nanoparticles as a function of particle size by single crystal microcalorimetry, *Phys. Chem. Chem. Phys.* **2011**, 13, 16800–16810.
6. Kong, D.; Wang, G.; Pan, Y.; Hu, S.; Hou, J.; Pan, H.; Campbell, C. T.; Zhu, J. F. Growth, structure and stability of Ag on CeO<sub>2</sub>(111): synchrotron radiation photoemission studies, *J. Physical Chemistry C* **2011**, 115, 6715–6725.
7. Campbell, C. T. Catalyst-Support Interactions: Electronic Perturbations, *Nature Chemistry (News and Views)* **2012**, 4, 597-598.
8. Yang, Y.; Mims, C.A.; Mei, D.H.; Peden, C.H.F.; Campbell, C.T. Mechanistic Studies of Methanol Synthesis over Cu from CO/CO<sub>2</sub>/H<sub>2</sub>/H<sub>2</sub>O Mixtures: the Source of C in Methanol and the Role of Water, *J. Catalysis* **2013**, 298, 10-17.
9. Campbell, C. T. The Energetics of Supported Metal Nanoparticles: Relationships to Sintering Rates and Catalytic Activity, *Accts. Chemical Research* **2013**, 46, 1712-1719.
10. Sharp, J. C.; Yao, Y. X.; Campbell, C. T. Silver Nanoparticles on Fe<sub>3</sub>O<sub>4</sub>(111): Energetics by Ag Adsorption Calorimetry and Structure by Surface Spectroscopies, *J. Phys. Chem. C* **2013**, 117, 24932–24936.
11. Campbell, C. T.; Sellers, J. R. V. Introductory Lecture: Anchored Metal Nanoparticles: Effects of Support and Size on Their Energy, Sintering Resistance and Reactivity, *Faraday Discussion* **2013**, 162, 9–30.
12. Campbell, C. T.; Sellers, J. R. V. Enthalpies and Entropies of Adsorption on Well-Defined Oxide Surfaces: Experimental Measurements, *Chem. Revs.* **2013**, 113, 4106–4135.
13. Campbell, C. T.; Sauer, J. Introduction: Surface Chemistry of Oxides, *Chemical Reviews* (special issue on Surface Chemistry of Oxides) 113, 3859–3862 (2013).
14. Campbell, C. T.; Árnadóttir, L.; Sellers, J. R. V. Kinetic Prefactors of Reactions on Solid Surfaces, *Z. Physikalische Chemie* (invited, for special issue celebrating famous Eyring / Polanyi paper introducing transition states) 227, 1–20, (2013).
15. Lu, P.; Campbell, C.T.; Xia, Y. A Sinter-resistant Catalytic System Fabricated by Maneuvering the Selectivity of SiO<sub>2</sub> Deposition onto TiO<sub>2</sub> Surface versus Pt Nanoparticle Surface, *Nano Letts* **2013**, 13, 4957-4962 (highlighted: IOP's *NanotechWeb.org* website).
16. Farmer, J. A.; Baricuatro, J. H.; Campbell, C. T. Correction to: Ag Adsorption on Reduced CeO<sub>2</sub>(111) Thin Films, *J. Physical Chemistry C* 117, 27167–27167 (2013).
17. Sellers, J. R.V.; James, T. E.; Farmer, J. A.; Hemmingson, S. L.; Campbell, C. T. Adsorption Calorimetry during Metal Vapor Deposition on Single Crystal Surfaces: Increased Flux, Reduced Optical Radiation, and Real-Time Flux and Reflectivity Measurements, *Review of Scientific Instruments* 84, art. 123901 (9 pages) (2013).
18. James, T. E.; Hemmingson, S. L.; Campbell, C. T. Adsorption Energetics of Cu Monomers on CeO<sub>2</sub>(111) Terrace Sites by Calorimetry, (in preparation).
19. James, T. E.; Hemmingson, S. L.; Campbell, C. T. Cu Nanoparticles CeO<sub>2</sub>(111) Steps and Terraces: Energetics and Electronic Structure (in preparation).

**Single-Molecule Nanocatalysis: from Intraparticle Catalytic Communication to Reactivity-Guided Engineering of Single-Particle Photoelectrocatalysts**

Peng Chen

Department of Chemistry and Chemical Biology, Cornell University, Ithaca, NY 14853

**Presentation Abstract**

This oral presentation will cover two topics: (1) The discovery and the mechanistic investigation of intraparticle catalytic communication among different reactive sites on the surface of a single nanocatalyst, phenomenologically in analogy to allosteric effects and cooperativity in enzymes. (2) Using single-molecule super-resolution imaging to map reactive sites for photoelectrocatalytic oxidation of water on semiconductor nanocrystals so as to guide the engineering and optimization of these nanocrystals by cocatalysts.

**DE-FG02-10ER16199: Chemical Imaging of Single-Particle Photo(electro)catalysis**

**Postdoc(s):** Justin Sambur (5%)

**Student(s):** Kaori Kubo (21%), Ace Santiago (21%), Eric Choudhary (48%), Guanqun Chen (21%), Ningmu Zou (35%), Danya Smart (18%)

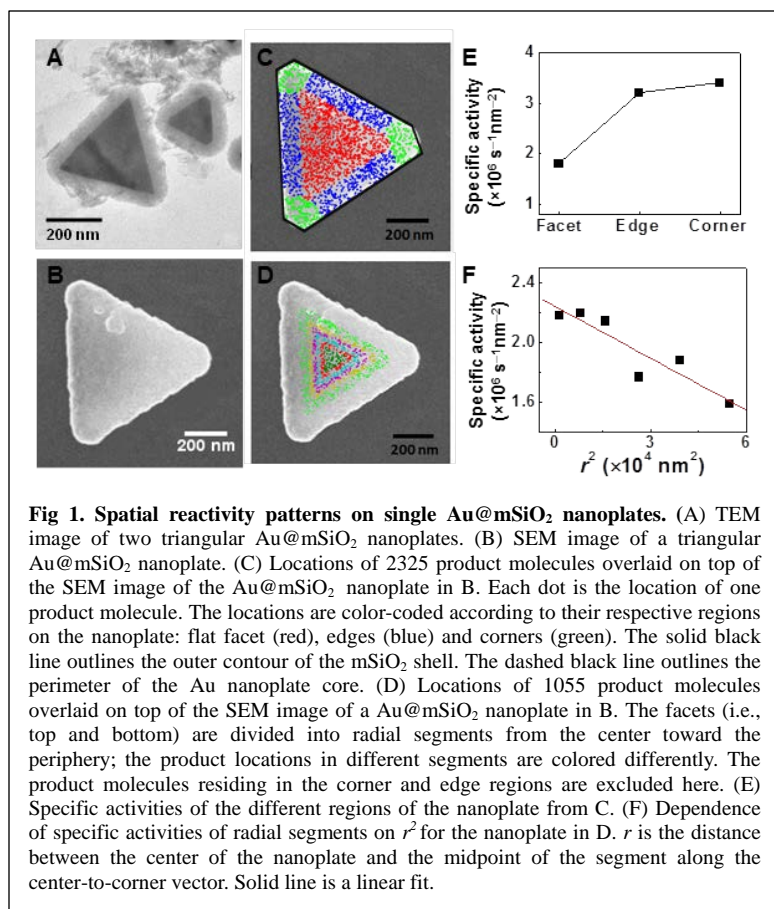
**RECENT PROGRESS**

***1. Site-specific activity mapping and discovery of radial activity gradients on single 2D nanocrystal catalysts***

We have used single-molecule super-resolution imaging to map catalytic N-deoxygenation reactions on single pseudo-2D nanocrystal catalysts, triangular and hexagonal Au@mSiO<sub>2</sub> nanoplates (**Fig 1A**). We localized the positions of individual catalytic products on single Au@mSiO<sub>2</sub> nanoplates, and mapped them onto their SEM images (**Fig 1B and C**). This mapping immediately allowed us to dissect individual Au@mSiO<sub>2</sub> nanoplates and the associated product locations into three types of regions: corners, edges, and flat top facets (**Fig 1C**), and within the top facets, further into different radial segments (**Fig 1D**). We found:

1) Within any single nanoplate, the specific activity follows the trend of corners > edges > flat facets (**Fig 1E**). This trend could be rationalized by the percentage of available low-coordination surface sites that decreases from corners to edges to facets.

2) The nanoplates, either each analyzed as a whole unit or each spatially dissected into different regions, show strong size-dependent specific catalytic activity, with larger ones having lower specific activity. This size dependence can be accounted for by their size-dependent chemical



potentials, similar to the size-dependent activity of pseudo-spherical Au nanoparticles we studied previously.

3) Surprisingly, but consistent with our findings on Au nanorods, the specific activities among the radial segments within the same flat facet of a single nanoplate are *not* uniform, and instead show a clear radial gradient, highest at the center of the facet and decays approximately linearly toward the periphery (**Fig 1D, F**). We attributed this radial activity gradient of Au nanoplates to an underlying radial gradient of surface defect density that came from the decaying growth rate when the nanoplate grew in 2D from a seed during their synthesis.

## 2. Development of a massively scalable, parallel method for screening catalyst activity at the single-particle level and sub-diffraction spatial resolution

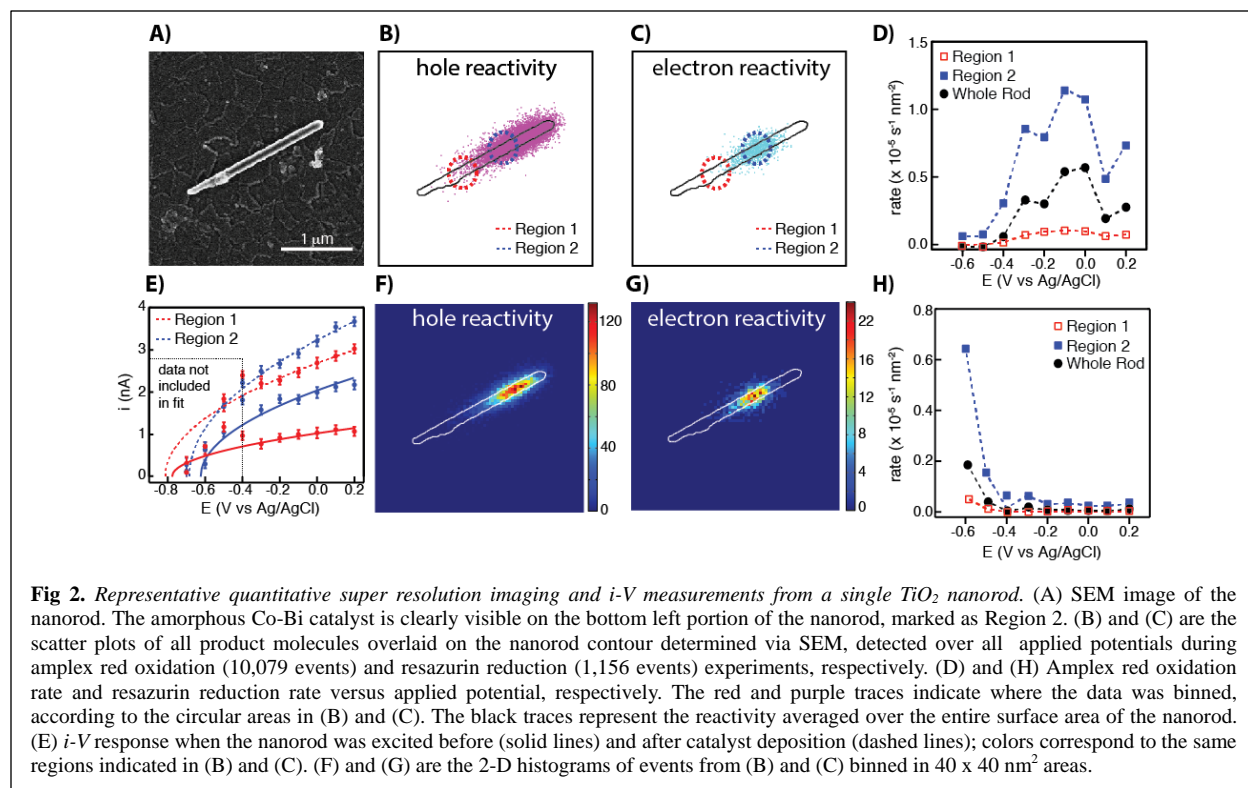
For catalyst discovery and optimization, once the catalysts are made or modified, one always needs to screen their activity, where high data throughput and quantitative activity information are desired. Along this line, we have further developed our single-molecule

fluorescence microscopy approach into a massively scalable, parallel method for screening catalyst activity, using two fluorogenic probe reactions: one oxidative deacetylation reaction and the other a reductive deoxygenation reaction. This method offers the following capabilities: 1) Its wide field imaging format allows imaging the catalysis on a large number of catalyst particles in parallel, giving high data throughput. 2) It offers sub-diffraction spatial resolution, i.e., super optical resolution, where individual particles can be resolved. 3) It offers quantitative activity information of every catalyst particle, which can be directly correlated to its structural properties, such as its size from SEM. 4) It can resolve subpopulations readily, such as in a binary mixture of catalyst particles. 5) Although it is based on fluorogenic probe reactions, we have shown that the activities of catalyst particles in the two fluorogenic catalytic reactions are directly correlated with standard model catalytic reactions such as 4-nitrophenol reduction and hydroquinone oxidation, so their activities in the fluorogenic probe reactions can be extrapolated and generalized to other non-fluorogenic reactions.

### ***3. Single-molecule super-resolution imaging of photoelectrocatalysis in correlation with single-particle current-voltage responses in photoelectrocatalytic oxidation of water by TiO<sub>2</sub> nanorods***

Here we have: (1) Applied the super-resolution imaging method to spatially resolve the *photoelectrocatalytic* reactivity of electrons and holes on TiO<sub>2</sub> nanorod surfaces. (2) Correlated the surface reactivity with current-voltage (*i-V*) behavior with sub-nanorod resolution. (3) Used photoelectrochemical deposition to deposit an oxygen evolution catalyst in a spatio-selectively and correlate the *i-V* response of the catalyst-modified nanorod with the intrinsic reactivity properties. (4) Used SEM to correlate nanorod surface structure with catalytic reactivity and *i-V* behavior.

**Fig 2** shows single-molecule imaging and *i-V* data from a single TiO<sub>2</sub> nanorod. A scatter plot of the localizations of every product molecule detected over all applied potentials is shown in **Fig 2B,C** for amplex red oxidation and resazurin reduction, respectively, where the locations of the reactions also represent the location of photo-excited minority (holes) and majority (electrons) carriers that react with either AR or S at the interface. The density of events on the nanorod surface are shown in the 2-D histograms in **Fig 2F,G**. **Fig 2D,H** shows the AR oxidation rate and S reduction rate ( $\text{s}^{-1} \text{nm}^{-2}$ ) versus applied potential for two regions of the



nanorod, as well as the whole rod averaged reactivity (black trace). These circular regions also represent the laser spot size relative to the rod contour determined by SEM imaging and correspond to the location used for sub-nanorod *i-V* measurements. **Fig 2D** shows that the AR oxidation rate increases with positive applied potentials, whereas the resazurin reduction rate increases sharply at negative potentials (**Fig 2G**). In addition, the region that exhibited higher AR oxidation rates over all potentials also exhibited higher resazurin reduction rates at negative potentials. The *i-V* behavior of the same two regions of the bare nanorod is shown in **Fig 2E**. The bare nanorod region with lower surface electron and hole reactivity exhibited lower photocurrent than the high activity region. The dotted lines in **Fig 2E** represent the *i-V* behavior from the same regions after modification with the Co-Bi oxygen evolution catalyst. The photocurrent increased for both nanorod regions; the *relative* increase in photocurrent was larger for the region with initially lower photocurrent, however.

### Publications Acknowledging this Grant in 2011-2014

1. Ochoa-Daza, M. A.; Zhou, X.; Chen, P.; Loring, R. F., Interpreting single turnover catalysis measurements with constrained mean dwell times. *J. Chem. Phys.* **2011**, *135*, 174509.

2. Zhou, X.; Andoy, N. M.; Liu, G.; Choudhary, E.; Han, K.-S.; Shen, H.; Chen, P., Quantitative Super-resolution Imaging Uncovers Reactivity Patterns on Single Nanocatalysts. *Nature Nanotech.* **2012**, *7*, 237–241.
3. Han, K. S.; Liu, G.; Zhou, X.; Medina, R. E.; Chen, P., How does a single Pt nanocatalyst behave in two different reactions? A single-molecule study. *Nano Lett.* **2012**, *12*, 1253-1259.
4. Andoy, N. M.; Zhou, X.; Choudhary, E.; Shen, H.; Liu, G.; Chen, P., Single-molecule catalysis mapping quantifies site-specific activity and uncovers radial activity gradient on single 2D nanocrystals. *J. Am. Chem. Soc.* **2013**, *135*, 1845–1852.
5. Zhou, X.; Choudhary, E.; Andoy, N. M.; Zou, N.; Chen, P., Scalable Parallel Screening of Catalyst Activity at the Single-Particle Level and Sub-diffraction Resolution. *ACS Catal.* **2013**, *3*, 1448-1453.
6. Ochoa, M. A.; Chen, P.; Loring, R. F., Single Turnover Measurements of Nanoparticle Catalysis Analyzed with Dwell Time Correlation Functions and Constrained Mean Dwell Times. *J. Phys. Chem. C* **2013**, *117*, 19074-19081.
7. Chen, P.; Zhou, X.; Andoy, N. M.; Han, K.-S.; Choudhary, E.; Zou, N.; Chen, G.; Shen, H., Spatiotemporal Catalytic Dynamics within Single Nanocatalysts Revealed by Single-Molecule Microscopy. *Chem. Soc. Rev.* **2014**, *43*, 1107-1117.
8. Sambur, J. B.; Chen, P., Approaches to Single Nanoparticle Catalysis. *Annu. Rev. Phys. Chem.* **2014**, *65*, 395-422.

This page is intentionally blank.

**Wednesday Morning**

**Oxidation Catalysis**

This page is intentionally blank.

David A. Dixon

## Catalytic Reactions of Alcohols on Transition Metal Oxide NanoClusters

David A. Dixon,<sup>1</sup> Zdenek Dohnálek,<sup>2</sup> Roger Rousseau,<sup>2</sup> Bruce D. Kay<sup>2</sup>

<sup>1</sup> Department of Chemistry, The University of Alabama

<sup>2</sup>Fundamental and Computational Sciences Directorate and Institute for Integrated Catalysis,  
Pacific Northwest National Laboratory

### Presentation Abstract

The reactions of alcohols (ROD, R = CH<sub>3</sub>, C<sub>2</sub>H<sub>5</sub>, n-C<sub>3</sub>H<sub>7</sub>, i-C<sub>3</sub>H<sub>7</sub>, n-C<sub>4</sub>H<sub>9</sub>, sec-C<sub>4</sub>H<sub>9</sub> and t-C<sub>4</sub>H<sub>9</sub>) over cyclic (MO<sub>3</sub>)<sub>3</sub> (M = Mo, W) clusters were studied experimentally and computationally. The cyclic clusters were prepared by sublimation of MoO<sub>3</sub> and WO<sub>3</sub> powders in vacuum. To evaluate the cluster activity in dehydration, dehydrogenation, and condensation reactions, they were suspended in an ethanol matrix on an inert substrate, graphene monolayer on Pt(111). The reaction products formed upon heating were followed and quantified using temperature programmed desorption. The experimental results were corroborated using coupled cluster CCSD(T) calculations at DFT optimized geometries that provide quantitative molecular-scale information of the reaction mechanisms. The dehydration and dehydrogenation of ethanol probe both the Lewis/Brønsted acid/base and redox properties of the metal centers. Reactions with one, two, and three alcohols per M<sub>3</sub>O<sub>9</sub> cluster have been studied computationally. Two alcohols are required to provide agreement with experiment for dehydration and dehydrogenation. The initial reaction step is a Lewis acid/base addition to the metal followed by the elimination of water via proton transfers to form a dialkoxy species which serves as the active intermediate. Dehydration is through a β hydrogen transfer to a terminal M=O. Dehydrogenation takes place via an α hydrogen transfer to an adjacent M<sup>VI</sup>=O atom or a W<sup>VI</sup> metal center with redox at the metal for M = Mo and no redox for M = W. Condensation requires the presence of 3 alcohol molecules with one alcohol sacrificed to form a metal hydroalkoxide, which is a strong gas phase Brønsted acid. The overall conversion of the alcohol (W > Mo) is governed by the Lewis acidity of the metal center and product selectivities, as determined by the relative weights of dehydrogenation and dehydration, are governed by the reducibility of the metal center (Mo > W). The results show that CCSD(T) is needed for agreement with experiment.

This work is part of the PNNL FWP 47319, “Multifunctional Catalysis to Synthesize and Utilize Energy Carriers”.

**Postdocs:** Monica Vasiliu (UA), Zhenjun Li (PNNL)

**Graduate Student:** Zongtang Fang (UA)

**Undergraduate Students:** Matthew S. Kelley (UA), Jamie, M. Hennigan (UA)

Closing the Materials and Pressure Gap: Selective Oxidation Catalysis using Gold

Cynthia M. Friend

Harvard University, Department of Chemistry and Chemical Biology/School of Engineering and Applied Sciences

Presentation Abstract

The overall goal of this project is to develop a molecular-scale mechanistic understanding for complex selective oxidation of alcohols on O-covered Au and Ag-Au alloys that guides the design of selective and energy efficient processes. On the basis of fundamental studies on single crystals, new classes of reactions have been discovered. The mechanisms derived from these fundamental studies have also been successfully applied over a wide range of pressures and materials complexity by demonstrating catalytic activity using nanoporous Au. We are focusing on selective oxidation of alcohols because it is a key technology for large-scale chemical synthesis and for biomass conversion.

Theory and experiment have been combined to establish a predictive framework for selective oxidation reactions on O-covered Au(111). Our recent significant accomplishments are: (i) development of molecular-scale mechanisms for selective alcohol oxidation over Au surfaces; (ii) discovery of two new classes of reactions on O/Au—amide synthesis from amines and aldehydes and carbonylation of alcohols; and, (iii) demonstration that the mechanisms derived from our fundamental work predict the conditions for efficient catalysis using nanoporous Au catalysts under flow conditions at atmospheric pressure. Our recent work has made an unprecedented connection between our fundamental studies and their implementation under catalytic conditions.

Grant Number: DE-FG02-84-ER13289

Grant Title: Molecular-scale Understanding of Selective Oxidative Transformations of Alcohols Promoted by Au and Au-based Alloys

Postdoc(s): Drs. Martin Schmid, Kara Stowers, Branko Zucic

Student(s): Cassandra Freyschlag Siler, Joshua E. Klobas

RECENT PROGRESS

Our DOE-sponsored work during the past three years has focused on oxidative transformations of alcohols induced by metallic Au surfaces, including

(A) Fundamental studies of selective reactions of alcohols on model gold surfaces:1

(i) development of a mechanistic framework for selective oxidation of alcohols by oxygen adsorbed on metallic Au allowing prediction analogous catalytic reactions; and,

(ii) discovery of two new classes of reactions—carbonylation and dimethylamide synthesis.

(B) Catalytic studies of alcohol oxidation using nanoporous Au catalysts and O<sub>2</sub> as an oxidant at atmospheric pressure that bridge the “pressure gap” by extension of the reaction principles derived from our fundamental studies to catalytic conditions.

These studies provide a foundation for understanding complex catalytic processes that are important for transformations of oxygenates into key chemicals and a means of predicting and developing new paradigms. We plan to build on this foundation in our future work in which Au-based alloys will be investigated for selective functionalization of alcohols and polyols in order to improve the catalytic performance relative to pure gold.

### Fundamental studies of selective oxidative processes on model gold surfaces

We have combined theory and experiment to understand selective oxidation reactions on Au because of the intense interest in using gold to promote reactions with high selectivity at low temperature. Our recent accomplishments have been to: (a) establish principles for oxidative reactions of key organic reagents; and, to use density functional theory (DFT) calculations to establish key aspects of bonding and reactivity for oxidative transformations on Au. Our work has demonstrated the high activity of oxygen on Au for oxidation of CO,<sup>2</sup> and alcohols.<sup>3-5</sup> We also showed that the local bonding of O and the presence of defects affect reactivity and selectivity.<sup>2,6-13</sup>

□

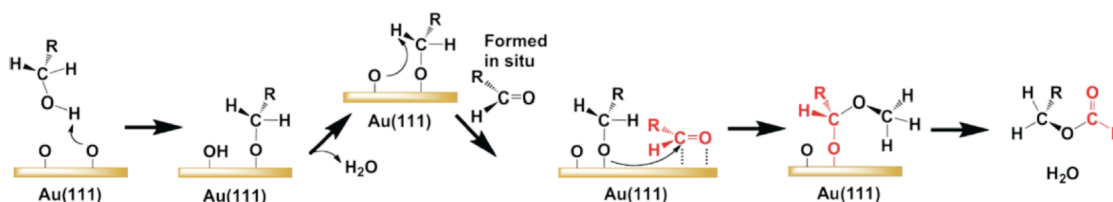


**Figure 1:** Schematic of the coupling of primary alcohols with methoxy formed from methanol on O-activated Au. The rate of C-H dissociation to form the aldehyde is a major factor in determining selectivity.

### Mechanistic principles for oxidation of alcohols on Au activated by atomic oxygen.

We have established *generalizable* principles of surface reactivity that predict oxygen-assisted processes on metallic gold. The key conclusions of our work are that (a) adsorbed O is required for bond activation on Au, leading to highly selective formation of key intermediates; and (b) coupling reactions that occur on Au are governed by the principle that electron rich centers attack electron-deficient carbon to form new bonds. Gold is particularly effective for coupling because surface intermediates are generally weakly bound and, therefore, readily diffuse and rearrange on the surface to assume the geometry necessary for coupling.<sup>3</sup> This paradigm, built on our investigations of a wide range of molecules, provides the basis for understanding known catalytic reactions, e.g. ester synthesis from alcohols, and for predicting entirely new classes of reactions, such as alcohol carbonylation.<sup>14</sup>

These principles are illustrated here by the oxidative coupling of methanol on gold to yield the ester, methyl formate. Ester synthesis from alcohols is an important class of reactions because of the widespread use of esters in many products, including in insulation, synthetic polymers, fragrances and flavorings. Our mechanistic understanding of ester production on Au activated by oxygen affords control of the selectivity for ester production from alcohols even for complex processes (Figure 1).<sup>4,5,15</sup> Oxygen adsorbed on Au (created either by O<sub>3</sub> in UHV or by O<sub>2</sub> at atmospheric pressure using nanoporous materials), activates the O-H bond in methanol (and higher alcohols) to produce methoxy (alkoxy) and OH. In vapor phase processes, two adsorbed OH species rapidly disproportionate to form water and adsorbed O. (In solution, adsorbed OH can be stabilized at high pH<sup>16</sup>.) A fraction of the methoxy, for example, further reacts to form formaldehyde, allowing its electron-deficient carbon to be attacked by another methoxy. The resultant hemiacetal intermediate subsequently yields methyl formate. Theoretical studies in our group show that formation of formaldehyde can be facilitated by

adsorbed O and also by other methoxy intermediates.<sup>3</sup> This mechanism predicts the catalytic behavior of nanoporous Au catalysts at atmospheric pressure (Section II.B).

We have also generalized the case of methanol oxidative coupling to a series of more complex reactions, including the coupling of dissimilar alcohols<sup>2,15,17</sup> and the coupling of methanol with other aldehydes.<sup>6,7,9,11,18</sup> We have further used our paradigmatic understanding of reactivity to *predict new catalytic reactions*. One such reaction is the carbonylation of methanol to produce *dimethyl carbonate* and other derivatives.

### **Development of new reactions derived from mechanistic principles.**

Dimethyl carbonate is an essential commodity chemical used in biofuel production and methylation processes. It is currently produced commercially in a catalytic process that yields HCl as a byproduct. A potential alternative pathway for dimethyl carbonate production was discovered in our group through our fundamental studies (Figure 2).<sup>4,5,14</sup> On Au this reaction is governed by the paradigm of reactivity in which the electron deficient C in CO is attacked by adsorbed methoxy. The only co-product of this process is water. Other competing processes yield CO<sub>2</sub> and methyl formate. This process occurs at moderate temperatures—just above room temperature—suggesting that low temperature carbonylation promoted by Au is feasible.

Our understanding of the mechanism for the carbonylation of methanol is based on fundamental studies that combine X-ray photoelectron and vibrational spectroscopies with reactivity studies. These spectroscopic studies identified the methoxy carbonyl intermediate on the surface that is formed from attack of CO by methoxy.<sup>2,8,10,12-14</sup> We used isotopic labeling and modeling of the vibrational modes based on DFT studies to make assignments and to definitively identify the intermediates depicted. This intermediate is a versatile synthetic reagent that allows for synthesis of other molecules that can serve as nucleophiles. Thus far, we demonstrated the synthesis of (CH<sub>3</sub>O)<sub>2</sub>C=O (dimethyl carbonate), (CH<sub>3</sub>O)(C<sub>2</sub>H<sub>5</sub>)O=C=O, (CH<sub>3</sub>O)(C<sub>6</sub>H<sub>5</sub>)O=C=O, and (CH<sub>3</sub>O)((CH<sub>3</sub>)<sub>2</sub>N)C=O.<sup>3,14</sup>

This example demonstrates **the value of a fundamental understanding** of surface reactions relevant to catalytic processes **for discovery of entirely new classes of reactions** on Au not previously reported. We plan to investigate this class of reactions on under catalytic conditions to determine if there is potential for a viable catalytic process.

### **Bridging the Pressure Gap: Implementation of Nanoporous Au catalysts based on mechanistic principles**

Nanoporous Au (NP Au) is a fascinating material that has efficacy for selective oxidative transformations at relatively low temperature.<sup>14,19-21</sup> NP Au is an unsupported, porous catalyst comprised primarily of metallic gold with a small amount of Ag (Figure 3). The Ag is present because the NP Au is synthesized by chemically dealloying a Au-Ag alloy.<sup>4,5,15,22</sup>

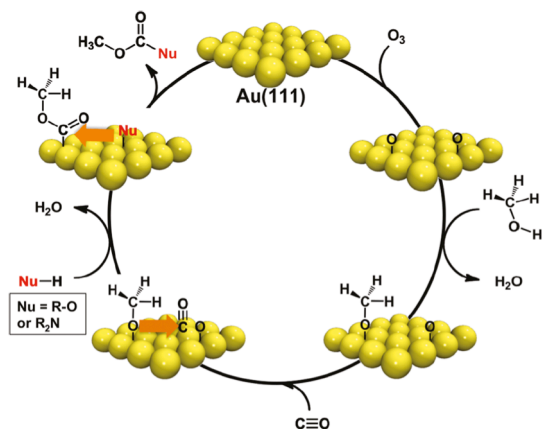


**Figure 2:** Schematic of the mechanism for methylcarbonate formation from carbonylation of methoxy on Au(111) and the ensuing reaction with a nucleophile (Nu). When Nu is CH<sub>3</sub>O<sub>ads</sub>, derived from methanol, dimethyl carbonate ((CH<sub>3</sub>O)<sub>2</sub>C=O) is produced.

We have already used NP Au as a catalyst for atmospheric pressure oxidation of methanol to methyl formate with essentially 100% selectivity at moderate temperatures (~60–80 °C) (Fig. 3). These studies establish that the principles derived from our fundamental studies of gold provide direct guidance to the catalytic process. Gold is an ideal material for this connection because the low intrinsic reactivity of Au itself results in low steady-state concentrations of reactants even at atmospheric pressure.

Recently, we have extended these investigations to higher alcohols.<sup>16,19</sup> As determined in our model studies, we found that the rate of C-H breaking in the alkoxides of higher alcohols occurs more rapidly than for methoxy. As a result, there is a propensity to form the corresponding aldehydes from selective oxidation of higher alcohols, whereas no formaldehyde is detected from methanol oxidation under the same conditions. There is also coupling of ethanol to form ethyl acetate via a mechanism analogous to that determined for methanol (Figure 1).

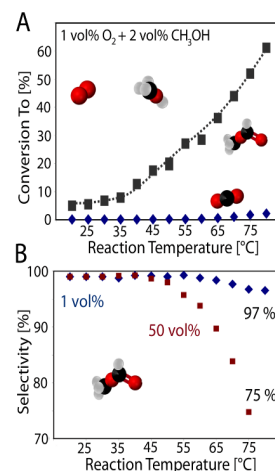
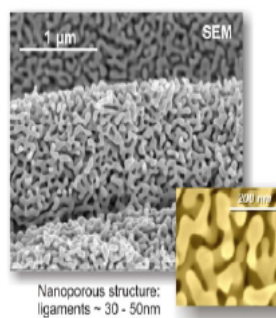


**Figure 3:** SEM image of nanoporous Au (left). Conversion and selectivity data as a function of temperature are shown for selective oxidative coupling of methanol over nanoporous Au using O<sub>2</sub> as an oxidant at atmospheric pressure on the right.

### Selective oxidation of methanol on Au-Ag alloys as a model for catalyst.

Nanoporous gold, a dilute alloy of Ag in Au activates molecular oxygen and promotes the oxygen-assisted catalytic coupling of methanol. Since this trace amount of Ag inherent to nanoporous gold has been proposed as the source of oxygen activation, a thin film Ag/Au alloy surface was studied as a model system for probing the origin of this reactivity.<sup>23</sup> Thin alloy layers of Ag<sub>x</sub>Au<sub>1-x</sub>, with 0.15 ≤ x ≤ 0.40, were examined for dioxygen activation and methanol self-coupling. These alloy surfaces recombine atomic oxygen at different temperatures depending on the alloy composition. Total conversion of methanol to selective oxidation products, i.e. formaldehyde and methyl formate, is achieved at low initial oxygen coverage and at low temperature. Reaction channels for methyl formate formation occur on both Au and Au/Ag mixed sites with a ratio as predicted from the local 2-dimensional composition.

### References

- (1) Xu, B.; Madix, R. J.; Friend, C. M. *Acc. Chem. Res.* **2014**.
- (2) Min, B. K.; Alemozafar, A. R.; Pinnaduwege, D.; Deng, X.; Friend, C. M. *J Phys Chem B* **2006**, *110*, 19833–19838.
- (3) Xu, B.; Baker, T. A.; Kaxiras, E.; Friend, C. M. *J. Phys. Chem. C* **2011**, *115*, 3703–3708.
- (4) Xu, B.; Liu, X.; Haubrich, J.; Madix, R. J.; Friend, C. M. *Angew. Chem. Int. Ed. Engl.* **2009**, *48*, 4206–4209.
- (5) Liu, X.; Xu, B.; Haubrich, J.; Madix, R. J.; Friend, C. M. *J. Am. Chem. Soc.* **2009**, *131*, 5757–5759.
- (6) Deng, X. Y.; Min, B. K.; Liu, X. Y.; Friend, C. M. *Journal of Physical Chemistry B* **2006**, *110*, 15982–15987.
- (7) Deng, X.; Friend, C. M. *J. Am. Chem. Soc.* **2005**, *127*, 17178–17179.
- (8) Baker, T. A.; Friend, C. M.; Kaxiras, E. *J Chem Theory Comp* **2009**, *6*, 279–287.
- (9) Liu, X.; Friend, C. M. *J. Phys. Chem. C* **2010**, *114*, 5141–5147.

- (10) Min, B. K.; Deng, X.; Liu, X.; Friend, C. M.; Alemozafar, A. R. *ChemCatChem* **2009**, *1*, 116–121.
- (11) Liu, X.; Baker, T. A.; Friend, C. M. *Dalton Transactions* **2010**, 39, 8521–8526.
- (12) Baker, T. A.; Xu, B.; Jensen, S. C.; Friend, C. M.; Kaxiras, E. *Cat. Sci. Tech.* **2011**, *1*, 1166–1174.
- (13) Baker, T. A.; Liu, X.; Friend, C. M. *Phys Chem Chem Phys* **2011**, *13*, 34–46.
- (14) Xu, B.; Madix, R. J.; Friend, C. M. *J. Am. Chem. Soc.* **2011**, *133*, 20378–20383.
- (15) Xu, B.; Haubrich, J.; Freyschlag, C. G.; Madix, R. J.; Friend, C. M. *Chemical Science* **2010**, *1*, 310–314.
- (16) Zope, B. N.; Hibbitts, D. D.; Neurock, M.; Davis, R. J. *Science* **2010**, *330*, 74–78.
- (17) Xu, B.; Madix, R. J.; Friend, C. M. *J. Am. Chem. Soc.* **2010**, *132*, 16571–16580.
- (18) Xu, B.; Liu, X.; Haubrich, J.; Friend, C. M. *Nat Chem* **2009**, *2*, 61–65.
- (19) Kosuda, K. M.; Wittstock, A.; Friend, C. M.; Bäumer, M. *Angew. Chem. Int. Ed. Engl.* **2012**, *51*, 1698–1701.
- (20) Wittstock, A.; Zielasek, V.; Biener, J.; Friend, C. M.; Baumer, M. *Science* **2010**, *327*, 319–322.
- (21) Zielasek, V.; Jürgens, B.; Schulz, C.; Biener, J.; Biener, M. M.; Hamza, A. V.; Bäumer, M. *Angew. Chem. Int. Ed.* **2006**, *45*, 8241–8244.
- (22) Ding, Y.; Kim, Y. J.; Erlebacher, J. *Adv. Mater.* **2004**, *16*, 1897–1900.
- (23) Xu, B.; Siler, C. G. F.; Madix, R. J.; Friend, C. M. *Chemistry-A European Journal* **2014**.

## 2.b. Future Objectives:

The next phase of our research is to investigate dilute Ag-Au alloys on the Au(110) surface in order to more closely mimic the nanoporous gold. The Ag(110) surface is known to dissociate O<sub>2</sub>; this, we selected the (110) orientation for these studies. Our plan is to use a combination of reactive measurements, spectroscopy (X-ray and vibrational) and scanning tunneling microscopy to characterize this class of materials. Subsequent chemical studies will provide a more detailed understanding of selective oxidation reactions and O<sub>2</sub> dissociation on these alloys.

## Publications Acknowledging this Grant in 2011-2014

1. Cremer, T.; Siler, C.G.F.; Rodriguez-Reyes, J.C.F.; Friend, C.M.; Madix, R.J. Tuning the Stability of Surface Intermediates Using Adsorbed Oxygen: Acetate on Au(111). *J. Phys. Chem Lett.* 2014, *5*, 1126-1130. DOI:10.1021/jz500192k.
2. Xu, B.J.; Madix, R.J.; Friend, C.M. Predicting Gold-Mediated Catalytic Oxidative-Coupling Reactions from Single Crystal Studies. *Acc. Chem. Res.* 2014, *47*, 761-772. DOI: 10.1021/ar4002476.
3. Stowers, K.J.; Madix, R.J.; Friend, C. M. From model studies on Au(111) to working conditions with unsupported nanoporous gold catalysts: Oxygen-assisted coupling reactions. *J. Cat.* 2013, *308*, 131-141. DOI:10.1016/j.jcat.2013.05.033.
4. Xu, Bingjun; Madix, Robert J.; Friend, Cynthia M. Alkyl groups as synthetic vehicles in gold-mediated oxidative coupling reactions. *Phys. Chem. Chem. Phys.* 2013, *15*, 31793185. DOI: 10.1039/c3cp43956a.
5. Siler, Cassandra G. F.; Xu, Bingjun; Madix, Robert J.; Friend, Cynthia M. Role of Surface-Bound Intermediates in the Oxygen-Assisted Synthesis of Amides by Metallic Silver and Gold. *J. Am. Chem. Soc.* 2012, *134*, 12604-12610. DOI 10.1021/ja303178z.

6. Rodriguez-Reyes, Juan Carlos F.; Friend, Cynthia M.; Madix, Robert J. Origin of the selectivity in the gold-mediated oxidation of benzyl alcohol. *Surf. Sci.* 2012, 606, 1129-1134. DOI 10.1016/j.susc.2012.03.013.
7. Xu, Bingjun; Madix, Robert J.; Friend, Cynthia M. Dual-Function of Alcohols in Gold-Mediated Selective Coupling of Amines and Alcohols. *Chem.—A Eur. J.* 2012, 18, 2313-2318. DOI 10.1002/chem.201103232.
8. Kosuda, Kathryn M.; Wittstock, Arne; Friend, Cynthia M.; Baeumer, Marcus. Oxygen-Mediated Coupling of Alcohols over Nanoporous Gold Catalysts at Ambient Pressures. *Ang. Chem. Int. Ed.* 2012, 51, 1698-1701. DOI 10.1002/anie.201107178.
9. Xu, Bingjun; Madix, Robert J.; Friend, Cynthia M. Activated Metallic Gold as an Agent for Direct Methoxycarbonylation. *J. Am. Chem. Soc.* 2011, 133, 20378-20383. DOI: 10.1021/ja207389z.
10. Xu, Bingjun; Haubrich, Jan; Baker, Thomas A.; Kaxiras, Efthimios; Friend, Cynthia M. Theoretical Study of O-Assisted Selective Coupling of Methanol on Au(111). *J. Phys. Chem. C.* 2011, 115, 3703-3708. DOI: 10.1021/jp110835w.
11. Baker, Thomas A.; Xu, Bingjun; Jensen, Stephen C.; Friend, Cynthia M. Kaxiras, Efthimios. Role of defects in propene adsorption and reaction on a partially O-covered Au(111) surface. *Catalysis Science & Technology*, 2011, 1(7), 1166- 1174. DOI: 10.1039/c1cy00076d.
12. Xu, B.J.; Friend, C.M.; Madix, R. J. A paradigm for predicting selective oxidation on noble metals: oxidative catalytic coupling of amines and aldehydes on metallic gold. *Faraday Discussions.* 2011, 152, 241-252. DOI: 10.1039/c1fd00012h.
13. Xu, B.J.; Friend, C.M. Oxidative coupling of alcohols on gold: Insights from experiments and theory. *Faraday Discussions*, 2011, 152, 307-320. DOI: 10.1039/c1fd00015b.
14. Baker, Thomas A.; Liu, Xiaoying; Friend, Cynthia M. The mystery of gold's chemical activity: local bonding, morphology and reactivity of atomic oxygen. *Physical Chemistry Chemical Physics (Invited Perspective article)*, 2011, 13, 34-46. DOI: 10.1039/c0cp01514h.

Shannon S. Stahl

**Aerobic Oxidation of Organic Molecules  
with Homogeneous, Nanoparticle and Heterogeneous Pd Catalysts**

Shannon S. Stahl

Department of Chemistry, University of Wisconsin - Madison

Palladium-based catalysts have widespread utility in liquid-phase aerobic oxidation of organic molecules. Most of our work in this area has focused on the development and mechanistic characterization of a new class of homogeneous Pd catalyzed reactions that employ ancillary ligands to promote direct aerobic catalytic turnover (without Cu cocatalysts) and to influence reaction chemoselectivity, regioselectivity and stereoselectivity (for leading references see: *Science* **2005**, *309*, 1824-1826 and *Acc. Chem. Res.* **2012**, *45*, 851-863). Recently, we have identified nanoparticle and heterogeneous Pd catalysts that offer complementary reaction selectivity in several different classes of aerobic oxidation reactions, including oxidative dehydrogenation of cyclohexanones, allylic acetoxylation of alkenes, alcohol oxidation, and oxidative coupling reactions of arenes. This presentation will highlight selected case studies from these reactions, emphasizing reactions mechanisms and insights relevant to the interface of homogeneous, nanoparticle and heterogeneous catalysis.

**Copper-Catalyzed Aerobic Oxidation of Alcohols and Arenes**

DE-FG02-05ER15690

**Postdocs:** Dr. Jessica M. Hoover

**Students:** Alison E. Wendlandt, Alison M. Suess, Lauren M. Huffman, Amanda E. King, Bradford L. Ryland, Jodie F. Greene, Janelle E. Steves

**Collaborators:** Prof. Thatcher W. Root (Dept. Chem. Biol. Engr., UW-Madison), Prof. Thomas C. Brunold (Dept. Chemistry UW-Madison), Prof. Christopher J. Cramer (Minnesota), Prof. Xavi Ribas (University of Girona)

**RECENT PROGRESS**

***Development and Mechanistic Characterization of (bpy)Cu/Nitroxyl-Catalyzed Aerobic Alcohol Oxidation.***

*Development of a Practical Method for Catalytic Aerobic Oxidation of Primary Alcohols.* Aldehydes and ketones are ubiquitous products and intermediates in industrial chemical synthesis. Effective alcohol oxidation reactions often must exhibit one or more types of "chemoselectivity", such as: A) oxidation of a primary alcohol to an aldehyde without over-oxidation to the carboxylic acid, B) selective oxidation of an alcohol in the presence of other oxidizable and/or potentially inhibitory functional groups, and C) oxidation of one alcohol in preference to another within a diol or polyol.

In 2011, we reported the development of a highly practical method for chemoselective aerobic oxidation of primary alcohols to aldehydes with a catalyst consisting of an inexpensive Cu<sup>I</sup> salt and TEMPO (2,2,6,6-tetramethylpiperidiny-*N*-oxyl) (Figure 1). The method is effective with both activated (benzylic, allylic, propargylic) and unactivated

(aliphatic, electron-deficient) alcohols, and many of the reactions, especially those with activated alcohols, reach completion within a few hours at room temperature, using ambient air as the oxidant. The method tolerates heterocycles and heteroatoms, including diverse oxygen, nitrogen, and sulfur-containing functional groups, and enables selective oxidation of primary alcohols, even within the molecules containing electronically more activated, unprotected secondary alcohols. The high activity of this catalyst system arose from the serendipitous discovery that use of a Cu<sup>I</sup> source results in dramatically higher rates relative to catalyst systems that employ a Cu<sup>II</sup> source.

The efficiency and synthetic scope of these Cu/TEMPO-catalyzed alcohol oxidation potentially also make them attractive for large-scale applications. In order to demonstrate safe and scalable operation of these reactions, we performed the reaction with dilute oxygen gas (9% O<sub>2</sub> in N<sub>2</sub>, 35 bar total pressure, which is outside the O<sub>2</sub>/CH<sub>3</sub>CN flammability limits) in a stainless steel tube reactor (Figure 2). The reactions performed in this manner achieved near-quantitative yields of aldehydes with residence times in the reactor as low as 5 min, and benzyl alcohol oxidation was demonstrated on 100 g scale. Aliphatic alcohols react more slowly, in part because they exhibit inherently slower reaction rates and also because the reaction temperature had to be lowered to 60 °C to minimize overoxidation of the aldehydes to carboxylic acids (carboxylic acids inhibit catalytic turnover, resulting in incomplete conversion of the starting alcohol).

#### *Mechanistic Studies of Cu/TEMPO-Catalyzed Aerobic Alcohol Oxidation Reactions.*

The practical utility of this new Cu/TEMPO catalyst system prompted us to undertake a systematic mechanistic study of the catalytic reaction. In early 2013, we reported a mechanistic study of (bpy)Cu<sup>I</sup>OTf/TEMPO/NMI-catalyzed alcohol oxidation. An oxoammonium pathway, in which TEMPO<sup>+</sup> serves as the active oxidant, had been proposed previously by Semmelhack for a different Cu/TEMPO catalyst system. However, this mechanism was excluded on the basis of several pieces of evidence, including electrochemical data showing that Cu<sup>II</sup> is not a strong enough oxidant to oxidize TEMPO to TEMPO<sup>+</sup>, a lack of kinetic competence of the TEMPO<sup>+</sup> oxoammonium species, and isotope effect analysis. Instead, the data suggest that Cu and TEMPO work in concert, as coupled one-electron oxidants, to achieve a net two-electron

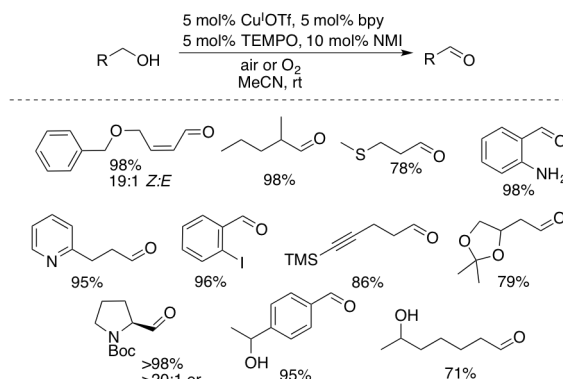


**Figure 1.** Aerobic oxidation of aliphatic alcohols with bpy/Cu<sup>I</sup>/NMI/TEMPO.

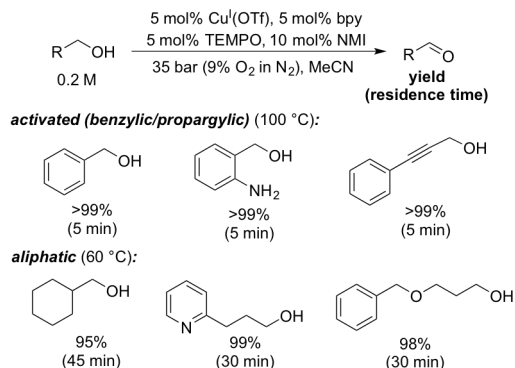
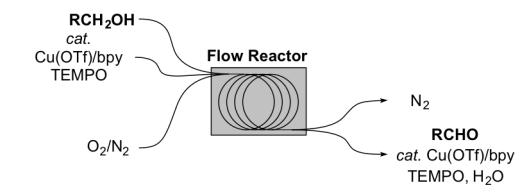


**Figure 2.** Continuous flow applications of Cu/TEMPO-catalyzed aerobic alcohol oxidation.

oxidation of the alcohol. Aerobic oxidation of  $\text{Cu}^{\text{I}}$  and TEMPOH affords a  $\text{Cu}^{\text{II}}\text{-OH}$  species and TEMPO. The unique effectiveness of a  $\text{Cu}^{\text{I}}$  catalyst precursor is evident from this sequence: aerobic oxidation of  $\text{Cu}^{\text{I}}$  generates a hydroxide base ( $\text{L}_n\text{Cu}^{\text{II}}\text{-OH}$ ) that is needed to deprotonate the alcohol in the substrate oxidation half-reaction.

A major component of this study focused on comparison of reactivity of benzylic and aliphatic alcohols, including analysis of catalytic rates by gas-uptake and in situ IR kinetic methods, and characterization of the catalyst speciation during the reaction by EPR and UV-visible spectroscopic methods. Overall, catalytic rate laws, kinetic isotope effects, and spectroscopic data provided evidence for different turnover-limiting steps for activated (benzylic and allylic) vs. unactivated (aliphatic) alcohols. Benzylic and other activated alcohols exhibit faster overall rates and show no kinetic dependence on [alcohol] or [TEMPO]. A rate dependence on [Cu] and  $[\text{O}_2]$  in these reactions suggests that aerobic oxidation of the Cu catalyst (step *i*, Figure 3) is the turnover-limiting step of the reaction. A second-order dependence on [Cu] at low Cu concentrations indicates that  $\text{O}_2$  activation involves two Cu centers. Aliphatic alcohols react more slowly than benzylic alcohols, and their rate exhibits a saturation dependence on [alcohol] and a first-order dependence on [TEMPO]. Alcohol oxidation proceeds via pre-equilibrium formation of a  $\text{Cu}^{\text{II}}$ -alkoxide species (step *iii*) followed by hydrogen transfer to TEMPO (step *iv*).

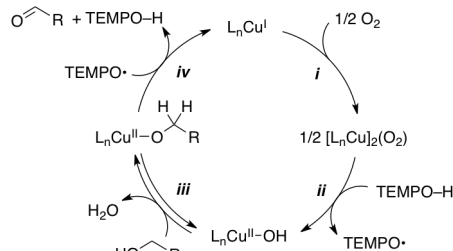


**Figure 3.** Expanded mechanism of (bpy)Cu-TEMPO-catalyzed alcohol oxidation.

*Development of a Practical Method for Catalytic Aerobic Oxidation of All Classes of Alcohols.* The insights obtained from the mechanistic studies described above provided a foundation to address two limitations of the (bpy)Cu/TEMPO/NMI

catalyst system: (1) the oxidation rates of unactivated aliphatic alcohols are significantly slower than those of activated alcohols and (2) secondary alcohols are unreactive. The latter feature is appealing because it underlies the reaction chemoselectivity (e.g., selective oxidation of unprotected diols), but it also limits the scope.

In 2013, we showed that replacement of TEMPO with a bicyclic nitroxyl, such as ABNO or ketoABNO, led to dramatic rate enhancements with aliphatic alcohols and rendered the catalyst compatible with secondary alcohols. Whereas the Cu/TEMPO catalyst system shows significantly different rates for different classes of alcohols (i.e., 1°

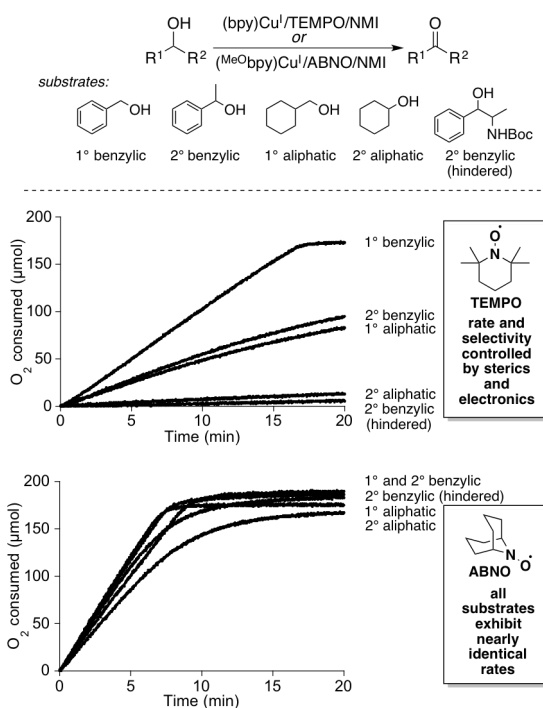
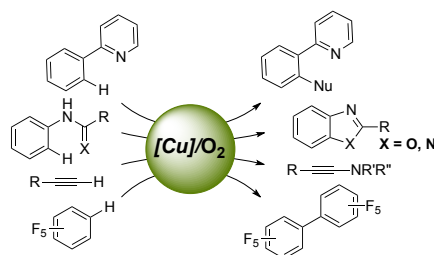


**Figure 4.** Rate comparison of five different alcohols with Cu/TEMPO and Cu/ABNO alcohol oxidation systems.

benzylic > 1° aliphatic/2° benzylic >> 2° aliphatic and/or sterically hindered 2° benzylic), the closely related Cu/ABNO catalyst system exhibits nearly identical rates with all classes of alcohols (Figure 4). These observations suggest that replacement of TEMPO with ABNO significantly increases the alcohol oxidation step (step *iv*, Figure 4) and that the rate is controlled by an alcohol-independent step, such as aerobic oxidation of Cu<sup>I</sup> (step *i*, Figure 4). This conclusion is supported qualitatively by the beneficial effect of an electron-rich bpy ligand (<sup>MeO</sup>bpy, 4,4'-dimethoxy-2,2'-bipyridyl) and the ability to lower the ABNO loading from 5 to 1 mol % without affecting the rate. The optimized Cu/ABNO catalyst system shows excellent reactivity with a broad range of activated and aliphatic primary and secondary alcohols, including those bearing diverse functional groups and stereocenters adjacent to the product aldehyde group. The good reactivity with secondary alcohols undoubtedly reflects the smaller steric profile of the bicyclic ABNO structure relative to TEMPO.

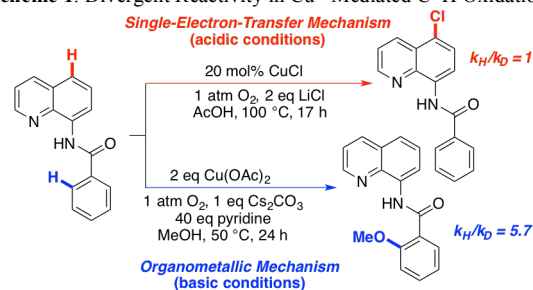
### Cu-Catalyzed Aerobic Oxidation of Aromatic C–H Bonds.

Copper(II) has an extensive history as a stoichiometric oxidant in organic chemistry, but such oxidation and oxidative coupling reactions are typically initiated by single-electron transfer (SET) from electron-rich organic molecules. In 2010, we reported the direct (spectroscopic) evidence for an aryl-Cu<sup>III</sup> intermediate in a Cu<sup>II</sup>-catalyzed C–H aerobic oxidation reaction. It seems reasonable that other Cu<sup>II</sup>-catalyzed oxidation reactions proceed via organometallic intermediates. In 2011, we reviewed "Copper-Catalyzed Aerobic Oxidative C–H Functionalizations", in which we classified reactions according to their probable mechanism, SET vs. organometallic. Recognition of these two distinct pathways provides a framework for the design of new catalytic reactions, and we are interested in elucidating the factors that dictate the mechanistic course of the reaction.



In a recent study of Cu<sup>II</sup>-mediated oxidation of *N*-(8-quinoliny)benzamide, we observed divergent reactivity, depending on the reaction conditions. Under basic conditions, the benzamide group undergoes directed C–H methoxylation or chlorination. Under acidic conditions, the quinoline group undergoes non-directed chlorination. Experimental and computational mechanistic studies implicate an organometallic C–H activation/functionalization mechanism under the former conditions and a single-electron transfer mechanism under the latter conditions. This rare observation of divergent, condition-dependent mechanisms for oxidation of a single substrate provides a valuable foundation for understanding Cu<sup>II</sup>-mediated C–H oxidation reactions.

Scheme 1. Divergent Reactivity in Cu<sup>II</sup>-Mediated C–H Oxidation.



### Publications Acknowledging this Grant in 2011-2014

1. Wendlandt, A. E.; Suess, A. M.; Stahl, S. S. Copper-Catalyzed Aerobic Oxidative C–H Functionalizations: Recent Trends and Mechanistic Insights. *Angew. Chem., Int. Ed.* **2011**, *50*, 11062-11087.
2. Huffman, L. M.; Casitas, A.; Font, M.; Canta, M.; Costas, M.; Ribas, X.; Stahl, S. S. Observation and Mechanistic Study of Facile C–O Bond Formation Between a Well-Defined Aryl-Copper(III) Complex and Oxygen Nucleophiles. *Chem., Eur. J.* **2011**, 10643–10650.
3. Huffman, L. M.; Stahl, S. S. Mechanistic Analysis of *trans* C–N Reductive Elimination From a Square-Planar Macrocyclic Aryl-Copper(III) Complex. *Dalton Trans.* **2011**, *40*, 8959-8963.
4. Wendlandt, A. E.; Stahl, S. S. Copper(II)-Mediated Oxidative Cyclization of Enamides to Oxazoles. *Org. Biomol. Chem.* **2012**, *10*, 3866-3870.
5. Wendlandt, A. E.; Stahl, S. S. Chemoselective Organocatalytic Aerobic Oxidation of Primary Amines to Secondary Imines. *Org. Lett.* **2012**, *14*, 2850–2853.
6. King, A. E.; Ryland, B. L.; Brunold, T. C.; Stahl, S. S. Kinetic and Spectroscopic Studies of Aerobic Cu(II)-Catalyzed Methoxylation of Arylboronic Esters and Insights into Aryl Transmetalation to Cu(II). *Organometallics*, **2012**, *31* 7948–7957.
7. Hoover, J. M.; Ryland, B. L.; Stahl, S. S. Mechanism of Copper(I)/TEMPO-Catalyzed Aerobic Alcohol Oxidation. *J. Am. Chem. Soc.* **2013**, *135*, 2357–2367.
8. Suess, A. M.; Ertem, M. Z.; Cramer, C. J.; Stahl, S. S. Divergence between Organometallic and Single-Electron Transfer Mechanisms in Copper(II)-Mediated Aerobic C–H Oxidation. *J. Am. Chem. Soc.* **2013**, *135*, 9797–9804.
9. Hoover, J. M.; Ryland, B. L.; Stahl, S. S. Copper/TEMPO-Catalyzed Aerobic Alcohol Oxidation: Mechanistic Assessment of Different Catalyst Systems. *ACS Catalysis*, **2013**, *3*, 2599–2605.
10. Greene, J. F.; Hoover, J. M.; Mannel, D. S.; Root, T. W.; Stahl, S. S. Continuous-Flow Aerobic Oxidation of Primary Alcohols with a Copper(I)/TEMPO Catalyst. *Org. Proc. Res. Devel.*, **2013**, *17*, 1247-1251.
11. Steves, J. E.; Stahl, S. S. Copper(I)/ABNO-Catalyzed Aerobic Alcohol Oxidation: Alleviating Steric and Electronic Constraints of Cu/TEMPO Catalyst Systems. *J. Am. Chem. Soc.* **2013**, *135*, 15742-15745.
12. Tsybizova, A.; Ryland, B. L.; Tsierkezos, N.; Stahl, S. S.; Roithová, J.; Schröder, D. Speciation Behaviour of Copper(II) Acetate in Simple Organic Solvents Revealing the Effect of Trace Water. *Eur. J. Inorg. Chem.* **2014**, *2014*, 1407-1412.
13. Ryland, B. R.; Stahl, S. S. Practical Aerobic Oxidations of Alcohols and Amines with Homogeneous Cu/TEMPO and Related Catalyst Systems. *Angew. Chem. Int. Ed.* **2014**, *53*, in press.

**Fundamental Studies of Oxidation Reactions on Model Catalysts  
Catalytic Sites for Propylene Epoxidation by O<sub>2</sub> and H<sub>2</sub> over Au/ titanium silicalite-1**

Fabio H. Ribeiro and W. Nicholas Delgass  
School of Chemical Engineering, 480 Stadium Mall Drive, West Lafayette, IN 47907

**Presentation Abstract**

The discovery by Haruta more than a decade ago that by co-feeding H<sub>2</sub> with propylene and O<sub>2</sub> and using Au/TiO<sub>2</sub> as the catalyst, one can produce PO with high selectivity provides the potential for a single-step, direct and green solution to this long standing catalytic partial oxidation challenge. Moreover, the catalytic chemistry of this system offers unique opportunities to study the role of *in situ* generated hydrogen peroxide as a selective olefin oxidant and to probe the catalytic properties of nanometer and subnanometer metal particles. We focus here on Au/TS-1 catalysts, which display the improved stability and activity associated with isolated Ti centers, and probed the nature and location of the active Au. Since proximity of Au and Ti is required for the catalysis, the activity of Au on a support made by coating TS-1 with an S-1 shell showed that Au clusters small enough to enter the MFI pore structure are active for PO production. Addition of Au to uncalcined TS-1, the pores of which were still blocked by the template, led to an unprecedented 20 hour activation period. Correlated changes in apparent surface area and other supported data showed that peroxide generated from H<sub>2</sub> and O<sub>2</sub> over the Au particles burned some of the template out of the pores, allowing Au migration to the Ti anchor points that create the active sites in the pores. Analysis of the most active catalysts yet reported, with a rate of reaction of 300 g<sub>poh</sub><sup>-1</sup>kg<sub>cat</sub><sup>-1</sup>, showed that the Cs salt used in deposition precipitation of the Au in these catalysts helps to stabilize the small Au particles in the TS-1 pores, thus maximizing the number of stable Au sites. These studies all confirm the importance of Au clusters small enough to enter the TS-1 pore structure as active sites for propylene epoxidation.

**Grant title: Fundamental Studies of Oxidation Reactions on Model Catalysts**

**Grant number: DE-FG02-03ER15408**

**PI: Fabio H. Ribeiro and W. Nicholas Delgass**

**Student(s): Viktor J. Cybulskis, Wen-Sheng Lee, Ian T. Smith**

**RECENT PROGRESS**

Recent work has focused three areas. The first is closure of the work on Au supported on uncalcined TS-1 supports, Au/U-TS-1. The motivation for that work was to force the gold to be deposited on the outer surface of the TS-1 crystallites by blocking the interior pore structure by not removing the template around which the TS-1 structure grows during its synthesis. Second is elaboration of the discovery that the reaction rate of Au/TS-1 can be dramatically enhanced by using Cs<sub>2</sub>CO<sub>3</sub> instead of our standard Na<sub>2</sub>CO<sub>3</sub> as the pH control agent during the deposition precipitation (DP) of the Au. The third is examination of the effects of the residual Na left from the standard DP process, the Cl left from the chloroauric acid gold precursor, and the method of activation.

**Au/U-TS-1:** The preliminary results of this approach given in last year's annual report have now

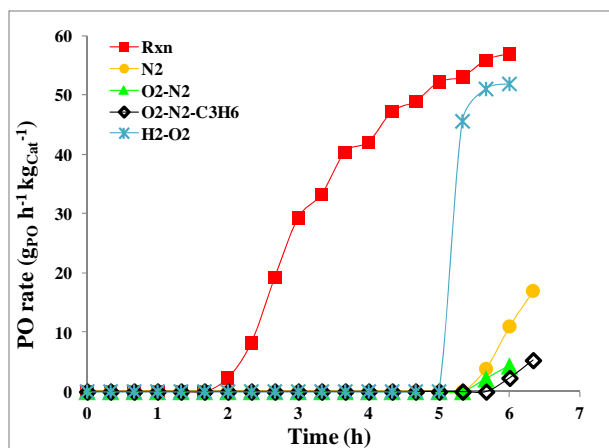


Figure 1 PO rate per gram of catalyst as a function of time for 0.05Au/UTS-1(119) samples first pretreated under different conditions for 5 h at  $\sim 200$  °C (including the time for temperature ramping with a ramping rate  $\sim 1$  °C  $\text{min}^{-1}$ ): (■) normal reaction conditions (10 vol% each of  $\text{H}_2, \text{O}_2, \text{C}_3\text{H}_6$  in  $\text{N}_2$ ), (●) pure  $\text{N}_2$  (▲) 10 vol%  $\text{O}_2$  in  $\text{N}_2$  (◇) 10 vol% each of  $\text{O}_2$  and  $\text{C}_3\text{H}_6$  in  $\text{N}_2$  (×) 10% each of  $\text{H}_2$  and  $\text{O}_2$  in  $\text{N}_2$ , and then tested under normal conditions for another 1-2 h. For reference, the BET apparent surface area of UTS-1(119) was  $21 \pm 1$   $\text{m}^2$   $\text{g}^{-1}$ .

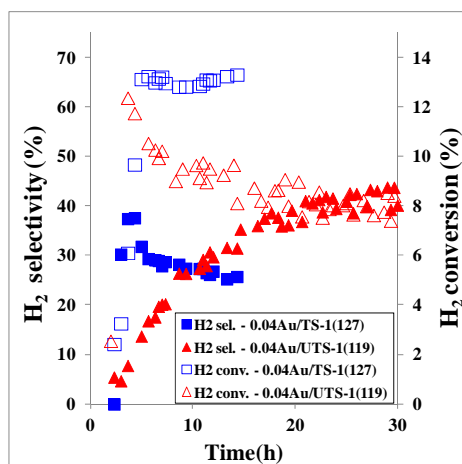


Figure 2.  $\text{H}_2$  selectivity/conversion as a function of time

**Effects of Cs on Au/TS-1:** We have known for some time that Au efficiency for the PO reaction is highest at the lowest loadings, an observation consistent with need for small, isolated Au clusters. Thus an optimal gold loading can be expected at a point where the increase in the number of sites with increasing loading is offset by the decrease in Au efficiency. This effect is illustrated in Fig 3. Fig 3b show clearly that the efficiency drops with loading regardless of the method of catalyst preparation. Fig 3a, however, shows a surprising effect of Cs vs. other alkali metals as the cation of the DP agent. With Cs the drop in efficiency is delayed as the rate increases, allowing

been published in the *Journal of Catalysis*. The unique feature of this catalyst is its slow activation, taking nearly 20 hours to reach full activation. In contrast, Au/TS-1 with the same Au loading rises almost immediately to its highest activity and then shows some deactivation over time. The fact that Au particles large enough to be seen by TEM form after Au deposition (before reaction) only on UTS-1 and not on calcined, open-pore TS-1 is further evidence that a significant amount of the Au enters the pore system when it is accessible during DP. The slight opening of the pores indicated by an increase in the area measured by BET and the loss of template in the near-surface region indicated by a decrease in the  $\text{N} 1s$  line in XPS confirm the correspondence of the opening of the pores with the increase in PO activity, while TEM shows that Au particle size does not correlate with the rate. Interestingly, Fig 1 shows clearly that it is the presence of  $\text{H}_2$  and  $\text{O}_2$  together in the reaction mixture that

drive the pore opening and thus the activation of the catalyst.

Also of particular interest in this system are the observations that, once activated, this catalyst has high stability and, over the entire time, a hydrogen selectivity that is significantly improved over that of Au/TS-1, as shown in Fig. 2. This is important because the hydrogen selectivity may well be the deciding factor on whether this catalyst will ever be applied commercially. We note that the sample 0.01Au/U-TS-1(119) showed the  $\text{H}_2$  selectivity at the level of  $\sim 55\%$  with PO rate  $\sim 60$   $\text{gPO h}^{-1} \text{kgCat}^{-1}$  at  $200$  °C, which is the highest  $\text{H}_2$  selectivity yet reported at similar conditions.

the rate to continue increasing to higher Au loading. The net effect is a doubling of the rate to the highest value yet recorded for PO production over Au catalysts.

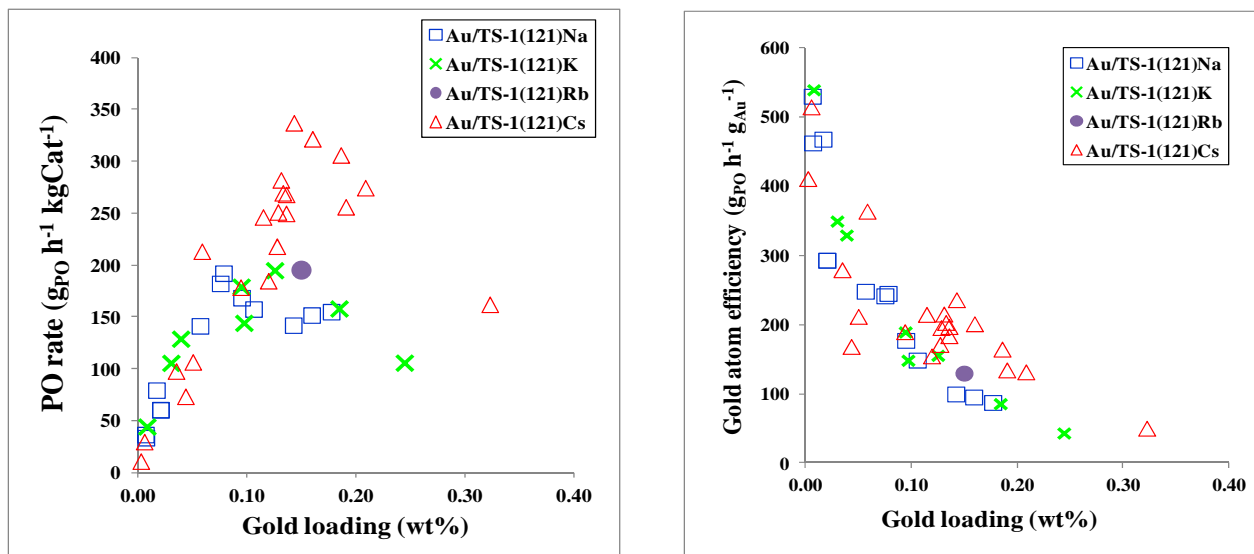


Figure 3. a) (left) PO rate per gram of catalyst and b) (right) PO rate per gram of gold for Au/TS-1(121) with different gold loadings prepared by using different precipitation agents:  $\text{Na}_2\text{CO}_3$ ,  $\text{K}_2\text{CO}_3$ ,  $\text{Rb}_2\text{CO}_3$ , and  $\text{Cs}_2\text{CO}_3$ . The data were taken as the average values of the first 1–2 h at 200 °C. The circled data points were the rates right at 200 °C (reacted at 200 °C for less than 0.5 h).

As shown in Figure 4, there is some deactivation of these high rate catalysts, but they still level out at well above 200  $\text{g}_{\text{PO}} \text{h}^{-1} \text{g}_{\text{Cat}}^{-1}$ . It is also interesting to note that we have found that the Cs enhances the catalyst performance even if it is added after DP with Na, provided the Au loading is high enough.

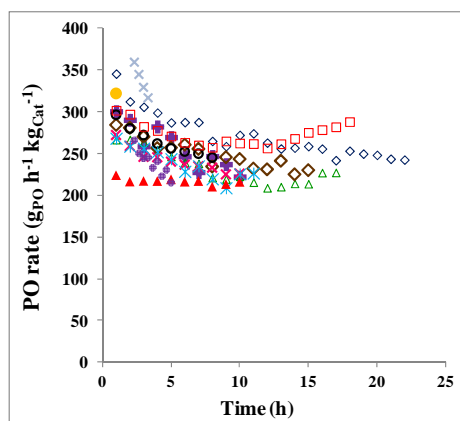


Figure 4. PO rates for 12 Au/TS-1 (121)Cs catalysts as a function of time on stream

At very low Au loading, sintering is not a problem and Cs is not needed. This can be seen in the low loading portion of Fig 3a, where the slopes are about the same for the Na and Cs samples. At higher loading, however, the presence of Cs retards sintering and preserves the population of optimal sites. The small Au clusters associated with those sites show a slightly higher hydrogen selectivity relative to the Na analogs (~20% vs. 12-15%), but not as high as that found for the uncalcined catalysts discussed above. There is clearly some chemical interaction of the Cs with both the TS-1 and the Au. With Cs DP, the Au capture onto the catalyst is enhanced by about a factor of 4 relative to that with Na and XPS of the Ti 2p region of the fresh catalyst shows some  $\text{Ti}^{3+}$ . Nevertheless, the activation energies and orders of reaction are independent of the alkali used, indicating that the chemistry of the Au sites is unchanged. We conclude, therefore, that the role of the Cs is to increase the number, but not the nature of the Au sites.

**Effects of Residual Alkali, Chlorine and Activation Method on the PO Rate:** Effects of both Na and particularly Cl might be expected for these catalysts, but as shown in Figs 5 and 6 they are not important descriptors of performance. In Fig. 5, a four times increase in the Na/Au ratio does

not affect the Au efficiency. Fig. 6 shows that post impregnation of additional NaCl or NaNO<sub>3</sub> also has little effect on the rate.

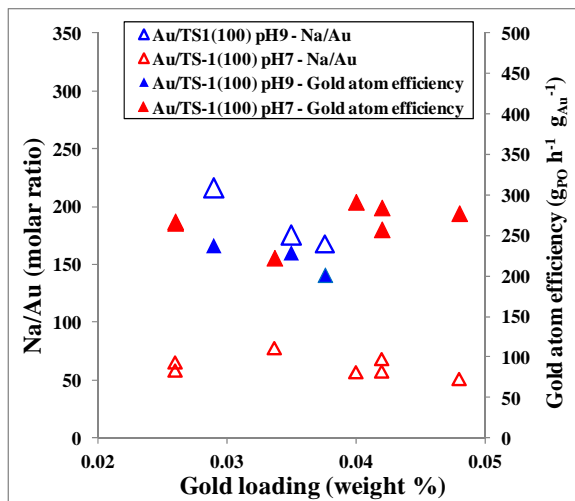


Figure 5. Na/Au molar ratio and the gold atom efficiency of the Au/TS-1(100) samples prepared at pH~7 and pH~9. The samples are prepared at different pH with different Na/Au molar ratios but have similar gold atom efficiency at ~250 gPO h<sup>-1</sup> gAu<sup>-1</sup>.

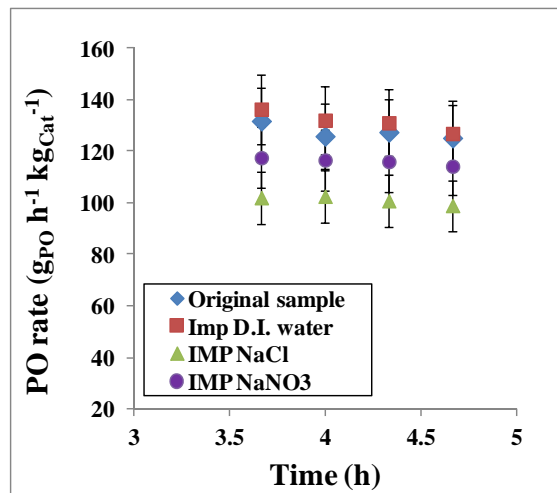


Figure 6. PO rate per gram of catalyst vs. time on stream

To study the effects the activation procedure on the rate of reaction, we compare H<sub>2</sub>, N<sub>2</sub>, and O<sub>2</sub> individually to the standard activation in the reaction mixture in Fig. 7. Pure hydrogen and oxygen are clearly poorer choices, while N<sub>2</sub> is only slightly below the reaction mixture activation.

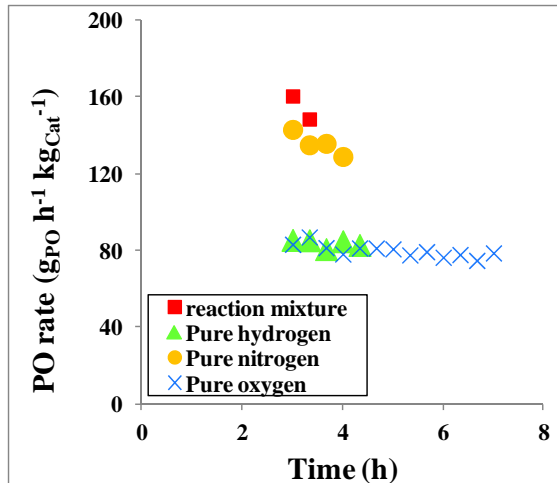


Figure 7. PO rate (gPO h<sup>-1</sup> kgCat<sup>-1</sup>) vs. time on stream for the 0.11Au/TS-1(121) samples activated in different environments: (triangle) pure H<sub>2</sub>, (round) pure N<sub>2</sub>, (cross) pure O<sub>2</sub>, and (square) reaction mixture from RT to ~200 °C with ramping rate ~1-1.5 °C min<sup>-1</sup>.

pure hydrogen and oxygen are clearly poorer choices, while N<sub>2</sub> is only slightly below the reaction mixture activation. TEM analysis of the activated samples showed that in hydrogen and oxygen the average particle sizes were 3.91 and 3.68 nm respectively, compared to 3.29 nm for activation in the reaction mixture. While the change is relatively small, coupled with the broadening of the distribution, it is in keeping with our findings that loss of the smallest particles is most detrimental. A complete study of the effects of the size of the particles that can be seen by TEM, i.e. larger than 1 nm, shows that the rate does not correlate with particle size or with the number of edge, corner, or surface sites. This finding again confirms that the TEM invisible small particles in the pores are the important active sites.

## Publications Acknowledging this Grant in 2011-2014

1. Lee, W.-S.; Zhang, R.; Akatay, M. C.; Baertsch, C.; Stach, E. A.; Ribeiro, F. H.; Delgass, W. N. Differences in Catalytic Sites for CO Oxidation and Propylene Epoxidation on Au Nanoparticles. *ACS Catal.* **2011**, 1, 1327–1330.
2. Lee, W.-S.; Akatay, M. C.; Stach, E. A.; Ribeiro, F. H.; Delgass, W. N. Reproducible Preparation of Au/TS-1 with High Reaction Rate for Gas Phase Epoxidation of Propylene. *J. Catal.* **2012**, 287, 178-189.
3. Lee, W.-S.; Lai, L.-C.; Akatay, M. C.; Stach, E. A.; Ribeiro, F. H.; Delgass, W. N. Probing the Gold Active Sites in Au/TS-1 for Gas Phase Epoxidation of Propylene in the Presence of Hydrogen and Oxygen. *J. Catal.* **2012**, 296, 31-42.
4. Lee, W.-S.; Akatay, M. C.; Stach, E. A.; Ribeiro, F. H.; Delgass, W. N. Enhanced Reaction Rate for Gas Phase Epoxidation of Propylene using H<sub>2</sub> and O<sub>2</sub> by Cs Promotion of Au/TS-1. *J. Catal.* **2013**, 308, 98–113.
5. Zemlyanov, D.; Klötzer, B.; Gabasch, H.; Smeltz, A.; Ribeiro, F. H.; Zafeiratos, S.; Teschner, D.; Schnörrch, P.; Vass, E.; Hävecker, M.; Knop-Gericke, A.; Schlögl, R. Kinetics of Palladium Oxidation in the mbar Pressure Range: Ambient Pressure XPS Study. *Top. Catal.* **2013**, 56, 885–895.
6. Lee, W.-S.; Akatay, M. C.; Stach, E. A.; Ribeiro, F. H.; Delgass, W. N. Gas Phase Epoxidation of Propylene in the Presence of H<sub>2</sub> and O<sub>2</sub> over Small Gold Ensembles in Uncalcined TS-1. *J. Catal.* **2014**, 313, 104–112.

This page is intentionally blank.

# Poster Presentations

This page is intentionally blank.

**Frank Abild-Pedersen**

**Trends in Nano Particle Catalysis**

Frank Abild-Pedersen, Lin Li, Hongliang Xin, Johannes Voss, Aleksandra Vojvodic and  
Jens K. Nørskov

SUNCAT Center for Interface Science and Catalysis, SLAC National Accelerator  
Laboratory 2575 Sand Hill Road, Menlo Park, CA 94025

**Presentation Abstract**

Understanding the workings of a catalyst at the atomic level and building on this knowledge to develop new and better catalysts is a scientific grand challenge that requires a close interplay between front-line experimental capabilities and significant theoretical efforts. The search for new materials based on computational screening approaches has proven to be a very cost-efficient way of identifying possible catalyst candidates if the right tools and methodologies are developed. Realizing that the complexity of a given process can be reduced significantly by a number of simple principles has been instrumental for the progress and the development of such simplification schemes for a larger group of materials, surface orientations, surface compositions and catalyst size regimes where the distinction between heterogeneity and homogeneity is unclear, is a necessity in order to take computational catalyst screening to a new level of predictability.

**Grant Number:** 10049

**Grant Title:** SUNCAT Center for Interface Science and Catalysis

**Staff Scientist:** Aleksandra Vojvodic

**Assoc. Staff:** Johannes Voss

**Post Doc:** Hongliang Xin

**Student:** Lin Li

## Recent Progress

The aim is to significantly enhance our understanding of chemistry at the nm size regime and through this, speed up the development of novel design strategies for computational catalyst screening that goes beyond extended systems.

The lateral interaction in the surface layer due to compressive strain or alloying and the interaction between the surface metal layer and a different host material in metal particles is expected to result in significant variations in reactivity of the active components in the surface.

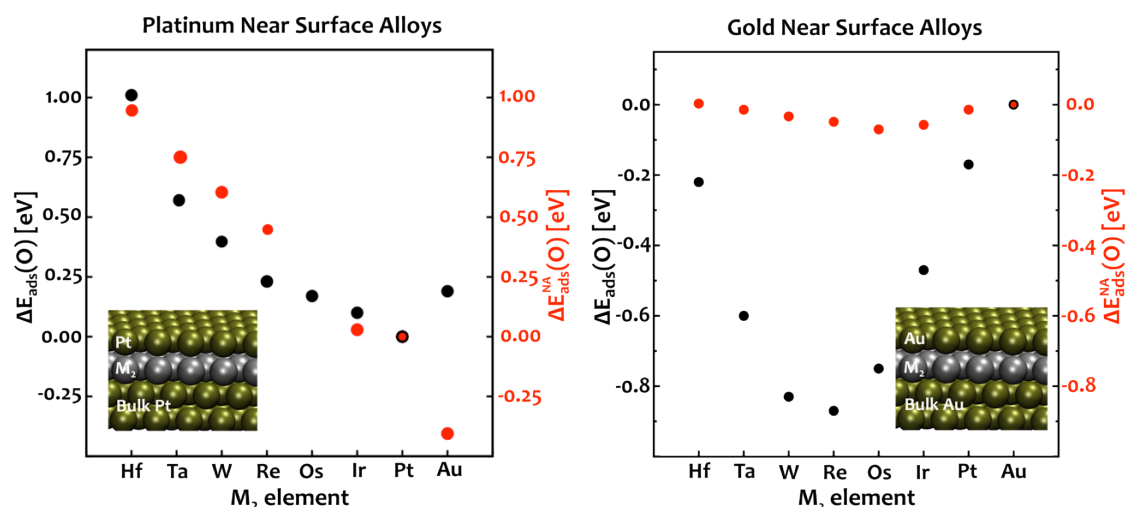


**Fig. 1** Oxygen binding energies on series of Pt and Au near-surface alloys. Black dots indicate full DFT calculations for oxygen adsorption in the fcc site on the close-packed metal surfaces. The red dots are oxygen binding energies calculated from the DFT extracted  $d$  density of states using the Newns-Anderson approach. On Au binding energies are seen to vary significantly between the DFT results and the Newns-Anderson results. This indicates that changes in bond strength on Au depend more on the overlap of metal states than coupling between adsorbate and surface  $d$ -states. On Pt on the other hand the agreement between the DFT and Newns-Anderson results is much better suggesting that the effects observed on Au only have a secondary contribution to the binding on Pt which in this case is mainly driven by the hybridization between the adsorbate states and the metal  $d$ -states.

We have studied this using a series of model systems that were designed explicitly to target each effect separately. Subsurface ligand effects were studied by looking at near-surface alloys where a different metal is substituted in the second layer of a surface slab. We found (see Fig. 1) that for coinage metal near surface alloys an increased binding energy could be obtained even though hybridization with the filled d-states should give a net zero variation in the bond strength. The effect is related to secondary interactions between the first two metal layers where variations in bond strength are governed by coupling between the small perturbations in the metal states in the first layer induced by the adsorbate and the second layer.

In the case when the metal surface has empty d-states this effect is still present but here variations in bond strength are mainly driven by adsorbate state and d-state hybridization.

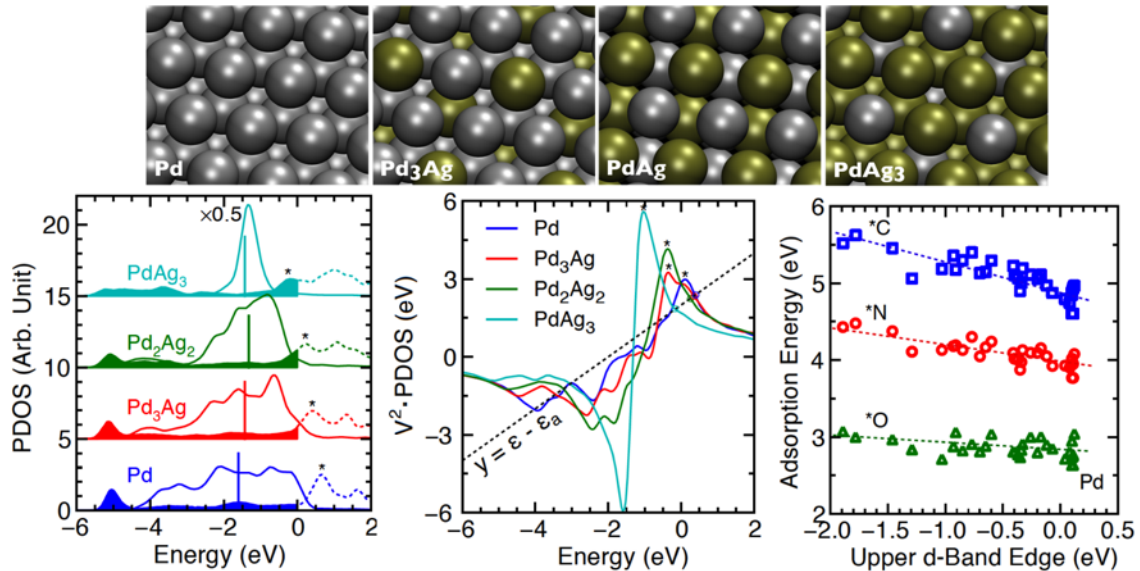


**Fig. 2** Left figure shows projected density of states (PDOS) on Pd 4d orbitals (solid lines) in Pd and Pd/Ag alloys together with the C 2p orbital PDOS (dashed lines) for C adsorbed on Pd and Pd/Ag alloys. The energy zero is the Fermi level and the vertical solid lines are used to denote the d-band center of the Pd atoms in the (111) surface of pure Pd and Pd alloys. The star (\*) is used to mark the position of C 2p-Pd 4d anti-bonding states. The middle figure shows Hilbert transforms of the local d-DOS of the surface Pd atoms in the pure Pd and Pd/Ag alloys. The dashed line represents the adsorbate function defined as  $y = \epsilon - \epsilon_a$  where  $\epsilon_a$  is the renormalized adsorbate state after the interaction with the sp-band of the substrate. The intersection between the adsorbate function and the upper part of the Hilbert transform

(marked with circles) represents the position of adsorbate-metal anti-bonding states. The upper d-band edge is defined as the peak position of the Hilbert transform of the local d-DOS and is marked with a star (\*). Right figure shows adsorption energies of C, N, and O on pure Pd and Pd alloys, with atomic metal ratio of 3:1, 1:1, and 1:3, plotted as function of the position of the upper d-band edge, given by the intersection between the Hilbert transform and the adsorbate function.

To understand ligand effects in the surface layer we studied a set of Pd/M alloys where M is chosen among the late transition metals. Here we found (see Fig. 2) that the simple d-band model that correlates d-state position and activity can be extended to include not only metals but also metal alloys by explicitly accounting for effects from the structure of the density of states. This effect is captured by the upper band edge of the d-band and it is most pronounced when the band structure of the active surface component is split into separate bands such that not only the position and the width become important but also the distribution of states in the vicinity of the Fermi-level.

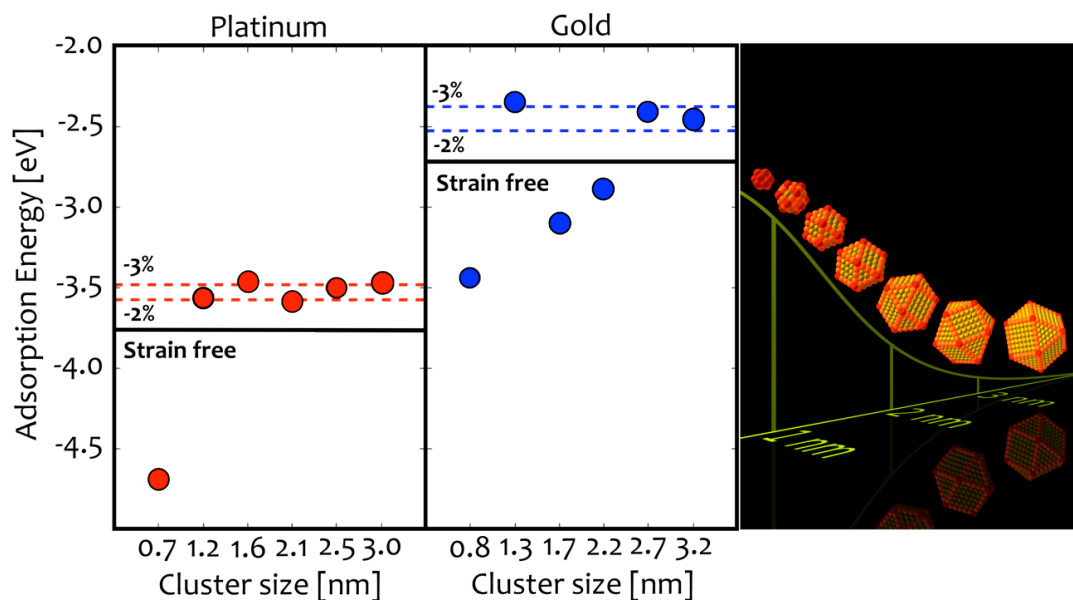


**Fig. 3** Oxygen adsorption energies calculated on different size cubo octahedral Pt and Au clusters. Quantum-size effects are observed for Au clusters giving rise to large fluctuations in the binding energies of small clusters an effect that is less pronounced for Pt clusters. Secondly, very slow size convergence towards the unstrained slab calculations for the binding energies

are observed for both Au and Pt clusters. This effect is mainly due to in-plane relaxations (lateral). A 2-3% compressive lateral relaxation of the clusters clearly underlines the necessity for a deeper understanding of the effects of cluster compression and how to incorporate that into existing models.

Studies of lateral compression in metal clusters and its effect on adsorption was made possible with the use of the super-computer at Argonne National Lab.

Fig. 3 shows the adsorption energies of oxygen on relaxed freestanding Pt and Au clusters. The adsorption energy on Pt clusters appears to approach a value that is around 0.3 eV weaker than the value on a strain-free surface. In addition, this limit corresponds to adsorption energies observed for Pt surfaces with 2-3% compression. The adsorption energy of oxygen on Pt clusters reaches this limit very quickly, already at 55 atoms. In contrast, the oxygen adsorption energy on Au clusters approach to a similar strained limit, however, this occurs first when the cluster size reaches 561 atoms. This difference in adsorption energies between large clusters and the traditional surface model has been identified to be due to self-compression of the metal clusters.

New materials discoveries have really only been possible through a careful understanding of the complex reaction network at the atomic level. Hence, expanding the model approach to a larger number of materials and structures and pushing our understanding into different size regimes where the boundaries between heterogeneity and homogeneity are unclear is a necessity in order to move the field forward.

### **Publications Acknowledging this Grant in 2011-2014<sup>1-33</sup>**

1. W. J. Durand, A. A. Peterson, F. Studt, F. Abild-Pedersen and J. K. Nørskov, Structure effects on the energetics of the electrochemical reduction of CO<sub>2</sub> by copper surfaces, *Surface Science*, **2011**, 605, 1354.
2. L. C. Grabow, F. Studt, F. Abild-Pedersen, V. Petzold, J. Kleis, T. Bligaard and J. K. Nørskov, Descriptor-Based Analysis Applied to HCN Synthesis from NH<sub>3</sub> and CH<sub>4</sub>, *Angewandte Chemie International Edition*, **2011**, 50, 4601.

3. G. Jones, F. Studt, F. Abild-Pedersen, J. K. Nørskov and T. Bligaard, Scaling relationships for adsorption energies of C<sub>2</sub> hydrocarbons on transition metal surfaces, *Chemical Engineering Science*, **2011**, 66, 6318.
4. J. K. Nørskov, F. Abild-Pedersen, F. Studt and T. Bligaard, Density functional theory in surface chemistry and catalysis, *Proceedings of the National Academy of Sciences of the United States of America*, **2011**, 108, 937.
5. S. Saadi, B. Hinnemann, C. C. Appel, S. Helveg, F. Abild-Pedersen and J. K. Nørskov, First-principles investigations of Ni<sub>3</sub>Al(111) and NiAl(110) surfaces at metal dusting conditions, *Surface Science*, **2011**, 605, 582.
6. A. Vojvodic, F. Calle-Vallejo, W. Guo, S. Wang, A. Toftelund, F. Studt, J. I. Martinez, J. Shen, I. C. Man, J. Rossmeisl, T. Bligaard, J. K. Nørskov and F. Abild-Pedersen, On the behavior of Bronsted-Evans-Polanyi relations for transition metal oxides, *Journal of Chemical Physics*, **2011**, 134, 244509.
7. S. Wang, V. Petzold, V. Tripkovic, J. Kleis, J. G. Howalt, E. Skulason, E. M. Fernandez, B. Hvolbaek, G. Jones, A. Toftelund, H. Falsig, M. Bjorketun, F. Studt, F. Abild-Pedersen, J. Rossmeisl, J. K. Nørskov and T. Bligaard, Universal transition state scaling relations for (de)hydrogenation over transition metals, *Physical Chemistry Chemical Physics*, **2011**, 13, 20760.
8. S. Wang, B. Temel, J. Shen, G. Jones, L. C. Grabow, F. Studt, T. Bligaard, F. Abild-Pedersen, C. H. Christensen and J. K. Nørskov, Universal Bronsted-Evans-Polanyi Relations for C-C, C-O, C-N, N-O, N-N, and O-O Dissociation Reactions, *Catalysis Letters*, **2011**, 141, 370.
9. M. Behrens, F. Studt, I. Kaatkin, S. Kuhl, M. Havecker, F. Abild-Pedersen, S. Zander, F. Girgsdies, P. Kurr, B. Kniep, M. Tovar, R. W. Fischer, J. K. Nørskov and R. Schlögl, Methanol Synthesis over Cu/ZnO/Al<sub>2</sub>O<sub>3</sub>: The Active Site in Industrial Catalysis, *Science*, **2012**, 336, 893.
10. S. H. Chou, J. Voss, I. Bargatin, A. Vojvodic, R. T. Howe and F. Abild-Pedersen, An orbital-overlap model for minimal work functions of cesiated metal surfaces, *Journal of Physics: Condensed Matter*, **2012**, 24, 445007.
11. J. S. Hummelshøj, F. Abild-Pedersen, F. Studt, T. Bligaard and J. K. Nørskov, CatApp: A Web Application for Surface Chemistry and Heterogeneous Catalysis, *Angewandte Chemie International Edition*, **2012**, 51, 272.
12. E. M. Karp, C. T. Campbell, F. Studt, F. Abild-Pedersen and J. K. Nørskov, Energetics of Oxygen Adatoms, Hydroxyl Species and Water Dissociation on Pt(111), *Journal of Physical Chemistry C*, **2012**, 116, 25772.
13. A. C. Lausche, J. S. Hummelshøj, F. Abild-Pedersen, F. Studt and J. K. Nørskov, Application of a new informatics tool in heterogeneous catalysis: Analysis of methanol dehydrogenation on transition metal catalysts for the production of anhydrous formaldehyde, *Journal of Catalysis*, **2012**, 291, 133.
14. A. J. Medford, A. Vojvodic, F. Studt, F. Abild-Pedersen and J. K. Nørskov, Elementary steps of syngas reactions on Mo<sub>2</sub>C(001): Adsorption thermochemistry and bond dissociation, *Journal of Catalysis*, **2012**, 290, 108.
15. S. Rajasekaran, S. Kaya, F. Abild-Pedersen, T. Anniyev, F. Yang, D. Stacchiola, H. Ogasawara and A. Nilsson, Reversible graphene-metal contact through hydrogenation, *Physical Review B*, **2012**, 86, 75417.

16. E. Skulason, T. Bligaard, S. Gudmundsdottir, F. Studt, J. Rossmeisl, F. Abild-Pedersen, T. Vegge, H. Jónsson and J. K. Nørskov, A theoretical evaluation of possible transition metal electro-catalysts for N<sub>2</sub> reduction, *Physical Chemistry Chemical Physics*, **2012**, 14, 1235.
17. F. Studt, F. Abild-Pedersen, Q. Wu, A. D. Jensen, B. Temel, J.-D. Grünwaldt and J. K. Nørskov, CO hydrogenation to methanol on Cu–Ni catalysts: Theory and experiment, *Journal of Catalysis*, **2012**, 293, 51.
18. A. Toftelund, I. C. Man, H. A. Hansen, F. Abild-Pedersen, T. Bligaard, J. Rossmeisl and F. Studt, Volcano Relations for Oxidation of Hydrogen Halides over Rutile Oxide Surfaces, *Chemcatchem*, **2012**, 4, 1856.
19. V. Tripković, F. Abild-Pedersen, F. Studt, I. Cerri, T. Nagami, T. Bligaard and J. Rossmeisl, Metal Oxide-Supported Platinum Overlayers as Proton-Exchange Membrane Fuel Cell Cathodes, *Chemcatchem*, **2012**, 4, 228.
20. M. García-Mota, A. Vojvodic, F. Abild-Pedersen and J. K. Nørskov, Electronic Origin of the Surface Reactivity of Transition-Metal-Doped TiO<sub>2</sub>(110), *Journal of Physical Chemistry C*, **2013**, 117, 460.
21. A. C. Lausche, F. Abild-Pedersen, R. J. Madix, J. K. Nørskov and F. Studt, Analysis of sulfur-induced selectivity changes for anhydrous methanol dehydrogenation on Ni(100) surfaces, *Surface Science*, **2013**, 613, 58.
22. A. C. Lausche, A. J. Medford, T. S. Khan, T. Bligaard, F. Abild-Pedersen, J. K. Nørskov and F. Studt, On the Effect of Coverage Dependent Adsorbate-Adsorbate Interactions for CO Methanation on Transition Metal Surfaces, *Journal of Catalysis*, **2013**, 307, 275.
23. L. Li, A. H. Larsen, N. A. Romero, V. A. Morozov, C. Glinsvad, F. Abild-Pedersen, J. Greeley, K. W. Jacobsen and J. K. Nørskov, Investigation of Catalytic Finite-Size-Effects of Platinum Metal Clusters, *Journal of Physical Chemistry Letters*, **2013**, 4, 222.
24. H. Öberg, T. Anniyev, A. Vojvodic, S. Kaya, H. Ogasawara, D. Friebel, D. J. Miller, D. Nordlund, U. Bergmann, M. P. Ljungberg, F. Abild-Pedersen, A. Nilsson and L. G. M. Pettersson, Stability of Pt-Modified Cu(111) in the Presence of Oxygen and Its Implication on the Overall Electronic Structure, *Journal of Physical Chemistry C*, **2013**, 117, 16371.
25. S. Rajasekaran, S. Kaya, F. Abild-Pedersen, H. Ogasawara and A. Nilsson, Hydrogen adsorption induced interlayer carbon bond formation in supported few layer graphene, *Physical Review Letters*, **2013**, 111, 85503.
26. F. Studt, F. Abild-Pedersen, J. B. Varley and J. K. Nørskov, CO and CO<sub>2</sub> Hydrogenation to Methanol Calculated Using the BEEF-vdW Functional, *Catalysis Letters*, **2013**, 143, 71.
27. F. Viñes, A. Vojvodic, F. Abild-Pedersen and F. Illas, Brønsted–Evans–Polanyi Relationship for Transition Metal Carbide and Transition Metal Oxide Surfaces, *Journal of Physical Chemistry C*, **2013**, 117, 4168.
28. J. Voss, A. Vojvodic, S. H. Chou, R. T. Howe, I. Bargatin and F. Abild-Pedersen, Thermionic current densities from first principles, *Journal of Chemical Physics*, **2013**, 138, 204701.

29. Y. Xu, A. C. Lausche, S. Wang, T. S. Khan, F. Abild-Petersen, F. Studt, J. K. Nørskov and T. Bligaard, In silico Search for Novel Methane Steam Reforming Catalysts, *New Journal of Physics*, **2013**, 15, 125021.
30. A. J. Medford, A. C. Lausche, F. Abild-Pedersen, B. Temel, N. C. Schjødt, J. K. Nørskov and F. Studt, Activity and Selectivity Trends in Synthesis Gas Conversion to Higher Alcohols, *Topics in Catalysis*, **2014**, 57, 135.
31. F. Studt, I. Sharafutdinov, F. Abild-Pedersen, C. F. Elkjær, J. S. Hummelshøj, S. Dahl, I. Chorkendorff and J. K. Nørskov, Discovery of a Ni-Ga Catalyst for CO<sub>2</sub> Reduction to Methanol, *Nature Chemistry*, **2014**, 6, 320.
32. A. Vojvodic, J. K. Nørskov and F. Abild-Pedersen, Electronic structure effects in transition metal surface chemistry, *Topics in Catalysis*, **2014**, 57, 25.
33. J. S. Yoo, F. Abild-Pedersen, J. K. Nørskov and F. Studt, Theoretical Analysis of Transition-Metal Catalysts for Formic Acid Decomposition, *ACS Catalysis*, **2014**, 4, 1226.

## Shape and Phase Transitions of Co Oxide Particles

M. Li<sup>1</sup>, A. Boscoboinik<sup>2</sup>, N. Levy<sup>2</sup>, U.D. Schwarz<sup>3</sup> and E.I. Altman<sup>1</sup>

<sup>1</sup>Yale University, Department of Chemical and Environmental Engineering

<sup>2</sup>Brookhaven National Laboratory, Center for Functional Nanomaterials

<sup>3</sup>Yale University, Department of Mechanical Engineering and Materials Science

### Presentation Abstract

The focus on Co oxide surfaces is motivated by the activity of Co-containing oxides for a wide range of reactions, yet continuing uncertainties regarding even the identity of the catalytically active phase. In the bulk, the thermodynamically stable phases of Co oxide are CoO and Co<sub>3</sub>O<sub>4</sub> with the latter favored at atmospheric pressure up to  $\approx 1100$  K. It will be shown, however, that a support can stabilize CoO nanoparticles under conditions where Co<sub>3</sub>O<sub>4</sub> is favored. On high energy substrates, the inherent bilayer structure of Co<sub>3</sub>O<sub>4</sub> dictates that the oxidation of CoO monolayers increases the exposed area of the substrate, thereby stabilizing CoO against oxidation. Further, the dewetting required to form Co<sub>3</sub>O<sub>4</sub> increases the occupancy of high energy edge sites, especially for small CoO islands. As a result, the oxidizability of CoO clusters decreases with size, the opposite of the usual trend. As CoO is difficult to reduce, this renders small Co oxide islands inactive for CO oxidation. It will be shown that specific island edges initiate oxidation of larger CoO islands leading to characteristic defect structures in the resulting Co<sub>3</sub>O<sub>4</sub> nanoparticles. Moreover, we find that even a weakly interacting support can modulate the favored shape of the CoO islands simply through lattice mismatch thereby altering the reactivity towards oxygen. One consequence of this modulation is that the particle shape does not converge to the continuum shape anticipated from surface and edge energies until the clusters contain thousands of atoms. Recent results characterizing the Co oxide particles under near ambient conditions using XPS and high pressure STM will be presented. Finally, a new direction for surface science models of transition metal cations and oxides on zeolite surfaces will be presented; this work builds upon two recent PI publications on 2D silica bilayers.

### **DE-FG02-98ER14882: Structure-Reactivity Relationships in Multi-Component Transition Metal Oxide Catalysts**

**Postdoc (Research Scientist):** Min Li

## RECENT PROGRESS

### *Shape, Morphology, and Phase Transitions During Co Oxide Growth on Au(111)*

The surface structure and morphology of cobalt oxide thin films grown on Au(111) were studied using scanning tunneling microscopy (STM) and ultra-violet and x-ray photoelectron spectroscopies. Initial growth in O<sub>2</sub> led to 2-D CoO clusters exhibiting a superstructure in STM images characteristic of the lattice mismatch between the rocksalt (111) surface and the substrate. The superstructure governed the CoO cluster shape; as a result, the shapes of clusters containing up to thousands of Co atoms were modulated by the most efficient packing of spheres. Continued growth led to a transition to 3-D, fully oxidized, spinel phase Co<sub>3</sub>O<sub>4</sub> clusters. These Co<sub>3</sub>O<sub>4</sub> clusters were embedded with characteristic “Y” shaped grain boundaries that result from high reactivity towards oxygen at specific edges of the CoO clusters, and the doubling of the periodicity when CoO is oxidized to Co<sub>3</sub>O<sub>4</sub>. Exposure of the Co<sub>3</sub>O<sub>4</sub> films to O atoms induced oxidation towards Co<sub>2</sub>O<sub>3</sub> which roughened the surface. Reducing these over-oxidized films produced CoO in a 3-D morphology. The results demonstrate how the shape and morphology of Co oxide nanostructures is intertwined with the support, the phase and the history of the structures.

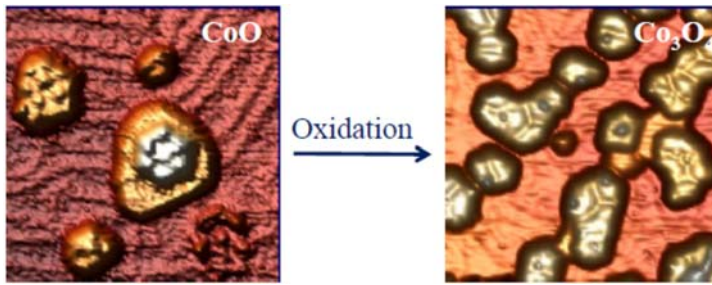


**Figure 1.** STM images of CoO islands (left) display a characteristic moiré pattern due to the lattice mismatch with Au. Oxidation to Co<sub>3</sub>O<sub>4</sub> (right) eliminates the lattice mismatch and the moiré pattern but creates characteristic "Y" shaped defects.

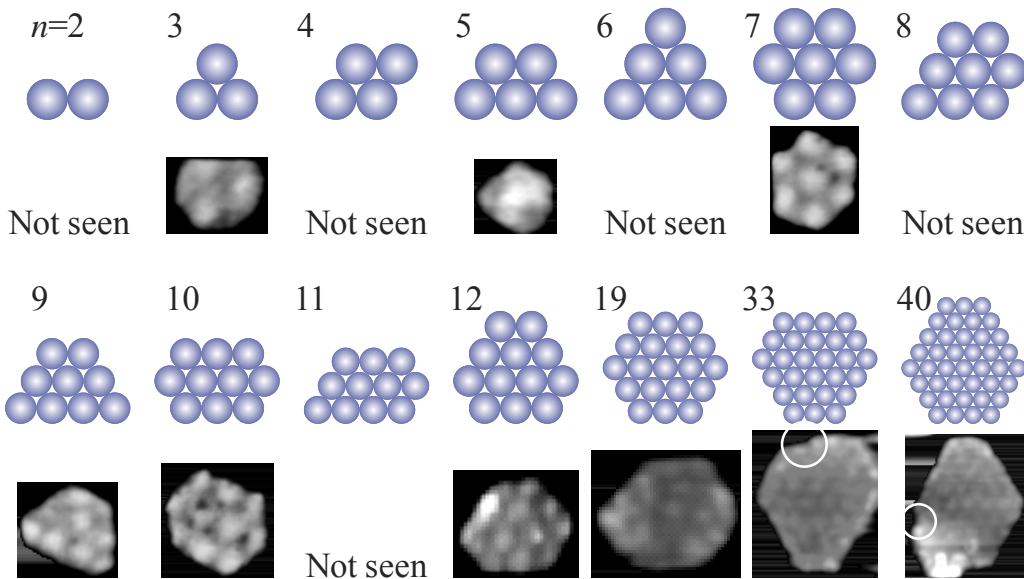


**Figure 2.** For CoO, the moiré maxima replace individual atoms as the building blocks that govern the particle shape. The shaded balls represent the observed white spots on moiré patterned CoO clusters in STM. The white circles highlight kinks resolved in the cluster edges for  $n = 33$  and  $40$ . Since each ball contains 110 Co atoms, the clusters exhibit “magic sizes” of hundreds of atoms.

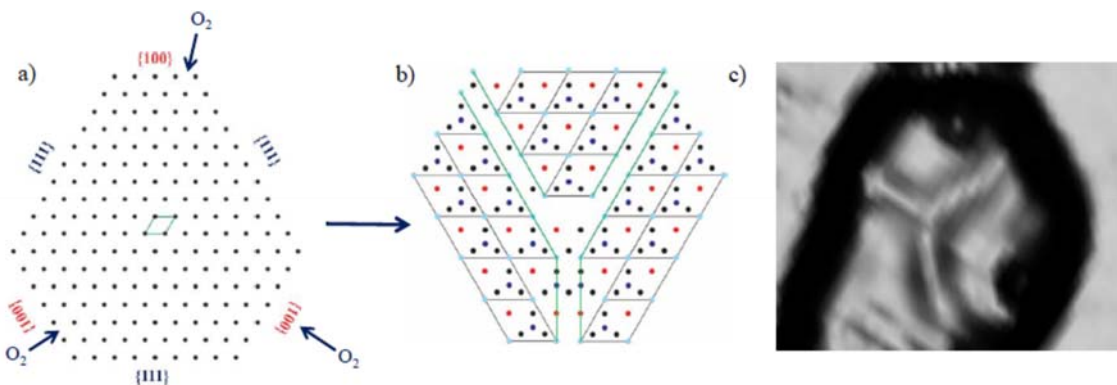


**Figure 3.** When oxidation of CoO (a) proceeds preferentially at the distinct alternating edges, the doubling of the periodicity in going to Co<sub>3</sub>O<sub>4</sub> (b) causes “Y” shaped grain boundaries highlighted in green to form. c) 3D rendering of an STM image showing the “Y” shaped groove.

### *Cluster-Size Dependent Phase Transitions of Co Oxides*

In the sub-monolayer regime, cobalt oxide nanoparticles on Au(111) undergo a phase transition from CoO to Co<sub>3</sub>O<sub>4</sub> as the coverage is increased. At low coverages, only CoO was observed even though the oxygen pressure was orders of magnitude higher than that required to form bulk Co<sub>3</sub>O<sub>4</sub>. The stabilization of the reduced phase is due to the higher surface energy of the substrate and the lower areal density of the more oxidized phase. These findings explain prior observations of transitions to more oxidized Co and Fe phases after initial layers of the monoxide form on various substrates. The distinction here is that the combination of the low surface energy of the Au substrate and the weaker interaction of Co with Au than Fe with either Au or ZrO<sub>2</sub>, where Fe oxide switches from FeO to Fe<sub>3</sub>O<sub>4</sub> after the monolayer is completed, dictates that the phase transition occurs well before the substrate is entirely covered. This indicates that an appropriate choice of substrate, be it a metal or an oxide, and particle size can allow a tuning of the oxidation/reduction properties of oxide clusters for catalysis. The results can be generalized to any system in which either a high substrate surface energy or strong attractive interfacial interaction favors wetting, and the reaction decreases the covered area of the substrate.

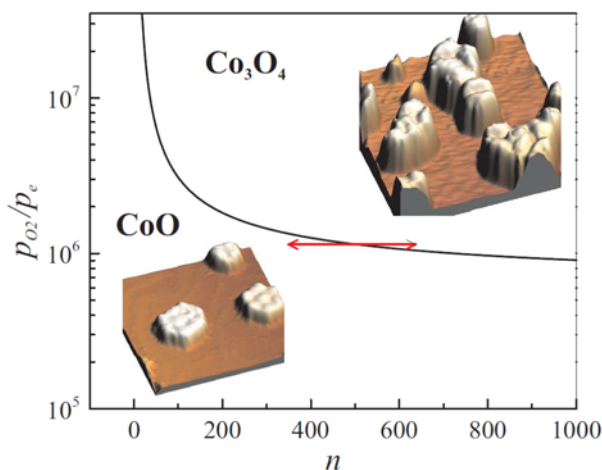


**Figure 4.** The plot shows the enhancement in the oxygen pressure required to form Co<sub>3</sub>O<sub>4</sub> clusters on Au(111) relative to the bulk oxygen equilibrium pressure at 670 K as a function of cluster size. The inset STM images show the structures of the two phases. The Co<sub>3</sub>O<sub>4</sub> above the equilibrium line is a bilayer compared to single layer CoO below the equilibrium line accounting for the height difference.

## **Publications Acknowledging this Grant in 2011-2014**

M. Li and E.I. Altman, "Shape, Morphology, and Phase Transitions During Co Oxide Growth on Au(111)," *Journal of Physical Chemistry C*, In Press.

M. Li and E.I. Altman, "Cluster-Size Dependent Phase Transition of Co Oxides on Au(111)," *Surface Science Letters* **619** (2014) L6.

### **Publications Acknowledging Other DOE Support**

E.I. Altman and U.D. Schwarz, "Structural and Electronic Heterogeneity of Two Dimensional Amorphous Silica Layers," *Advanced Materials Interfaces*, In Press.

E.I. Altman, J. Götzen, N. Samudrala, and U.D. Schwarz, "Growth and Crystallization of Crystalline Silica Films on Pd(100)," *Journal of Physical Chemistry C* **117** (2013) 26144.

H. Mönig, M. Todorović, M.Z. Baykara, T.C. Schwendemann, L. Rodrigo, E.I. Altman, R. Pérez, U.D. Schwarz, "Understanding Scanning Tunneling Microscopy Contrast Mechanisms on Metal Oxides: A Case Study," *ACS Nano* **7** (2013) 10233.

M.Z. Baykara, M. Todorović, H. Mönig, T.C. Schwendemann, Ö. Ünverdi, L. Rodrigo, E.I. Altman, R. Pérez, and U.D. Schwarz, "Atom-specific Forces and Defect Identification on Surface-oxidized Cu(100) with Combined 3D-AFM and STM Measurements," *Physical Review B* **87** (2013) 155414.

M.Z. Baykara, T.C. Schwendemann, B.J. Albers, N. Pilet, H. Mönig, E.I. Altman and U.D. Schwarz, "Exploring Atomic-Scale Lateral Forces in the Attractive Regime: A Case Study on Graphite (0001)," *Nanotechnology* **40** (2012) 405073.

Perla B. Balbuena

**Roles of Catalyst-Substrate  
and Growing Structure-  
Catalyst Interactions during  
Nucleation and Growth of  
Single-Walled Carbon  
Nanotubes**

Perla B. Balbuena, Juan C. Burgos, and J.  
Leonardo Gomez-Ballesteros  
Texas A&M University, Department of Chemical Engineering

**Presentation Abstract**

A strong interaction between the catalyst surface and the graphitic lattice of the nanotube was found necessary for healing and formation of defects during growth of single-walled carbon nanotubes. Defects can be healed independently of their degree of embedment of the defective structure into the tube structure. Diffusion and catalytic events at the catalyst/tube interface are the main sources of nanotube structural recovery on the catalyst surface. Optimal growth conditions are identified that allow significant structural healing in nanotubes. On quartz supports, selective functionalization of low-coordinated surface sites may cause exposure of low-coordinated Si atoms that bond strongly to nanotube walls. On the other hand, saturation of low-coordinated oxygen also favors carbon nanotube adhesion to the substrate. A chirality preference towards zigzag over armchair nanotubes was found on functionalized quartz surfaces. Magnetization effects on the surface originated by the presence of adsorbed functional groups were found to enhance adsorption of arm-chair nanotubes compared to that on clean surfaces. Based on the findings, it was suggested that surfaces may be engineered to favor horizontal adsorption of specific chiralities along preferential directions. Catalyst nanoparticles have adjacent surfaces with different works of adhesion for graphene. This difference is crucial for nanotube growth efficiency because it offers the required anchoring and lift-off sites. Our results indicate that the faceting geometry of the nanoparticles determines the nanotube cap structure, thus defining both the diameter and the chiral angle of the single-walled carbon nanotubes during their birth.

**DE-FG02-06ER15836: Modeling  
catalyzed growth of single-walled  
carbon nanotubes**

**Student(s):** D. A. Gomez-Gualdrón, J. C. Burgos, J. L. Gomez-Ballesteros, G. D. McKenzie, J. Beetge, and E. Jones.

**RECENT PROGRESS**

***Dynamics of defects on nanotube walls during CVD growth***

The type of topological defect that nucleates in the nanotube wall is linked to the catalyst shape and therefore to the metal-support interaction energy ( $E_{MS}$ ). The 5-7 type of defect was found in every nanotube grown from our reactive molecular dynamics (RMD) simulations independently of the  $E_{MS}$  value, because of their low formation energy, the dynamic nature of the growth process, and the high growth rates. For stronger  $E_{MS}$  the catalyst becomes flatter, and 5-7 defects are more frequently found in the tube structure

(Figure 1). Although Stone-Wales (SW) defects can be found at low  $E_{MS}$  interactions (associated with low amount of defects), their presence in the nanotube sidewall results from local concentrations of 5-7's that recombine into 5-7-7-5 arrangements. Vacancy defects were seen more often in nanotubes grown on bi/mono-layer catalysts. At these conditions, carbon caps lift-off so rapidly that they are not able to minimize dangling bond through structural rearrangements on the catalyst surface. Therefore, low coordinated carbon atoms were frequently observed in the tube sidewall during growth on catalysts with these particular shapes.

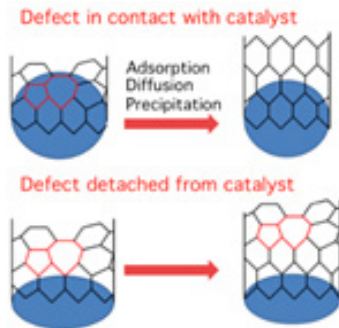


**Figure 1.** Role of the catalyst surface in healing defects. Defects can be healed on the catalyst surface via three mechanisms: Carbon adsorption, carbon surface diffusion, or carbon precipitation from bulk (top). Once the defect lifts off, the defect cannot be healed (bottom).

Figure 2 illustrates a defect formation mechanism valid for vacancy and di-vacancy defects. The mechanism follows six steps after starting with the formation of nanotube edge delimited by carbon atoms potentially forming a defect. Rapid addition of catalyzed carbon to the edge as a result of high pressures, leads to the fast growth of carbon chains in close interaction with the support.

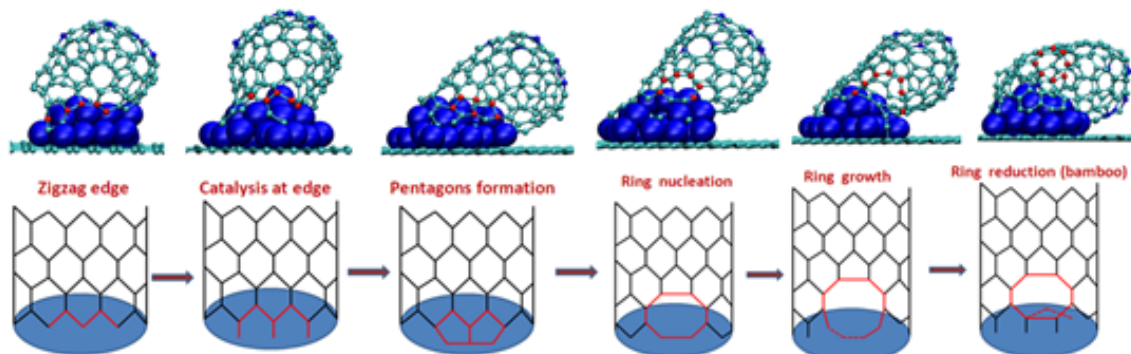


**Figure 2.** Formation mechanism for vacancy type of defects (mono and di-vacancy). The flatness of the catalyst is the key factor to the nucleation of large rings due to their fast stabilization on the nanotube wall. Red dots represent the atoms that will finally form the large ring.

Carbon chains formed in the 2<sup>nd</sup> step bend because of substrate repulsion to neighbor carbon atoms. Highly unstable pentagons are formed due to rapid formation of rings, which leads to ring recombination into larger rings assisted by carbon diffusion on the catalyst surface. Part of the large ring lifts off the catalyst surface. The size of the ring grows, as the flatness of the catalyst does not allow the healing of this defect through further carbon diffusion. Catalysis of carbon atoms at the edge leads to formation of even less stable carbon squares and triangles that end incorporated into a bigger carbon ring. However, very large rings are also unstable and low coordinated carbon atoms from the large ring try to interact with metal atoms at the top of the catalyst. This favors the ring size reduction by imposing a bamboo growth through formation of carbon chains at the inner part of the nanotube cap. Once the large ring lifts off from the catalyst surface eliminating any kind of interaction with it, the defect becomes stable and the catalytic healing is impossible. This mechanism differs in some details for different growths at the same conditions.

Intermediate states may vary (Figure 2), such as the number of pentagons formed at the edge, the size of the first ring, and/or the extent of ring growth and reduction. Nonetheless, the overall defect formation mechanism remains the same, and vacancy/di-vacancy defects are generally related to bamboo growth.

The analysis of defect equilibration within the nanotubes structure, as shown in Figure 1 applies to most kind of defects. However, Stone-Wales (SW) arrangements are not included in this hypothesis and stabilize along the nanotube structure as soon as all carbon atoms belonging to the defect stop interacting with the catalyst surface. Figure 3 illustrates the formation mechanism of a SW defect elucidated by the RMD trajectory. Unlike what it has been said about SW defects, the nucleation of this defect does not involve a bond rotation in the graphitic structure of the tube. Although carbon diffusivity makes bond rotations plausible on catalyst surfaces, we observe that the net rotation of the main bond (green bond in Figure 3) is practically null.

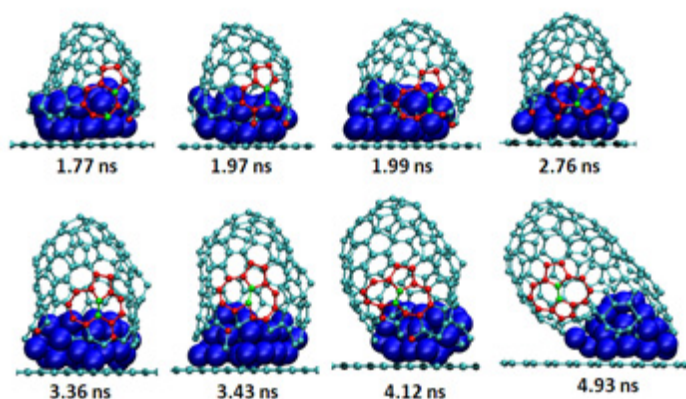
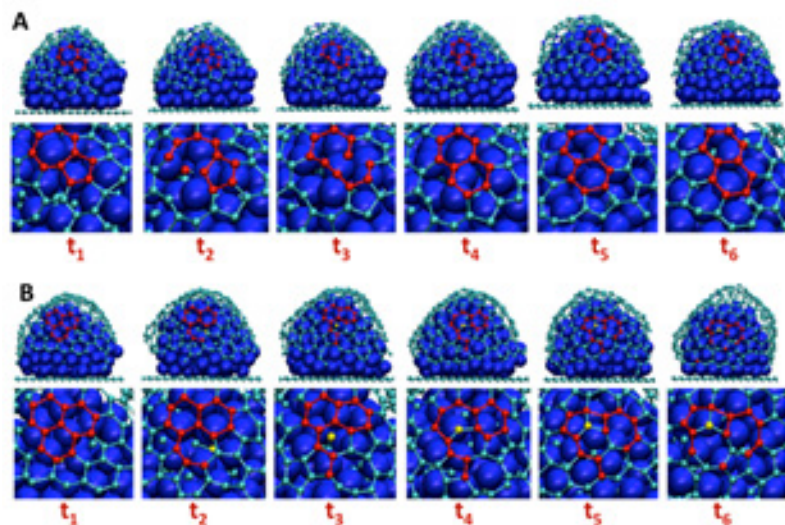


**Figure 3.** Formation mechanism for Stone-Wales defects. The green bond represents the principal bond separating the two heptagons in the 5-7-7-5 configuration. The rest of atoms involved in the defect represented by red dots.

Only ~3 ns elapse since the main bond is initially formed until the SW defect is finally stabilized outside the reach of the catalyst surface. During these 3 ns, the main C-C bond undergoes insignificant alterations in its orientation respect to the nanotube principal axis, despite catalytic phenomena taking place around it. This bond becomes part of different carbon rings before permanently settle in the center of the 5-7-7-5 configuration of the SW defects. The SW defects are then nucleated as a result of the incorporation of a newly created 5-7 defect into a preexistent 5-7 defect (1.99 ns). This phenomenon is frequently observed in our RMD simulations due to high local concentration of 5-7 defects because of the use of elevated growth rates.

Accounting the presence and measuring the concentration of SW defects in nanotubes



represents an experimental challenge since this defect affects only four adjacent hexagons without having repercussions on the physical behavior.

**Figure 4.** Reconstruction mechanism of embedded carbon networks. Systems were analyzed by the time ( $t_i$ ), where  $t_6 > t_5 > t_4 > t_3 > t_2 > t_1$ . A. Embedded 5-7 defect healed on the catalyst surface via carbon surface diffusion. B. Embedded

hexagonal network disrupted via carbon surface diffusion and precipitation of carbon atom (yellow) from bulk.

The enhanced surface area of the largest catalyst particle does not only assist defect healing but also favors defect formation. Hexagons embedded into a near perfect graphitic network are exposed to network reconstruction, as they remain deposited on the catalyst surface. The stability of the hexagonal network might be then jeopardized by the high kinetic energy at the catalyst-cap interface and the mass transfer from the bulk of the catalyst toward the interface. As seen in Figure 4B, an embedded network comprising three adjacent hexagons (t1) is disrupted by surface diffusion and reorganization into a transitional 6-6-7 configuration (t2). The instability of this arrangement allows the reconfiguration of the network back to six adjacent hexagons (t3). A single carbon (yellow atom in Figure 4B) is precipitated into the nanotube-catalyst interface at t3 and favors breaking of a C-C bond in order to accommodate in the middle of two heptagons at t4. After this event takes place, the original perfect hexagonal network is never recovered despite the probability for defect healing inherent to the cap-catalyst interaction. The carbon precipitation at the interface has a significant repercussion on the concentration of defects.

### ***Factors that influence horizontal growth on quartz surfaces***

A general scenario of depletion and accumulation of charges before and after nanotube adsorption provides insightful information about the repulsive/attractive nature of each interaction and the migration of charges upon adsorption. Charge depletion and accumulation were computed for an isosurface value of  $0.8 \text{ e}/\text{\AA}^3$  for nanotubes along the [100](2) direction of the monohydrated surface. The results confirm the repulsion experienced by the (4,4) tube as charges are depleted at the interface and accumulated inside the nanotube. In the top half of the (4,4) nanotube, charges are also displaced in the positive direction of the z-axis. This overall charge shift in the SWCNT (4,4) denotes a strong repulsion undergone by the nanotube after contact with the surface that results in a displacement of carbon nuclei away from the surface. In contrast, SWCNT (6,0) shows the strongest adsorption energy along the same direction of the monohydrated surface, and allows a significant charge accumulation at the interface. Electron depletion is found at the inner part for the lower nanotube half, as well as accumulation in the inner and depletion in the outer part of the upper half of the nanotube wall.

Electron cloud depletion at the interface was occasionally observed for hydrated surfaces, unlike the behavior on clean surfaces. Localized migration of charges away from the interface combined with accumulation at Si-C connections, are a result of structural deformation of strongly adsorbed nanotubes. As a consequence of these deformations, nuclei might move away from the surface at specific locations, such as stiff OH functional groups, and approach lower energy spots such as unsaturated Si sites. Therefore, simultaneous electron depletion and accumulation is observed at different points of the interface, shown for the (6,0) tube along the [110] direction of the di-hydrated surface. This analysis allows us to conclude that low-coordinated Si atoms guide preferential alignment of carbon nanotubes on the ST-surface of quartz. It was previously reported that unsaturated O atoms at the surface were critical on defining preferential alignment through partial oxidation of nanotubes. However, we demonstrate that if the low-coordinated O is bonded to low-coordinated Si, as in the case of the ST-cut, the unsaturated Si is most likely to cause the attraction and charge concentration at the interface. We believe these results can be extended to any kind of silica surface no matter the spatial arrangement of atoms within the lattice. Only the coordination states of the Si and O atoms will define the adsorption strength of carbon nanotubes on the surface, and therefore, the surface concentration and distribution of this kind of atoms will establish the directions of preferential alignment.

### **Publications Acknowledging this Grant in 2011-2014**

1. J. C. Burgos, E. Jones, and P. B. Balbuena, Dynamics of Topological Defects in Single-Walled Carbon Nanotubes during Catalytic Growth, *J. Phys. Chem. C*, **2014**, *118*, 4808-4817.
2. D. A. Gomez-Gualdrón, J. M. Beetge, J. C. Burgos, and P. B. Balbuena, Effects of precursor type on the CVD growth of single-walled carbon nanotubes, *J. Phys. Chem. C*, **2013**, *117*, 10397-10409;
3. D. A. Gomez-Gualdrón, J. M. Beetge, and P. B. Balbuena, Characterization of metal nanocatalyst state and morphology during simulated single-walled carbon nanotube growth, *J. Phys. Chem. C*, **2013**, *117*, 12061-12070;
4. J. C. Burgos and P. B. Balbuena, Preferential Adsorption of Zigzag Single-Walled Carbon Nanotubes on the ST-cut Surface of Quartz, *J. Phys. Chem. C*, **2013**, *117*, 4639-4646.
5. D. A. Gomez-Gualdrón and P. B. Balbuena, "Characterization of Carbon Atomistic Pathways during Single-Walled Carbon Nanotube Growth on Supported Metal Nanoparticles, *Carbon*, **2013**, *57*, 298-309;
6. D. A. Gómez-Gualdrón, G. D. McKenzie, J. F. J. Alvarado, and P. B. Balbuena, Dynamic Evolution of Supported Metal Nanocatalyst/Carbon Structure during Single-Walled Carbon Nanotube Growth, *ACS Nano*, **2012**, *6*, 720-735;
7. J. C. Burgos, E. Jones, and P. B. Balbuena, Effect of the metal-substrate interaction strength on the growth of single-walled carbon nanotubes, *J. Phys. Chem. C.*, **2011**, *115*, 7668-7675;
8. Diego A. Gómez-Gualdrón, Jin Zhao, and Perla B. Balbuena, Nanocatalyst structure as a template to define chirality of nascent single-wall carbon nanotubes, *J. Chem. Phys.*, **2011**, *134*, 014705.

**Multiscale Imaging and DFT analysis of Reactant Interactions on Single-Layer MoS<sub>2</sub> and related Molybdenum-Sulfur Materials**

Ludwig Bartels, Talat S. Rahman\*, Wenhao Lu, Koichi Yamaguchi, Duy Le,\* Takat B. Rawal,\* Chen Wang, Quan Ma, Miguel Isarraraz, Michael Gomez, Cindy Merida

University of California at Riverside (\*=University of Central Florida)

**Presentation Abstract**

We present experimental and theoretical investigations of the structure and chemical interaction of single-layer films/islands of MoS<sub>2</sub> and related molybdenum-sulfur compounds on Cu(111) and SiO<sub>2</sub>/Si substrates. In particular, our work focuses on the properties of sub-stoichiometric sulfides and sulfur vacancies, which we find to have a significantly higher affinity for reactants than – unsurprisingly – the MoS<sub>2</sub> basal plane but also the brims/edges of MoS<sub>2</sub> islands. Our multipronged effort involves scanning tunneling microscopy imaging, density functional theory simulation, photoluminescence spectroscopy and submicron optical imaging. The latter two approaches required the setup of dedicated instrumentation; they offer a complementary approach to the properties of this catalyst material that permits probing at ambient pressures and above.

Additional work in this project addressed the role of the support in facilitating reactions on supported metal catalysts. This is described in a separate poster.

**DE-FG02-07ER15842: Controlling Structural, Electronic, and Energy Flow Dynamics of Catalytic Processes through Tailored Nanostructures**

**PI:** Talat S. Rahman

**Postdocs:** Duy Le, Sampyo Hong

**Students:** Wenhao Lu, Koichi Yamaguchi, Chen Wang, Quan Ma, Miguel Isarraraz, Michael Gomez, Cindy Merida, Takat B. Rawal, Maral Aminpour, S. Islamuddin Shah, Ghazal Shafai

**RECENT PROGRESS**

***Atomic Scale Imaging***

In extension of our prior work on adsorption of anthraquinone on MoSCs grown on Cu(111) we further evaluated the binding of small oxygenate species (formic acid and ethanol). This project revealed images like in the figure, showing exclusive binding of formic acid to Mo<sub>2</sub>S<sub>3</sub> (and not to MoS<sub>2</sub> or its edges).

We also performed mass spectrometry during backfilling and heating of the chamber in order to evaluate the activity of the material and find traces of conversion of formic acid to ethanol (even at typical UHV pressures, Fig. 1 center).

***Atomic Scale Modification***

In a parallel effort we address the formation of vacancies in MoS<sub>2</sub> and their activity. Computational modeling shows far higher activity at vacancies and vacancy clusters than on the basal plane or even at the cluster edges. As a prototype we have evaluated the propensity for catalytic activity of an MoS<sub>2</sub> layer with two types of sulfur-vacancy structures (row and patch) and find the energetics for alcohol synthesis

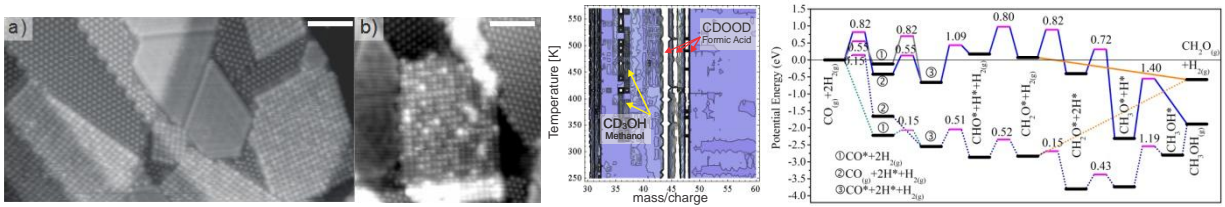


Fig. 1 Left panel: a) MoS<sub>2</sub> (central), Mo<sub>2</sub>S<sub>3</sub> (nearly square) and S-terminated Cu (hexagonal) on a Cu(111) surface. Formic acid molecules exclusively stick on the Mo<sub>2</sub>S<sub>3</sub> (and not on the MoS<sub>2</sub> step edges), as highlighted on the left, b). The center panel shows TPD from the surface under constant formic acid pressure. The right panel depicts the potential energies along the reaction pathway of the formation of CH<sub>3</sub>OH via the CO hydrogenation on MoS<sub>2</sub> with a row of sulfur-vacancies (Solid connections) and with a patch of 7 sulfur-vacancies (dotted connections). Thicker-longer bars represent the intermediate states while thinner-shorter bars represent transition states. Numbers (in eV) are energetic barriers. Superscript \* indicates adsorbed specie. Subscript (g) indicates gas phase.

from syngas to be more favorable for the layer with a sulfur-vacancy patch. The comparative reaction energetics for the two types of vacancy structures in Fig. 1 (right panel) show that while the vacancy patch is better suited for conversion of syn gas to methanol, there are still hurdles that need to be overcome before we arrive at optimal configurations that would facilitate the reaction. We have obtained similar results for water gas-shift reaction on defect laden MoS<sub>2</sub>, a manuscript of which is available.

An interesting finding in our DFT calculations for vacancy formation on one side of an MoS<sub>2</sub> layer is that vacancies tend to form rows: the formation energy per sulfur vacancy is the lowest when the vacancies form a row and that the longer the row, the lower the formation energy. In addition, we find that the lowest energy barrier for the diffusion of sulfur vacancy at the row structures through the exchange of a vacancy with a nearby sulfur atom is 0.79 eV and that this barrier increases as the row elongates. Guided by the above theoretical findings, we have fabricated vacancies on MoS<sub>2</sub> by means of sputtering of the substrate using low energy Ar<sup>+</sup> ions. To this end, we set up a vacuum system that allows in-vacuo photoluminescence spectroscopy. This task required integration of a laser system and a spectrometer with the vacuum chamber.

Since we found that MoS<sub>2</sub> grows as an inverted catalyst on Cu(111) only on the 10nm scale, we have also developed capabilities for the fabrication of MoS<sub>2</sub> monolayers on the micron (optical wavelength) scale. This was accomplished by using SiO<sub>2</sub>/Si as a substrate, which provides the added benefit of being inert/dielectric and, hence, does not quench the PL yield.

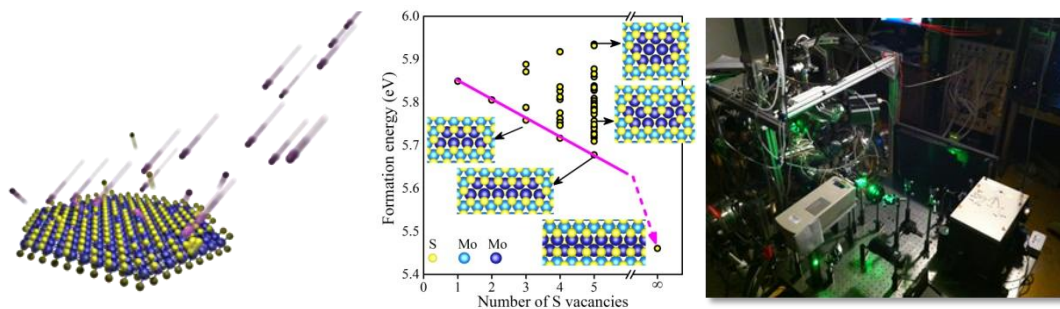


Fig. 2 (left) schematic representation of sulfur removal from MoS<sub>2</sub> via sputtering with low-energy Ar<sup>+</sup> ions. (center) Calculated formation energy of sulfur-vacancies on MoS<sub>2</sub>. Each data point (circle) represents the formation energy of a vacancy structure. The magenta line connects the data of sulfur-vacancy row. (right) UHV chamber (back) with attached setup for in-vacuo PL spectroscopy (front)

To utilize sputtering to create a defined number of vacancies, the first question we had to answer was whether sputtering allows the material to remain integral overall or leads to a randomized structure. We used XPS to ascertain that the core level signature (i.e., oxidation states) of the material's components

remain unchanged. After sputtering we find the material to be sulfur deficient (by up to ¼ of the initial amount) and air sensitive, validating that we indeed activated it.

Concurrent PL measurements reveal a vacancy induced dimming of the native photoluminescence (PL) yield of MoS<sub>2</sub>. PL spectroscopy, once a system is set up for it, is a very facile and rapid way of monitoring material quality and the presence/absence of defects. Our research effort in the first year of the current grant was to ascertain that we can utilize PL spectroscopy for real-time following of surface reactions. In this context, we deposited a sulfur source (benzenethiol) both on an unperturbed and a sputtered MoS<sub>2</sub> film. In the case of the unperturbed film, we deposited the sulfur source at cryogenic temperature and see a decrease of the PL intensity due to the presence of the physisorbed species. The material regains its original PL yield once a temperature is reached, at which benzenethiol desorbs thermally (Fig. 3, bottom left). At higher temperatures, the PL intensity resembles that of the untreated substrate. In contrast, if we first sputter the sample, we see low PL intensity both at low and high temperature (Fig. 3, bottom right). Annealing in the presence of the sulfur source recovers the PL intensity almost completely. This finding verifies that we can create vacancies that are sufficiently localized and embedded in an intact MoS<sub>2</sub> film, so as to serve as a test bed for local surface reactivity. Currently, we are setting up a manipulator whose heating elements remain dark (and, thus, do not interfere with PL measurements) at realistic process temperatures of MoS<sub>2</sub>, so that we can monitor activity of the film under realistic conditions.

### Submicron Scale Monitoring of Catalyst Performance

PL measurements have over the past year attained interest in the DOE BES Catalysis community because efforts such as those led by Peng Chen at Cornell or Suzanne Blum in Irvine have shown that PL permits real-time monitoring of catalytic reactions. MoS<sub>2</sub> offers an advantage over other catalytic systems, that here the untreated catalyst is PL active so that no specific chromophores as reactants or spectators are required. We are currently setting up a reactor chamber, in which we can rapidly vary the pressure over more than 10 orders of magnitude (UHV to a few atmospheres) and the temperatures from cryogenic to beyond the decomposition temperature of MoS<sub>2</sub> while maintaining sub-micron optical resolution of a set of MoS<sub>2</sub> catalyst islands. Fig. 4 shows a set of MoS<sub>2</sub> catalyst islands on the left as optical image and on the right by their PL emission in the spectral range between 675 and 685 nm.

In the first data from this setup (Fig. 4), each MoS<sub>2</sub> single-layer islands is about 1-3 micron in size) with jagged edges reflecting their domain structure. Variation of the nitrogen

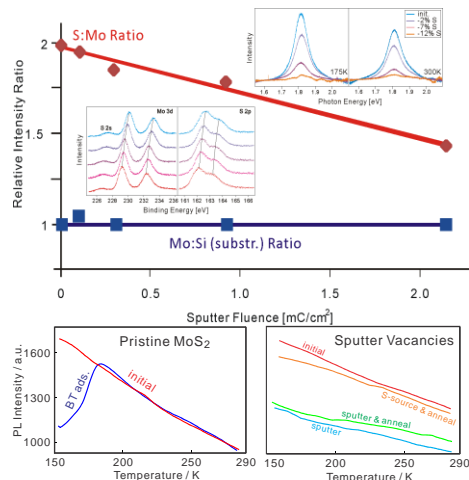


Fig. 3 (too) Molybdenum to substrate and sulfur to molybdenum ratios as obtained by XPS measurements (left inset) during the sputtering of an MoS<sub>2</sub> film. The absence of a marked change in the spectra indicates that the MoS<sub>2</sub> stays overall intact. The right inset shows the concurrent reduction in PL yield. (bottom left) PL intensity of an MoS<sub>2</sub> film before (red) and after adsorption of benzenethiol (BT) at cryogenic temperatures. The recovery of PL signal at 180K coincides with the desorption of intact BT. (bottom right) PL intensity of an MoS<sub>2</sub> film prior to (red) and after (blue) creating sputter-induced vacancies, after subsequent anneal (green) and after exposure to BT and renewed anneal (orange).

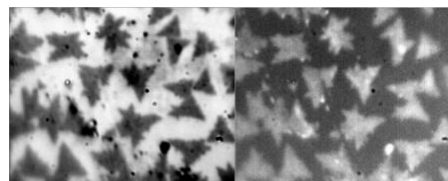


Fig. 4: (left) visible light image of about 1 micron size single-layer MoS<sub>2</sub> islands on SiO<sub>2</sub> in high vacuum. (right) direct imaging of photoluminescence from these islands during excitation with a 532 nm filter. Exclusively PL light in the 675-685 nm range was used to acquire this image.



## Publications Acknowledging this Grant in 2011-2014

1. Tenney, S.; He, W.; Ratliff, J.; Mullins, D.; Chen, D., Characterization of Pt–Au and Ni–Au Clusters on TiO<sub>2</sub>(110). *Top. Catal.* **2011**, *54* (1-4), 42-55.
2. Zhao, L.; Rim, K. T.; Zhou, H.; He, R.; Heinz, T. F.; Pinczuk, A.; Flynn, G. W.; Pasupathy, A. N., Influence of copper crystal surface on the CVD growth of large area monolayer graphene. *Solid State Commun.* **2011**, *151* (7), 509-513.
3. Tenney, S. A.; He, W.; Roberts, C. C.; Ratliff, J. S.; Shah, S. I.; Shafai, G. S.; Turkowski, V.; Rahman, T. S.; Chen, D. A., CO-Induced Diffusion of Ni Atoms to the Surface of Ni-Au Clusters on TiO<sub>2</sub>(110). *J. Phys. Chem. C* **2011**, *115* (22), 11112-11123.
4. Hong, S.; Rahman, T. S.; Ciftlikli, E. Z.; Hinch, B. J., Stress balance in nanopatterned N/Cu(001) surfaces. *Phys. Rev. B* **2011**, *84* (16), 165413.
5. Le, D.; Sun, D. Z.; Lu, W. H.; Bartels, L.; Rahman, T. S., Single layer MoS<sub>2</sub> on the Cu(111) surface: First-principles electronic structure calculations. *Phys. Rev. B* **2012**, *85* (7), 075429
6. Sun, D.; Lu, W.; Le, D.; Ma, Q.; Aminpour, M.; Alcantara Ortigoza, M.; Bobek, S.; Mann, J.; Wyrick, J.; Rahman, T. S.; Bartels, L., An MoS<sub>x</sub> Structure with High Affinity for Adsorbate Interaction. *Angew. Chem. Int. Ed.* **2012**, *51* (41), 10284-10288.
7. Le, D.; Kara, A.; Schroder, E.; Hyldgaard, P.; Rahman, T. S., Physisorption of nucleobases on graphene: a comparative van der Waals study. *J. Phys.: Condens. Matter* **2012**, *24* (42), 424210.
8. Turkowski, V.; Babu, S.; Le, D.; Kumar, A.; Haldar, M. K.; Wagh, A. V.; Hu, Z.; Karakoti, A. S.; Gesquiere, A. J.; Law, B.; Mallik, S.; Rahman, T. S.; Leuenberger, M. N.; Seal, S., Linker-induced anomalous emission of organic-molecule conjugated metal-oxide nanoparticles. *ACS Nano* **2012**, *6* (6), 4854-4863.
9. Le, D.; Aminpour, M.; Kiejna, A.; Rahman, T. S., The role of van der Waals interaction in the tilted binding of amine molecules to the Au(111) surface. *J. Phys.: Condens. Matter* **2012**, *24* (22), 222001.
10. Lewis, E. A.; Le, D.; Murphy, C. J.; Jewell, A. D.; Mattera, M. F. G.; Liriano, M. L.; Rahman, T. S.; Sykes, E. C. H., Dissociative Hydrogen Adsorption on Close-Packed Cobalt Nanoparticle Surfaces. *J. Phys. Chem. C* **2012**, *116* (49), 25868-25873.
11. Ge, L.; Zuo, F.; Liu, J.; Ma, Q.; Wang, C.; Sun, D.; Bartels, L.; Feng, P., Synthesis and Efficient Visible Light Photocatalytic Hydrogen Evolution of Polymeric g-C<sub>3</sub>N<sub>4</sub> Coupled with CdS Quantum Dots. *J. Phys. Chem. C* **2012**, *116* (25), 13708-13714.
12. Hou, Y.; Zuo, F.; Ma, Q.; Wang, C.; Bartels, L.; Feng, P., Ag<sub>3</sub>PO<sub>4</sub> Oxygen Evolution Photocatalyst Employing Synergistic Action of Ag/AgBr Nanoparticles and Graphene Sheets. *J. Phys. Chem. C* **2012**, *116* (38), 20132-20139.
13. Yeming, Z.; Jonathan, W.; Kamelia, D. C.; Katie Marie, M.; Connor, H.; Daniel, S.; Quan, M.; Dezheng, S.; Ludwig, B., Acetylene on Cu(111): imaging a molecular surface arrangement with a constantly rearranging tip. *J. Phys.: Condens. Matter* **2012**, *24* (35), 354005.
14. Galhenage, R. P.; Ammal, S. C.; Yan, H.; Duke, A. S.; Tenney, S. A.; Heyden, A.; Chen, D. A., Nucleation, Growth, and Adsorbate-Induced Changes in Composition for Co–Au Bimetallic Clusters on TiO<sub>2</sub>. *J. Phys. Chem. C* **2012**, *116* (46), 24616-24629.
15. Tenney, S. A.; Cagg, B. A.; Levine, M. S.; He, W.; Manandhar, K.; Chen, D. A., Enhanced activity for supported Au clusters: Methanol oxidation on Au/TiO<sub>2</sub>(110). *Surf. Sci.* **2012**, *606* (15-16), 1233-1243.
16. Mak, K. F.; He, K.; Lee, C.; Lee, G. H.; Hone, J.; Heinz, T. F.; Shan, J., Tightly bound triions in monolayer MoS<sub>2</sub>. *Nat Mater* **2013**, *12* (3), 207-11.
17. Berciaud, S.; Deshpande, V. V.; Caldwell, R.; Miyauchi, Y.; Voisin, C.; Kim, P.; Hone, J.; Heinz, T. F., All-optical structure assignment of individual single-walled carbon nanotubes from Rayleigh and Raman scattering measurements. *Phys. Status Solidi B* **2012**, *249* (12), 2436-2441.
18. Le, D.; Rahman, T. S., Joined edges in MoS<sub>2</sub>: metallic and half-metallic wires. *J. Phys.: Condens. Matter* **2013**, *25* (31), 312201-1–5.

19. Ma, Q.; Odenthal, P. M.; Mann, J.; Le, D.; Wang, C. S.; Zhu, Y.; Chen, T.; Sun, D.; Yamaguchi, K.; Tran, T.; Wurch, M.; McKinley, J. L.; Wyrick, J.; Magnone, K.; Heinz, T. F.; Rahman, T. S.; Kawakami, R.; Bartels, L., Controlled Argon Beam-Induced Desulfurization of Monolayer Molybdenum Disulfide. *J. Phys.: Condens. Matter* **2013**, *25*, 252201-1-5.
20. Hong, S.; Le, D.; Rahman, T., Deactivation of Cu<sub>2</sub>O(100) by CO Poisoning. *Top. Catal.* **2013**, *56* (12), 1082-1087.
21. Le, D.; Sun, D.; Lu, W.; Aminpour, M.; Wang, C.; Ma, Q.; Rahman, T. S.; Bartels, L., Growth of aligned Mo<sub>6</sub>S<sub>6</sub> nanowires on Cu(111). *Surf. Sci.* **2013**, *611*, 1-4.
22. Restrepo, D. T.; Giesler, K. E.; Penabe, R. A.; Aminpour, M.; Le, D.; Rahman, T. S.; Blair, R. G., Heterogeneous Metal-Free Hydrogenation Over Defect Hexagonal Boron Nitride. **Resubmit to Science**.
23. Shah, S. I.; Hong, S.; Rahman, T. S., Combined Density Functional Theory and Kinetic Monte Carlo Study of Selective Oxidation of NH<sub>3</sub> on Rutile RuO<sub>2</sub>(110) at Ambient Pressures. *J. Phys. Chem. C* **2014**, *118* (10), 5226-5238.
24. Hong, S.; Rahman, T. S., Rationale for the Higher Reactivity of Interfacial Sites in Methanol Decomposition on Au<sub>13</sub>/TiO<sub>2</sub>(110). *J. Am. Chem. Soc.* **2013**, *135* (20), 7629-7635.
25. Mann, J.; Ma, Q.; Odenthal, P. M.; Isarraraz, M.; Le, D.; Preciado, E.; Barroso, D.; Yamaguchi, K.; von Son Palacio, G.; Nguyen, A.; Tran, T.; Wurch, M.; Nguyen, A.; Klee, V.; Bobek, S.; Sun, D.; Heinz, T. F.; Rahman, T. S.; Kawakami, R.; Bartels, L., 2-Dimensional Transition Metal Dichalcogenides with Tunable Direct Band Gaps: MoS<sub>2(1-x)</sub>Se<sub>2x</sub> Monolayers. *Adv. Mater.* **2014**, *26* (9), 1399-404.
26. Le, D.; Rawal, T. B.; Rahman, T. S., Single-Layer MoS<sub>2</sub> with Sulfur Vacancies: Structure and Catalytic Application. *J. Phys. Chem. C* **2014**, *118* (10), 5346-5351.
27. Ma, Q.; Isarraraz, M.; Wang, C. S.; Preciado, E.; Klee, V.; Bobek, S.; Yamaguchi, K.; Li, E.; Odenthal, P. M.; Nguyen, A.; Barroso, D.; Sun, D.; von Son Palacio, G.; Gomez, M.; Nguyen, A.; Le, D.; Pawin, G.; Mann, J.; Heinz, T. F.; Rahman, T. S.; Bartels, L., Post-Growth Tuning of the Bandgap of Single-Layer Molybdenum Disulfide Films by Sulfur/Selenium Exchange. *ACS Nano* **2014**, DOI 10.1021/nm5004327.
28. Mann, J.; Sun, D. Z.; Ma, Q.; Chen, J. R.; Preciado, E.; Ohta, T.; Diaconescu, B.; Yamaguchi, K.; Tran, T.; Wurch, M.; Magnone, K.; Heinz, T. F.; Kellogg, G. L.; Kawakami, R.; Bartels, L., Facile growth of monolayer MoS<sub>2</sub> film areas on SiO<sub>2</sub>. *Eur. Phys. J. B* **2013**, *86* (5), 226-1-4.
29. Lewis, E. A.; Le, D.; Jewell, A. D.; Murphy, C. J.; Rahman, T. S.; Sykes, E. C. H., Visualization of Compression and Spillover in a Coadsorbed System: Syngas on Cobalt Nanoparticles. *ACS Nano* **2013**, *7* (5), 4384-4392.
30. Lewis, E. A.; Le, D.; Jewell, A. D.; Murphy, C. J.; Rahman, T. S.; Sykes, E. C. H., Segregation of Fischer-Tropsch reactants on cobalt nanoparticle surfaces. *Chem. Commun.* **2014**, DOI 10.1039/C4CC01680G.

**Bridging Molecules and Surfaces for Energy-Relevant Catalytic Chemical Transformations**

Bart M. Bartlett, Benjamin M. Klepser, James J. Brancho, and Kayla J. Pyper  
University of Michigan, Department of Chemistry  
bartmb@umich.edu

**Presentation Abstract**

Converting solar energy to chemical energy is a major challenge for generating hydrogen from water and for improving the atom economy of small-molecule transformations. For activating water, molecular catalysts can help overcome the kinetic limitations of water oxidation and typically generate oxygen faster than do semiconductor photoelectrocatalysts. However, molecular catalysts typically require sacrificial oxidants (e.g.—Ce<sup>4+</sup> or S<sub>2</sub>O<sub>8</sub><sup>2-</sup>), and they only operate in the dark unless a separate photosensitizing component is added. To address these drawbacks, an iron complex, Fe(tebppmcn)Cl<sub>2</sub> (**1**, tebppmcn = tetraethyl*N,N'*-bis(2-methylpyridyl-4-phosphonate)-*N,N'*-dimethyl-cyclohexyldiamine) has been tethered to the semiconductor, WO<sub>3</sub> through its phosphonate linker to generate a solar-responsive oxygen-evolving system (**1**-WO<sub>3</sub>). **1**-WO<sub>3</sub> exhibits a 61% increase in selectivity for water oxidation (over sulfate oxidation) in acidic sulfate solution. Preliminary data for the copper analog shows nearly *quantitative* conversion to O<sub>2</sub> with 14 hours of continuous 1-sun illumination. Copper is of particular interest because other work in our group establishes that the copper-based hole in the semiconductor CuWO<sub>4</sub> is not as oxidizing as •OH generated on WO<sub>3</sub>, allowing this strategy to translate to organic transformations. As proof of concept, CuWO<sub>4</sub> can perform selective oxidative coupling of amines to imines. These efforts present a new avenue toward bridging homogeneous catalysts and substrates and semiconductor photoelectrodes to eliminate the need for sacrificial oxidants for energy-relevant chemistry.

**DE-FG02-11ER16262: Bridging Homogeneous and Heterogeneous Catalysis through Ion-Exchangeable Materials**

**Students: Tanya M. Breault and Benjamin M. Klepser**

**RECENT PROGRESS**

***Synthesis and Characterization of Visible-Light Absorbing TiO<sub>2</sub>:(Nb,N) Semiconductors***

Synthesizing narrow band gap semiconductors that absorb longer wavelengths of the solar spectrum ( $\lambda \leq 550$  nm) is an active research area focusing on using sunlight and a photocatalyst for water splitting to evolve hydrogen gas as renewable energy. Harnessing the energy of sunlight through electron transfer is also useful for environmental remediation since industrial effluents often contain a high concentration of organic dyes that require degradation. The goal of this project was to create lower band-gap materials by alloying donor-acceptor pairs. Ti<sub>1-x</sub>Nb<sub>x</sub>O<sub>2-x</sub>N<sub>x</sub> is our target composition for visible-light dye degradation and water oxidation

photocatalysts. Furthermore, knowing the mechanistic pathways by which organic dyes are degraded allows us to target new catalytic organic transformations relevant to energy science.

A series of co-incorporated compounds,  $\text{TiO}_2:(\text{Nb},\text{N})$ , were synthesized via a facile sol-gel process. This technique allows us to synthesize mono-alloyed compositions,  $\text{Ti}_{1-(5x/4)}\text{Nb}_x\text{O}_2$ , which are converted to co-incorporated forms by annealing under flowing ammonia to afford  $\text{Ti}_{1-(5x/4)}\text{Nb}_x\text{O}_{2-y-\delta}\text{N}_y$ , referred to as NbN- $x$ , where  $x = 1 - 30\%$  niobium. The series of compounds crystallize in the anatase structure, determined by powder X-ray diffraction. Diffuse reflectance UV-vis spectroscopy in Figure 1 shows that the indirect band gap

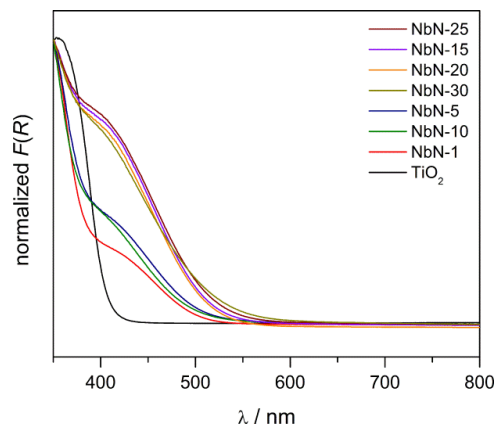


**Figure 1.** Optical gap changes as a function of Nb loading in  $\text{TiO}_2:(\text{Nb},\text{N})$ .

ranges from 2.37 eV ( $x = 1$ ) to 2.20 eV ( $x = 30$ ). Without the nitridation treatment, *all* compounds display a band-gap energy of  $\sim 3.1$  eV, the same as that of pure anatase  $\text{TiO}_2$ .

The XP spectra for the N(1s) peak in all samples exhibit peaks centered around 400 eV, which are attributed to interstitial nitrogen ( $\text{N}_i$ ) in an N–O–Ti chemical environment. The line at 396 eV is the reference line for substitutional nitrogen ( $\text{N}_s$ ) in TiN, forming a N–Ti–N environment. The intensity of the peak increases with increasing niobium incorporation, suggesting the amount of nitrogen replacing oxygen on the titania lattice increases with increasing mole-percent of niobium. This result is also consistent with the decrease in band gap with increasing niobium content, suggesting that high mole-percent niobium allows for increased solubility of nitrogen ( $\text{N}_s$ ). Furthermore, EPR results support this concept: the  $\text{Ti}^{3+}$  signal decreases with increasing mole-percent niobium. This observation also provides evidence for greater charge compensation between niobium and nitrogen at high mole-percents niobium, resulting in less  $\text{Ti}^{3+}$ .

### ***Photocatalytic Activity on Visible-Light Absorbing $\text{TiO}_2:(\text{Nb},\text{N})$ Semiconductors***

Methylene blue (MB) degradation was performed in order to interrogate the photocatalytic activity of these compounds. We note that as the mole-percent of niobium increases, the rate of dye degradation also increases ( $k_{40 \text{ ppm MB, max}} \sim 0.779 \text{ h}^{-1}$ , NbN-25). The fastest degradation rates also correspond to the compounds with the smallest band-gap values by UV-vis spectroscopy, the weakest  $\text{Ti}^{3+}$  signals in the EPR spectra, and the greatest quantity of substitutional nitrogen by XPS analysis. We proposed that in addition to giving rise to larger band gaps,  $\text{Ti}^{3+}$  sites can act as charge recombination centers for small  $x$  and decrease the rate of dye degradation for these compounds with low mole-percent niobium incorporation. We probed the mechanistic pathway for dye degradation, and found that degradation was favored over simple photobleaching, with identified reactive species including superoxide radicals and hydroxyl radicals. Upon illumination, the photogenerated active species results in products such as the azure dyes and thionine, as well as ring breaking products that include 4-((hydroxymethyl)(methyl)amino)benzene-1,2-diol, benzenesulfonic acid, and dimethylaniline, illustrated in Figure 2.

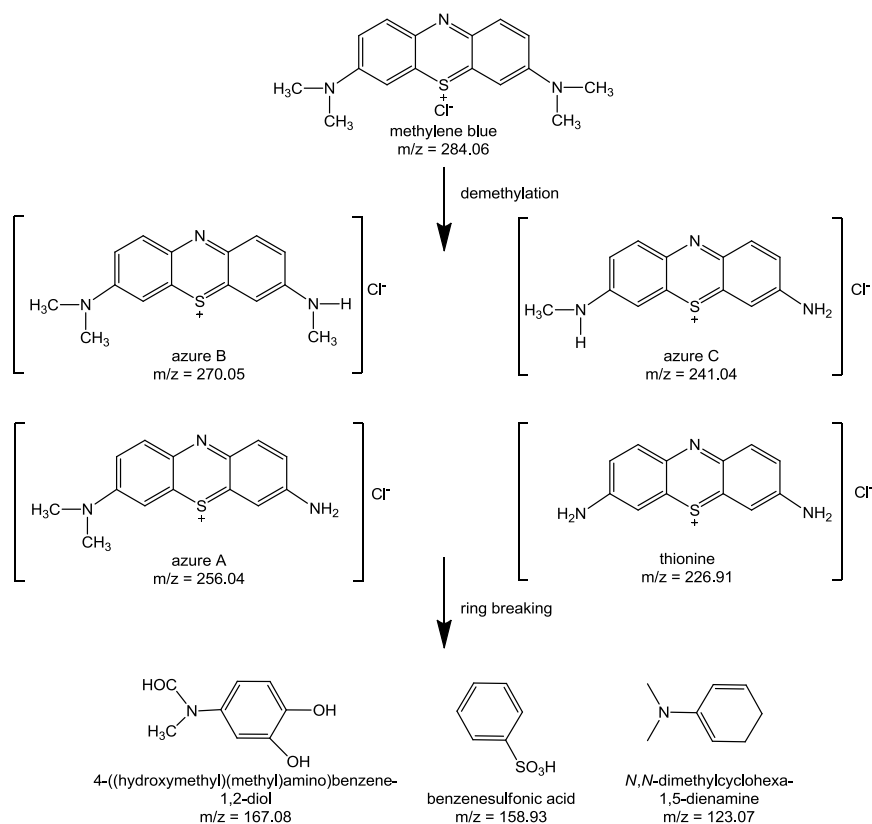


**Figure 2.** Methylene blue dye degradation products observed by ESI-MS analysis.

yielding the fastest rate for water oxidation ( $\sim 7 \mu\text{mol O}_2 \text{ h}^{-1}$ ). NbN-25 was tested as a water oxidation photocatalyst in 1 mM  $\text{NaIO}_3$  under solar simulated irradiation (AM1.5G filter). Without added  $\text{RuO}_2$ , no oxygen is evolved, even when the irradiance is increased to  $\sim 600 \text{ mW/cm}^2$ . Under 6-sun illumination of a 1 mM  $\text{NaIO}_3$  solution with 1 wt%  $\text{RuO}_2$  loaded onto NbN-25, 16  $\mu\text{mol O}_2$  are observed after 3 hours of irradiation. Notably, the control experiment shows that no oxygen is generated in the dark with 1 wt%  $\text{RuO}_2$  loaded.

Important to photo-catalysis, we investigated the visible light response of this compound by using a 150 W Xe lamp fitted with a water filter to eliminate IR light that can cause fluctuating temperatures that occur upon illumination ( $T = 23 \pm 3 \text{ }^\circ\text{C}$ ). The reaction conditions included 50 mg of catalyst in 30 mL of  $\text{N}_2$ -purged 1 mM  $\text{NaIO}_3$  solution in an air tight cell. The cut-on filters used to probe oxygen evolution at longer wavelengths included  $\lambda \geq 295, 400, 455$  and 515 nm. The irradiance for each experiment was  $\sim 600 \text{ mW/cm}^2$ . Figure 3 highlights that oxygen evolution tracks the absorption profile of the semiconductor; maximum  $\text{O}_2$  is evolved ( $\sim 33 \mu\text{mol}$ ) when UV light is included ( $\lambda \geq 295$ ), but  $\text{O}_2$  evolution persists under solely visible wavelengths. Oxygen detection at longer wavelengths suggests that the N-based impurity levels formed above the  $\text{O}(2p)$  valence

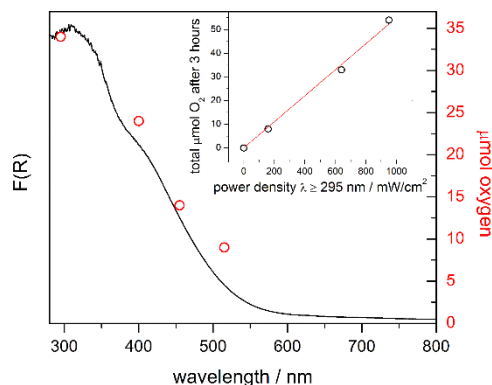


**Figure 3.** Dependence of  $\text{O}_2$  evolution after 3 h irradiation with cut-on filters for NbN-25 loaded with 1wt%  $\text{RuO}_2$  (red). The diffuse reflectance spectrum of NbN-25 is also shown (black). Reaction conditions: 50 mg catalyst, 1 mM  $\text{NaIO}_3$  (30 mL), 150 W Xe lamp with water filter, custom built Pyrex cell fit with quartz window.

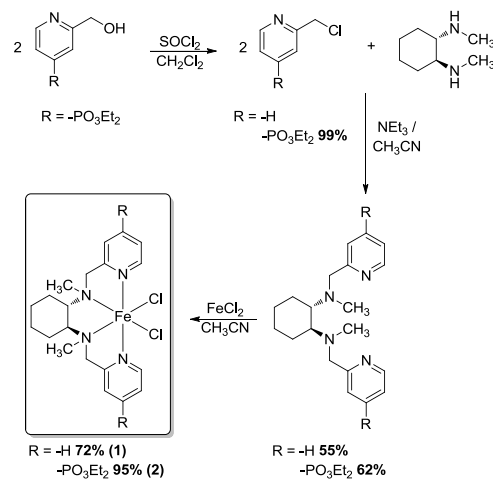
We also showed that in addition to redox chemistry leading to dye degradation by active oxygen species, our champion compound, NbN-25, acts as a visible-light responsive water oxidation photocatalyst in the presence of a cocatalyst and an electron acceptor. An impregnation technique was used to load the desired quantity of  $\text{RuO}_2$  cocatalyst, starting from  $\text{RuCl}_3 \cdot 3\text{H}_2\text{O}$  followed by annealing for 1 hour at  $350 \text{ }^\circ\text{C}$  to maintain  $\text{N}_5$  in the compound, confirmed by X-ray photoelectron spectroscopy. The cocatalyst loading percent was optimized, with 1 wt%  $\text{RuO}_2$

band, formed by introducing both  $\text{Nb}^{5+}$  and  $\text{N}^{3-}$  in anatase, contribute to the photocatalytic activity of this co-incorporated compound for water oxidation.  $\text{O}_2$  evolution after 3 h using the 295 nm cut-on filter increases linearly with spectral irradiance (shown as the inset of Figure 3).

### Tethering Molecular Catalysts to the Visible-Light Absorbing Solid-State Semiconductor, $\text{WO}_3$

Molecular catalysts are attractive because of their chemo-selectivity, fast reaction rates, and readily characterized mechanisms. However, many molecular catalysts for high-energy transformations such as water oxidation require sacrificial reagents such as ceric ammonium nitrate (CAN). As a result, the atom economy of these reactions is often limited to the selected oxidant. Since the primary function of the sacrificial oxidant is to accept electrons irreversibly, we recently proposed that the electrons stored in the catalyst could be transferred to photogenerated holes from semiconductor electrodes under illumination. However, for rapid reaction rates, the molecular catalyst must be tethered to the electrode surface. We have recently

demonstrated that we can covalently anchor a derivative of the known molecular water oxidation catalyst  $\text{Fe}(\text{bpmcn})\text{Cl}_2$  (bpmcn = bis- $N,N'$ -(2-pyridylmethyl)- $N,N'$ -dimethyl-transcyclohexyldiamine) using a diethyl-phosphonate anchor (**2** =  $\text{Fe}(\text{tebpmcn})\text{Cl}_2$ ) illustrated in Scheme 1. Since this catalyst best functions under acidic conditions, we synthesized  $\text{WO}_3$  as the semiconducting photoelectrode since it gives the highest photocurrent in acids. We observe a nearly two-fold enhancement the current density and also the chemoselectivity for water oxidation in the presence of sulfate anions (the electrolyte) as depicted in Figure 4. This finding demonstrates the proof of concept that we initially proposed: the sacrificial oxidant CAN is replaced by photoelectrochemically generated holes in  $\text{WO}_3$ .



**Scheme 1**

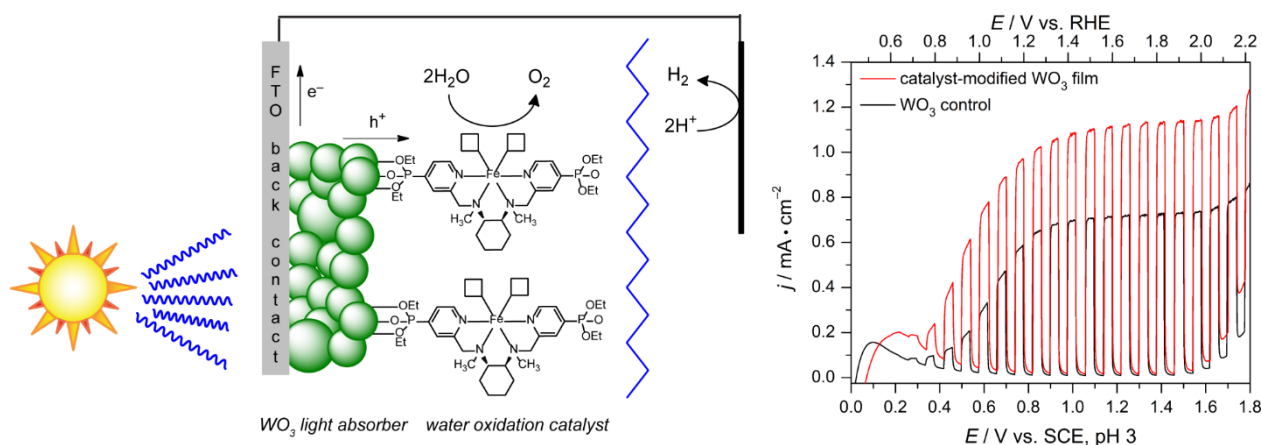


**Figure 4.** Photocurrent enhancement of **1**- $\text{WO}_3$  electrodes in pH 3  $\text{Na}_2\text{SO}_4$  under  $100 \text{ mW cm}^{-2}$  AM 1.5G at 1.23 V vs. NHE.

### Publications Acknowledging this Grant in 2011-2014

1. Breault, T. M.; Bartlett, B. M. Lowering the Band Gap of Anatase-structured  $\text{TiO}_2$  by Co-Alloying with Nb and N: Electronic Structure and Photocatalytic Degradation of Methylene Blue Dye. *J. Phys. Chem. C* **2012**, *116*, 5986-5994.
2. Breault, T. M.; Bartlett, B. M. Composition-Dependence of  $\text{TiO}_2:(\text{Nb},\text{N})-x$  Compounds on the Rate of Photocatalytic Methylene Blue Dye Degradation. *J. Phys. Chem. C* **2013**, *117*, 8611-8618.
3. Breault, T. M.; Brancho, J. J.; Guo, P.; Bartlett, B. M. Visible Light Water Oxidation Using a Co-Catalyst Loaded Anatase-Structured  $\text{Ti}_{1-(5x/4)}\text{Nb}_x\text{O}_{2-y-\delta}\text{N}_y$  Compound. *Inorg. Chem.* **2013**, *52*, 9363-9368.
4. Klepser, B. M.; Bartlett, B. M. Anchoring a Molecular Iron Catalyst to Solar-Responsive  $\text{WO}_3$  Improves the Rate and Selectivity of Photoelectrochemical Water Oxidation *J. Am. Chem. Soc.* 2014, *136*, 1694-1697.

## Catalysts for the Selective Oxidation of Hydrocarbons

Alexis T. Bell

Lawrence Berkeley National Laboratory  
 Division of Chemical Science  
 Berkeley, CA 94720

## Abstract

## FWP CH030201; Catalysis Research Program

## RECENT PROGRESS

*Synthesis and characterization of high-surface area oxides*

Highly dispersed metal oxide species exhibit high activity for the selective oxidation of hydrocarbons and alcohols, for the metathesis of alkenes, and alcohol dehydration. The activity and selectivity of such species are particularly sensitive to the local composition and structure of the active site. The goal of our research is to relate the local composition and structure of catalytically active sites to their activity and selectivity. This effort has focused on the preparation of isolated-site metal oxo species, and in particular vanadate species supported on either silica or silica modified by a layer of titania, zirconia, or ceria grafted onto the silica using organometallic precursors.<sup>1-3</sup> Characterization of the modifier by Raman and UV-Visible spectroscopy, XANES, and EXAFS revealed that deposited layer is two-dimensional in structure anchored to the silica surface by M-O-Si bonds. Isolated vanadates species were then grafted onto the support using  $\text{VO}(\text{O}^i\text{Pr})_3$  as the precursor. Spectroscopic characterization of the supported vanadate species revealed that they are present as  $\text{O}=\text{V}(\text{O}-\text{Si})_3$  or  $\text{O}=\text{V}(\text{O}-\text{M})_3$  (M = Ti, Zr, or Ce) species. The oxidation of methanol to formaldehyde was then used to probe the activity of these catalysts. Figure 1 shows that the activity of supported vanadate units is influenced to a greater degree by the coverage of silica by the modifier than by its composition.

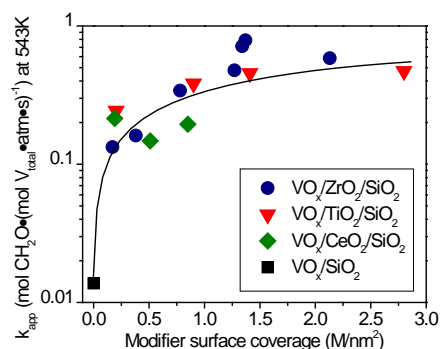


Fig. 1 Apparent rate constants for  $\text{VO}_x/\text{TiO}_2/\text{SiO}_2$ ,  $\text{VO}_x/\text{ZrO}_2/\text{SiO}_2$ , and  $\text{VO}_x/\text{CeO}_2/\text{SiO}_2$  as a function of  $\text{MO}_2$  surface density (M = Ce, Ti, Zr) at 543 K.

Sample Name	$k_{\text{app}}^0$ (mol $\text{CH}_2\text{O} \cdot (\text{mol V} \cdot \text{atm} \cdot \text{s})^{-1}$ )	$E_{\text{app}}$ (kcal $\text{mol}^{-1}$ )
$\text{VO}_x/\text{SiO}_2$	$2.3 \times 10^7$	23
$\text{VO}_x/\text{TiO}_2/\text{SiO}_2$	$1.8 \times 10^6$	18
$\text{VO}_x/\text{ZrO}_2/\text{SiO}_2$	$4.0 \times 10^6$	16
$\text{VO}_x/\text{CeO}_2/\text{SiO}_2$	$2.2 \times 10^6$	18

Table 1 Apparent pre-exponential factors and activation energies for  $\text{VO}_x/\text{TiO}_2/\text{SiO}_2$ ,  $\text{VO}_x/\text{ZrO}_2/\text{SiO}_2$ , and  $\text{VO}_x/\text{CeO}_2/\text{SiO}_2$ . All rate parameters were determined for a modifier coverage of  $1.5 \text{ M/nm}^2$  (M = Ti, Zr, Ce).

The rate parameters for formaldehyde oxidation are also significantly different for vanadate units supported on a monolayer of modifier oxide than on silica itself, but the differences in the rate parameters for the former group do not differ significantly. Quantum chemical simulation of methanol oxidation on silica- and titania- supported vanadate species indicate that while the first step of the reaction mechanism is the same for both systems and involves the equilibrated addition of methanol across a V-O-M (M = Si or Ti) bond, e.g.,  $\text{CH}_3\text{OH} + \text{O}=\text{V}(-\text{OM})_3 \leftrightarrow \text{O}=\text{V}(-\text{OM})_2(-\text{OCH}_3) + \text{M}-\text{OH}$ , the second, rate-limiting step is different.<sup>4</sup> For silica-supported vanadate species the rate limiting step is  $\text{O}=\text{V}(-\text{OM})_2(-\text{OCH}_3) \rightarrow \text{HO}-\text{V}(-\text{OM})_2(\text{OCH}_2)$ , whereas for titania-supported vanadate species the rate-limiting step is  $\text{O}=\text{V}(-\text{OM})_2(-\text{OCH}_3) + \text{M}-\text{O}-\text{M} \rightarrow \text{O}=\text{V}(-\text{OM})_2(-\text{OCH}_2) + \text{M}-\text{OH}-\text{M}$ .

### *Investigations of the mechanism and kinetics of hydrocarbon oxidation*

The selective oxidation of organic molecules is central to the production of both commodity and specialty products (e.g., aldehydes, alcohols, carboxylic acids, epoxides). While both mono- and multi-metallic oxides are used extensively for such applications, their selection is largely empirical. The goal of our work is to understand the roles of different metals in mixed oxides on the activity and selectivity of these oxides and to find descriptors that could relate the activity and oxide to its physical properties. To this end, we have focused first on the preparation, characterization, and evaluation of  $\text{Bi}_{(1-x)/3}\text{V}_{1-x}\text{Mo}_x\text{O}_4$  because this series of oxides can be prepared with only minor changes in the crystal structure as x is varied from 0 to 1.0. Experimental studies were conducted to establish the role of composition on the activity and the rate parameters for propene oxidation to acrolein and this work was complemented by theoretical studies.

The activity and selectivity of  $\text{Bi}_{1-x/3}\text{V}_{1-x}\text{Mo}_x\text{O}_4$  for the oxidation of propene to acrolein changes in a systematic manner with  $x = \text{Mo}/(\text{Mo}+\text{V})$ .<sup>5</sup> The maximum activity for acrolein formation occurs at  $x = 0.45$ , whereas the maximum in the selectivity to acrolein (85%) occurs at  $x = 0.15$ . At temperatures above 573 K, the rate of acrolein formation is first order in the partial pressure of propene and zero order in the partial pressure of oxygen of all values of x between 0 and 1.0, suggesting that the catalyst is fully oxidized and that the formation of acrolein does not involve gas-phase  $\text{O}_2$ . Powder x-ray diffraction demonstrates that the crystal structure of  $\text{Bi}_{1-x/3}\text{V}_{1-x}\text{Mo}_x\text{O}_4$  varies only slightly with composition. XANES data reveal that  $\text{Bi}^{3+}$  is not reduced, but that  $\text{Mo}^{6+}$  is reduced to  $\text{Mo}^{5+}$  and  $\text{V}^{5+}$  is reduced to  $\text{V}^{4+}$  upon reaction with propene. Based on these observations and the measured kinetics for acrolein formation, we have proposed a mechanism for acrolein formation on  $\text{Bi}_2\text{Mo}_3\text{O}_{12}$  (see Figure 2). The rate-limiting step in this scheme involves abstraction of a hydrogen atom from the methyl group of propene to form an allylic species, which then rapidly reacts with a  $\text{Mo}=\text{O}$  group to form a  $\text{Mo}-\text{OCH}_2-\text{CH}=\text{CH}_2$  group. The resulting rate expression is fully consistent with the reaction kinetics. A model for the dependence of catalyst activity on catalyst composition was developed that correctly describes the experimental results. According to this model, vanadium and molybdenum are randomly distributed to form three types of sites (Mo-Mo, Mo-V, and V-V) each associated with its own set of rate parameters. Mo-V sites exhibit the highest activity. Since vanadium affects the ease of H abstraction, V-V and Mo-V sites are characterized by lower apparent activation energies compared to Mo-Mo site. The proposed model gives a very good description of the effects of catalyst composition on the rate of acrolein formation as a function of catalyst composition, and reactant partial pressures.

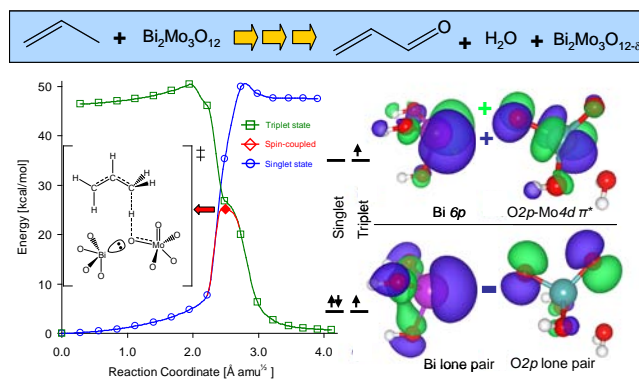


Figure 2. Mechanism for propene activation over  $\text{Bi}_2\text{Mo}_3\text{O}_{12}$ .

Figure 3. Energy profile for rate-limiting step and illustration of orbital overlap for Bi lone pair with  $\text{O}_{\text{eq}}$  of  $\text{Mo}=\text{O}$ .

Density functional theory calculations were performed using both the RPBE+U and M06-L functionals to study the conversion of propene to acrolein over the (010) surface of  $\alpha$ - $\text{Bi}_2\text{Mo}_3\text{O}_{12}$ .<sup>6,8</sup> The most active site for the initial, rate-determining hydrogen abstraction on the most abundant exposed surface is molybdenyl oxygen weakly coordinated to a proximal bismuth atom, designated as  $\text{O}_{\text{eq}}$ . Orbital interactions of bismuth with the O of the  $\text{Mo}=\text{O}$  center destabilizes the HOMO and stabilizes the LUMO on the molybdate unit, thereby facilitating the promotion of an electron into a  $\text{Mo}-\text{O} \pi^*$  orbital that must accompany the abstraction of hydrogen from propene. Figure 3 shows the energy profile for this rate-limiting step and the overlap of the Bi lone pair with  $\text{O}_{\text{eq}}$  of  $\text{Mo}=\text{O}$ .

The development of a descriptor or descriptors that can relate the activity of catalysts to their physical properties is a major objective of catalysis research. We have found that the apparent activation energy for the oxidation of propene to acrolein over scheelite-structured, multicomponent mixed metal oxides ( $\text{Bi}_3\text{FeMo}_2\text{O}_{12}$ ,  $\text{Bi}_2\text{Mo}_{2.5}\text{W}_{0.5}\text{O}_{12}$ , and  $\text{Bi}_{1-x/3}\text{V}_{1-x}\text{Mo}_x\text{O}_4$ , where  $0 \leq x \leq 1$ ) correlates with the band-gap of the catalyst measured at reaction temperature.<sup>10</sup> Theoretical analysis of the energy components comprising the activation energy show why the band-gap energy is the primary component dependent on catalyst composition and, hence, why one should expect the activation energy for propene oxidation to correlate with the band-gap energy. A further finding is that the change in band-gap energy with composition arises from the interplay between the sizes and energies of the V 3d, Fe 3d, Mo 4d, and W 5d orbitals that give rise to the lowest unoccupied crystal orbitals. Both the utility of the band gap energy as a descriptor for catalytic activity and the role of orbital overlap in determining the band gap are likely to be general features in mixed metal oxide oxidation catalysts, enabling the rational design of catalysts with greater activity for oxidation reactions.

#### *A novel approach for the synthesis of high surface area mixed metal oxide catalysts*

A significant limitation for our studies of metal oxide catalysts has been their low surface area ( $\sim 0.1 \text{ m}^2/\text{g}$ ) when prepared by conventional methods making it impossible to carry out studies of adsorbed species. To overcome this limitation, we have investigated the preparation of  $\text{Bi}_{1-x/3}\text{V}_{1-x}\text{Mo}_x\text{O}_4$  using high surface area silica and carbon templates.<sup>9</sup> The preparation of such oxides in mesoporous silica, MCM-48 and KIT-6, produced materials with high surface areas but removal of the silica template contaminated the surface of the oxide rendering it catalytically inactive. We therefore developed a double templating method. In this approach MCM-48 or KIT-6 was used as a template to form mesoporous carbon frameworks, CMK-1 or CMK-8. The silica template

was then removed, leaving behind the mesoporous carbon. The mesoporous carbon was then used as the template to form the mixed metal oxide via incipient wetness impregnation followed by drying and calcination in air. At the end of the last step, the carbon template was destroyed by combustion leaving behind a mesoporous monometallic or mixed metal oxide.  $\text{BiVO}_4$ ,  $\text{Bi}_{0.85}\text{V}_{0.55}\text{Mo}_{0.45}\text{O}_4$ , and  $\text{Bi}_2\text{Mo}_3\text{O}_{12}$  catalysts by this method had surface areas  $> 15 \text{ m}^2/\text{g}$  and catalytically active for propene oxidation to acrolein. Measured surface areas for  $\text{BiVO}_4$ ,  $\text{Bi}_{0.85}\text{V}_{0.55}\text{Mo}_{0.45}\text{O}_4$ , and  $\text{Bi}_2\text{Mo}_3\text{O}_{12}$  produced using a mesoporous carbon template are 350x, 90x, and 180x higher than reference materials prepared using conventional synthetic techniques.  $\text{Bi}_{0.85}\text{V}_{0.55}\text{Mo}_{0.45}\text{O}_4$  and  $\text{Bi}_2\text{Mo}_3\text{O}_{12}$  formed single phase materials, while partial segregation of  $\text{V}_2\text{O}_5$  was observed in the  $\text{BiVO}_4$  sample. The per-gram activities of the high-surface area oxides for propene oxidation to acrolein are 14-85 fold higher than those of catalysts produced via conventional hydrothermal synthesis and are stable over a 24 h period. While the acrolein selectivities of high-surface area  $\text{Bi}_{0.85}\text{V}_{0.55}\text{Mo}_{0.45}\text{O}_4$ , and  $\text{Bi}_2\text{Mo}_3\text{O}_{12}$  are comparable to those of conventionally prepared materials, high surface area  $\text{BiVO}_4$  has lower acrolein selectivity than its low-surface area analog. This difference is attributed to  $\text{V}_2\text{O}_5$  formation during the preparation of high-surface area  $\text{BiVO}_4$ .

#### Publication Acknowledging this Grant in 2011-2014

1. Strunk, J.; Vining, W. C.; Bell, A. T. Synthesis of Different  $\text{CeO}_2$  Structures on Mesoporous Silica and Characterization of Their Reduction Properties, *J. Phys. Chem. C* **2011**, *115*, 4114-4126.
2. Vining, W. C.; Strunk, J.; Bell, A. T. Investigation of the structure and activity of  $\text{VO}_x/\text{ZrO}_2/\text{SiO}_2$  catalysts for methanol oxidation to formaldehyde, *J. Catal.* **2011**, *281*, 222-230.
3. Vining, W. C.; Strunk, J.; Bell, A. T. Investigation of the structure and activity of  $\text{VO}_x/\text{CeO}_2/\text{SiO}_2$  catalysts for methanol oxidation to formaldehyde, *J. Catal.*, **2012** *285*, 160-167.
4. Shapovalov, V.; Fievez, T.; Bell, A. T., A Theoretical Study of Methanol Oxidation Catalyzed by Isolated Vanadia Clusters Supported on the (101) Surface of Anatase, *Journal of Physical Chemistry C* **2012**, *116*, 18728.
5. Zhai, Z.; Getsoian, A. B.; Bell, A. T., The kinetics of selective oxidation of propene on bismuth vanadium molybdenum oxide catalysts, *J. Catal.* **2013**, *305*, 25-36.
6. Getsoian, A. B.; Shapovalov, V.; Bell, A.T. DFT+U Investigation of Propene Oxidation over Bismuth Molybdate: Active Sites, Reaction Intermediates, and the Role of Bismuth, *J. Phys. Chem. C* **2013**, *117*, 7123.
7. Rumberger, E. M.; Ahn, H. S.; Bell, A. T.; Tilley, T. D. Water oxidation via immobilization of the dimanganese complex  $[\text{Mn}-2(\mu\text{-O})(2)(\mu\text{-O}_2\text{CCH}_3)\text{-}(\text{bpy})(2)(\text{H}_2\text{O})]$  onto silica, *Dalton Trans.* **2013**, *42*, 12238-12247.
8. Getsoian, A.; Bell, A. T. The Influence of Functionals on Density-Functional Theory Calculations of Reducible Transition Metal Oxide Catalysts, *J. Phys. Chem. C*, **2013**, *117*, 25562-25578.
9. Nell, A.; Getsoian, A.; Werner, S.; Kiwi, L.; Bell, A. T. Preparation and Characterization of High Surface Area  $\text{Bi}_{1-x/3}\text{V}_{1-x}\text{Mo}_x\text{O}_4$  Catalysts, *Langmuir* **2014**, *30*, 873-880.
10. Getsoian, A.; Zhai, Z.; Bell, A. T. Band Gap Energy as a Descriptor of Catalytic Activity for Propene Oxidation over Mixed Metal Oxide Catalysts, *J. Am. Chem. Soc.*, submitted.

## Catalytic deoxygenation

Aditya Bhan

Department of Chemical Engineering and Materials Science, University of Minnesota

### Abstract

The  $(\text{CH}_2\text{O})_n$  stoichiometry of biomass implies that its conversion to energy carriers and other petroleum-derived hydrocarbons centers on the removal of oxygen. This presentation will discuss cases studies of hydrodeoxygenation chemistry on metal carbide catalysts. Specifically, it will include a discussion of: (i) the potential for using  $\text{CH}_4$  – instead of molecular hydrogen – so that in essence,  $\text{CH}_4$  serves as a surrogate for molecular hydrogen for biomass deoxygenation while biomass serves as the oxygen carrier for hydrogen removal from  $\text{CH}_4$ ; and (ii) the site requirements and mechanism for selectively cleaving C=O and C-O linkages in sugar and lignin monomers for the synthesis of bulk and specialty chemicals.

### **DE-SC000084818: One-pot catalytic conversion of biomass and alkanes: Kinetically coupling deoxygenation and dehydrogenation pathways**

Postdoc(s): None

Student(s): Jeremy Bedard, Mark Sullivan, Cha-Jung Chen

Affiliation: University of Minnesota, 421 Washington Ave SE, Minneapolis, MN 55455;

### Recent Progress

*Dehydroaromatization of  $\text{CH}_4$ ,  $\text{CH}_4/\text{H}_2$ , and  $\text{CH}_4/\text{C}_x\text{H}_y\text{O}_z$  mixtures:*

(a)  $\text{C}/\text{H}_{\text{eff}} < 0.25$ : Co-processing acetic acid, formic acid, or carbon dioxide with methane on Mo/ZSM-5 catalysts at 950 K resulted in reforming of the  $\text{CH}_4$ /oxygenate co-feed to produce CO and  $\text{H}_2$  upstream while concurrently oxidizing a part of the catalyst bed deeming it unavailable for  $\text{CH}_4$  dehydroaromatization. Oxygen is stoichiometrically removed as CO irrespective of the concentration or identity of the oxygenate and no change in the forward rate of benzene synthesis was observed at varying CO concentrations in the effluent. The  $\text{C}/\text{H}_{\text{eff}}$  ratio, defined as  $(\text{C-H})/\text{O}$ , represents a descriptor for all co-feeds that are stoichiometrically oxygen rich with respect to methane – the addition of all such co-feeds results in a decrease in the net rate of benzene synthesis because of (i) a fraction of the catalyst being unavailable for methane pyrolysis and (ii)

upstream production of hydrogen which consequently results in higher thermodynamic reversibility of CH<sub>4</sub> decomposition to benzene.

(b)  $C/H_{\text{eff}} > 0.25$ : The addition of co-feeds that are stoichiometrically carbon rich with respect to methane (e.g., CH<sub>3</sub>COCH<sub>3</sub> or CH<sub>3</sub>CH<sub>2</sub>CHO) resulted in an increase in the net benzene synthesis rate when co-processed with CH<sub>4</sub> (oxygenate/CH<sub>4</sub> = 0.01-0.1) over Mo/ZSM-5 formulations at 950 K. Isotopic and chemical transient studies suggest that benzene synthesis pathways in presence of oxygenates with  $C/H_{\text{eff}} > 0.25$  differ from those present when co-processing oxygen-rich hydrocarbons and that a fraction of the benzene is directly formed from the oxygenate.

*Hydrodeoxygenation on self-supporting metal carbide catalysts:* We report the selective deoxygenation of biomass-derived C<sub>2-3</sub> and C<sub>5-6</sub> oxygenates, and phenyl ethers over non-precious metal carbide catalysts for the synthesis of olefin and aromatic chemical precursors at atmospheric pressure and 420-520 K. Two characteristics of metal carbide formulations, the high selectivity for C-O bond cleavage and the near absence of sequential hydrogenation reactions of carbon-carbon double bonds, are distinct from what has been observed for hydrodeoxygenation on noble metal or hydrotreating catalysts, and these selectivity characteristics clearly demonstrate the potential of using metal carbides as deoxygenation catalysts. Chemical and structural characterization was combined with transient and steady state kinetic measurements, isotopic tracer methods, and probe reaction studies to infer that (i) high-surface area β-Mo<sub>2</sub>C formulations initially synthesized are modified in presence of the oxygenate such that sequential hydrogenation pathways are inhibited on the oxygen-modified catalyst, (ii) distinct sites are required for the activation of the oxygenate and molecular H<sub>2</sub>, and (iii) turnover rates normalized by the number of CO adsorption centers are nearly invariant suggesting that metallic sites are involved.

#### **Publications (2013-2014)**

1. J. W. Bedard, D-Y. Hong, A. Bhan “Co-processing CH<sub>4</sub> and oxygenates on Mo/H-ZSM-5: 2. CH<sub>4</sub>/CO<sub>2</sub> and CH<sub>4</sub>/HCOOH Mixtures” *Physical Chemistry Chemical Physics* **15** (2013) 12173-12179
2. J. W. Bedard, D-Y. Hong, A. Bhan “CH<sub>4</sub> dehydroaromatization on Mo/H-ZSM-5: 1. Effects of co-processing H<sub>2</sub> and CH<sub>3</sub>COOH” *Journal of Catalysis* **306** (2013) 58-67.

## Single-Molecule Fluorescence Microscopy Tools for Catalysis and Chemistry: Polymerization

Prof. Suzanne A. Blum  
University of California, Irvine

### Presentation Abstract

*DOE Interest and Global Interest in Catalysis:* Polymers are workhorse materials. The macroscopic properties of a polymer, e.g., its flexibility, melting point, chemical degradation, and optical characteristics, are determined partially by the microscopic arrangements of individual polymer strands. Multiple physical and chemical processes over the course of the reaction often determine this polymer morphology. Identification of the steps involved in these processes, their relative rates, and the mechanisms through which they dictate polymer morphology are therefore central for creating polymerization catalysts that produce materials of desired properties (project period schematic, Figure 1).

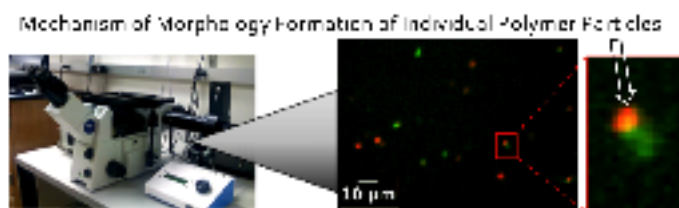


**Figure 1.** Project period schematic, single-particle and -molecule microscopy studies; showing green and orange fluorescent tools developed in our laboratory that enabled mechanistic insight into polymerization.

### Single-Molecule Fluorescence Imaging for Studying Organic, Organometallic, and Inorganic Reaction Mechanisms DE-FG02-08ER15994

**PI:** Prof. Suzanne A. Blum

**Postdocs:** Eva Hensle

**Students:** Alexander Fast, Quinn Easter, N. Melody Esfandiari, Yong Wang, Jonathan Y. Bass

**Affiliations:** University of California, Irvine

### RECENT PROGRESS

We established a single-particle and -molecule fluorescence imaging technique to address these questions. This thrust involved the synthesis of new organic probe molecules, development of microscopy conditions, image collection and data evaluation. This imaging revealed a precipitation polymerization process, the relative rates of certain chemical and physical steps, and an aggregation mechanism responsible for “dumbbell” polymer morphology in the polymerization of dicyclopentadiene catalysed by a ruthenium carbene complex, Grubbs 2nd generation catalyst. This information was obtained because of the ability of the technique to probe individual polymer particles (Figure 2).

Efficient catalysts exhibit high selectivity for the desired product. The structure of the catalyst can change over the course of the reaction—sometimes to degrade, sometimes to reveal a more selective cat-

alyst after an induction period. The ability to determine the time at which an individual product molecule of particular selectivity formed would allow more accurate modelling of the structure of the catalyst at that time. Single-particle fluorescence microscopic imaging permitted the identification of the time of formation of individual particles of polymer in this proof-of-concept study. These polymer particles were formed during the course of the ruthenium-catalyzed polymerization reaction described in Figure 3.

A timestamp or “pulse/chase” experiment swapped the solution of green BODIPY probe for a solution of orange BODIPY probe after 2.4 minutes of reaction. Otherwise identical polymers then could be identified by color as has having formed early in the reaction (green) or later in the reaction (orange) regardless of when the polymer precipitated (Figure 3). In this way, the ability to determine the timing of the chemical reaction that resulted in polymerization of an individual polymer molecule was decoupled from the timing of the observed physical precipitation process.

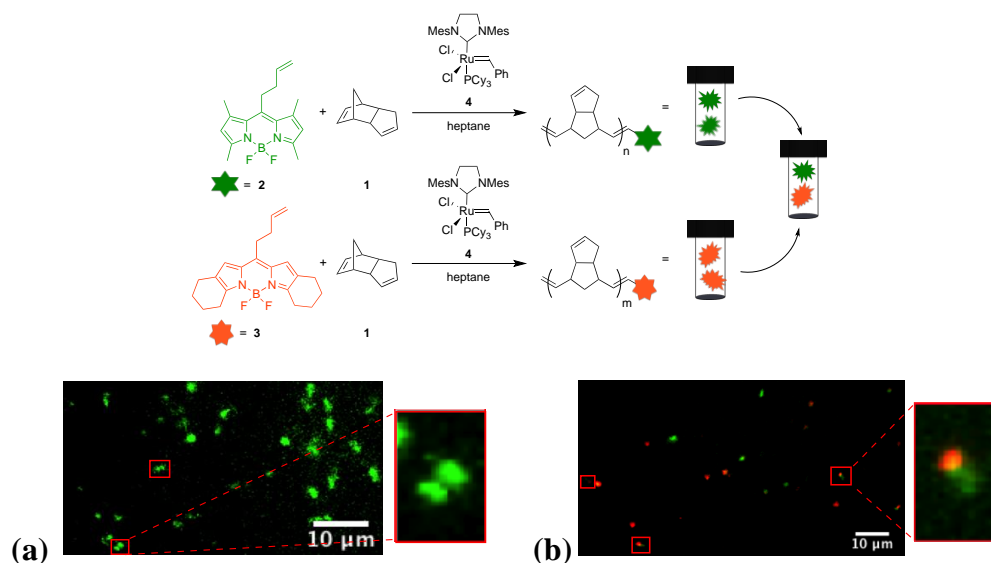


**Figure 2.** (a) Fluorescence microscopy image of DCPD polymerization at  $t = 187$  s showing dumbbell morphology of polymer particles (examples in red boxes). (b) Mixing experiment of DCPD polymerization using both fluorophores 2 and 3 revealed that aggregation of two preformed polymer particles is responsible for the dumbbell formation.

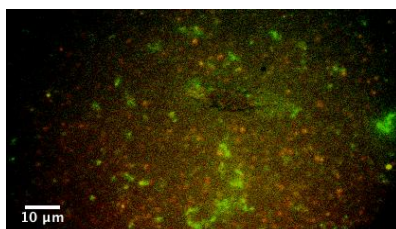


**Figure 3.** Timestamp or “pulse-chase” experiment with green and orange fluorescent polymers in same sample. Color of polymer particle indicates time of chemical synthesis, with green polymers synthesized at earlier reaction stages ( $<2.4$  min) and orange polymers synthesized at later reaction stages ( $>2.4$  min).

These experiments also determined that the active catalyst in a widely used polymerization system is exclusively homogeneous though fluorescence microscopy imaging; as the first such application, it demonstrated a new analytical tool for chemists to address this long-standing challenge of catalyst iden-

tification. Specifically, the location change microscopy method was employed to image the location of nascent polymers relative to a solid surface of a crystal of ruthenium metathesis catalyst at early reaction stages this way, the early stage polymers could be probed for their location: on the crystals (growing from them, heterogeneous catalysis) or in solution (homogenous catalysis).

Specifically, polymerization of dicyclopentadiene by Grubbs catalysts is used in the industrial synthesis of polydicyclopentadiene and in self-healing materials. In the case of self-healing materials, the catalytic reaction occurs in the presence of solid particles of metathesis catalyst embedded in wax, raising the possibility that the solid catalyst could contribute to the polymerization reactivity. Similarly, in the course of our studies, we noted that Grubbs II catalyst polymerized dicyclopentadiene in proximity to particles of solid Grubbs II, such that polydicyclopentadiene encapsulated the solid (Figure 3a).

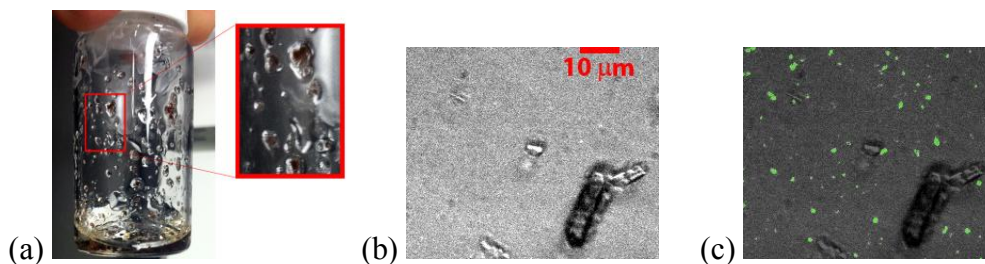


**Figure 3.** (a) Photograph of bench-scale experiment. Dicyclopentadiene polymerizes around solid particles of Grubbs II, encapsulating the solid maroon-colored precatalyst in clear polydicyclopentadiene. (b) A  $53 \mu\text{m} \times 63 \mu\text{m}$  microscope image with ambient light, showing individual crystals of Grubbs II on the surface of a glass microscope slide. (c) Overlay reveals that polymer growth is not spatially associated with solid particles of Grubbs II precatalyst. Fluorescent polymers are false colored green to facilitate spatial comparison. The location of the polymerization differentiates between homogeneous and heterogeneous catalysis.

This macroscale colocalization was consistent with the possibility that the polymerization could be occurring on the solid surface, as has been suggested recently for other polymerization catalysts. We then asked the fundamental question: Does this reaction occur by heterogeneous catalysis, homogeneous catalysis, or both? We developed and applied an analytical technique capable of directly imaging the location of polymer growth to differentiate between homogeneous and heterogeneous catalysis.

Our microcopy data revealed that dicyclopentadiene polymer growth occurred exclusively in solution by soluble homogeneous Grubbs II catalysts (Figure 3c). The solid precatalyst was unreactive toward polymerization and even single metathesis reactions. This method therefore provided an understanding of the nature of the active catalyst at a level of detail that would not be available from prior methods.

## Publications Acknowledging this Grant in 2011-2014

9. "BODIPY Fluorophore Toolkit for Probing Chemical Reactivity and for Tagging Reactive Functional Groups," Hensle, E. M.; Esfandiari, N. M.; Lim, S.-G.; Blum, S. A. **2014**. *Euro. J. Org. Chem.* Early View.
8. "Location Change Method for Imaging Chemical Reactivity and Catalysis with Single-Molecule and -Particle Fluorescence Microscopy," Blum, S. A. *Phys. Chem. Chem. Phys.* **2014**. Early view. *Invited Perspective*.
7. "Opportunities and Challenges in Single-Molecule and -Particle Fluorescence Microscopy for Mechanistic Studies of Chemical Reactions," Cordes, T.; Blum, S. A. *Nat. Chem.* **2013**, 5, 993–999. *Invited Perspective*.
6. "Small Number of Active Sites and Single-Locus Kinetics Revealed in (salph)Co-Catalyzed Ethylene Oxide Polymerization," Fast, A.; Esfandiari, N. M.; Blum, S. A. *ACS Catal.* **2013**, 3, 2150–2153.
5. "Phase Separation Polymerization of Dicyclopentadiene Characterized by In Operando Fluorescence Microscopy," Hensle, E. M.; Blum, S. A. *J. Am. Chem. Soc.* **2013**, 135, 12324–12328.
4. "Organometallics Roundtable 2011," Gladysz, J. A.; Ball, Z. T.; Bertrand, G.; Blum, S. A.; Dong, V. M.; Dorta, R.; Hahn, F. E.; Humphrey, M. G.; Jones, W. D.; Klosin, J.; Manners, I.; Marks, T. J.; Mayer, J. M.; Rieger, B.; Ritter, J.; Sattelberger, A. P.; Schomaker, J. M.; Yam, V. W. W. *Organometallics* **2012**, 31, 1–18.
3. "Homogeneous vs Heterogeneous Polymerization Catalysis Revealed by Single-Particle Fluorescence Microscopy," Esfandiari, N. M.; Blum, S. A. *J. Am. Chem. Soc.* **2011**, 133, 18145–18147.  
**Highlighted Editor's Choice, Science 2011, 334, 1034. "A Probe of Homogeneity."**
2. "Deconvoluting Subensemble Chemical Reaction Kinetics of Platinum–Sulfur Ligand Exchange Detected with Single-Molecule Fluorescence Microscopy," Esfandiari, N. M.; Wang, Y.; Bass, J. Y.; Blum, S. A. *Inorg. Chem.* **2011**, 50, 9201–9203.
1. "Real-Time Imaging of Platinum–Sulfur Ligand Exchange Reactions at the Single-Molecule Level via a General Chemical Technique." Esfandiari, N. M.; Wang, Y.; McIntire, T. M.; Blum, S. A. *Organometallics* **2011**, 30, 2901–2907.

## Interaction of D<sub>2</sub>O, CO<sub>2</sub> and Na with Manganese Oxide and NaMnO<sub>2</sub>-Like Surfaces

David F. Cox  
Virginia Tech, Department of Chemical Engineering

### Presentation Abstract

Our work on transition metal oxide surface chemistry has previously focused on structure-function relationships in the reaction of hydrocarbon fragments on  $\alpha$ -Cr<sub>2</sub>O<sub>3</sub> and  $\alpha$ -Fe<sub>2</sub>O<sub>3</sub> surfaces. Both materials crystallize in the corundum structure, and examination of similar low-index surface among the two materials allows for an examination of a nearly pure electronic effect since Cr<sup>3+</sup> has a 3d<sup>3</sup> electronic configuration, and Fe<sup>3+</sup> a 3d<sup>5</sup> configuration. In that work, it has been demonstrated that the electronic structure of the 3+ cations have a far greater impact on reaction selectivity than surface atomic structure. Manganese oxide provides an alternative look at the dependence of reactivity on electronic structure since it can be manipulated in UHV to several different forms: MnO (Mn<sup>2+</sup>, 3d<sup>5</sup>), Mn<sub>3</sub>O<sub>4</sub> (Mn<sup>2+</sup> and Mn<sup>3+</sup>), and Mn<sub>2</sub>O<sub>3</sub> (Mn<sup>3+</sup>, 3d<sup>4</sup>). Alloying with alkali metals like sodium also provides an additional route to Mn<sup>3+</sup> via the formation of NaMnO<sub>2</sub>-like surfaces. In this work, we start with a well-defined MnO(001) single crystal surface in ultra-high vacuum (UHV), then modify the system by thermal and oxidative treatments and the deposition of Na metal. The surface compounds generated by of these treatments have been characterized by X-ray photoelectron spectroscopy (XPS) and low-energy electron diffraction (LEED). Oxidation and UHV annealing of the Na-precovered MnO(001) surface yields a surface compound with a composition close to NaMnO<sub>2</sub>.

Water and CO<sub>2</sub> have proven to be useful probe molecules for characterizing oxide surfaces. Therefore, temperature programmed desorption (TPD) of D<sub>2</sub>O and CO<sub>2</sub> and co-adsorbed D<sub>2</sub>O and CO<sub>2</sub> were investigated on manganese oxide surfaces, NaMnO<sub>2</sub>-like surfaces, and Na-precovered MnO(001). H<sub>2</sub>O interacts with preadsorbed CO<sub>2</sub> to stabilize the binding through the formation of carbonates and bicarbonates. Results will also be presented for the interaction of water and carbon dioxide with Na-precovered MnO(001). These results are related to the Na<sub>2</sub>CO<sub>3</sub>/MnO low-temperature (850°C) system for the catalytic production of hydrogen via thermochemical water splitting that has been identified recently by the Davis group at Caltech.

## DE-FG02-97ER14751: Hydrocarbon Oxidation, Dehydrogenation and Coupling over Model Metal Oxide Surfaces

**Postdoc(s):** Dr. Yujung Dong

**Student(s):** Ms. Yujung Dong; Mr. Xu Feng; Mr. Han Chen

### RECENT PROGRESS

#### *C<sub>1</sub> Reactions on Chromia Surfaces*

Chromia was chosen as a target material because it exhibits an ability to selectively dehydrogenate butanes to butylenes, although the selectivity for ethane dehydrogenation or oxidative dehydrogenation is limited. For butane dehydrogenation, coordinately unsaturated Cr<sup>3+</sup> centers are thought to be the primary reaction sites for the dehydrogenation chemistry.

Reactions were studied on the  $\alpha$ -Cr<sub>2</sub>O<sub>3</sub>(10 $\bar{1}$ 2) and  $\alpha$ -Cr<sub>2</sub>O<sub>3</sub>(0001) surfaces to examine the structure sensitivity of the methyl, CH<sub>3</sub>, dehydrogenation reaction and the diffusion and coupling of methylene, :CH<sub>2</sub>, to ethylene, CH<sub>2</sub>=CH<sub>2</sub>. These chromia surfaces, because of the 3d<sup>3</sup> electronic configuration of the Cr<sup>3+</sup> cations, are highly nonreducible in UHV, even when exposed to hydrogen atoms. As a result, no oxygen-containing products are observed in TPD from these surfaces.

The (10 $\bar{1}$ 2) and (0001) surfaces expose Cr<sup>3+</sup> cations with coordination numbers of five (one coordination vacancy relative to the bulk) and three (three coordination vacancies), respectively. We have shown experimentally that methyl dehydrogenation is structure insensitive, showing no significant variation in the activation barrier to dehydrogenation to methylene with changes in cation coordination or local site geometry. Methylene coupling to ethylene is associated with a rate-limiting surface diffusion step on both  $\alpha$ -Cr<sub>2</sub>O<sub>3</sub>(10 $\bar{1}$ 2) and (0001) surfaces, and shows a significant structure sensitivity. The rate-limiting step shows a 85 K increase in the reaction temperature in TPD on the (0001) due to the lower accessibility of surface O atoms on the stoichiometric (0001) surface. The local site geometry also requires longer, less-stable bonds as the methylene diffuses across the surface.

For both surfaces, DFT gives an interesting picture of the methylene surface diffusion process. DFT suggests methylene can  $\pi$ -bond to a surface cation, or bridge bond between a surface cation and anion on either surface. The diffusion process is simply a thermally-driven rehybridization in which methylene varies between  $\pi$ -bonded (*sp*<sup>2</sup>) and bridge-bonded (*sp*<sup>3</sup>) configurations, with the barrier to diffusion significantly lower than that for methylene dehydrogenation to surface carbon.

#### *C<sub>1</sub> Reactions on $\alpha$ -Fe<sub>2</sub>O<sub>3</sub>*

Because  $\alpha$ -Cr<sub>2</sub>O<sub>3</sub> and  $\alpha$ -Fe<sub>2</sub>O<sub>3</sub> both crystallize in the corundum bulk structure with only minor (less than 2%) differences in the lattice parameters, a comparison of surface chemistry over similar terminations of the two materials allows one to test the impact of a nearly-pure electronic effect associated with the 3d<sup>3</sup> and 3d<sup>5</sup> electronic structure of Cr<sup>3+</sup> and Fe<sup>3+</sup> cations, respectively. The iron oxide is known to be much more reducible than the chromia, so differences in selectivity due to the reactivity of surface lattice oxygen were anticipated.

Variations in the  $M^{3+}$  d-electron density cause dramatic but predictable changes in the surface chemistry of methylene,  $:CH_2$ , fragments on stoichiometric corundum-structure (10 $\bar{1}2$ ) surfaces when  $Cr^{3+}$  cations are replaced with  $Fe^{3+}$ . The reaction selectivity on stoichiometric  $\alpha$ - $Fe_2O_3$  (10 $\bar{1}2$ ) is entirely towards the non selective oxidation products CO and CO<sub>2</sub> for small submonolayer doses of the reactant, consistent with the reducible nature of the surface. CO and CO<sub>2</sub> evolve simultaneously (often an indication of a carboxylate surface intermediate) at 630 K in TPD. The reaction of formate formed from the adsorption of formic acid occurs in a similar temperature range to give CO and CO<sub>2</sub>, in support of this assignment. No other products are observed from the stoichiometric surface. However, for consecutive TPD runs, the production of CO and CO<sub>2</sub> drop off quickly with the first few doses of reactant, and formaldehyde ( $H_2C=O$ ) and ethylene ( $H_2C=CH_2$ ) appear as major products.

From the products formed, it is clear that methylene fragments reduce the surface via the extraction of lattice oxygen to make CO, CO<sub>2</sub> and  $H_2C=O$ . The shift in the product slate from nonselective oxidation products (CO, CO<sub>2</sub>) to selective oxidation ( $H_2C=O$ ) and  $H_2C=CH_2$  occurs as the surface becomes reduced. For methylene coupling to ethylene, the generation of reduced  $Fe^{2+}$  surface sites is clearly important, although the specific site requirements (if any) for the coupling reaction are unclear because of a lack of information about the surface structure.

#### Publication Acknowledging this Grant in 2011-2014

1. Dong, Y.; Brooks, J.D.; Chen, T.L.; Mullins, D.R.; Cox, D.F. Methylene migration and coupling on a non-reducible metal oxide: the reaction of dichloromethane on stoichiometric  $\alpha$ - $Cr_2O_3$ (0001). *Surface Science*, Submitted.
2. Gibbs, G.V.; Ross, N.L.; Cox, D.F.; Rosso, K.M. Insights into the crystal chemistry of earth materials rendered by electron density distributions: Pauling's rules revisited, *American Mineralogist*. **2014**, *99*, 1071-1084.
3. Gibbs, G.V.; Ross, N.L.; Cox, D.F.; Rosso, K.M.; Iversen, B.B.; Spackman, M.A. Pauling Bond Strength, Bond Length and Electron Density Distribution, *Physics and Chemistry of Minerals*. **2014**, *41*, 17-25.
4. Gibbs, G.V.; Ross, N.L.; Cox, D.F.; Rosso, K.M.; Iversen, K.M.; Spackman, M.A. Bonded radii and the contraction of the electron density of the oxygen atom by bonded interactions, *The Journal of Physical Chemistry A*. **2013**, *117*, 1632-1640.
5. Gibbs, G.V.; Wang, D.; Hin, C.; Ross, N.L.; Cox, D.F.; Crawford, T.D.; Spackman, R.J. Properties of atoms under pressure: Bonded interactions of the atoms in three perovskites, *The Journal of Chemical Physics*, **2012**, *137*, 164313.
6. Gibbs, G.V.; Crawford, T.D.; Wallace, A.F.; Cox, D.F.; Parrish, R.M.; Hohenstein, E.G.; Sherrill, C.D. Role of Long-Range Intermolecular Forces in the Formation of Inorganic Nanoparticle Clusters, *The Journal of Physical Chemistry A*, **2011**, *115*, 12933-12940.
7. Brooks, J.D.; Chen, T.L.; Mullins, D.R.; Cox, D.F. Reactions of ethylidene on a model chromia surface:1,1-dichloroethane on stoichiometric  $\alpha$ - $Cr_2O_3$  (10 $\bar{1}2$ ), *Surface Science*, **2011**, *605*, 1170-1176.

8. Gibbs, G.V.; Wallace, A.F.; Downs, R.T.; Ross, N.L.; Cox, D.F.; Rosso, K.M. Thioarsenides: van der Waals bonded Interactions and bond paths, *Physics and Chemistry of Minerals*, **2011**, 38, 267-291.

## Heterogeneous and Homogeneous Catalyst Design by Discovery Informatics

W. Nicholas Delgass  
Purdue University, School of Chemical Engineering

### Abstract

Work on an informatics protocol for design of heterogeneous catalysts is currently focused on the metal-support interface of catalysts for the water gas shift reaction. Studies of supported Au on Fe-doped  $\text{TiO}_2$  have shown an increase in rate and strong effects of Fe on both the activation energy and the CO order of reaction. The influence of Fe on the CO bonding to metal sites is supported by *in situ* FTIR spectra. Removal of Co from PtCo/MWCNT, on the other hand, shows promotion by oxidized Co. Oxidized Mo sites also promote Pt/Mo<sub>2</sub>C. Detailed DFT modeling of Pd and Pt (111) surfaces confirms the importance of carboxyl intermediates but also shows that: i) the metal alone cannot account for experimental results, and ii) that coverage effects of the CO binding energy can be accounted for with a new cluster expansion approach. Calculations on metal nanowire models of Pt on  $\text{Al}_2\text{O}_3$  and Au on MgO confirm the carboxyl kinetic model and clearly show enhanced water activation at the metal/oxide interface and CO bonding to the interfacial metallic sites. The theory work is aimed ultimately at developing descriptors and scaling for the metal-support effects. Homogeneous catalyst studies have moved to non-Cp coordination catalysts for olefin polymerization and oligomerization. A binuclear catalyst complex is invoked to account for changes in rate and molecular weight distribution at sub-stoichiometric activator conditions and effects the electronics of the pendant group on the rate constants for propagation, misinsertion, and recovery correlate with corresponding changes in HOMO energy. Effects of catalyst structure on oligomer formation, extraction of activation energies for individual rate constants, the kinetic consequences of Ti, Zr, and Hf in a family of catalyst complexes, and co-polymerization of 1-hexene with styrene are current research activities. Kinetic modeling capabilities have been expanded with a new algorithm based on Dynamic Monte Carlo methods.

### DOE Grant No. DE-FG02-03ER15466 CATALYSIS SCIENCE INITIATIVE: Catalyst Design by Discovery Informatics

**Co-PIs:** M. Abu-Omar (Chemistry), J. M. Caruthers, F. H. Ribeiro, K. T. Thomson, W. F. Schneider (University of Notre Dame), **Research Associate:** G. Medvedev, **Postdocs:** Z. Zhao and Houyu Zhu (Notre Dame), **Students:** J. Clay (N. D.), Y. Cui, , T. Gunanskera (Chem.), J. Kim, P. Pletcher (Chem.), S. Pradhan, A. Preston (Chem.), S. McDonough (N. D.), K. Sabnis, K. Steelman (Chem.), J. Switzer, S. Xiong, **Collaborators:** J. P. Greeley, Purdue; J. T. Miller, Argonne Nat. Lab.; E. A. Stach, Brookhaven Nat. Lab.; M. Neurock, University of Virginia.

### Recent Progress

**Water Gas Shift Reaction: Au supported on Fe-doped Rutile ( $\text{TiO}_2$ ):** The negative apparent order with respect to CO for Au/Fe<sub>2</sub>O<sub>3</sub> (-0.7~-0.43) found in previous results implies much stronger CO adsorption on that catalyst compared to Au supported on other oxides. To pursue the possibility that Fe electronically modifies the CO adsorption strength on Au and thus changes the catalyst activity, we prepared a series of different Fe-doped rutile ( $\text{TiO}_2$ ) supports loaded with ~1wt% Au by the deposition-precipitation method. WGS rate per mole of Au at 120 °C was promoted by a factor of 4 for 1 wt% Fe content. Significant changes in kinetic parameters were observed at varying Fe contents. Apparent orders with respect to CO decreased (from 0.7 to -0.3) and apparent activation energy increased (from 53 to 98 kJ (mol)<sup>-1</sup>) with Fe content increasing from 0 wt% to 5 wt%, leading to a maximum WGS rate versus CO order, Figure 1.

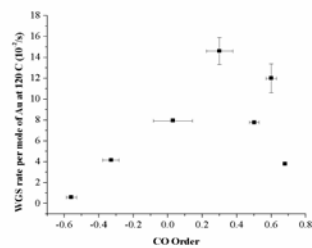


Figure 1 WGS rate versus CO order

To examine the CO binding more closely, *operando* Fourier Transform Infrared Spectroscopy (FTIR) was performed on the 1 wt% Fe-doped catalyst and the result compared with Au supported on undoped rutile. IR peaks at wavenumbers of 2097  $\text{cm}^{-1}$ , 2015  $\text{cm}^{-1}$ , 2044  $\text{cm}^{-1}$ , 1967  $\text{cm}^{-1}$  and 1888  $\text{cm}^{-1}$  were observed. The peak at 2097  $\text{cm}^{-1}$  can be assigned to CO adsorbed on metallic Au, while the lower frequencies of 2044  $\text{cm}^{-1}$  and 1967  $\text{cm}^{-1}$  have been associated with CO adsorbed on partially negatively charged Au. The IR bands at frequencies below 2050  $\text{cm}^{-1}$  were stronger than the corresponding peaks of Au supported on undoped rutile and thus suggest a participation of Fe in the neighborhood of the CO bonding site. The results show that Fe-doping can modify the CO adsorption properties of Au/Rutile and that WGS rates can be optimally promoted with appropriate Fe content.

**WGS on Metal Surfaces:** We used the VASP code and density functional theory to compute the adsorption energies, reaction energies, and activation barriers for four candidate reaction pathways over Pd and Pt. Figure 2 summarizes the computed free energy surfaces at representative low-temperature WGS conditions. The two metals exhibit similar reaction profiles at these conditions. We then developed analytical representations of the kinetics based on these models which allow us to decompose the rates into contributions from each pathway. Using DFT-only numbers, we find that (a) the surfaces are CO-covered, (b) routes involving carboxyl (COOH) are preferred, (c) the computed kinetics underestimate observed rates and do not recover observed kinetic parameters. The high CO coverage is a consequence of the neglect of coverage-dependent CO binding. We systematically varied the CO binding energies (as well as binding entropies) upwards from the low-coverage limit and recomputed the kinetics. Rates increase dramatically as the coverage attains more reasonable values, activity over Pd is always higher than over Pt, consistent with observation, and the rate-limiting step shifts from water dissociation to carboxyl formation. Over the whole space of model values, the model kinetics cannot capture experimental observations. We conclude that even over “inert”  $\gamma$ -alumina, the support is participating materially in the catalysis.

**WGS at the metal-support interface:** We have initially chosen systems that exhibit minimal lattice mismatch between the oxide surface and the (111) and (100) surfaces of transition metals. We construct quasi-two-dimensional transition metal nanowires, containing multiple rows and 2-3 metal layers on a supercell model of the oxide surfaces. A Pd stripe on  $\alpha\text{-Al}_2\text{O}_3(0001)$  illustrates through charge density differences and Bader charge analysis that the electronic communication between metal and support is localized to the interface. Consistent with these results, models containing as few as two metal layers represent the interface similarly, while a single metal layer behaves qualitatively differently.

We used the DFT models to compare adsorption of WGS reactants and intermediates at various Pd/ $\alpha\text{-Al}_2\text{O}_3(0001)$  interface sites with that on isolated Pd(111) and  $\alpha\text{-Al}_2\text{O}_3(0001)$  sites (Figure 3). Based on these results and additional work on Au/ $\alpha\text{-Al}_2\text{O}_3(0001)$  and Au/MgO(100) (below), we find several important general conclusions: CO prefers the metal sites and its binding is relatively unaffected by the oxide;  $\text{H}_2\text{O}$  prefers metal cation sites right at the metal/oxide boundary; and water dissociation barriers are decreased at the metal/oxide boundary relative to the metal alone. In addition, these results begin to isolate the sensitivity of computed results to the model details, for instance that the description of the bottom of the oxide slab can have substantial influence on the chemistry at the slab top.

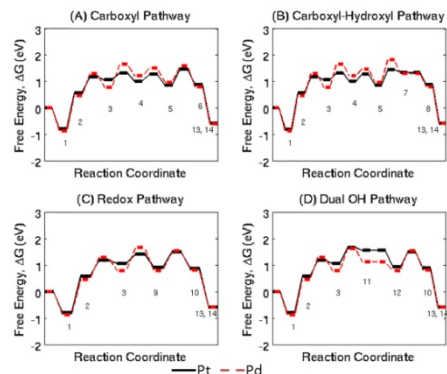


**Figure 2:** Free Energy Surfaces for the (A) Carboxyl pathway, (B) Carboxyl-Hydroxyl Pathway, (C) Redox Pathway, (D) Dual OH pathway on Pt and Pd(111). Conditions:  $P=1$  atm,  $T=553$  K,  $y_{\text{CO}}=6.8\%$ ,  $y_{\text{CO}_2}=8.5\%$ ,  $y_{\text{H}_2\text{O}}=21.9\%$ ,  $y_{\text{H}_2}=37.4\%$ , balance inert.

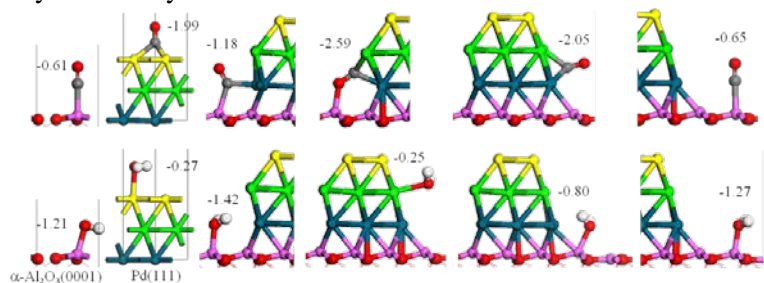


**Figure 3:** Stable CO and  $\text{H}_2\text{O}$  binding configurations on  $\alpha\text{-Al}_2\text{O}_3(0001)$ , Pd(111) and 3-layers Pd stripe/ $\alpha\text{-Al}_2\text{O}_3(0001)$ , along with the corresponding adsorption energy (eV).

We have also extensively analyzed WGS catalysis on Au particles. Previous theoretical studies have shown that pure gold is not a good WGS catalyst due to its very high barrier ( $> 2$  eV) for water dissociation. In contrast, our efforts have demonstrated that the catalytic properties of Au/MgO can be favorable for WGS (Figure 4). Using the quasi-two dimensional oxide-supported nanowire models described above, we have found that the barrier for water dissociation is dramatically decreased at the Au/MgO interface, to essentially zero. We have traced this important interfacial effect to stronger binding of the OH product between an  $Mg^{2+}$  and the Au nanowire edge and to similar strong interaction of the H product with available oxygen atoms on the MgO surface. This result hints that a Bronsted-Evans-Polanyi type of relationship may govern molecular activation at metal/oxide interfaces, as has been previously shown on pure metal and oxide surfaces, and further exploration of this potential relationship will be a central focus of our future efforts.

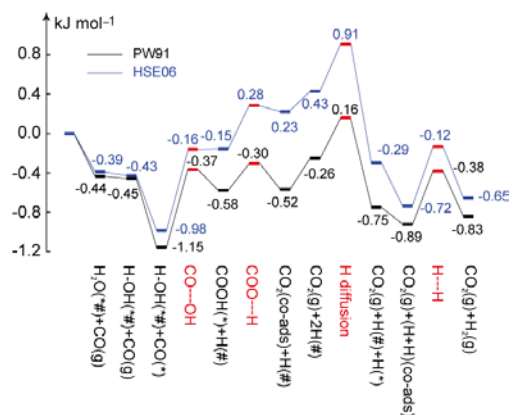


**Figure 4:** Energy profile of carboxyl mechanism at Au/MgO interface. Red ones indicate a transition state.

Our calculation implies that after water dissociation, the reaction follows a carboxyl mechanism. The highest barrier is 0.78 eV for the formation of COOH via CO and OH combination. The calculated PW91 reaction energies and barriers have been further refined by single point calculations with the highly accurate hybrid functional HSE06. As expected, weaker binding is predicted by HSE06, especially for the CO adsorption. However, the rate-limiting activation barriers between these two functionals are quite similar, with a difference of less than 0.05 eV.

**Olefin Polymerization: Selective Degenerative Benzyl Group Transfer in Olefin Polymerization:** A comprehensive kinetic study of the  $Zr[tBu-ON^{THF}O]Bn_2/B(C_6F_5)_3$  system under sub-stoichiometric activator conditions has shown that decreasing the amount of activator causes (i) the rate of monomer consumption to decrease and (ii) the molecular weight distribution (MWD) to narrow and shift to lower values. The proposed mechanism includes the formation of a binuclear complex (BNC) consisting of the neutral catalytic species and an active site connected via degenerative transfer of a benzyl ligand, as shown in Fig. 5. Bridging via methyl and chloral ligands has been previously postulated, but not bridging via a benzyl ligand, which has been argued to not be feasible. The BNC can be formed when a pre-catalyst species reacts with an active catalyst thereby providing a second channel for activation. The most significant finding of this study is that the BNC is only formed by the normally inserting active sites and not by mis-inserting sites, resulting in narrowing of the MWD of the polymer as compared to the case of stoichiometric activator, where the BNC is not formed. Although the BNC concentration is small compared to the total concentration of active sites, due to the small equilibrium constant of BNC formation, it is shown to play an important role in initiation which is faster via the BNC, and dominates the product distribution.

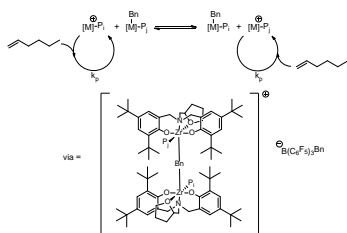


**Figure 5:** 1-Hexene polymerization

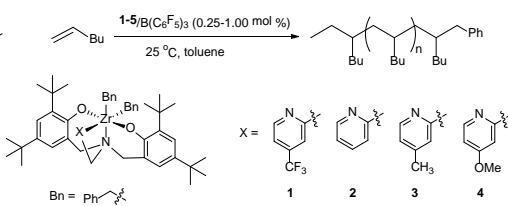


**Figure 6:** Catalysts studied in pendant electronics analysis by the BNC

**Effects of Pendant Electronics on Olefin Polymerization:** A detailed kinetic study of the four catalytic systems shown in Fig.6, based on Zr amine bis-phenolate complexes bearing an electronically modified pyridyl pendant, has been completed. The mechanism includes initiation, normal propagation, misinsertion, recovery, and chain transfer. The most significant finding is a correlation between the HOMO energy in the precatalyst structure and the first order rate constants for propagation, misinsertion, and recovery from mis-

insertion. Specifically, for catalysts 1-4, the logarithm of the rate constants ( $k_p$ ,  $k_{mis}$ , and  $k_{rec}$ ) decreases linearly with the HOMO energy. This indicates that the systematic addition of electron withdrawing character to the pendant results in a lowering of the energy barrier associated with each monomer insertion event. Chain transfer rates across catalysts 1-4 were relatively unaffected, indicating that the electronic nature of the pendant is selective.

**Alpha Olefin Copolymerization with Styrene Using Salan and Amino Bis(phenoxide) Catalysts:** We have recently begun a focus on the copolymerization between 1-hexene and styrene monomer feeds in an effort to further tune the final polymer product and to expand our modeling capability to copolymers. Initial work with a dichloride phenoxide substituted Zr Salan catalyst has shown rapid consumption of styrene (up to 30% of the initial styrene feed) during the conversion of 85% of the 1-hexene. Studies of the effects of styrene and other monomers with 1-hexene on the copolymerization mechanism are currently underway.

#### Publications Acknowledging this Grant in 2011-2014

1. Pazmiño, J. H.; Shekhar, M.; Williams, W. D.; Akatay, M. C.; Miller, J. T.; Delgass, W. N.; Ribeiro, F. H. Metallic Pt as active sites for the Water-Gas Shift reaction on alkali-promoted supported catalysts. *J. Catal.* **2012**, *286*, 279-286.
2. Shekhar, M.; Wang, J.; Lee, W.-S.; Williams, W. D.; Kim, S. M.; Stach, E. A.; Miller, J. T.; Delgass, W. N.; Ribeiro, F. H. Size and Support Effects for the Water-Gas Shift Catalysis over Gold Nanoparticles Supported on Model Al<sub>2</sub>O<sub>3</sub> and TiO<sub>2</sub>. *J. Am. Chem. Soc.* **2012**, *134*, 4700-4708.
3. Wang, J.; Kispersky, V. F.; Delgass, W. N.; Ribeiro, F. H. Determination of the Au active site and surface active species via *operando* transmission FTIR and isotopic transient experiments on 2.3 wt% Au/TiO<sub>2</sub> for the WGS reaction. *J. Catal.* **2012**, *289*, 171-178.
4. Switzer, J.; Travia, N.; Steelman, D. K.; Medvedev, G.; Thomson, K.; Delgass, W. N.; Abu-Omar, M. M.; Caruthers, J. M. Kinetic Modeling of 1-Hexene Polymerization Catalyzed by Zr(tBu-ONNMe<sub>2</sub>O)Bn<sub>2</sub>/B(C<sub>6</sub>F<sub>5</sub>)<sub>3</sub>. *Macromolecules* **2012**, *45*, 4978-4988.
5. Williams, W. D.; Bollmann, L.; Miller, J. T.; Delgass, W. N.; Ribeiro, F. H. Effect of Molybdenum Addition on Supported Platinum Catalysts for the Water-Gas Shift Reaction. *Appl. Catal. B* **2012**, *125*, 206-214.
6. Shekhar, M.; Wang, J.; Lee, W.-S.; Akatay, M. C.; Stach, E. A.; Delgass, W. N.; Ribeiro, F. H. Counting Au Catalytic Sites for the Water-Gas Shift Reaction. *J. Catal.* **2012**, *293*, 94-102.
7. Manz, T. A.; Caruthers, J. M.; Sharma, S.; Phomphrai, K.; Thomson, K. T.; Delgass, W. N.; Abu-Omar, M. M. Structure-Activity Correlation for Relative Chain Initiation to Propagation Rates in Single-Site Olefin Polymerization Catalysis. *Organometallics* **2012**, *31*, 602-618.
8. Steelman, D. K.; Xiong, S.; Pletcher, P. D.; Smith, E.; Switzer, J. M.; Medvedev, G. A.; Delgass, W. N.; Caruthers, J. M.; Abu-Omar, M. M. Effects of pendant ligand binding affinity on chain transfer for 1-hexene polymerization catalyzed by single-site zirconium amine bis-phenolate complexes. *J. Am. Chem. Soc.* **2013**, *135*, 6280-6288.
9. Steelman, D. K.; Pletcher, P. D.; Switzer, J. M.; Xiong, S.; Medvedev, G. A.; Delgass, W. N.; Caruthers, J. M.; Abu-Omar, M. M. Comparison of Selected Zirconium and Hafnium Amine Bis(phenolate) Catalysts for 1-Hexene Polymerization. *Organometallics* **2013**, *32*, 4862-4867.
10. Xiong, S.; Steelman, D. K.; Medvedev, G. A.; Delgass, W. N.; Abu-Omar, M. M.; Caruthers, J. M. Selective Degenerative Benzyl Group Transfer in Olefin Polymerization. *ACS Catal.* **2014**, *4*, 1162-1170.
11. Brown, H. A.; Silei Xiong, S.; Medvedev, G. A.; Chang, Y. A.; Abu Omar, M. M.; Caruthers, J. M.; Waymouth, R. M. Zwitterionic Ring-Opening Polymerization: Kinetic Models for the Synthesis of Cyclic Poly(caprolactones). *Macromolecules*, Accepted

**Water Dynamics on RuO<sub>2</sub>(110)**

Zdenek Dohnálek, Roger Rousseau, Igor Lyubinetsky and Michael A Henderson  
Fundamental and Computational Sciences Directorate and Institute for Integrated Catalysis,  
Pacific Northwest National Laboratory

**Presentation Abstract**

The interaction of water with solid surfaces is of great interest and importance in many areas including heterogeneous catalysis, photocatalysis, electrochemistry, and others. In this study, we prepared stoichiometric, reduced and oxidized RuO<sub>2</sub>(110) surfaces and examined water adsorption, dissociation, and diffusion using time-lapsed scanning tunneling microscopy. On stoichiometric RuO<sub>2</sub>(110) we show that water monomers adsorb on top of the Ru sites and are immobile below ~225 K. At temperatures above ~240 K, the monomers are found to diffuse along Ru rows and form water dimers, trimers and tetramers with dimers being the most stable configuration. The onset for dimer diffusion is observed at ~280 K indicating higher diffusion barrier than that for monomers. The diffusion barrier for water dimers is determined to be ~0.73 eV, which is significantly higher compared to 0.35 eV determined previously on the isostructural TiO<sub>2</sub> (110).<sup>1</sup> On reduced RuO<sub>2</sub>(110), we find that water molecules dissociate in bridging oxygen vacancies forming pairs of bridging hydroxyls. Subsequently, both the along- and across-row diffusion of proton is observed at room temperature. On oxidized RuO<sub>2</sub>(110), water molecules react with oxygen adatoms on Ru rows and form pairs of terminal hydroxyl groups that can reversibly dissociate back to water and adatom. Along- and across-row diffusion of water molecules at room temperature is tracked by following the position of hydroxyl pairs. Further mechanistic insight is obtained from detailed density functional calculations and *ab initio* molecular dynamics simulations.

This work was performed in EMSL, a national scientific user facility sponsored by the Department of Energy's Office of Biological and Environmental Research and located at Pacific Northwest National Laboratory. PNNL is a multiprogram national laboratory operated for DOE by Battelle.

<sup>1</sup> J. Matthiesen, J. Hansen, S. Wendt, E. Lira, R. Schaub, E. Lægsgaard, F. Besenbacher, and B. Hammer, Phys. Rev. Lett. **102**, 226101 (2009).

**DE-AC06-76RLO 1830: Multifunctional  
Catalysis to Synthesize and Utilize  
Energy Carriers**

**PI: Johannes Lercher**

**Postdoc(s):** Rentao Mu, David Cantu

**Zooming in on active species: Correlative, *operando* XAS and TEM studies of catalytic mechanisms**

Y. Li,<sup>1</sup> A. I. Frenkel,<sup>1</sup> E. A. Stach,<sup>2</sup> S. Zhao,<sup>3</sup> U. Jung,<sup>3</sup> A. Elsen,<sup>3</sup> R. G. Nuzzo,<sup>3</sup> J. Kas,<sup>4</sup> F. Vila,<sup>4</sup> J. J. Rehr,<sup>4</sup> C. S. Bonifacio<sup>5</sup>  
J. C. Yang,<sup>5</sup>

<sup>1</sup>Dept. of Physics, Yeshiva University, New York, <sup>2</sup>Center for Functional Nanomater., Brookhaven National Lab., Upton, NY, <sup>3</sup>Dept. of Chemistry, Univ. of Illinois Urbana-Champaign, Urbana, IL, <sup>4</sup>Dept. of Physics, Univ. of Washington, Seattle, <sup>5</sup>Dept. of Mat. Science and Eng. and Dept. of Chem. Eng., Univ. of Pittsburgh, Pittsburgh

**Presentation Abstract**

Elucidating the complex structure-property-rate relationships of catalysis calls for the use of multiple characterization techniques. X-ray Absorption Spectroscopy (XAS) and Transmission Electron Microscopy (TEM) are the premier methods for obtaining ensemble-average and local, statistical information about nanocatalyst structure. The major challenge toward combining multiple probes to study the same reaction is the strong sensitivity of reaction mechanisms to the environmental conditions that vary between different in situ cells. In our approach, the application of same catalytic conditions to these two probes is implemented by using a portable micro-cell that is fully compatible with the sampling requirements for XAS, TEM (and a few other probes). This cell is developed by E. Stach and is used by our group to investigate a model reaction of ethylene hydrogenation over Pt/SiO<sub>2</sub> catalysts. XAS measurements were done at beamline X27A (NSLS, BNL) with focused (10 μm) beam. STEM images and EELS data were taken at Titan E-TEM (CFN, BNL). For these two measurements, identical gas input/output system was used in which reaction process was monitored by quadruple mass spectrometer. Combination of EXAFS and STEM results reveal the restructuring of Pt catalysts during the reaction and indicate formation of nanophases of platinum carbide. Calculation of absorption spectra of Si L edges by *ab initio* x-ray absorption code FEFF 8 by J. J. Rehr's group sheds light on the effects of Si-O bond length, Si-Si distance and Si-O bond valence on SiO<sub>2</sub> support, the changes of which are evidenced in *operando* EELS data.

**Grant Number: DE FG02-03ER15476**

**Grant Title: The Reactivity and Structural Dynamics of Supported Metal Nanoclusters Using Electron Microscopy, *in situ* X-Ray Spectroscopy, Electronic Structure Theories, and Molecular Dynamics Simulations.**

**PIs:** Ralph G. Nuzzo, Anatoly I. Frenkel, Judith C. Yang, John J. Rehr  
**Postdocs:** A. Elsen, C. Bonifacio, U. Jung, S. Zhao, J. Kas, Y. Li, F. Vila

**RECENT PROGRESS**

A major goal to better understand catalytic reaction mechanisms being addressed in our current work is to provide means that will make it possible to inter-operably explore catalytic materials with multiple techniques, with the hope of using this combined data to elucidate the complex structure-property-rate relationships of catalysis with unprecedented clarity. A main challenge we have surmounted is to establish how to best combine the ensemble-average and local information about nanoscale structure that is commonly provided by XAS and TEM measurements. The chief problem is that these two probes are usually applied at different conditions, complicating interpretations relevant to *in operando* conditions. Our efforts are highlighting new means to investigate catalytic systems *in operando* using a portable/inter-operable cell that is fully compatible with the sampling requirements for most relevant probes. In the first experiment of this kind, we investigated a model reaction system by XAS and STEM, the ethylene hydrogenation reaction carried out over Pt/SiO<sub>2</sub> catalysts in the micro-cell, in collaboration with E. Stach (CFN, BNL) and with help of R. Tappero (NSLS, BNL). In each experiment (at the focusing XAS beamline X27A at NSLS and the Titan E-TEM at CFN) we used an identical setup: a micro-cell for sample

analysis by XAS and TEM, and a coupled quartz capillary plug-flow cell placed downstream from the micro-cell for product analysis. The new results emerging from this work revealed that the changes in the SiO<sub>2</sub> support evidenced in Si EELS data correlate with the atomistic changes evidenced in the bonding environment of Pt atoms before, during and after the reaction. These impacts are highly responsive to the reactant atmosphere composition and conversion regime of the reaction (Fig. 1).

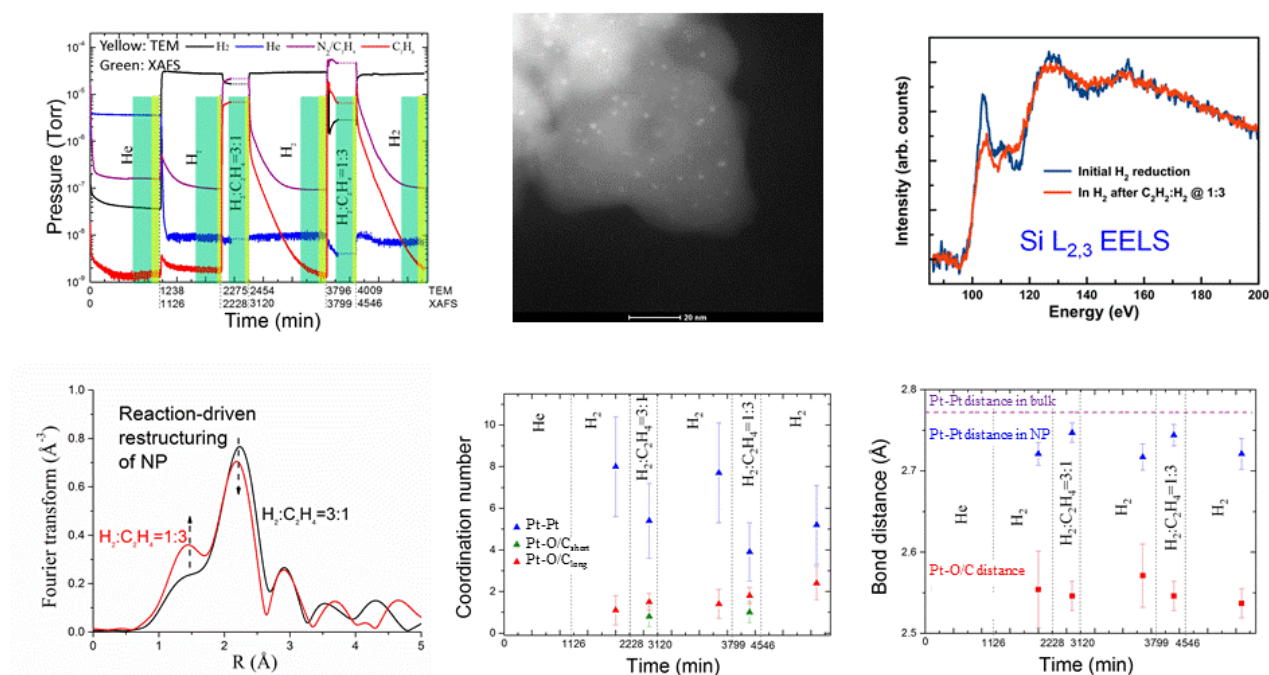


**Figure 1.** Data and results of the combined, *in operando* XAFS-TEM ethylene hydrogenation reaction experiment over Pt/SiO<sub>2</sub> nanocatalysts in the portable micro-cell. Top row, from left to right: RGA data taken during XAFS and TEM measurements. HAADF image during the 3:1 C<sub>2</sub>H<sub>4</sub>: H<sub>2</sub> flow at 1 atm in the cell, Si L<sub>2,3</sub> edges EELS data taken *in operando* conditions during different stages of the reaction. Bottom row, from left to right: EXAFS data in r-space taken for the 3:1 and 1:3 ratios of C<sub>2</sub>H<sub>4</sub> to H<sub>2</sub>, analysis results for the coordination numbers and bond distances illustrating restructuring of the nanoparticles during the reaction.

#### Publications Acknowledging this Grant in 2011-2014

1. Erickson, E.M.; Oruc, M.E.; Small, M.W.; Wetzel, D.J.; Cason, M.W.; Hoang, T.T.H.; Li, D.; Marinkovic, N.S.; Frenkel, A.I.; Gewirth, A.A.; Nuzzo, R.G. A Comparison of Atomistic and Continuum Approaches to the Study of Bonding Dynamics in Electrocatalysis: Microcantilever Stress and In-Situ EXAFS Observations of Platinum Bond Expansion Due to Oxygen Adsorption During the Oxygen Reduction Reaction, *Anal. Chemistry*, **submitted**.
2. Frenkel, A.I.; van Bokhoven, J.A. X-Ray Spectroscopy for Chemical and Energy Sciences (invited) *J. Sync. Rad.*, **submitted**.
3. Shan, J.; Zhang, S.; Choksi, T.; Zhu, W.; Zhang, Y.; Li, Y.; Nguyen, L.; Chafe, A.; Greeley, J.; Frenkel, A.I.; Tao, F. Tuning catalytic performance through a single or sequential post-synthesis reaction in a gas phase. *Nature Comm.*, **submitted**.
4. Huang, W.; Shan, J.; Nguyen, L.; Li, Y.; Zhang, S.; Frenkel, A.I.; Tao, F. Catalytic conversion of methane to methanol and formic acid on singly dispersed palladium oxide species on internal surface of ZSM5. *Angew. Chem. Int. Ed.*, **submitted**.
5. Shan, J.; Huang, W.; Nguyen, L.; Yu, Y.; Zhang, S.; Li, Y.; Frenkel, A.I.; Tao, F. Conversion of methane to methanol in gas phase on a bent mono( $\mu$ -oxo)dinickel anchored on internal surface of micro-pores. *Langmuir*, **submitted**.

6. Zhang, S.; Nguyen, L.; Liang, J.; Li, J.; Shan, J.; Frenkel, A.I.; Patlolla, A.; Liu, J.; Huang, W.; Tao, F. Catalysis on an isolated bimetallic site. *Nature Chem.*, **submitted**.
7. Zhang, L.; Yang, C.; Frenkel, A.I.; Wang, S.; Xiao, G.; Brinkman, K.; Chen, F. Co-generation of electricity and chemicals from propane fuel in solid oxide fuel cells with anode containing nano-bimetallic catalyst. *J. Power Sources*, **2014**, *262*, 421-428
8. Rehr, J.J.; Vila, F.D. Dynamic Structural Disorder in Supported Nanoscale Catalysts. *J. Chem. Phys.* **2014**, *140*, 134701.
9. Small, M.W.; Kas, J.; Kvashnina, K.O.; Rehr, J.J.; Nuzzo, R.G.; Tromp, M.; Frenkel, A.I. Effects of adsorbate coverage and bond length disorder on the d-band center in carbon-supported Pt catalysts. *Chem. Phys. Chem.* **2014**, DOI: 10.1002/cphc.201400055
10. Frenkel, A.I.; Cason, M.; Elsen, A.; Jung, U.; Small, M.W.; Nuzzo, R.G.; Vila, F.D.; Rehr, J.J.; Stach, E.A.; Yang, J.C. Effects of complex interactions on structure and dynamics of supported metal catalysts. *J. Vac. Sci. Tech. (Invited Critical Review)* **2014**, *32*, 020801-0208017.
11. Frenkel, A.I.; Small, M.W.; Smith, J.G.; Nuzzo, R.G.; Kvashnina, K.O.; Tromp, M. An In-Situ Study of Bond Strains in 1 nm Pt Catalysts and Their Sensitivities to Cluster-Support and Cluster-Adsorbate Interactions. *J. Phys. Chem. C* **2013**, *117*, 23286-23294.
12. Frenkel, A.I.; Wang, Q.; Sanchez, S.I.; Small, M.W.; Nuzzo, R.G. Short range order in bimetallic nanoalloys: An extended X-ray absorption fine structure study. *J. Chem. Phys.* **2013**, *138*, 064202.
13. Zhang, Z.; Li, L.; Yang, J.C. Adhesion of Pt nanoparticles supported on  $\gamma$ -Al<sub>2</sub>O<sub>3</sub> single crystal. *J. Phys. Chem. C* **2013**, *117*, 21407-21412.
14. Li, L.; Wang, L.-L.; Johnson, D.D.; Zhang, Z.; Sanchez, S.I.; Kang, J.H.; Nuzzo, R.G.; Wang, Q.; Frenkel, A.I.; Ciston, J.; Stach, E.A.; Yang, J.C. Noncrystalline-to-crystalline transformations in Pt nanoparticles. *J. Am. Chem. Soc.* **2013**, *135*, 13062-13072.
15. Stach, E.A.; Zakharov, D.; Akatay, M.C.; Baumann, P.; Ribeiro, F.; Zvienevich, Y.; Li, Y.; Frenkel, A.I. Developments in environmental transmission electron microscopy for catalysis research *Microsc. Microanal.* **2013**, *19*, Suppl. 2, 1174-1175.
16. Zhang, S.; Tao, F.; Frenkel, A.I.; Takeda, S. Singly anchored Pt and Pd atoms on Co<sub>3</sub>O<sub>4</sub> and their catalytic performance. *Microsc. Microanal.* **2013**, *19*, Suppl. 2, 1620-1621.
17. Stach, E.A.; Baumann, P.; Li, Y.; Zakharov, D.; Frenkel, A.I. Using operando methods to characterize working catalysts with TEM, XAS, EXAFS and Raman Spectroscopy. *Microsc. Microanal.* **2013**, *19*, Suppl. 2, 1674-1675.
18. Zhang, S.; Shan, J.-J.; Zhu, Y.; Frenkel, A.I.; Patlolla, A.; Huang, W.; Yoon, S.; Wang, L.; Yoshida, H.; Takeda, S.; Tao, F. WGS Catalysis and in-situ studies of CoO(1-x)PtCo(n)/Co<sub>3</sub>O<sub>4</sub> and Pt(m)Co(m')/CoO(1-x) nanorod catalysts. *J. Am. Chem. Soc.* **2013**, *135*, 8283-8293.
19. Merte, L.R.; Ahmadi, M.; Behafarid, F.; Ono, L.K.; Lira, E.; Matos, J.; Li, L.; Yang, J.C.; Cuenya, B.R. Correlating Catalytic Methanol Oxidation with the Structure and Oxidation State of Size-Selected Pt Nanoparticles. *ACS Catal.* **2013**, *3*, 1460-1468.
20. Korobko, R.; Lerner, A.; Li, Y.; Frenkel, A.I.; Lubomirsky, I. Electric field increases local symmetry in Gd-doped ceria. *Nature Mater.*, **submitted**.
21. Wu, L.-b.; Wu, L.-h.; Yang, W.-m.; Frenkel, A.I. Study of the local structure and oxidation state of iron in complex oxide catalysts for propylene ammoxidation. *Cat. Sci. & Technol.*, 2014, **in press**.
22. He, L.; Liu, F.; Hautier, G.; Oliveira, M.J.T.; Marques, M.A.L.; Vila, F.D.; Rehr, J.J.; Rignanese, G.-M.; Zhou, A. Accuracy of generalized gradient approximation functionals for density-functional perturbation theory calculations. *Phys. Rev. B* **2014**, *89*, 064305.
23. Frenkel, A.I.; Khalid, S.; Hanson, J.C.; Nachtegaal, M. QEXAFS in Catalysis Research: Principles, Data Analysis and Applications. In *In-situ Characterization of Heterogeneous Catalysts*, Chupas, P.; Hanson, J.; Rodriguez, J.A., Eds., John Wiley and Sons **2013**.
24. Frenkel, A.I.; Hanson, J.C. Combined XAFS-XRD methods in Catalysis Research. In *In-situ Characterization of Heterogeneous Catalysts*, Chupas, P.; Hanson, J.; Rodriguez, J. A., Eds., John Wiley and Sons **2013**.
25. Kossov, A.; Wang, Q.; Korobko, R.; Grover, V.; Feldman, Y.; Wachtel, E.; Tyagi, A.K.; Frenkel, A.I.; Lubomirsky, I. Evolution of the local structure at the phase transition in CeO<sub>2</sub>-Gd<sub>2</sub>O<sub>3</sub> solid solutions. *Phys. Rev. B* **2013**, *87*, 054101.
26. Perelshtein, I.; Ruderman, E.; Perkash, N.; Tzanov, T.; Beddow, J.; Joyce, E.; Mason, T.; Blanes, M.; Molla, K.; Patlolla, A.; Frenkel, A.I.; Gedanken, A., Chitosan and chitosan-ZnO-based complex nanoparticles: formation, characterization, and antibacterial activity. *J. Mater. Chem. B* **2013**, *1*, 1968-1976.
27. Sanchez, S.I.; Small, M.W.; Bozin, E.S.; Wen, J.-G.; Zuo, J.-M.; Nuzzo, R.G., Metastability and Structural Polymorphism in Noble Metals: the Role of Composition and Metal Atom Coordination in Mono- and Bimetallic Nanoclusters. *ACS Nano* **2013**, *7*, 1542-1557.

28. Amit, Y.; Eshet, H; Faust, A.; Patlolla, A.; Rabani, E.; Banin, U.; Frenkel, A.I. Unraveling the Impurity Location and Binding in Heavily Doped Semiconductor Nanocrystals: The Case of Cu in InAs Nanocrystals. *J. Phys. Chem. C* **2013**, *117*, 13688-13696.
29. Amit, Y.; Eshet, H; Milo, O.; Rabani, E.; Frenkel, A.I.; Banin, U. How to dope a semiconductor nanocrystal. *ECS Trans.* **2013**, *58*, 127-133.
30. Yancey, D.F.; Chill, S.T.; Zhang, L.; Frenkel, A.I.; Henkelman, G.; Crooks, R.M. A theoretical and experimental examination of systematic ligand-induced disorder in Au dendrimer-encapsulated nanoparticles. *Chem. Science* **2013**, *4*, 2912-2921.
31. Wang, L.; Zhang, S.; Zhu, Y.; Patlolla, A.; Shan, J.-J.; Yoshida, H.; Takeda, S.; Frenkel, A.I.; Tao, F. Catalysis and In-situ Studies of Rh/Co<sub>3</sub>O<sub>4</sub> Nanorods in Reduction of NO with H<sub>2</sub>. *ACS Catalysis* **2013**, *3*, 1011-1019.
32. Patlolla, A.; Baumann, P.; Xu, W.; Senanayake, S.; Rodriguez, J.A.; Frenkel, A.I. Characterization of Metal-Oxide Catalysts in Operando Conditions by Combining X-Ray Absorption and Raman Spectroscopies in the Same Experiment. *Top. Catal.* **2013**, *56*, 896-904.
33. Amakawa, K.; Sun, L.; Guo, C.; Havecker, M.; Kube, P.; Wachs, I.E.; Lwin, S.; Frenkel, A.I.; Patlolla, A.; Hermann, K.; Schlögl, R.; Trunschke, A. How strain affects the reactivity of surface metal oxide catalysts. *Angew. Chem. Int. Ed.* **2013**, *52*, 13553-13557.
34. Frenkel, A.I., Applications of extended X-ray absorption fine-structure spectroscopy to studies of bimetallic nanoparticle catalysts. *Chem. Soc. Rev.* **2012**, *41*, 8163-8178.
35. Yang, J.C.; Small, M.W.; Grieshaber, R.V.; Nuzzo, R.G., Recent Developments and Applications of Electron Microscopy to Heterogeneous Catalysis. *Chem. Soc. Rev.* **2012**, *41*, 8179-8194.
36. Zhang, Z.; Gleeson, B.; Jung, K.; Li, L.; Yang, J.C., A Diffusion Analysis of Transient Subsurface gamma-Ni<sub>3</sub>Al Formation During beta-NiAl Oxidation, *Acta. Mater.* **2012**, *60*, 5273-5283.
37. Zhang, Z.; Jung, K.; Li, L.; Yang, J.C., Kinetic Aspects of Initial Stage Thin gamma-Al<sub>2</sub>O<sub>3</sub> Film Formation on Single Crystalline beta-NiAl (110). *J. Appl. Phys.* **2012**, *111*, 34312.
38. Erickson, E. M.; Thorum, M. S.; Vasic, R.; Marinkovic, N.; Frenkel, A. I.; Gewirth, A. A.; Nuzzo, R. G., In-Situ Electrochemical X-ray Absorbance Spectroscopy Oxygen Reduction Catalysis with High Oxygen Flux. *J. Am. Chem. Soc.* **2012**, *134*, 197-200.
39. Small, M. W.; Sanchez, S. I.; Marinkovic, N. S.; Frenkel, A. I.; Nuzzo, R. G., Influence of Adsorbates on the Electronic Structure, Bond Strain, and Thermal Properties of an Alumina-Supported Pt Catalyst. *ACS Nano*, **2012**, *6*, 5583-5595.
40. Yan, W.; Vasic, R.; Frenkel, A. I.; Koel, B. E., Intra-particle reduction of arsenite (As(III)) by nanoscale zerovalent iron (nZVI) investigated with *in-situ* X-ray absorption spectroscopy. *Environ. Sci. & Technology* **2012**, *46*, 7018-7026.
41. Patlolla, A.; Zunino III, J.; Frenkel, A. I.; Iqbal, Z., Thermochromism in Polydiacetylene-metal oxide nanocomposites *J. Mater. Chem.* **2012**, *22*, 7028-7035.
42. Myers, S. V.; Frenkel, A. I.; Crooks, R. M., In Situ Structural Characterization of Platinum Dendrimer-Encapsulated Oxygen Reduction Electrocatalysts. *Langmuir* **2012**, *28*(2), 1596-1603.
43. Ryu, H.; Lei, H.; Frenkel, A. I.; Petrovic, C., Local structural disorder-induced superconductivity in K(x)Fe(2-y)Se(2) materials *Phys. Rev. Lett.* **2012**, *85*, 224515.
44. Chen, W.-F.; Sasaki, K.; Ma, C.; Frenkel, A. I.; Marinkovic, N.; Muckerman, J. T.; Zhu, Y.; Adzic, R. R., Noble metal-free hydrogen-evolution catalysts based on NiMo nitride nanosheets. *Angew. Chemie Int. Ed.* **2012**, *51*, 6131-6135.
45. Yadgarov, L.; Rosentsveig, R.; Leitun, G.; Albu-Yaron, A.; Moshkovitz, A.; Perfiliev, V.; Vasic, R.; Frenkel, A. I.; Enyashin, A. N.; Seifert, G.; Rapoport, L.; Tenne, R., Controlled doping of MS<sub>2</sub> (M=W, Mo) nanotubes and fullerene-like nanoparticles *Ang. Chemie, Int. Ed.* **2012**, *51*, 1148-1151.
46. Yih, K.; Hamdemir, I.K.; Mondoch, J.E.; Bayrem, E.; Ozkar, S.; Vasic, R.; Frenkel, A.I.; Anderson, O.P.; Finke, R.G., Synthesis and Characterization of [Ir(1,5-Cyclooctadiene)(μ-H)]<sub>4</sub>: A Tetrametallic Ir<sub>4</sub>H<sub>4</sub>-core, Coordinatively Unsaturated Cluster. *Inorg. Chem.* **2012**, *51*, 3186-3193.
47. Frenkel, A.I.; Vasic, R.; Dukesz, B.; Li, D.; Chen, M.; Zhang, L.; Fujita, T.; Thermal Properties of Nanoporous Gold. *Phys. Rev. B* **2012**, *85*, 195419.
48. Landon, J.; Demeter, E.; Inoglu, N.; Keturakis, C.; Wachs, I.E.; Vasic R.; Frenkel, A.I.; Kitchin, J.R., Spectroscopic Characterization of Mixed Fe-Ni Oxide Electrocatalysts for the Oxygen Evolution Reaction in Alkaline Electrolytes. *ACS Catalysis* **2012**, *2*, 1793-1801.
49. Korobko, R.; Patlolla, A.; Kossoy, A.; Wachtel, E.; Tuller, H.L.; Frenkel, A.I.; Lubomirsky, I., Giant Electrostriction in Gd-doped Ceria. *Adv. Mater.* **2012**, *24*, 5857-5861.
50. Lyahovitskaya, V.; Feldman, Y.; Zon, I.; Yoffe, A.; Frenkel, A.I., Strain-arranged structure in amorphous films. *J. Mater. Res.* **2012**, *27*, 2819-2828.
51. Coppage, R.; Slocik, J. M.; Briggs, B. D.; Frenkel, A. I.; Naik, R. R.; Knecht, M. R., Determining peptide sequence effects that control the size, structure and function of nanoparticles. *ACS Nano* **2012**, *6*, 1625-1636.

52. Patlolla, A.; Carino, E.V.; Ehrlich, S.N.; Stavitski, E.; Frenkel, A.I., Application of Operando XAS, XRD, and Raman Spectroscopy for Phase Speciation in Water Gas Shift Reaction Catalysts. *ACS Catalysis* **2012**, *2*, 2216-2223.
53. Lei, H.; Ryu, H.; Ivanovski, V.; Warren, J.B.; Frenkel, A.I.; Cekic, B.; Yin, W.-G.; Petrovic, C., Structure and physical properties of the layered iron oxychalcogenide BaFe<sub>2</sub>Se<sub>2</sub>O. *Phys. Rev. B* **2012**, *86*, 195133.
54. M. W. Small, S. I. Sanchez, L. D. Menard, J. H. Kang, A. I. Frenkel and R. G. Nuzzo, The Atomic Structural Dynamics of  $\gamma$ -Al<sub>2</sub>O<sub>3</sub> Supported Ir-Pt Nanocluster Catalysts Prepared From a Bimetallic Molecular Precursor: A Study Using Aberration-Corrected Electron Microscopy and X-ray Absorption Spectroscopy, *Journal of the American Chemical Society*, **2011**, *133*, 3582-3591.
55. W. Du, D. Su, Q. Wang, A. I. Frenkel, X. Teng, Promotional effects of Bismuth on the formation of Platinum-Bismuth nanowires and the electrocatalytic activity toward ethanol oxidation, *Crystal Growth & Design*, **2011**, *11*, 594-599.
56. A. Piovano, G. Agostini, A. I. Frenkel, T. Bertier, C. Prestipino, M. Ceretti, W. Paulus, C. Lamberti, Time-resolved in situ XAFS study of the electrochemical oxygen intercalation in SrFeO<sub>2.5</sub> Brownmillertite structure: comparison with the homologous SrCoO<sub>2.5</sub> system, *J. Phys. Chem. C* **2011**, *115*, 1311-1322.
57. Alley, W. M.; Hamdemir, I. K.; Wang, Q.; Frenkel, A. I.; Li, L.; Yang, J. C.; Menard, L. D.; Nuzzo, R. G.; Ozkar, S.; Yih, K.; Johnson, K. A.; Finke, R. G., Industrial Ziegler-Type Hydrogenation Catalysts Made from Co(neodecanoate)(2) or Ni(2-ethylhexanoate)(2) and AlEt<sub>3</sub>: Evidence for Nanoclusters and Sub-Nanocluster or Larger Ziegler-Nanocluster Based Catalysis. *Langmuir* **2011**, *27*, 6279-6294.
58. Danh, N.-T.; Frenkel, A. I.; Wang, J.; O'Brien, S.; Akins, D. L., Cobalt-polypyrrole-carbon black (Co-PPY-CB) electrocatalysts for the oxygen reduction reaction (ORR) in fuel cells: Composition and kinetic activity. *Applied Catalysis B-Environmental* **2011**, *105*, 50-60.
59. Du, W.; Su, D.; Wang, Q.; Frenkel, A. I.; Teng, X., Promotional Effects of Bismuth on the Formation of Platinum-Bismuth Nanowires Network and the Electrocatalytic Activity toward Ethanol Oxidation. *Cryst. Growth Des.* **2011**, *11*, 594-599.
60. Du, W.; Wang, Q.; LaScala, C. A.; Zhang, L.; Su, D.; Frenkel, A. I.; Mathur, V. K.; Teng, X., Ternary PtSnRh-SnO<sub>2</sub> nanoclusters: synthesis and electroactivity for ethanol oxidation fuel cell reaction. *J. Mater. Chem.* **2011**, *21*, 8887-8892.
61. Du, W.; Wang, Q.; Saxner, D.; Deskins, N. A.; Su, D.; Krzanowski, J. E.; Frenkel, A. I.; Teng, X., Highly Active Iridium/Iridium-Tin/Tin Oxide Heterogeneous Nanoparticles as Alternative Electrocatalysts for the Ethanol Oxidation Reaction. *J. Am. Chem. Soc.* **2011**, *133*, 15172-15183.
62. Frenkel, A. I.; Wang, Q.; Marinkovic, N.; Chen, J. G.; Barrio, L.; Si, R.; Lopez Camara, A.; Estrella, A. M.; Rodriguez, J. A.; Hanson, J. C., Combining X-ray Absorption and X-ray Diffraction Techniques for *in-situ* Studies of Chemical Transformations in Heterogeneous Catalysis: Advantages and Limitations. *J. Phys. Chem. C* **2011**, *115*, 17884-17890.
63. Frenkel, A. I.; Yevick, A.; Cooper, C.; Vasic, R., Modeling the Structure and Composition of Nanoparticles by Extended X-Ray Absorption Fine-Structure Spectroscopy. *Annual Review Of Analytical Chemistry, Vol 4* **2011**, *4*, 23-39.
64. Li, L.; Zhang, Z.; Ciston, J.; Stach, E. A.; Wang, L.-l.; Johnson, D. D.; Wang, Q.; Frenkel, A. I.; Sanchez, S. I.; Small, M. W.; Nuzzo, R. G.; Yang, J. C., H<sub>2</sub>-driven crystallization of supported Pt nanoparticles observed with aberration-corrected Environmental TEM. *Microsc. Microanal.* **2011**, *17*, 1604-1605.
65. Marinkovic, N. S.; Wang, Q.; Barrio, L.; Ehrlich, S. N.; Khalid, S.; Cooper, C.; Frenkel, A. I., Combined *in-situ* X-ray absorption and diffuse reflectance infrared spectroscopy: An attractive tool for catalytic investigations. *Nuclear Instruments & Methods In Physics Research Section A* **2011**, *649*, 204-206.
66. Marinkovic, N. S.; Wang, Q.; Frenkel, A. I., *In-situ* diffuse reflectance IR spectroscopy and X-ray absorption spectroscopy for fast catalytic processes. *Journal Of Synchrotron Radiation* **2011**, *18*, 447-455.
67. Paredis, K.; Ono, L. K.; Behafarid, F.; Zhang, Z.; Yang, J. C.; Frenkel, A. I.; Cuenya, B. R., Evolution of the Structure and Chemical State of Pd Nanoparticles during the *in-situ* Catalytic Reduction of NO with H<sub>2</sub>. *J. Am. Chem. Soc.* **2011**, *133*, 13455-13464.
68. Paredis, K.; Ono, L. K.; Mostafa, S.; Li, L.; Zhang, Z.; Yang, J. C.; Barrio, L.; Frenkel, A. I.; Cuenya, B. R., Structure, chemical composition, and reactivity correlations during the *in-situ* oxidation of 2-propanol. *J. Am. Chem. Soc.* **2011**, *133*, 6728-6735.
69. Sasaki, K.; Kuttiyiel, K. A.; Barrio, L.; Su, D.; Frenkel, A. I.; Marinkovic, N.; Mahajan, D.; Adzic, R. R., Carbon-Supported IrNi Core-Shell Nanoparticles: Synthesis, Characterization, and Catalytic Activity. *J. Phys. Chem. C* **2011**, *115*, 9894-9902.
70. Zhang, Z.; Li, L.; Wang, L.-l.; Sanchez, S. I.; Wang, Q.; Johnson, D. D.; Frenkel, A. I.; Nuzzo, R. G.; Yang, J. C., The Role of  $\gamma$ -Al<sub>2</sub>O<sub>3</sub> Single Crystal Support to Pt Nanoparticles Construction. *Microsc. Microanal.* **2011**, *17*, 1324-1325.
71. Zhang, Z.; Li, L.; Yang, J. C.,  $\gamma$ -Al<sub>2</sub>O<sub>3</sub> thin film formation via oxidation of  $\beta$ -NiAl(1 1 0). *Acta Mater.* **2011**, *59*, 5905-5916.
72. Lei, H.; Ryu, H.; Frenkel, A. I.; Petrovic, C., Anisotropy in BaFe<sub>2</sub>Se<sub>3</sub> single crystals with double chains of FeSe tetrahedra *Physical Review B* **2011**, *84*, 214511.

73. Shen, X.-F.; Morey, A.; Liu, J.; Ding, Y.-S.; Durand, J.; Wang, Q.; Wen, W.; Hines, W. A.; Hanson, J. C.; Bai, J.; Frenkel, A. I.; Reiff, W.; Aindow, M.; Suib, S. L.; Cai, J., Characterization of the Fe-doped mixed-valent tunnel structure manganese oxide KOMS-2 *J. Phys. Chem. C* **2011**, *115*, 21610-21619.
74. Coppage, R.; Slocik, J. M.; Briggs, B. D.; Frenkel, A. I.; Heinz, H.; Naik, R. R.; Knecht, M. R., Crystallographic Recognition Controls Peptide Binding for Bio-Based Nanomaterials. *J. Am. Chem. Soc.* **2011**, *133*, 12346-12349.

**Competing Forces in Enantioselective Heterogeneous Catalysis and Separations:  
Enantiospecific Energetics and Auto-Amplification**

Andrew J. Gellman, Yongju Yun, Bharat S. Mhatre  
Dept. of Chemical Engineering, Carnegie Mellon University

**Presentation Abstract**

One of the critical limitations of past studies of the surface chemistry of adsorbed enantiomers was the inability to distinguish one enantiomer from the other when adsorbed as mixtures. A methodology has been developed that uses mixtures of amino acids in which the L-enantiomer is labelled with  $^{13}\text{C}$ , thus allowing enantiomer differentiation using mass spectrometry. Using a racemic mixture of D- and  $^{13}\text{C}$ -L-aspartic acid it has been possible, for the first time, to demonstrate enantiospecific adsorption and separation on naturally chiral metal surfaces,  $\text{Cu}(3,1,17)^{\text{R\&S}}$ . Exposure of these surfaces to a racemic vapor phase with an enantiomeric excess of  $ee_g = 0$  results in the adsorption of a mixture with  $ee_s = 39 \pm 3\%$ . This translates to an enantiospecific difference in the adsorption energies of D- and L-Asp of  $\Delta\Delta G_{ads} = 3.2 \pm 0.3$  kJ/mole. The new methodology has allowed us to discover a phenomenon that would never have been observed without  $^{13}\text{C}$  labelling. Not surprisingly, exposure of a racemic mixture of D- and  $^{13}\text{C}$ -L-aspartic acid to the achiral Cu(111) results in the adsorption of a racemic mixture; in other words, a gas phase mixture with  $ee_g = 0$  results in an adsorbed mixture with  $ee_g = 0$ . However, exposure of the achiral Cu(111) surface to a gas phase mixture with  $ee_g = 0.2$  results in an adsorbed phase with  $ee_s = 0.4$ . In spite of the fact that the surface is achiral, adsorption results in auto-amplification of enantiomeric excess. Although the mechanism of this auto-amplification has not been confirmed, one can show that this can be a simple consequence of adsorption of gas phase monomers in the form of homochiral clusters  $L_n$  or  $D_n$ . Auto-amplification and enantiospecific adsorption energetics must be ubiquitous to enantiomer adsorption and catalysis.

**DOE Grant No. DE-FG02-12ER16330**

**Molecular-Level Design of Heterogeneous Chiral Catalysts**

**PI:** W.T. Tysoe (PI), N. Shukla, F. Zaera

**Postdoc(s):** M. Garvey, S. Devarajan, I. Lee, A. Gordon, S. Karakalos

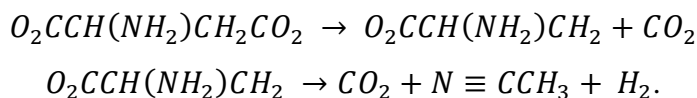
**Student(s):** J. Hong, C. Janini, J. Kestell, C. Lin, M. Mahapatra, A. Reinkicker, X. Xing

**Affiliations(s):** University of Wisconsin – Milwaukee, University of California - Riverside

**RECENT PROGRESS**

*Naturally Chiral Surfaces*

*Catalytic decomposition of D- and \*L-Asp.* Recently, we have demonstrated that the decomposition of D- and \*L-Asp can be performed catalytically and in steady state on the Cu(111) surface. The decomposition mechanism for aspartic acid on Cu(111) is:



Because all of the decomposition products desorb from the surface, the decomposition reaction can be performed catalytically in steady state at a fixed temperature and in a flux of gas phase Asp. The reaction has been performed to ~50 turnovers at 600 K without signs of deactivating the surface (Figure 1). The enantiospecific catalytic decomposition of D- and \*L-Asp or mixtures of the two can now be studied in steady state on achiral and chiral Cu surfaces.

*Spatial mapping of enantiospecific decomposition.* We have now begun to collect data on the decomposition of tartaric acid decomposition on Structure Spread Single Crystal Surfaces (S<sup>4</sup>Cs). These are spherical sections of Cu single crystals that expose a distribution of crystal planes that span a continuous region of the stereographic projection. Explosive decomposition of tartaric acid has been shown in our prior work to be highly enantiospecific on chiral single crystal surfaces. We have mapped the structure sensitivity of TA decomposition across a Cu(111) S<sup>4</sup>C surface that spans all crystallographic orientations within 6° of the Cu(111) pole. The explosive decomposition has been initiated by isothermal heating and then quenched at different extents of reaction. Following the quench, imaging XPS is used to map the local coverages TA on the surface (Figure 2). These initial experiments clearly show structure sensitivity in that the decomposition is more rapid along the directions which expose (100) steps than along those directions that expose (111) step edges. Furthermore, the decomposition kinetics clearly depend on step density and the rate of decomposition increases as one moves away from the (111) pole.

### Templated Chiral Surfaces

Work on chiral templates has focused on our ability to correlate surface structures with the enantioselective adsorption of a chiral probe on modified surfaces, primarily using propylene oxide as the probe molecule. First, the Tysoe group has extended the range of chiral modifiers to TA, a chiral modifier for the hydrogenation of β-ketoesters, and to using other chiral probes, glycidol. Tysoe has also used density functional theory to identify the nature of the dimer, tetramer or dimer row structures formed from aminoacids on Pd(111) surfaces, where the tetrameric structures are found to be enantioselective.

In the second area, the Zaera group is exploring auto-enantioselective effects by using propylene oxide as a modifier for itself. The idea underlying this approach is that different packing structures may be available for chiral and racemic mixtures of propylene

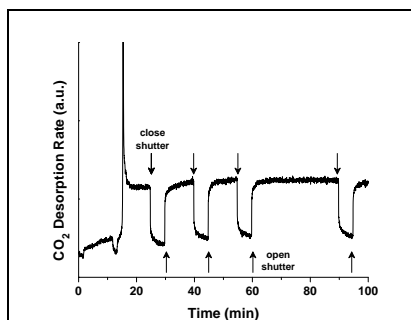


**Figure 1.** CO<sub>2</sub> production during steady state decomposition of D-Asp on Cu(111). The spike at 16 min is explosive decomposition of the Asp monolayer during initial heating to 600 K, after which the Cu(111) is held at 600 K in a flux of D-Asp. A shutter is periodically closed and then re-opened during steady-state decomposition.

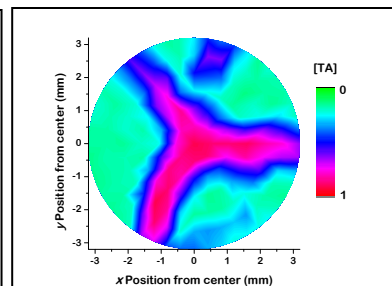


**Figure 2.** Coverage map of TA remaining on the Cu(111)±6° surface after heating a saturated surface at 440K until the extent of the decomposition reaction reached 70%. The remaining TA is clearly distributed along the directions that expose straight (111) step edges. The TA remaining at the top of the sample is due to a defect in the surface around that point.

oxide that modify the attainable saturation coverages. Enantiospecific, adsorbate-enhancement of the sticking coefficient is found for propylene oxide on Pt(111).

In the last year, the Zaera group has focused on contrasting the differences in adsorption of chiral compounds on platinum surfaces when dealing with enantiopure compounds *versus* racemic or mixed R-S adsorbates. In general, the enantiomers of chiral compounds are mirror images of each other, and exhibit identical chemical and physical properties. However, many mixtures of enantiomers of single

chiral compounds exhibit different properties than each of the enantiomers alone. This is because opposite enantiomers usually pair up and form racemic compounds *via* strong interactions such as hydrogen bonding. In Zaera's study of the uptake of propylene oxide (PO) on Pt(111), a unique behavior was observed where the differences are due to a kinetic effect instead. First, temperature-programmed desorption (TPD) data showed that the density of the saturated monolayers of propylene oxide (PO) adsorbed on a Pt(111) single-crystal surface changes monotonically with enantiomeric composition, decreasing by approximately 20% when going from enantiopure to racemic layers (Figure 3).

Scanning tunneling microscopy (STM) images were then used to corroborate the coverage changes, and also to reveal that there is no racemate formation or long-range ordering on these surfaces. This work was done in collaboration with Prof. Charles Sykes, of Tufts University. It was found that the density of the racemic PO layers could be increased slightly, if the uptake is carried out at higher temperatures, an indication that the observed behavior is kinetically controlled. However, this effect was found to be limited by competition with desorption from the surface. Additional STM work is currently being carried out by the Tysoe group on trifluoropropylene on Pd(111) to supplement this information. Here, the fluorinated molecules were used to enhance the contrast in STM. Preliminary results are shown in Figure 4 suggesting that there are attracting lateral interactions between the molecules.

### New Chiral Materials

One of the possible routes to formation of chiral catalytic materials on a large scale is the imprinting of chirality by molecular adsorbates into initially achiral materials. This phenomenon differs from chiral templating in which the adsorbed layer is chiral but does not cause reconstruction of the underlying substrate. During the decomposition of TA on Cu(110) we have observed that Cu atoms are extracted from the surface to form a chiral structure whose handedness depends on the chirality of the TA decomposing on the surface. LEED patterns show this reconstructed surface to have  $(2, \bar{1}; 6, 7)$  periodicity when formed from L-TA and  $(2, 1; 6, \bar{7})$  when formed from D-TA. This type of imprinting phenomenon may be quite common and may well occur with the Asp being used in these studies.

We have continued to develop the synthesis of chiral Au

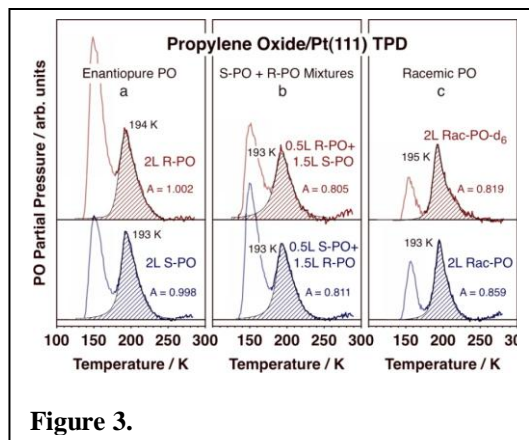


Figure 3.

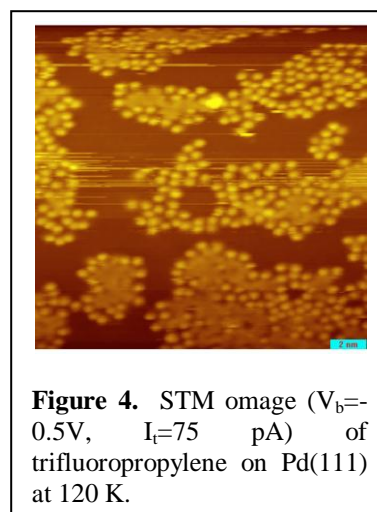
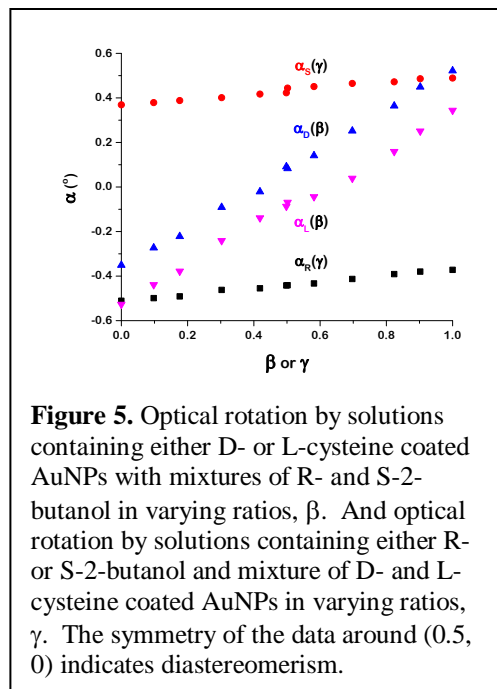


Figure 4. STM image ( $V_b = -0.5V$ ,  $I_t = 75$  pA) of trifluoropropylene on Pd(111) at 120 K.

nanoparticles and our methodology for studying enantioselective adsorption using optical polarimetry. Over the past year we have developed and published a methodology for using polarimetry measurements as the basis for a robust means of measuring the enantiospecificity of adsorption equilibrium constants for chiral molecules on chiral Au NPs. In one experiment we measure optical rotation,  $\alpha$ , for solutions containing either D- or L-modified Au NPs (at constant concentration) and R- and S-probe molecules in varying ratios,  $\beta$ . In a complementary experiment, we measure optical rotation for solutions containing either R- or S-probe molecule (at constant concentration) and D- and L-modified Au NPs in varying ratios,  $\gamma$ . Examples are shown in Figure 5 for R- and S-2-butanol in solutions containing D- or L-cysteine coated AuNPs. The following expression can be used for parameter estimation of the enantiospecific adsorption equilibrium constants,  $K_D$  and  $K_L$ , from the optical rotation data.



**Figure 5.** Optical rotation by solutions containing either D- or L-cysteine coated AuNPs with mixtures of R- and S-2-butanol in varying ratios,  $\beta$ . And optical rotation by solutions containing either R- or S-2-butanol and mixture of D- and L-cysteine coated AuNPs in varying ratios,  $\gamma$ . The symmetry of the data around (0.5, 0) indicates diastereomerism.

$$\alpha'_D(\beta) = \frac{\alpha(\beta)}{x_{tot}\alpha_{sol}} = -\left(\frac{1 + \bar{\alpha}\bar{K}_D}{1 + \bar{K}_D}\right) + \left[\left(\frac{1 + \bar{\alpha}\bar{K}_L}{1 + \bar{K}_L}\right) + \left(\frac{1 + \bar{\alpha}\bar{K}_D}{1 + \bar{K}_D}\right)\right]\beta$$

$$\alpha'_L(\beta) = \frac{\alpha(\beta)}{x_{tot}\alpha_{sol}} = -\left(\frac{1 + \bar{\alpha}\bar{K}_L}{1 + \bar{K}_L}\right) + \left[\left(\frac{1 + \bar{\alpha}\bar{K}_L}{1 + \bar{K}_L}\right) + \left(\frac{1 + \bar{\alpha}\bar{K}_D}{1 + \bar{K}_D}\right)\right]\beta$$

$$\alpha'_S(\gamma) = \frac{1 + \bar{\alpha}(\gamma\bar{K}_D + (1 - \gamma)\bar{K}_L)}{1 + (\gamma\bar{K}_D + (1 - \gamma)\bar{K}_L)}$$

$$\alpha'_R(\gamma) = \frac{1 + \bar{\alpha}(\gamma\bar{K}_L + (1 - \gamma)\bar{K}_D)}{1 + (\gamma\bar{K}_L + (1 - \gamma)\bar{K}_D)}$$

Recently, we have developed syntheses of Au NPs that are coated with N-acetyl-L-cysteine (N-acetyl-D-cysteine) or with N-isobutyryl-L-cysteine (N-isobutyryl-D-cysteine). These sets of optical rotation measurements are now being extended to AuNPs coated with these chiral ligands and using new chiral probes that include known chiral pharmaceuticals for which we can purchase both enantiomers. Finally, we have learned how to synthesize nanoparticle that with tetrahedral shapes, exposing 24 facets that have high Miller index orientations. Because these expose a single crystal surface, these ought to be superior nanoparticles for enantioselective adsorption once they are modified by adsorption of chiral ligands. Current work is aimed at chiral modification of these nanoparticles.

### Publications Acknowledging this Grant in 2011-2014

1. Identifying Molecular Species on Surfaces by Scanning Tunneling Microscopy: Methyl Pyruvate on Pd(111), Michael Garvey, Yun Bai, J. Anibal Boscoboinik, Luke Burkholder, T.E. Sorensen and W.T. Tysoe., *J. Phys. Chem. C*, **117**, 4505-4514 (2013)
2. Formation of Chiral Self-Assembled Structures of Amino Acids on Transition-Metal Surfaces: Alanine on Pd(111), Mausumi Mahapatra , Luke Burkholder, Yun Bai, Michael Garvey, J. Anibal Boscoboinik, Carol Hirschmugl and Wilfred T. Tysoe, *Journal of Physical Chemistry C*, **118**, 6856–6865 (2014)
3. Structure and Decomposition Pathways of D-(-)-Tartaric Acid on Pd(111), Mausumi Mahapatra and Wilfred T. Tysoe, *Surface Science*, In press (2014)
4. Adsorption and Reaction Pathways of a Chiral Probe Molecule, S-glycidol on a Pd(111) Surface, Mausumi Mahapatra and Wilfred T. Tysoe, *Catalysis Science & Technology*, submitted (2014). INVITED.
5. W.Y. Cheong, A.J. Gellman “Enantiospecific desorption of R- and S-propylene oxide from D- or L-lysine Modified Cu(100) Surfaces” *Langmuir*, **28**, (2012), 15251–15262
6. Y. Yun, A.J. Gellman, “Enantioselective separation of DL-aspartic acid on naturally chiral Cu(3,1,7)<sup>R&S</sup> surfaces” *Angewandte Chemie International Edition*, **52**, (2013), 3394-3397
7. B. Mahtre, V.V. Pushkarev, B. Holsclaw, T.J. Lawton, E.C.H. Sykes, A.J. Gellman, “A Window on Surface Explosions: Tartaric Acid on Cu(110)” *Journal of Physical Chemistry C*, **117**, (2014) 7577-7588
8. A.J. Gellman, Y. Huang, F. Xu, V.V. Pushkarev, B. Holsclaw, B. Mhatre, “Super-enantioselective chiral surface explosions” *Journal of the American Chemical Society*, **135(51)**, (2013), 19208-19214
9. N. Shukla, N. Ondeck, A.J. Gellman, “Quantitation of Enantiospecific Adsorption on Chiral Nanoparticles from Optical Rotation” *Surface Science* (2014), *in press*
10. N. Shukla, N. Ondeck, N. Khosla, S. Klara, A. Petti, A.J. Gellman “Effect of wavelength and temperature on measurements of optical rotation during enantiospecific adsorption on chiral Au nanoparticles” *in preparation*
11. Y. Yun, A.J. Gellman, “Auto amplification of enantiomeric excess by adsorption on achiral surfaces” *in preparation*
12. B.S. Mhatre, Y. Yun, A.J. Gellman, “Kinetics and mechanism of aspartic acid decomposition on Cu(110)” *in preparation* Stavros Karakalos, Timothy J. Lawton, Felicia R. Lucci, E. Charles H. Sykes, and Francisco Zaera, Enantiospecific Kinetics in Surface Adsorption: Propylene Oxide on Pt(111) Surfaces, *J. Phys. Chem. C*, **117(36)**, 18588-18594 (2013).
13. Alexander D. Gordon, Stavros Karakalos, and Francisco Zaera, Dependence of the Adsorption of Chiral Compounds on their Enantiomeric Composition, *Surf. Sci.*, DOI: 10.1016/j.susc.2014.02.003 (2014). INVITED, Topical Special Issue of Surface Science on "Chirality at Surfaces".

14. Junghyun Hong, Ilkeun Lee, and Francisco Zaera, Cinchona Alkaloids Anchored on Porous Silica as Enantioselective Heterogeneous Catalysts, *Top. Catal.*, **54(19/20)**, 1340-1347 (2011). INVITED (Special Issue, Chiral Surface Chemistry and Catalysis)
15. Junghyun Hong and Francisco Zaera, Interference by the Solid on the Performance of Tethered Molecular Catalysts, *J. Am. Chem. Soc.*, **134(31)**, 13056–13065 (2012)
16. Alexander D. Gordon and Francisco Zaera, Adsorption of 1-(1-Naphthyl)ethylamine from Solution onto Pt Surfaces: Implications for the Chiral Modification of Heterogeneous Catalysts, *Angew. Chem., Int. Ed.*, **52(12)**, 3453–3456 (2013)
17. N. Ondeck, N. Khosla, S. Klara, P. Downey, A. Petti, N. Shukla, A.J. Gellman “Effect of wavelength and temperature on measurements of optical rotation during enantiospecific adsorption on chiral Au nanoparticles” *in preparation*
18. N. Ondeck, N. Khosla, N. Shukla, A.J. Gellman “Quantitative analysis of optical rotation measurements of chiral probe molecules adsorbed on chiral metal nanoparticles” *in preparation*
19. Y. Yun, D. Wei, D.S. Sholl, and A.J. Gellman, “Equilibrium adsorption of D- and L-alanine mixtures on naturally chiral Cu{3,1,17}<sup>R&S</sup> surfaces” submitted to *Journal of Physical Chemistry C*
20. J.R. Boes, G. Gumuslu, J.B. Miller, A.J. Gellman, John R. Kitchin, “Estimating bulk composition dependent H<sub>2</sub>dissociative adsorption energies on Cu<sub>x</sub>Pd<sub>1-x</sub> alloy(111) surfaces” *in preparation*
21. B.S. Mhatre, A.J. Gellman, “Review of the surface reaction mechanisms leading to auto-catalysis and explosion kinetics” *in preparation*
22. M. Payne, J.B. Miller, A.J. Gellman, “High-throughput characterization of alloyoxidation behavior across Al<sub>x</sub>Fe<sub>y</sub>Ni<sub>1-x-y</sub> composition space” *in preparation*
23. Francisco Zaera, Shape-Controlled Nanostructures in Heterogeneous Catalysis, *ChemSusChem*, 6(10), 1797-1820 (2013). INVITED, SPECIAL ISSUE: "Shape-Controlled Nanostructures for Energy and Sustainability Applications"
24. Jie Li, Xiaoliang Liang, Ji Bong Joo, Ilkeun Lee, Yadong Yin, and Francisco Zaera, Mass Transport Across the Porous Oxide Shells of Core-Shell and Yolk-Shell Nanostructures in Liquid Phase, *J. Phys. Chem. C*, 117(39), 20043–20053 (2013).
25. Francisco Zaera, New Advances in Infrared Absorption Spectroscopy for the Characterization of Heterogeneous Catalytic Reactions, *Chem. Soc. Rev.*, DOI:10.1039/C3CS60374A (2014). INVITED, "Catalysis for Production of Renewable Energy" Special Issue

26. W.D. Michalak, J.B. Miller, C. Yoclu, A.J. Gellman “Fabrication of metallic nanoparticles by spinodal dewetting of thin films: A high-throughput approach” *Thin solid Films* **522**, (2012), 473-479
27. F. Braun, J.B. Miller, A.J. Gellman, A.M. Tarditi, B. Fleutot, P. Kondrayuk, L.M. Cornaglia, “PdAgAu alloy with high resistance to corrosion by H<sub>2</sub>S” *International Journal of Hydrogen Energy*, **37(23)**, (2012), 18547-18555
28. P. Kondratyuk, G. Gumuslu, S. Shukla, J.B. Miller, B.D. Morreale, A.J. Gellman “A Microreactor Array for Spatially-Resolved Measurement of Catalytic Activity on Composition Spread Alloy Films: a Device for High-Throughput Catalyst Evaluation” *Journal of Catalysis*, **300**, (2013), 55–62
29. W.D. Michalak, A.J. Gellman, “Reaction Path Analysis of Dynamic Systems: Identifying the Dominant Transition and Intermediate States” *Journal of Physical Chemistry B*, submitted
30. Francisco Zaera, Surface Chemistry at the Liquid/Solid Interface, *Surf. Sci.*, **605(13/14)**, 1141-1145 (2011). INVITED, PROSPECTIVE
31. Menno Bouman and Francisco Zaera, Reductive Eliminations from Amido Complexes, *J. Electrochem. Soc.*, **158(8)**, D524-D526 (2011).
32. Qiao Zhang, Diana Q. Lima, Ilkeun Lee, Francisco Zaera, Miaofang Chi and Yadong Yin, A Highly Active TiO<sub>2</sub>-Based Visible-Light Photocatalyst with Nonmetal Doping and Plasmonic Metal Decoration, *Angew. Chem., Int. Ed.*, **50(31)**, 7088-7092 (2011).
33. Qiang Ma, Roy G. Gordon, and Francisco Zaera, Surface Chemistry of Copper(I) Acetamidates in Connection with Atomic Layer Deposition (ALD) Processes, *Chem. Mater.*, **23(14)**, 3325-3334 (2011).
34. Huaxing Sun, Xiangdong Qin, and Francisco Zaera, Chemical Nature of the Thin Films that Grow on SiO<sub>2</sub>/Si(100) Surfaces Upon Manganese Deposition, *J. Phys. Chem. Lett.*, **2 (20)**, 2525–2530 (2011).
35. Ilkeun Lee, Ji Bong Joo, Yadong Yin and Francisco Zaera, A New York@Shell Nanoarchitecture for Au/TiO<sub>2</sub> Catalysts, *Angew. Chem., Int. Ed.*, **50(43)**, 10208–10211 (2011). INVITED
36. Xiangdong Qin, Huaxing Sun, and Francisco Zaera, Thermal Chemistry of Mn<sub>2</sub>(CO)<sub>10</sub> during Deposition of Thin Manganese Films on Silicon Oxide and on Copper Surfaces, *J. Vac. Sci. Technol. A*, **30(1)**, 01A112/1-01A112/10 (2012). SPECIAL ISSUE: ALD
37. Qiang Ma, Roy G. Gordon, and Francisco Zaera, Thermal Chemistry of Copper(I)-N,N'-di-sec-butylacetamidate on Cu(110) Single-Crystal Surfaces, *J. Vac. Sci. Technol. A*, **30(1)**, 01A114/1-01A114/10 (2012). SPECIAL ISSUE: ALD

38. Ji Bong Joo, Qiao Zhang, Ilkeun Lee, Michael Dahl, Francisco Zaera, and Yadong Yin, Mesoporous Anatase Titania Hollow Nanostructures through Silica-Protected Calcination, *Adv. Funct. Mater.*, **22**, 166-174 (2012).
39. Ji Bong Joo, Qiao Zhang, Michael Dahl, Ilkeun Lee, James Goebel, Francisco Zaera, and Yadong Yin, Control of the Nanoscale Crystallinity in Mesoporous TiO<sub>2</sub> Shells for Enhanced Photocatalytic Activity, *Energy Environ. Sci.*, **5**, 6321-6327 (2012).
40. Taeseung Kim and Francisco Zaera, X-Ray-Initiated Metal-Promoted Thin Film Growth, *J. Phys. Chem. C*, **116(15)**, 8594-8600 (2012).
41. Layer Depositions of Solid Thin Films, *J. Phys. Chem. Lett.*, **3**, 1301-1309 (2012). INVITED
42. Francisco Zaera, New Challenges in Heterogeneous Catalysis for the 21st Century, *Catal. Lett.*, **142(5)**, 501-516 (2012). INVITED PERSPECTIVE
43. Francisco Zaera, Probing Liquid/Solid Interfaces at the Molecular Level, *Chem. Rev.*, **112(5)**, 2920-2986 (2012).
44. Xiaoliang Liang, Jie Li, Ji Bong Joo, Alejandro Gutiérrez, Aashani Tillekaratne, Ilkeun Lee, Yadong Yi, and Francisco Zaera, Diffusion through the Shells of Yolk@Shell and Core@Shell Nanostructures in Liquid Phase, *Angew. Chem., Int. Ed.*, **51(32)**, 8034-8036 (2012).
45. Huaxing Sun, Xiangdong Qin, and Francisco Zaera, Activation of Metalorganic Precursors by Electron Bombardment in the Gas Phase for Enhanced Deposition of Solid Films, *J. Phys. Chem. Lett.*, **3**, 2523-2527 (2012).
46. Francisco Zaera, Infrared Absorption Spectroscopy of Adsorbed CO: New Applications in Nanocatalysis for an Old Approach, *ChemCatChem*, **4(10)**, 1525-1533 (2012). INVITED
47. Qiang Ma and Francisco Zaera, The Chemistry of Cu(acac)<sub>2</sub> on Ni(110) and Cu(110) Surfaces: Implications for Atomic Layer Deposition (ALD) Processes, *J. Vac. Sci. Technol. A*, **31(1)**, A01A112/1-A01A112/10 (2013).
48. Huaxing Sun and Francisco Zaera, Chemical Deposition of Manganese Metallic Films on Silicon Oxide Substrates, *J. Phys. Chem. C.*, **116 (44)**, 23585-23595 (2012).
49. Robert J. Dillon, Ji-Bong Joo, Francisco Zaera, Yadong Yin, and Christopher J. Bardeen, Correlating the excited state relaxation dynamics as measured by photoluminescence and transient absorption with the photocatalytic activity of Au@TiO<sub>2</sub> core-shell nanostructures, *Phys. Chem. Chem. Phys.*, **15**, 1488-1496 (2013).
50. Ji Bong Joo, Qiao Zhang, Michael Dahl, Francisco Zaera, Yadong Yin, Synthesis, Crystallinity Control, and Photocatalysis of Nanostructured TiO<sub>2</sub> Shells, *J. Mater. Res.*, **28(03)**, 362-368 (2013).
51. Francisco Zaera, Nanostructured Materials for Applications in Heterogeneous Catalysis, *Chem. Soc. Rev.*, **42(7)**, 2746-2762 (2013). INVITED

52. Qiao Zhang, Ilkeun Lee, Ji Bong Joo, Francisco Zaera and Yadong Yin, Core-Shell Nanostructured Catalysts, *Acc. Chem. Res.*, DOI: 10.1021/ar300230s (2013). INVITED
53. Ji Bong Joo, Ilkeun Lee, Michael Dahl, Geondae Moon, Francisco Zaera, Yadong Yin, Controllable Synthesis of Mesoporous TiO<sub>2</sub> Hollow Shells: Toward an Efficient Photocatalyst, *Adv. Func. Mater.*, DOI: 10.1002/adfm.201300255 (2013).

**Michael A. Henderson**

**Partial Oxidation of Alkenes on TiO<sub>2</sub>(110) Through Photochemistry**

Michael A Henderson

Physical Sciences Division, Fundamental and Computational Sciences Directorate,  
and Institute for Integrated Catalysis, Pacific Northwest National Laboratory

The partial oxidation of alkenes (ethene, propene and isomers of butene) was examined on the model rutile TiO<sub>2</sub>(110) surface using temperature programmed desorption and photostimulated desorption.<sup>1,2</sup> This class of molecules interacts weakly with most semiconducting oxide surfaces, with little reactivity to partial oxidation products at low temperature. Photooxidation reactions offer a means of low temperature partial oxidation if the selectivity can be controlled and the extent of reaction limited (to prevent full oxidation). These factors pose significant challenges to researchers interested in using oxide surfaces to photocatalyze partial oxidation reactions. Fundamental studies with these molecules on TiO<sub>2</sub>(110) demonstrate a variety of photochemical phenomena that include direct activation (involving charge transfer between the molecule and the surface), indirect activation (in which secondary species, such as O<sub>2</sub>, are photochemically activated first), competition between photochemical pathways, and variations in oxidation selectivity depending on the form of activating oxygen. For example, atomic oxygen leads to undesirable C=C bond activation (to acetone) in isobutene, but physisorbed O<sub>2</sub> promotes photochemical formation of methacrolein and isobutanal. In the general case of 2-butenes, methyl configurations about the C=C play a major factor in the molecule's photoactivity. Understanding these processes is key toward controlling photocatalytic selectivity and ultimately being able to use semiconductor photocatalysis for performing selective chemistry.

This work was supported by the US Department of Energy, Office of Basic Energy Sciences, Division of Chemical Sciences, Geosciences & Biosciences. Pacific Northwest National Laboratory (PNNL) is a multiprogram national laboratory operated for DOE by Battelle. The research was performed using EMSL, a national scientific user facility sponsored by the Department of Energy's Office of Biological and Environmental Research and located at Pacific Northwest National Laboratory.

<sup>1</sup> Henderson, M. A. Comparison of the Photodesorption Activities of cis-Butene, trans-Butene, and Isobutene on the Rutile TiO<sub>2</sub>(110) Surface." *J. Phys. Chem. C* **2013**, *117*, 23840-23847.

<sup>2</sup> Henderson, M. A. Photooxidation and Photodesorption in the Photochemistry of Isobutene on TiO<sub>2</sub>(110). *J. Phys. Chem. C* **2013**, *117*, 14113-14124.

**DE-AC05-76RL0 1830:  
Multifunctional Catalysis to Synthesize  
and Utilize Energy Carriers**

**PI: Johannes Lercher**

**Theoretical Investigation of Heterogeneous Catalysis at the Solid-Liquid Interface for the Conversion of Lignocellulosic Biomass Model Molecules**

Andreas Heyden, Jianmin Lu, Muhammad Faheem, Sina Behtash  
University of South Carolina, Department of Chemical Engineering

**Presentation Abstract**

The *objectives* of this research program are to develop and validate a hierarchy of multi-scale methods for computing reaction and activation free energies of elementary processes occurring at metal-water interfaces and to apply these methods to the rational design of novel heterogeneous catalysts with exceptional activity and selectivity for the liquid-phase conversion of lignocellulosic biomass into transportation fuels or commodity and specialty chemicals. An overarching theme of our method developments has been practicability and rapid applicability such that we aim at limiting the computational cost of our novel methods for computing free energies of elementary processes at metal-liquid interfaces to a cost of only two orders of magnitude higher than that of similar calculations at solid-gas interfaces. To achieve at the same time high accuracy in our free energy calculations, we rely on adapting and optimizing previously developed computational tools in the enzyme and homogeneous catalysis communities. In particular, by adapting already parameterized and validated methods from these communities, we reap the benefits of experience of many decades of computational studies in liquid phase environments. Consequently, we can minimize our own parameterization effort which is often very time consuming and dependent on the availability of a large and well-balanced set of experimental or “high-level” computational data. In the heterogeneous catalysis community these data are often lacking due to the extreme complexity of heterogeneous catalysis. As model systems for our computational study, we investigate selectivity issues in the reductive deoxygenation of ethylene glycol, glycerol, guaiacol, and propionic acid over transition metal catalysts under liquid-phase processing conditions.

**DE-FG02-11ER16268: Theoretical Investigation of Heterogeneous Catalysis at the Solid-Liquid Interface for the Conversion of Lignocellulosic Biomass Model Molecules**

PI: Andreas Heyden  
Postdoc: Jianmin Lu  
Students: Muhammad Faheem, Sina Behtash

**RECENT PROGRESS**

***Explicit Solvation for Metal Surfaces (eSMS)***

We report the development of a quantum mechanics/molecular mechanics free energy perturbation (QM/MM-FEP) method for modeling chemical reactions at metal-water interfaces. This novel solvation scheme combines planewave density function theory (DFT), periodic electrostatic embedded cluster method (PEECM) calculations using Gaussian-type orbitals, and classical molecular dynamics (MD) simulations to obtain a free energy description of a complex

metal-water system. We derive a potential of mean force (PMF) of the reaction system within the QM/MM framework. A fixed-size, finite ensemble of MM conformations is used to permit precise evaluation of the PMF of QM coordinates and its gradient defined within this ensemble. Local conformations of adsorbed reaction moieties are optimized using sequential MD-sampling and QM-optimization steps. An approximate reaction coordinate is constructed using a number of interpolated states and the free energy difference between adjacent states is calculated using the QM/MM-FEP method. By avoiding on-the-fly QM calculations and by circumventing the challenges associated with statistical averaging during MD sampling, a computational speedup of multiple orders of magnitude is realized. The method is systematically validated against the results of *ab initio* QM calculations and demonstrated for C–C cleavage in double-dehydrogenated ethylene glycol on a Pt (111) model surface.<sup>1</sup>

#### ***Applications of our Implicit Solvation Model for Metal Surfaces: HDO of Propionic Acid***

We recently developed an implicit solvation model for metal surfaces (*iSMS*) that permits rapid computation of approximate reaction free energies of elementary reactions occurring at solid–liquid interfaces within the framework of planewave DFT and implicit solvation models developed for nonperiodic clusters.<sup>2</sup> Here, we report the application of our *iSMS* method to identify the effects of liquid water, n-octane, and n-butanol on the hydrodeoxygenation (HDO) of propanoic acid over Pd (111) model surfaces. We developed a microkinetic model for the HDO based on parameters obtained from first principles and studied the reaction mechanism in vapor and liquid phase environments at a temperature of 473 K.<sup>3-5</sup> Our model predicts that for all reaction media, decarbonylation pathways are favored over decarboxylation pathways. However, in the presence of polar solvents like water, decarboxylation routes become competitive with decarbonylation routes. The activity of the Pd surface varies as a function of the environment as follows: water > n-butanol > octane  $\approx$  gas phase. Finally, a sensitivity analysis of our models suggests that both C–OH and C–H bond cleavages control the overall rate of the catalyst in all environments and are likely to be activity descriptors for the HDO of organic acids. The importance of C–H bond cleavage for the HDO over Pd catalysts has recently been experimentally confirmed by us by observing a primary kinetic isotope effect (KIE) on labeled propionic acid ( $\text{CH}_3\text{CD}_2\text{COOH}$ ). The experimental KIE of 1.6 is in excellent agreement with the computed one of 1.49.

#### ***Applications of our Implicit Solvation Model for Metal Surfaces: HDO of Guaiacol***

As a second application for *iSMS*, we investigated the reaction mechanism of the HDO of guaiacol to aromatic products over Ru (0001) and Pt (111) model surfaces in vapor and aqueous environments. Coverage dependent adsorption energies have been considered in the models that suggest that over Ru catalysts<sup>6</sup> the dominant HDO pathway proceeds via O–H cleavage of guaiacol,  $\text{C}_6\text{H}_4(\text{OH})(\text{OCH}_3)$ , to  $\text{C}_6\text{H}_4(\text{O})(\text{OCH}_3)$ , followed by dehydrogenation of the methoxy group to  $\text{C}_6\text{H}_4(\text{O})(\text{OC})$ , decarbonylation to  $\text{C}_6\text{H}_4\text{O}$ , and finally hydrogenation to phenol. In agreement with experimental results, phenol is predicted to be the major product and further deoxygenation of phenol to benzene is very slow. In contrast, over Pt catalysts catechol is the main reaction product which does not involve removal of any oxygen atoms.<sup>7</sup>

#### ***Applications of our Implicit Solvation Model for Metal Surfaces: HDO of Ethylene Glycol***

Finally, a third application of *iSMS* and our test bed system for our *eSMS* method development has been the HDO of ethylene glycol and glycerol over Pt (111) catalysts. Ethylene glycol is the

simplest molecule containing C-C, C-O, C-H, and O-H bonds and having a C/O stoichiometry of 1:1 as it is common in most biomass-derived polyols. As a result, ethylene glycol is an ideal model molecule to study solvent effects in the catalytic HDO of polyols over metal catalysts where the product distribution critically depends on competing C-C and C-O bond scissions. We developed a detailed microkinetic model for both the vapor and aqueous phase HDO of ethylene glycol over Pt (111) model surfaces and observe that a liquid phase environment facilitates C-O bond scissions relative to C-C bond dissociations.<sup>8</sup>

#### **Publications Acknowledging this Grant in 2012-2014**

1. Faheem, M.; Heyden, A. Hybrid quantum mechanics/molecular mechanics solvation scheme for computing free energies of reactions at metal-water interfaces. Under Review.
2. Faheem, M.; Suthirakun, S.; Heyden, A. New Implicit Solvation Scheme for Solid Surfaces. *J. Phys. Chem. C* **2012**, *116*, 22458-22462.
3. Lu, J.; Behtash, S.; Heyden, A. Theoretical Investigation of the Reaction Mechanism of the Decarboxylation and Decarbonylation of Propanoic Acid on Pd (111) Model Surfaces. *J. Phys. Chem. C* **2012**, *116*, 14328-14341.
4. Lu, J.; Behtash, S.; Faheem, M.; Heyden, A. Microkinetic Modeling of the Decarboxylation and Decarbonylation of Propanoic Acid over Pd (111) Model Surfaces Based on Parameters Obtained from First Principles. *J. Catal.* **2013**, *305*, 56-66.
5. Behtash, S.; Lu, J.; Faheem, M.; Heyden, A. Solvent Effects on the Hydrodeoxygenation of Propanoic Acid over Pd (111) Model Surfaces. *Green Chemistry* **2014**, *16*, 605-616.
6. Lu, J.; Heyden, A. Theoretical Investigation of the Reaction Mechanism of the Hydrodeoxygenation of Guaiacol over Ru (0001) Model Surfaces. Under Review.
7. Lu, J.; Behtash, S.; Heyden, A. Theoretical Investigation of the Reaction Mechanism of Guaiacol Hydrotreatment over Pt (111) Model Surfaces. To be submitted.
8. Faheem, M.; Heyden, A. To be submitted.

**Immobilized Molecular Catalysts in Cooperative Catalysis and Cascade Reactions**

Marcus Weck,<sup>1</sup> Seung Soon Jang,<sup>2</sup> C. David Sherrill<sup>2</sup>  
<sup>1</sup>New York University, <sup>2</sup>Georgia Institute of Technology

**Presentation Abstract**

**DE-FG02-03ER15459: Immobilized Molecular Catalysts:  
Cooperative Catalysis to Cascade Reactions**

**Postdocs:** Jonas Dimroth (NYU), Niels ten Brummelhuis (NYU), Lori Burns (GT), Nicholas Brunelli (GT), Yan Feng (GT), Eric Moschetta (GT)

**Students:** Michael Kahn (NYU), Jie Lu (NYU), Aaron Cohen (NYU), Byeong Jae Chun (GT), Matthew Kennedy (GT), Caroline Hoyt (GT), Wei Long (GT)

**RECENT PROGRESS**

This collaborative research program has focused on the design and understanding of cooperative catalysts that combine two distinct catalytic sites (e.g. acid and base) into a single material or molecule to effect catalytic reactions that are accelerated by cooperative interactions with the two sites, relative to catalysis by a single site. In a new direction within the team, these cooperative reactions are being extended to cascade reactions, whereby multiple individual catalytic steps are catalyzed in a series using different active centers. Cooperative catalysis and cascade catalysis are two examples of the use of designed, multi-functional catalysts, with both sites interacting with a substrate(s) simultaneously to effect a reaction in the former case, and with different sites working independently in a series in the latter case.

A major initiative in the past years has been the development of cooperative Co-Salen catalysts for epoxide ring-opening reactions (Weck, Jones), whereby some of the most efficient catalysts known have been synthesized and characterized. In recent work, the team has sought to understand on the molecular level the catalytic reaction pathway (Sherrill, Ludovice, Weck, Jones), which was proposed by Jacobsen and Blackmond ten years ago based on kinetic studies.

We (Sherrill) have used density functional theory (DFT) to study the rate-determining step for the hydrolytic kinetic resolution (HKR) of terminal epoxides as catalyzed by Co(III)-Salen-X, with X a counterion. The rate-determining step is thought to involve activation of the epoxide through its coordination to one Co(III)-Salen-X catalyst, concomitant with a ring-opening attack by activated OH<sup>-</sup> from Co(III)-Salen-OH [*in-situ* generated by loss of counterion from Co(III)-Salen-X]. Our previous studies of Metal-Salen complexes suggest an intricate electronic structure, hence we have used both the B3LYP and BP86 functionals to test variation in DFT results. We find quantitative differences but overall similar qualitative trends. Semi-empirical London dispersion corrections (DFT-D) lead to slight differences in the relative energies of attack at secondary vs tertiary carbons in the epoxide. Co(III)-Salen-OH by itself, without the presence of Co(III)-Salen-X (X being some other counterion), is not active in HKR. This might seem a result of Co(III)-Salen-OH being insufficiently Lewis acidic to activate the epoxide. Our computations indicate, however, that X=OH<sup>-</sup> binds epoxide nearly as well as X=Cl<sup>-</sup> (gas-phase or with implicit solvent correction). We are thus seeking the transition state with X=OH<sup>-</sup> to verify that its inactivity is primarily due to transition state destabilization and to probe the origin of this destabilization relative to active counterions. The computed barrier height for X=OAc<sup>-</sup> is less than half that of X=Cl<sup>-</sup>, consistent with the higher experimental reaction rate at half-conversion observed for OAc<sup>-</sup>. Propylene oxide and 1-hexene oxide exhibit similar barrier heights, meaning that observed differences in experimental reaction rates are due to other factors [such as different rates for initial counterion loss to create Co(III)-Salen-OH]. To date, significant new insights into the epoxide ring-opening reaction have been obtained, but the complete catalytic cycle is not yet defined.

Building on the above work, which involves cooperative activation of substrates by electrophilic and nucleophilic centers, we (Jones, Weck) are working on silica-supported and polymer-supported organocatalytic acid-base catalyzed (aldol, nitroaldol) reactions. Having determined that weakly acidic silanols were better cooperative partners than carboxylic acids in aldol reactions, we elucidated the optimal distance between the amines and silanols for aldol and nitroaldol reactions, showing they depend on the pore curvature and nature of the coupling partners in the reaction (ketone/aldol vs. nitroalkane/nitroaldol). By synthesizing a homologous series of aminosilanes (C1-C5 linkers), we showed that we could alter the catalytic activity by an order of magnitude by changing only the pore curvature and linker length in the nitroaldol

reaction. In contrast, the aldol reaction was much less sensitive to linker length, suggesting significant differences in reaction pathway of these seemingly similar reactions. Most recently, in addition to our linker length and pore size studies, we also examined the effect of incorporating heteroatoms (B, Al, Ga, Ti, Zr, and Ce) into the framework of the silica support for amine-silanol bifunctional catalysts. For the nitroaldol condensation, four of the six heteroatoms (B, Al, Ga, and Ti) increased the catalytic activity compared to the supported amine-silanol catalyst with no heteroatom substitution. Incorporating Ce into the silica did not change the catalytic activity, but incorporating Zr decreased the catalytic activity. We observed a decrease in catalytic activity for the aldol condensation for all heteroatom substitutions compared to the catalyst with no heteroatom substitution. These differences will be the subject of future theoretical/computational investigations by the team (Sherrill, Jang).

Moving from cooperative reactions to consecutive, cascade reactions, a major initiative within the team is the design of well-defined reaction environments to promote or control cascade reactions (Weck, Jang, Jones). Operation of multiple catalytic reactions in one pot is often limited by incompatibilities of the catalysts and reaction conditions. Inspired by nature where the compartmentalization of cells enables metabolism pathways to proceed simultaneously, we have designed and synthesized metal catalyst containing shell cross-linked micelles (SCMs) as well as multi compartment micelles (MCMs) that enable the site isolation of two or more incompatible catalytic systems. The SCMs were prepared from amphiphilic poly(2-oxazoline) triblock copolymers with orthogonal functional handles in the side-chains of hydrophobic and hydrophilic blocks to attach different metal catalysts and a cross-linkable middle block to stabilize the micelle structure from disassembly. As a test system, we immobilized Ru(II)-porphyrin in the shell and Co(III)-Salen complexes in the core respectively for tandem catalytic reactions. The first step of the tandem reaction is the Ru(II)-porphyrin-catalyzed epoxidation of terminal olefins and the second step is the Co(III)-Salen-catalyzed HKR of the racemic epoxide intermediate. We are also developing another class of tandem catalysis supported by SCMs combining transition metal- and organocatalysis. We use the immobilization of a Rh-TsDPEN complex that catalyzes the asymmetric transfer hydrogenation (ATH) for the enantioselective reduction of prochiral ketones in combination with a DMAP-derived organocatalyst (DMAP: 4-dimethylaminopyridine) for the acylation of secondary alcohols.

Multicompartment micelles are a particular type of supramolecular assembly, which features an additional level of microphase separation within a micellar core. Such a phenomenon is accessible using a triblock copolymer consisting of hydrophilic, hydrophobic, and fluorophilic blocks. The former of these three blocks solubilizes the polymer in an aqueous environment while the latter two are both internalized into the micellar core, where they phase separate to form discrete hydrophobic and fluorophilic domains. To date multicompartment micelles have been prepared and visualized but their applied uses remain non-existent. We are preparing multicompartment micelles where each block possesses a functional "handle," through which a series of modified catalysts can be covalently attached to during post-polymerization functionalization. Such a modified multicompartment micelle can be viewed as a nano-reactor, capable of carrying out a wide variety of multistep "cascade reactions."

To achieve predictive and mechanistic understanding of the correlation between the transport of reactant/product molecules and the structures of multicompartment micelles, full-atomistic molecular modeling simulations have been performed using the molecular dynamics simulation method (Jang, Weck). For this purpose, first, using density functional theory, thermodynamic characteristics such as the solvation free energies of key molecules such as reactants, products and blocks of micelle have been calculated to assess their hydrophilicity/hydrophobicity, which determines how regions of the micelle are associated with water molecules. The molecular interactions of reactants/products with the various blocks of the micelle and the segment-segment interactions between the blocks in the micelle have been evaluated by calculating the Chi-parameter based on Flory-Huggins theory to characterize the association of reactants/products with each compartment in the micelle and the block-block immiscibility, respectively, since it is desirable that the reactants/products have miscibility to some extent, while the individual blocks of the polymer need to attain a compartmentalized via the segregation among the blocks. To investigate the structure of overall multicompartment micelle, the distribution of compartments, the water content in each compartment, and the thickness of interphase between the compartments have been characterized from the equilibrated micelle structure via molecular dynamics simulations. For direct assessment of the transport properties of reactants/products, the energy barriers for molecular diffusion are being estimated using the potential of mean force via steered molecular dynamics simulations.

### Publications Acknowledging this Grant in 2011-2014

1. Madhavan, M.; Sommer, W.; Weck, M.; Supporting Multiple Organometallic Catalysts on Poly(norbornene) for Cyanide Addition to  $\alpha,\beta$ -Unsaturated Imides. *J. Mol. Catal. A. Chem.* **2011**, 334, 1-7. Editor's Choice Paper.
2. Liu, Y.; Rawlston, J.; Swann, A.T.; Takatani, T.; Sherrill, C.D.; Ludovice, P.J.; Weck, M.; The Bigger, the Better: Ring-size Effects of Macrocyclic Oligomeric Co(III)-salen Catalysts. *Chem. Sci.* **2011**, 2, 429-438.
3. Liu, Y.; Pinon, V.; Weck, M.; Poly(norbornene) Block Copolymer-Based Shell Cross-linked Micelles with Co(III)-salen Cores. *Polym. Chem.* **2011**, 2, 1964-1975.
4. Liu, Y.; Wang, Y.; Wang, Y.; Lu, J.; Pinon, V.; Weck, M.; Shell Cross-linked Micelle-Based Nanoreactors for the Substrate-Selective Hydrolytic Kinetic Resolution of Epoxides. *J. Am. Chem. Soc.* **2011**, 133, 14260-14263.
5. Venkatasubbaiah, K. Kays, E.; Hardcastle, K. I.; Jones, C. W.; Co(III)-Porphyrin Mediated Highly Regioselective Ring Opening of Terminal Epoxides with Alcohols and Phenols. *ACS. Catal.* **2011**, 1, 489-492.
6. Long, W.; Jones, C. W.; Hybrid Sulfonic Acid Catalysts Based on Silica-Supported Poly(Styrene Sulfonic Acid) Brush Materials and Their Application in Ester Hydrolysis. *ACS. Catal.* **2011**, 1, 674-681.
7. Kahn M. G. C.; Weck, M.; Highly Crosslinked Polycyclooctyl-Salen Cobalt (III) for the Hydrolytic Kinetic Resolution of Terminal Epoxides. *Catal. Sci. Tech.* **2012**, 2, 386-389.
8. Kahn, M. G. C.; Stenlid, J. H.; Weck, M.; Poly(styrene) Resin-Supported Co (III) Salen Cyclic Oligomers: Highly Active and Easily Recycled HKR Catalysts. *Adv. Synth. Catal.* **2012**, 354, 3016-3024.
9. Brunelli, N. A.; Didas, S. A.; Venkatasubbaiah, K.; Jones, C. W.; Tuning Cooperativity by Controlling the Linker Length of Silica-Supported Amines in Catalysis and CO<sub>2</sub> Capture. *J. Am. Chem. Soc.* **2012**, 134, 13950-13953.
10. Brunelli, N. A.; Venkatasubbaiah, K.; Jones, C. W.; Cooperative Catalysis with Acid-Base Bifunctional Mesoporous Silica: Impact of Grafting and Co-condensation Synthesis Methods on Material Structure and Catalytic Properties. *Chem. Mater.* **2012**, 24, 2433-2442.
11. Brunelli, N. A.; Long, W.; Venkatasubbaiah, K.; Jones, C. W.; Catalytic Regioselective Epoxide Ring Opening with Phenol using Homogeneous and Supported Analogues of Dimethylaminopyridine. *Top. Catal.* **2012**, 55, 432-438.

12. Brunelli, N. A.; Jones, C. W.; Tuning Acid-Base Cooperativity to Create Next Generation Silica-Supported Organocatalysts. *J. Catal.* **2013**, 308, 60-72.
13. Key, R. E.; Venkatasubbaiah, K.; Jones, C. W.; Evaluation of Enantiopure and Non-Enantiopure Co(III)-Salen Catalysts and their Counter-ion Effects in the Hydrolytic Kinetic Resolution (HKR) of Racemic Epichlorohydrin. *J. Mol. Catal. A. Chem.* **2013**, 366, 1-7. Editor's Choice Paper.
14. Long, W.; Brunelli, N. A.; Didas, S. A.; Ping, E. W.; Jones, C. W.; Aminopolymer-Silica Composite Supported Pd Catalysts for Selective Hydrogenation of Alkynes. *ACS. Catal.* **2013**, 3, 1700-1708.
15. Feng, Y.; Lydon, M. E.; Jones, C. W.; Cobalt Salen Catalysts Supported on a Highly Cross-linked Polymer Resin: Role of Co(II) Salen species in the Heterogeneous Cooperative Regioselective Ring Opening of 1,2-Epoxyhexane with Methanol. *ChemCatChem* **2013**, 5, 3636-3643.
16. Brummelheis, N. T.; Weck, M.; RAFT Polymerization of Alternating Styrene-Pentafluorostyrene Copolymers. *J. Polym. Sci. Polym. Chem.* **2014**, 52, 1555-1559.
17. Lu, J.; Brummelheis, N. T.; Weck, M.; Intramolecular Folding of Triblock Copolymers via Quadrupole Interactions between Poly(styrene) and Poly(pentafluorostyrene) Blocks. *Chem. Commun.* **2014**, 50, 6225-6227.

## Tuning Catalytic Properties of Molecular Metal Clusters on Supports

PIs: Ilke Arslan (Pacific Northwest National Laboratory), David Dixon (U. of Alabama), Bruce Gates (U. of California, Davis, UCD), Alexander Katz (U. of California, Berkeley, UCB)

Post-docs: Alexander Okrut (UCB), Andrew Solovyov (UCB)

Graduate Students: Jing Lu (UCD), Ceren Aydin (UCD), Joseph D. Kistler (UCD), Mingyang Chen (UA), Shengjie Zhang (UA)

Collaborators: Nigel Browning (PNNL), C. Y. Chen (Chevron), Sonjong Hwang (Caltech), Kathy Durkin (UCB), Olayinka Olatunji-Ojo (UCB), Tobin Marks (Northwestern), L. Wang (Southern Illinois)

### Goals

The analysis and control of catalytic properties of essentially molecular supported metals by choice of metal (e.g., Rh, Ir, Os), metal nuclearity (e.g., Ir, Ir<sub>4</sub>, Os, Os<sub>3</sub>, Os<sub>4</sub>, Os<sub>5</sub>, Os<sub>10</sub>), ligands, and support (which can also be considered to be a ligand), including control of metal surface reactivity in a supported Ir<sub>4</sub> cluster catalyst, is leading to a better understanding of catalytic properties and the design of new catalysts. These systems can be viewed as simple mimics of enzymes – whose metal active sites function in water and are able to direct selective chemical transformations by virtue of their ability to control binding in an even off-on fashion at an active site.

### DOE Interest

The ability to program an electronic environment at will on a metal catalyst surface, in a way that switches bonding of a molecule back and forth from an on state to an off state, has profound implications (e.g., carbon dioxide (CO<sub>2</sub>) electroreduction to give alkane fuels and hydrodesulfurization of compounds in petroleum for production of clean-burning low-sulfur fuels), whereby one molecule present in a mixture is prevented from poisoning the site by bonding too strongly to it and blocking reaction of other molecules that must bond to be converted. Indeed, the enabling molecular-scale structure-function relationships in catalysis that control such electronic environments and their performance constitute a central catalysis grand challenge. This project focuses on harnessing the power of synthesis, self assembly, spectroscopy, atomic-resolution microscopy, electronic structure theory, and catalyst performance testing to understand well-defined, essentially molecular metal clusters as catalysts on support surfaces. Our intent is to lead the forefront in the synthesis, characterization, and imaging of metal cluster catalysts consisting of well-defined sites for catalysis, encompassing fundamental understanding of catalysts and discovery of active sites with new selective properties.

### Recent Progress

By changing the ligand-imposed electronic environment, the bonding of ethylene to the same cluster was turned on, as illustrated by the molecular modeling image in Figure 1 below. We thereby demonstrated that this could be used to turn off and on ethylene poisoning during H-D exchange catalysis, as well as the catalytic activity of the cluster site for ethylene hydrogenation. This progress opens the way to new structures for on-off control of binding and activation of molecules via programming of the electronic environment at active sites in metal-containing

nanostructures and other surface-catalytic structures, offering an attractive strategy to control reactivity and poisoning at a catalyst active site.

Our design builds on one of the simplest metal surfaces, using the  $\text{Ir}_4(\text{phosphine})_3(\text{CO})_9$  family of clusters. Active sites for binding and catalysis are created on this surface by selective and controlled removal of CO ligands, which consist of open coordination sites on iridium atoms. The other ligands present consist of phosphines and a weakly interacting mesoporous silica surface. While the silica, being a support, was chosen for site isolation of the clusters, the phosphine ligands facilitate selective access to open sites on the underlying metal surface. The phosphines also act as a steric barrier against aggregation/coalescence of the clusters. We elucidated the essential role of the nanoscale calixarene phosphine ( $1.4 \text{ nm} \times 1.3 \text{ nm}$ ) in a comparative study involving the less bulky non-calixarene ( $\text{PPh}_2\text{CH}_3$ ) phosphine ( $1.0 \text{ nm} \times 0.7 \text{ nm}$ ) ligand. These are represented schematically in Figure 1 by clusters **1** (calixarene) and **2** (non-calixarene). A key role of the calixarene phosphines is to donate electron density to the metal core and facilitate thermally driven decarbonylation at basal-plane Ir atoms in the presence of a flowing gas that sweeps away dissociated CO – all while keeping the cluster stable. Such stability is impossible to accomplish with **2** under similar conditions. We demonstrate that the resulting open “CO vacancy” sites are within nanoenvironments that readily take up newly added CO while completely excluding ethylene, even when treated with just ethylene for a prolonged period of time. We also demonstrate the synthesis—by reactive decarbonylation—of open sites in a different nanoenvironment as shown by cluster **3**, involving the apical iridium atom, which leads to binding of both CO and ethylene. These results are supported by infrared spectroscopy, as well as density functional theory (DFT) calculations, which are based on the structure of **1** (previously determined by single-crystal X-ray diffraction) as a starting point. We also used catalytic reactions consisting of H-D exchange and ethylene hydrogenation to contrast the two different open-site nanoenvironments on the tetrairidium cluster. Our results illustrate a clear influence of the differing reactivities of the separate open sites on the metal surface. The data demonstrate one site where CO binds and ethylene does not—and no ethylene hydrogenation catalysis occurs on it and no ethylene poisoning of H-D exchange occurs on it. On the other open site, both ethylene and CO bind, and ethylene hydrogenation catalysis takes place, as does ethylene poisoning of H-D exchange catalysis. Such a distinction between equally accessible active sites is unusual, since they differ so markedly in their relative binding energy of ethylene, which is otherwise known to bind and interact strongly with Ir metal surfaces.

In addition, the adsorption of dinitrogen on structurally well-defined dealuminated HY zeolite-supported iridium diethylene complexes synthesized by the adsorption  $\text{Ir}(\text{C}_2\text{H}_4)_2(\text{acac})$  was investigated experimentally and computationally. Iridium-dinitrogen complexes formed when the supported iridium diethylene complex was exposed to  $\text{N}_2$  in the presence of a pulse of  $\text{H}_2$  at 298 K. The structures and reactivities of the iridium dinitrogen species were investigated with isotopically labeled  $\text{N}_2$  as infrared spectra were measured during changes in the supported structures in various flowing gases. Four supported iridium dinitrogen complexes formed:  $\text{Ir}(\text{N}_2)$ ,  $\text{Ir}(\text{N}_2)(\text{N}_2)$ ,  $\text{Ir}(\text{C}_2\text{H}_5)(\text{N}_2)$ , and  $\text{Ir}(\text{H})(\text{N}_2)$ . Conversion of  $\text{Ir}(\text{N}_2)$  to  $\text{Ir}(\text{N}_2)(\text{N}_2)$  or  $\text{Ir}(\text{H})(\text{N}_2)$  was reversible, but conversion of  $\text{Ir}(\text{C}_2\text{H}_5)(\text{N}_2)$  to  $\text{Ir}(\text{N}_2)$  was not. In the presence of  $\text{N}_2$ ,  $\text{Ir}(\text{N}_2)$  was the predominant dinitrogen species at temperatures between 273 and 373 K.  $\text{Ir}(\text{CO})(\text{N}_2)$  formed transiently as CO flowed over the sample, forming the highly stable  $\text{Ir}(\text{CO})_2$ . In the presence of  $\text{H}_2$ , rather stable iridium hydride complexes compete with iridium dinitrogen complexes. The

experimental results are in good agreement with calculations at the level of density functional theory with two different models of the zeolite. Calculated ligand dissociation energies were used to propose a reaction network.

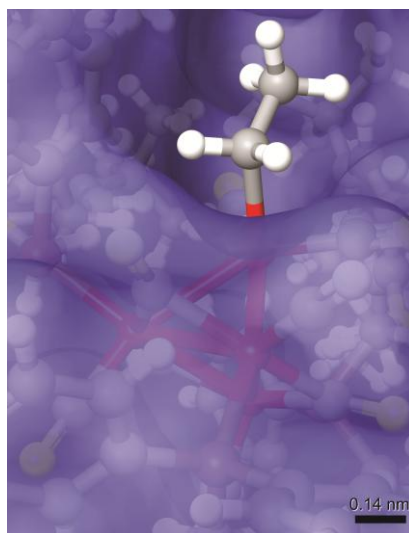


**Fig. 1.** Ethylene binding and activation in a supported tetrairidium cluster catalyst are controlled by selective nanoenvironments at the metal surface, formed by three calixarene-phosphine ligands surrounding and bonding to the cluster at sites neighboring the site where reactivity is switched off and on.

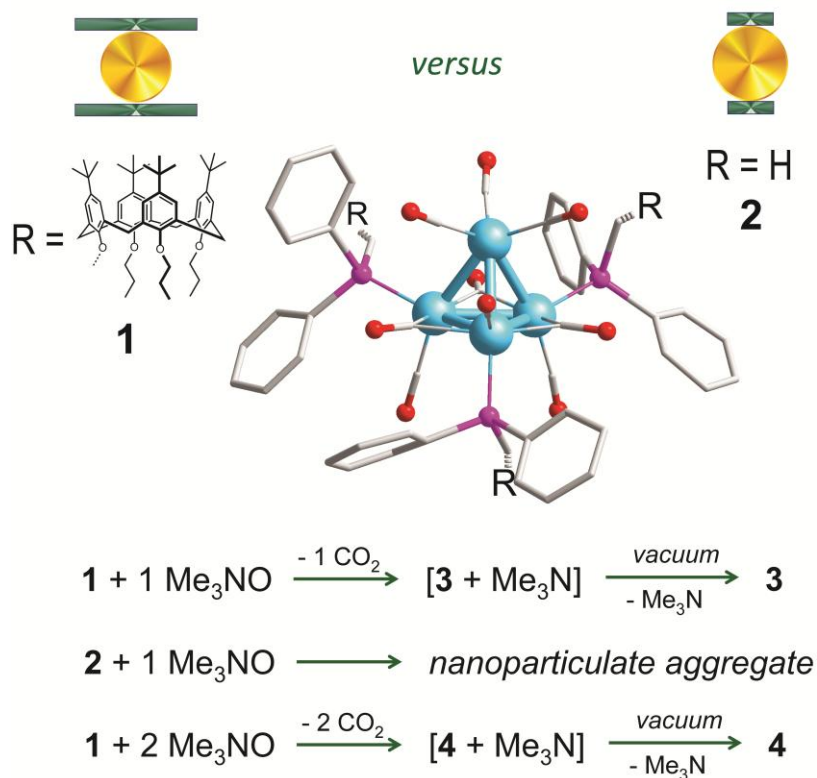


**Fig. 2.** Schematic representation of  $\text{Ir}_4(\text{CO})_9(\text{phosphine})_3$  clusters consisting of calixarene phosphine **1** and  $\text{PPh}_2\text{Me}$  in **2**. Bottom panel represents the method of synthesizing a vacancy by reactive decarbonylation using TMAO. This procedure is used to synthesize stable calixarene-bound open clusters **3** and **4**.

There are significant differences in the reactivities of zeolite-supported  $\text{Rh}(\text{C}_2\text{H}_5)_2$  and  $\text{Ir}(\text{C}_2\text{H}_5)_2$  with  $\text{N}_2$ : (a)  $\text{Ir}(\text{N}_2)$  is the predominant dinitrogen species other than  $\text{Ir}(\text{N}_2)(\text{N}_2)$  in the presence of  $\text{N}_2$  at temperatures between 273 and 373 K, whereas  $\text{Rh}(\text{N}_2)$  is totally converted to  $\text{Rh}(\text{N}_2)(\text{N}_2)$  under the same conditions and (b) iridium hydrides incorporating dinitrogen ligands are more stable than the corresponding rhodium complexes, so that the dinitrogen ligands tend to predominate on the rhodium complexes more than on the iridium complexes.

The structures and energetics of low energy isomers of the  $\text{Ir}_x(\text{PH}_3)_y(\text{CO})_z$  complexes ( $n=1, 2, 4$ ) were studied using density functional theory and coupled cluster theory. The  $\omega\text{B97X-D}$  functional gave the most consistent ligand dissociation energies as compared to the CCSD(T) benchmark calculations, so it was used to predict the ligand dissociation energies for the larger  $n = 4$  clusters. The ligand dissociation energies of CO depended on the position of  $\text{PH}_3$ . The steric bulk of the phosphine leads to *cis*- $\text{IrPH}_3(\text{CO})_2$ , *trans*- $\text{Ir}(\text{PH}_3)_2\text{CO}$  and *trans*- $\text{Ir}(\text{PH}_3)_2(\text{CO})_2$  being more stable than the other isomers. The calculations predict three fundamental structures for  $\text{Ir}_2(\text{PH}_3)_y(\text{CO})_z$ :  $\text{C}_{2v}$  ( $\text{C}_s$ ),  $\text{C}_2$  and  $\text{D}_{3d}$  with the lowest energy structure dependent on the position of the  $\text{PH}_3$ 's and CO's. The  $\text{C}_{3v}$  structures of  $\text{Ir}_4(\text{PH}_3)_y(\text{CO})_z$  clusters have lower energies than the  $\text{T}_d$  isomers and become even more favored as more phosphines are introduced due to less steric interactions. Dissociation of a bridging CO ligand often involved hydrogen atom transfer from the  $\text{PH}_3$  to the Ir, and such reaction products always had the lowest relative energies. Except for the bridge ligands with dissociation involving hydrogen transfer, the ligands at the equatorial positions have the highest LDEs, while those at apical positions have the lowest. Carbonyls are strong  $\pi$ -electron acceptor and phosphines act as a strong  $\sigma$ -electron donor and weak  $\pi$ -electron acceptor. These electronic effects strengthen the Ir-C and Ir-P bonds and increase the LDEs. However, phosphines are easier to dissociate as more are substituted for CO due to steric interactions. The larger increase in the CO LDEs is predicted to make it difficult to get very highly substituted phosphine iridium carbonyl clusters.

### Publications (2012–2014)

"Hydrogen Activation and Metal Hydride Formation Trigger Cluster Formation from Supported Iridium Complexes," J. Lu, C. Aydin, N. D. Browning, and B. C. Gates, *J. Am. Chem. Soc.*, **134**, 5022 (2012).

"Electron Tomography: Seeing Atoms in Three Dimensions," I. Arslan and E. A. Stach, *Nat. Matls.*, **11**, 911 (2012).

"A Smart Catalyst: Sinter-resistant Supported Iridium Clusters Visualized with Electron Microscopy," C. Aydin, J. Lu, N. D. Browning, and B. C. Gates, *Angew. Chem., Int. Ed.*, **51**, 5929 (2012).

"Structures and Stability of  $\text{Ir}_n(\text{CO})_m$ ," M. Y. Chen, J. E. Dyer, B. C. Gates, A. Katz, and D. A. Dixon, *Mol. Phys.*, **110**, 1977 (2012).

"Defragmenting Catalysis" (editorial), B. C. Gates and T. J. Marks, *Angew. Chem., Int. Ed.*, **51**, 11644 (2012).

"Gold nanoparticle-catalyzed reduction in a model system: Quantitative determination of reactive heterogeneity of a supported nanoparticle surface," M. M. Nigra, I. Arslan, and A. Katz, *J. Catal.*, 115–121 (2012).

"Sinter-Resistant Catalysts: Supported Iridium Nanoclusters with Intrinsically Limited Sizes," J. Lu, C. Aydin, N. D. Browning, L. Wang, and B. C. Gates, *Catal. Lett.*, **142**, 1445 (2012).

"Computational Study of the Low-lying Electronic States of Ir<sub>n</sub> Clusters with n = 2 – 8 at the DFT, CASSCF, and CCSD(T) Levels," M. Chen and D. A. Dixon *J. Phys. Chem. A*, **117**, 3676 (2013).

"Selective molecular recognition by nanoscale environments in a supported iridium cluster catalyst," A. Okrut, R. Runnebaum, X. Ouyang, J. Lu, C. Aydin, S. -J. Hwang, S. Zhang, O. Olatunji-Ojo, K. Durkin, D. Dixon, B. Gates, and A. Katz, *Nature Nanotech.*, pub online April 20, 2014, doi:10.1038/nnano.2014.72.

**Harold H. Kung**

**Exploring New Chemistry with Molecular Nanocages**

Harold H. Kung, Jingmei Shen, Mayfair Kung, Zhongliang Shen, Zhen Wang  
William A. Gunderson<sup>1</sup>, Brian M. Hoffman<sup>1</sup>  
Department of Chemical and Biological Engineering and <sup>1</sup>Department of Chemistry  
Northwestern University, Evanston, IL 60208

**Abstract**

Functionalized molecular nanocages have demonstrated interesting chemical and catalytic properties. Recently, we have synthesized a discrete nanocage of a core-shell design, in which carboxylic acid groups were tethered to the core and silanol to the interior of the carbosilane shell, possessed a hydrophilic interior and a hydrophobic shell. The hydrophilic interior also enabled internalization of metal salts in an organic medium. The interior carboxylic acid groups were found to react with  $\text{Co}_2(\text{CO})_8$  to form and stabilize a  $\text{Co(I)-CO}$  species. The singular CO stretching band of this new Co species at  $1958\text{ cm}^{-1}$  and its magnetic susceptibility were consistent with  $\text{Co(I)}$  compounds. When exposed to  $\text{O}_2$ , it transformed from an EPR inactive to an EPR active species indicative of oxidation of  $\text{Co(I)}$  to  $\text{Co(II)}$  with the formation of  $\text{H}_2\text{O}_2$ . It could be oxidized also by organoazide or water. Its residing in the nanocage interior was confirmed by size selectivity in the oxidation process and the fact that the entrapped Co species could not be accessed by an electrode.

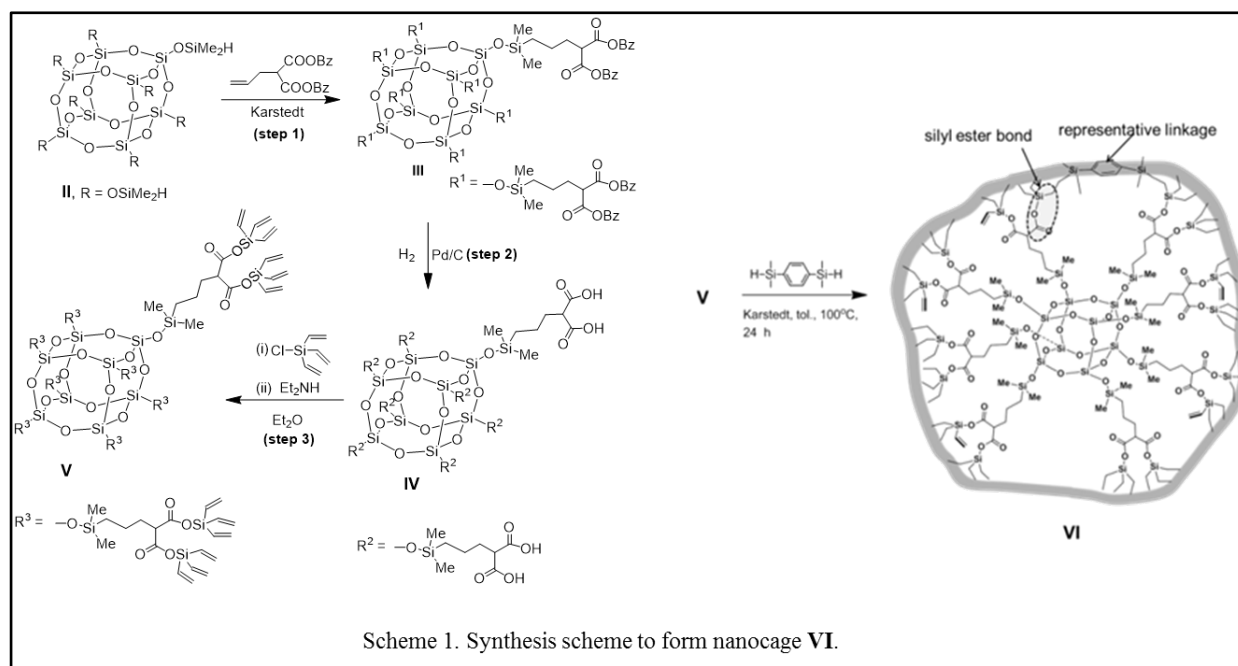
**Grant DE-FG-02-01ER15184; Molecular Engineering for Selective Catalysis**

PI: Harold H. Kung  
Postdoc(s): Jingmei Shen  
Student(s): John Galloway, Delrae Haag, Zhen Wang

**RECENT PROGRESS**

Discrete nanocages have been shown to stabilize ionic reaction intermediates and moisture sensitive materials, and alter molecular conformation, reaction regioselectivity, reaction rates and extent of sequential reaction, as well as protonation affinity. Recently, we have extended our study of molecular nanocages to bifunctional structures of a core-shell design, in which the core and the shell interior harbor different functionalities.

We constructed the structure starting with a spherosilicate with 8 silane groups, one at each of the corners, that was converted by hydrosilylation with dibenzyl allylmalonate to **IV**,  $[\text{Si}_8\text{O}_{12}]-(\text{OSiMe}_2\text{CH}_2\text{CH}_2\text{CH}_2\text{CH}(\text{COOH})_2)_8$  which had 16 carboxylate groups at the periphery (Scheme 1). Subsequent hydrolysis of the carboxylate groups followed by condensation with trivinylchlorosilane generated a dendrimer  $[\text{Si}_8\text{O}_{12}]-(\text{OSiMe}_2\text{CH}_2\text{CH}_2\text{CH}_2\text{CH}(\text{COOSi}-(\text{CH}=\text{CH}_2)_3)_2)_8$  **V** with 48 peripheral vinyl groups and labile silyl ester bonds. Intramolecular cross-linking of the vinyl groups in **V** by hydrosilylation with 1,4-bis-dimethylsilylbenzene created a nanosphere in which the core and the shell are covalently linked. Finally, cleaving the silyl ester bonds by hydrolysis resulted in a core-shell nanosphere, in which the shell was detached from the core.

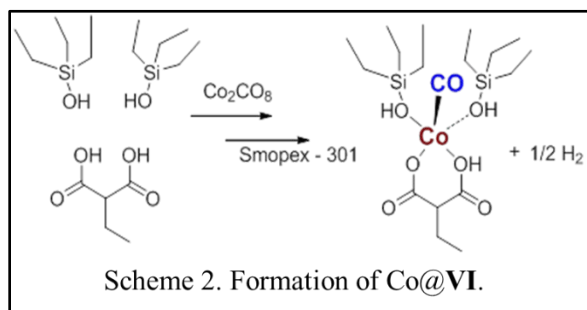


The identity of each of these compounds in the synthesis scheme was confirmed by a combination of analytical techniques, including  $^1\text{H}$ ,  $^{13}\text{C}$ , and  $^{29}\text{Si}$  NMR spectroscopy and mass spectrometry. For example,  $^1\text{H}$  NMR spectrum of **V** did not show any signal of carboxylic proton, and its  $^{29}\text{Si}$  NMR spectrum only contained three peaks for the Si in three different environments, indicating complete conversion of  $-\text{COOH}$  to  $-\text{COOSi}(\text{CH}=\text{CH}_2)_3$  in its formation. Its ESI-MS signal was detected at  $m/z = 1969.5$  (for  $(\text{V} + 2 \text{NH}_4^+)^{2+}$ ). In the formation of **VI**, the cross-linking reaction could be monitored by the disappearance and broadening of

multiplets at  $\delta$  6.1 (vinyl region of **V**) and the appearance of a broad peak at  $\delta$  7.6 (aromatic H from the reacted linker) in  $^1\text{H}$  NMR spectroscopy, and the presence of four major peaks in the  $^{29}\text{Si}$  NMR spectrum.

Hydrolysis of the silyl ester bonds in **VI** with a controlled amount of water generated carboxylic acid groups inside the structure. Although the nanocage was hydrophobic and soluble in toluene because of the carbosilane nanocage shell, the carboxylic acid groups rendered the interior hydrophilic. These acid sites were potential metal binding sites, and we observed that a toluene solution containing **VI** and solid  $\text{PdCl}_2$  or  $\text{TiCl}_3$  turned yellow slowly, whereas the toluene without **VI** remained colorless, suggesting transfer of Pd or Ti ions into **VI**.

Reaction of **VI** with  $\text{Co}_2(\text{CO})_8$  (Scheme 2) followed by purification to removal excess



$\text{Co}_2(\text{CO})_8$  generated Co@**VI**, which contained  $\sim 4$  Co per nanocage at saturation (M.W. III $\sim$ 7900/g). Evidence that Co@**VI** contained Co(I) inside the nanocage included: a single intense CO stretch at  $1958\text{ cm}^{-1}$  (Fig. 1), absence of redox peaks between  $-2$  and  $1\text{ V}$  vs SCE from the  $\text{Co}^{+1}/\text{Co}^0$  couple in the CV curve, absence of a EPR signal but appearance of a signal at  $g = 4.0$  upon exposure of Co@**VI** to  $\text{O}_2$  (Fig. 2), a room temperature effective magnetic moment of  $3.55\ \mu_{\text{B}}$ , and size-selective reaction with organoazide with concomitant change of the orange solution to pale yellow.

Thus, we have demonstrated that a molecular nanocage with a core-shell structure, containing a prescribed number of common functional groups and restricted interior space for movement of complexes, can be used to generate and stabilize metal complexes of an uncommon oxidation state with a high degree of uniformity.

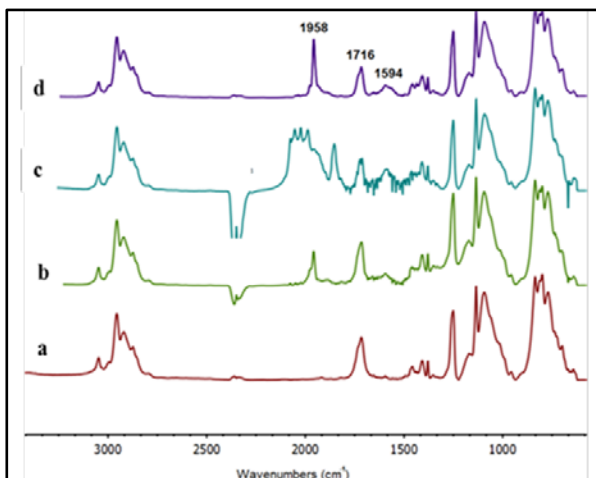


Figure 1. IR spectra of (a) **III**, (b) **III** + 1 equivalent of  $\text{Co}_2(\text{CO})_8$  after 34 h at r.t.; (c) **III** + 12 equivalents of  $\text{Co}_2(\text{CO})_8$ , (d) **Co@III** which is sample c after removal of unreacted  $\text{Co}_2(\text{CO})_8$  with Smopex-301 at 50 °C in 4 h.

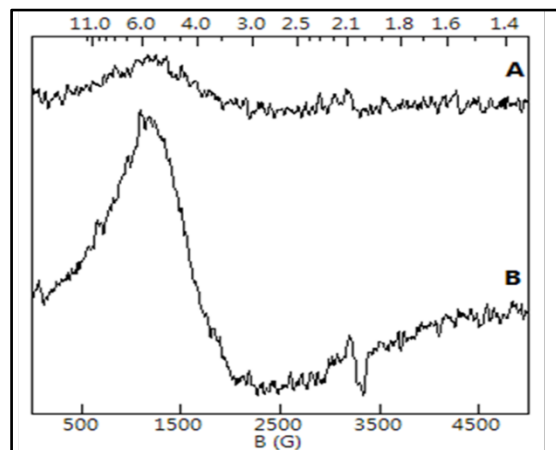


Figure 2. EPR spectra of (A) **Co@III** (and (B) **Co@III** after 90 minute exposure to  $\text{O}_2$ . Spectral Conditions: microwave frequency = 9.36 GHz, microwave attenuation = 20 dB, modulation amplitude = 13.2 G, modulation frequency = 100 kHz,  $T = 7\text{K}$ .

#### Publications Acknowledging this Grant in 2011-2014

1. Shen, J.; Kung, M. C.; Shen, Z.; Wang, Z.; Gunderson, W. A.; Hoffman, B. M.; Kung, H. H. Generating and Stabilizing Co(I) in a Nanocage Environment. *J. Amer. Chem. Soc.* **2014**, *36* (14), 5185–5188.
2. Kung, M. C.; Riofski, M. V.; Missaghi, M. N.; Kung, H. H. Organosilicon Platform: Bridging Homogeneous, Heterogeneous, and Bioinspired Catalysis. *Chem. Commun.* **2014**, *50*, 3262–3276.
3. “Metal Free Graphene Based Catalysts. A Review,” Haag, D., Kung, H. H. Metal Free Graphene Based Catalysts. A Review. *Topics Catal.* **2014**, *57*, 762–773.
4. Zhongliang Shen, Z.; Jongsik Kim, J.; Jingmei Shen, J.; Downing, C. M.; Lee, S.; Kung, H. H.; Kung, M. C. Spherosilicates with Malonic Acid and Vinyl End Groups. *Chem. Commun.* **2013**, *49*, 3357–3359.
5. Missaghi, M.N.; Kung, M. C., Kung, H. H. Polysiloxanes in Catalysis and Catalyst Preparation: Opportunities for Control of Catalytic Processes. *Topics Catal.* **2012**, *55*, 99–107.
6. Downing, C. M.; Kung, H. H. Diethyl sulfide stabilization of Platinum-Complex Catalysts for Hydrosilylation of Olefins. *Catal. Commun.* **2011**, *12*, 1166–1169.
7. Downing, C. M.; Missaghi, M. N.; Kung, M. C.; Kung, H. H. Design and Synthesis of Readily Degradable Acyloxysilane Dendrimers. *Tetrahedron* **2011**, *67*(39), 7502–7509.
8. Missaghi, M. N.; Galloway, J. M.; Kung, H. H. Bis(pyridyl)siloxane-Pd(II) Complex Catalyzed Oxidation of Alcohol to Aldehyde: Effect of Ligand Tethering on Catalytic Activity and Deactivation Behavior. *Appl. Catal. A: Gen.* **2011**, *391*, 297–304.

**Multifunctional Solid Catalysts for Lignin to Hydrocarbons**  
**Understanding and Controlling Scalable Catalytic Routes in Aqueous Phase**

Johannes A. Lercher, Donald M. Camaioni, John L. Fulton,

Jian Zhi Hu, Donghai Mei, Yong Wang

Pacific Northwest National laboratory, Institute for Integrated Catalysis

TU München, Department of Chemistry, Catalysis Research Center

Washington State University, School of Chemical and Biological Engineering

**Presentation Abstract**

The catalyzed conversion of lignin to hydrocarbon energy carriers requires a cascade of reactions for deconstructing and reducing the polymeric, highly oxofunctionalized material. While lignin is the most intractable component of lignocellulose, its conversion to useful products is particularly important, because the carbon in lignin is the most reduced fraction of lignocellulose. Our main focus has been on understanding the properties of catalysts in aqueous environments and the catalytic chemistry of lignin fragments in aqueous and biphasic oil-water environments. We have studied the catalysis of ether hydrogenolysis and hydrolysis, the reduction of phenols, hydrodeoxygenation of alcohols, and the hydroalkylation of (substituted) phenols in the aqueous phase. Hydrogenation, hydrogenolysis, and even hydrolysis were found to be effectively catalyzed by supported noble and base metals allowing for higher reaction rates than observed previously by molecular catalysts. Catalysts with dual functions, consisting of highly dispersed nickel nanoparticles on acidic supports including sulfonated carbons and zeolites (HZSM5 and HBEA), have been synthesized and characterized. The catalysts efficiently convert liquid phase lignin components to cycloalkanes, the nickel particles catalyzing hydrogenation of unsaturated C=C and C=O bonds and the acidic sites on the support catalyzing dehydration of cycloalkanols. As these measurements and simulations have led the way to better catalysts for lignin conversion, we now also work to address the challenge of quantitatively and qualitatively exploring all individual steps of these reactions to use this information to synthesize tailored catalysts that combine the functions in catalysts organized at a mesoscale level.

## Multifunctional Catalysts to Synthesize and Utilize Energy Carriers

Additional PIs: A. Appel, T. Autrey, M. Bullock, D. Camaioni, H. Cho, D. Dixon (U of AL), Z. Dohnalek, F. Gao, V. Glezakou, M. Henderson, J. Hu, E. Iglesia (U of CA), A. Karkamkar, B. Kay, G. Kimmel, J. Linehan, J. Liu, I. Lyubinetsky, D. Mei, C. Peden, R. Rousseau, G. Schenter, W. Shaw, J. Szanyi, Y. Wang, Z. Wang, R. Weber

**Contact:** Johannes Lercher, P.O. Box 999, MS: K2-12, Institute for Integrated Catalysis, Pacific Northwest National Laboratory, Richland, Washington; johannes.lercher@pnnl.gov

### Background

The central role and critical importance of catalysis in a future based on sustainability, together with the insight that developments have to be knowledge-based have motivated significant efforts to better understand catalyzed processes and to develop new catalytic routes from this knowledge. Overall, three main energy carriers are used worldwide, carbon (and hydrocarbons), hydrogen, and electrons. Conventionally, the stored energy is accessed by oxidizing carbon and hydrogen, forming O-H and C-O bonds and performing work with the produced heat or electricity. Conversely, to synthesize energy carriers sustainably, it is consequently required to reverse the direction, i.e., to break C-O and O-H bonds and form C-C, C-H and H-H bonds.

### Structure of the program

To address these challenges, PNNL's BES-sponsored program comprises three thrust areas with subtasks, focusing on the fundamentals of biomass conversion processes, direct and indirect CO<sub>2</sub> reduction, and on elementary studies aimed at generating and using H<sub>2</sub>. Multi-functionality, i.e., the simultaneous interaction of more than one catalytically active site with the substrate is the key to achieving the atom and energy efficiency in individual steps. The combination of several types of these sites with carefully selected energetics and rate constants is used to generate complex catalysts able to enhance the rates of multistep processes.

Conversion of biogenic molecules with and without water	Reduction of CO <sub>2</sub> to energy carriers	Generation and conversion of H <sub>2</sub>
Multifunctional solid catalysts for lignin to hydrocarbons – Understanding and controlling scalable catalytic routes in aqueous phase (ST 1.1) Well-defined metal oxide catalysts – Understanding fundamental chemical transformations and the role of water for catalyzed reactions (ST1.2)	Multifunctional catalyst for CO <sub>2</sub> reduction (ST2.1)  An energy-based approach to bifunctional molecular catalysis for CO <sub>2</sub> reduction and fuel utilization (ST 2.2)	Fundamental studies of photocatalysis (ST3.1)  Activation of small molecules with bi-functional ambiphilic catalyst complexes (ST 3.2)  H <sub>2</sub> activation and conversion catalyzed by ambiphilic surfaces (ST3.3)

Overview of thrusts and project clusters for understanding principles of multifunctional catalysis to synthesize and utilize

**Thrust Area 1: Conversion of biogenic molecules in the presence and absence of water** addresses the multi-step conversion of polar molecules on multifunctional surfaces. The aim is to develop a better understanding of the role the metal as well as the acid-base functions on oxide surfaces as they interact with increasingly complex polar biogenic molecules. Hydrodeoxygenation and hydroalkylation will be the reactions we will use to exemplify potential routes from lignocellulosic biomass to alkane energy carriers requiring several catalytic functions acting sequentially. Since most reactions will either involve water or will occur in the presence of water, we will explore its role on catalytic transformations.

**Thrust Area 2: Conversion of CO<sub>2</sub> to energy carriers** is focused on mechanistic understanding of the catalytic reduction of CO<sub>2</sub> to energy carriers (e.g. methane, methanol, formaldehyde, and formic acid, as well as C<sub>2</sub> and higher fuels). The bifunctional sites for CO<sub>2</sub> reduction in enzymes motivate us to design and test potential heterogeneous and homogeneous catalysts with bifunctional motifs. Our primary goal is to compare and contrast various mechanistic aspects of the observed chemistries, gain a molecular level understanding of the fundamental reaction steps, identify the reaction intermediates and their stability, and determine the role that reaction conditions can have on the energetics and kinetics.

**Thrust 3: Generation and conversion of H<sub>2</sub>** assumes as its central hypothesis that efficient production and utilization of molecular hydrogen is key to sustainable synthesis of energy carriers; i.e., for storing energy chemically. The three tasks described in this thrust address formation and activation of molecular hydrogen by

multifunctional catalysts. All of the tasks focus on the fundamental understanding of properties and chemistry at polar interfaces; i.e., the hydrogen formation from water notably in the absence of bulk water, as well as the activation by sterically well-defined Lewis acid - base pairs (frustrated Lewis pairs, of FLPs) and the subsequent utilization of  $H^-$  and  $H^+$  for hydrogenation reactions.

## Examples of Recent Results:

### Subtask 1.1.: From lignin to hydrocarbon energy carriers – understanding and controlling scalable catalytic routes in aqueous phase

The catalyzed conversion of lignin to hydrocarbon energy carriers requires a cascade of reactions for deconstructing and reducing the polymeric, highly oxofunctionalized material. In our current work, we are studying ether hydrogenolysis and hydrolysis, the reduction of phenols, HDO of alcohols, and the alkylation of (substituted) phenols in the aqueous phase using supported noble and base metals as well as zeolites. Hydrogenation, hydrogenolysis, and even hydrolysis were found to be effectively catalyzed by supported palladium and nickel catalysts allowing for higher reaction rates on these metal particles than observed previously by molecular catalysts.

The impact of water on the supported metal has been explored, using X-ray absorption spectroscopy. We followed the state of palladium and catalysts under reaction conditions. We have demonstrated that both metals were not oxidized and interacted only weakly with water in the presence of 30 bar  $H_2$ . We showed that under typical operating conditions with temperatures up to 200°C, the metal surfaces were in equilibrium with  $H_2$ . The high partial pressure of the  $H_2$  kept the metals in a reduced state even in acidic solutions (0.5 wt%  $H_3PO_4$  or 15 wt%  $CH_3CO_2H$ ) at 200°C. The results also demonstrate that neither the palladium particles nor the hydrogen/palladium ratio in the nanoparticle are influenced by water, but dynamically adapts to reaction conditions. In support of these observations, density functional theory (DFT) ab initio molecular dynamic (AIMD) simulations have shown that palladium-water interactions are relatively weak for metallic palladium metal and that these interactions become even weaker in presence of  $H_2$  and when hydrogen atoms are incorporated into the metal particles. We also modeled the effects of liquid water on metal-catalyzed hydrogenation of phenol.

Zeolites have been shown to be uniquely effective at cleaving carbon-oxygen bonds, and are also effective in forming carbon-carbon bonds. Using in situ  $^{13}C$  magic angle spinning nuclear magnetic resonance (NMR) spectroscopy, cyclohexanol dehydration was shown to be reversible and the protonation/deprotonation of cyclohexene was shown to be fast compared to the addition of water. To perform these experiments, we developed

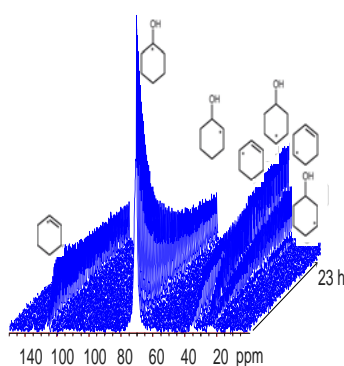
a micro-autoclave/solid-state NMR rotor capable of withstanding temperatures up to 200°C and pressures up to 20 bar. As an example, our  $^{13}C$  spectra show that the conversion of cyclohexanol is accompanied by significant migration of the hydroxyl group in cyclohexanol and the double bond in cyclohexene with respect to the initial position of the labelled carbon.

The degree of substitution of  $Si^{4+}$  by  $Al^{3+}$  in zeolite framework determines the concentration of Brønsted acid sites. As the location of these aluminum-tetrahedral sites will influence the subtle steric requirements for the catalyzed reactions, quantitative information about the location of aluminum T-sites in the framework is critical to rationalize catalytic properties and to design new catalysts. Using a combination of extended X-ray absorption fine structure analysis and  $^{27}Al$  MAS NMR spectroscopy supported by DFT-based molecular dynamics simulations, a first quantitative distribution of  $Al^{3+}$  in the HBEA zeolite framework has been attained. The distribution of aluminum T-sites in samples of HBEA150 and HBEA25 differed markedly and in neither zeolite did the distribution follow the predicted thermodynamic stability of the aluminum T-sites. This strongly suggests

that the incorporation of aluminum into the zeolite lattice during hydrothermal synthesis is controlled by kinetics and primarily determined by the templating constituent. While the details of this dealumination process are yet to be explored, the analysis using a combination of extended X-ray absorption fine structure, NMR, and theory demonstrates the potential to analyze zeolite active sites in a depth and detail, which were not available hitherto.

### Subtask 1.2: Well-defined metal oxide catalysts - understanding fundamental chemical transformations and the role of water for catalyzed reactions

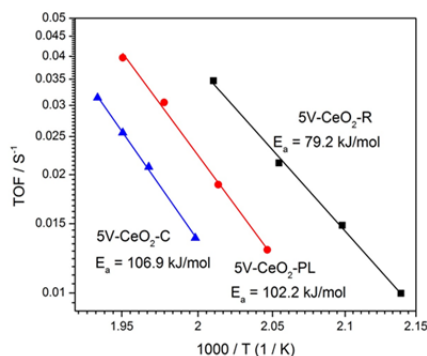
Catalytic materials for upgrading biomass-derived molecules to fuels include metals dispersed on oxide- and



$^{13}C$  NMR spectra acquired during hydrolysis of cyclohexanol over HBEA150 at 130 °C in liquid water.

carbon-support materials, and oxide materials themselves (including zeolites) that are essential as catalysts for acid/base and redox reactions. Among these materials, oxides have been the subject of far fewer fundamental studies aimed at developing structure/function relationships. Current oxide-based heterogeneous catalysts are structurally and chemically complex and their experimental assessment can seldom be interpreted with atomic-level precision. We seek to reduce the complexity to levels addressable and controllable at the atomistic level – structurally and mechanistically – while maintaining rigorous connections with the conditions and materials relevant to catalysis.

**High Surface Area Model Catalysts.** We are synthesizing dispersed transition metal oxides with controlled domain size and atomic connectivity supported on high surface area scaffolds with nominally inert and homogeneous surfaces and then providing a detailed characterization.



Arrhenius plots of 5V-CeO<sub>2</sub>-R/C/PL catalysts in oxidative dehydrogenation of methanol

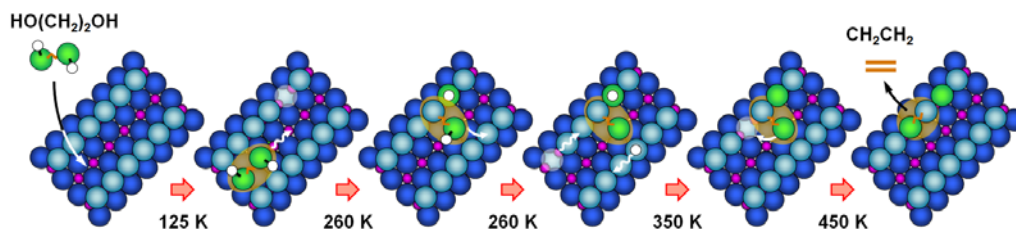
supported on high surface area scaffolds with nominally inert and homogeneous surfaces and then providing a detailed characterization. Recently, we prepared CeO<sub>2</sub> supports including nanocubes, nanorods, and nanopolyhedras with dominating low index (100), (110) and (111) facets. In the presence of mixed facets, infrared and Raman spectroscopic measurements demonstrate that surface vanadia species preferentially deposit on the (100) facet of CeO<sub>2</sub>, presumably because of its higher surface energy. At the same surface vanadium densities, VO<sub>x</sub> species on (100) facets show better dispersion, followed by (110) and (111) facets. The VO<sub>x</sub> species on CeO<sub>2</sub> nanorods with an approximately equal amount of (110) and (100) facets display higher oxidative dehydrogenation activity and lower apparent reaction activation energies compared to VO<sub>x</sub> species on CeO<sub>2</sub> nanopolyhedras with dominating (111) facets and CeO<sub>2</sub> nanocubes with dominating (100) facets. The higher activity for VO<sub>x</sub>/CeO<sub>2</sub>(110) might be related to the fact that more abundant oxygen vacancies are present on the (110) facets, evidenced from Raman spectroscopic measurements.

vacancies are present on the (110) facets, evidenced from Raman spectroscopic measurements.

**Planar Model Catalysts.** In our recent studies, we have followed a complete sequence of elemental steps in the reaction of both ethylene glycol and 1,3-propylene glycol on TiO<sub>2</sub>(110) at low coverages using STM, TPD measurements and DFT simulations. The use of ethylene glycol and 1,3-propylene glycol allowed us to compare and contrast the chemistries of two functionally similar molecules with different steric constraints and yielded information about how molecular geometry may influence the observed chemical reactivity. Our temperature-dependent studies provided evidence for:

- Oxygen-hydrogen dissociation of titanium-row-bound diols at temperatures as low as 125 K
- Diol diffusion to and dissociation in bridging oxygen vacancy sites via both carbon-oxygen and oxygen-hydrogen bond cleavage above ~230 K.

Coverage-dependent temperature-programmed desorption studies further showed that alkenes and aldehydes are the major carbon-containing products formed from ethylene glycol and 1,3-propylene glycol. While the alkenes are observed from the lowest coverages, aldehydes form primarily at high coverages.



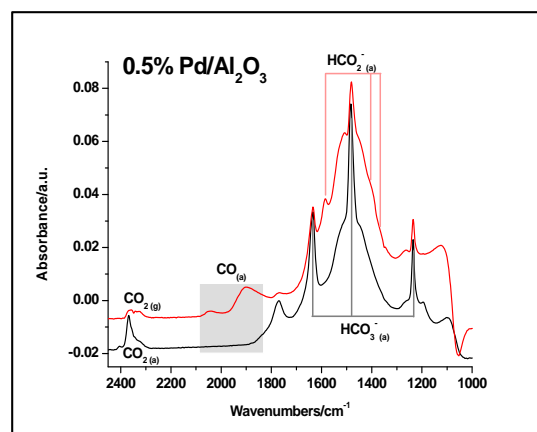
A sequence of elemental steps in the conversion of diols on TiO<sub>2</sub>(110).

### Subtask 2.1: Multifunctional catalysts for CO<sub>2</sub> reduction to fuels.

Experimental and theory capabilities are combined to investigate the mechanistic chemistry of catalytic CO<sub>2</sub> conversion to value added fuels by well characterized multifunctional catalysts in a wide range of media.

**High Surface Area Model Catalysts: Synthesis, Characterization, and Kinetics Studies.** We have prepared active metals (palladium and ruthenium) in geometries ranging from atomically dispersed metals to two-dimensional rafts and three-dimensional metal particles and tested their activity for carbon dioxide reduction with hydrogen. Our work has also substantiated the critical role oxides play in providing a Lewis acidic site for the activation of carbon dioxide. Intriguingly, we have recently observed the formation of bicarbonates under catalytic operating conditions, suggesting that these species may be intermediates in the overall reduction mechanism.

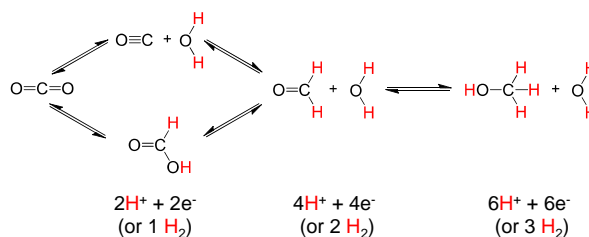
**Homotopic Polyoligomeric Silesquioxane (POSS) Clusters – Synthesis, Catalysis and Kinetics.** A series of ruthenium-supported POSS catalysts have been synthesized and deployed in either homogeneous solution and/or supported on surfaces to function as heterogeneous catalysts. We have demonstrated that homogeneous catalysts can be tethered to POSS without loss of reactivity. Moreover, catalysts where ruthenium is directly integrated into the POSS framework can reduce carbon dioxide to formate in solution as well and carbon dioxide to carbon monoxide when supported on alumina. Indeed, we found the reactivity of the ruthenium-supported POSS sites is equal to that of the monoatomic sites employed in the high surface area studies.



*In situ* Fourier transform infrared spectroscopy measurements on palladium/ $\text{Al}_2\text{O}_3$  samples during  $\text{CO}_2$  hydrogenation at 473 K.

### Subtask 2.2: An energy-based approach to bifunctional molecular catalysis for $\text{CO}_2$ reduction and fuel utilization

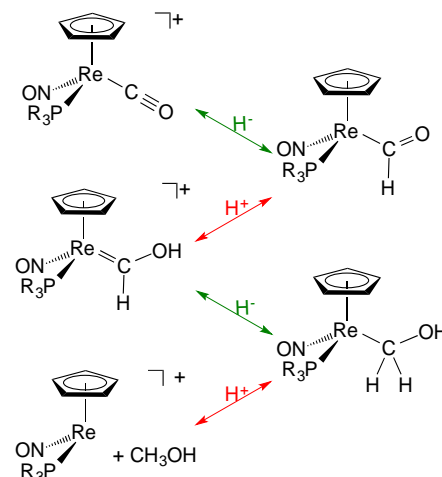
In this subtask, the goal is to learn how to rationally design catalysts for the interconversion of energy and fuels, specifically for the reduction of carbon dioxide to C1 species, including carbon monoxide, formic acid, formaldehyde, and methanol. By controlling the energies of the catalytic intermediates, artificial barriers in the overall transformation can be avoided by stepping smoothly in energy from the reactants to the products. Use multiple catalyst-substrate interactions, as ubiquitously observed in enzyme catalyzed reactions, gives multifunctional catalysts typically more active than their monofunctional analogs.



**Hydrogenation of Carbon Dioxide to Formic Acid.** The first step in carbon dioxide hydrogenation is the transfer of a hydride from the catalyst to carbon dioxide. Based on thermochemical data, we have designed an active catalyst system utilizing a molecular cobalt complex that efficiently operates at 1 atm and 21°C. At elevated pressure, this complex of a first-row transition metal has comparable catalytic performance to the fastest precious metal-based molecular catalysts for carbon dioxide hydrogenation.

**Reduction of Carbon Monoxide to Methanol.** The development of molecular catalysts for carbon monoxide reduction has been a long-standing challenge. In initial work, the energetics of a series of possible catalytic intermediates have been characterized, revealing that the classic rhenium complexes that have been studied for this transformation will always be energetically unfavorable.

**Ketone Hydrogenation.** Reduction of carbon dioxide to a liquid fuel will require multiple catalytic transformations, including hydrogenation of the carbon-oxygen double bond in formaldehyde to produce methanol. To understand the requirements for the reduction of carbon-oxygen double bonds, we are examining the use of molybdenum and tungsten complexes as catalysts for hydrogenation of ketones and aldehydes to alcohols. We are currently investigating the effects of incorporating bifunctionality into these catalysts for ionic hydrogenations, so that the catalytic activity can be improved by independently tuning.

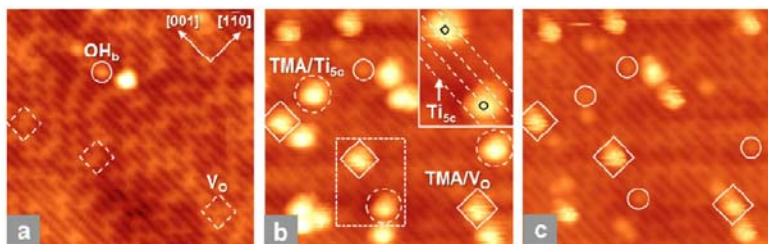


Thermochemical studies have been performed to understand how to design molecular catalysts for the reduction of carbon monoxide to methanol.

### Subtask 3.1: Fundamental studies of water splitting on model mixed TiO<sub>2</sub>, RuO<sub>2</sub> catalysts.

The objective of this subtask is to provide fundamental insight into catalytic and photocatalytic water-splitting reactions using model TiO<sub>2</sub>, RuO<sub>2</sub> and mixed titanium dioxide-ruthenium dioxide materials. The exciting potential of combining STM and photochemistry is highlighted in our recent invited article in Chemical Review.

**The Importance of Diffusion in Photocatalysis on Titanium Dioxide.** Using methanol photochemistry on TiO<sub>2</sub>(110), we have shown that thermal processes can be as important in photocatalysis as those associated with charge transfer. Under conditions in which diffusion is hindered (such as at low temperature and coverage or when

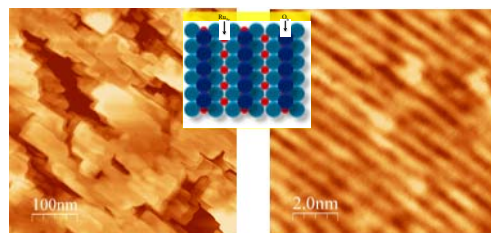


STM images (at 250 K) of the same TiO<sub>2</sub>(110) surface area: (a) before and (b) after TMAA exposure, and (c) after UV irradiation. Inset in panel (b) displays the magnified area marked by a rectangle, with positions of TMA's and Ti<sub>5c</sub> rows indicated.

the surface is packed with competing species), the rate of methanol dissociation to methoxy, and hence the rate of methanol photodecomposition, will depend on the thermally activated process of diffusion. We have recently illustrated the importance of diffusional limitations to photochemistry in a combined temperature-programmed desorption and STM study. The amount of photoreaction is fairly limited for preheating temperatures below ~200 K, while the yield of the photoreaction significantly increased above 200 K.

**Preparation of Well-Defined RuO<sub>2</sub>(110) Surfaces.** RuO<sub>2</sub> is a promising oxide-based co-catalyst in many catalytic and photocatalytic processes. We have proposed to examine the role of ruthenium dioxide as a photochemical co-

catalyst on TiO<sub>2</sub>(110). The first step in this process is to prepare well-characterized ruthenium dioxide surfaces and understand how small probe molecules interact with these surfaces. RuO<sub>2</sub> is stable in the rutile bulk structure and its (110) surface is thermodynamically stable, resembling the TiO<sub>2</sub>(110) surface. Oxidation of Ru(0001) at 550 K in ~10<sup>-5</sup> Torr oxygen resulted in large (110) terraces with atomically well-defined structures.

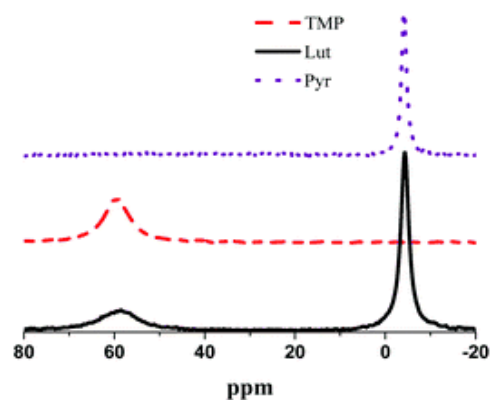


STM images of the RuO<sub>2</sub> film formed on Ru(0001) after oxidation in UHV at 550 K.

### Subtask 3.2: Activation of small molecules with bi-functional ambiphilic catalyst complexes.

This subtask is studying the chemical and physical properties of bifunctional ambiphilic molecular complexes using a combination of experiment and theory to study the relationship between structure and reactivity in Lewis acid-Lewis base pairs involved in the catalytic reduction of polar substrates.

We are studying the quantum effects in hydrogen-bonding and hydrogen-activation reactions, the role of large amplitude motions and anharmonics in strained molecular complexes, and how weak interactions, such as van der Waals, and electrostatic interactions affect the structure and dynamics in the ionic salts of Lewis acid-Lewis base pair complexes. We are developing new reaction calorimetry techniques and approaches to provide a direct measure of kinetics and thermodynamics simultaneously. These approaches are providing the first detailed experimental insights into the energy landscape describing the catalytic reduction of polar substrates by frustrated Lewis pairs. Specifically, using a unique approach to reaction calorimetry, we have shown that the activation of hydrogen by the inter-molecular frustrated Lewis pairs is well described by a termolecular reaction between the Lewis acid, Lewis base, and molecular hydrogen with a very low activation barrier,  $E_a \approx 20\text{-}25$  kJ/mol. We have also studied the catalytic reduction of t-butylbenzylimine (imine) using the linked frustrated Lewis pair (Mes)<sub>2</sub>P-(CH<sub>2</sub>CH<sub>2</sub>)-B(C<sub>6</sub>F<sub>5</sub>)<sub>2</sub>. The overall reaction enthalpy for the reduction of the imine,  $\Delta H$ , is ca. -75 kJ/mol. It is also notable that hydrogen activation is rate limiting. This suggests that the disappearance of the imine will appear linear as a function of time. Our initial measurement of the catalytic reduction of the imine using in situ NMR is consistent with this prediction.



<sup>11</sup>B NMR spectra of three distinct Lewis acid-base equilibrium conditions: (1) tris(pentafluorophenyl)borane (BCF) with pyridine, (2) BCF with 2,2,6,6-tetramethylpiperidine or TMP, and (3) BCF with 2,6-lutidine or Lut.

## Subtask 1.1 – JA Lercher – From Lignin to Hydrocarbon Energy Carriers – Understanding and Controlling Scalable Catalytic Routes in Aqueous Phase

### 2012

Zhao, C; DM Camaioni, and JA Lercher, “Selective Catalytic Hydroalkylation and Deoxygenation of Substituted Phenols to Bicycloalkanes.” *J. Catal.* **288** (2012) 92-103.

Hu, MY; J Feng, DM Camaioni, RVF Turcu, CHF Peden, JA Lercher, and JZ Hu, “In-situ MAS-NMR Investigations on Catalytic Conversion of Biogenic Molecules in the Presence of Aqueous Water.” *Prepr. Pap.-Am. Chem. Soc., Div. Energy Fuels Chem.* **57** (2012) 215.

### 2013

Shi, H; OY Gutiérrez, GL Haller, D Mei, R Rousseau, and JA Lercher, “Structure Sensitivity of Hydrogenolytic Cleavage of Endocyclic and Exocyclic C–C Bonds in Methylcyclohexane over Supported Iridium Particles.” *J. Catal.* **297** (2013) 70-78.

Chase, Z; JL Fulton, V-T Pham, DM Camaioni, M Balasubramanian, D Mei, R Weber, C Zhao, and JA Lercher, “X-Ray Absorption Spectroscopy of Supported Palladium Catalysts during Hydrodeoxygenation of Phenol in Water.” *Prepr. Pap.-Am. Chem. Soc., Div. Energy Fuels Preprints* **58** (2013) 1066.

Chase, Z. A.; Fulton, J. L.; Camaioni, D. M.; Mei, D.; Balasubramanian, M.; Pham, V. T.; Zhao, C.; Weber, R. S.; Wang, Y.; Lercher, J. A., State of Supported Pd during Catalysis in Water. *J. Phys. Chem. C* 2013, *117*, 17603-17612.

### 2014

Vjunov, A.; Fulton, J. L.; Huthwelker, T.; Pin, S.; Mei, D.; Schenter, G.K.; Govind, N.; Camaioni, D. M.; Hu, J. Z.; Lercher, J. Towards Quantitatively Probing the Al Distribution in Zeolites. *J. Am. Chem. Soc.*, Just Accepted Manuscript.

Vjunov, A.; Hu, M. Y.; Feng, J.; Camaioni, D. M.; Mei, D.; Hu, J. Z.; Zhao, C.; Lercher, J. A. Following Solid Acid Catalyzed Reactions by MAS NMR Spectroscopy in Liquid Phase- Zeolite Catalyzed Conversion of Cyclohexanol in Water. *Angewandte Chemie International Edition*, **2014**, *53*, 479-482.

He, J. Y.; Lu, L.; Zhao, C.; Mei, D.; Lercher, J. A. Mechanisms of Catalytic Cleavage of Benzyl Phenyl Ether in Aqueous and Apolar Phases. *J. Catal.* **2014**, *311*, 41-51.

He, J.; Zhao, C.; Lercher, J. A., Impact of solvent for individual steps of phenol hydrodeoxygenation with Pd/C and HZSM-5 as catalysts. *J. Catal.* **2014**, *309*, 362-375.

He, J. Y.; Zhao, C.; Mei, D.; Lercher, J. A. On the Mechanisms of Selective Cleavage of C–O Bonds in Di-aryl Ethers in the Aqueous Phase. *J. Catal.* **2014**, *309*, 280-290.

## Subtask 1.2 - Charles HF Peden – Well-Defined Metal-Oxide Catalysts to Understand Fundamental Chemical Transformations, and the Role of Water for Catalyzed Reactions

### 2012

Zhu, KK; JM Sun, H Zhang, J Liu, and Y Wang, “Carbon as a Hard Template for Nano Material Catalysts.” *J. Nat. Gas Chem.* **21**(3), (2012) 215-232.

Zhang, L; AM Karim, MH Engelhard, ZH Wei, DL King, and Y Wang, “Correlation of Pt-Re Surface Properties with Reaction Pathways for the Aqueous-phase Reforming of Glycerol.” *J. Catal.* **287** (2012) 37-43.

Wei, ZH; JM Sun, Y Li, AK Datye, and Y Wang, “Bimetallic Catalysts for Hydrogen Generation.” *Chem. Soc. Rev.* **41**(24), (2012) 7994-8008.

Mei, DH; AM Karim, and Y Wang, “On the Reaction Mechanism of Acetaldehyde Decomposition on Mo(110).” *ACS Catal.* **2**(4), (2012) 468-478.

Karim, AM; C Howard, B Roberts, L Kovarik, L Zhang, DL King, and Y Wang, “In Situ X-ray Absorption Fine Structure Studies on the Effect of pH on Pt Electronic Density during Aqueous Phase Reforming of Glycerol.” *ACS Catal.* **2**(11), (2012) 2387-2394.

Halevi, B; EJ Peterson, A Roy, A DeLariva, E Jerero, F Gao, Y Wang, JM Vohs, B Kiefer, E Kunkes, M Havecker, M Behrens, R Schlogl, and AK Datye, "Catalytic Reactivity of Face Centered Cubic PdZn Alpha for the Steam Reforming of Methanol." *J. Catal.* **291** (2012) 44-54.

Li, SC; Z Li, Z Zhang, BD Kay, R Rousseau, and Z Dohnálek, "Preparation, Characterization, and Catalytic Properties of Tungsten Trioxide Cyclic Trimers on FeO(111)/Pt(111)." *J. Phys. Chem. C* **116** (2012) 908-916.

Simonetti, DA; RT Carr, and E Iglesia, "Acid Strength and Solvation Effects on Methylation, Hydride Transfer, and Isomerization Rates during Catalytic Homologation of C-1 Species." *J. Catal.* **285** (2012) 19-30.

Hu, JZ; JA Sears, HS Mehta, JJ Ford, JH Kwak, K Zhu, Y Wang, J Liu, DW Hoyt, and CHF Peden, "A Large Volume Magic Angle Spinning Nuclear Magnetic Resonance Probe for *In Situ* Investigations with Constant Flow of Reactants." *Phys. Chem. Chem. Phys.* **14** (2012) 2105-2532.

Szanyi, J; M Daturi, G Clet, DR Baer, and CHF Peden, "Well-Studied Cu-BTC Still Serves Surprises: Evidence for Facile  $\text{Cu}^{2+}/\text{Cu}^+$  Interchange." *Phys. Chem. Chem. Phys.* **14** (2012) 4383-4390.

Li, S; H-J Zhai, L-S Wang, and DA Dixon, "Structural and Electronic Properties of Reduced Transition Metal Oxide Clusters,  $\text{M}_4\text{O}_{10}$  and  $\text{M}_4\text{O}_{10}^-$  (M = Cr, W), from Photoelectron Spectroscopy and Quantum Chemical Calculations." *J. Phys. Chem. A.* **116** (2012) 5256-5271.

Jeong, SY; HJ Kim, J-H Bae, DH; Kim, CHF Peden, Y-K Park, and JK Jeon, "Synthesis of Butenes through 2-butanol Dehydration over Mesoporous Materials Produced from Ferrierite." *Catal. Today* **185** (2012) 191-197.

Kim, B; Z Li, BD Kay, Z Dohnálek, and YK Kim, "Unexpected Nondissociative Binding of  $\text{N}_2\text{O}$  on Oxygen Vacancies on a Rutile  $\text{TiO}_2(110)-1\times 1$ ." *J. Phys. Chem. C* **116** (2012) 1145-1150.

Peterson KA; D Feller, and DA Dixon, "Chemical Accuracy in ab initio Thermochemistry and Spectroscopy: Current Strategies and Future Challenges." *Theor. Chem. Acc.* **131** (2012) 1079-1098, DOI 10.1007/s00214-011-1079-5.

Gounder, R; A Jones, RT Carr, and E Iglesia, "Solvation and Acid Strength Effects on Catalysis by Faujasite Zeolites." *J. Catal.* **286**, (2012) 214-223.

Haiges, R; M Rahm, DA Dixon, EB Garner, III, and KO Christe, "Binary Group 15 Polyazides. Structural Characterization of  $[\text{Bi}(\text{N}_3)_4]^-$ ,  $[\text{Bi}(\text{N}_3)_5]^{2-}$ ,  $[\text{bipy}\cdot\text{Bi}(\text{N}_3)_5]^{2-}$ ,  $[\text{Bi}(\text{N}_3)_6]^{3-}$ ,  $\text{bipy}\cdot\text{As}(\text{N}_3)_3$ ,  $\text{bipy}\cdot\text{Sb}(\text{N}_3)_3$  and  $[(\text{bipy})_2\cdot\text{Bi}(\text{N}_3)_3]_2$ , and the Free Pair Activation of Valence Electrons." *Inorg. Chem.* **51** (2012) 1127-1141.

She, X; JH Kwak, J Sun, J Hu, MY Hu, CM Wang, CHF Peden, and Y Wang, "A Comparative Study of SBA-15 Mesoporous Silica Supported Tungsten Oxide and Rhenium Oxide Catalysts for 2-Butanol Dehydration." *ACS Catal.* **2** (2012) 1020-1026.

Vasiliiu, M; DJ Grant, DA Dixon, and D Feller, "Heats of Formation of  $\text{MH}_x\text{Cl}_y$  (M = P, Si, As, Sb) Compounds and Main Group Fluorides from High Level Electronic Structure Calculations." *J. Phys. Chem. A* **116** (2012) 3717-3727.

Fang, Z; M Outlaw, K Smith, N Gist, S Li, DA Dixon, and JL Gole, "Computational Study of the Hydrolysis Reactions of Small  $\text{MO}_2$  (M= Zr and Hf) Nanoclusters with Water." *J. Phys. Chem. C* **116** (2012) 8475-8492.

Kim, B; ZJ Li, BD Kay, Z Dohnálek, and YK Kim, "The Effect of Oxygen Vacancies on the Binding Interactions of  $\text{NH}_3$  with Rutile  $\text{TiO}_2(110)-1\times 1$ ." *PCCP* **14** (2012) 15060-15065.

Stott, AC; TP Vaid, EJ Bylaska, and DA Dixon, "Tuning Band Gap Energies in  $\text{Pb}_3(\text{C}_6\text{X}_6)$  Extended Solid-State Structures." *J. Phys. Chem. C* **116** (2012) 8370-8378.

Feller, D; KA Peterson, and DA Dixon, "Further Benchmarks of a Composite, Convergent, Statistically-calibrated Coupled Cluster-based Approach for Thermochemical and Spectroscopic Studies." *Mol. Phys.* **110** (2012) 2381-2399.

Li, ZJ; B Smid, YK Kim, V Matolin, BD Kay, R Rousseau, and Z Dohnálek, "Alcohol Dehydration on Monooxo  $\text{W}=\text{O}$  and Dioxo  $\text{O}=\text{W}=\text{O}$  Species." *J. Phys. Chem. Lett.* **3** (2012) 2168-2172.

Dixon, DA; D Feller, and KA Peterson, "A Practical Guide to Reliable First Principles Computational Thermochemistry Predictions across the Periodic Table." In *Annual Reports in Computational Chemistry*, Vol. 8, ed. R. A. Wheeler, Section Ed. G. S. Tschumper, Elsevier, Amsterdam, 2012, Chapt. 1, pp. 1-28.

Lin, X; Y Yoon, NG Petrik, ZJ Li, ZT Wang, VA Glezakou, BD Kay, I Lyubinetsky, GA Kimmel, R Rousseau, and Z Dohnálek, "Structure and Dynamics of  $\text{CO}_2$  on Rutile  $\text{TiO}_2(110)-1\times 1$ ." *J. Phys. Chem. C* **116** (2012) 26322-26334.

Mikulas, T; Z Fang, JL Gole, MG White, and DA Dixon, "The Presence of Ti(II) Centers in Doped Nanoscale TiO<sub>2</sub> and TiO<sub>2-x</sub>N<sub>x</sub>." *Chem. Phys. Lett.* **539-540** (2012) 58-63.

Wu, L; Y Liu, C Zhang, S Li, DA Dixon, and D-S Yang, "Mass-analyzed Threshold Ionization of an Excited State of Lanthanum Dioxide." *J. Chem. Phys.* **137** (2012) 034307 (8 pgs.)

Gong, Y; L Andrews, CA Bauschlicher, Jr., KS Thanthiriwatte, and DA Dixon, "Infrared Spectroscopic and Theoretical Studies of the OTiF<sub>2</sub>, OZrF<sub>2</sub> and OHfF<sub>2</sub> Molecules with Terminal Oxo Ligands." *Dalton Trans.* **41** (2012) 11706-11715.

Zhao YF; R Rousseau, J Li, and D Mei, "Theoretical Study of Syngas Hydrogenation to Methanol on the Polar Zn-terminated ZnO(0001) Surface." *J. Phys. Chem. C* **116** (2012) 15952-15961.

Vasiliu, M; A Jones, K Guynn, and DA Dixon, "Prediction of the Thermodynamic Properties of Key Products and Intermediates from Biomass – II." *J. Phys. Chem. C* **116** (2012) 20738-20754.

Smid, B; ZJ Li, A Dohnalkova, BW Arey, RS Smith, V Matolin, BD Kay, and Z Dohnálek, "Characterization of Nanoporous WO<sub>3</sub> Films Grown via Ballistic Deposition." *J. Phys. Chem. C* **116** (2012) 10649-10655.

Thanthiriwatte, KS; M Vasiliu, DA Dixon, and KO Christe, "Structural and Energetic Properties of Closed Shell XF<sub>n</sub> (X = Cl, Br and I; n = 1-7) and XO<sub>n</sub>F<sub>m</sub> (X = Cl, Br and I; n = 1-3; m = 0 – 6) Molecules and Ions Leading to Stability Predictions for Yet Unknown Compounds." *Inorg. Chem.* **51** (2012) 10966-10982.

Peterson, KA; DA Dixon, and H Stoll, "The Use of Explicitly Correlated Methods on XeF<sub>6</sub> Predicts a C<sub>3v</sub> Minimum with a Sterically Active, Free Valence Electron Pair on Xe." *J. Phys. Chem. A* **116** (2012) 9777-9782.

Zhang, ZR; Y Yoon, X Lin, D Acharya, BD Kay, R Rousseau, and Z Dohnálek, "OH group dynamics of 1,3-propanediol on TiO<sub>2</sub>(110)." *J. Phys. Chem. Lett.* **3** (2012) 3257-3263.

Chen, M; R Craciun, N Hoffman, and DA Dixon, "Ligand Bond Energies in *cis*- and *trans*- [L-Pd(PH<sub>3</sub>)<sub>2</sub>Cl]<sup>+</sup> Complexes: Benchmarking Density Functional Theory vs. CCSD(T)." *Inorg. Chem.* **51** (2012) 13195-13203.

## **2013**

Kovarik, L; A Genc, CM Wang, A Qiu, CHF Peden, J Szanyi, and JH Kwak, "Tomography and High Resolution Electron Microscopy Study of Surfaces and Porosity in a Plate-like  $\gamma$ -Al<sub>2</sub>O<sub>3</sub>." *J. Phys. Chem. C* **117** (2013) 179-186.

Shi H; OY Gutierrez, GL Haller, D Mei, R Rousseau, and JA Lercher, "Structure Sensitivity of Hydrogenolytic Cleavage of Endocyclic and Exocyclic C-C Bonds in Methylcyclohexane over Supported Iridium Particles." *J. Catal.* **297** (2013) 70-78.

Yang, Y; CA Mims, DH Mei, CHF Peden, and CT Campbell, "Mechanistic Studies of Methanol Synthesis over Cu from CO/CO<sub>2</sub>/H<sub>2</sub>/H<sub>2</sub>O Mixtures: The Source of C in Methanol and the Role of Water." *J. Catal.* **298** (2013) 10-17.

Lin, X; Z-T Wang, I Lyubinsky, BD Kay, and Z Dohnálek, "Interaction of CO<sub>2</sub> with Oxygen Adatoms on Rutile TiO<sub>2</sub>(110)." *PCCP* **15** (2013) 6190-6195.

Li, Y; Z Wei, J Sun, F Gao, CHF Peden, and Y Wang, "Effect of Sodium on the Catalytic Properties of VO<sub>x</sub>/CeO<sub>2</sub> Catalysts for Oxidative Dehydrogenation of Methanol." *J. Phys. Chem. C* **117** (2013) 5722-5729.

Clayton, DA; TE McPherson, S Pan, M Chen, DA Dixon, and D Hu, "Spatial and Temporal Variation of Surface-Enhanced Raman Scattering at Ag Nanowires in Aqueous Solution." *PCCP* **15** (2013) 850-859.

Appel, A.M.; Bocarsly, A.B.; Bercaw, J. E.; Dobbek, H.; Dupuis, M.; DuBois, D. L.; Ferry, J. G.; Fujita, E.; Hille, R.; Kenis, P. J. A.; Kerfeld, C. A.; Morris, R. H. Peden, C. H. F.; Portis, A.; Ragsdale, S.; Rauchfuss, T. B.; Reek, J. N. H.; Seefeldt, L. C.; Spitler, M.; Stack, R. J.; Thauer, R. K.; Waldrop, G. L., Frontiers, Opportunities, and Challenges in Biochemical and Chemical Catalysis of CO<sub>2</sub>. *Chem. Rev.* **2013**, *113*, 6621-6658.

Li, S and DA Dixon, "Structural and Electronic Properties of Group 6 Transition Metal Oxide Clusters." Invited Chapter in *Catalysis by Nanoparticles*, Ed. S. Suib, Elsevier, 2013, Chapt. 2, pp. 21-61.

Li, W-Z; L Kovarik, DH Mei, J Liu, Y Wang, and CHF Peden, "Anti-sintering Pt Nanoparticles Stabilized by MgAl<sub>2</sub>O<sub>4</sub> Spinel {111} Facets." *Nature Comm.* **4:2481** (2013) 7 pages.

Fang, Z.; Dixon, D. A. "Hydrolysis of MCl<sub>4</sub> (M = Zr, Hf): The Initial Steps in the Production of MO<sub>2</sub>. *J. Phys. Chem. C*, **2013**, *117*, 7459-7474.

Li, Z.; Kay, B. D.; Dohnálek, Z., "Dehydration and Dehydrogenation of Ethylene Glycol on Rutile TiO<sub>2</sub>(110)." *Phys. Chem. Chem. Phys.* **2013**, *15* (29), 12180-12186.

Fang, Z.; Dixon, D. A. Computational Study of H<sub>2</sub> and O<sub>2</sub> Production from Water Splitting by using Small MO<sub>2</sub> Nanoclusters (M = Ti, Zr, Hf). *J. Phys. Chem. A*, **2013**, *117*, 3539–3555.

Acharya, D. P.; Yoon, Y.; Li, Z.; Zhang, Z.; Lin, X.; Mu, R.; Chen, L.; Kay, B. D.; Rousseau, R.; Dohnálek, Z., Site-Specific Imaging of Elemental Steps in Dehydration of Diols on TiO<sub>2</sub>(110). *ACS Nano* **2013**, *7* (11), 10414-10423.

Sung, Y. M.; Vasiliu, M.; Dixon, D. A.; Bonizzoni, M.; Kim, D.; Vaid T. P. Electronic Structure and Photophysics of (C=C)tetra-*p*-tolylporphyrin. *Photochem. Photobio. Sci.*, **2013**, *12*, 1774-1779. (cover).

Kovarik, L.; Genc, A.; Wang, C. M.; Qiu, A. N.; Peden, C. H. F.; Szanyi, J.; Kwak, J. H., Tomography and High-Resolution Electron Microscopy Study of Surfaces and Porosity in a Plate-Like Gamma-Al<sub>2</sub>O<sub>3</sub>. *J. Phys. Chem. C* **2013**, *117* (1), 179-186.

Wang, J.; Pan, S.; Chen, M.; Dixon, D. A. Gold Nanorod-Enhanced Light Absorption and Photoelectrochemical Performance of α-Fe<sub>2</sub>O<sub>3</sub> Thin-Film Electrodes for Renewable Energy Conversion and Electromagnetic Enhancement Mechanism. *J. Phys. Chem. C*, **2013**, *117*, 22060.

## **2014**

Kovarik, L.; Bowden, M.; Genc, A.; Szanyi, J.; Peden, C.H.F.; Kwak, J.H., The Structure of δ-Al<sub>2</sub>O<sub>3</sub>: Toward the Atomic Level Understanding of Transition Alumina Phases. *J. Phys. Chem. C* **2014**. In Press.

Li, Y.; Wei, Z.; Gao, F.; Peden, C.H.F.; Wang, Y., Effects of CeO<sub>2</sub> Support Facets on VO<sub>x</sub>/CeO<sub>2</sub> Catalysts for Oxidative Dehydrogenation of Methanol. *J. Catal.* **2014**, *315*, 15-24.

Sun, J.; Wang, Y. Review of ethanol conversion to chemicals and fuels. *ACS Catalysis* **2014**, dx.doi.org/10.1021/cs4011343. (featured on cover of the 2014 April issue).

Kwak, J.; Dagle, R.; Tustin, G.; Zoeller, J.; Allard, L.; Wang, Y. Molecular active sites in heterogeneous Ir-La/C catalyzed carbonylation of methanol to acetates. *J.Phys.Chem.Lett.* **2014**, dx.doi.org/10.1021/jz402728e

Davidson, S.; Sun, J.; Wang, Y. The effect of ZnO addition on Co/C catalyst for vapor and aqueous phase reforming of ethanol. *Catal.Today* **2014**, dx.doi.org/10.1016/j.cattod.2013.12.044.

Li, Z.; Fang, Z.; Kelley, M. S.; Kay, B. D.; Rousseau, R.; Dohnálek, Z.; Dixon, D. A., Ethanol Conversion on Cyclic (MO<sub>3</sub>)<sub>3</sub> (M = Mo, W) Clusters. *J. Phys. Chem. C* **2014**, *118* (9), 4869-4877.

Garner, III, E. B.; Arduengo, III, A. J.; Streubel, R.; Dixon, D. A. Electronic Structure Predictions of the Properties of Non-innocent P-Ligands in Group 6B Transition Metal Complexes. *Dalton Trans* **2014**, *43*, 2069-2078.

Rousseau, R.; Dixon, D. A.; Kay, B.; Dohnálek, Z., Dehydration, Dehydrogenation, and Condensation of Alcohols on Supported Oxide Catalysts Based on Cyclic (WO<sub>3</sub>)<sub>3</sub> and (MoO<sub>3</sub>)<sub>3</sub> Clusters. *Chem. Soc. Rev.* **2014**, DOI: 10.1039/C3CS60445D.

Smith, R. S.; Li, Z.; Chen, L.; Dohnálek, Z.; Kay, B. D., Adsorption, Desorption, and Displacement Kinetics of H<sub>2</sub>O and CO<sub>2</sub> on TiO<sub>2</sub>(110). *J. Phys. Chem. B* **2014**, DOI: 10.1021/jp501131v.

Chen, L.; Li, Z.; Smith, R. S.; Kay, B. D.; Dohnálek, Z., Molecular Hydrogen Formation from Proximal Glycol Pairs on TiO<sub>2</sub>(110). *J. Am. Chem. Soc.* **2014**, DOI: 10.1021/ja500992b.

Kim, B.; Li, Z.; Kay, B.; Dohnálek, Z.; Kim, Y. K., Low-Temperature Desorption of N<sub>2</sub>O from NO on Rutile TiO<sub>2</sub>(110)-1×1. *J. Phys. Chem. C* **2014**, DOI: 10.1021/jp501179y.

## **Subtask 2.1 – Roger Rousseau – Multifunctional Catalysts for CO<sub>2</sub> Reduction**

### **2012**

Szanyi, J; M Daturi, G Clet, D Baer, and CHF Peden, “Well-studied Cu-BTC Still Serves Surprises: Evidence for Facile Cu<sup>2+</sup>/Cu<sup>+</sup> Interchange.” *Phys. Chem. Chem. Phys.* **14**(13) (2012) 4383-4390.

Mudiyanselage, K and J Szanyi, “NO<sub>2</sub> Uptake under Practically Relevant Conditions on BaO/Pt(111).” *Catal. Today* **181**(1) (2012) 116-123.

Kwak, JH; R Tonkyn, D Tran, CHF Peden, and J Szanyi, “Size-Dependent Catalytic Performance of CuO on gamma-Al<sub>2</sub>O<sub>3</sub>: NO Reduction versus NH<sub>3</sub> Oxidation.” *ACS Catal.* **2** (2012) 1432-1440.

### **2013**

- Kovarik, L; A Genc, C Wang, JA Kwak, J Szanyi, and CHF Peden, "Tomography and High-Resolution Electron Microscopy Study of Surfaces and Porosity in a Plate-like gamma-Al<sub>2</sub>O<sub>3</sub>." *J. Phys. Chem. C* **117** (2013) 179-186.
- Ho, M. H.; Chen, S.; Rousseau, R.; Dupuis, M.; Bullock, R. M.; Raugei, S. Bio-Inspired Molecular Catalysts for Hydrogen Oxidation and Hydrogen Production. Chapter 6 in Application of Molecular Modeling to Challenges in Clean Energy. *ACS Symposium Series*, **2013**, vol. 1133, ed. G Fitzgerald and N Govind, pp. 89-111. American Chemical Society, Washington, DC.
- Ho, M. H.; Raugei, S.; Rousseau, R.; Dupuis, M.; Bullock, R. M. Evaluation of the Role of Water in the H<sub>2</sub> Bond Formation by Ni(II)-based Electrocatalysts. *Journal of Chemical Theory and Computation* **2013**, 9(8):3505-3514. doi:10.1021/ct400396s
- Mock, M. T.; Chen, S.; O'Hagan, M. J.; Rousseau, R.; Dougherty, W. G.; Kassel, W. S.; Bullock, R. M. Dinitrogen Reduction by a Chromium (0) Complex Supported by a 16-membered Phosphorus Macrocyclic. *Journal of the American Chemical Society* **2013**, 135(31):11493-11496. doi:10.1021/ja405668u
- Wang, Y.; Mei, D.; Li, J.; Rousseau, R. DFT+U Study on the Localized Electronic States and Their Potential Role During H<sub>2</sub>O Dissociation and CO Oxidation Processes on CeO<sub>2</sub>(111) Surface. *Journal of Physical Chemistry* **2013**, C 117(44):23082-23089. doi:10.1021/jp409953u
- Wang, Y.; Yoon, Y.; Glezakou, V. A.; Li, J.; Rousseau, R. The Role of Reducible Oxide-Metal Cluster Charge Transfer in Catalytic Processes: New Insights on The Catalytic Mechanism of CO Oxidation on Au/TiO<sub>2</sub> from Ab Initio Molecular Dynamics. *Journal of the American Chemical Society* **2013**, 135(29):10673-10683. doi:10.1021/ja402063v
- Heiden, Z. M.; Chen, S.; Mock, M. T.; Dougherty, W. G.; Kassel, W. S.; Rousseau, R.; Bullock, R. M. Protonation of Ferrous Dinitrogen Complexes Containing a Diphosphine Ligand with a Pendant Amine. *Inorganic Chemistry* **2013**, 52(7):4026-4039. doi:10.1021/ic4000704
- 2014**
- Rousseau, R.; Dixon, D. A.; Kay, B. D.; Dohnálek, Z. Dehydration, dehydrogenation, and condensation of alcohols on supported oxide catalysts based on cyclic (WO<sub>3</sub>)<sub>3</sub> and (MoO<sub>3</sub>)<sub>3</sub> clusters. *Chem. Soc. Rev.* **2014**, doi: 10.1039/C3CS60445D
- Li, S; Fang, Z.; Kelley, M. S.; Kay, B. D.; Rousseau, R.; Dohnalek, Z.; Dixon, D. A. Ethanol Conversion on Cyclic (MO<sub>3</sub>)<sub>3</sub> (M= Mo, W) Clusters. *Journal of Physical Chemistry*, **2014**, C118: 4869-4877. doi: 10.1021/jp500255f
- Chen, S.; Ho, M. H.; Bullock, R. M.; DuBois, D. L.; Dupuis, M.; Rousseau, R.; Raugei, S. Computing Free Energy Landscapes: Application to Ni-based Electrocatalysts with Pendant Amines for H<sub>2</sub> Production and Oxidation. *ACS Catalysis* **2014**, 4 229-242. doi: 10.1021/cs401104w
- Acharya, D. P.; Yoon, Y.; Li, Z.; Zhang, Z.; Lin, X.; Mu, R.; Chen, L.; Kay, B. D.; Rousseau, R.; Dohnalek, Z. Site-Specific Imaging of Elemental Steps in Dehydration of Diols on TiO<sub>2</sub>(110). *ACS Nano* **2014**, 7(11):10414-10423. doi:10.1021/nn404934q

## Subtask 2.2 – Aaron Appel - An Energy-Based Approach to Bifunctional Molecular Catalysis for CO<sub>2</sub> Reduction and Fuel Utilization

### 2012

- Jain, A; ML Reback, ML Lindstrom, CE Thogerson, ML Helm, AM Appel, and WJ Shaw, "Investigating the Role of the Outer-Coordination Sphere in [Ni(P<sup>Ph<sub>2</sub></sup>N<sup>Ph-R<sub>2</sub></sup>)<sub>2</sub>]<sup>2+</sup> Hydrogenase Mimics." *Inorg. Chem.* **51** (2012) 6592.
- Lense, S; M-H Ho, S Chen, A Jain, S Raugei, JC Linehan, JAS Roberts, AM Appel, and W Shaw, "Incorporating Amino Acid Esters into Catalysts for Hydrogen Oxidation: Steric and Electronic Effects and the Role of Water as a Base." *Organometallics* **31** (2012) 6719.
- Liu, T; S Chen, MJ O'Hagan, M Rakowski DuBois, RM Bullock, and DL DuBois, "Synthesis, Characterization, and Reactivity of Fe Complexes Containing Cyclic Diazadiphosphine Ligands: The Role of the Pendant Base in Heterolytic Cleavage of H<sub>2</sub>." *J. Am. Chem. Soc.* **134** (2012) 6257.

Seu, CS; AM Appel, MD Doud, DL DuBois, and CP Kubiak, "Formate oxidation via  $\beta$ -deprotonation in  $[\text{Ni}(\text{P}^{\text{R}}_2\text{N}^{\text{R}'}_2)_2(\text{CH}_3\text{CN})]^{2+}$  complexes." *Energy Environ. Sci.* **5** (2012) 6480.

van der Eide, EF; T Liu, DM Camaioni, ED Walter, and RM Bullock, "Facile Thermal W-W Bond Homolysis in the N-Heterocyclic Carbene-Containing Tungsten Dimer  $[\text{CpW}(\text{CO})_2(\text{IME})_2]$ ." *Organometallics* **31** (2012) 1775.

van der Eide, EF; P Yang, ED Walter, T Liu, and RM Bullock, "Dinuclear Metalloradicals Featuring Unsupported Metal–Metal Bonds." *Angew. Chem. Int. Ed.* **51** (2012) 8361.

Wiedner, ES; JY Yang, S Chen, S Raugei, WG Dougherty, WS Kassel, ML Helm, RM Bullock, M Rakowski DuBois, and DL DuBois, "Stabilization of Nickel Complexes with  $\text{Ni}^0\cdots\text{H-N}$  Bonding Interactions Using Sterically Demanding Cyclic Diphosphine Ligands." *Organometallics* **31** (2012) 144.

### **2013**

van der Eide, EF; G-L Hou, SHM Deng, H Wen, P Yang, RM Bullock, and X-B Wang, "Metal-Centered 17-Electron Radicals  $\text{CpM}(\text{CO})_3\cdot$  (M = Cr, Mo, W): A Combined Negative Ion Photoelectron Spectroscopic and Theoretical Study." *Organometallics* **32** (2013) 2084.

Liu, T; DL DuBois, and RM Bullock, "An Iron Complex with Pendent Amines as a Molecular Electrocatalyst for Oxidation of Hydrogen." *Nat. Chem.* **5** (2013) 228.

Appel, A. M.; Bercaw, J. E.; Bocarsly, A. B.; Dobbek, H.; Dupuis, M.; DuBois, D. L.; Ferry, J. G.; Fujita, E.; Hille, R.; Kenis, P. J. A.; Kerfeld, C. A.; Morris, R. H.; Peden, C. H. F.; Portis, A. R.; Ragsdale, S. W.; Rauchfuss, T. B.; Reek, J. N. H.; Seefeldt, L. C.; Thauer, R. K.; Waldrop, G. L., Frontiers, Opportunities, and Challenges in Biochemical and Chemical Catalysis of  $\text{CO}_2$  Fixation. *Chem. Rev.* **2013**, *113*, 6621-6658.

Jeletic, M. S.; Mock, M. T.; Appel, A. M.; Linehan, J. C., A Cobalt-Based Catalyst for the Hydrogenation of  $\text{CO}_2$  under Ambient Conditions. *J. Am. Chem. Soc.* **2013**, *135*, 11533-11536.

Hulley, E. B.; Welch, K. D.; Appel, A. M.; DuBois, D. L.; Bullock, R. M., Rapid, Reversible Heterolytic Cleavage of Bound  $\text{H}_2$ . *J. Am. Chem. Soc.* **2013**, *135*, 11736-11739.

Wiedner, E. S.; Appel, A. M.; DuBois, D. L.; Bullock, R. M., Thermochemical and Mechanistic Studies of Electrocatalytic Hydrogen Production by Cobalt Complexes Containing Pendant Amines. *Inorg. Chem.* **2013**, *52*, 14391-14403.

Franz, J. A.; O'Hagan, M.; Ho, M. H.; Liu, T.; Helm, M. L.; Lense, S.; DuBois, D. L.; Shaw, W. J.; Appel, A. M.; Raugei, S.; Bullock, R. M., Conformational Dynamics and Proton Relay Positioning in Nickel Catalysts for Hydrogen Production and Oxidation. *Organometallics* **2013**, *32*, 7034-7042.

Hoffert, W. A.; Mock, M. T.; Appel, A. M.; Yang, J. Y., Incorporation of Hydrogen-Bonding Functionalities into the Second Coordination Sphere of Iron-Based Water-Oxidation Catalysts. *Eur. J. Inorg. Chem.* **2013**, 3846-3857.

Horvath, S.; Fernandez, L. E.; Appel, A. M.; Hammes-Schiffer, S., pH-Dependent Reduction Potentials and Proton-Coupled Electron Transfer Mechanisms in Hydrogen-Producing Nickel Molecular Electrocatalysts. *Inorg. Chem.* **2013**, *52*, 3643-3652.

Galan, B. R.; Reback, M. L.; Jain, A.; Appel, A. M.; Shaw, W. J., Electrocatalytic Oxidation of Formate with Nickel Diphosphine Dipeptide Complexes: Effect of Ligands Modified with Amino Acids. *Eur. J. Inorg. Chem.* **2013**, *30*, 5366-5371.

Das, A. K.; Engelhard, M. H.; Liu, F.; Bullock, R. M.; Roberts, J. A. S., The Electrode as Organolithium Reagent: Catalyst-Free Covalent Attachment of Electrochemically Active Species to an Azide-Terminated Glassy Carbon Electrode Surface. *Inorg. Chem.* **2013**, *52*, 13674-13684.

Wiese, S.; Kilgore, U. J.; Ho, M.-H.; Raugei, S.; DuBois, D. L.; Bullock, R. M. Helm, M. L., Hydrogen Production using Nickel Electrocatalysts with Pendant Amines: Ligand Effects on Rates and Overpotentials. *ACS Catalysis*, **2013**, *3*, 2527-2535.

### **2014**

Appel, A. M.; Helm, M. L., Determining the Overpotential for a Molecular Electrocatalyst. *ACS Catal.* **2014**, *4*, 630-633.

Bullock, R. M.; Appel, A. M.; Helm, M. L., Production of Hydrogen by Electrocatalysis: Making the H-H Bond by Combining Protons and Hydrides. *Chem. Commun.* **2014**, *50*, 3125-3143.

Das, P.; Ho, M. H.; O'Hagan, M.; Shaw, W. J.; Bullock, R. M.; Raugei, S.; Helm, M. L., Controlling proton

movement: electrocatalytic oxidation of hydrogen by a nickel(II) complex containing proton relays in the second and outer coordination spheres. *Dalton Trans.* **2014**, 43, 2744-54. **Featured on the cover of issue 7.**

Chen, S.; Ho, M.-H.; Bullock, R. M.; DuBois, D. L.; Dupuis, M.; Rousseau, R.; Raugei, S., Computing Free Energy Landscapes: Application to Ni-based Electrocatalysts with Pendant Amines for H<sub>2</sub> Production and Oxidation. *ACS Catalysis* **2014**, 4, 229-242.

Lewandowska-Andralojc, A.; Grills, D. C.; Zhang, J.; Bullock, R. M.; Miyazawa, A.; Kawanishi, Y.; Fujita, E., Kinetic and Mechanistic Studies of Carbon-to-Metal Hydrogen Atom Transfer Involving Os-Centered Radicals: Evidence for Tunneling. *J. Am. Chem. Soc.* **2014**, 136, 3572-3578.

Heiden, Z. M.; Chen, S.; Labios, L. A.; Bullock, R. M.; Walter, E. D.; Tyson, E. L.; Mock, M. T., Proton and Electron Additions to Iron(II) Dinitrogen Complexes Containing Pendant Amines. *Organometallics* **2014**, 33, 1333-1336.

Liu, T.; Wang, X. Hoffmann, C.; DuBois, D. L.; Bullock, R. M., Heterolytic Cleavage of Hydrogen by an Iron Hydrogenase Model: An Fe-H···H-N Dihydrogen Bond Characterized by Neutron Diffraction. *Angew. Chem.* **2014**, in press, (designated as a "Very Important Paper")

### **Subtask 3.1 – Michael A. Henderson – Fundamental Studies of Water Splitting on Model TiO<sub>2</sub>, RuO<sub>2</sub> and Mixed TiO<sub>2</sub>-RuO<sub>2</sub> Catalysis**

#### **2012**

Du, Y; NG Petrik, NA Deskins, Z Wang, MA Henderson, GA Kimmel, and I Lyubinetsky, "Hydrogen Reactivity on Highly-hydroxylated TiO<sub>2</sub>(110) Surfaces Prepared via Carboxylic Acid Adsorption and Photolysis." *Phys. Chem. Chem. Phys.* **14**(9): (2012) 3066-3074.

Du, Y; DJ Kim, TC Kaspar, SE Chamberlin, I Lyubinetsky, and SA Chambers, "In-situ Imaging of the Nucleation and Growth of Epitaxial Anatase TiO<sub>2</sub>(001) Films on SrTiO<sub>3</sub>(001)." *Surf. Sci.* **606**(17-18): (2012) 1443-1449.

Henderson, MA, "Visible Light Induced Photodesorption of NO from the Alpha-Cr<sub>2</sub>O<sub>3</sub>(0001) Surface." *Surf. Sci.* **606**(3-4): (2012) 505-509. (Corrigendum: *Surface Science* **606**(17-18): 1467)

Kim, B; ZJ Li, BD Kay, Z Dohnalek, and YK Kim, "The effect of Oxygen Vacancies on the Binding Interactions of NH<sub>3</sub> with Rutile TiO<sub>2</sub>(110)-1 x 1." *Phys. Chem. Chem. Phys.* **14**(43): (2012) 15060-15065.

Kim, B; ZJ Li, BD Kay, Z Dohnalek, and YK Kim, "Unexpected Nondissociative Binding of N<sub>2</sub>O on Oxygen Vacancies on a Rutile TiO<sub>2</sub>(110)-1 x 1." *J. Phys. Chem. C* **116**(1): (2012) 1145-1150.

Lin, X; Y Yoon, NG Petrik, ZJ Li, ZT Wang, VA Glezakou, BD Kay, I Lyubinetsky, GA Kimmel, R Rousseau, and Z Dohnalek, "Structure and Dynamics of CO<sub>2</sub> on Rutile TiO<sub>2</sub>(110)-1x1." *J. Phys. Chem. C* **116**(50): (2012) 26322-26334.

Shen, M; DP Acharya, Z Dohnalek, and MA Henderson, "Importance of Diffusion in Methanol Photochemistry on TiO<sub>2</sub>(110)." *J. Phys. Chem. C* **116**(48): (2012) 25465-25469.

Shen, MM and MA Henderson, "Role of Water in Methanol Photochemistry on Rutile TiO<sub>2</sub>(110)." *J. Phys. Chem. C* **116**(35): (2012) 18788-18795.

Wang, ZT; NA Deskins, and I Lyubinetsky, "Direct Imaging of Site-Specific Photocatalytical Reactions of O<sub>2</sub> on TiO<sub>2</sub>(110)." *J. Phys. Chem. Lett.* **3**(1): (2012) 102-106.

Wang, ZT; NA Deskins, MA Henderson, and I Lyubinetsky, "Inhibitive Influence of Oxygen Vacancies for Photoactivity on TiO<sub>2</sub>(110)." *Phys. Rev. Lett.* **109**(26): (2012) 266103.

#### **2013**

Henderson, MA, M Shen, ZT Wang, and I Lyubinetsky, "Characterization of the Active Surface Species Responsible for UV-Induced Desorption of O<sub>2</sub> from the Rutile TiO<sub>2</sub>(110) Surface." *J. Phys. Chem. C* **117**(11): (2013) 5774-5784.

Henderson, MA and I Lyubinetsky, "Molecular-Level Insights into Photocatalysis from Scanning Probe Microscopy Studies on TiO<sub>2</sub>(110)." *Chem. Rev.* (2013 in press.)

Herman, GS; ZT Zehr, and MA Henderson, "Characterization of Oxygen and Titanium Diffusion at the Anatase TiO<sub>2</sub>(001) Surface." *Surf. Sci.* **612**(1): (2013) L5-L8.

Lin, X; Z-T Wang, I Lyubinetsky, BD Kay, and Z Dohnalek, "Interaction of CO<sub>2</sub> with Oxygen Adatoms on Rutile TiO<sub>2</sub>(110)." *Phys. Chem. Chem. Phys.* **15**(17): (2013) 6190-6195.

Petrik, N. G.; Kimmel, G. A., Multiple Non-Thermal Reaction Steps for the Photooxidation CO to CO<sub>2</sub> on Reduced TiO<sub>2</sub>(110), *Journal of Physical Chemistry Letters* **2013**, 4, 344.

#### **2014**

Petrik, N. G.; Kimmel, G. A., Probing the photochemistry of chemisorbed oxygen on TiO<sub>2</sub>(110) with Kr and other co-adsorbates, *Physical Chemistry Chemical Physics* **2014**, 16, 2338 – 2346.

### **Subtask 3.2 – S. Thomas Autrey - Activation of Small Molecules with Bi-functional Amphiphilic Catalyst Complexes**

#### **2012**

Dang, LX; GK Schenter, T-M Chang, SM Kathmann, and ST Autrey. "The Role of Solvent on the Thermodynamics and Kinetics of Forming Frustrated Lewis Pairs." *J. Phys. Chem. Lett.* **3** (2012) 3312. DOI: 10.1021/jz301533a.

Camaioni, DM; B Ginovska-Pangovska, GK Schenter, SM Kathmann, and ST Autrey. "Analysis of the Activation and Heterolytic Dissociation of H<sub>2</sub> by "Frustrated" Lewis Pairs: NH<sub>3</sub> and BX<sub>3</sub> (X = H, F and Cl)." *J. Phys Chem A* **116** (2012) 7228. 10.1021/jp3039829.

Aijaz, Arshad; A Karkamkar, YJ Choi, N Tsumori, E Rönnebro, T Autrey, H Shioyama, and Q Xu. "Immobilizing Highly Catalytically Active Pt Nanoparticles inside the Pores of Metal-Organic Framework: A Double Solvents Approach." *J. Am. Chem. Soc.* **134** (2012) 13926. DOI: 10.1021/ja3043905.

Nielsen, TK; A Karkamkar, M Bowden, F Besenbacher, TR Jensen, and T Autrey. "Methods to Stabilize and Destabilize Ammonium Borohydride." Invited *Dalton Trans.* **42** (2012) 680. DOI: 10.1039/C2DT31591B.

Huang, Z and T Autrey. "Boron-nitrogen-hydrogen ("BNH") Compounds: Recent Developments in Hydrogen Storage, Applications in Hydrogenation and Catalysis, and New Syntheses." *Energy Environ. Sci.* **5** (2012) DOI:10.1039/C2EE23039A. Invited Review

Kathmann, SM; CJ Mundy, GK Schenter, T Autrey, P Aeberhard, B David, MO Jones, and T Ramirez-Cuesta. "Understanding Vibrational Anharmonicity and Phonon Dispersion in Solid Ammonia Borane." *J. Phys. Chem C* **116** (2012) 5926.

#### **2013**

Nielsen, T. K.; Karkamkar, A.; Bowden, M.; Besenbacher, F.; Jensen, T. R.; Autrey, T., Methods to Stabilize and Destabilize Ammonium Borohydride. *Dalton Trans.* **2013**, 42, 680-687.

Karkamkar, A; K Parab, D Neiner, TK Nielsen, H Cho, DM Camaioni, and T Autrey. "Thermodynamic Study of Heterolytic Hydrogen Activation by Frustrated Borane-Amine Lewis Pairs." *Dalton Trans.* **42** (2013) 615. DOI: 10.1039/c2dt31628e. Invited

#### **2014**

Kathmann, S. M.; Cho, H.; Chang, T. M.; Schenter, G. K.; Parab, K. P.; Autrey, S. T., Experimental and Theoretical Study of Molecular Response of Amine Bases in Organic Solvents. *J. Phys. Chem. B* **in press**.

**Ping Liu**

**Water gas shift reactions on metal-oxide catalysts: mechanistic understanding  
and rational catalyst optimization**

Ping Liu, Jose A. Rodriguez, Dario Stacchiola, Sanjaya Senanayake and Mike G.  
White  
Brookhaven National Laboratory

**Presentation Abstract**

Optimization of catalyst behaviors in a rational way is one of great importance in catalysis. Here, we made a coordinated experimental and theoretical efforts to better understand promising transition metal-doped nanostructured oxide catalysts, and to develop concepts for their improvement for the water gas shift (WGS,  $\text{CO} + \text{H}_2\text{O} \rightarrow \text{H}_2 + \text{CO}_2$ ) reaction. The calculations based on DFT and kinetic modeling identified that water dissociation is the key step to control the WGS activity on Au,Cu-oxide systems, where the calculated reaction energy for water dissociation correlates well with the experimental measured WGS activity. Accordingly, the calculated reaction energy for water dissociation was used as the scaling descriptor to screen the inverse model catalysts, oxide/Cu(111), for the better WGS activity. During the process, both Cu and oxides participate in the reaction directly. The strong oxide-Cu interaction is able to tune the electronic structure of oxides and therefore the activity towards water dissociation.

## FWP: CO-027

### Mechanisms for the Water Gas Shift Reaction

**PI:** Jose A. Rodriguez

**Postdoc(s):** Wenqian Xu (current), Alba Vidal (previous), Liang Yu (partly)

**Student(s):** John Lofaro (Stony Brook University)

**Affiliations(s):** Brookhaven National Laboratory; Stony Brook University; Xiamen University

### RECENT PROGRESS

We made a coordinated experimental and theoretical effort to better understand promising transition metal-doped nanostructured oxide catalysts, and to develop concepts for their improvement for the water gas shift (WGS,  $\text{CO} + \text{H}_2\text{O} \rightarrow \text{H}_2 + \text{CO}_2$ ) reaction. It combines three thrusts: (i) *in-situ* studies to determine catalyst structure, oxidation state and chemistry under reaction conditions; (ii) studies of relevant model systems, primarily based on nanoparticles supported on single crystal substrates; and (iii) computational modeling.

#### *In-situ studies of WGS catalysts with XRD, PDF, XAFS and TEM*

The active phase of a series of metal/oxide powder catalysts (Pt/CeO<sub>2</sub>, Pt-Ru/CeO<sub>2</sub>, Pt/CeO<sub>x</sub>/TiO<sub>2</sub>, Au/CeO<sub>x</sub>/TiO<sub>2</sub>, Ce<sub>1-x</sub>Ni<sub>x</sub>O<sub>2-y</sub>, CeO<sub>x</sub>/CuO) was investigated using a combination of *in-situ* time-resolved X-ray diffraction (XRD), Pair-distribution function (PDF) analysis, X-ray absorption fine structure (XAFS) and environmental TEM. Under reaction conditions most of these WGS catalysts underwent chemical

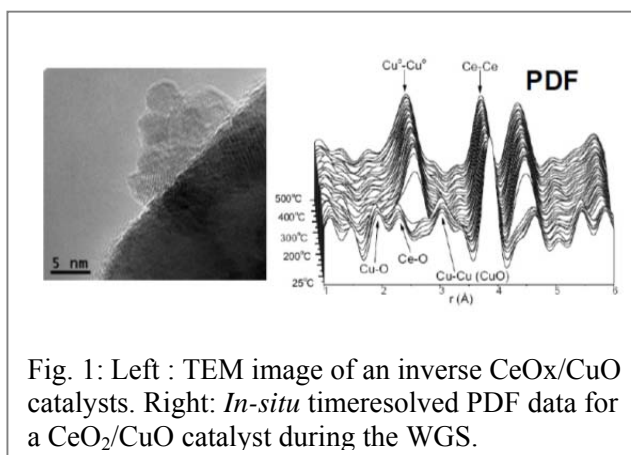


Fig. 1: Left : TEM image of an inverse CeO<sub>x</sub>/CuO catalysts. Right: *In-situ* timeresolved PDF data for a CeO<sub>2</sub>/CuO catalyst during the WGS.

transformations that drastically modified their composition with respect to that obtained during the synthesis process. The active phase of catalysts which combine Cu, Ni, Au or Pt with oxides such as CeO<sub>2</sub>, TiO<sub>2</sub> and CeO<sub>x</sub>/TiO<sub>2</sub> essentially involved nanoparticles of the reduced metals. The oxide support underwent partial reduction and was not a simple spectator, facilitating the dissociation of water and in some cases modifying the chemical properties of the supported metal. Therefore, to optimize the performance of these catalysts one must take into consideration the properties of the metal and oxide phases. Figure 1 shows a TEM image and PDF data for an inverse CeO<sub>x</sub>/CuO powder catalyst. In the TEM image, taken for the as-prepared catalysts, one can see crystallites that in many cases exhibit a (111) surface termination. The

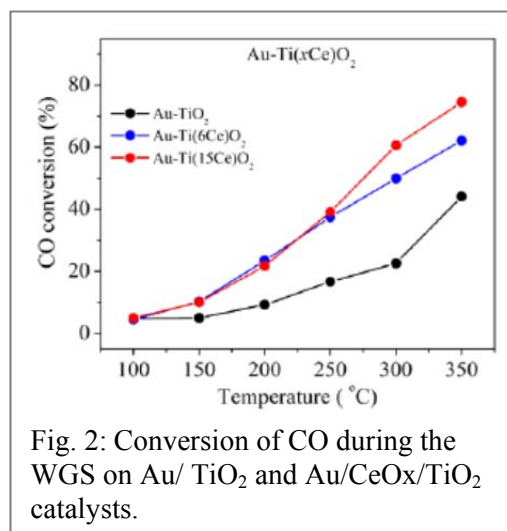


Fig. 2: Conversion of CO during the WGS on Au/ TiO<sub>2</sub> and Au/CeO<sub>x</sub>/TiO<sub>2</sub> catalysts.

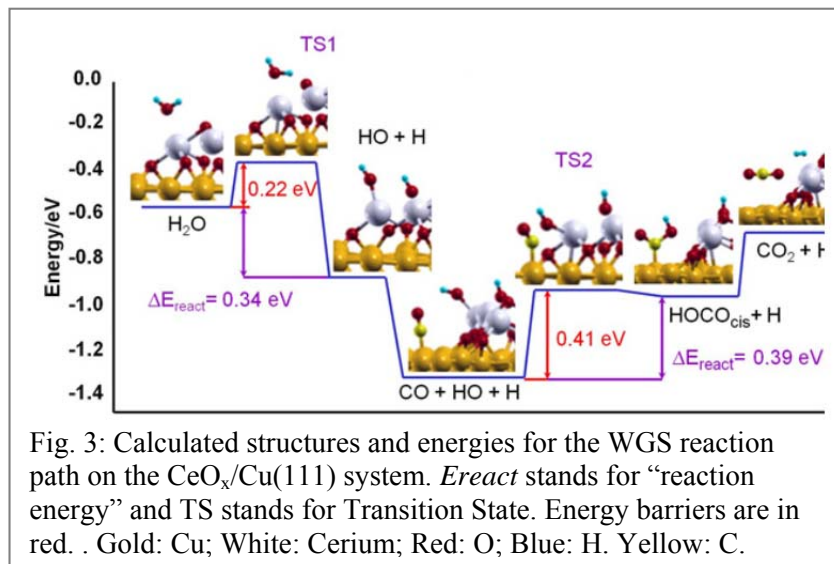
PDF results illustrate the effects of WGS reaction conditions and show a simultaneous disappearance of the Cu-O vector of CuO with the appearance of a Cu-Cu vector for metallic copper. These data, and *in-situ* results obtained for other catalysts in our group, indicate that a WGS metal/oxide catalyst is a dynamic entity that changes with reaction conditions.

Previous studies at BNL indicated that the Au/CeO<sub>x</sub>/TiO<sub>2</sub>(110) and Pt/CeO<sub>x</sub>/TiO<sub>2</sub>(110) model surfaces are excellent catalysts for the WGS. We have prepared and characterized powder samples of Au/CeO<sub>x</sub>/TiO<sub>2</sub> and Pt/CeO<sub>x</sub>/TiO<sub>2</sub>. The activity data in Figure 2 indicate that the Au/CeO<sub>x</sub>/TiO<sub>2</sub> catalysts are more active than plain Au/TiO<sub>2</sub>. The improvement in activity is very pronounced at 300°C. The ceria nanoparticles deposited on the titania powder act as anchoring sites for Au, reducing the sintering of the admetal and, thus, improving the long term stability of the Au/CeO<sub>x</sub>/TiO<sub>2</sub> catalysts. Powders of Pt/CeO<sub>x</sub>/TiO<sub>2</sub> were also excellent catalysts for the WGS. As a result of complex Pt↔ceria and ceria↔titania interactions,

Pt/CeO<sub>x</sub>/TiO<sub>2</sub> catalysts are much more active and stable than Pt/CeO<sub>2</sub> or Pt/TiO<sub>2</sub> catalysts. The characterizations using a combination of TEM, XAFS or NEXAFS, and EELS point to the existence of a mixed-oxide interface in which the Ce<sup>3+</sup> is trapped. Furthermore, *in situ* measurements with XANES indicate that the Ce<sup>4+</sup> cations in the ceria nanoparticles are much easier to reduce than in bulk ceria. The Pt L<sub>3</sub>-edge spectra pointed to the initial presence of a PtO<sub>x</sub> that got reduced to Pt under WGS reaction conditions at temperatures as low as 100°C. The ceria nanoparticles in contact with titania do have special electronic and spatial properties that contribute to the very high catalytic activity of Pt/CeO<sub>x</sub>/TiO<sub>2</sub>.

#### Mechanistic study of WGS on well-defined model Catalysts

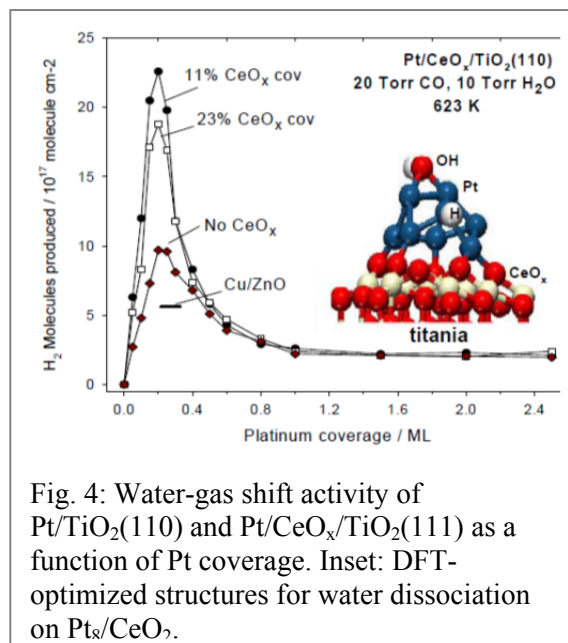
A series of model catalysts (CeO<sub>x</sub>/Cu(111), CeO<sub>x</sub>/Au(111), Pt/CeO<sub>2</sub>(111), Ni/CeO<sub>2</sub>(111), Pt/TiO<sub>2</sub>(110), Pt/CeO<sub>x</sub>/TiO<sub>2</sub>(110)) was used to study fundamental aspects of the WGS reaction. These studies revealed that the oxide component of the catalyst can affect the reaction process in two different ways. First, the presence of O



vacancies in the oxide greatly facilitates the dissociation of water and the rest of reactions occur at the metal-oxide interface (bifunctional effect). And

second, the electronic properties of the metal can be affected by interactions with the oxide producing special chemical properties to catalyze the WGS reaction (electronic effect).

The WGS reaction on inverse  $\text{CeO}_x/\text{Cu}(111)$  model catalysts was studied using combined ambient-pressure XPS, infrared spectroscopy and DFT. Under reaction conditions no adsorbed formate was detected, instead a  $\text{CO}_2$ -like species was formed at the metal-oxide interface. The results of DFT calculations indicate that the  $\text{CO}_2$ -like intermediate is a product of the decomposition of an unstable HOCO species (Figure 3). The DFT results suggest that the high performances of  $\text{CeO}_x/\text{Cu}(111)$  in the WGS reaction is a consequence of a bifunctional effect by coupling the moderate chemical activity of Cu to the more reactive  $\text{CeO}_x$  nanoparticle.  $\text{H}_2\text{O}$  dissociation takes place on  $\text{CeO}_x$  with a barrier much lower than that on Cu. CO adsorbs on sites of the Cu substrate located nearby. Then all the subsequent steps occur at the oxide-metal interface via the carboxyl (HOCO) intermediate at a reasonable speed. The energy released by chemisorption of CO on Cu(111) and the dissociation of  $\text{H}_2\text{O}$  on  $\text{CeO}_x$  can be used for the formation of carboxyl and the final release of  $\text{CO}_2$  and  $\text{H}_2$  at the metal-oxide interface.



In contrast, the electronic effect plays an essential role for the WGS on Pt/CeO<sub>2</sub>(111) and Pt/CeO<sub>x</sub>/TiO<sub>2</sub>(110). The large electronic perturbations seen for small Pt particles in contact with ceria significantly enhanced the ability of the admetal to adsorb and dissociate water and made it a highly active catalyst for the WGS (Figure 4). When going from Pt(111) to Pt<sub>8</sub>/CeO<sub>2</sub>(111), the results of DFT calculations indicate that dissociation of water becomes a very exothermic process. The ceria-supported Pt<sub>8</sub> appears as a fluxional system that can change geometry and charge distribution to better accommodate adsorbates. Compared to other WGS catalysts (Cu(111), Pt(111), Cu/CeO<sub>2</sub>(111) and Au/CeO<sub>2</sub>(111)), the Pt/CeO<sub>2</sub>(111) surface has

the unique property that the admetal is able to dissociate water in an efficient way. Furthermore, for the codeposition of Pt and CeO<sub>x</sub> nanoparticles on TiO<sub>2</sub>(110), we found a transfer of O from the ceria to Pt that opens new paths for the WGS process and makes the mixed-metal oxide an extremely active catalyst for the production of hydrogen. The behavior seen for Ni/CeO<sub>2</sub>(111), Pt/CeO<sub>2</sub>(111) and Pt/CeO<sub>x</sub>/TiO<sub>2</sub>(110) systems illustrates the positive effects derived from electronic metal-support interactions and points to a promising approach for improving or optimizing the performance of metal/oxide catalysts.

*Theoretical optimization of the components in metal-oxide catalysts for the WGS reaction*

The key for theoretical catalyst optimization is to identify the key factors, which are able to scale well with the overall activity. What we learn from our studies of working catalysts set up a strong basis for theoretical optimization of better WGS catalysts. That is, a good WGS catalyst should be active enough to dissociate H<sub>2</sub>O, but still being able to oxidize and remove CO efficiently. Accordingly, two optimization cycles are considered. The key kinetic parameter for the first cycle is the energetics for H<sub>2</sub>O dissociation. As shown in Figure 5, our DFT-calculated reaction energy and activation barrier for

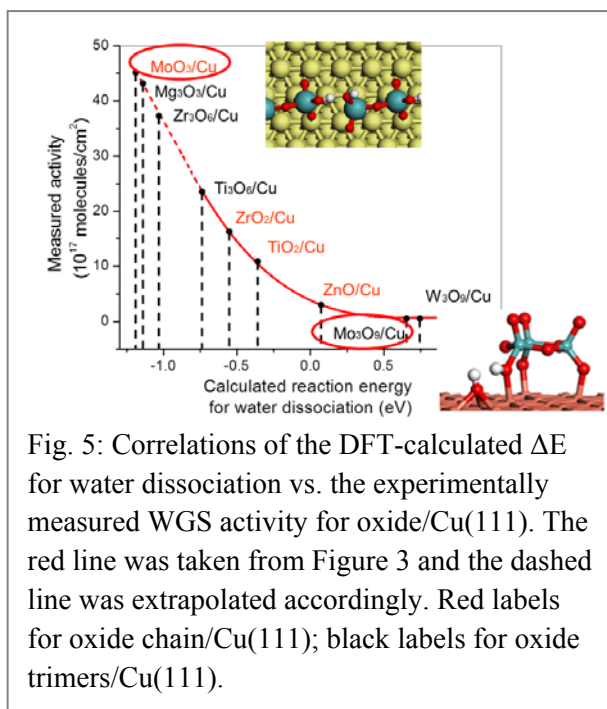


Fig. 5: Correlations of the DFT-calculated  $\Delta E$  for water dissociation vs. the experimentally measured WGS activity for oxide/Cu(111). The red line was taken from Figure 3 and the dashed line was extrapolated accordingly. Red labels for oxide chain/Cu(111); black labels for oxide trimers/Cu(111).

H<sub>2</sub>O dissociation on pure metal (Au, Cu) and metal (Au,Cu)-oxide correlates with the WGS activity measured experimentally. By using oxides, an enhanced WGS

activity is observed due to the fact that the oxides help the rate-limiting H<sub>2</sub>O dissociation via bifunctional effects. As a result, moving from non-reducible oxides to reducible and reduced oxides, H<sub>2</sub>O dissociation is more exothermic with a strengthened interaction with dissociated H and OH, the barrier for H<sub>2</sub>O dissociation is lowered and an increasing WGS activity is observed experimentally. The second-cycle optimization is based on the reaction of CO with catalysts which are active for H<sub>2</sub>O dissociation.

Recently, we performed the catalyst optimization on Oxide/Cu(111) systems. Two different models are considered for the optimization (Figure 5). One is oxide chain (M<sub>x</sub>O<sub>x</sub>), which is constructed according to the bulk structure. It is a reasonable model to represent the brim of relatively big oxide islands on metal surfaces, which was observed in STM. The other is oxide trimer (M<sub>3</sub>O<sub>3x</sub>) to simulate the relatively small particles of oxides. Our first-cycle optimization based on H<sub>2</sub>O dissociation show that the size of oxides matters (Figure 6). The most significant difference is observed for Mo oxide/Cu(111). Although Mo:O ratio is same in both case, the chain is able to break O-H bond with no barrier, while the trimer does not adsorb H<sub>2</sub>O molecule at all. In addition, the stable MgO in such small size and a unique hexagonal conformation can be further oxidized, which facilitate the O-H bond cleavage. However, we also notice that some data points for the catalysts with facile H<sub>2</sub>O dissociation are not in range of the previously determined red line (Figure 5), but in the extrapolated dash line region. As indicated previously, the estimated WGS activity may not be valid. Therefore, currently we move to the second-cycle optimization based on the CO reaction of the catalysts, which are active towards H<sub>2</sub>O dissociation.

Overall, our systematic study using combined in-situ measurements of real catalysts with experimental and theoretical studies on well-defined model systems takes advantage of unique capabilities for in-situ studies in the BNL catalysis programs and at BNL facilities. Our approach allows more insight into the active sites and reaction mechanism for the WGS on promising metal-oxide catalysts.

## Publications Acknowledging this Grant in 2011-2014

### 2011

1. Senanayake, S.D.; Evans, J.; Agnoli, S.; Barrio, L.; Chen, T.-L.; Hrbek J.; Rodriguez, J.A. Water-Gas Shift and CO Methanation Reactions over Ni-CeO<sub>2</sub>(111) Catalysts, *Topics in Catal.* **2011**, *54*, 34-41.
2. Ciston, J.; Si, R.; Rodriguez, J.A.; Hanson, J.C.; Martínez-Arias, A.; Fernandez-García, M.; Zhu, Y. Morphological and Structural Changes during the Reduction and Reoxidation of CuO/CeO<sub>2</sub> and Ce<sub>1-x</sub>Cu<sub>x</sub>O<sub>2</sub> Nanocatalysts: In-situ Studies with Environmental TEM, XRD and XAS, *J. Phys. Chem. C*, **2011**, *115*, 13851-13859.
3. Rodriguez, J.A. Gold-based Catalysts for the Water-gas Shift Reaction: Active Sites and Reaction Mechanism, *Catal. Today*, **2011**, *160*, 3-10.

### 2012

4. Barrio, L.; Zhou, G.; González, I. D.; Estrella, M.; Hanson, J.; Rodriguez, J. A.; Navarro R. M.; Fierro J. L. G. In situ characterization of Pt catalysts supported on ceria modified TiO<sub>2</sub> for the WGS reaction: influence of ceria loading on catalytic behavior, *Phys. Chem. Chem. Phys.*, **2012**, *14*, 2192-2202.
5. Senanayake, S. D.; Sadowski, J.; Evans, J.; Kundu, S.; Agnoli, S.; Yang, F.; Stacchiola, D.; Flege, J.I.; Hrbek, J.; Rodriguez, J.A. Nanopatterning in CeO<sub>x</sub>/Cu(111): A New Mechanism for Surface Reconstruction and Enhancement of Catalytic Activity, *J. Phys. Chem. Lett.*, **2012**, *3*, 839-843.
6. Vidal, A.B.; Liu, P. Density Functional Study of Water-gas Shift Reaction on M<sub>3</sub>O(3x)/Cu(111), *Phys. Chem. Chem. Phys.* **2012**, *14*, 16626-16632.
7. Bruix, A.; Rodriguez, J.A.; Ramirez, P.J.; Senanayake, S.D.; Evans, J.; Park, J.B.; Stacchiola, D.; Liu, P.; Hrbek, J.; Illas, F. A New Type of Strong Metal-

- Support Interaction and the Production of H<sub>2</sub> through the Transformation of Water on Pt/CeO<sub>2</sub>(111) and Pt/CeO<sub>x</sub>/TiO<sub>2</sub>(110) Catalysts, *J. Am. Chem. Soc.* **2012**, *134*, 8968-8974.
8. Xu, W.; Si, R.; Senanayake, S. D.; Llorca, J.; Idriss, H.; Stacchiola, D.; Hanson, J. C.; Rodriguez, J.A. In situ Studies of CeO<sub>2</sub>-supported Pt, Ru, and Pt–Ru Alloy Catalysts for the Water–gas Shift Reaction: Active Phases and Reaction Intermediates, *J. Catal.* **2012**, *291*, 117-126.
  9. Kubacka, A.; Si, R.; Michorczyk, P.; Martínez-Arias, A.; Xu, W.; Hanson, J. C.; Rodriguez, J. A.; Fernández-García, M. Tungsten as an Interface Agent Leading to Highly Active and Stable Cu-Ce Water Gas Shift Catalyst, *Applied Catal. B: Environmental*, **2012**, *132/133*, 423-432.
  10. Si, R.; Tao, J.; Evans, J.; Park, J. B.; Barrio, L.; Hanson, J. C.; Zhu, Y.; Hrbek J.; Rodriguez, J.A. Effect of Ceria on Gold-Titania Catalysts for the Water-Gas Shift Reaction: Fundamental Studies for Au/CeO<sub>x</sub>/TiO<sub>2</sub>(110) and Au/CeO<sub>x</sub>/TiO<sub>2</sub> Powders, *J. Phys. Chem. C*, **2012**, *116*, 23547-23555.
  11. Rodriguez, J.A. Supported Gold in CO Oxidation, the Water-gas Shift, and DeSO<sub>x</sub> Reactions, book chapter for *Supported Metals in Catalysis*, 2<sup>nd</sup> Edition (Editors: James Anderson and Marcos Fernandez-Garcia), Imperial College Press, London, 2012 (**invited book chapter**).

## **2013**

12. Ramírez Reina, T.; Xu, W.; Ivanova, S.; Centeno, M. A.; Hanson, J.; Rodriguez, J. A.; Odriozola, J. A. Operando Characterization of Iron-promoted Ceria-alumina Gold Catalysts during the Water-gas Shift Reaction, *Catal. Today*, **2013**, *205*, 41- 48.
13. Rodriguez, J.A.; Hanson, J. C.; Stacchiola D.; Senanayake S., In-situ/Operando Studies for the Production of Hydrogen through the Water-Gas

- Shift on Metal Oxide/Catalysts, *Phys. Chem. Chem. Phys.* **2013**, *15*, 12004-12025 (**invited**).
14. Mudiyansele, K.; Senanayake, S. D.; Ferial, L.; Kundu, S.; Baber, A. E.; Graciani, J.; Vidal, A. B.; Agnoli, S.; Evans, J.; Chang, R.; Axnanda, S.; Liu, Z.; Sanz, J. F.; Liu, P.; Rodriguez, J. A.; Stacchiola D. J. Importance of the Metal–Oxide Interface in Catalysis: In Situ Studies of the Water–Gas Shift Reaction by Ambient-Pressure X-ray Photoelectron Spectroscopy, *Angew. Chem. Intl. Ed.* **2013**, *52*, 5101-5105.
  15. Johnston-Peck, A.C.; Senanayake, S. D.; Plata, J. J.; Kundu, S.; Xu, W.; Barrio, L.; Graciani, J.; Fdez. Sanz, J.; Navarro, R. M.; Fierro, J.L.G.; Stach, E. A.; Rodriguez, J. A., Nature of the mixed-oxide interface in Ceria–Titania catalysts: clusters, chains, and nanoparticles, *J. Phys. Chem. C*, **2013**, *117*, 14463-14471.
  16. Senanayake, S.D.; Rodriguez J.A.; Stacchiola, D. Electronic Metal–Support interactions and the production of hydrogen through the Water-Gas Shift reaction and ethanol steam reforming: fundamental studies with well-defined model catalysts, *Top. Catal.* **2013**, *56*, 1488-1498.
  17. Senanayake, S.D.; Stacchiola, D.; Rodriguez, J. A. Unique Properties of Ceria Nanoparticles Supported on Metals: Novel Inverse Ceria/Copper catalysts for CO Oxidation and the Water-Gas Shift Reaction, *Acc. Chem. Res.*, **2013**, *46*, 1702–1711 (**invited**).
  18. Mudiyansele, K.; Kim, H-Y.; Senanayake, S.D.; Baber, A.E.; Liu, P.; Stacchiola, D. Probing adsorption sites for CO on ceria, *Phys. Chem. Chem. Phys.*, **2013**, *15*, 15856-15862.
  19. Liu, P. Synergistic Effect of metal/oxide catalysts in the water-gas shift reactions: a theory-guided rational design of better catalysts” in *New and Future Developments in Catalysis: Hybrid Materials, Composites, and Organocatalysts*, 1st Edition, S. Suib (Ed.), Elsevier (2013) 213-241132 (**invited book chapter**).

## **2014**

20. Rodriguez, J. A.; Senanayake, S. D.; Stacchiola, D.; Liu, P.; Hrbek, J. The Activation of Gold and the Water-Gas Shift Reaction: Insights from Studies with Model Catalysts, *Acc. Chem. Res.*, **2014**, *47*, 773–782 (**invited**).
21. Zhao, F.; Liu, Z.; Xu, W.; Yao, S.; Kubacka, A.; Johnston-Peck, A. C.; Senanayake, S. D.; Zhang, A.-Q.; Stach, E.A.; Fernández-García, M.; Rodriguez, J.A. Water Gas Shift Reaction on Ni-W-Ce Catalysts: Catalytic Activity and Structural Characterization, *J. Phys. Chem. C*, **2014**, doi 10.1021/jp410790z.

**Tobin J. Marks**

**Supported Organometallic Complexes: Surface Chemistry, Spectroscopy, Catalysis and Homogeneous Models**

**Presentation Abstract (Poster)**

Tobin J. Marks

Department of Chemistry and the Center for Catalysis and Surface Science, Northwestern University, Evanston IL 60208-3113

This presentation outlines efforts to model, understand at a fundamental level, expand, and exploit the unique pathways by which organometallic molecules of varying nuclearity undergo chemisorptive activation and catalytic activity enhancement on solid surfaces. These processes connect to real-world, large-scale industrial hydrocarbon processes and to manufacturing cleaner, greener, more environmentally acceptable products, including those from sustainable resources. The research effort combines catalyst synthesis, surface chemistry and spectroscopy, homogeneous analogue catalysis, structural analysis, and computation, and involves collaboration with US national laboratories and industry. Advances in the past year include: 1) Investigating mononuclear and binuclear organometallic chemisorption on “super Brønsted acid” oxides, and the polymerization and hydrogenation catalytic properties of these unusual species, 2) Synthesizing and characterizing mononuclear and polynuclear catalyst precursors for the above chemisorption and comparing the results to homogeneous catalytic properties in solution, 3) Computationally modeling both the chemisorbed catalysts and their reactivity/selectivity modalities, 4) Employing this information to design and catalytically produce new types of efficient, nanocomposite energy storage materials.

**DE-FG02-86ER13511: Supported Organometallic Complexes: Surface Chemistry, Spectroscopy, Catalysis and Homogeneous Models**

**PI:** Tobin J. Marks  
**Postdoc:** Maximilliano Delferro, Shaofeng Liu, Weixing Gu  
**Graduate students:** Madelyn Staltzer  
**Affiliations:** Department of Chemistry and the Center for Catalysis and Surface Science, Northwestern University, Evanston IL 60208-3113  
[t-marks@northwestern.edu](mailto:t-marks@northwestern.edu) <http://chemgroups.northwestern.edu/marks/>  
**Collaborators:** Mark Ratner (Northwestern U.), Ignazio Fragala, Alessandro Motta (U. Catania, Italy), Alceo Macchioni, Cristiano Zuccaccia (U. Perugia, Italy), Jeffery Miller, Chris Marshall (Argonne Nat. Lab.), Michael Lanagan (Pennsylvania State U.), Peter Nickias (Dow Chemical Co.), Christopher Nicholas, Jeffery Bricker (UOP Honeywell).

**Recent Progress**

The program consists of three complementary, interlinked and synergistic efforts: 1) Metal Hydrocarbyl Chemisorption on Brønsted “Super Acid” Surfaces to Produce Single-Site Heterogeneous Catalysts, 2) Catalyst Nuclearity Effects on Homogeneous and Heterogeneous Catalysis, 3) Heterogeneous Catalytic Synthesis of Energy Storage Materials. The catalytic transformations

of interest here involve modification of small hydrocarbon molecules, including polymerization and hydrogenation, asking how and why the environment of molecule-based catalysts (e.g., support, presence of other metal centers) can so profoundly alter activity and selectivity, and how these fundamental phenomena can be used to produce unusual functional materials.

*Metal Hydrocarbyl Chemisorption on Sulfated Metal Oxide Surfaces.* Electrophilic Zr surface alkyls are created in high coverages by protonolytic chemisorption of group 4 alkyls, and these species exhibit extreme activity and selectivity for arene and olefin hydrogenation as well as for olefin polymerization--benzene hydrogenation rates exceed those of Pt metal catalysts. The kinetics and mechanism were characterized, revealing that almost 100% of the surface Zr species are catalytically significant--unusual for any heterogeneous catalyst. Density functional theory (DFT) was used to study the sulfated  $\gamma$ -alumina (AlS) surface as well as the pathway for  $\text{Cp}_2\text{Zr}(\text{CH}_3)_2$  (**2**;  $\text{Cp} = \eta^5\text{-C}_5\text{H}_5$ ) chemisorption. Using the most stable configuration of the sulfated surface, it is found that Zr-CH<sub>3</sub> protonolysis yields cationic species which interact with the surface sulfate species to form electrostatically anchored cations. Computed changes in sulfate vibrational spectra on zirconocene chemisorption are in good agreement with experiment. Furthermore, Zr K-edge XAFS and XANES characterization of  $\text{Cp}_2\text{ZrH}_2$  (**1**), **2**,  $\text{Cp}^*\text{ZrH}_2$  (**3**) ( $\text{Cp}^* = \eta^5\text{-(CH}_3)_5\text{C}_5$ ) and  $\text{Cp}'\text{ZrMe}_3$  (**4**) and as well as their AlS-supported product catalysts **1**/AlS, **3**/AlS and **4**/AlS are used to elucidate the metrical nature of the Zr...AlS interaction, complemented by high-resolution solid state NMR. The XAFS data yield key structural information: the supported cationic organozirconium catalysts have electrostatic interactions with the surface sulfate O atoms at average (long) Zr...O distances of 2.25 - 2.36 Å, in good agreement with the DFT results. EXAFS analysis of benzene dosing experiments with **4**/AlS reveals that benzene is captured by essentially all of the Zr centers and is bound in an  $\eta^6$  fashion, with an average Zr-C bond distance of 2.27 Å. These results are in excellent agreement with the computational and catalytic mechanistic results.

*Metal Nuclearity Effects on the Homogeneous/Heterogeneous Catalytic Interface.* The hetero-bimetallic complexes,  $(\eta^5\text{-indenyl})[1\text{-Me}_2\text{Si}(\text{tBuN})\text{TiCl}_2]\text{-3-C}_n\text{H}_{2n}\text{-}[N,N\text{-bis}(2\text{-(ethylthio)ethyl})\text{-amine}]\text{CrCl}_3$  ( $n = 0$ , **Ti-C<sub>0</sub>-Cr<sup>SNS</sup>**;  $n = 2$ , **Ti-C<sub>2</sub>-Cr<sup>SNS</sup>**;  $n = 6$ , **Ti-C<sub>6</sub>-Cr<sup>SNS</sup>**),  $(\eta^5\text{-indenyl})[1\text{-Me}_2\text{Si}(\text{tBuN})\text{TiCl}_2]\text{-3-C}_2\text{H}_4\text{-}[N,N\text{-bis}((o\text{-OMe-C}_6\text{H}_4)_2\text{P})\text{amine}]\text{CrCl}_3$  (**Ti-C<sub>2</sub>-Cr<sup>PNP</sup>**), and  $(\eta^5\text{-indenyl})[1\text{-Me}_2\text{Si}(\text{tBuN})\text{TiCl}_2]\text{-3-C}_2\text{H}_4\text{-}[N,N\text{-bis}((\text{diethylamine})\text{ethyl})\text{-amine}]\text{CrCl}_3$  (**Ti-C<sub>2</sub>-Cr<sup>NNN</sup>**), were synthesized, fully characterized, and employed as olefin polymerization catalysts. With ethylene as the feed and MAO as cocatalyst/activator, SNS-based complexes **Ti-C<sub>0</sub>-Cr<sup>SNS</sup>**, **Ti-C<sub>2</sub>-Cr<sup>SNS</sup>** and **Ti-C<sub>6</sub>-Cr<sup>SNS</sup>** afford linear low-density polyethylenes (LLDPEs) with exclusive *n*-butyl branches (6.8 – 25.8 branches/1000C), while under identical polymerization conditions **Ti-C<sub>2</sub>-Cr<sup>PNP</sup>** and **Ti-C<sub>2</sub>-Cr<sup>NNN</sup>** produce polyethylenes with heterogeneous branching (C<sub>2</sub>, C<sub>4</sub>, and C<sub>>6</sub>) or negligible branching, respectively. Under identical ethylene polymerization conditions, **Ti-C<sub>0</sub>-Cr<sup>SNS</sup>** produces polyethylenes with higher activity (4.5x and 6.1x, respectively), M<sub>w</sub> (1.3x and 1.8x, respectively), and branch density (1.4x and 3.8x, respectively), than **Ti-C<sub>2</sub>-Cr<sup>SNS</sup>** and **Ti-C<sub>6</sub>-Cr<sup>SNS</sup>**. Versus a CGC<sup>Et</sup>Ti + SNSCr tandem catalyst, **Ti-C<sub>0</sub>-Cr<sup>SNS</sup>** yields polyethylene with lower activity, but with 22.6x higher M<sub>w</sub>, and 4.0x greater branching density under identical conditions. In the ethylene + 1-pentene competition experiments, **Ti-C<sub>0</sub>-Cr<sup>SNS</sup>** yields *n*-propyl branches as low as 5.5% of the total, predominantly *n*-butyl branches, while the tandem CGC<sup>Et</sup>Ti + SNSCr tandem yields 91.0% *n*-propyl branches. The homopolymerization and 1-pentene competition results argue that Ti...Cr spatial proximity, as also supported by DFT computation, significantly influences relative 1-hexene enchainment and chain transfer rates and that such proximity effects are conversion insensitive but are cocatalyst and solvent sensitive.

### Heterogeneous Catalytic Synthesis and Characterization of New Energy Storage Materials.

Low-cost materials combining the processability and mechanical properties of inexpensive polymers with the high dielectric constants of ferroelectric oxides are highly desirable for energy storage as in large-scale capacitors. In this work we find that chemisorption of the activated metallocene propylene polymerization catalyst derived from [*rac*-ethylenebisindenyl]zirconium dichloride (EBIZrCl<sub>2</sub>) on the native Al<sub>2</sub>O<sub>3</sub> surfaces of metallic aluminum nanoparticles, followed by exposure to polypropylene, affords 0–3 metal-isotactic polypropylene nanocomposites. The microstructures of these nanocomposites were characterized by XRD (X-ray diffraction), TEM (transmission electron microscopy), SEM (scanning electron microscopy), and AFM (atomic force microscopy). Electrical measurements show that increasing concentrations of the filler nanoparticles increases the effective permittivity of the nanocomposites to  $\epsilon_r$  values as high as 15.4. Because of the high contrast in the complex permittivities and conductivities between the metallic aluminum nanoparticles and the polymeric polypropylene matrix, these composites obey the percolation law for two-phase composites, reaching maximum permittivities just before the percolation threshold volume fraction,  $v_f < 0.16$ . These Al-polypropylene nanocomposites perform well as pulse-power capacitor materials, with leakage current densities of  $\sim 10^{-7} - 10^{-9}$  A/cm<sup>2</sup> at an applied field of 10<sup>5</sup> V/cm, low dielectric loss in the 100 Hz – 1 MHz frequency range, and a remarkable recoverable energy storage as high as 14.4 J/cm<sup>3</sup>.

### **Publications (2011-2014)**

1. Delferro, M.; Marks, T.J. Multinuclear Olefin Polymerization Catalysis: Structure, Function, and Cooperativity, *Chem. Rev.* **2011**, *111*, 2450–2485.
2. Williams, L.A.; Marks, T.J. Synthesis, Characterization, and Heterogeneous Catalytic Implementation of Sulfated Alumina Nanoparticles. Arene Hydrogenation and Olefin Polymerization Properties of Supported Organo-Group 4 Complexes, *ACS Catalysis*, **2011**, *1*, 238–245.
3. Weberski, M.P.; Chen, C.; Delferro, M.; Marks, T.J. Catalyst Center-Catalyst Center Cooperativity and Deactivation Mechanisms in Bimetallic Nickel(II) Phenoxyiminato-Based Ethylene Polymerization Catalysts, *Chem. Euro. J.* **2012**, *18*, 10715 - 10732.
4. Weberski, M.P.; Chen, C.; Delferro, M.; Zuccaccia, C.; Macchioni, A.; Marks, T.J. Suppression of  $\beta$ -H Chain Transfer in Ni(II) Catalyzed Ethylene Polymerization via Weak Secondary Ligand Interactions, *Organometallics*, **2012**, *31*, 3773–3789.
5. Fredin, L.A.; Li, Z.; Lanagan, M.T.; Ratner, M.A.; Marks, T.J. Enhancing Energy Storage and Suppressing Dielectric Loss in Oxide Core-Shell-Polyolefin Nanocomposites by Decreasing Internal Surface Area and Increasing Shell Thickness, *Advan. Mater.* **2012**, *24*, 5946–5953.
6. Fredin, L.A.; Li, Z.; Lanagan, M.T.; Ratner, M.A.; Marks, T.J. Substantial Recoverable Energy Storage in Percolative Metallic Aluminum-Polypropylene Nanocomposites, *Advan. Funct. Mater.*, **2013**, *23*, 3560–3569.
7. Williams, L.A.; Guo, N.; Motta, A.; Delferro, M.; Fragala, I.L.; Miller, J.T.; Marks, T.J. Surface Structural-Chemical Characterization of a Single-Site d<sup>0</sup> Heterogeneous Arene Hydrogenation Catalyst Having 100% Active Sites, *Proc. Nat. Acad. Sci.*, **2013**, *110*, 413–418.
8. Fredin, L.A.; Li, Z.; Ratner, M.A.; Marks, T.J.; Lanagan, M.T. Metallic Aluminum-Polypropylene Nanocomposites with Sustainable High Capacitance at High Frequencies, *ACS Nano*, **2013**, *7*, 396–407.
9. Liu, S.; Motta, A.; Delferro, M.; Marks, T.J. Synthesis, Characterization, and Heterobimetallic Cooperation in Titanium-Chromium Catalyst for Highly Branched Polyethylenes, *J. Am. Chem. Soc.*, **2013**, *135*, 8830–8833.
10. Stephenson, C.J.; McInnis, J.P.; Chen, C.; Weberski Jr., M.P.; Motta, A.; Delferro, M.; Marks, T.J. Ni(II) Phenoxyiminato Olefin Polymerization Catalysis: Striking Coordinative Modulation of Hyperbranched Polymer Microstructure and Stability by a Proximate Sulfonyl Group, *ACS Catalysis*,

**2014**, 4, 999-1004.

11. Gu, W.; Delferro, M.; Motta, A.; Miller, J.T. Marks, Nicholas, C.P. T.J. Molecule-Based Heterogeneous Catalysts for Selective Arene Hydrogenation. Scope, Ligand Structure Effects, and Mechanism, **2014**, submitted for publication.

12. Fredin, L.A.; Ratner, M.A.; Marks, Lanagan, M.T.; T.J. Using Single-Site Heterogeneous Olefin Polymerization Catalysts for the Synthesis of High-Capacity Energy Storage Materials, **2014**, submitted for publication.

13. Liu, S.; Motta, A.; Mouat, A.R.; Delferro, M.; Marks, T.J.; Remarkable Cooperative Effects in Heterobimetallic Titanium-Chromium Catalysts for Ethylene Polymerization/Copolymerization, **2014**, submitted for publication.

14. McInnis, J.P.; Delferro, M.; Marks, T.J.; Multinuclear Catalysis: Olefin Polymerization Pathways Modified by Strong Cooperative Effects, **2014**, submitted for publication.

15. Bachrach, M.; Morlanes-Sanchez, N.; Canlas, C.P.; Miller, J.T.; Marks, T.J.; Notestein, J.; Highly Dispersed  $\text{TiO}_x\text{-Al}_2\text{O}_3$ ,  $\text{TaO}_x\text{-Al}_2\text{O}_3$ , and  $\text{MoO}_x\text{-Al}_2\text{O}_3$  Materials: Unexpected Reactivity in Heterocycle Hydrogenation and C-N Bond Cleavage, **2014**, submitted for publication.

## Organometallic Reactivity of Paramagnetic Late Transition Metal Complexes

Liviu M. Mirica

Washington University in St. Louis, Department of Chemistry

### Presentation Abstract

The long term goal of this project is to develop novel transition metal catalysts by combining successful approaches from organometallic chemistry for the functionalization of unactivated organic molecules with strategies from bioinorganic chemistry for the activation of small molecules (e.g., O<sub>2</sub> and CO<sub>2</sub>). We have recently investigated energy-related chemical transformations such as the aerobically induced C-C and C-heteroatom bond formation reactions relevant to the oxidative oligomerization of methane and hydrocarbon functionalization reactions. Current studies are focused on Pd complexes – given their extensive use in catalysis, and future studies will include Rh and Ir systems. These investigations take advantage of our ability to judiciously design ligands that tune the electronic properties and catalytic reactivity of metal ions in various oxidation states. We are also distinctively equipped to study the electronic properties and reactivity of both paramagnetic and diamagnetic systems through an extensive series of spectroscopic, mechanistic, and computational approaches.

The targeted energy-related chemical transformations would allow for a more efficient use of natural gas reserves as an inexpensive energy resource and thus should have a major impact on our society and the environment. In addition, the development of novel catalytic systems for efficient C-H functionalization reactions has far-reaching energy-related implications, in line with the mission of the *Basic Energy Sciences – Catalysis Science Program* of the Department of Energy.

### Grant Number DE-FG02-11ER16254

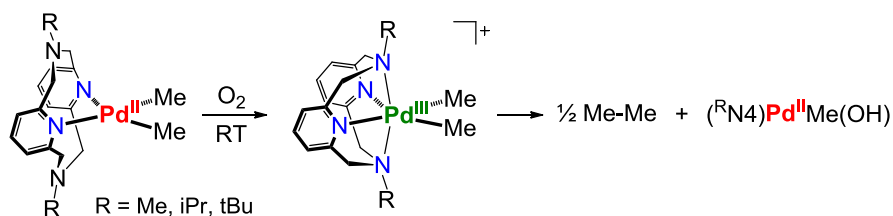
### Novel Palladium Catalysts for the Oxidative Oligomerization of Methane & Carbon Dioxide Reduction

Postdocs: Julia Khusnutdinova, Bo Zheng  
Students: Fengzhi Tang, Fengrui Qu, Jia Luo, Jason Schultz, Kei Fuchigami  
Collaborators: Nicolai Lehnert (Univ. of Michigan), Jeffrey T. Miller (Argonne National Lab)  
Contacts: Liviu M. Mirica, Washington University, Dept. of Chemistry, CB 1134, 1 Brookings Drive, St. Louis, MO 63130; Tel. 314-935-3464; mirica@wustl.edu

### RECENT PROGRESS

*Aerobically-induced C-C bond formation from organometallic Pd<sup>II</sup> complexes.* In 2010 we have employed the flexible tetradentate ligand <sup>t</sup>BuN4 (N,N'-di-*tert*-butyl-2,11-diaza[3.3](2,6)pyridinophane) to stabilize the first mononuclear organometallic Pd<sup>III</sup> complexes and we have investigated their C-C and C-heteroatom bond formation reactivity. We have also reported that (<sup>t</sup>BuN4)Pd<sup>II</sup>Me<sub>2</sub> undergoes facile aerobic oxidation to generate the Pd<sup>III</sup> species [(<sup>t</sup>BuN4)Pd<sup>III</sup>Me<sub>2</sub>]<sup>+</sup>, followed by formation of ethane and the monomethyl complex

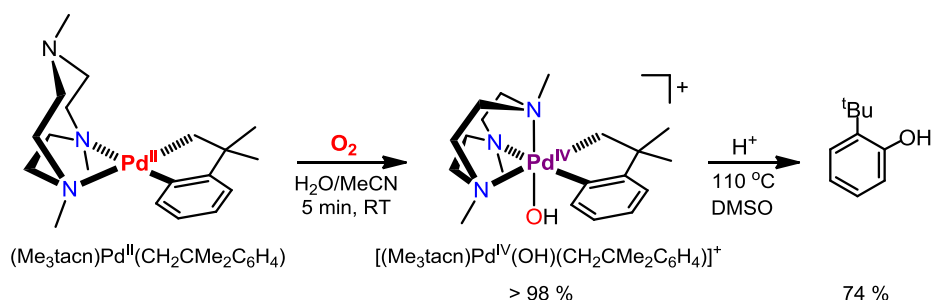
(<sup>t</sup>BuN<sub>4</sub>)Pd<sup>II</sup>Me(OH) (Scheme 1). Continuing our study of high-valent Pd chemistry, we have employed the N-methyl (<sup>Me</sup>N<sub>4</sub>) and N-isopropyl (<sup>iPr</sup>N<sub>4</sub>) substituted N<sub>4</sub> ligands, which lead to the isolation and characterization of mononuclear Pd<sup>III</sup> and Pd<sup>IV</sup> complexes and allowed a direct structural and reactivity comparison. Detailed mechanistic studies suggest an inner-sphere mechanism for the (<sup>R</sup>N<sub>4</sub>)Pd<sup>II</sup>Me<sub>2</sub> oxidation by O<sub>2</sub> to generate a Pd<sup>III</sup>-superoxide intermediate, *implying that one-electron oxidation and formation of a Pd<sup>III</sup> center is a pre-requisite for the aerobic oxidation of Pd<sup>II</sup> complexes*. Subsequent protonation of the Pd<sup>III</sup>-superoxide intermediate generates detectable Pd<sup>IV</sup>-hydroperoxo and Pd<sup>IV</sup>-hydroxo intermediates, similar to Pt systems, and comproportionation in the presence of the Pd<sup>II</sup>Me<sub>2</sub> precursor yields the Pd<sup>III</sup>Me<sub>2</sub> complex. Experimental results are consistent with a non-radical mechanism that involves Me group transfer and formation of the [(<sup>R</sup>N<sub>4</sub>)Pd<sup>IV</sup>Me<sub>3</sub>]<sup>+</sup> species as the key intermediate responsible for ethane elimination. Overall, this study represented one of the first examples of C-C bond formation upon aerobic oxidation of a Pd<sup>II</sup> dimethyl complex, with implications in the development of Pd catalysts for aerobic oxidative coupling of C-H bonds.



**Scheme 1.** Aerobic oxidative C-C bond formation reactivity of (<sup>R</sup>N<sub>4</sub>)Pd<sup>II</sup>Me<sub>2</sub> complexes.

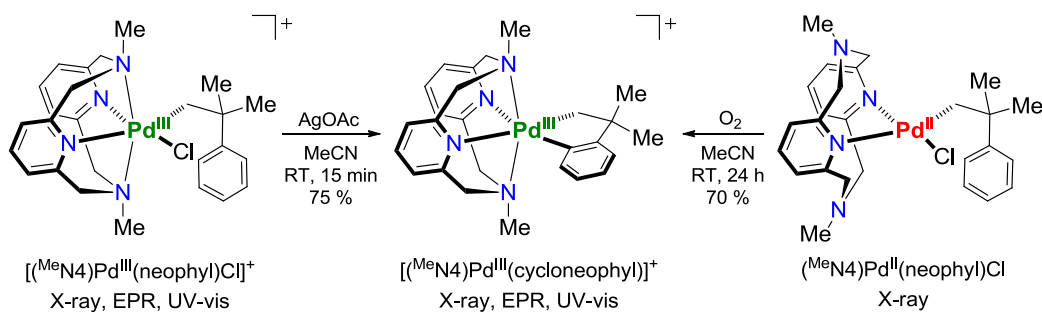
Formation of isolable Pd<sup>V</sup> complexes by aerobic oxidation of Pd<sup>II</sup> precursors and subsequent selective C-C or C-O bond formation. In addition to the studies using tetradentate <sup>R</sup>N<sub>4</sub> ligands, we have shown that the tridentate ligand N,N',N''-trimethyltriazacyclononane (Me<sub>3</sub>tacn) can stabilize both dinuclear Pd<sup>III</sup> and mononuclear Pd<sup>IV</sup> complexes upon sequential one-electron oxidations of mononuclear Pd<sup>II</sup> precursors. We have also reported that the dimethyl Pd<sup>II</sup> complex (Me<sub>3</sub>tacn)Pd<sup>II</sup>Me<sub>2</sub> undergoes facile aerobic oxidation to yield the stable [(Me<sub>3</sub>tacn)Pd<sup>IV</sup>Me<sub>3</sub>]<sup>+</sup> species, which eliminates ethane at elevated temperatures.

In addition, we have recently shown that the palladacycle complex (Me<sub>3</sub>tacn)Pd<sup>II</sup>(CH<sub>2</sub>CMe<sub>2</sub>C<sub>6</sub>H<sub>4</sub>) – or (Me<sub>3</sub>tacn)Pd<sup>II</sup>(cycloneophyl), undergoes rapid oxidation with O<sub>2</sub> or H<sub>2</sub>O<sub>2</sub> to directly generate the isolable complex [(Me<sub>3</sub>tacn)Pd<sup>IV</sup>(OH)(CH<sub>2</sub>CMe<sub>2</sub>C<sub>6</sub>H<sub>4</sub>)]<sup>+</sup> without the need for alkyl group transfer (Scheme 2). Interestingly, thermolysis of the organometallic Pd<sup>IV</sup>-OH complex leads to selective C(sp<sup>2</sup>)-O vs. C(sp<sup>3</sup>)-O bond formation and formation of 2-tert-butylphenol. This represents a rare example of a selective C<sub>aryl</sub>-O reductive elimination from a Pd<sup>IV</sup>-OH complex that is formed via aerobic oxidation of a Pd<sup>II</sup> precursor and thus is relevant to Pd-catalyzed aerobic hydroxylation reactions. Additional reactivity studies suggest that the tridentate ligand Me<sub>3</sub>tacn employed herein leads to selective C(sp<sup>2</sup>)-O bond formation, while no C-halide bond formation was observed for the analogous Pd<sup>IV</sup>-halide complexes, suggesting that ligand denticity can be used to control the selectivity of these high-valent Pd complexes in various C-heteroatom bond formation reactions.



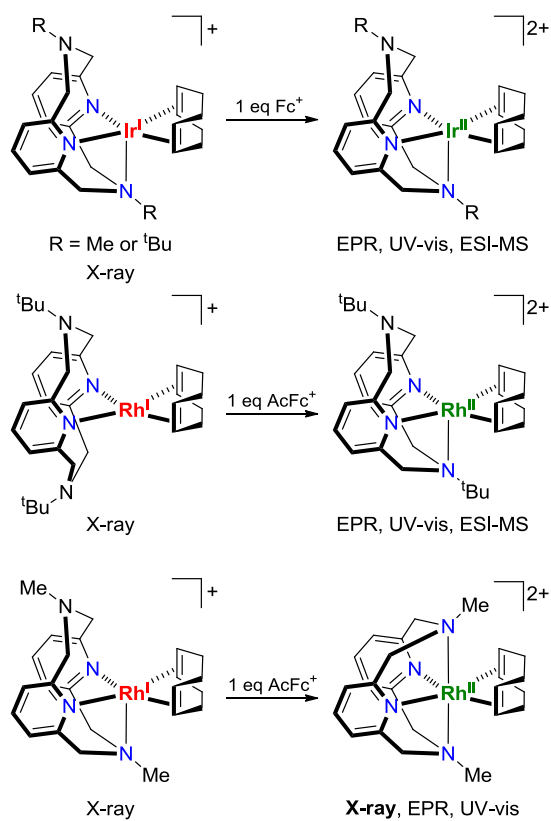
**Scheme 2.** Aerobic reactivity of the  $(\text{Me}_3\text{tacn})\text{Pd}^{\text{II}}$  complex and subsequent  $\text{C}_{\text{aryl}}\text{-O}$  bond formation.

**C-H bond activation at a  $\text{Pd}^{\text{III}}$  center.** The activation of strong C-H bonds is the key step required for achieving the long term goal of methane oligomerization and/or functionalization. In this regard, we began investigating whether C-H activation can occur at high-valent Pd centers, with possibly different chemo- and regioselectivity than the C-H activation at  $\text{Pd}^{\text{II}}$  centers. Recently, C-H bond activation at  $\text{Pd}^{\text{IV}}$  centers has been proposed in several systems and unambiguously shown to occur in two related cases by Sanford et al. By comparison, no C-H activation has ever been observed at a  $\text{Pd}^{\text{III}}$  center, likely due to the dearth of isolated or well-characterized  $\text{Pd}^{\text{III}}$  complexes. In this context, we first evaluated the ability of a  $(^{\text{Me}}\text{N}4)\text{Pd}^{\text{III}}$  complex to undergo intramolecular C-H activation by using an alkyl ligand that contains a tethered phenyl ring (i.e., a neophyl group, Scheme 3). Interestingly, the isolated  $[(^{\text{Me}}\text{N}4)\text{Pd}^{\text{III}}(\text{neophyl})\text{Cl}]^+$  complex reacts with 1 equiv  $\text{AgOAc}$  in MeCN at RT to yield the C-H activated product  $[(^{\text{Me}}\text{N}4)\text{Pd}^{\text{III}}(\text{cycloneophyl})]^+$  in 75 % yield in 15 min, as confirmed by UV-Vis, EPR, and X-ray characterization. Additional experiments suggest that  $\text{Ag}^+$  is needed to remove the  $\text{Cl}^-$  ligand and open a coordination site at the Pd center, while the acetate anion likely assists the C-H cleavage by acting as an intramolecular base. By comparison, the  $(^{\text{Me}}\text{N}4)\text{Pd}^{\text{II}}(\text{neophyl})\text{Cl}$  precursor reacts much slower under the same reaction conditions to yield the corresponding cyclopalladated  $\text{Pd}^{\text{II}}$  product, while the  $\text{Pd}^{\text{IV}}$  analog  $[(^{\text{Me}}\text{N}4)\text{Pd}^{\text{IV}}(\text{neophyl})\text{Cl}]^{2+}$  does not undergo C-H activation. Most exciting is the observation of aerobic oxidatively-induced C-H activation of  $(^{\text{Me}}\text{N}4)\text{Pd}^{\text{II}}(\text{neophyl})\text{Cl}$  to generate the  $\text{Pd}^{\text{III}}$  species  $[(^{\text{Me}}\text{N}4)\text{Pd}^{\text{III}}(\text{neophyl})\text{Cl}]^+$  (Scheme 3). This provides evidence that mono-alkyl  $\text{Pd}^{\text{II}}$  complexes supported by  $^{\text{Me}}\text{N}4$  can be oxidized aerobically – an important requirement for aerobic C-H functionalization. In addition, these preliminary results demonstrate the viability of C-H activation at a  $\text{Pd}^{\text{III}}$  center and suggest that such step could be incorporated into a catalytic cycle for aerobic oxidative coupling of C-H bonds.



**Scheme 3.** Unprecedented C-H activation at a  $\text{Pd}^{\text{III}}$  center.

*Synthesis and characterization of (<sup>R</sup>N<sub>4</sub>)Rh<sup>II</sup> and Ir<sup>II</sup> complexes.* There are a large number of examples of Rh<sup>I/III</sup> and Ir<sup>I/III</sup> systems that can activate strong C-H bonds, including those in alkanes and methane, as well as promote C-C and C-heteroatom bond formation reactions. Given our long term interest in the oxidative oligomerization of methane, we began exploring the redox reactivity of analogous (<sup>R</sup>N<sub>4</sub>)Rh and (<sup>R</sup>N<sub>4</sub>)Ir complexes, including the paramagnetic Rh<sup>II</sup> and Ir<sup>II</sup> oxidation states. Both <sup>t</sup>BuN<sub>4</sub> and <sup>Me</sup>N<sub>4</sub> ligands were employed to generate (<sup>R</sup>N<sub>4</sub>)Rh<sup>I</sup> and Ir<sup>I</sup> precursors that were crystallographically characterized and shown to exhibit square planar as well as less-common square pyramidal geometries (Scheme 4). Interestingly, all these complexes exhibit at least one oxidation wave at accessible potentials (0.0 - 0.3 V vs. Fc) and their chemical oxidation generates both Rh<sup>II</sup> and Ir<sup>II</sup> species that exhibit characteristic anisotropic EPR spectra, suggesting a metal-based radical along with superhyperfine coupling to the axial N donor(s). For example, oxidation of the five-coordinate [<sup>Me</sup>N<sub>4</sub>)Rh<sup>I</sup>(COD)]<sup>+</sup> complex generates the six-coordinate [<sup>Me</sup>N<sub>4</sub>)Rh<sup>II</sup>(COD)]<sup>2+</sup> complex that was crystallographically characterized, and whose EPR confirms the coordination of both axial N donors in solution as well. By comparison, oxidation of the four-coordinate [(<sup>t</sup>BuN<sub>4</sub>)Rh<sup>I</sup>(COD)]<sup>+</sup> complex generates the corresponding [(<sup>t</sup>BuN<sub>4</sub>)Rh<sup>II</sup>(COD)]<sup>2+</sup> complex that is proposed to adopt a five-coordinate geometry based on its EPR spectrum (Scheme 4). Overall, these preliminary results suggest that the <sup>R</sup>N<sub>4</sub> ligands can stabilize paramagnetic Rh<sup>II</sup> and Ir<sup>II</sup> complexes and control their structure and likely their reactivity profiles in a similar fashion to our well-established Pd systems. Thus, we will investigate in detail the oxidative reactivity of these Rh and Ir systems aimed toward the development of catalytic systems for aerobic oxidative C-C coupling of hydrocarbons and C-H functionalization.



**Scheme 4.** Synthesis and characterization of (<sup>R</sup>N<sub>4</sub>)Ir<sup>II</sup> and Rh<sup>II</sup> complexes.

## Relevant Publications

*Publications acknowledging this Grant in 2011-2014:*

13. Qu, F.; Khusnutdinova, J. R.; Rath, N. P.; Mirica, L. M.\* “An Organometallic Pd(IV)-OH Complex Formed upon Aerobic Oxidation of a Pd(II) Precursor and Its C-O Bond Formation Reactivity”, *Chem. Comm.*, **2014**, *50*, 3036-3039.
12. Luo, J.; Rath, N. P.; Mirica, L. M.\* “Oxidative Reactivity of (N<sub>2</sub>S<sub>2</sub>)PdRX Complexes (R = Me, Cl; X = Me, Cl, Br): Involvement of Palladium(III) and Palladium(IV) Intermediate”, *Organometallics*, **2013**, *32*, 3343-3353.
11. Khusnutdinova, J. R.; Luo, J.; Rath, N. P.; Mirica, L. M.\* “Late First Row Transition Metal Complexes of a Tetradentate Pyridinophane Ligand: Electronic Properties and Reactivity Implications”, *Inorg. Chem.*, **2013**, *52*, 3920-3932.
10. Khusnutdinova, J. R.; Mirica, L. M.\* “Organometallic Pd(III) Complexes in C-C and C-Heteroatom Bond Formation Reactions”, invited book chapter in *C-H Activation and Functionalization, Transition Metal Mediation*, Ribas, X., Ed.; Royal Society of Chemistry, 2013.
9. Mirica L. M.,\* Khusnutdinova J. R., “Structure and Electronic Properties of Pd(III) Complexes”, *Coord. Chem. Rev.*, **2013**, *257*, 299-314.
8. Tang, F.; Qu, F.; Khusnutdinova, J. R.; Rath, N. P.; Mirica, L. M.\* “Structural and Reactivity Comparison of Analogous Organometallic Pd(III) and Pd(IV) Complexes”, *Dalton Trans.*, **2012**, *41*, 14046-14050.
7. Tang, F.; Zhang, Y.; Rath, N. P.; Mirica, L. M.\* “Detection of Pd(III) and Pd(IV) Intermediates during the Aerobic Oxidative C-C Bond Formation from a Pd(II) Dimethyl Complex”, *Organometallics*, **2012**, *31*, 6690-6696.
6. Khusnutdinova, J. R.; Qu, F.; Zhang, Y.; Rath, N. P.; Mirica, L. M.\* “Formation of the Pd(IV) Complex [(Me<sub>3</sub>tacn)Pd<sup>IV</sup>Me<sub>3</sub>]<sup>+</sup> through Aerobic Oxidation of (Me<sub>3</sub>tacn)Pd<sup>II</sup>Me<sub>2</sub> (Me<sub>3</sub>tacn = N,N',N''-trimethyl-1,4,7-triazacyclononane)”, *Organometallics*, **2012**, *31*, 4627-4630. Featured on the cover.
5. Khusnutdinova J. R., Rath N. P., Mirica L. M.\* “The Aerobic Oxidation of a Pd(II) Dimethyl Complex Leads to Selective Ethane Elimination from a Pd(III) Intermediate” *J. Am. Chem. Soc.*, **2012**, *134*, 2414-2422.

*Earlier Relevant Publications:*

4. Luo, J., Khusnutdinova J. R., Rath N. P., Mirica L. M.\* “Unsupported d<sup>8</sup>-d<sup>8</sup> interactions in cationic Pd<sup>II</sup> and Pt<sup>II</sup> complexes: Evidence for a significant metal-metal bonding character” *Chem. Comm., Emerging Investigators issue* **2012**, *48*, 1532-1534.
3. Luo, J.; Rath, N. P.; Mirica, L. M.\* “Dinuclear Co(II)Co(III) Mixed-Valence and Co(III)Co(III) Complexes with N- and O- Donor Ligands: Characterization and Water Oxidation Studies”, *Inorg. Chem.*, **2011**, *50*, 6152-6157.
2. Khusnutdinova, J. R.; Rath, N. P.; Mirica, L. M.\* “Dinuclear Pd(III) Complexes with a Single Unsupported Bridging Halide Ligand: Reversible Formation from Mononuclear Pd(II) or Pd(IV) Precursors”, *Angew. Chem. Int. Ed.*, **2011**, *50*, 5532-5536.
1. Khusnutdinova, J. R.; Rath, N. P.; Mirica, L. M.\* “Stable Mononuclear Organometallic Pd(III) Complexes and Their C-C Bond Formation Reactivity”, *J. Am. Chem. Soc.*, **2010**, *132*, 7303-7305. Featured as “News of the Week” in *Chem. & Eng. News*, **2010**, *88*, 21, 9.

**Variations in Reactivity on Different  
Crystallographic Orientations of Cerium Oxide\***

David R. Mullins, De-en Jiang, Ye Xu, Steven H. Overbury,  
Peter M. Albrecht, Tsung-Liang Chen and Florencia Calaza  
Oak Ridge National Laboratory, Chemical Sciences Division

Cerium oxide is a principal component in many heterogeneous catalytic processes. Recent work has demonstrated how the reactivity and selectivity of various molecules are dramatically altered on different crystallographic faces of cerium oxide. The structure and composition of different faces determine the number of coordination vacancies (CV) surrounding surface atoms, the availability of adsorption sites and the spacing between adsorption sites. These properties in turn influence the acid/base character and the reducibility of surface.

To investigate the role of surface orientation on reactivity, CeO<sub>2</sub> films with different orientations were grown by two different methods. CeO<sub>2</sub>(100) films were grown ex situ by pulsed laser deposition on Nb-doped SrTiO<sub>3</sub>(100). CeO<sub>2</sub>(111) films were grown in situ by thermal deposition of Ce metal onto Ru(0001) in an oxygen atmosphere. The chemical reactivity was characterized by the adsorption and decomposition of various molecules such as CO<sub>2</sub>, H<sub>2</sub>O, alcohols, aldehydes and organic acids. In general the CeO<sub>2</sub>(100) surface was found to be more active, i.e. molecules adsorbed more readily and reacted to form new products, especially on a fully oxidized substrate. However the CeO<sub>2</sub>(100) surface was less selective with a greater propensity to produce CO, CO<sub>2</sub> and water as products. This is related to the higher basicity of the more highly under-coordinated O anions on this surface. It is possible to synthesize high surface area shape-selected nanoparticles (octahedra and cubes), i.e. powders that expose a single, well-defined surface. It will therefore be possible transfer the results from model surfaces to real catalysts.

\*This research is part of FWP ERKCC96. For a full description of recent progress see the Abstract submitted by Steven H. Overbury.

C. Buddie Mullins

## **The Effects of Surface Hydroxyl and Oxygen Species on the Partial Oxidation of Allylic Alcohols on Au(111)**

G. M. Mullen, L. Zhang, E. J. Evans, Jr., T. Yan, G. Henkelman, C. B. Mullins  
University of Texas at Austin, Departments of Chemical Engineering and Chemistry

### **Presentation Abstract**

Partial oxidation of alcohols is a topic of great interest in the field of gold catalysis. In this work, we provide evidence that the partial oxidation of allyl alcohol to its corresponding aldehyde, acrolein, over oxygen precovered gold surfaces occurs via multiple reaction pathways. Utilizing temperature programmed desorption (TPD) with isotopically-labeled water and oxygen species, reactive molecular beam scattering, and density functional theory (DFT) calculations, we demonstrate that the reaction mechanism for allyl alcohol oxidation is influenced by the relative proportions of atomic oxygen and hydroxyl species on the gold surface. Both atomic oxygen and hydroxyl species are shown to be active for allyl alcohol oxidation but each displays a different pathway of oxidation as indicated by TPD measurements and DFT calculations. The hydroxyl hydrogen of allyl alcohol is readily abstracted by either oxygen adatoms or adsorbed hydroxyl species on the gold surface to generate a surface bound allyloxide intermediate, which then undergoes  $\alpha$ -dehydrogenation via interaction with an oxygen adatom or surface hydroxyl species to generate acrolein. Mediation of a second allyloxide with the hydroxyl species lowers the activation barrier for the  $\alpha$ -dehydrogenation process. A third pathway exists in which two hydroxyl species recombine to generate water and an oxygen adatom, which subsequently dehydrogenates allyloxide. This work may aid in the understanding of oxidative catalysis over gold and the effect of water therein.

### **Grant # DE-FG02-04ER15587: Surface Chemistry of Gold Model Catalysts**

**PI:** Charles Buddie Mullins

**Postdocs:** N/A

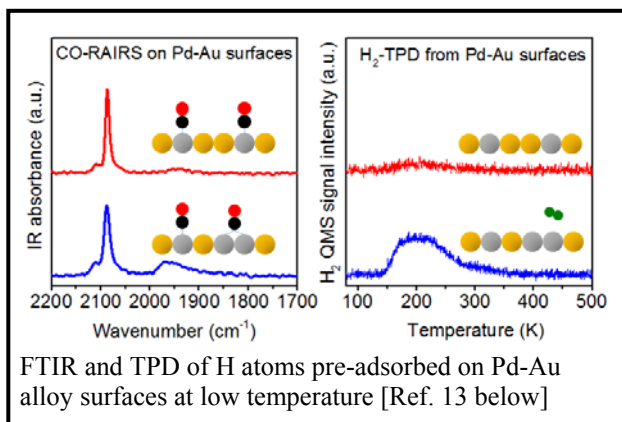
**Students:** Gregory M. Mullen, Adrian J. Brush, Wen-Yueh Yu, Edward J. Evans, Jr.

### **RECENT PROGRESS**

#### ***Hydrogen adsorption and absorption with Pd-Au bimetallic surfaces***

Pd-Au bimetallic catalysts have shown promising performance in numerous reactions that involve hydrogen. In this study, the interactions of hydrogen (*i.e.*, adsorption, absorption, diffusion and desorption) with Pd/Au(111) model surfaces were studied using temperature-programmed desorption (TPD) under ultrahigh vacuum conditions.

Our experimental results reveal Pd-Au bimetallic surfaces readily dissociates H<sub>2</sub> and yet also weakly binds H adatoms, properties that could be beneficial for catalytic reactions

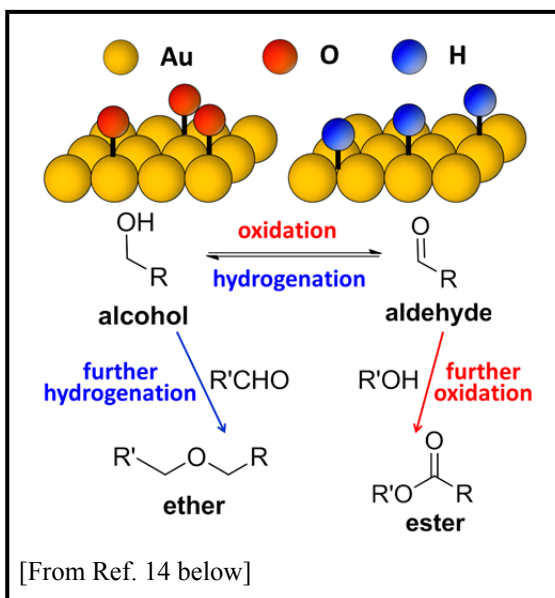


involving hydrogen. The presence of contiguous Pd sites, characterized by reflection-absorption infrared spectroscopy using CO as a probe molecule (CO-RAIRS), was found to be vital for the dissociative adsorption of H<sub>2</sub> at 77 K. The H adatom binds to Pd-Au alloy sites more strongly than to Au(111) but more weakly than to Pd(111) as indicated by its desorption temperature (~200 K). With

hydrogen exposure at slightly higher temperatures (i.e., 100 - 150 K), extension of a low temperature desorption feature was observed, suggesting the formation of subsurface H atoms (or H absorption).

### **Model studies with gold: A versatile oxidation and hydrogenation catalyst**

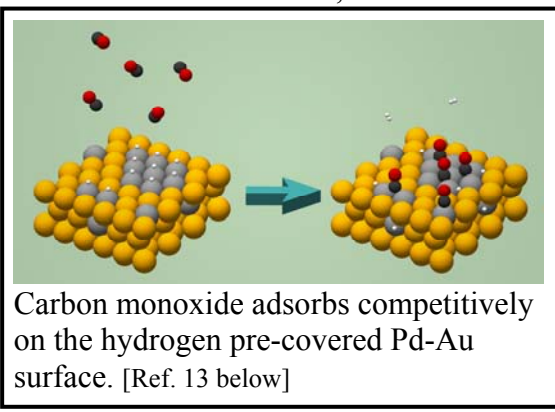
Here, we compare two inverse reactions, alcohol oxidation and aldehyde hydrogenation, on a Au(111) surface. Beyond the expected different chemistry, there are intriguing similarities observed since the same surface is employed. First, both molecular oxygen and hydrogen have high barriers to dissociation on Au(111) and frequently atomic O and H are employed to populate surfaces for the study of chemical reactions. Recombinative desorption features of oxygen and hydrogen are apparent at ~500 K and ~110 K, lower temperatures compared to other transition metals. These results indicate that oxygen and hydrogen have low desorption activation energies and weakly chemisorb on the surface, likely leading to selective reactions. On the oxygen-pre-covered Au(111) surface, alcohols are selectively oxidized to aldehydes. Similarly, weakly bound hydrogen atoms on Au(111) also shows chemoselective reactivity for hydrogenation of propionaldehyde and acetone. The second similarity is that the gold surface activates self-coupling of alcohol or aldehyde with oxygen or hydrogen, resulting in the formation of esters and ethers, respectively in alcohol oxidation and aldehyde hydrogenation. During these two reactions, the different reaction



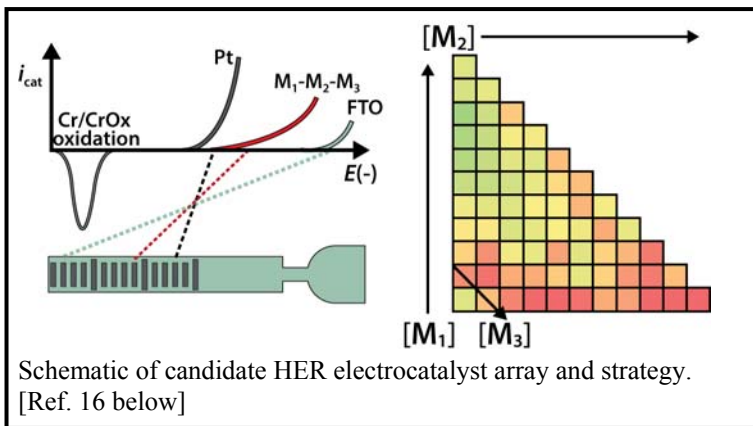
intermediates, alkoxy groups and alcohol-like species, are produced, which likely play a key role in the formation of coupling products. In addition, the cross coupling reaction between alcohol and aldehyde occurs on both O- and H-modified surfaces, yielding the production of esters and ethers, respectively. Thus, the synthesis of ester and ether can be tuned regarding the molecular structure via selecting the corresponding aldehyde and alcohol for the coupling reaction.

***Interactions of hydrogen and carbon monoxide on Pd-Au bimetallic surfaces***

Pd-Au bimetallic catalysts have shown potential applications in numerous heterogeneous reactions in which hydrogen and CO act as reactants, intermediates or products. In this study, the interactions of hydrogen and CO with Pd/Au(111) model surfaces were investigated by temperature-programmed desorption (TPD) and molecular beam scattering (MBS) experiments. Our results reveal that CO adsorbs competitively on the hydrogen-precovered Pd-Au surface, causing surface H adatoms to diffuse away from stronger-binding sites (e.g., Pd(111)-like islands) to weaker-binding sites (e.g., Pd-Au alloy sites and subsurface) as evidenced by a shift of the H<sub>2</sub> desorption feature to lower temperatures in TPD measurements. Additionally, evolution of H<sub>2</sub> was observed when a CO molecular beam was impinged onto the H-precovered Pd-Au surface, providing direct evidence that CO induces recombinative desorption of H adatoms. The presence of H adatoms on the Pd-Au surface was found to decrease the initial sticking probability of CO during MBS experiments but had little influence on CO desorption during subsequent TPD measurements.



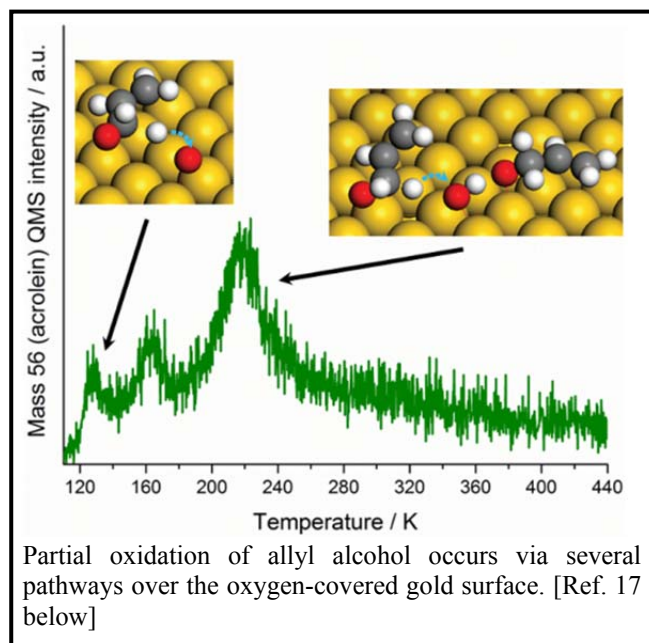
***Evaluating electrocatalysts for the hydrogen evolution reaction based on bi- and trimetallic combinations of Co, Fe, Ni, Mo, and W using bipolar electrode arrays***



We reported on the development of a parallel electrocatalyst screening platform for the hydrogen evolution reaction (HER) using bipolar electrodes (BPEs). Electrocatalyst candidates are subjected to screening in a N<sub>2</sub>-purged bipolar electrochemical cell where a pair of driving electrodes produce an

electric field in the electrolyte solution. The HER occurring at the BPE cathodes is electrically coupled to the electrodisolution of an array of Cr microbands present at the BPE anodes. The readout of this device is simple, where the species that dissolve the most Cr microbands are identified as the most promising electrocatalyst candidates for further evaluation. We demonstrate the utility of this technique by comparing several bi- and trimetallic systems involving Co, Fe, Ni, Mo, and W, which are compared directly to pure Pt. Of all the compositions tested, Ni<sub>8</sub>-Mo<sub>2</sub> is demonstrated to be the most active for the HER in a neutral electrolyte solution.

***Oxygen and hydroxyl species induce multiple reaction pathways for the partial oxidation of allyl alcohol on gold***



Partial oxidation of alcohols is a topic of great interest in the field of gold catalysis. In this work, we provide evidence that the partial oxidation of allyl alcohol to its corresponding aldehyde, acrolein, over oxygen precovered gold surfaces occurs via multiple reaction pathways. Utilizing temperature programmed desorption (TPD) with isotopically-labeled water and oxygen species, reactive molecular beam scattering, and density functional theory (DFT) calculations, we demonstrate that the reaction mechanism for allyl alcohol oxidation is influenced by the relative proportions of

atomic oxygen and hydroxyl species on the gold surface. Both atomic oxygen and hydroxyl species are shown to be active for allyl alcohol oxidation but each displays a different pathway of oxidation as indicated by TPD measurements and DFT calculations. The hydroxyl hydrogen of allyl alcohol is readily abstracted by either oxygen adatoms or adsorbed hydroxyl species on the gold surface to generate a surface bound allyloxide intermediate, which then undergoes  $\alpha$ -dehydrogenation via interaction with an oxygen adatom or surface hydroxyl species to generate acrolein. Mediation of a second allyloxide with the hydroxyl species lowers the activation barrier for the  $\alpha$ -dehydrogenation process. A third pathway exists in which two hydroxyl species recombine to generate water and an oxygen adatom, which subsequently dehydrogenates allyloxide. This work may aid in the understanding of oxidative catalysis over gold and the effect of water therein.

## Publications Acknowledging this Grant in 2011-2014

1. Pan, M.; Hoang, S.; Mullins, C. B. Interaction of water with the clean and oxygen precovered Ir(111) surface. *Catal. Today* **2011**, *160*, 198-203. <http://dx.doi.org/10.1016/j.cattod.2010.05.008>
2. Yan, T.; Gong, J.; Flaherty, D. W.; Mullins, C. B. The effect of adsorbed water in CO oxidation on Au/TiO<sub>2</sub>(110). *J. Phys. Chem. C* **2011**, *115*, 2057–2065. <http://dx.doi.org/10.1021/jp109295u>
3. Pan, M.; Flaherty, D. W.; Mullins, C. B. Low-temperature hydrogenation of acetaldehyde to ethanol on H-precovered Au(111). *J. Phys. Chem. Lett.* **2011**, *2*, 1363-1367. <http://dx.doi.org/10.1021/jz200577n>
4. Flaherty, D. W.; Yu, W.-Y.; Pozun, Z. D.; Henkelman, G.; Mullins, C. B. Mechanism for the water-gas shift reaction on monofunctional platinum and cause of catalyst deactivation. *J. Catal.* **2011**, *282*, 278-288. <http://dx.doi.org/10.1016/j.jcat.2011.06.024>
5. Pan, M.; Pozun, Z. D.; Yu, W.-Y.; Henkelman, G.; Mullins, C. B. Structure revealing H/D exchange with co-adsorbed hydrogen and water on gold. *J. Phys. Chem. Lett.* **2012**, *3*, 1894-1899. <http://dx.doi.org/10.1021/jz3007707>
6. Pan, M.; Pozun, Z. D.; Brush, A. J.; Henkelman, G.; Mullins, C. B. Low-temperature chemoselective gold-surface-mediated hydrogenation of acetone and propionaldehyde. *ChemCatChem* **4**, 1241-1244 (2012). <http://dx.doi.org/10.1002/cctc.201200311>
7. Yan, T.; Redman, D. W.; Yu, W.-Y.; Flaherty, D. W.; Rodriguez, J. A.; Mullins, C. B. CO oxidation on inverse Fe<sub>2</sub>O<sub>3</sub>/Au(111) model catalysts. *J. Catal.* **2012**, *294*, 216-222. <http://dx.doi.org/10.1016/j.jcat.2012.07.024>
8. Pan, M.; Brush, A. J.; Dong, G.; Mullins, C. B. Tunable ether production via coupling of aldehydes or aldehyde/alcohol over hydrogen-modified gold catalysts at low temperature. *J. Phys. Chem. Lett.* **2012**, *3*, 2512-2516. <http://dx.doi.org/10.1021/jz301105e>
9. Brush, A. J.; Pan, M.; Mullins, C. B. Methanol O-H bond dissociation on H-precovered gold originating from a structure with a wide range of surface stability. *J. Phys. Chem. C* **2012**, *116*, 20982-20989. <http://dx.doi.org/10.1021/jp308099y>
10. Pan, M.; Ham, H. C.; Yu, W.-Y.; Hwang, G. S.; Mullins, C. B. Highly selective, facile NO<sub>2</sub> reduction to NO at cryogenic temperatures on H precovered gold. *J. Am. Chem. Soc.* **2013**, *135*, 436-442. <http://dx.doi.org/10.1021/ja3096575>

11. Pan, M.; Brush, A. J.; Pozun, Z. D.; Ham, H. C.; Yu, W.-Y.; Henkelman, G.; Hwang, G. S.; Mullins, C. B. Model studies of heterogeneous catalytic hydrogenation reactions with gold. *Chem. Soc. Rev.* **2013**, *42*, 5002-5013. <http://dx.doi.org/10.1039/c3cs35523c>
12. Mullen, G. M.; Pan, M.; Yan, T.; Gong, J.; Mullins, C. B. The effects of adsorbed water on gold catalysis and surface chemistry. *Top. Catal.* **2013**, *56*, 1499-1511. <http://dx.doi.org/10.1007/s11244-013-0143-x>
13. Yu, W.-Y.; Mullen, G. M.; Mullins, C. B. Hydrogen adsorption and absorption with Pd-Au bimetallic surfaces. *J. Phys. Chem. C* **2013**, *117*, 19535-119543. <http://dx.doi.org/10.1021/jp406736b>
14. Pan, M.; Yan, T.; Gong, J.; Dong, G.; Mullins, C. B. Model studies with gold: A versatile oxidation and hydrogenation catalyst. *Acc. Chem. Res.* **2014**, *47*, 750-760. <http://dx.doi.org/10.1021/ar400172u>
15. Yu, W.-Y.; Mullen, G. M.; Mullins, C. B. Interactions of hydrogen and carbon monoxide on Pd-Au bimetallic surfaces. *J. Phys. Chem. C* **2014**, *118*, 2129-2137. <http://dx.doi.org/10.1021/jp411299e>
16. Fosdick, S. E.; Berglund, S. P.; Mullins, C. B.; Crooks, R. M. Evaluating electrocatalysts for the hydrogen evolution reaction based on bi- and trimetallic combinations of Co, Fe, Ni, Mo, and W using bipolar electrode arrays. *ACS Catal.* **2014**, *4*, 1332-1339. <http://dx.doi.org/10.1021/cs400168t>
17. Mullen, G. M.; Zhang, L.; Evans Jr., E. J.; Yan, T.; Henkelman, G.; Mullins, C. B. Oxygen and hydroxyl species induce multiple reaction pathways for the partial oxidation of allyl alcohol on gold. *J. Am. Chem. Soc.* **2014**, *136*, 6489-6498. <http://dx.doi.org/10.1021/ja502347d>

## Institute for Catalysis in Energy Processes

PI: Peter C. Stair

Department of Chemistry and Center for Catalysis and Surface Science  
Northwestern University

### Project Abstract

The Institute for Catalysis in Energy Processes (ICEP) is a multi-investigator project in the Northwestern University Center for Catalysis and Surface Science (NU). It has strong connections to the catalysis research group at Argonne National Laboratory (ANL) through joint appointments of several PIs. The overarching theme of ICEP research is *Chemical Catalysis: Manipulation and Understanding of Oxidation Catalysts*. The objectives of the project are 1) Elucidate the structure-function relationships in oxidation catalysts of several forms, *supported molecular oxides*, *supported metal nanoparticles*, and *supported metal atoms* and 2) Understand the roles of different oxidizing species in catalytic oxidation. Recent objectives for the project year have been 1) Develop the oxidation of cyclohexene as a versatile and informative probe reaction for oxidation pathways, 2) Develop the capability to carry out catalytic reaction experiments with a variety of oxidants: O<sub>2</sub>, H<sub>2</sub>O<sub>2</sub>, NO, N<sub>2</sub>O, organic hydroperoxides and begin reaction studies, 3) Synthesize and characterize new catalytic materials with novel structures designed to probe specific questions about structure-function relationships, and 4) Advance our characterization methodologies, both experimental and computational, to obtain an atomic scale picture of our catalytic materials and their function.

### Grant No: DE-FG02-03ER15457: Institute for Catalysis in Energy Processes

**PI:** Peter C. Stair

**Co-PI's:** Michael Bedzyk, Linda Broadbelt, Donald Ellis, Joseph Hupp, Harold Kunk, Laurence Marks, Tobin Marks, SonBinh Nguyen, Kenneth Poepelmeier, Randal Snurr

**Postdocs:** Sven Eric Stoltz, Weiqiang Wu

**Students:** Bor Rong Chen, Yi-Yi Wu, Yuyuan Lin, Chuandao Wang, Houg Giang Lian, James McCarthy, Stephanie Kwon, Tasha Drake, Sicelo Masango, Jeffrey Miles Tan

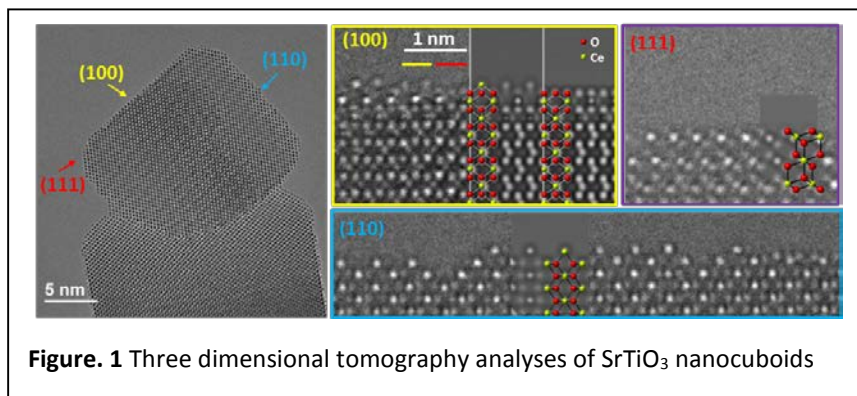
### RECENT PROGRESS

ICEP research is focused on the understanding and advancement of heterogeneous catalytic oxidation by supported late transition metals and supported early transition metal oxides. The report is organized into two sections, each addressing one of these materials systems. Our work combines the preparation of highly uniform, designed materials and state-of-the-art, atomic-scale characterization measurements and theory in order to understand catalytic function.

#### *Supported Late Transition Metals*

The synthesis of supported Pt, Au, Pd, Ag, etc. catalysts begins with the support. The support imparts stability to metallic nanoparticle (NP) and can influence their shape and electronic properties. It may also participate directly in the active site.

The systematic investigation of how support structure and composition influences metal NPs has been carried out using cuboidal, crystalline, perovskite nanoparticles having the composition Ba<sub>x</sub>Sr<sub>1-x</sub>TiO<sub>3</sub> with x in the range 0-1. We have demonstrated both (i) the general synthesis with lamellar microemulsions of crystalline nanocuboids with uniform size and tunable composition and (ii) their subsequent assembly into two-dimensional arrays by bent oleic acid in a nonpolar solvent. A porous version of these materials has also been synthesized with a BET surface area of 46m<sup>2</sup>/g compared to 20m<sup>2</sup>/g for our previously synthesized nonporous materials. BJH pore diameters of 2.5nm, 9nm, and 18nm were obtained indicating that the porous SrTiO<sub>3</sub> nanocuboids should be an excellent support for precious metal catalysts.



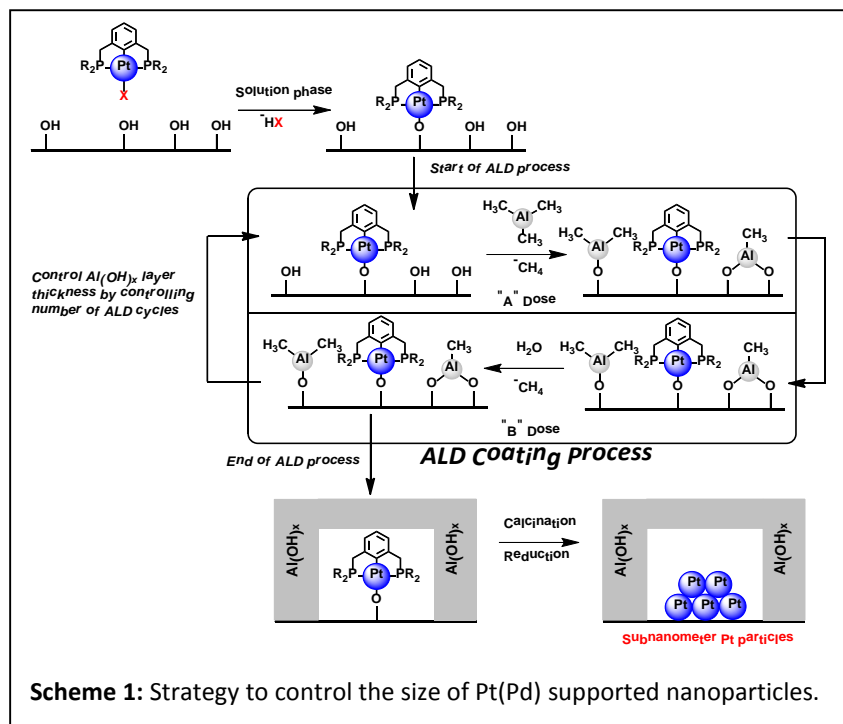
It was unknown whether the different processes can result in a surface structural change. An example is the SrTiO<sub>3</sub> nanocuboids. We have obtained SrTiO<sub>3</sub> nanocuboids with three hydrothermal processes. We performed aberration-corrected HREM in the profile imaging mode and found that the atomic surface structures are synthesis-dependent. The ones obtained by using

organic ligands (oleic acid) result in SrTiO<sub>3</sub> nanocuboids with SrO termination. The ones prepared by acetic acid synthesis result in a TiO<sub>2</sub> double-layer termination. The acetic acid synthesis conducted in a microwave oven lead to a mixed termination, which indicates a surface which is closer to being stoichiometric. We attributed the SrO termination to the preferably bonding between the oleate ligands to the surface Sr ions. Organic ligands are usually believed to influence the electronic structures of catalysts or blocking the reactants to reach the catalysts' surfaces; this study demonstrates the ligands can also change the atomic structures.

Detailed studies using X-ray absorption near edge structure (XANES) and extended X-ray absorption fine structure (EXAFS) combined with HRTEM examined the influence of SrTiO<sub>3</sub> termination on the structure and composition of supported Pd nanoparticles prepared by ALD. On the SrO termination the average Pd particle size is 2-3 nm independent of the loading. On the TiO<sub>2</sub> termination the size increases with loading. The Pd particle composition shifts with increasing numbers of ALD cycles from oxide to metallic state.

The size of Pt NPs (measured by HRTEM) prepared using three different atomic layer deposition (ALD) procedures (AB-type, ABC-type, and static ABC-type) on SrTiO<sub>3</sub> nanocuboids was determined as a function of Pt loading and preparation temperature in order to study the mechanism of NP formation.

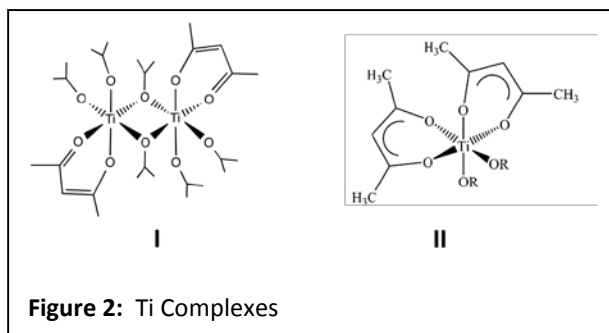
Methods for the preparation of single-atom supported Pt and Pd materials have been explored. The strategies involve grafting of a stable Pt(Pd)-organometallic pincer compound onto a support, followed by encapsulation with an ALD-deposited oxide, and finished by high temperature calcination to remove the ligands and open the encapsulating layers. Evidence from TEM and CO FTIR is consistent with the formation of either ultra-



small clusters or single-atom species. Future work will target more definitive characterization of the Pt and Pd species and catalytic oxidation reactions.

A second support material we have studied is  $\text{CeO}_2$  in collaboration with Oak Ridge National Lab. Its excellent catalytic properties are attributed to the remarkable redox capabilities of its surfaces. Direct observation of the  $\text{CeO}_2$  surface atomic structures can provide insight about the atomic origin for surface-dependent catalysis. We successfully imaged the Ce and O atom positions on the different surfaces of  $\text{CeO}_2$  nanoparticles by using the aberration-corrected high resolution electron microscopy (HREM). The (100) surface has a mixture of Ce, O and reduced CeO terminations on the outermost surface as well as partially occupied lattice sites in the near-surface region (~1 nm from the surface). The (110) surface has a combination of reduced flat  $\text{CeO}_{2-x}$  surface termination and “sawtooth-like” (111) nanofacets. The  $\text{CeO}_2$  (111) surface is O-terminated. The surface structures derived from this HREM study are consistent with results from the infrared spectroscopy investigation performed by our collaborators.

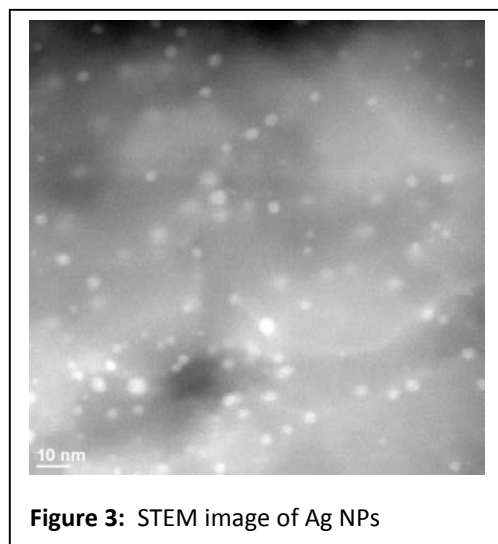
To study the direct participation of support atoms in the catalytic site responsible for selective propane oxidation by supported Au, well-defined ligands for the Au particles have been created that: (1) can serve as a surrogate of the metal-support interface; (2) can be precisely tuned with respect to the molecularity and environment; (3) can be treated under mild conditions to remove unnecessary ancillary components. This approach was used to study how the presence of Ti species influences oxidation catalysis, since  $\text{TiO}_2$  is a common support used for Au. We have found that the activity of the Au catalysts for the selective oxidation of propane to acetone required the presence of such Ti species, and the activity increased with increasing density of Ti, but decreased when the Ti species was positioned farther away from the Au surface. During the past year the focus was on manipulating the spatial distribution of Ti species around the Au NP and on whether there was any effect caused by the number of Ti cations in these species. Preliminary experiments were performed to compare Ti species prepared using dinuclear complexes with mononuclear complexes. Both materials oxidized propane primarily to acetone, but the catalyst prepared from the dinuclear complex also formed propene.



In order to expand the scope of catalytic materials that can be prepared by ALD, we have developed synthesis strategies for supported Ag nanoparticles. Ag is an active and selective catalyst for the epoxidation of olefins using  $\text{O}_2$ . Trimethylphosphine(hexafluoroacetylacetonato)silver (I) was the Ag-containing precursor and formalin (AB-type) or trimethylaluminum and  $\text{H}_2\text{O}$  (ABC-type) were used as the secondary reagents for AB-type and ABC-type ALD, respectively. Metallic nanoparticles with an average diameter of 2.2-2.5 nm (determined by HR-TEM) were prepared on an alumina support.

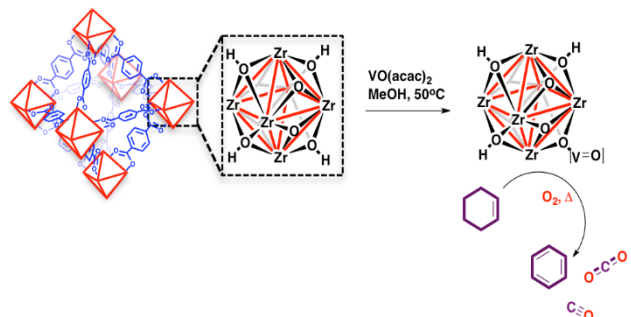
#### *Supported Early Transition Metal Oxides*

Vanadium oxide, molybdenum oxide, chromium oxide, manganese oxide, and other early transition metals in the form of monolayer or isolated molecular species supported on a high surface area refractory oxide are active and selective oxidation catalysts. During the past year, ICEP has targeted



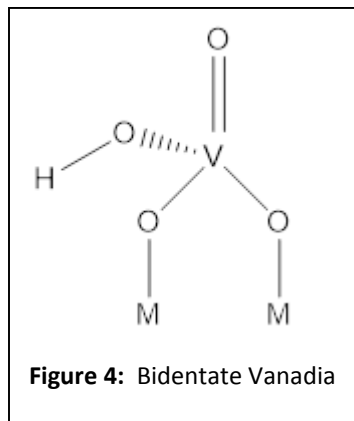
the synthesis of vanadium oxide on novel support materials that are expected to afford novel molecular vanadia structures as well as the preparation of mixed oxide monolayers of vanadium and molybdenum.

One novel support material is a metal organic framework (MOF) structure termed UiO-66. UiO-66 exhibits high thermal stability and catalytic activity for the oxidative dehydrogenation (ODH) of cyclohexene after grafting of vanadyl groups to zirconium oxide nodes in the structure (Scheme 1). At low conversion (<2%) benzene is the sole product. At higher conversions the selectivity to benzene decreases to 83% with the remaining products being CO and CO<sub>2</sub>. The activation energy was measured to be 110 ± 10 kJ/mol, which is comparable to values obtained for vanadium oxide supported on alumina.



**Scheme 2.** Synthesis of VUiO-66 and its catalytic activity in the oxidative dehydrogenation of cyclohexene using molecular oxygen as oxidant.

The SrTiO<sub>3</sub> nanocuboids, described above, represent a second novel support. Supported vanadium oxide has been prepared on this support using ALD of vanadyl-triisopropoxide (VOTP). Surface science studies of VOTP reactions on SrTiO<sub>3</sub> (001) single crystals have shown that the surface vanadia species bond to the support through only two, not three, bridging oxygen atoms. ODH of cyclohexene using O<sub>2</sub> catalyzed by SrTiO<sub>3</sub>-supported vanadium oxide produced primarily benzene but cyclohexadiene was also observed.



The catalytic properties of supported vanadium oxide species can be tuned by changing the support or by introducing a second oxide component on the surface. We have studied the influence of molybdenum and tungsten oxides as a modifiers of vanadium oxide supported on alumina. The studies have examined the role of preparation method on the interaction between surface molybdena/tungsta and vanadia by comparing samples prepared by conventional wet impregnation and by ALD. Changes in the structural motifs exhibited by vanadia and molybdena have been probed using UV Raman spectroscopy. In general, the ALD preparation method produces more highly dispersed oxide species on the support.

Catalytic oxidation by supported vanadium oxide materials has been studied using the oxidation of cyclohexene as a probe reaction for kinetics and mechanisms. The reaction pathways open to cyclohexene provide a rich platform for the investigating the factors that govern several classes of oxidation reactions, especially oxidative dehydrogenation, epoxidation, and alcohol formation. A special flow reactor that makes use of gas phase H<sub>2</sub>O<sub>2</sub> as the oxidant has been developed to make possible a comparison to the more commonly studied O<sub>2</sub> under identical reaction conditions. Reactions performed using gas phase H<sub>2</sub>O<sub>2</sub> are also free of solvent effects that may complicate the elucidation of reaction mechanisms. Proof for the delivery of intact H<sub>2</sub>O<sub>2</sub> into the catalyst bed has been obtained through the observation of cyclohexene epoxidation using titanium-silicate as a catalyst. Preliminary experiments using vanadium oxide supported on SiO<sub>2</sub>, Al<sub>2</sub>O<sub>3</sub>, TiO<sub>2</sub>, and ZrO<sub>2</sub> as catalysts for the oxidation of cyclohexene by H<sub>2</sub>O<sub>2</sub>. Oxidative dehydrogenation to benzene has been observed as the major reaction pathway; however, small quantities of cyclohexane diol have been obtained when SiO<sub>2</sub> is the support. Interestingly, in-situ FTIR measurements using O<sub>2</sub> as the oxidant have detected formation of both the diol and the epoxide of cyclohexane using these same catalysts whereas these oxygenates are not detectable in conventional catalytic reaction experiments.

## Publications Acknowledging this Grant in 2011-2014

1. Allotta, P. M.; Stair, P. C., Time-Resolved Studies of Ethylene and Propylene Reactions in Zeolite H-MFI by In-Situ Fast IR Heating and UV Raman Spectroscopy. *ACS Catalysis* **2012**, *2* (11), 2424-2432.
2. Amirjalayer, S.; Snurr, R. Q.; Schmid, R., Prediction of structure and properties of boron-based covalent organic frameworks by a first principles derived force field. *J Phys Chem C* **2012**, *116*, 4921-4929.
3. Atesin, A. C.; Ray, N. A.; Stair, P. C.; Marks, T. J., Etheric C-O Bond Hydrogenolysis Using a Tandem Lanthanide Triflate/Supported Palladium Nanoparticle Catalyst System. *Journal of the American Chemical Society* **2012**, *134* (36), 14682-14685.
4. Bae, Y. S.; Lee, C. Y.; Kim, K. C.; Farha, O. K.; Nickias, P.; Hupp, J. T.; Nguyen, S. T.; Snurr, R. Q., High Propene/Propane Selectivity in Isostructural Metal-Organic Frameworks with High Densities of Open Metal Sites. *Angew Chem Int Edit* **2012**, *51* (8), 1857-1860.
5. Bae, Y.-S.; Hauser, B. G.; Colon, Y. J.; Hupp, J. T.; Farha, O. K.; Snurr, R. Q., High xenon/krypton selectivity in a metal-organic framework with small pores and strong adsorption sites. *Microporous and Mesoporous Materials* **2013**, *169*, 176-179.
6. Bao, X. Y.; Sung, C. Y.; Snurr, R. Q.; Broadbelt, L. J., Rate-Determining Step in the NO<sub>x</sub> Reduction Mechanism on BaY Zeolites and the Importance of Long-Range Lattice Effects. *ACS Catalysis* **2012**, *2* (3), 350-359.
7. Becerra-Toledo, A. E.; Enterkin, J. A.; Kienzle, D. M.; Marks, L. D., Water adsorption on SrTiO<sub>3</sub>(001): II. Water, water, everywhere. *Surface Science* **2012**, *606* (9-10), 791-802.
8. Bhattacharyya, K.; Danon, A.; Vijayan, B. K.; Gray, K. A.; Stair, P. C.; Weitz, E., Role of the Surface Lewis Acid and Base Sites in the Adsorption of CO<sub>2</sub> on Titania Nanotubes and Platinized Titania Nanotubes: An in Situ FT-IR Study. *J Phys Chem C* **2013**, *117* (24), 12661-12678.
9. Buchbinder, A. M.; Gibbs-Davis, J. M.; Stokes, G. Y.; Peterson, M. D.; Weitz, E.; Geiger, F. M., Method for Evaluating Vibrational Mode Assignments in Surface-Bound Cyclic Hydrocarbons Using Sum-Frequency Generation. *J Phys Chem C* **2011**, *115* (37), 18284-18294.
10. Buchbinder, A. M.; Ray, N. A.; Lu, J. L.; Van Duyne, R. P.; Stair, P. C.; Weitz, E.; Geiger, F. M., Displacement of Hexanol by the Hexanoic Acid Overoxidation Product in Alcohol Oxidation on a Model Supported Palladium Nanoparticle Catalyst. *Journal of the American Chemical Society* **2011**, *133* (44), 17816-17823.
11. Burd, S. D.; Ma, S.; Perman, J. A.; Sikora, B. J.; Snurr, R. Q.; Thallapally, P. K.; Tian, J.; Wojtas, L.; Zaworotko, M. J., Highly selective carbon dioxide uptake by [Cu(bpy-n)<sub>2</sub>(SiF<sub>6</sub>)] (bpy-1 = 4,4'-bipyridine; bpy-2 = 1,2-bis(4-pyridyl)ethene. *Journal of the American Chemical Society* **2012**, *134*, 3663-3666.
12. Canlas, C.; Lu, J.; Ray, N. A.; Grosso-Giordano, N.; Lee, S.; Elam, J. W.; Winans, R.; Stair, P. C.; Van Duyne, R. P.; Notestein, J., Shape-selective sieving layers on an oxide catalyst surface. *Nature Chemistry* **2012**, *4*, 1030-1036.
13. Chattopadhyay, S.; Lipson, A. L.; Karmel, H. J.; Emery, J. D.; Fister, T. T.; Fenter, P. A.; Hersam, M. C.; Bedzyk, M. J., In Situ X-ray Study of the Solid Electrolyte Interphase (SEI) Formation on Graphene as a Model Li-ion Battery Anode. *Chemistry of Materials* **2012**, *24* (15), 3038-3043.
14. Comstock, D. J.; Elam, J. W.; Pellin, M. J.; Hersam, M. C., High aspect ratio nanoneedle probes with an integrated electrode at the tip apex. *Rev Sci Instrum* **2012**, *83* (11).
15. Danon, A.; Bhattacharyya, K.; Vijayan, B. K.; Lu, J. L.; Sauter, D. J.; Gray, K. A.; Stair, P. C.; Weitz, E., Effect of Reactor Materials on the Properties of Titanium Oxide Nanotubes. *ACS Catalysis* **2012**, *2* (1), 45-49.

16. Danon, A.; Stair, P. C.; Weitz, E., Mechanistic and Adsorption Studies of Relevance to Photocatalysts on Titanium Grafted Mesoporous Silicalites. *Catal Lett* **2011**, *141* (8), 1057-1066.
17. Danon, A.; Stair, P. C.; Weitz, E., FTIR Study of CO<sub>2</sub> Adsorption on Amine-Grafted SBA-15: Elucidation of Adsorbed Species. *J Phys Chem C* **2011**, *115* (23), 11540-11549.
18. Danon, A.; Weitz, E.; Stair, P. C., Molecular nature and site requirements of adsorbed CO<sub>2</sub>. *Abstr Pap Am Chem S* **2012**, *243*.
19. DeSario, P. A.; Wu, J. S.; Grahm, M. E.; Gray, K. A., Nanoscale structure of Ti<sub>1-x</sub>Nb<sub>y</sub>O<sub>2</sub> mixed-phase thin films: Distribution of crystal phase and dopants. *J Mater Res* **2012**, *27* (6), 944-950.
20. Deshpande, A.; Sham, C. H.; Alaboson, J. M. P.; Mullin, J. M.; Schatz, G. C.; Hersam, M. C., Self-Assembly and Photopolymerization of Sub-2 nm One-Dimensional Organic Nanostructures on Graphene. *Journal of the American Chemical Society* **2012**, *134* (40), 16759-16764.
21. Dickey, A. N.; Yazaydin, A. O.; Willis, R. R.; Snurr, R. Q., Screening CO<sub>2</sub>/N<sub>2</sub> selectivity in metal-organic frameworks using Monte Carlo simulations and ideal adsorbed solution theory. *Canadian Journal of Chemical Engineering* **2012**, *90*, 825-832.
22. Downing, C. M.; Kung, H. H., Diethyl sulfide stabilization of platinum-complex catalysts for hydrosilylation of olefins. *Catalysis Communications* **2011**, *12* (12), 1166-1169.
23. Downing, C. M.; Missaghi, M. N.; Kung, M. C.; Kung, H. H., Design and Synthesis of Readily Degradable Acyloxysilane Dendrimers. *Tetrahedron* **2011**, doi:10.1016/j.tet.2011.07.068.
24. Ebben, C. J.; Martinez, I. S.; Shrestha, M.; Buchbinder, A. M.; Corrigan, A. L.; Guenther, A.; Karl, T.; Petaja, T.; Song, W. W.; Zorn, S. R.; Artaxo, P.; Kulmala, M.; Martin, S. T.; Russell, L. M.; Williams, J.; Geiger, F. M., Contrasting organic aerosol particles from boreal and tropical forests during HUMPPA-COPEC-2010 and AMAZE-08 using coherent vibrational spectroscopy. *Atmos Chem Phys* **2011**, *11* (20), 10317-10329.
25. Enterkin, J. A.; Kennedy, R. M.; Lu, J. L.; Elam, J. W.; Cook, R. E.; Marks, L. D.; Stair, P. C.; Marshall, C. L.; Poepelmeier, K. R., Epitaxial Stabilization of Face Selective Catalysts. *Topics in Catalysis* **2013**, 1-6.
26. Enterkin, J. A.; Poepelmeier, K. R.; Marks, L. D., Oriented Catalytic Platinum Nanoparticles on High Surface Area Strontium Titanate Nanocuboids (vol 11, pg 993, 2011). *Nano Letters* **2011**, *11* (8), 3510-3510.
27. Enterkin, J. A.; Poepelmeier, K. R.; Marks, L. D., A Chemical Approach to Understanding Oxide Surfaces. *Surface Science* **2012**, *606*, 334-355.
28. Fairen-Jimenez, D.; Colon, Y. J.; Farha, O. K.; Bae, Y.-S.; Hupp, J. T.; Snurr, R. Q., Understanding excess uptake maxima for hydrogen adsorption isotherms in frameworks with rhf topology. *Chemical Communications* **2012**, *48*, 10496-10498.
29. Farha, O. K.; Eryazici, I.; Jeong, N. C.; Hauser, B. G.; Wilmer, C. E.; Sarjeant, A. A.; Snurr, R. Q.; Nguyen, S. T.; Yazaydin, A. O.; Hupp, J. T., Metal-organic framework materials with ultrahigh surface areas: Is the sky the limit? *Journal of the American Chemical Society* **2012**, *134*, 15016-15021.
30. Farha, O. K.; Wilmer, C. E.; Eryazici, I.; Hauser, B. G.; Parilla, P. A.; O'Neill, K.; Sarjeant, A. A.; Nguyen, S. T.; Snurr, R. Q.; Hupp, J. T., Designing higher surface area metal-organic frameworks: Are triple bonds better than phenyls? *Journal of the American Chemical Society* **2012**, *134*, 9860-9863.
31. Feng, Z.; Lu, J.; Feng, H.; Stair, P. C.; Elam, J. W.; Bedzyk, M. J., Catalysts Transform While Molecules React: An Atomic-Scale View. *Journal of Physical Chemistry Letters* **2013**, *4* (2), 285-291.

32. Feng, Z. X.; Cheng, L.; Kim, C. Y.; Elam, J. W.; Zhang, Z.; Curtiss, L. A.; Zapol, P.; Bedzyk, M. J., Atomic-Scale Study of Ambient-Pressure Redox-Induced Changes for an Oxide-Supported Submonolayer Catalyst: VOx/ $\alpha$ -TiO<sub>2</sub>(110). *Journal of Physical Chemistry Letters* **2012**, *3* (19), 2845-2850.
33. Feng, Z. X.; Kazimirov, A.; Bedzyk, M. J., Atomic Imaging of Oxide-Supported Metallic Nanocrystals. *ACS Nano* **2011**, *5* (12), 9755-9760.
34. Finkelstein-Shapiro, D.; Buchbinder, A. M.; Vijayan, B.; Bhattacharyya, K.; Weitz, E.; Geiger, F. M.; Gray, K. A., Identification of Binding Sites for Acetaldehyde Adsorption on Titania Nanorod Surfaces Using CIMS. *Langmuir* **2011**, *27* (24), 14842-14848.
35. Finkelstein-Shapiro, D.; Hurst, S. J.; Gray, K. A.; Dimitrijevic, N. M.; Rajh, T.; Tarakeshwar, P.; Mujica, V., CO<sub>2</sub> pre-activation via charge transfer states of TiO<sub>2</sub>-aminosalicylic acid complexes. *Journal of Physical Chemistry Letters* **2013**, *4* (3), 475-479.
36. Finkelstein-Shapiro, D.; Tsai, C. Y. H.; Li, S. Y.; Gray, K. A., Synthesis of high-energy anatase nanorods via an intermediate nanotube morphology. *Chem Phys Lett* **2012**, *546*, 106-108.
37. Frontiera, R. R.; Gruenke, N. L.; Van Duyne, R. P., Fano-like resonances arising from long-lived molecule-plasmon interactions in colloidal nanoantennas. *Nano Letters* **2012**, *12*, 5989-5994.
38. Fu, B.; Lu, J.; Stair, P. C.; Xiao, G.; Kung, M. C.; Kung, H. H., Oxidative dehydrogenation of ethane over alumina-supported Pd catalysts. Effect of alumina overlayer. *J Catal* **2013**, *297*, 289-295.
39. Gassensmith, J. J.; Smaldone, R. A.; Forgan, R. S.; Wilmer, C. E.; Cordes, D. B.; Botros, Y. Y.; Slawin, A. M. Z.; Snurr, R. Q.; Stoddart, J. F., Polyporous metal-coordination frameworks. *Organic Letters* **2012**, *14*, 1460-1463.
40. Getman, R. B.; Bae, Y.-S.; Wilmer, C. E.; Snurr, R. Q., Review and analysis of molecular simulations of methane, hydrogen, and acetylene storage in metal-organic frameworks. *Chemical Reviews* **2012**, *112*, 703-723.
41. Hayner, C. M.; Zhao, X.; Kung, H. H., Materials for rechargeable lithium-ion batteries. *Annual Review of Chemical and Biomolecular Engineering* **2012**, *3*, 445-471.
42. Hossain, M. Z.; Johns, J. E.; Bevan, K. H.; Karmel, H. J.; Liang, Y. T.; Yoshimoto, S.; Mukai, K.; Koitaya, T.; Yoshinobu, J.; Kawai, M.; Lear, A. M.; Kesmodel, L. L.; Tait, S. L.; Hersam, M. C., Chemically homogeneous and thermally reversible oxidation of epitaxial graphene. *Nature Chemistry* **2012**, *4* (4), 305-309.
43. Hu, L. H.; Wang, C. D.; Lee, S.; Winans, R. E.; Marks, L. D.; Poepelmeier, K. R., SrTiO<sub>3</sub> Nanocuboids from a Lamellar Microemulsion. *Chemistry of Materials* **2013**, *25* (3), 378-384.
44. Jaber-Ansari, L.; Hersam, M. C., Solution-processed graphene materials and composites. *Mrs Bull* **2012**, *37* (12), 1167-1175.
45. Jiang, N.; Foley, E. T.; Klingsporn, J. M.; Sonntag, M. D.; Valley, N. A.; Dieringer, J. A.; Seideman, T.; Schatz, G. C.; Hersam, M. C.; Van Duyne, R. P., Observation of Multiple Vibrational Modes in Ultrahigh Vacuum Tip-Enhanced Raman Spectroscopy Combined with Molecular-Resolution Scanning Tunneling Microscopy. *Nano Letters* **2012**, *10*, 5061-5067.
46. Johnson, A. M.; Quezada, B. R.; Marks, L. D.; Stair, P. C., Influence of the Metal Oxide Substrate Structure on Vanadium Oxide Monomer Formation. *Topics in Catalysis* **2013**, *57* (1-4), 177-187.
47. Kang, B.; Totten, R. K.; Weston, M. H.; Hupp, J. T.; Nguyen, S. T., Cyclic metalloporphyrin dimers and tetramers: tunable shape-selective hosts for fullerenes. *Dalton Transactions* **2012**, *41* (39), 12156-12162.

48. Kim, H.; Ferguson, G. A.; Cheng, L.; Zygmunt, S. A.; Stair, P. C.; Curtiss, L. A., Structure-Specific Reactivity of Alumina-Supported Monomeric Vanadium Oxide Species. *J Phys Chem C* **2012**, *116* (4), 2927-2932.
49. Kim, T.; Assary, R. S.; Marshall, C. L.; Gosztola, D. J.; Curtiss, L. A.; Stair, P. C., Conversion of furfuryl alcohol into polyfurfuryl alcohol: reaction mechanism, thermodynamic properties, and solvent effects. *Preprints of Symposia - American Chemical Society, Division of Fuel Chemistry* **2012**, *57* (1), 470-471.
50. Kim, T.; Assary, R. S.; Marshall, C. L.; Gosztola, D. J.; Curtiss, L. A.; Stair, P. C., Studies of the Raman spectra of cyclic and acyclic molecules: Combination and prediction spectrum methods. *Chem Phys Lett* **2012**, *531*, 210-215.
51. Leever, B. J.; Bailey, C. A.; Marks, T. J.; Hersam, M. C.; Durstock, M. F., In Situ Characterization of Lifetime and Morphology in Operating Bulk Heterojunction Organic Photovoltaic Devices by Impedance Spectroscopy. *Adv Energy Mater* **2012**, *2* (1), 120-128.
52. Leung, C. Y.; Palmer, L. C.; Qiao, B. F.; Kewalramani, S.; Sknepnek, R.; Newcomb, C. J.; Greenfield, M. A.; Vernizzi, G.; Stupp, S. I.; Bedzyk, M. J.; de la Cruz, M. O., Molecular Crystallization Controlled by pH Regulates Mesoscopic Membrane Morphology. *ACS Nano* **2012**, *6* (12), 10901-10909.
53. Liang, Y. T.; Hersam, M. C., Towards Rationally Designed Graphene-Based Materials and Devices. *Macromol Chem Phys* **2012**, *213* (10-11), 1091-1100.
54. Liang, Y. T.; Vijayan, B. K.; Gray, K. A.; Hersam, M. C., Minimizing Graphene Defects Enhances Titania Nanocomposite-Based Photocatalytic Reduction of CO<sub>2</sub> for Improved Solar Fuel Production. *Nano Letters* **2011**, *11* (7), 2865-2870.
55. Liang, Y. T.; Vijayan, B. K.; Lyandres, O.; Gray, K. A.; Hersam, M. C., Effect of Dimensionality on the Photocatalytic Behavior of Carbon-Titania Nanosheet Composites: Charge Transfer at Nanomaterial Interfaces. *Journal of Physical Chemistry Letters* **2012**, *3* (13), 1760-1765.
56. Lin, S. Y.; Yang, J.; Kung, H. H., Transition metal-decorated activated carbon catalysts for dehydrogenation of NaAlH<sub>4</sub>. *International Journal of Hydrogen Energy* **2012**, *37* (3), 2737-2741.
57. Lin, Y. Y.; Becerra-Toledo, A. E.; Silly, F.; Poepplmeier, K. R.; Castell, M. R.; Marks, L. D., The (2 x 2) reconstructions on the SrTiO<sub>3</sub> (001) surface: A combined scanning tunneling microscopy and density functional theory study. *Surface Science* **2011**, *605* (17-18), L51-L55.
58. Lin, Y. Y.; Wen, J.; Hu, L. H.; Kennedy, R. M.; Stair, P. C.; Poepplmeier, K. R.; Marks, L. D., Synthesis-Dependent Atomic Surface Structures of Oxide Nanoparticles. *Physical Review Letters* **2013**, *111* (15), 156101.
59. Lin, Y. Y.; Wu, Z.; Wen, J.; Poepplmeier, K. R.; Marks, L. D., Imaging the Atomic Surface Structures of CeO<sub>2</sub> Nanoparticles. *Nano Letters* **2014**, *14* (1), 191-196.
60. Lipson, A. L.; Chattopadhyay, S.; Karmel, H. J.; Fister, T. T.; Emery, J. D.; Dravid, V. P.; Thackeray, M. M.; Fenter, P. A.; Bedzyk, M. J.; Hersam, M. C., Enhanced Lithiation of Doped 6H Silicon Carbide (0001) via High Temperature Vacuum Growth of Epitaxial Graphene. *J Phys Chem C* **2012**, *116* (39), 20949-20957.
61. Lu, J.; Fu, B.; Kung, M. C.; Xiao, G.; Elam, J. W.; Kung, H. H.; Stair, P. C., Coking- and Sintering-Resistant Palladium Catalysts Achieved Through Atomic Layer Deposition. *Science (Washington, DC, United States)* **2012**, *335* (6073), 1205-1208.
62. Lu, J.; Liu, B.; Greeley, J. P.; Feng, Z.; Libera, J. A.; Lei, Y.; Bedzyk, M. J.; Stair, P. C.; Elam, J. W., Porous Alumina Protective Coatings on Palladium Nanoparticles by Self-Poisoned Atomic Layer Deposition. *Chemistry of Materials* **2012**, *24* (11), 2047-2055.

63. Luo, J.; Zhao, X.; Wu, J. S.; Jang, H. D.; Kung, H. H.; Huang, J., Crumpled Graphene-Encapsulated Si Nanoparticles for Lithium Ion Battery Anodes. *Journal of Physical Chemistry Letters* **2012**, *3* (13), 1824-1829.
64. Lyandres, O.; Chakthranont, P.; Finkelstein-Shapiro, D.; Graham, M.; Gray, K., The effects of preferred orientation in sputtered TiO<sub>2</sub> thin films on the photooxidation efficiency of acetaldehyde. *Chemistry of Materials* **2012**, *24* (17), 3355-3362.
65. Martynova, Y.; Liu, B. H.; McBriarty, M. E.; Groot, I. M. N.; Bedzyk, M. J.; Shaikhutdinov, S.; Freund, H. J., CO oxidation over ZnO films on Pt(111) at near-atmospheric pressures. *J Catal* **2013**, *301*, 227-232.
66. Mashayekhi, N. A.; Kung, M. C.; Kung, H. H., Selective oxidation of propane to acetone over Au-(oxoTi) catalysts. *Preprints - American Chemical Society, Division of Energy & Fuels* **2013**, *58* (1), 1284.
67. Mashayekhi, N. A.; Kung, M. C.; Kung, H. H., Selective oxidation of hydrocarbons on supported Au catalysts. *Catalysis Today* **2014**, Ahead of Print.
68. Mashayekhi, N. A.; Wu, Y. Y.; Kung, M. C.; Kung, H. H., Metal nanoparticle catalysts decorated with metal oxide clusters. *Chemical Communications* **2012**, *48* (81), 10096-10098.
69. Missaghi, M. N.; Galloway, J. M.; Kung, H. H., Bis(pyridyl)siloxane-Pd(II) complex catalyzed oxidation of alcohol to aldehyde: Effect: of ligand tethering on catalytic activity and deactivation behavior. *Appl Catal a-Gen* **2011**, *391* (1-2), 297-304.
70. Missaghi, M. N.; Kung, M. C.; Kung, H. H., Polysiloxanes in Catalysis and Catalyst Preparation: Opportunities for Control of Catalytic Processes. *Topics in Catalysis* **2012**, *55* (1-2), 99-107.
71. Mondloch, J. E.; Bury, W.; Fairen-Jimenez, D.; Kwon, S.; DeMarco, E. J.; Weston, M. H.; Sarjeant, A. A.; Nguyen, S. T.; Stair, P. C.; Snurr, R. Q.; Farha, O. K.; Hupp, J. T., Vapor-Phase Metalation by Atomic Layer Deposition in a Metal-Organic Framework. *Journal of the American Chemical Society* **2013**, *135* (28), 10294-10297.
72. Nguyen, H. G. T.; Weston, M. H.; Farha, O. K.; Hupp, J. T.; Nguyen, S. T., A catalytically active vanadyl(catecholate)-decorated metal organic framework via post-synthesis modifications. *CrystEngComm* **2012**, *14* (12), 4115-4118.
73. Nguyen, H. G. T.; Weston, M. H.; Sarjeant, A. A.; Gardner, D. M.; An, Z.; Carmieli, R.; Wasielewski, M. R.; Farha, O. K.; Hupp, J. T.; Nguyen, S. T., Design, Synthesis, Characterization, and Catalytic Properties of a Large-Pore Metal-Organic Framework Possessing Single-Site Vanadyl(monocatecholate) Moieties. *Crystal Growth & Design* **2013**, *13* (8), 3528-3534.
74. Odom, S. A.; Tyler, T. P.; Caruso, M. M.; Ritchey, J. A.; Schulmerich, M. V.; Robinson, S. J.; Bhargava, R.; Sottos, N. R.; White, S. R.; Hersam, M. C.; Moore, J. S., Autonomic restoration of electrical conductivity using polymer-stabilized carbon nanotube and graphene microcapsules. *Appl Phys Lett* **2012**, *101* (4).
75. Ostojic, G. N.; Hersam, M. C., Biomolecule-Directed Assembly of Self-Supported, Nanoporous, Conductive, and Luminescent Single-Walled Carbon Nanotube Scaffolds. *Small* **2012**, *8* (12), 1840-1845.
76. Peng, Y.; Srinivasa, G.; Wilmer, C. E.; Eryazici, I.; Snurr, R. Q.; Hupp, J. T.; Yildirim, T.; Farha, O. K., Simultaneously high gravimetric and volumetric methane uptake characteristics of the metal-organic framework NU-111. *Chemical Communications* **2013**, *49*, 2992-2994.
77. Pozzi, E.; Sonntag, M. D.; Jiang, N.; Klingsporn, J. M.; Hersam, M. C.; Van Duyne, R. P., Tip-Enhanced Raman Imaging: An Emergent Tool for Probing Biology at the Nanoscale. *ACS Nano* **2013**, *7*, 885-888.

78. Prieto-Centurion, D.; Boston, A. M.; Notestein, J. M., Structural and electronic promotion with alkali cations of silica-supported Fe(III) sites for alkane oxidation. *J Catal* **2012**, *296*, 77-85.
79. Proffit, D. E.; Harvey, S. P.; Klein, A.; Schafrank, R.; Emery, J. D.; Buchholz, D. B.; Chang, R. P. H.; Bedzyk, M. J.; Mason, T. O., Surface studies of crystalline and amorphous Zn-In-Sn-O transparent conducting oxides. *Thin Solid Films* **2012**, *520* (17), 5633-5639.
80. Proffit, D. E.; Ma, Q.; Buchholz, D. B.; Chang, R. P. H.; Bedzyk, M. J.; Mason, T. O., Structural and Physical Property Studies of Amorphous Zn-In-Sn-O Thin Films. *J Am Ceram Soc* **2012**, *95* (11), 3657-3664.
81. Ray, N. A.; Van Duyne, R. P.; Stair, P. C., Synthesis Strategy for Protected Metal Nanoparticles. *J Phys Chem C* **2012**, *116* (14), 7748-7756.
82. Reuter, M. G.; Hersam, M. C.; Seideman, T.; Ratner, M. A., Signatures of Cooperative Effects and Transport Mechanisms in Conductance Histograms. *Nano Letters* **2012**, *12* (5), 2243-2248.
83. Sangwan, V. K.; Ortiz, R. P.; Alaboson, J. M. P.; Emery, J. D.; Bedzyk, M. J.; Lauhon, L. J.; Marks, T. J.; Hersam, M. C., Fundamental Performance Limits of Carbon Nanotube Thin-Film Transistors Achieved Using Hybrid Molecular Dielectrics. *ACS Nano* **2012**, *6* (8), 7480-7488.
84. Schwartzenberg, K. C.; Gray, K. A., Nanostructured Titania: the current and future promise of Titania nanotubes. *Catalysis Science & Technology* **2012**, *2* (8), 1617-1624.
85. Sharma, B.; Frontiera, R. R.; Henry, A.-I.; Ringe, E.; Van Duyne, R. P., SERS: Materials, Applications, and the Future. *Materials Today* **2012**, (15), 16-25.
86. Shen, Z.; Kim, J. H.; Shen, J.; Downing, C. M.; Lee, S.; Kung, H. H.; Kung, M. C., Spherosilicates with peripheral malonic acid and vinyl end groups. *Chemical Communications* **2013**, *49* (32), 3357-3359.
87. Shultz, A. M.; Farha, O. K.; Adhikari, D.; Sarjeant, A. A.; Hupp, J. T.; Nguyen, S. T., Selective Surface and Near-Surface Modification of a Noncatenated, Catalytically Active Metal-Organic Framework Material Based on Mn(salen) Struts. *Inorganic Chemistry* **2011**, *50* (8), 3174-3176.
88. Shultz, A. M.; Farha, O. K.; Hupp, J. T.; Nguyen, S. T., Synthesis of catalytically active porous organic polymers from metalloporphyrin building blocks. *Chemical Science* **2011**, *2* (4), 686-689.
89. Shultz, A. M.; Sarjeant, A. A.; Farha, O. K.; Hupp, J. T.; Nguyen, S. T., Post-Synthesis Modification of a Metal-Organic Framework To Form Metallosalen-Containing MOF Materials. *Journal of the American Chemical Society* **2011**, *133* (34), 13252-13255.
90. Sikora, B. J.; Wilmer, C. E.; Greenfield, M. L.; Snurr, R. Q., Thermodynamic analysis of Xe/Kr selectivity in over 137,000 hypothetical metal-organic frameworks. *Chemical Science* **2012**, *3*, 2217-2223.
91. Song, K.; Sauter, D. J.; Wu, J. S.; Dravid, V. P.; Stair, P. C., Evolution of High-Energy Electron Beam Irradiation Effects on Zeolite Supported Catalyst: Metal Nanoprecipitation. *ACS Catalysis* **2012**, *2* (3), 384-390.
92. Sonntag, M. D.; Klingsporn, J. M.; Garibay, L. K.; Roberts, J. M.; Dieringer, J. A.; Seideman, T.; Scheidt, K. A.; Jensen, L.; Schatz, G. C.; Van Duyne, R. P., Single-Molecule Tip-Enhanced Raman Spectroscopy. *J Phys Chem C* **2012**, *116* (1), 478-483.
93. Stair, P. C., Synthesis of supported catalysts by atomic layer deposition. *Topics in Catalysis* **2012**, *55* (1-2), 93-98.
94. Strutt, N. L.; Fairen-Jimenez, D.; Iehl, J.; Lalonde, M. B.; Snurr, R. Q.; Farha, O. K.; Hupp, J. T.; Stoddart, J. F., Incorporation of an A1/A2-difunctionalized pillar[5]arene into a metal-organic framework. *Journal of the American Chemical Society* **2012**, *134*, 17436-17439.

95. Trahey, L.; Kung, H. H.; Thackeray, M. M.; Vaughey, J. T., Effect of Electrode Dimensionality and Morphology on the Performance of Cu<sub>2</sub>Sb Thin Film Electrodes for Lithium-Ion Batteries. *European Journal of Inorganic Chemistry* **2011**, 2011 (26), 3984-3988.
96. Tuci, G.; Kwon, S.; Stair, P. C.; Snurr, R. Q.; Rossin, A., Chiral Co(II) metal-organic framework in the heterogeneous catalytic oxidation of alkenes under aerobic and anaerobic conditions. *ACS Catalysis* **2014**, 4, 1032-1039
97. Tyler, T. P.; Lin, P. A.; Tian, Y.; Gao, H. J.; Gao, X. P. A.; Sankaran, R. M.; Hersam, M. C., Centrifugal Shape Sorting of Faceted Gold Nanoparticles Using an Atomic Plane-Selective Surfactant. *Journal of Physical Chemistry Letters* **2012**, 3 (11), 1484-1487.
98. Tyler, T. P.; Shastry, T. A.; Leever, B. J.; Hersam, M. C., Narrow Diameter Distributions of Metallic Arc Discharge Single-Walled Carbon Nanotubes via Dual-Iteration Density Gradient Ultracentrifugation. *Adv Mater* **2012**, 24 (35), 4765-4768.
99. Vijayan, B. K.; Dimitrijevic, N. M.; Finkelstein-Shapiro, D.; Wu, J. S.; Gray, K. A., Coupling Titania Nanotubes and Carbon Nanotubes To Create Photocatalytic Nanocomposites. *ACS Catalysis* **2012**, 2 (2), 223-229.
100. Wegener, S. L.; Kim, H.; Marks, T. J.; Stair, P. C., Precursor Nuclearity Effects in Supported Vanadium Oxides Prepared by Organometallic Grafting. *Journal of Physical Chemistry Letters* **2011**, 2 (3), 170-175.
101. Wegener, S. L.; Marks, T. J.; Stair, P. C., Design Strategies for the Molecular Level Synthesis of Supported Catalysts. *Accounts of Chemical Research* **2012**, 45 (2), 206-214.
102. Williams, L. A.; Marks, T. J., Synthesis, Characterization, and Heterogeneous Catalytic Implementation of Sulfated Alumina Nanoparticles. Arene Hydrogenation and Olefin Polymerization Properties of Supported Organozirconium Complexes. *ACS Catalysis* **2011**, 1 (4), 238-245.
103. Wilmer, C. E.; Farha, O. K.; Bae, Y.-S.; Hupp, J. T.; Snurr, R. Q., Structure-property relationships of porous materials for carbon dioxide separation and capture. *Energy & Environmental Science* **2012**, 5, 9849-9856.
104. Wilmer, C. E.; Farha, O. K.; Yildirim, T.; Eryazici, I.; Krungleviciute, V.; Sarjeant, A. A.; Snurr, R. Q.; Hupp, J. T., Gram-scale, high-yield synthesis of a robust metal-organic framework for storing methane and other gases. *Energy & Environmental Science* **2013**, 6, 1158-1163.
105. Wilmer, C. E.; Leaf, M.; Lee, C. Y.; Farha, O. K.; Hauser, B. G.; Hupp, J. T.; Snurr, R. Q., Large-scale screening of hypothetical metal-organic frameworks. *Nature Chemistry* **2012**, 4, 83-89.
106. Wu, W. Q.; Bhattacharyya, K.; Gray, K.; Weitz, E., Photoinduced Reactions of Surface-Bound Species on Titania Nanotubes and Platinized Titania Nanotubes: An in Situ FTIR Study. *J Phys Chem C* **2013**, 117 (40), 20643-20655.
107. Wu, Y. Y.; Mashayekhi, N. A.; Kung, H. H., Au-metal oxide support interface as catalytic active sites. *Catalysis Science & Technology* **2013**, 3 (11), 2881-2891.
108. Yoon, T.; Chae, C.; Sun, Y.; Zhao, X.; Kung, H. H.; Lee, J. K., Bottom-up in situ formation of Fe<sub>3</sub>O<sub>4</sub> nanocrystals in a porous carbon foam for lithium-ion battery anodes. *Journal of Materials Chemistry* **2011**, 21 (43), 17325-17330.
109. Yuan, D.; Getman, R. B.; Wei, Z.; Snurr, R. Q.; Zhou, H.-C., Stepwise adsorption in a mesoporous metal-organic framework: Experimental and computational analysis. *Chemical Communications* **2012**, 48, 3297-3299.

110. Zhao, X.; Hayner, C. M.; Kung, H. H., Self-assembled lithium manganese oxide nanoparticles on carbon nanotube or graphene as high-performance cathode material for lithium-ion batteries. *Journal of Materials Chemistry* **2011**, *21* (43), 17297-17303.
111. Zhao, X.; Hayner, C. M.; Kung, M. C.; Kung, H. H., Flexible Holey Graphene Paper Electrodes with Enhanced Rate Capability for Energy Storage Applications. *ACS Nano* **2011**, *5* (11), 8739-8749.
112. Zhao, X.; Hayner, C. M.; Kung, M. C.; Kung, H. H., In-plane vacancy-enabled high-power Si-graphene composite electrode for lithium-ion batteries. *Adv Energy Mater* **2011**, *1* (6), 1079-1084.
113. Zhao, X.; Hayner, C. M.; Kung, M. C.; Kung, H. H., Photothermal-assisted fabrication of iron fluoride-graphene composite paper cathodes for high-energy lithium-ion batteries. *Chemical Communications* **2012**, *48* (79), 9909-9911.

**Uptake of Dihydrogen by  
Paramagnetic Metal  
Complexes**

Jack R. Norton  
Columbia University Department of Chemistry

**Presentation Abstract**

Hydrogen atom transfers from metal hydride catalysts can be used in olefin hydrogenations and isomerizations, radical cyclizations, and chain transfer during radical polymerizations. These transfers leave metalloradicals, which can sometimes react with hydrogen gas to reform the hydride complexes and make these reactions catalytic. We have studied the mechanism of these termolecular ( $2 M\cdot + H_2$ ) reactions in an attempt to improve catalyst efficiency.

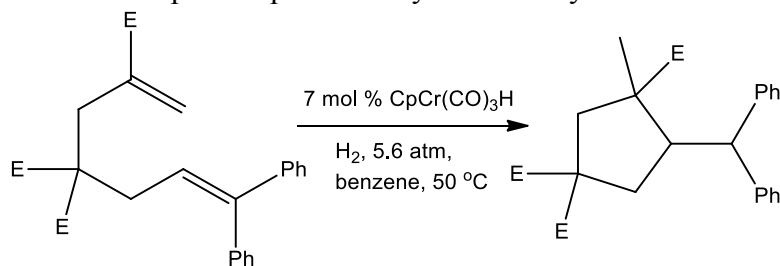
We have investigated the hydrogenation of  $2 \text{ CpCr(CO)}_3\cdot / [\text{CpCr(CO)}_3]_2$  to  $\text{CpCr(CO)}_3\text{H}$  as well as the thermodynamically unfavorable reaction of  $\text{Co(dmgBF}_2)_2\text{L}_2$  with hydrogen, and have found that both of these reactions are termolecular (first order in  $[H_2]$ , second order in  $[M\cdot]$ ). DFT calculations on the Cr reaction suggest that a sideways-bound  $H_2$  complex is too high in energy to be an intermediate, but that an end-on  $H_2$  complex is plausible. The mechanism probably involves either a collinear Cr..H..H..Cr transition state, or the heterolytic cleavage of an  $H_2$  between one Cr and a carbonyl oxygen on the other Cr. The cobaloximes must dissociate a ligand before  $H_2$  activation step occur — only the five-coordinate Co(II) species is reactive. We have quantified the position of the equilibrium for the reaction of cobaloximes with  $H_2$ , and have confirmed that the reaction is uphill, with a Co–H Bond Dissociation Free Energy of 50.5 kcal/mol. We believe these cobaloxime hydrides are involved in a tautomeric equilibrium with a ligand-protonated Co(I) species.

**DE-FG02-97ER14807: Catalytic Regeneration  
of Transition-Metal Hydrides for H Atom  
Transfer**

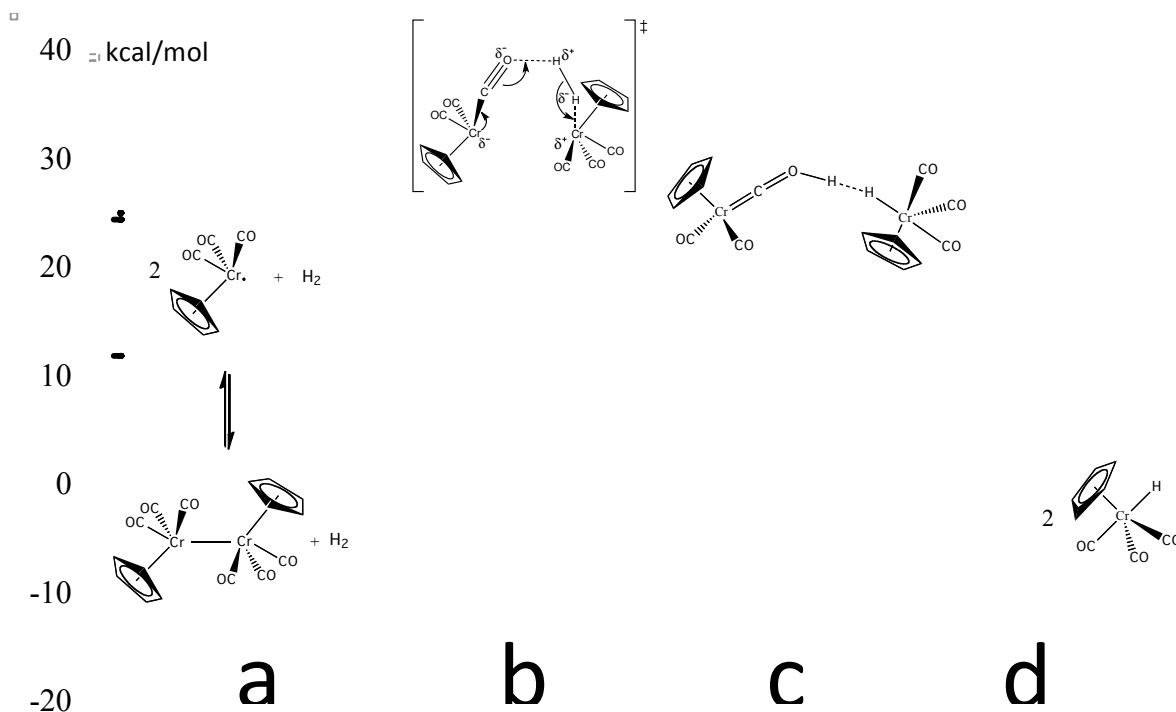
**Student(s):** Deven Estes and Gang Li

**RECENT PROGRESS**

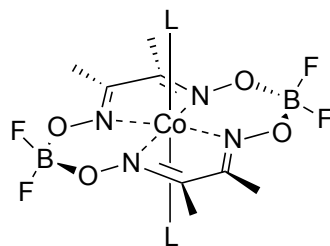
Hydrogen atom transfers from metal hydride catalysts can be used in olefin hydrogenations and isomerizations, radical cyclizations, and chain transfer during radical polymerizations. These transfers leave metalloradicals, which can sometimes react with hydrogen gas to reform the hydride complexes and make these reactions catalytic. We have studied the mechanism of these termolecular ( $2 M\cdot + H_2$ ) reactions in an attempt to improve catalyst efficiency.



One reaction we have studied is the hydrogenation of 2 CpCr(CO)<sub>3</sub>•/[CpCr(CO)<sub>3</sub>]<sub>2</sub> to CpCr(CO)<sub>3</sub>H. The reaction is second-order in Cr and first-order in H<sub>2</sub>, with a rate constant (if the rate law is written with [CpCr(CO)<sub>3</sub>•]<sup>2</sup>) of 12(2) M<sup>-2</sup>s<sup>-1</sup> at 25 °C in benzene. DFT calculations rule out a *side-on* H<sub>2</sub> complex as an intermediate, and suggest either (1) *homolytic* cleavage via a collinear Cr-H-H-Cr transition state, or (2) *end-on* approach of H<sub>2</sub> to one Cr as charge is transferred to the other, followed by *heterolytic* cleavage of the coordinated H<sub>2</sub> between the first Cr and the O of a carbonyl ligand on the second Cr, and eventual isomerization of the resulting *O*-protonated intermediate to CpCr(CO)<sub>3</sub>H.



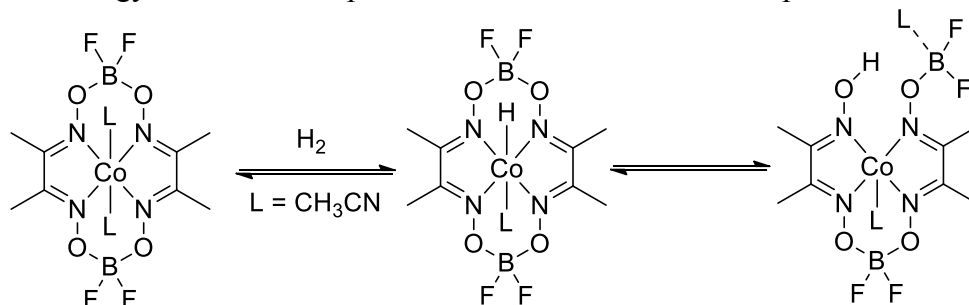
We have also studied the hydrogenation of cobaloximes, which are usually prepared as six-coordinate complexes with two solvent molecules (THF, MeOH, H<sub>2</sub>O, MeCN) as axial ligands. By using the tris(*p*-*tert*-butylphenyl)methyl radical Ar<sub>3</sub>C• as H• acceptor we have been able to study the kinetics of H<sub>2</sub> activation by cobaloximes. The reaction is independent of [Ar<sub>3</sub>C•], second-order in [Co], and first order in [H<sub>2</sub>]. By varying the concentration of added ligand we have shown that the mechanism involves a dissociative pre-equilibrium and obeys the rate law given below.



$$\frac{d[\text{Ar}_3\text{C-H}]}{dt} = k \left( \frac{K[\text{Co}]}{K + [\text{L}]} \right)^2 [\text{H}_2]$$

The reactive metalloradical is thus a five-coordinate cobalt(II) with a single axial ligand. Of the ligands examined, THF is the most weakly bound and gives the fastest reaction with H<sub>2</sub>. Strongly bound ligands like acetonitrile make the reaction very slow. The addition of PPh<sub>3</sub> to a cobaloxime produces only a five-coordinate species (a second phosphine does not bind), so additional PPh<sub>3</sub> has no effect on the rate of the reaction with H<sub>2</sub>.

The thermodynamics of H<sub>2</sub> uptake are important in catalyst choice. The production of a cobalt hydride by the reaction of cobaloximes with hydrogen gas is an unfavorable equilibrium at pressures around one atmosphere. While such hydrides have been proposed as intermediates in many catalytic cycles, they have not been directly observed. At pressures above 70 atm we can prepare and observe the formation of a Co(III) hydride from a cobaloxime, and can see a second species as well; we believe that the second species arises from tautomerism of the “hydride” to a ligand oxygen, as shown below. By varying the hydrogen pressure we have determined the bond dissociation free energy of the second species to be 50.5 kcal/mol and its pK<sub>a</sub> to be 13.4.



#### Publications Acknowledging this Grant in 2011-2014

1. Estes, D. P.; Vannucci, A. K.; Hall, A. R.; Lichtenberger, D. L. Thermodynamics of the metal-hydrogen bonds in ( $\eta^5\text{-C}_5\text{H}_5$ )M(CO)<sub>2</sub>H (M = Fe, Ru, Os). *Organometallics* **2011**, 30, 3444-3447.
2. Li, G.; Han, A.; Pulling, M. E.; Estes, D. P.; Norton, J. R. Evidence for Formation of a Co–H Bond from (H<sub>2</sub>O)<sub>2</sub>Co(dmgBF<sub>2</sub>)<sub>2</sub> under H<sub>2</sub> : Application to Radical Cyclizations. *J. Am. Chem. Soc.* **2012**, 134, 14662–14665.
3. Estes, D. P.; Norton, J. R.; Jockusch, S.; Sattler, W. Mechanisms by which Alkynes React with CpCr(CO)<sub>3</sub>H. Application to Radical Cyclization. *J. Am. Chem. Soc.* **2012**, 134, 15512– 15518.
4. Norton, J. R.; Spataru, T.; Camaioni, D. M.; Lee, S. J.; Li, G.; Choi, J.; Franz, J. A. Kinetics and Mechanism of the Hydrogenation of the CpCr(CO)<sub>3</sub>/[CpCr(CO)<sub>3</sub>]<sub>2</sub> Equilibrium to CpCr(CO)<sub>3</sub>H. *Organometallics* **2014**, Article ASAP, DOI: 10.1021/om4012399
5. Han, A.; Spataru, T.; Hartung, J.; Li, G.; Norton, J. R. Effect of Double Bond Substituents on the Rate of Cyclization of  $\alpha$ - Carbomethoxy Hex-5-enyl Radicals. *J. Org. Chem.* **2014** 79 (5), 1938–1946.

## Quantifying Active Sites in Supported Oxide Catalysts

Todd Eaton,[1] Andrew Boston, [1] Anthony Thompson, [1] Kimberly Gray, [2, 3] Justin Notestein [1, 3]

Northwestern University Department of Chemical and Biological Engineering  
Northwestern University Department of Civil and Environmental Engineering  
Northwestern University Center for Catalysis and Surface Science

### Presentation Abstract

The rational design and understanding of supported catalysts is greatly aided by the quantification of the number and nature of active sites. While direct particle imaging and EXAFS fitting are available for some materials, and a variety of chemisorption or redox probes exist for strong acid or reducible sites on supported oxides, quantification of weaker Lewis sites, especially for lighter oxides, is not routine, or minimally, requires *ex situ* spectroscopy. This is problematic, as many supported oxide catalysts undergo significant structural changes as surface densities increase from statistically isolated sites to monolayers and crystallites, so the number of kinetically relevant sites should not be assumed to be either the total or the geometrically-accessible surface sites. As part of a larger research program, herein are described selective titration methods for SiO<sub>2</sub>-supported TiO<sub>x</sub> and mixed TiO<sub>2</sub>-SiO<sub>2</sub> via phenylphosphonic acid (PPA) to quantify both the total fluid-accessible surface area and the number of sites participating in epoxidation of cyclooctene with H<sub>2</sub>O<sub>2</sub>. The latter method is entirely *in situ* and requires no additional spectroscopy or other experiments to quantify specifically the undercoordinated sites for H<sub>2</sub>O<sub>2</sub> activation. From these studies, we provide quantitative comparisons of TiO<sub>x</sub> dispersion on more than 22 materials; show that materials with poor average properties, as revealed by typical spectroscopy, can actually have large numbers of undercoordinated active sites; and unify observed rates over all materials, giving a single intrinsic turnover frequency when counting only the active sites. The latter measurement shows that different catalyst preparations principally control the number, but not the intrinsic reactivity, of these sites. Additional characterization of the chemisorbed PPA, and extensions of the technique to other materials will be shown.

## DE-SC0006718: Templating Routes to Supported Oxide Catalysts by Design

**Students:** Todd Eaton, [1] Zhenyu Bo, [2] Matthew Ardagh, [1] Andrew Korinda [1]

**Internal Student Collaborators:** Anthony Thompson, [1] Andrew Boston, [1] Mark Bachrach, [3] Nicholas Thornburg, [1] Scott Nauert, [1] Fabian Schax [4]

**Affiliations:** [1] Northwestern University Department of Chemical and Biological Engineering, [2] Northwestern University Department of Materials Science and Engineering, [3] Northwestern University Department of Chemistry, [4] Humbolt University Institute for Chemistry

### RECENT PROGRESS

**Goals and DOE Interest.** Supported oxide catalysts are critically important for fuels conversion, emissions control, and in the chemical industry. The foundations of catalyst development and understanding lie in the development of tools for investigating their structure, methods of interpreting reaction mechanisms, and techniques to design and synthesize supported oxide domains on the atomic scale. The latter remains a long-standing DOE grand challenge, and it is essential for advancements in catalysis since it enables findings from structural and functional studies to be translated into new catalyst designs in a rational manner.

Specifically sought is an understanding of the requirements for synthesizing and stabilizing isolated metal cations and small, supported oxide clusters and methods for evaluating these nanoscale domains, including new quantitative titration techniques and nanoparticle tagging. Small clusters, in particular, are believed to be present in important metalloenzyme active sites and exchanged zeolites, and have been assigned high reactivity in several transformations. However, such mimics are challenging to make unambiguously and as the dominant or only species on a surface (i.e. 'single-site materials'). Progress towards understanding and developing new oxide catalysts has been along three directions: 1) Developing synthesis-structure-function maps for catalytic metal oxides, 2) Templating catalytic domains via well-defined oxide cluster precursors, and 3) Templating catalytic domains via support design.

**Refining Synthesis-Structure-Function Relationships.** Since 2011, the PI has developed a route to controlling surface speciation of supported FeOx catalysts using the chelating ligand ethylenediamine tetraacetic acid (EDTA). The bulky, strongly-chelating, and net anionic Fe-EDTA complexes enforce unusually high levels of dispersion for FeOx-SiO<sub>2</sub> catalysts, as judged by XPS, XANES, DRUV-vis, and TPR, particularly when alkali countercations are used in catalyst precursors (e.g. NaFeEDTA). [1] The latter precursor gives verifiably 'single-site' oxide catalysts (**Fig. 1**) and using it as a starting point, a full map was developed for the reactivity of particular FeOx surface structures. It was shown that alkane oxidation rates (with H<sub>2</sub>O<sub>2</sub>) increased with increasingly basic alkali countercations, and that the alkali was required to be in stoichiometric equivalence with Fe. Rates were shown to be independent of structure for isolated cations and very small clusters, but that the latter were relatively uncommon (<10%) for more typical catalyst preparation routes. These results were expanded to understanding and controlling the redox activity of CeO<sub>2</sub> with FeOx, CuOx, and CoOx dopants. The M-EDTA precursors result in ~50% more redox active doped sites than for more traditional precursors, improving activity in, for example NO H<sub>2</sub>-SCR catalysis. [2] This work is also the basis for a recent patent application.

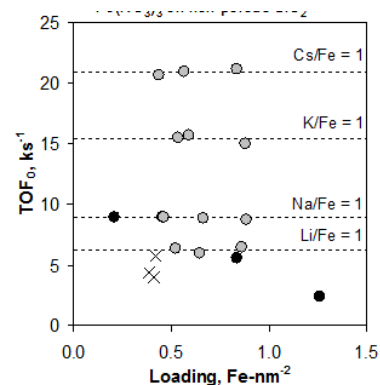


**Figure 1.** Alkali-dependent, single-site behavior (grey circles) in alkane oxidation using a Fe-EDTA precursor [1].

Parallel work partially supported by this program has focused on developing and understanding precursors for a variety of highly-dispersed metal oxides (TiO<sub>x</sub>, ZrO<sub>x</sub>, HfO<sub>x</sub>, NbO<sub>x</sub>, TaO<sub>x</sub>, MoO<sub>x</sub>, and WO<sub>x</sub>) on SiO<sub>2</sub> and Al<sub>2</sub>O<sub>3</sub> for use in epoxidation and, in a novel approach, hydrogenolysis. In the latter, it is shown that highly dispersed metal oxides (Ti, Ta, and Mo) on Al<sub>2</sub>O<sub>3</sub> are all capable of an unusual direct C-N bond cleavage of anilines and quinolines under 20 bar H<sub>2</sub> and relatively mild conditions, although the reactions are stoichiometric. [3]

In 2013 we determined structure and reactivity trends of TiO<sub>x</sub>-SiO<sub>2</sub> catalysts for benzyl alcohol photooxidation. [4] Here, phosphonic acid titration was developed as a surface-sensitive complement to XRD, XANES, and DRUV-vis. It was first shown that two precursors (an ethoxide and a bulky titanocene) give very different TiO<sub>x</sub> structures as judged by UV-edge energies, XANES pre-edge features, and crystallinity. Moreover, the number and surface density of geometrically-accessible sites, as titrated by phenylphosphonic acid, was very dependent on the synthesis method. A synthesis-structure-function map was developed, including fine gradations between, for example, polymeric TiO<sub>x</sub>, 2D anatase-like surfaces, and nanocrystalline anatase, which have not been previously proposed. In addition the geometrically accessible surface area from phenyl phosphonic acid titration was used to normalize all benzyl alcohol oxidation rates of the supported oxides, in spite of large differences in the aforementioned properties.

More recently, an *in situ* phosphonic acid titration method (Fig. 2) was used to assess the number of sites active in a liquid phase oxidation by TiO<sub>x</sub>-SiO<sub>2</sub> catalysts. [5] Added phenylphosphonic acid monotonically decreases the rate of cyclooctene epoxidation with H<sub>2</sub>O<sub>2</sub> in acetonitrile over all materials tested. From such plots, the intercept is the number of catalytically relevant sites; no assumptions or further characterization of the material is needed and thus this technique can be applied to 'unknown' samples. This data set has three significant findings: 1) some synthesis methods, such as the metalocalixarene route pioneered by the PI while still a PhD student, are quantitatively proven as the most disperse oxides, 2) mixed oxides that show evidence of aggregation into crystallites are not necessarily poor catalysts, due to the simultaneous presence of highly dispersed active sites not counted by most bulk characterization techniques, and 3) using the *in situ* titration data, epoxidation rates are normalized over 22 different supported oxide catalysts, showing that it is the number, not the intrinsic activity, that differs amongst the various materials. This method is now being applied to many other classes of catalyst.

**Templating via Well-Defined Oxide Precursors.** Here, we seek to control supported oxide catalyst structure via precursor design. Recent activity focused on completing a series of investigations with Mn triazacyclononane (TACN) complexes of different nuclearity as precursors to supported MnO<sub>x</sub>-SiO<sub>2</sub> catalysts that are more dispersed than typical precursors. Since 2011, we have sought to control the synthesis of multinuclear domains in supported oxides via choice of the precursor. We originally investigated the use of supported Mn(IV) triazacyclononane (TACN) complexes of different nuclearity

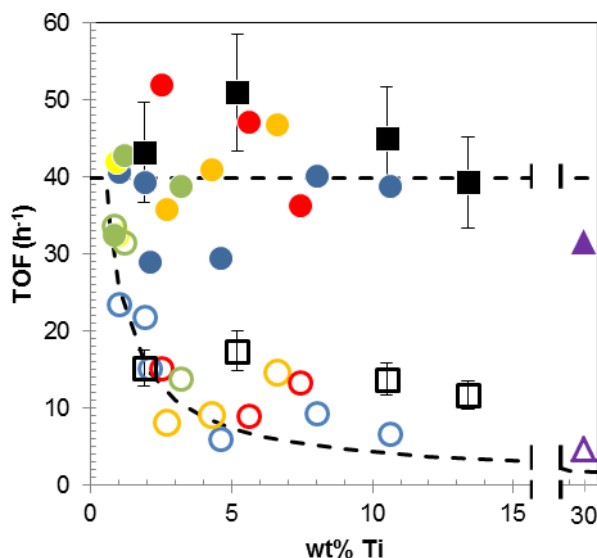


**Figure 2.** Cyclooctene epoxidation rates of 22 catalysts are normalized by phenylphosphonic acid titration (filled) in ways not captured by typical correlations against total Ti content. (open) [5]

(mononuclear **Mn1**, dinuclear **Mn2**, and tetranuclear **Mn4**, Mn(IV) oxide complexes) as alkane oxidation catalysts. Immobilized onto carboxylate-functionalized surfaces, these are catalysts for room-temperature alkane oxidation from the formation of carboxylate bridged structures of reduced oxidation state, as determined by EXAFS and XANES. [6]

In parallel, precursors **Mn1**, **Mn2**, and **Mn4** lead to unique structures of supported MnOx. After the complexes are deposited intact on SiO<sub>2</sub>, all catalysts autoreduce to Mn(III) oxides at 250°C or above, when the ligand decomposes. After this mild calcination temperature, 1<sup>st</sup> shell Mn-O fits increase monotonically from the **Mn1**, **Mn2**, and **Mn4** precursors. While unambiguous fits of such complex oxide structures are challenging, these results are consistent with higher nuclearity clusters from increasing nuclearity of the deposited precursor. [7] With more aggressive calcination, **Mn1**, **Mn2**, and **Mn4** precursors have similar coordination environments, and with no strong evidence of Mn-Mn interactions, unlike for a typical Mn(NO<sub>3</sub>)<sub>2</sub> precursor, which as begin to form small microcrystalline domains, even at 0.5 wt% loading.

In recent work, we have collaborated with researchers from the Humboldt University of Berlin to immobilize a hexameric Cu(I) complex on SiO<sub>2</sub> through wet impregnation from dry THF. This and related complexes have relatively short Cu-Cu distances (0.27 nm) and highly multidentate silanol ligands. These complexes are unstable in solution and oxidize irreversibly, but we have collected preliminary evidence that they remain as stable Cu(I) complexes in the solid state to ~450°C, much like Cu-exchanged zeolites. Preliminary experiments show these catalysts to have activity in cyclohexane ODH at 250-350°C, which is extraordinarily rare for Cu catalysts.

**Templating via Support Design.** Since 2011, we and collaborators have developed a new class of materials by partially overcoating a carrier (oxide) particle with <2nm of a second oxide by repetitive growth methods such as ALD. Molecular templates are used to generate nanocavities (nc) 1-2 nm in diameter whose walls and floor can be different oxide compositions. We have first shown that Al<sub>2</sub>O<sub>3</sub>-nc-TiO<sub>2</sub> imparts reactant selectivity to oxidations and reductions catalyzed by the underlying TiO<sub>2</sub>. [8] For example, in the oxidation of equimolar benzyl alcohol and more bulky alcohols to their respective aldehydes, relative rates increased from ~1.5:1 for TiO<sub>2</sub> to nearly 10:1 for the overcoated materials. Such selectivity had not, to our knowledge, been previously demonstrated in a formally non-porous oxide catalyst. We are developing a library of supports, templates, and oxide deposition techniques to expand this approach.

An open goal is to use the nanocavity space to template the growth of other catalytic domains, or to tag these sites with metal nanoparticles, which will also aid in imaging. In preliminary work, we have developed two techniques to 'backfill' these nanocavities with catalytic domains of a defined size: selective photoreduction onto partially masked TiO<sub>2</sub> surfaces, and selective strong electrostatic adsorption of cations onto exposed SiO<sub>2</sub> domains under near-neutral pH. In the first route, the nanoparticle density is limited by nucleation events, but the nanoparticle size is restricted by the nanocavity dimensions. (**Fig. 3**) In the second case, metal deposition is in proportion to the number of cavities, while their ultimate size is relatively constant. This work remains under development.

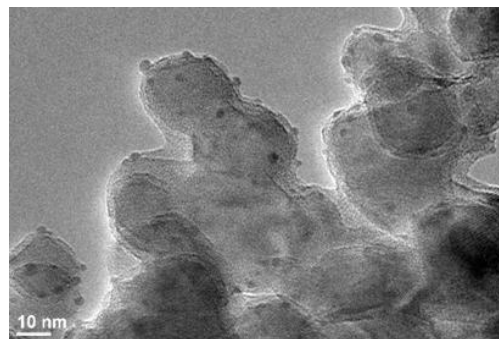


**Figure 3.** Representative TEM of Ag nanoparticles are deposited by photoreduction onto exposed TiO<sub>2</sub> domains on a SiO<sub>2</sub>-nc-TiO<sub>2</sub> nanocavity material. Nanoparticle sizes are controlled by the nanocavity.

### Publications Acknowledging this Grant in 2011-2014

1. Prieto-Centurion, D.; Boston, A.M.; Notestein, J.M., Structural and electronic promotion with alkali cations of silica-supported Fe(III) sites for alkane oxidation, *J. Catal.*, **2012**, *296*, 77-85.
2. Prieto-Centurion, D.; Roberts, C.A.; Fanson, P.A.; Notestein, J.M., H<sub>2</sub> SCR of NO over highly dispersed FeOx-CeO<sub>2</sub> catalysts. *J. Catal.* In preparation.
3. Bachrach, M.; Morlanes, N.; Canlas, C.P.; Miller, J.T.; Marks, T.J.; Notestein, J.M. Enhanced Hydrodenitrogenation Selectivity with Pd on Lewis acid-doped Alumina," *Catal. Lett.* **2014**, submitted.
4. Eaton, T.R.; Campos, M.P.; Gray, K.A.; Notestein, J.M. Quantifying accessible sites and reactivity on titania-silica (photo)catalysis: Refining TOF calculations, *J. Catal.* **2014**, *309*, 156-165.
5. Eaton, T.R.; Boston, A.M.; Thompson, A.B.; Gray, K.A.; Notestein, J.M. Counting Active Sites on TiOx-SiO<sub>2</sub> Catalysts via in situ Poisoning with Phenylphosphonic Acid. *Angew. Chem.* **2014**, submitted.
6. Korinda, A.W.; Schoenfeldt, N.J.; Notestein, J.M. Supported Mn triazacyclonane complexes as alkane oxidation catalysts. *ACS Catal.* In preparation.
7. Korinda, A.W.; Notestein, J.M. Mn triazacyclonane complexes as precursors to supported MnOx domains. *Appl. Catal. A*. In preparation.
8. Canlas, C.P.; Lu, J.L.; Ray, N.A.; Grosso-Giordano, N.A.; Elam, J.W.; Lee, S.; Winans, R.E.; Stair, P.C.; Van Duyne, R.P.; Notestein, J.M. Shape-Selective Sieving Layers on an Oxide Catalyst Surface, *Nature Chem.*, **2012**, *4*, 1030-1036.

## Catalysts for the Dehydrogenation of Formic acid and for the Functionalization of CO<sub>2</sub>

Wesley Sattler, Michelle C. Neary, Gerard Parkin  
Columbia University, Department of Chemistry

### Abstract

Formic acid has received considerable attention with respect to its potential as a chemical storage medium for hydrogen fuel *via* its catalytic dehydrogenation into CO<sub>2</sub> and H<sub>2</sub>. In this regard, we have observed that molybdenum complexes such as CpMo(CO)<sub>x</sub>(PMe<sub>3</sub>)<sub>3-x</sub>H ( $x = 1, 2, 3$ ) are capable of serving as catalysts for this transformation. Furthermore, these complexes are also capable of converting formic acid into methanol, which is subsequently converted to methyl formate. There is also much interest in converting CO<sub>2</sub> into useful chemicals and, in this regard, the zinc hydride complex, [*tris*(2-pyridylthio)methyl]zinc hydride ( $[\kappa^3\text{-Tptm}]\text{ZnH}$ ) is effective for the catalytic hydrosilylation of CO<sub>2</sub>. Specifically,  $[\kappa^3\text{-Tptm}]\text{ZnH}$  catalyzes the addition of (EtO)<sub>3</sub>SiH to CO<sub>2</sub> to give (EtO)<sub>3</sub>SiO<sub>2</sub>CH, which may subsequently be converted into useful chemicals such as ethyl formate or *N,N*-dimethylformamide. In addition to the direct reduction of CO<sub>2</sub>, the reduction of bicarbonate to formate has also garnered interest due to the fact that bicarbonates are easier to handle than CO<sub>2</sub> and, of relevance to this issue, we have demonstrated that the zinc bicarbonate complex  $[\kappa^4\text{-Tptm}]\text{ZnOCO}_2\text{H}$  reacts with PhSiH<sub>3</sub> at room temperature to give the formate derivative  $[\kappa^4\text{-Tptm}]\text{ZnO}_2\text{CH}$ .

### Fundamental Studies of Metal Centered Transformations Relevant to Catalysis

Students: Ahmed Al-Harbi, Ashley Zuzek, Yi Rong, Michelle Neary  
Contact: Department of Chemistry, Columbia University, New York, NY 10027;  
parkin@columbia.edu.

### Goals

The specific objectives and research goals of the research performed during the recent grant period have been to obtain information that is relevant to metal mediated transformations that produce useful chemicals from natural resources. For example, considerable effort is currently being directed towards (i) the implementation of a “hydrogen economy”, in which hydrogen serves as a fuel, and (ii) the use of ubiquitous carbon dioxide as a renewable C<sub>1</sub> source for the synthesis of useful chemicals. However, the practical realization of both of these objectives presents daunting challenges. For example, a principal problem with respect to the utilization of carbon dioxide as a chemical feedstock is concerned with the fact that it is not only thermodynamically a very stable molecule, but it is also kinetically resistant to many chemical transformations. Likewise, the energy efficient storage of hydrogen with a high volumetric energy density is a critical prerequisite to the implementation of a hydrogen economy. The discovery of new catalytic methods for (i) the rapid generation of hydrogen and (ii) the functionalization of CO<sub>2</sub> are crucial for advancing the use of hydrogen as a fuel and for utilizing CO<sub>2</sub> as an effective C<sub>1</sub> source for commodity chemicals.

## DOE Interest

An important objective of the Mission of the U. S. Department of Energy is to “Catalyze the timely, material, and efficient transformation of the nation’s energy system and secure U.S. leadership in clean energy technologies”. The research performed is of direct relevance to this goal because on demand production of hydrogen is essential for establishing a future hydrogen economy to transform the nation’s energy system. In addition, the effective utilization of carbon dioxide as a raw material for the chemical industry will contribute considerably to the efficient implementation of clean energy technologies. Furthermore, a fundamental understanding of the chemical aspects of catalysis is important because, as emphasized by the Catalysis Science core research area of the Department of Energy, Basic Energy Sciences: “Catalysts are crucial to creating new, energy-efficient routes for the production of basic chemical feedstocks and value-added chemicals.”

## Recent Progress

### 1. Reduction of Bicarbonate to Formate in Molecular Zinc Complexes

The use of carbon dioxide as a renewable C<sub>1</sub> source for the synthesis of useful chemicals is an important objective that is also of interest due to concerns regarding the impact of CO<sub>2</sub> on the environment. For example, the conversion of CO<sub>2</sub> to formic acid and formates has received much attention, not only because the principal industrial method involves an energy intensive sequence of transformations, but also because formic acid can serve as a material for energy storage *via* the release of H<sub>2</sub>. In addition to the direct reduction of CO<sub>2</sub>, the reduction of bicarbonate to formate has also garnered interest due to the fact that bicarbonates are easier to handle than CO<sub>2</sub>. For example, formic acid has been obtained by reduction of bicarbonate by using a formate-utilizing methanogen as a biocatalyst. There are, however, few reports concerned with the reduction of bicarbonate to formate in well-defined molecular systems. It is, therefore, significant that we have discovered that the bicarbonate complex  $[\kappa^4\text{-Tptm}]\text{ZnOCO}_2\text{H}$  reacts with PhSiH<sub>3</sub> at room temperature to give the formate derivative  $[\kappa^4\text{-Tptm}]\text{ZnO}_2\text{CH}$ . Isotopic labeling studies, however, indicate that the mechanism does not proceed *via* a direct exchange between the bicarbonate ligand and PhSiH<sub>3</sub>, but rather occurs *via* the initial formation of the zinc hydride complex  $[\kappa^3\text{-Tptm}]\text{ZnH}$  *via* metathesis of the Zn–OCO<sub>2</sub>H and PhH<sub>2</sub>Si–H bonds. Subsequent decomposition of the incipient silyl bicarbonate PhSiH<sub>2</sub>OCO<sub>2</sub>H releases CO<sub>2</sub> that is trapped by the zinc hydride  $[\kappa^3\text{-Tptm}]\text{ZnH}$  to give the formate derivative  $[\kappa^4\text{-Tptm}]\text{ZnO}_2\text{CH}$ .

### 2. Catalysts for the Release of H<sub>2</sub> from Formic Acid

Recent interest has focused on the use of formic acid as a hydrogen storage medium because it is a liquid at room temperature and, as such, is easy to handle and transport. It is, therefore, of considerable interest to develop more efficient catalysts for the release of H<sub>2</sub> from formic acid that incorporate earth abundant metals. As such, we have investigated the ability of the series of molybdenum compounds, CpMo(PMe<sub>3</sub>)<sub>3-x</sub>(CO)<sub>x</sub>H and Cp\*Mo(PMe<sub>3</sub>)<sub>3-x</sub>(CO)<sub>x</sub>H (*x* = 1, 2, or 3), because the electronic impact of progressively substituting PMe<sub>3</sub> for CO ligands will provide a means to evaluate mechanistic possibilities. Significantly, although all of the compounds, CpMo(PMe<sub>3</sub>)<sub>3-x</sub>(CO)<sub>x</sub>H and Cp\*Mo(PMe<sub>3</sub>)<sub>3-x</sub>(CO)<sub>x</sub>H, serve as catalysts for the release of H<sub>2</sub> and CO<sub>2</sub> from formic acid, their activity varies considerably. For example, the bis(trimethylphosphine) compounds Cp<sup>R</sup>Mo(PMe<sub>3</sub>)<sub>2</sub>(CO)H are much more active than either Cp<sup>R</sup>Mo(PMe<sub>3</sub>)(CO)<sub>2</sub>H or Cp<sup>R</sup>Mo(CO)<sub>3</sub>H (Cp<sup>R</sup> = Cp, Cp\*). Interestingly,

while H<sub>2</sub> and CO<sub>2</sub> are the primary products of decomposition of formic acid, methanol and methyl formate are also formed. The methanol that is formed is a product of hydrogenation of the formic acid, while the methyl formate is a result of subsequent esterification. The amount of methanol/methyl formate that is produced relative to the amount of formic acid consumed is dependent on the catalyst, with the tricarbonyl compounds CpMo(CO)<sub>3</sub>H and Cp\*Mo(CO)<sub>3</sub>H exhibiting greater selectivities than the PMe<sub>3</sub> derivatives, Cp<sup>R</sup>Mo(PMe<sub>3</sub>)(CO)<sub>2</sub>H and Cp<sup>R</sup>Mo(PMe<sub>3</sub>)<sub>2</sub>(CO)H. Furthermore, CpMo(PMe<sub>3</sub>)<sub>2</sub>(CO)H is more selective for formation of methanol/methyl formate than is Cp\*Mo(CO)(PMe<sub>3</sub>)<sub>2</sub>H.

### 3. Si–H and Si–C Bond Cleavage Reactions

The interaction of Si–H bonds with transition metal compounds is of fundamental interest, not only because it is a key step in hydrosilylation, dehydrogenative Si–H/O–H coupling, and dehydrogenative polymerization of silanes, but also because it provides a model for the corresponding interactions of C–H bonds with metal centers. By comparison to substituted silanes, however, the reactivity of SiH<sub>4</sub> towards transition metal compounds has received relatively little attention. Therefore, it is significant that we have now demonstrated that Mo(PMe<sub>3</sub>)<sub>6</sub> cleaves the Si–H bond of SiH<sub>4</sub> at room temperature to give the bis(silyl) compound Mo(PMe<sub>3</sub>)<sub>4</sub>(SiH<sub>3</sub>)<sub>2</sub>H<sub>2</sub>. The latter compound reacts with H<sub>2</sub> to generate Mo(PMe<sub>3</sub>)<sub>4</sub>(SiH<sub>3</sub>)H<sub>3</sub> and measurement of the equilibrium constant provides the estimate that the Mo–H BDE is *ca.* 7 kcal mol<sup>-1</sup> stronger than the Mo–SiH<sub>3</sub> bond. While a simple mechanism for the formation of Mo(PMe<sub>3</sub>)<sub>4</sub>(SiH<sub>3</sub>)H<sub>3</sub> upon treatment of Mo(PMe<sub>3</sub>)<sub>4</sub>(SiH<sub>3</sub>)<sub>2</sub>H<sub>2</sub> with H<sub>2</sub> could involve reductive elimination of SiH<sub>4</sub> followed by oxidative addition of H<sub>2</sub>, isotope labeling studies indicate that such a mechanism, which is commonly invoked for non-*d*<sup>0</sup> metal phosphine hydride compounds, does not operate. Rather, the mechanism is proposed to involve metathesis between the Mo–H and D–SiD<sub>3</sub> bonds. Mo(PMe<sub>3</sub>)<sub>6</sub> also undergoes facile oxidative addition of Si–H bonds of PhSiH<sub>3</sub> at room temperature to give the bis(phenylsilyl) compound, Mo(PMe<sub>3</sub>)<sub>4</sub>(SiH<sub>2</sub>Ph)<sub>2</sub>H<sub>2</sub>, which, in the presence of excess PhSiH<sub>3</sub> forms the *silyl* (SiH<sub>3</sub>) compounds Mo(PMe<sub>3</sub>)<sub>4</sub>(SiH<sub>2</sub>Ph)(SiH<sub>3</sub>)H<sub>2</sub>, Mo(PMe<sub>3</sub>)<sub>4</sub>(SiH<sub>3</sub>)<sub>2</sub>H<sub>2</sub> and Mo(PMe<sub>3</sub>)<sub>4</sub>(SiH<sub>3</sub>)H<sub>3</sub>. Interestingly, the reactivity of Ph<sub>2</sub>SiH<sub>2</sub> towards Mo(PMe<sub>3</sub>)<sub>6</sub> is quite distinct from that of either PhSiH<sub>3</sub> or SiH<sub>4</sub> and has resulted in the isolation of several novel compounds, namely Mo(PMe<sub>3</sub>)<sub>4</sub>(κ<sup>2</sup>-H<sub>2</sub>-H<sub>2</sub>SiPh<sub>2</sub>)H, Mo(PMe<sub>3</sub>)<sub>3</sub>(κ<sup>2</sup>-H<sub>2</sub>-H<sub>2</sub>Si<sub>2</sub>Ph<sub>4</sub>)H<sub>2</sub> (the first example of a disilane complex) and Mo(PMe<sub>3</sub>)<sub>3</sub>(σ-HSiHPh<sub>2</sub>)H<sub>4</sub>.

### 4. Application of [O<sub>3</sub>] Ligands as Platforms for Early Transition Metal Olefin Polymerization

#### Catalysts

While cyclopentadienyl ligands are ubiquitous in olefin polymerization catalysis, we rationalize that related L<sub>2</sub>X donor ligands that present an [O<sub>3</sub>] array could also provide catalysts with useful properties. Specifically, we postulate that the oxygen rich environment provided by the *tris*(oxoimidazolyl)hydroborato ligand system, [To<sup>R</sup>], could provide more robust catalysts for oxophilic metal centers that are less sensitive towards degradation. In this regard, we have synthesized a series of zirconium benzyl compounds, namely [To<sup>RBenz</sup>]Zr(CH<sub>2</sub>Ph)<sub>3</sub> (R = Me, Bu<sup>t</sup>, 1-Ad). Treatment of [To<sup>Bu<sup>t</sup>Benz</sup>]Zr(CH<sub>2</sub>Ph)<sub>3</sub> with [PhNM<sub>2</sub>H][B(C<sub>6</sub>F<sub>5</sub>)<sub>4</sub>] in ether gives cationic {[To<sup>Bu<sup>t</sup>Benz</sup>]Zr(CH<sub>2</sub>Ph)<sub>2</sub>(OEt<sub>2</sub>)}[B(C<sub>6</sub>F<sub>5</sub>)<sub>4</sub>], which has been isolated and structurally characterized by X-ray diffraction. Although six-coordinate {[To<sup>Bu<sup>t</sup>Benz</sup>]Zr(CH<sub>2</sub>Ph)<sub>2</sub>(OEt<sub>2</sub>)}[B(C<sub>6</sub>F<sub>5</sub>)<sub>4</sub>] exhibits low ethylene

polymerization activity, activation of  $[\text{To}^{\text{RBenz}}]\text{Zr}(\text{CH}_2\text{Ph})_3$  ( $\text{R} = \text{Bu}^t, 1\text{-Ad}$ ) in benzene solution generates a five-coordinate species  $\{[\text{To}^{\text{RBenz}}]\text{Zr}(\text{CH}_2\text{Ph})_2\}^+$  that exhibits very high activity.

### Future Plans

Future studies will include, for example, further development of (i) molybdenum and tungsten compounds as catalysts for decarboxylation and disproportionation of formic acid, and as hydrosilylation catalysts, (ii) the use of  $[\text{O}_2]$  and  $[\text{O}_3]$  as platforms early metal catalysts, and (iii) the use of zinc compounds in the functionalization of  $\text{CO}_2$  and other substrates.

### Publications (2011 – 2014)

1. Al-Harbi, A.; Sattler, W.; Sattler, A.; Parkin, G. "Synthesis and Structural Characterization of Tris(2-oxo-1-t-butylimidazolyl) and Tris(2-oxo-1-methylbenzimidazolyl)hydroborato Complexes: A New Class of Tripodal Oxygen Donor Ligand." *Chem. Commun.* **2011**, 47, 3123-3125.
2. Sattler, A.; Parkin, G. "Carbon–Sulfur Bond Cleavage and Hydrodesulfurization of Thiophenes by Tungsten." *J. Am. Chem. Soc.* **2011**, 133, 3748-3751.
3. Sattler, A.; Janak, K. E.; Parkin, G. "Modeling Aspects of Hydrodesulfurization by Molybdenum Hydride Compounds: Desulfurization of Thiophene and Benzothiophene and C–S Bond Cleavage of Dibenzothiophene." *Inorg. Chim. Acta* **2011**, 369, 197-202.
4. Sattler, A.; Rucolo, S.; Parkin, G. "Structural Characterization of  $\text{TaMe}_3\text{Cl}_2$  and  $\text{Ta}(\text{PMe}_3)_2\text{Me}_3\text{Cl}_2$ , a Pair of Five and Seven-Coordinate  $d^0$  Tantalum Methyl Compounds." *Dalton Trans.* **2011**, 40, 7777-7782.
5. Sattler, A.; Parkin, G. "Formation of a Cationic Alkylidene Complex via Formal Hydride Abstraction: Synthesis and Structural Characterization of  $[\text{W}(\text{PMe}_3)_4(\eta^2\text{-CHPMe}_2)\text{H}]\text{X}$  ( $\text{X} = \text{Br}, \text{I}$ )." *Chem. Commun.* **2011**, 47, 12828–12830.
6. Sattler, A.; Parkin, G. "A New Class of Transition Metal Pincer Ligand: Tantalum Complexes that Feature a  $[\text{CCC}] \text{X}_3$ -Donor Array Derived from a Terphenyl Ligand." *J. Am. Chem. Soc.* **2012**, 134, 2355–2366.
7. Sattler, W.; Parkin, G. "Zinc Catalysts for On Demand Hydrogen Generation and Carbon Dioxide Functionalization." *J. Am. Chem. Soc.* **2012**, 134, 17642-17465.8. Rong, Y.; Al-Harbi, A.; Parkin, G. "Highly Variable Zr–CH<sub>2</sub>–Ph Bond Angles in Tetrabenzylzirconium: Analysis of Benzyl Ligand Coordination Modes." *Organometallics* **2012**, 31, 8208-8217.
9. Green, J. C.; Green, M. L. H.; Parkin, G. "The Occurrence and Representation of Three-Centre Two-Electron Bonds in Covalent Inorganic Compounds." *Chem. Commun.* **2012**, 48, 11481–11503.
10. Shin, J. H.; Churchill, D. G.; Parkin, G. "Bis( $\eta^5$ -pentamethylcyclopentadienyl) Complexes of Molybdenum." *Inorganic Syntheses*, **2014**, 36, 58-62.
11. Sattler, W.; Parkin, G. "Reduction of Bicarbonate and Carbonate to Formate in Molecular Zinc Complexes." *Catal. Sci. Tech. Catal. Sci. Tech.* **2014**, 4, 1578–1584.
12. Zuzek, A. A.; Parkin, G. "Si–H and Si–C Bond Cleavage Reactions of Silane and Phenylsilanes with  $\text{Mo}(\text{PMe}_3)_6$ : Silyl, Hypervalent Silyl, Silane, and Disilane Complexes." *J. Am. Chem. Soc.* <http://dx.doi.org/10.1021/ja503368j>.

**A Combined DFT+KMC Study of Selective Oxidation of NH<sub>3</sub> on Rutile RuO<sub>2</sub>(110) at Ambient Pressures**

Talat S. Rahman, Sampyo Hong and S. Islamuddin Shah

University of Central Florida

**Presentation Abstract**

Ruthenium dioxide has attracted considerable interest as a possible substitute for platinum-based industrial catalysts for ammonia oxidation ever since Wang et al [1] showed RuO<sub>2</sub>(110) to exhibit NO selectivity around 530 K, under UHV conditions. Related density functional theory (DFT) based kinetic Monte Carlo (KMC) simulations [2] provided further support for this selectivity. Perez et al [3], however, find N<sub>2</sub> to be the dominant product in experiments at ambient pressure on polycrystalline RuO<sub>2</sub> samples. To address possible pressure and/or material gap in the products, we have extended our DFT-based KMC calculations to include reactions rates for a large set of reaction intermediates that may be found under ambient conditions. We have also carried out simulations using data-bases proposed by Perez et al [3] and others. Interestingly, our KMC simulations [4] using any of the above databases show NO to be the dominant species under UHV conditions at or above the peak NO desorption temperature, in accordance with Wang et al. [1]. On the other hand, we find N<sub>2</sub> to be the dominant product under ambient conditions. The rationale for the pressure gap is the activation of secondary reaction of NO i.e. active formation and decomposition of N<sub>2</sub>O to N<sub>2</sub>, owing to sufficient supply of N species, which is a result of active NH<sub>x</sub> decomposition by plentiful O species on RuO<sub>2</sub>(110). Furthermore, we show that reliable prediction of selectivity requires consideration of competing reaction processes as made feasible in kinetic simulations such as KMC.

[1] Y. Wang, K. Jacobi, W. -D Schone, G. Ertl, *J. Phys. Chem.B* 109, 7883 (2005)

[2] S. Hong, A. Karim, T.S. Rahman, K. Jacobi, and G. Ertl, *J. Catal.*, 276, 371 (2010).

[3] J. Perez-Ramirez, N. Lopez, and E. V. Kondratenko, *J. Phys. Chem. C* 114, 16660 (2010).

[4] S.I. Shah, S. Hong, and T.S. Rahman, *J. Phys. Chem. C* 118, 5226-5238 (2014).

**DE-FG02-07ER15842: Controlling Structural, Electronic, and Energy Flow Dynamics of Catalytic Processes through Tailored Nanostructures**

**PI:** Talat S. Rahman ; **Co PI :** Ludwig Bartels

**Postdocs:** Duy Le, Sampyo Hong

**Students:** Wenhao Lu, Koichi Yamaguchi, Chen Wang, Quan Ma, Miguel Isarraraz, Michael Gomez, Cindy Merida, Takat B. Rawal, Maral Aminpour, S. Islamuddin Shah, Ghazal Shafai

**Affiliations:** University of Central Florida and University of California, Riverside

**RECENT PROGRESS**

(See main abstract with Bartels as presenter)

***Ab Initio* Studies of CO Adsorption and Oxidation on Graphene–Pt<sub>13</sub> Nanocomposites**

Ashwin Ramasubramaniam, Ioanna Fampiou  
Department of Mechanical & Industrial Engineering, University of Massachusetts Amherst

**Presentation Abstract**

Pt nanoclusters on carbon supports have been shown to possess superior catalytic activity and increased selectivity in a variety of electrochemical reactions as compared to bulk Pt electrodes; however, the underlying mechanisms remain poorly understood. We examine the interaction of Pt nanoclusters with point defects in graphene using first-principles density functional theory. The presence of defects in graphene supports enhances the Pt-carbon bonding, which can suppress cluster sintering thus allowing for sustained catalytic performance. Furthermore, stronger binding of clusters at defects is found to substantively decrease the strength of CO binding thus increasing the tolerance of bound Pt nanoparticles towards CO poisoning. Finally, we examine the role of defective graphene supports on the activity of the cluster for the CO oxidation reaction and obtain estimates for CO-oxidation kinetics. Our results suggest possible avenues for controlling the dispersion and catalytic activity of Pt nanoclusters on carbon supports via defect engineering.

**DE-SC0010610: Computational Design of Graphene–Nanoparticle Catalysts**

**PI:** Dr. Ashwin Ramasubramaniam

**Students:** Ms. Ioanna Fampiou, Mr. Raymond Gasper, Mr. Hongbo Shi

**RECENT PROGRESS**

***CO Adsorption and Oxidation on Graphene-Supported Pt<sub>13</sub> Nanoclusters***

We have systematically investigated the binding of CO to catalytically active Pt<sub>13</sub> nanoclusters. CO is a well-known catalyst poison and also the thermodynamic sink in several energy conversion pathways of interest to us such as methanol or formic acid decomposition. Efficient removal of CO by oxidation is thus critical for ensuring sustained catalytic performance. Graphene-supported Pt nanoclusters have been shown in experiments to possess improved tolerance towards CO poisoning although the precise mechanism that leads to this effect is not understood. We have made significant progress in unraveling, at the electronic structure level, the cause of this improved tolerance and establishing the key role of cluster–substrate interactions. [1]

In previous work we established that defects in graphene substrates act as strong binding sites for Pt nanoclusters through the formation of strong Pt–C bonds. In addition to stabilizing clusters against sintering, the formation of these strong Pt–C bonds causes a downshift in the average position of the cluster *d*-band, which is then expected to lead to weaker adsorption of molecules on the cluster. [2] In our most recent work, [1] we have explicitly investigated CO binding on unsupported and graphene-supported clusters. In general, the adsorption energy of CO to a

binding site depends sensitively upon the coordination of cluster the atom(s) at the binding site. For Pt nanoclusters, which typically display several near-degenerate isomers, this variability in local coordination results in variations in CO binding energy of  $\sim 0.2$  eV, an order of magnitude smaller than the binding energy. [1] To a good approximation then, variability in coordination of cluster atoms can be averaged out by statistical sampling over several configurations of adsorbed CO molecules. The remaining differences in CO binding energies can then be attributed to cluster–substrate interactions and systematically analyzed. Figure 1 displays the average adsorption energy of CO on unsupported and supported Pt<sub>13</sub> clusters as a function of the cluster  $d$ -band center, which in turn is affected by the strength of binding between the cluster and the graphene support. For defective support, the cluster–support binding is much stronger leading to a downshift of the  $d$ -band center relative to the Fermi level. This in turn leads to weaker adsorption of CO on the cluster and provides one possibility for employing defect engineering of substrates as a means of controlling cluster catalytic activity. Similar results have been obtained for oxygen binding as well.

While the weaker adsorption energy of CO on defective-graphene-supported Pt nanoclusters provides a possible explanation for improved CO tolerance of Pt-graphene nanocomposites, it does not furnish proof (other than through indirect Bronsted-Evans-Polyani arguments) of a reduced reaction barrier for CO oxidation. To conclusively establish this, we are now in the process of performing systematic DFT calculations of CO oxidation on supported and unsupported Pt<sub>13</sub> nanoclusters. [3] Given that CO binding to Pt<sub>13</sub> clusters is substantially stronger (by 0.7-0.8 eV) than O, the Pt cluster is expected to be *fully saturated* by CO under normal operating conditions. Therefore, we have gone beyond looking at single-CO adsorption studies and systematic saturated and optimized Pt<sub>13</sub> clusters with DFT. Studies of CO oxidation on these clusters via a CO\*-assisted O<sub>2</sub> activation without the involvement of adsorbed O<sub>2</sub>\* precursors, which is expected to be favored over the Langmuir-Hinshelwood mechanism, [4] are currently underway. An interesting and unexpected outcome of

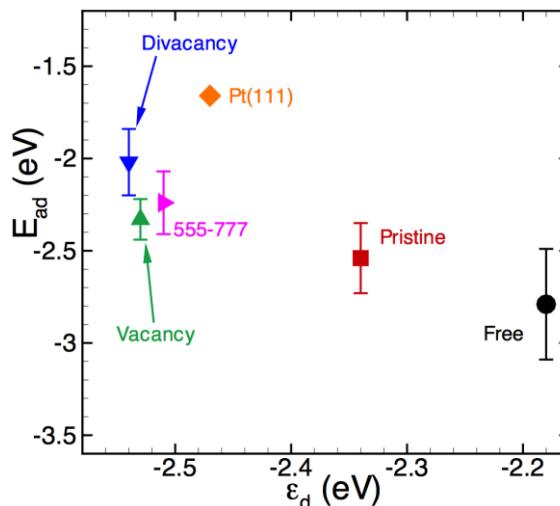


**Figure 1:** CO adsorption energy ( $E_{ad}$ ) as a function of  $d$ -band center ( $\epsilon_d$ ) relative to the Fermi energy for supported Pt<sub>13</sub> clusters, free Pt<sub>13</sub> clusters, and Pt(111) surface. A downshift of the cluster  $d$ -band center with respect to the Fermi level (more negative  $\epsilon_d$ ) is directly correlated with weaker adsorption of CO on the cluster. Error bars indicate 95% confidence intervals obtained from sampling over multiple adsorption sites on the cluster.

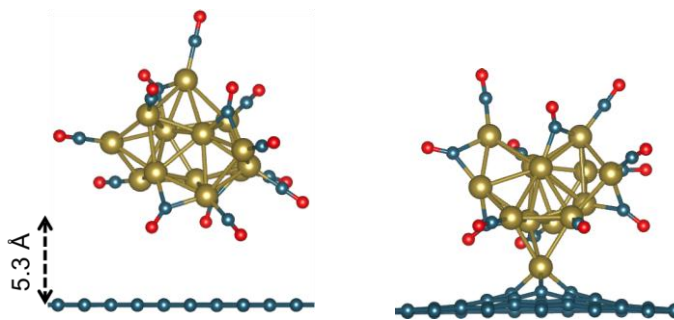


**Figure 2:** (Left) Spontaneous desorption of a Pt<sub>13</sub> cluster from a pristine graphene support upon saturation with CO. (Right) CO-saturated Pt<sub>13</sub> cluster bound to a vacancy in the graphene support.

studies of CO saturation of Pt<sub>13</sub> clusters is shown in Figure 2. As seen, for a cluster supported on pristine graphene, CO can intercalate between the support and the cluster, bind to the cluster, and cause complete desorption of the cluster from the support, leading to catalyst loss. Such cluster desorption does not occur when a cluster is bound to a support defect though (which we have confirmed more thoroughly with high-temperature *ab initio* MD simulations) further emphasizing the role of support defects in stabilizing catalyst clusters.

### **References**

- [1] Fampiou, I.; Ramasubramaniam, A. CO Adsorption on Defective Graphene-Supported Pt<sub>13</sub> Nanoclusters, *J. Phys. Chem. C* **2013**, *117*, 19927-19933.
- [2] Fampiou, I.; Ramasubramaniam, A. Binding of Pt nanoclusters to defects in graphene: adsorption, morphology, and electronic structure, *J. Phys. Chem. C* **2012**, *116*, 6543-6555.
- [3] Fampiou, I.; Ramasubramaniam, A. The Influence of Support Effects on CO Oxidation Kinetics on Graphene-Supported Pt<sub>13</sub> Nanoclusters, in preparation.
- [4] Allian, A. D.; Takanabe, K.; Fajdala, K. L.; Hao, X.; Trues, T. J.; Cai, J.; Buda, C.; Neurock, M.; Iglesia, E. Chemisorption of CO and mechanism of CO oxidation on supported platinum clusters, *Journal of the American Chemical Society* **2011**, *133*, 4498-4517

### **Publications Acknowledging this Grant in 2011-2014**

1. Fampiou, I.; Ramasubramaniam, A. CO Adsorption on Defective Graphene-Supported Pt<sub>13</sub> Nanoclusters, *J. Phys. Chem. C* **2013**, *117*, 19927.

John J. Rehr

**Understanding supported Pt nanoparticles by combining theoretical and experimental spectroscopy and ab initio molecular dynamics**

J. J. Rehr,<sup>1</sup> F. D. Vila,<sup>1</sup> J. J. Kas,<sup>1</sup> Y. Li,<sup>2</sup> A. I. Frenkel,<sup>2</sup> U. Jung,<sup>3</sup> A. Elsen,<sup>3</sup> R. G. Nuzzo,<sup>3</sup> C. S. Bonifacio<sup>4</sup>  
J. C. Yang,<sup>4</sup>

<sup>1</sup>Dept. of Physics, Univ. of Washington, Seattle,<sup>2</sup>Dept. of Physics, Yeshiva University, New York, <sup>3</sup>Dept. of Chemistry, Univ. of Illinois Urbana-Champaign, Urbana, IL, <sup>4</sup>Dept. of Mat. Science and Eng. and Dept. of Chem. Eng., Univ. of Pittsburgh, Pittsburgh

**Presentation Abstract**

Supported Pt nanoparticles are of wide interest in nanoscale physics and chemical sciences, and have many industrial applications in energy research. Yet, a microscopic understanding of their structure and catalytic behavior is far from complete. Experimental probes such as x-ray absorption spectroscopy (XAS) typically yield globally averaged properties, e.g., mean bond distances, which alone can give a misleading characterization of their behavior. Here we present a combination of ab initio molecular dynamics simulations and theoretical and experimental spectroscopy methods to obtain a more detailed microscopic understanding that includes their interactions with adsorbates and the support. For example, experimental observations by our team show that CO absorption affects both their conformational and electronic structure: First, the mean Pt-Pt bond lengths increase with CO coverage. Second, the non-resonant XES L<sub>3</sub>-alpha emission line and XANES L<sub>3</sub> absorption edge show opposite shifts with increasing temperature. Third, experimental RIXS data have a main peak that shifts toward higher energy loss with increasing CO coverage. Remarkably our theoretical simulations for small supported Pt clusters reproduce all three observations. Also the shifts in RIXS spectra are explained in terms of movement of the d-band center relative to the Fermi level. Finally, finite temperature density functional theory molecular dynamics (DFT/MD) simulations of Pt nanoclusters under *operando* conditions show that the nanoscale cluster structure and charge distribution are inhomogeneous and dynamically fluctuating over several time-scales, ranging from fast (200-400 fs) bond vibrations to slow fluxional bond breaking (>10 ps). Indeed, we find that this anomalous behavior can be attributed to “dynamic structural disorder” (DSD) driven by stochastic motion of the center of mass over 1-4 ps time-scales.

**Grant Number: DE FG02-03ER15476**

**Grant Title: The Reactivity and Structural Dynamics of Supported Metal Nanoclusters Using Electron Microscopy, *in situ* X-Ray Spectroscopy, Electronic Structure Theories, and Molecular Dynamics Simulations.**

**PIs:** Ralph G. Nuzzo, John J. Rehr, Anatoly I. Frenkel, Judith C. Yang,  
**Postdocs:** F. D. Vila J. J. Kas, A. Elsen, C. Bonifacio, U. Jung, S. Zhao, Y. Li

**RECENT PROGRESS**

1) *Effects of adsorbate coverage and bond length disorder on the d-band behavior in carbon-supported Pt catalysts*  
Determination of the factors that affect the d-band center of catalysts is required to explain their catalytic properties. Resonant inelastic X-ray scattering (RIXS) enables direct imaging of electronic transitions in the d-band of Pt catalysts in real time and in realistic environmental conditions. Through a combination of *in situ*, temperature-resolved RIXS measurements and theoretical simulations we isolated and quantified the effects of bond-length disorder and adsorbate coverage (CO and H<sub>2</sub>) on the d-band center of 1.25 nm size Pt catalysts supported on carbon. We obtained that the decrease in adsorbate coverage at elevated temperatures is responsible for the d-band shifts towards higher energies relative to the Fermi level, whereas the effect of the increase in bond-length disorder on the d-band center is negligible. Although these results were

obtained for a specific case of non-interacting support and weak temperature dependence of the metal-metal bond length in a model catalyst, this work can be extended to a broad range of catalysts in real catalytic reactions. Our RIXS experiments were performed at the ESRF beamline ID26, in collaboration with **M. Tromp** (TUM, Germany). **J. Rehr** and his group have developed the simulation method to calculate RIXS theoretically and compare with experimental data (Fig. 1). These methods allow to directly compare the effects of coverage and strain on the d-band center behavior and, hence, catalytic activity of supported noble metal catalysts. This work has been published in *Small, M.W. et al., Chem. Phys. Chem. 2014, DOI: 10.1002/cphc.201400055*.

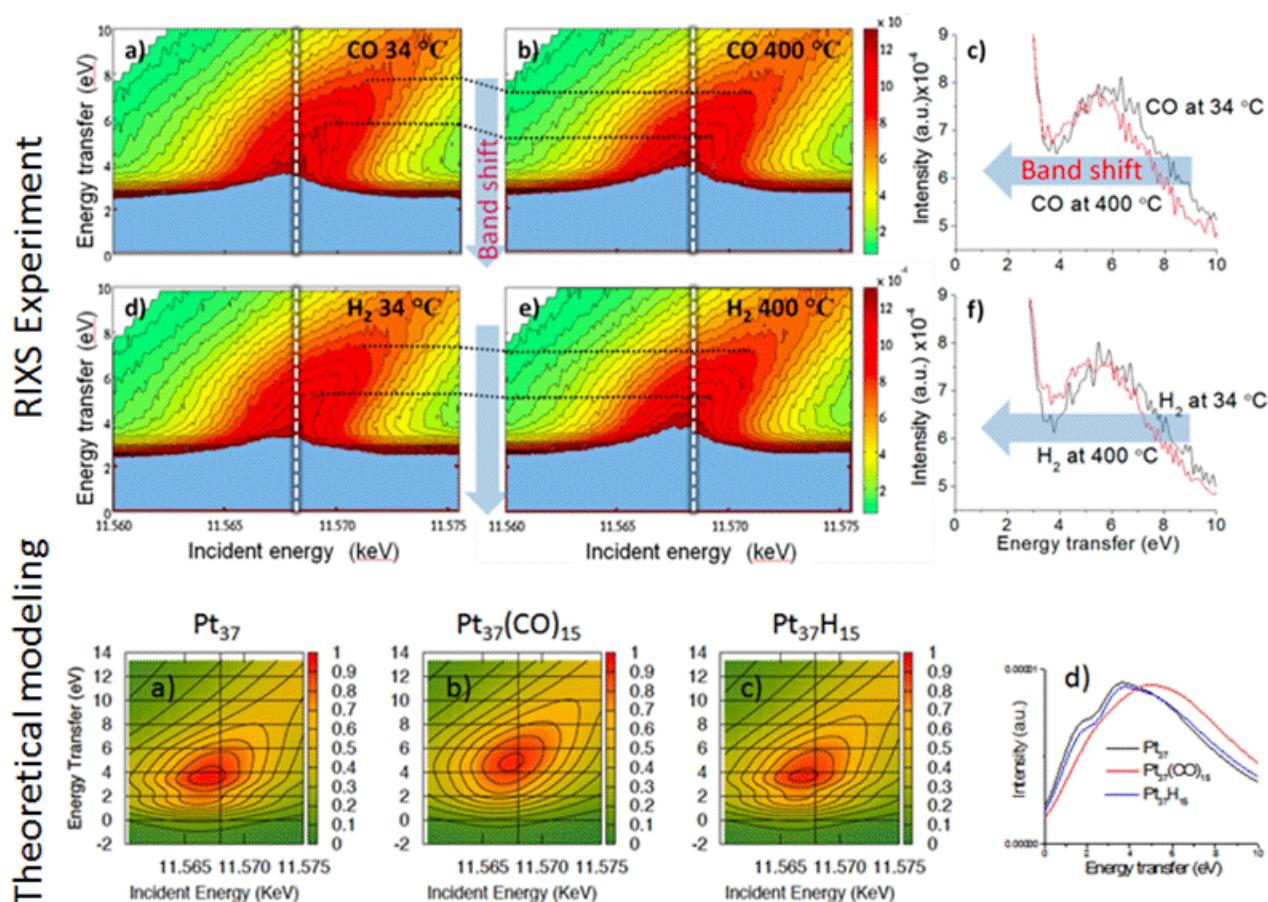


**Figure 1.** Experiment: RIXS maps and their intensity profiles visualizing the density of photo-excited electronic transitions between Pt 5d states in Pt/C nanoparticles for different atmospheres. The transition densities shown in (a, d) are shifted toward lower energy transfers in (b, e) at elevated temperatures for both gases. Vertical dashed lines illustrate the direction of the intensity profiles obtained for each map at the same incident energy of 11568.4 eV and are shown in (c, f). Theoretical modeling: Simulated RIXS data for a 37-atom Pt cluster: bare (a), with CO (b) and H (c) adsorbed. The profile along the 11586 eV energy [shown as a vertical line in (a–c)] is shown in (d).

## 2) Investigation of CO-induced electronic evolution of supported heterogeneous catalysts with HERFD and RIXS

An *in operando* study using resonant inelastic X-ray scattering (RIXS) and high energy resolution fluorescence detection (HERFD) was performed to understand the temperature-dependent adsorption of CO on nm-sized Pt nanoparticles on different supports (C, SiO<sub>2</sub>, Al<sub>2</sub>O<sub>3</sub>) and complemented with *in situ* XAS and DRIFTS experiments as well as pre- and post-measurement characterization of the nanoparticle structure by STEM. In particular, the following points were addressed: (i) the binding motifs of CO to Pt and how they change, (ii) the influence of metal-support interaction, (iii) metal-metal bond length and (iv) metal-metal bond length disorder and, hence, strain. The supported Pt nanoparticles were prepared in the

group of **R. Nuzzo**, the RIXS and HERFD experiments were carried out at the SuperXAS beamline at the Swiss Light Source (SLS) at the Paul Scherrer Institute by the groups of **A. Frenkel** and **R. Nuzzo** in collaboration with **M. Tromp**, the XAS and DRIFTS measurements at the NSLS, BNL (beamlines X18B and 19A, groups of **A. Frenkel** and **R. Nuzzo**) and the STEM measurements by the groups of **R. Nuzzo** and **J. Yang**. The RIXS measurements provide information on both absorption and emission properties of the investigated system and therefore directly measure characteristics of bonding interactions between particles and adsorbates. With HERFD characteristic spectral features of specific binding sites of the CO could be resolved and, as was also demonstrated in our previous work (*Frenkel, A.I. et al., J. Phys. Chem. C* **2013**, *117*, 23286), it is sensitive to strain and electronic perturbations due to temperature changes. Both methods allow to directly compare the effects of coverage on the d-band center behavior and, hence, catalytic activity of supported noble metal catalysts. Together with the XAS and DRIFTS measurement our findings allowed the identification of the temperature-dependent adsorption of the different CO species (e.g. a-top, bridge, three-fold hollow) and to unravel the effects of the different support materials. In particular, a distinct temperature-dependent shift in the HERFD white line energy of  $\sim 1$  eV and a change in white line area were observed with decreasing coverage and an opposite and less pronounced shift was observed for the non-resonant line in the RIXS maps (Fig. 2). **J. Rehr** and his group are currently performing theoretical calculations to unravel the origin of these changes in the electronic structure of the Pt nanoparticles. Preliminary results show similar trends induced by a change in Pt atom charge upon CO adsorption.

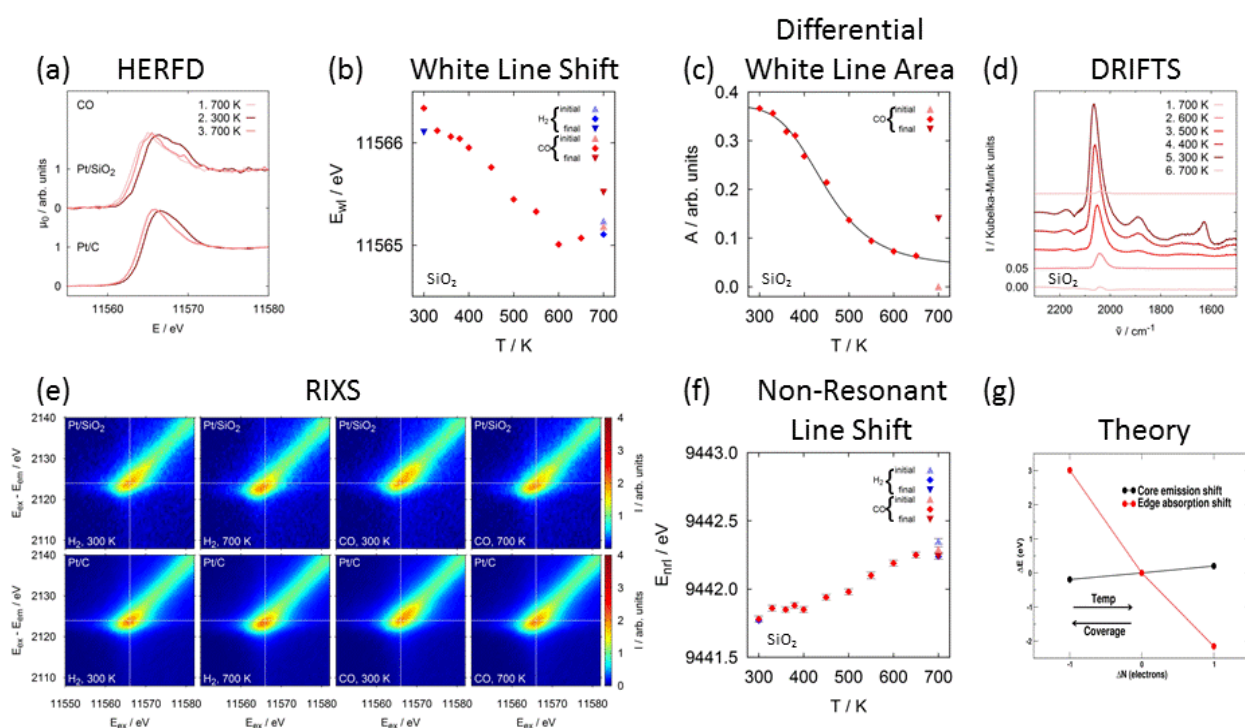


**Figure 2.** HERFD and RIXS data of the CO adsorption on C- and SiO<sub>2</sub>- supported Pt nanoparticles. (a) Selected HERFD spectra. (b) Temperature dependence of the HERFD white line energy for Pt/SiO<sub>2</sub>. (c) differential white line area for Pt/SiO<sub>2</sub>. (d) DRIFTS spectra for Pt/SiO<sub>2</sub>. (e) RIXS maps for Pt/C and Pt/SiO<sub>2</sub>. (f) Non-resonant line energy for Pt/SiO<sub>2</sub>. (g) Theoretical simulations showing the experimentally observed absorption edge and core emission shift induced by charge transfer between the CO adsorbate and the Pt atom.

### Publications Acknowledging this Grant in 2011-2014

1. Erickson, E.M.; Oruc, M.E.; Small, M.W.; Wetzel, D.J.; Cason, M.W.; Hoang, T.T.H.; Li, D.; Marinkovic, N.S.; Frenkel, A.I.; Gewirth, A.A.; Nuzzo, R.G. A Comparison of Atomistic and Continuum Approaches to the Study of Bonding Dynamics in Electrocatalysis: Microcantilever Stress and In-Situ EXAFS Observations of Platinum Bond Expansion Due to Oxygen Adsorption During the Oxygen Reduction Reaction, *Anal. Chemistry*, **submitted**.
2. Frenkel, A.I.; van Bokhoven, J.A. X-Ray Spectroscopy for Chemical and Energy Sciences (invited) *J. Sync. Rad.*, **submitted**.
3. Shan, J.; Zhang, S.; Choksi, T.; Zhu, W.; Zhang, Y.; Li, Y.; Nguyen, L.; Chafe, A.; Greeley, J.; Frenkel, A.I.; Tao, F. Tuning catalytic performance through a single or sequential post-synthesis reaction in a gas phase. *Nature Comm.*, **submitted**.
4. Huang, W.; Shan, J.; Nguyen, L.; Li, Y.; Zhang, S.; Frenkel, A.I.; Tao, F. Catalytic conversion of methane to methanol and formic acid on singly dispersed palladium oxide species on internal surface of ZSM5. *Angew. Chem. Int. Ed.*, **submitted**.
5. Shan, J.; Huang, W.; Nguyen, L.; Yu, Y.; Zhang, S.; Li, Y.; Frenkel, A.I.; Tao, F. Conversion of methane to methanol in gas phase on a bent mono( $\mu$ -oxo)dinickel anchored on internal surface of micro-pores. *Langmuir*, **submitted**.
6. Zhang, S.; Nguyen, L.; Liang, J.; Li, J.; Shan, J.; Frenkel, A.I.; Patlolla, A.; Liu, J.; Huang, W.; Tao, F. Catalysis on an isolated bimetallic site. *Nature Chem.*, **submitted**.
7. Zhang, L.; Yang, C.; Frenkel, A.I.; Wang, S.; Xiao, G.; Brinkman, K.; Chen, F. Co-generation of electricity and chemicals from propane fuel in solid oxide fuel cells with anode containing nano-bimetallic catalyst. *J. Power Sources*, **2014**, *262*, 421-428
8. Rehr, J.J.; Vila, F.D. Dynamic Structural Disorder in Supported Nanoscale Catalysts. *J. Chem. Phys.* **2014**, *140*, 134701.
9. Small, M.W.; Kas, J.; Kvashnina, K.O.; Rehr, J.J.; Nuzzo, R.G.; Tromp, M.; Frenkel, A.I. Effects of adsorbate coverage and bond length disorder on the d-band center in carbon-supported Pt catalysts. *Chem. Phys. Chem.* **2014**, DOI: 10.1002/cphc.201400055
10. Frenkel, A.I.; Cason, M.; Elsen, A.; Jung, U.; Small, M.W.; Nuzzo, R.G.; Vila, F.D.; Rehr, J.J.; Stach, E.A.; Yang, J.C. Effects of complex interactions on structure and dynamics of supported metal catalysts. *J. Vac. Sci. Tech.* (Invited Critical Review) **2014**, *32*, 020801-0208017.
11. Frenkel, A.I.; Small, M.W.; Smith, J.G.; Nuzzo, R.G.; Kvashnina, K.O.; Tromp, M. An In-Situ Study of Bond Strains in 1 nm Pt Catalysts and Their Sensitivities to Cluster-Support and Cluster-Adsorbate Interactions. *J. Phys. Chem. C* **2013**, *117*, 23286-23294.
12. Frenkel, A.I.; Wang, Q.; Sanchez, S.I.; Small, M.W.; Nuzzo, R.G. Short range order in bimetallic nanoalloys: An extended X-ray absorption fine structure study. *J. Chem. Phys.* **2013**, *138*, 064202.
13. Zhang, Z.; Li, L.; Yang, J.C. Adhesion of Pt nanoparticles supported on  $\gamma$ -Al<sub>2</sub>O<sub>3</sub> single crystal. *J. Phys. Chem. C* **2013**, *117*, 21407-21412.
14. Li, L.; Wang, L.-L.; Johnson, D.D.; Zhang, Z.; Sanchez, S.I.; Kang, J.H.; Nuzzo, R.G.; Wang, Q.; Frenkel, A.I.; Ciston, J.; Stach, E.A.; Yang, J.C. Noncrystalline-to-crystalline transformations in Pt nanoparticles. *J. Am. Chem. Soc.* **2013**, *135*, 13062-13072.
15. Stach, E.A.; Zakharov, D.; Akatay, M.C.; Baumann, P.; Ribeiro, F.; Zvienevich, Y.; Li, Y.; Frenkel, A.I. Developments in environmental transmission electron microscopy for catalysis research *Microsc. Microanal.* **2013**, *19*, Suppl. 2, 1174-1175.
16. Zhang, S.; Tao, F.; Frenkel, A.I.; Takeda, S. Singly anchored Pt and Pd atoms on Co<sub>3</sub>O<sub>4</sub> and their catalytic performance. *Microsc. Microanal.* **2013**, *19*, Suppl. 2, 1620-1621.
17. Stach, E.A.; Baumann, P.; Li, Y.; Zakharov, D.; Frenkel, A.I. Using operando methods to characterize working catalysts with TEM, XAS, EXAFS and Raman Spectroscopy. *Microsc. Microanal.* **2013**, *19*, Suppl. 2, 1674-1675.
18. Zhang, S.; Shan, J.-J.; Zhu, Y.; Frenkel, A.I.; Patlolla, A.; Huang, W.; Yoon, S.; Wang, L.; Yoshida, H.; Takeda, S.; Tao, F. WGS Catalysis and in-situ studies of CoO(1-x)PtCo(n)/Co<sub>3</sub>O<sub>4</sub> and Pt(m)Co(m')/CoO(1-x) nanorod catalysts. *J. Am. Chem. Soc.* **2013**, *135*, 8283-8293.
19. Merte, L.R.; Ahmadi, M.; Behafarid, F.; Ono, L.K.; Lira, E.; Matos, J.; Li, L.; Yang, J.C.; Cuenya, B.R. Correlating Catalytic Methanol Oxidation with the Structure and Oxidation State of Size-Selected Pt Nanoparticles. *ACS Catal.* **2013**, *3*, 1460-1468.
20. Korobko, R.; Lerner, A.; Li, Y.; Frenkel, A.I.; Lubomirsky, I. Electric field increases local symmetry in Gd-doped ceria. *Nature Mater.*, **submitted**.
21. Wu, L.-b.; Wu, L.-h.; Yang, W.-m.; Frenkel, A.I. Study of the local structure and oxidation state of iron in complex oxide catalysts for propylene ammoxidation. *Cat. Sci. & Technol.*, 2014, **in press**.
22. He, L.; Liu, F.; Hautier, G.; Oliveira, M.J.T.; Marques, M.A.L.; Vila, F.D.; Rehr, J.J.; Rignanese, G.-M.; Zhou, A. Accuracy of generalized gradient approximation functionals for density-functional perturbation theory calculations. *Phys. Rev. B* **2014**, *89*, 064305.

23. Frenkel, A.I.; Khalid, S.; Hanson, J.C.; Nachtegaal, M. QEXAFS in Catalysis Research: Principles, Data Analysis and Applications. In *In-situ Characterization of Heterogeneous Catalysts*, Chupas, P.; Hanson, J.; Rodriguez, J.A., Eds., John Wiley and Sons **2013**.
24. Frenkel, A.I.; Hanson, J.C. Combined XAFS-XRD methods in Catalysis Research. In *In-situ Characterization of Heterogeneous Catalysts*, Chupas, P.; Hanson, J.; Rodriguez, J. A., Eds., John Wiley and Sons **2013**.
25. Kossoy, A.; Wang, Q.; Korobko, R.; Grover, V.; Feldman, Y.; Wachtel, E.; Tyagi, A.K.; Frenkel, A.I., Lubomirsky, I. Evolution of the local structure at the phase transition in CeO<sub>2</sub>-Gd<sub>2</sub>O<sub>3</sub> solid solutions. *Phys. Rev. B* **2013**, *87*, 054101.
26. Perelshtein, I.; Ruderman, E.; Perkas, N.; Tzanov, T.; Beddow, J.; Joyce, E.; Mason, T.; Blanes, M.; Molla, K.; Patlolla, A.; Frenkel, A.I.; Gedanken, A., Chitosan and chitosan-ZnO-based complex nanoparticles: formation, characterization, and antibacterial activity. *J. Mater. Chem. B* **2013**, *1*, 1968-1976.
27. Sanchez, S.I.; Small, M.W.; Bozin, E.S.; Wen, J.-G.; Zuo, J.-M.; Nuzzo, R.G., Metastability and Structural Polymorphism in Noble Metals: the Role of Composition and Metal Atom Coordination in Mono- and Bimetallic Nanoclusters. *ACS Nano* **2013**, *7*, 1542-1557.
28. Amit, Y.; Eshet, H; Faust, A.; Patlolla, A.; Rabani, E.; Banin, U.; Frenkel, A.I. Unraveling the Impurity Location and Binding in Heavily Doped Semiconductor Nanocrystals: The Case of Cu in InAs Nanocrystals. *J. Phys. Chem. C* **2013**, *117*, 13688-13696.
29. Amit, Y.; Eshet, H; Milo, O.; Rabani, E.; Frenkel, A.I.; Banin, U. How to dope a semiconductor nanocrystal. *ECS Trans.* **2013**, *58*, 127-133.
30. Yancey, D.F.; Chill, S.T.; Zhang, L.; Frenkel, A.I.; Henkelman, G.; Crooks, R.M. A theoretical and experimental examination of systematic ligand-induced disorder in Au dendrimer-encapsulated nanoparticles. *Chem. Science* **2013**, *4*, 2912-2921.
31. Wang, L.; Zhang, S.; Zhu, Y.; Patlolla, A.; Shan, J.-J.; Yoshida, H.; Takeda, S.; Frenkel, A.I.; Tao, F. Catalysis and In-situ Studies of Rh/Co<sub>3</sub>O<sub>4</sub> Nanorods in Reduction of NO with H<sub>2</sub>. *ACS Catalysis* **2013**, *3*, 1011-1019.
32. Patlolla, A.; Baumann, P.; Xu, W.; Senanayake, S.; Rodriguez, J.A.; Frenkel, A.I. Characterization of Metal-Oxide Catalysts in Operando Conditions by Combining X-Ray Absorption and Raman Spectroscopies in the Same Experiment. *Top. Catal.* **2013**, *56*, 896-904.
33. Amakawa, K.; Sun, L.; Guo, C.; Havecker, M.; Kube, P.; Wachs, I.E.; Lwin, S.; Frenkel, A.I.; Patlolla, A.; Hermann, K.; Schlogl, R.; Trunschke A. *How strain affects the reactivity of surface metal oxide catalysts. Angew. Chem. Int. Ed.* **2013**, *52*, 13553-13557.
34. Frenkel, A.I., Applications of extended X-ray absorption fine-structure spectroscopy to studies of bimetallic nanoparticle catalysts. *Chem. Soc. Rev.* **2012**, *41*, 8163-8178.
35. Yang, J.C.; Small, M.W.; Grieshaber, R.V.; Nuzzo, R.G., Recent Developments and Applications of Electron Microscopy to Heterogeneous Catalysis. *Chem. Soc. Rev.* **2012**, *41*, 8179-8194.
36. Zhang, Z.; Gleeson, B.; Jung, K.; Li, L.; Yang, J.C., A Diffusion Analysis of Transient Subsurface gamma-Ni<sub>3</sub>Al Formation During beta-NiAl Oxidation, *Acta. Mater.* **2012**, *60*, 5273-5283.
37. Zhang, Z.; Jung, K.; Li, L.; Yang, J.C., Kinetic Aspects of Initial Stage Thin gamma-Al<sub>2</sub>O<sub>3</sub> Film Formation on Single Crystalline beta-NiAl (110). *J. Appl. Phys.* **2012**, *111*, 34312.
38. Erickson, E. M.; Thorum, M. S.; Vasic, R.; Marinkovic, N.; Frenkel, A. I.; Gewirth, A. A.; Nuzzo, R. G., In-Situ Electrochemical X-ray Absorbance Spectroscopy Oxygen Reduction Catalysis with High Oxygen Flux. *J. Am. Chem. Soc.* **2012**, *134*, 197-200.
39. Small, M. W.; Sanchez, S. I.; Marinkovic, N. S.; Frenkel, A. I.; Nuzzo, R. G., Influence of Adsorbates on the Electronic Structure, Bond Strain, and Thermal Properties of an Alumina-Supported Pt Catalyst. *ACS Nano*, **2012**, *6*, 5583-5595.
40. Yan, W.; Vasic, R.; Frenkel, A. I.; Koel, B. E., Intra-particle reduction of arsenite (As(III)) by nanoscale zerovalent iron (nZVI) investigated with *in-situ* X-ray absorption spectroscopy. *Environ. Sci. & Technology* **2012**, *46*, 7018-7026.
41. Patlolla, A.; Zunino III, J.; Frenkel, A. I.; Iqbal, Z., Thermochromism in Polydiacetylene-metal oxide nanocomposites *J. Mater. Chem.* **2012**, *22*, 7028-7035.
42. Myers, S. V.; Frenkel, A. I.; Crooks, R. M., In Situ Structural Characterization of Platinum Dendrimer-Encapsulated Oxygen Reduction Electrocatalysts. *Langmuir* **2012**, *28*(2), 1596-1603.
43. Ryu, H.; Lei, H.; Frenkel, A. I.; Petrovic, C., Local structural disorder-induced superconductivity in K(x)Fe(2-y)Se(2) materials *Phys. Rev. Lett.* **2012**, *85*, 224515.
44. Chen, W.-F.; Sasaki, K.; Ma, C.; Frenkel, A. I.; Marinkovic, N.; Muckerman, J. T.; Zhu, Y.; Adzic, R. R., Noble metal-free hydrogen-evolution catalysts based on NiMo nitride nanosheets. *Angew. Chemie Int. Ed.* **2012**, *51*, 6131-6135.
45. Yadgarov, L.; Rosentsveig, R.; Leitun, G.; Albu-Yaron, A.; Moshkovitz, A.; Perfiliev, V.; Vasic, R.; Frenkel, A. I.; Enyashin, A. N.; Seifert, G.; Rapoport, L.; Tenne, R., Controlled doping of MS<sub>2</sub> (M=W, Mo) nanotubes and fullerene-like nanoparticles *Ang. Chemie, Int. Ed.* **2012**, *51*, 1148-1151.

46. Yih, K.; Hamdemir, I.K.; Mondoch, J.E.; Bayrem, E.; Ozkar, S.; Vasic, R.; Frenkel, A.I.; Anderson, O.P.; Finke, R.G., Synthesis and Characterization of [Ir(1,5-Cyclooctadiene)( $\mu$ -H)]<sub>4</sub>: A Tetrametallic Ir<sub>4</sub>H<sub>4</sub>-core, Coordinatively Unsaturated Cluster. *Inorg. Chem.* **2012**, *51*, 3186-3193.
47. Frenkel, A.I.; Vasic, R.; Dukesz, B.; Li, D.; Chen, M.; Zhang, L.; Fujita, T.; Thermal Properties of Nanoporous Gold. *Phys. Rev. B* **2012**, *85*, 195419.
48. Landon, J.; Demeter, E.; Inoglu, N.; Keturakis, C.; Wachs, I.E.; Vasic R.; Frenkel, A.I.; Kitchin, J.R., Spectroscopic Characterization of Mixed Fe-Ni Oxide Electrocatalysts for the Oxygen Evolution Reaction in Alkaline Electrolytes. *ACS Catalysis* **2012**, *2*, 1793-1801.
49. Korobko, R.; Patlolla, A.; Kossoy, A.; Wachtel, E.; Tuller, H.L.; Frenkel, A.I.; Lubomirsky, I., Giant Electrostriction in Gd-doped Ceria. *Adv. Mater.* **2012**, *24*, 5857-5861.
50. Lyahovitskaya, V.; Feldman, Y.; Zon, I.; Yoffe, A.; Frenkel, A.I., Strain-arranged structure in amorphous films. *J. Mater. Res.* **2012**, *27*, 2819-2828.
51. Coppage, R.; Slocik, J. M.; Briggs, B. D.; Frenkel, A. I.; Naik, R. R.; Knecht, M. R., Determining peptide sequence effects that control the size, structure and function of nanoparticles. *ACS Nano* **2012**, *6*, 1625-1636.
52. Patlolla, A.; Carino, E.V.; Ehrlich, S.N.; Stavitski, E.; Frenkel, A.I., Application of Operando XAS, XRD, and Raman Spectroscopy for Phase Speciation in Water Gas Shift Reaction Catalysts. *ACS Catalysis* **2012**, *2*, 2216-2223.
53. Lei, H.; Ryu, H.; Ivanovski, V.; Warren, J.B.; Frenkel, A.I.; Cekic, B.; Yin, W.-G.; Petrovic, C., Structure and physical properties of the layered iron oxychalcogenide BaFe<sub>2</sub>Se<sub>2</sub>O. *Phys. Rev. B* **2012**, *86*, 195133.
54. M. W. Small, S. I. Sanchez, L. D. Menard, J. H. Kang, A. I. Frenkel and R. G. Nuzzo, The Atomic Structural Dynamics of  $\gamma$ -Al<sub>2</sub>O<sub>3</sub> Supported Ir-Pt Nanocluster Catalysts Prepared From a Bimetallic Molecular Precursor: A Study Using Aberration-Corrected Electron Microscopy and X-ray Absorption Spectroscopy, *Journal of the American Chemical Society*, **2011**, *133*, 3582-3591.
55. W. Du, D. Su, Q. Wang, A. I. Frenkel, X. Teng, Promotional effects of Bismuth on the formation of Platinum-Bismuth nanowires and the electrocatalytic activity toward ethanol oxidation, *Crystal Growth & Design*, **2011**, *11*, 594-599.
56. A. Piovano, G. Agostini, A. I. Frenkel, T. Bertier, C. Prestipino, M. Ceretti, W. Paulus, C. Lamberti, Time-resolved in situ XAFS study of the electrochemical oxygen intercalation in SrFeO<sub>2.5</sub> Brownmillertite structure: comparison with the homologous SrCoO<sub>2.5</sub> system, *J. Phys. Chem. C* **2011**, *115*, 1311-1322.
57. Alley, W. M.; Hamdemir, I. K.; Wang, Q.; Frenkel, A. I.; Li, L.; Yang, J. C.; Menard, L. D.; Nuzzo, R. G.; Ozkar, S.; Yih, K.; Johnson, K. A.; Finke, R. G., Industrial Ziegler-Type Hydrogenation Catalysts Made from Co(neodecanoate)(2) or Ni(2-ethylhexanoate)(2) and AlEt<sub>3</sub>: Evidence for Nanoclusters and Sub-Nanocluster or Larger Ziegler-Nanocluster Based Catalysis. *Langmuir* **2011**, *27*, 6279-6294.
58. Danh, N.-T.; Frenkel, A. I.; Wang, J.; O'Brien, S.; Akins, D. L., Cobalt-polypyrrole-carbon black (Co-PPY-CB) electrocatalysts for the oxygen reduction reaction (ORR) in fuel cells: Composition and kinetic activity. *Applied Catalysis B-Environmental* **2011**, *105*, 50-60.
59. Du, W.; Su, D.; Wang, Q.; Frenkel, A. I.; Teng, X., Promotional Effects of Bismuth on the Formation of Platinum-Bismuth Nanowires Network and the Electrocatalytic Activity toward Ethanol Oxidation. *Cryst. Growth Des.* **2011**, *11*, 594-599.
60. Du, W.; Wang, Q.; LaScala, C. A.; Zhang, L.; Su, D.; Frenkel, A. I.; Mathur, V. K.; Teng, X., Ternary PtSnRh-SnO<sub>2</sub> nanoclusters: synthesis and electroactivity for ethanol oxidation fuel cell reaction. *J. Mater. Chem.* **2011**, *21*, 8887-8892.
61. Du, W.; Wang, Q.; Saxner, D.; Deskins, N. A.; Su, D.; Krzanowski, J. E.; Frenkel, A. I.; Teng, X., Highly Active Iridium/Iridium-Tin/Tin Oxide Heterogeneous Nanoparticles as Alternative Electrocatalysts for the Ethanol Oxidation Reaction. *J. Am. Chem. Soc.* **2011**, *133*, 15172-15183.
62. Frenkel, A. I.; Wang, Q.; Marinkovic, N.; Chen, J. G.; Barrio, L.; Si, R.; Lopez Camara, A.; Estrella, A. M.; Rodriguez, J. A.; Hanson, J. C., Combining X-ray Absorption and X-ray Diffraction Techniques for *in-situ* Studies of Chemical Transformations in Heterogeneous Catalysis: Advantages and Limitations. *J. Phys. Chem. C* **2011**, *115*, 17884-17890.
63. Frenkel, A. I.; Yevick, A.; Cooper, C.; Vasic, R., Modeling the Structure and Composition of Nanoparticles by Extended X-Ray Absorption Fine-Structure Spectroscopy. *Annual Review Of Analytical Chemistry, Vol 4* **2011**, *4*, 23-39.
64. Li, L.; Zhang, Z.; Ciston, J.; Stach, E. A.; Wang, L.-l.; Johnson, D. D.; Wang, Q.; Frenkel, A. I.; Sanchez, S. I.; Small, M. W.; Nuzzo, R. G.; Yang, J. C., H<sub>2</sub>-driven crystallization of supported Pt nanoparticles observed with aberration-corrected Environmental TEM. *Microsc. Microanal.* **2011**, *17*, 1604-1605.
65. Marinkovic, N. S.; Wang, Q.; Barrio, L.; Ehrlich, S. N.; Khalid, S.; Cooper, C.; Frenkel, A. I., Combined *in-situ* X-ray absorption and diffuse reflectance infrared spectroscopy: An attractive tool for catalytic investigations. *Nuclear Instruments & Methods In Physics Research Section A* **2011**, *649*, 204-206.
66. Marinkovic, N. S.; Wang, Q.; Frenkel, A. I., *In-situ* diffuse reflectance IR spectroscopy and X-ray absorption spectroscopy for fast catalytic processes. *Journal Of Synchrotron Radiation* **2011**, *18*, 447-455.

67. Paredis, K.; Ono, L. K.; Behafarid, F.; Zhang, Z.; Yang, J. C.; Frenkel, A. I.; Cuenya, B. R., Evolution of the Structure and Chemical State of Pd Nanoparticles during the *in-situ* Catalytic Reduction of NO with H<sub>2</sub>. *J. Am. Chem. Soc.* **2011**, *133*, 13455-13464.
68. Paredis, K.; Ono, L. K.; Mostafa, S.; Li, L.; Zhang, Z.; Yang, J. C.; Barrio, L.; Frenkel, A. I.; Cuenya, B. R., Structure, chemical composition, and reactivity correlations during the *in-situ* oxidation of 2-propanol. *J. Am. Chem. Soc.* **2011**, *133*, 6728-6735.
69. Sasaki, K.; Kuttiyiel, K. A.; Barrio, L.; Su, D.; Frenkel, A. I.; Marinkovic, N.; Mahajan, D.; Adzic, R. R., Carbon-Supported IrNi Core-Shell Nanoparticles: Synthesis, Characterization, and Catalytic Activity. *J. Phys. Chem. C* **2011**, *115*, 9894-9902.
70. Zhang, Z.; Li, L.; Wang, L.-l.; Sanchez, S. I.; Wang, Q.; Johnson, D. D.; Frenkel, A. I.; Nuzzo, R. G.; Yang, J. C., The Role of  $\beta$ -Al<sub>2</sub>O<sub>3</sub> Single Crystal Support to Pt Nanoparticles Construction. *Microsc. Microanal.* **2011**, *17*, 1324-1325.
71. Zhang, Z.; Li, L.; Yang, J. C.,  $\gamma$ -Al<sub>2</sub>O<sub>3</sub> thin film formation via oxidation of  $\beta$ -NiAl(1 1 0). *Acta Mater.* **2011**, *59*, 5905-5916.
72. Lei, H.; Ryu, H.; Frenkel, A. I.; Petrovic, C., Anisotropy in BaFe<sub>2</sub>Se<sub>3</sub> single crystals with double chains of FeSe tetrahedra *Physical Review B* **2011**, *84*, 214511.
73. Shen, X.-F.; Morey, A.; Liu, J.; Ding, Y.-S.; Durand, J.; Wang, Q.; Wen, W.; Hines, W. A.; Hanson, J. C.; Bai, J.; Frenkel, A. I.; Reiff, W.; Aindow, M.; Suib, S. L.; Cai, J., Characterization of the Fe-doped mixed-valent tunnel structure manganese oxide KOMS-2 *J. Phys. Chem. C* **2011**, *115*, 21610-21619.
74. Coppage, R.; Slocik, J. M.; Briggs, B. D.; Frenkel, A. I.; Heinz, H.; Naik, R. R.; Knecht, M. R., Crystallographic Recognition Controls Peptide Binding for Bio-Based Nanomaterials. *J. Am. Chem. Soc.* **2011**, *133*, 12346-12349.

**Influence of Multi-Valency, Electrostatics and Molecular Recognition on the Adsorption of Transition Metal Complexes on Metal Oxides: A Molecular Approach to Supported Catalyst Synthesis (DE-FG02-12ER16364)**

Ahana Mukhopadhyay<sup>1</sup>, Charlie S. Spanjers<sup>1</sup>, Mitchell Cornwall<sup>1</sup>, Megan Strayer<sup>2</sup>, Robert M. Rioux<sup>1</sup>  
<sup>1</sup>Department of Chemical Engineering and <sup>2</sup>Department of Chemistry, The Pennsylvania State University, University Park, PA 16802-4400, rioux@enr.psu.edu

**Presentation Abstract**

The project introduces a quantitative, molecular approach to the catalysis synthesis, which will aid the development of methods for the synthesis of single-site or nanoparticle-based catalysts. The *in-situ* approach will provide a direct correlation between the mechanism of transition metal complex (TMC) adsorption and the pretreatment regime with the overall properties of the final catalyst. A molecular-level treatment of catalyst synthesis will be developed via the application of novel *in-situ* techniques that provide quantitative data on the thermodynamics and kinetics of the adsorption of TMCs, and *in-situ* methods to probe morphological changes due to particle nucleation and growth during pretreatment. This proposal represents a unique molecular-level picture of catalyst synthesis with a direct quantitative comparison of its catalytic properties with the mechanism of TMC adsorption. We have applied isothermal titration calorimetry to quantify the thermodynamics associated with the adsorption of TMCs (Pt primarily) under interface conditions of ion-exchange (strong electrostatic adsorption) and inner-sphere (covalent) to refractory metal oxides (silica and alumina) and perovskites. The measured thermodynamics were then compared with catalyst properties after calcination-reduction pretreatments to determine if these properties correlated with other. In effect, these experiments probed whether a memory effect, or whether the final properties of the catalyst were influenced by the solution-phase conditions. We find that the strength of adsorption (as measured by the apparent heat of adsorption) during strong electrostatic adsorption displays a direct correspondence with the difference between the PZC of the support and pH of the solution when the appropriate TMC (cation or anion) source is utilized. The correspondence between adsorption conditions are correlated with the final properties of the supported Pt catalysts as determined by high energy x-ray diffraction – pair distribution function (PDF) analysis, x-ray absorption spectroscopy and high-resolution transmission electron microscopy. We demonstrate through an identical experimental approach that this memory effect is persistent in covalent bonding systems. We demonstrate the latter with the adsorption of Rh(OH)<sub>3</sub> nanoparticles onto the surface of Nb-based Dion-Jacobsen perovskite supports.

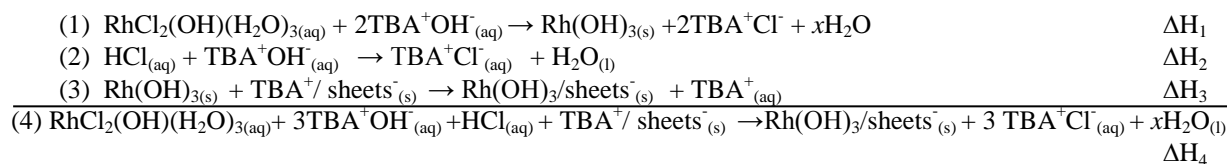
**Recent Progress**

Rhodium oxide and rhodium metal nanoparticles on niobate and tantalate supports are anomalously stable. To understand this, the nanoparticle-support interaction was studied by isothermal titration calorimetry (ITC), environmental transmission electron microscopy (ETEM), and synchrotron X-ray absorption and scattering techniques. Nanosheets derived from the layered oxides KCa<sub>2</sub>Nb<sub>3</sub>O<sub>10</sub>, K<sub>4</sub>Nb<sub>6</sub>O<sub>17</sub>, and RbTaO<sub>3</sub> were compared as supports to nanosheets prepared from Na-TSM, a synthetic fluoromica (Na<sub>0.66</sub>Mg<sub>2.68</sub>(Si<sub>3.98</sub>Al<sub>0.02</sub>)O<sub>10.02</sub>F<sub>1.96</sub>), and  $\alpha$ -Zr(HPO<sub>4</sub>)<sub>2</sub>·H<sub>2</sub>O. High surface area SiO<sub>2</sub> and  $\gamma$ -Al<sub>2</sub>O<sub>3</sub> supports were also used for comparison in the ITC experiments. A Born-Haber cycle analysis of ITC data revealed an exothermic interaction between Rh(OH)<sub>3</sub> nanoparticles and the layered niobate and tantalate supports, with  $\Delta H$  values in the range -32 kJ·mol<sup>-1</sup> Rh to -37 kJ·mol<sup>-1</sup> Rh. In contrast, the interaction enthalpy was positive with SiO<sub>2</sub> and  $\gamma$ -Al<sub>2</sub>O<sub>3</sub> supports. The strong interfacial bonding in the former case led to “reverse” ripening of micron-size Rh(OH)<sub>3</sub>, which dispersed as 0.5 nm to 2 nm particles on the niobate and tantalate supports. In contrast, particles grown on Na-TSM and  $\alpha$ -Zr(HPO<sub>4</sub>)<sub>2</sub>·H<sub>2</sub>O nanosheets were larger and had a broad size distribution. ETTEM, x-ray absorption

spectroscopy, and pair distribution function analyses were used to study the growth of supported nanoparticles under oxidizing and reducing conditions, as well as the transformation from  $\text{Rh}(\text{OH})_3$  to Rh nanoparticles. The behavior of these nanoparticles on layered niobate and tantalates is not consistent with local reduction of the oxide support or encapsulation of the metal nanoparticles, as are often invoked in models of the strong metal-support interaction. Rather, it appears that interfacial covalent bonding, possibly strengthened by d-electron acid/base interactions, is responsible for the stability of  $\text{Rh}(\text{OH})_3$ ,  $\text{Rh}_2\text{O}_3$ , and Rh nanoparticles on niobate and tantalate supports.

Isothermal titration calorimetry (ITC) was used to investigate the strength of bonding between rhodium hydroxide nanoparticles and oxide supports. During a deposition reaction, several reactions occur simultaneously, and the overall process can be represented by the Born-Haber cycle shown in **Scheme 1**. The enthalpy associated with the interaction of the  $\text{Rh}(\text{OH})_3$  nanoparticles and the oxide support (Reaction 3) is determined by taking the difference between the overall reaction (Reaction 4) and the heats of hydrolysis (Reaction 1,  $\Delta H_1 = (-27 \pm 5) \text{ kJ}\cdot\text{mol}^{-1}$ ) and neutralization (Reaction 2,  $\Delta H_2 = (-58 \pm 2) \text{ kJ}\cdot\text{mol}^{-1}$ ). (See Supporting Information for details of the determination of  $\Delta H_1$  and  $\Delta H_2$ ) In this cycle, there is also a surface energy term that is dependent on the size of the particles produced. In order to obtain a reliable comparison of bonding energies for different supports, the final sizes of the  $\text{Rh}(\text{OH})_3$  nanoparticles should be similar.  $\text{Rh}(\text{OH})_3$  particles deposited on Na-TSM ( $(5 \pm 1) \text{ nm}$ ,  $n = 101$ ) are significantly larger than those deposited on Nb oxide nanosheets ( $< 1 \text{ nm}$  diameter).

**Scheme 1.** Born Haber cycle for deposition of rhodium hydroxide particles onto nanosheet supports in ITC experiments.



Therefore, high surface area  $\text{SiO}_2$  and  $\gamma\text{-Al}_2\text{O}_3$  were used as non-transition metal oxide supports in the ITC experiments, as they gave  $\text{Rh}(\text{OH})_3$  nanoparticle sizes of  $(0.7 \pm 0.2) \text{ nm}$  ( $n = 100$ ) and  $(1.3 \pm 0.4) \text{ nm}$  ( $n = 100$ ), respectively. The  $\gamma\text{-Al}_2\text{O}_3$  used in these experiments had an average particle diameter of  $(50 \pm 40) \text{ nm}$  ( $n = 127$ ) and a surface area of  $(35.8 \pm 0.1) \text{ m}^2\cdot\text{g}^{-1}$ . The  $\text{SiO}_2$  support had an average particle diameter of  $(17 \pm 6) \text{ nm}$  ( $n = 101$ ) and a surface area of  $(408 \pm 8) \text{ m}^2\cdot\text{g}^{-1}$ . Both of these high surface area oxides are used widely as supports for rhodium and platinum nanoparticles. In addition, nanoparticles deposited on these supports are known to coalesce at temperatures as low as  $550 \text{ }^\circ\text{C}$ .

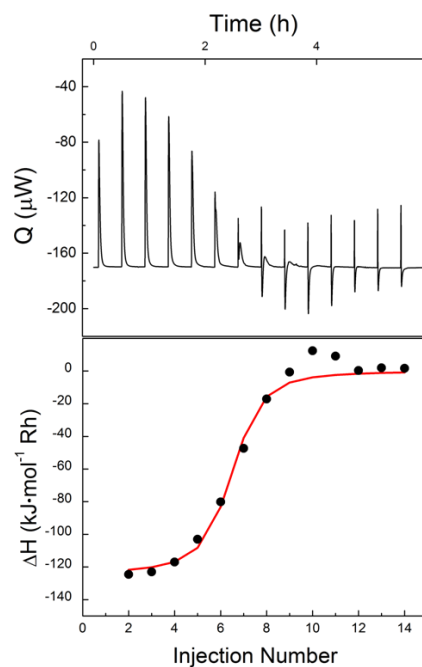


**Figure 1.** A) Real-time ITC thermogram for the addition of  $\text{RhCl}_3$  aqueous solution to  $\text{TBA}_{0.24}\text{H}_{0.76}\text{Ca}_2\text{Nb}_3\text{O}_{10}$  sheets in excess  $\text{TBA}^+\text{OH}^-$  solution and B) the integrated heat fit data with an independent model fit.

A representative ITC isotherm for  $\text{Rh}(\text{OH})_3$  deposition onto  $\text{TBA}_{0.24}\text{H}_{0.76}\text{Ca}_2\text{Nb}_3\text{O}_{10}$  sheets and the associated integrated area plot are shown in Figure 1. The adsorption of  $\text{Rh}(\text{OH})_3$  to  $\text{TBA}_{0.24}\text{H}_{0.76}\text{Ca}_2\text{Nb}_3\text{O}_{10}$ ,  $\text{TBA}_{0.7}\text{H}_{2.2}\text{K}_{1.1}\text{Nb}_6\text{O}_{17}$ , and  $\text{TBA}_{0.1}\text{H}_{0.8}\text{Rb}_{0.1}\text{TaO}_3$  is exothermic, with  $\Delta H_3$  values in the range of  $-32 \text{ kJ}\cdot\text{mol}^{-1}$  Rh to  $-37 \text{ kJ}\cdot\text{mol}^{-1}$  Rh. These three layered oxides are structurally different:  $\text{KCa}_2\text{Nb}_3\text{O}_{10}$  contains only corner-sharing  $\text{NbO}_6$  octahedra, whereas the corrugated sheets of  $\text{K}_4\text{Nb}_6\text{O}_{17}$  and  $\text{RbTaO}_3$  contain both edge and corner-shared octahedra. Nevertheless the  $\Delta H_3$  values are all exothermic and quite similar. In contrast,  $\Delta H_3$  values obtained with  $\text{SiO}_2$  and  $\gamma\text{-Al}_2\text{O}_3$  were both endothermic,  $(25 \pm 6) \text{ kJ}\cdot\text{mol}^{-1}$  and  $(55 \pm 6) \text{ kJ}\cdot\text{mol}^{-1}$ , respectively. These differences are consistent with a relatively strong covalent interaction between  $\text{Rh}(\text{OH})_3$  and the layered niobate and tantalate supports. The difference in  $\Delta H_3$  between  $\text{SiO}_2$  and  $\gamma\text{-Al}_2\text{O}_3$  may, in part, reflect a difference in the electrostatic energy of bringing negatively charged  $\text{Rh}(\text{OH})_3$  particles to the surfaces of these supports.  $\text{SiO}_2$  and  $\gamma\text{-Al}_2\text{O}_3$  have zeta-potentials of  $(-37 \pm 1) \text{ mV}$  and  $(-44 \pm 1) \text{ mV}$ , respectively. The less negative zeta-potential of  $\text{SiO}_2$  results in less electrostatic repulsion and therefore, a smaller endothermic heat of interaction than with  $\gamma\text{-Al}_2\text{O}_3$ .

Rh metal nanoparticles on oxide supports are used widely in catalysis, and the temperature at which they can be used under reducing conditions is limited by their stability against growth. Therefore, *in situ* TEM was used to investigate the growth of Rh nanoparticles on both Nb oxide nanosheets and Na-TSM under reducing conditions. Figure 2A shows a plot of average nanoparticle diameter versus temperature for samples heated in hydrogen. The nanoparticles were too small to retrieve size information when deposited on  $\text{KCa}_2\text{Nb}_3\text{O}_{10}$  and imaged at temperatures up to  $200^\circ\text{C}$ . The nanoparticles deposited on  $\text{K}_4\text{Nb}_6\text{O}_{17}$  were  $(0.5 \pm 0.2) \text{ nm}$  in diameter at  $200^\circ\text{C}$  when heated in  $200 \text{ Pa}$  of hydrogen, compared to  $(1.1 \pm 0.4) \text{ nm}$  when heated in vacuum ( $1 \times 10^{-6} \text{ Pa}$ ). When samples were heated in  $\text{H}_2$ , the growth of the nanoparticles was retarded for all supports relative to samples heated in vacuum (Figures 2B-E). Interestingly, nanoparticles deposited on  $\text{KCa}_2\text{Nb}_3\text{O}_{10}$  and  $\text{K}_4\text{Nb}_6\text{O}_{17}$  remain smaller than  $2 \text{ nm}$  diameter up to  $700^\circ\text{C}$ . Since the nanoparticles do not aggregate, they retain active surface area at increased temperatures, and thus niobates are likely to stabilize Rh nanoparticles under catalytic conditions. Nanoparticles deposited on Na-TSM also remain small ( $3.6 \pm 0.9 \text{ nm}$ ) at  $600^\circ\text{C}$  but they are not evenly dispersed. Below  $600^\circ\text{C}$ , the particles are present only at the sheet edges (Figure 2D). At  $600^\circ\text{C}$ , the nanoparticles move from the edges onto basal planes of the sheets (Figure 2E). This behavior differs from the other supports heated in  $\text{H}_2$ , where the nanoparticles were less than  $2 \text{ nm}$  and evenly distributed at all temperatures studied.  $\text{Rh}(\text{OH})_3$  nanoparticles deposited on Na-TSM and heated under vacuum also behaved differently. Under vacuum, the nanoparticles were unevenly distributed but did not segregate to the edges of the sheets. The  $\text{Rh}_2\text{O}_3$  nanoparticles also grew rapidly with temperature under vacuum conditions. Possible beam effects were investigated to confirm that the increase in particle size was due to the intended increase in temperature and not due to irradiation. An area of the support  $\text{K}_4\text{Nb}_6\text{O}_{17}$  with deposited nanoparticles was bombarded with the electron beam for  $12 \text{ min}$  at  $550^\circ\text{C}$  (electron density of  $3 \times 10^7 \text{ electrons}\cdot\text{nm}^{-1}$ ), which is the approximate length of time spent

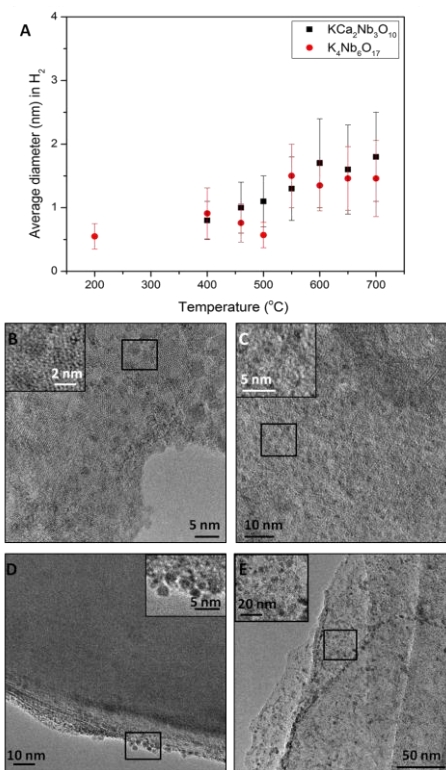


**Figure 2.** A) Plot of the average diameter of nanoparticles heated *in situ* in  $200 \text{ Pa}$   $\text{H}_2$  at increasing temperatures on  $\text{KCa}_2\text{Nb}_3\text{O}_{10}$  and  $\text{K}_4\text{Nb}_6\text{O}_{17}$ . The uncertainty reported for each measured value is one standard deviation of the mean for  $n$  measurements. TEM images of nanoparticles on B)  $\text{KCa}_2\text{Nb}_3\text{O}_{10}$  at  $600^\circ\text{C}$ ; C)  $\text{K}_4\text{Nb}_6\text{O}_{17}$  at  $600^\circ\text{C}$ ; D) Na-TSM at  $200^\circ\text{C}$  and E) Na-TSM at  $600^\circ\text{C}$ .

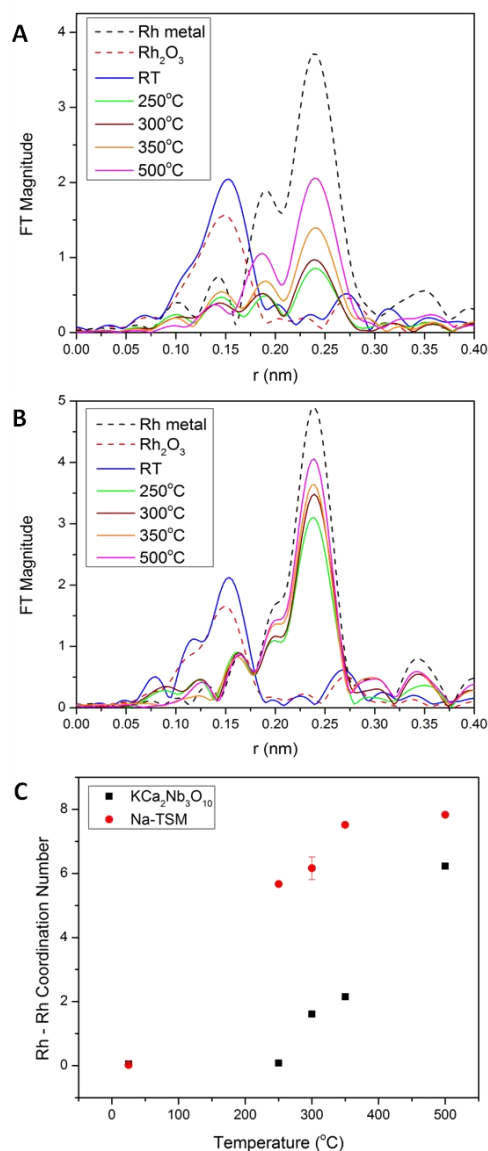


**Figure 3.** EXAFS spectra of rhodium catalyst on A)  $\text{KCa}_2\text{Nb}_3\text{O}_{10}$  and B) Na-TSM heated *ex situ* in hydrogen for half an hour at each temperature. The spectra were taken at ambient conditions; C) Plot of Rh – Rh coordination number versus temperature for  $\text{KCa}_2\text{Nb}_3\text{O}_{10}$  and Na-TSM shows the quicker reduction to rhodium metal nanoparticles on Na-TSM versus  $\text{KCa}_2\text{Nb}_3\text{O}_{10}$ .

under ambient conditions. X-ray Absorption Near Edge Structure (XANES) analysis of samples reduced in 100 kPa  $\text{H}_2$  indicates that Rh(III) is 80 % reduced to Rh(0) by 250 °C and 90 % by 500 °C on both  $\text{KCa}_2\text{Nb}_3\text{O}_{10}$  and Na-TSM (Figure 3). While the rhodium is being reduced at the same rate for both supports, the coordination number increases more rapidly for the particles on Na-TSM than  $\text{KCa}_2\text{Nb}_3\text{O}_{10}$ . As noted above, the difference can be attributed to differences in the size of the precursor  $\text{Rh}(\text{OH})_3$  particles.

at each temperature during TEM imaging. During this time, no nanoparticle growth was evident. This leads to the conclusion that beam effects did not induce significant changes in nanoparticle size.

Short timescale studies were also done *in situ* in the TEM to determine if kinetics played a role in the growth of the nanoparticles. During a typical TEM analysis, stabilization at a given temperature took up to 30 min. Samples with nanoparticles deposited on  $\text{KCa}_2\text{Nb}_3\text{O}_{10}$  and Na-TSM were heated at 600 °C for 2.5 h and the particle sizes did not increase on either support. To further investigate kinetic effects, nanoparticles deposited on  $\text{KCa}_2\text{Nb}_3\text{O}_{10}$  were heated *ex situ* at atmospheric pressure in pure hydrogen at 600 °C for 24 h and 48 h, and the average diameters of the nanoparticles were  $(4 \pm 2)$  nm ( $n = 116$ ) and  $(4 \pm 3)$  nm ( $n = 192$ ), respectively.

As noted above, many previous studies of SMSI show evidence, especially from TEM and chemisorption data, that encapsulation of late transition metal nanoparticles occurs under reducing conditions. With oxide nanosheet supports under the conditions investigated here, there was no evidence in HRTEM images of encapsulation of the nanoparticles. Thus it appears in the present case that the unusual stabilization of Rh nanoparticles arises from a covalent bonding interaction with the layered niobate supports. Rhodium oxide nanoparticles have previously been deposited on  $\text{SiO}_2$ ,  $\text{CeZrO}_2$ ,  $\text{ZrO}_2$  and  $\text{CeO}_2$  supports and heated in  $\text{H}_2$  to reduce the particles. It was found that the activity of the catalyst for CO oxidation increased as  $\text{SiO}_2 < \text{ZrO}_2 < \text{CeZrO}_2 < \text{CeO}_2$ . It was suggested the activity increases in this manner because of the distribution of rhodium oxide on the support. This trend correlates with the d-electron acidity of the support, which increases in the order of increasing catalyst activity. Another study showed zirconia retarded the growth of Pd nanoparticles, whereas  $\text{SiO}_2$  and  $\gamma\text{-Al}_2\text{O}_3$  supports did not have the same effect at 900 °C. These trends are not easily explained by an SMSI model involving reduction of the support. Zirconia is not easily reduced nor does it suppress  $\text{H}_2$  chemisorption, but it does maintain small particle sizes for late transition elements such as Rh and Pd.

The transformation of supported  $\text{Rh}(\text{OH})_3$  to elemental Rh was studied using extended x-ray absorption spectroscopy (EXAFS). Samples were heated *ex situ* in hydrogen for 30 min at each temperature before x-ray absorption data were obtained

### **Publications Acknowledging this Grant in 2011-2014**

1. Strayer, M.; Binz, J. M.; Tanase, M.; Kamali Shahri, S. M.; Sharma, R.; Rioux, R. M.; Mallouk, T. E. Interfacial bonding stabilizes rhodium and rhodium oxide nanoparticles on layered Nb- and Ta oxide supports. *J. Am. Chem. Soc.* 2014, 136, 5687-5696.
2. Spanjers, C. S.; Senftle, T. P.; van Duin, A. C. T.; Janik, M. J.; Frenkel, A. I.; Rioux, R. M.; Illuminating Surface Atoms in Nanoclusters by Differential X-ray Absorption Spectroscopy. Submitted to *Phys. Chem. Chem. Phys.* (2014).

**José A. Rodriguez**

## **Catalysis for Advanced Fuels**

**José A Rodriguez, Ping Liu, Dario Stacchiola, Sanjaya Senanayake, Mike G. White and Jonathan C. Hanson.**

**Chemistry Department , Brookhaven National Laboratory**

### **Presentation Abstract**

This program pursues an improved understanding of chemical catalysis for advanced fuels synthesis and energy conversion processes by elucidating catalytically important properties of well-defined surfaces, powders and nanostructures. Complexities stemming from the inherent multi-component aspects of heterogeneous catalysis are explored using both ultra-high-vacuum surface science investigations of well-defined model systems, and powder diffraction and x-ray absorption studies of "real-world" systems. We have found very efficient catalysts for desulfurization and the production of methanol from CO<sub>2</sub> hydrogenation that take advantage of the chemical properties of metal-carbide interfaces such as Au-TiC and Cu-TiC. Small clusters of Au and Cu in direct contact with TiC undergo a polarization of charge which enhances the chemical reactivity of the admetals. The metal-carbide interfaces contain special binding sites which are able to adsorb and transform molecules that have a low reactivity (CO<sub>2</sub>, CH<sub>4</sub>, thiophene, etc). In contrast, the formation of a Ni-ceria interface reduces the ability of Ni to break C-O bonds making the Ni/ceria system an excellent catalyst for ethanol steam reforming. In the future, we plan to study and manipulate in a systematic way a series of multifunctional catalysts which contain metal-oxide, metal-carbide or metal-sulfide interfaces. One of our main objectives is to develop instrumentation or methodologies for *in-situ* imaging (STM, TEM) of working catalysts. Part of our efforts focus on the coupling of XRD and XAFS with infrared spectroscopy and in the development of instrumentation for transient measurements and kinetic studies.

## **BNL FWP CO-009: Catalysis for Advanced Fuels**

### **Subtask 1: Catalysis, Structure and Reactivity**

**Postdoctoral fellows: Shankamala Kundu, Rui Si, Fuzhen Zhao**

**Students: Si Luo, Zongyen Liu, Siyu Yao**

## RECENT PROGRESS

The research themes in this FWP are inspired by challenges in the production and use of chemical fuels [1-34]. Specific themes are (i) the cleaning of oil-derived fuels through hydrodesulfurization [1,9,10], (ii) the reforming of alcohols [12,21,28], (iii) the synthesis of higher (C<sub>1</sub>-C<sub>4</sub>) alcohols by the hydrogenation of CO<sub>2</sub> or CO [2,30], and (iv) CO oxidation [3-7,13,23,29,31]. The last two topics are associated with C1 chemistry. These research efforts are also linked by an interest in the properties of oxides [4,5,11,14,27,28], carbides [1,9,15-17] and sulfides [9], materials which may be able to replace scarce noble metals in energy-related catalysis involving hydrogen transfer, e.g. hydrogenation and hydrodesulfurization processes [2,9,30]. In many of our studies, the catalytic processes are carried out on multifunctional catalysts which contain metal-oxide, metal-carbide or metal-sulfide interfaces [1,5,9,28]. The research team has a strong interest in the development of tools for the *in-situ* characterization of model and powder catalysts under reaction conditions [8,12,18-20,23,29]. Since 2011, more than 30 papers have been published showing the work done under this FWP [1-34].

### *Activation of Noble Metals on Metal-Carbide Surfaces: Novel Catalysts for Desulfurization, CO Oxidation and Hydrogenation Reactions*

Transition-metal carbides exhibit broad and amazing physical and chemical properties. These properties may be viewed as resulting from a combination of those of covalent solids, ionic crystals and transition metals. High-resolution photoemission, scanning tunneling microscopy (STM) and first-principles periodic density-functional (DF) calculations have been used to study the interaction of metals of Groups 9, 10 and 11 with MC(001) (M= Ti, Zr, V, Mo) surfaces [1,2,16]. DF calculations give adsorption energies that range from 2 eV (Cu, Ag, Au) to 6 eV (Co, Rh, Ir) [1,15,16]. STM images show that Au, Cu, Ni and Pt grow on the carbide substrates forming two-dimensional islands at very low coverage, and three-dimensional islands at medium and large coverage [1]. In many systems, the results of DF calculations point to the preferential formation of admetal-C bonds with significant electronic perturbations in the admetal, see Figure 1. A comparison of the

behavior of Au deposited on MC(001) (M= Ti, Mo, V, Zr) indicates that the electronic perturbations on the admetal vary depending on the nature of the carbide substrate [1,15,16]. TiC(001) and ZrC(001) transfer some electron density to the admetals facilitating bonding of the adatom with electron-acceptor molecules (CO, O<sub>2</sub>, C<sub>2</sub>H<sub>4</sub>, SO<sub>2</sub>, thiophene, etc) [1,10]. In spite of the very poor HDS performance of TiC(001) or Au(111), a Au/TiC(001) surface displays an activity for the HDS of thiophene higher than that of conventional Ni/MoS<sub>x</sub> catalysts [1,9]. In

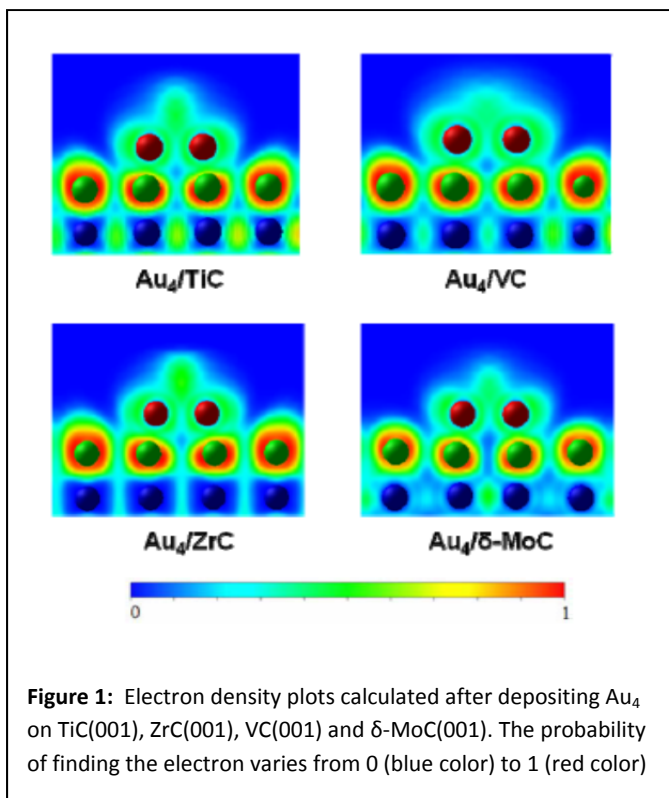


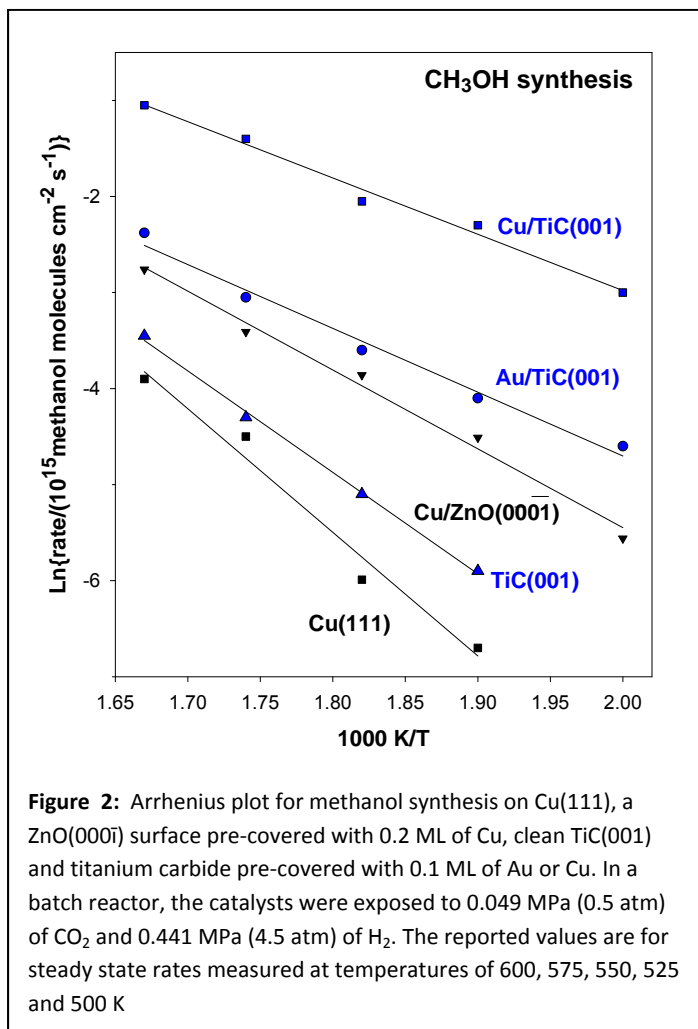
**Figure 1:** Electron density plots calculated after depositing Au<sub>4</sub> on TiC(001), ZrC(001), VC(001) and δ-MoC(001). The probability of finding the electron varies from 0 (blue color) to 1 (red color)

general, the Au/TiC system is more chemically active than systems generated by depositing Au nanoparticles on oxide surfaces [1,2,9,10,15,16]. Thus, metal carbides are excellent supports for enhancing the chemical reactivity of noble metals.

#### *Methanol synthesis from CO<sub>2</sub> Hydrogenation on Au/TiC(001) and Cu/TiC(001)*

CO<sub>2</sub> chemistry has become a very attractive area of research not only because environmental concerns but also due to the potential use of CO<sub>2</sub> as an alternative and economical feedstock. This is a difficult task in C1 chemistry due to the challenges associated with the chemical activation of CO<sub>2</sub>. In the area of heterogeneous catalysis, a lot of attention has been focused on the synthesis of methanol through the hydrogenation of carbon dioxide (CO<sub>2</sub> + 3H<sub>2</sub> → CH<sub>3</sub>OH + H<sub>2</sub>O) on metal and metal/oxide catalysts. Our studies indicate that small Cu and Au particles in contact with a TiC(001) surface undergo a charge polarization (Fig 1)

which makes them very active for CO<sub>2</sub> activation and the catalytic synthesis of



methanol [2,30]. The binding energy of CO<sub>2</sub> on these systems is in the range of 0.6 to 1.1 eV, much larger than those observed on surfaces or nanoparticles of Cu and Au. Thus, in spite of the poor CO<sub>2</sub> hydrogenation performance of Cu(111) and Au(111), the Cu/TiC(001) and Au/TiC(001) systems display a catalytic activity for methanol synthesis substantially higher than that of conventional Cu/ZnO catalysts, see Fig 2 [2,30]. The turnover frequencies for methanol production on Cu/TiC(001) are 170-500 times much larger than on Cu(111) [2]. Thus, our study

illustrates the advantages of using a metal carbide as a support for noble metals for CO<sub>2</sub> hydrogenation.

#### *Studies on Ethanol Steam Reforming on a NiO/CeO<sub>2</sub> Catalyst*

In recent years, ethanol has received significant attention as a source of energy. One objective is the production of hydrogen from steam reforming (C<sub>2</sub>H<sub>5</sub>OH + 3H<sub>2</sub>O → 2CO<sub>2</sub> + 6H<sub>2</sub>) and there is also a strong interest in directly using ethanol as a fuel for mobile fuel cell applications. A major issue is the identification of non-expensive and stable catalysts which can accomplish the cleavage of the C-C bond in ethanol without subsequent deactivation by coke deposition. Our studies have

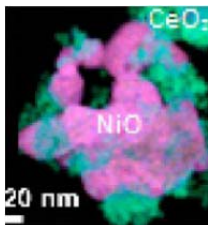


**Figure 3.** TEM image of a NiO-CeO<sub>2</sub> catalyst used for ethanol reforming

shown that the NiO/CeO<sub>2</sub> can accomplish this [12]. The steam reforming of ethanol on a Ni-based CeO<sub>2</sub>-supported catalyst, see Figure 3, was studied using *in-situ* X-ray XRD, operando DRIFTS, and mass spectroscopy with a focus on the structural characterization of the catalysts, chemical identification of the reaction pathway, and understanding of the interaction between Ni and the CeO<sub>2</sub> support [11,12]. The results of TEM and XRD indicate that the fresh catalyst consists of a mixture of NiO and CeO<sub>2</sub>. Upon exposure to a mixture of ethanol and water, or even pure ethanol, the NiO undergoes reduction at temperatures above 300 °C. At the conditions in which ethanol is transformed into H<sub>2</sub> and CO<sub>2</sub> (T > 300 °C), the sample contains nanoparticles of Ni dispersed on a partially reduced ceria support [12]. Ethoxy, acetate, carbonate, and hydroxyl species were identified by DRIFTS as surface intermediates that appear during the reaction process. The oxidation of ethoxy to acetate and the decomposition of acetate were two key steps in the steam reforming process on Ni/CeO<sub>2</sub> [12]. Electronically perturbed Ni adatoms exhibited an unusual chemical reactivity [11,28]. In general, we have found that the small Ni particles supported by CeO<sub>2</sub> are highly active towards ethanol steam reforming displaying a better performance than the best catalyst reported in the literature, Rh/CeO<sub>2</sub>. Thus, in Ni/CeO<sub>2</sub> we have a highly efficient and non-expensive catalysts for ethanol steam reforming [12,28].

#### *CO Oxidation of Well-defined Surfaces of Mixed-Metal Oxides*

Within the realm of C1 chemistry, the oxidation of CO ( $\text{CO} + 0.5\text{O}_2 \rightarrow \text{CO}_2$ ) is the simplest reaction that can be used to test the catalytic properties of novel materials. In automotive exhaust emission control, the complete oxidation of carbon monoxide is of prime importance to meet increasingly stringent environmental regulations in a practical way. Our group has found that mixed-metal oxides of the CeO<sub>2</sub>/CuO<sub>x</sub>, TiO<sub>x</sub>/CuO<sub>x</sub> and RuO<sub>2</sub>/TiO<sub>2</sub> types are quite active for the oxidation of CO [3,4,13,23,29,34]. In a set of experiments, the combination of XPS and STM established that supported nanoparticles of CeO<sub>x</sub> and RuO<sub>x</sub> were quite efficient for adsorbing and dissociating the O<sub>2</sub> molecule [3,4], with a subsequent spilling of O to

the oxide support. The configuration of these mixed-metal oxide catalysts opens interesting routes for technological applications.

*Development of Techniques for In-situ Characterization of Powder Catalysts: Time-resolved PDF, XAFS/XRD, XAFS/IR and XAFS/Raman*

The development of techniques for characterizing the structural properties of catalysts under the high-pressure conditions of industrial processes is widely recognized as a top priority in the area of heterogeneous catalysis. In the last years, the Catalysis Group at BNL has been very active in developing instrumentation for the characterization of catalysts with pair-distribution function (PDF) analysis and the integration of XAFS and XRD or XAFS and IR or Raman [18-20,23,25]. The integration of IR and Raman with XAFS (Fig 4) allows a simultaneous determination of the reaction intermediates on the surface and the chemical state and structure of the catalyst [23]. Raman spectroscopy adds sensitivity to crystallographic phase and long range order that both XANES and EXAFS are lacking. *In-situ* PDF has been used to study the structure of amorphous metal and metal oxide nanoparticles under reaction [31]. Using a XAFS/IR combination, we have investigated reaction mechanisms and correlations between structure/reactivity for CO oxidation [29].

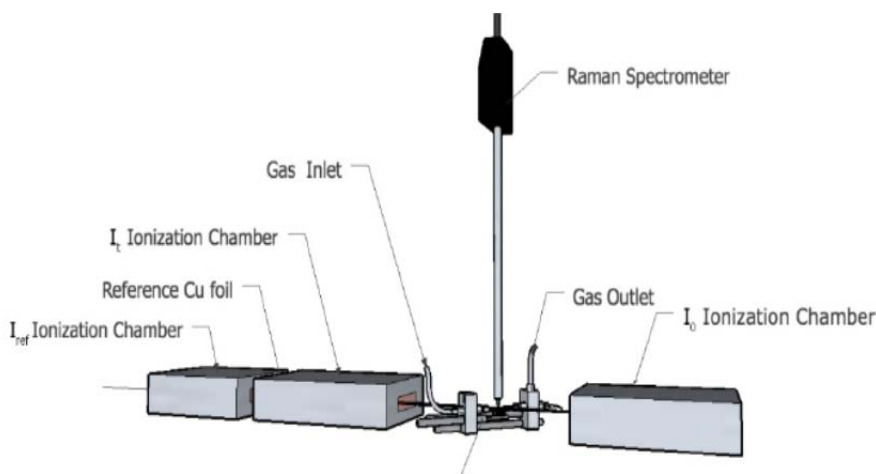


Figure 4. Instrumental set-up for combining XAFS and Raman [23].

## Publication list

1. Rodriguez, J.; Illas, F. *Physical Chemistry Chemical Physics*, **2012**, *14*, 427-438.
2. Vidal, A., et al., *Journal of Physical Chemistry Letters*, **2012**, *3*, 2275-2280.
3. Yang, F., et al., *Journal of the American Chemical Society*, **2011**, *133*, 3444-3451.
4. Yang, F., et al., *Angewandte Chemie-International Edition*, **2011**, *50*, 10198-10202.
5. Stacchiola, D.J., et al., *Chemical Reviews*, **2013**, *113*, 4373-4390.
6. Yang, F., et al., *Journal of Physical Chemistry C*, **2011**, *115*, 23062-23066.
7. Liu, P., *Journal of Physical Chemistry C*, **2012**, *116*, 25337-25343.
8. Mudiyansele, K., et al., *Angewandte Chemie International Edition*, **2013**, *52*, 5101-5105.
9. Rodriguez, J., et al., *Catalysis Today*, **2011**, *166*, 2-9.
10. Feria, L., et al., *Journal of Catalysis*, **2011**, *279*, 352-360.
11. Carrasco, J., et al., *Journal of Physical Chemistry C*, **2013**, *117*, 8241-8250.
12. Xu, W., et al., *ACS Catalysis*, **2013**, *3*, 975-984.
13. Yan, T., et al., *Journal of Catalysis*, **2012**, *294*, 216-222.
14. Wang, H., et al., *Journal of the American Chemical Society*, **2013**, *135*, 4149-4158.
15. Gomez, T., et al., *Journal of Physical Chemistry C*, **2011**, *115*, 11666-11672.
16. Florez, E., et al., *Physical Chemistry Chemical Physics*, **2011**, *13*, 6865-6871.
17. Asara, G., et al., *Journal of Physical Chemistry C*, **2011**, *115*, 22495-22504.
18. Frenkel, A.I.; Rodriguez, J.A.; Chen, J.G. *ACS Catalysis*, **2012**, *2*, 2269-2280.
19. Frenkel, A., et al., *Journal of Physical Chemistry C*, **2011**, *115*, 17884-17890.
20. Rodriguez, J.A.; Hanson, J.C.; Chupas, P. *Goals and Challenges for the In-situ Characterization of Heterogeneous Catalysts*, in *In-situ Characterization of Heterogeneous Catalysts*, J.A. Rodriguez, J.C. Hanson, and P. Chupas, Editors. 2013, Wiley: New York.
21. Choi, Y.M.; Liu, P. *Catalysis Today*, **2011**, *165*, 64-70.
22. Kundu, S., et al., *Journal of Physical Chemistry C*, **2012**, *116*, 4767-4773.
23. Platolla, A., et al., *Topics in Catalysis*, **2013**, *56*, 896-904.
25. Rodriguez, J.A., et al., *Physical Chemistry Chemical Physics*, **2013**, *15*, 12004-12025.

26. Senenayake, S.D.; Stacchiola, D.; Rodriguez, J.A. *Accounts of Chemical Research*, **2013**, *46*, 1702-1711.
27. Johnston-Peck, A., et al., *Journal of Physical Chemistry C*, **2013**, *117*, 14463-14471.
28. Senenayake, S.D.; Rodriguez, J.A.; Stacchiola, D., *Topics in Catalysis*, **2013**, *56*, 1488-1498.
29. Yao, S.Y. et al., *ACS Catalysis*, **2014**, *4*, 1650-1661.
30. Rodriguez, J.A. et al., *Journal of Catalysis*, **2013**, *307*, 162-169.
31. Hanson, J.C. et al, *Catalysis Today*, **2014**, *229*, 64-71.
32. Guzman-Blas, R. et al, *Electrocatalysis*, **2014**, *5*, 50-61.
33. Wang, H. et al, *Angew. Chem. Int. Ed.* **2013**, *52*, 9210-9214.
34. Baber, A.E. et al, *Angew. Chem. Int. Ed.* **2014**, doi: 10.1002/anie.201402435.

## Solution-phase and Immobilized Ligands in Catalytic Carbonyl Chemistry

Andreja Bakac, Takeshi Kobayashi, Oleg Pestovsky, Marek Pruski, Aaron D. Sadow, Igor I. Slowing  
Ames Laboratory, U.S. DOE, Iowa State University, Ames, IA 50011-3111

### Presentation Abstract

This work is part of Ames Laboratory research on "Homogeneous and Interfacial Catalysis in 3D Controlled Environment", described in detail elsewhere.

To prepare single site interfacial catalysts for conversions of oxygenated and partly oxidized organic compounds, we have reacted  $To^M Rh(CO)_2$  ( $To^M = \text{tris}(4,4\text{-dimethyl-2-oxazolinyl})\text{phenylborate}$ ) with benzenesulfonic acid functionalized mesoporous silica (MSN- $PhSO_3H$ ). The product,  $[HTo^M Rh(CO)_2]^+[MSN-PhSO_3]^-$ , is assigned based on a comparison to soluble analogues, namely the reactions of  $To^M Rh(CO)_2$  and  $PhSO_3H$  or  $F_3CSO_3H$ .<sup>1</sup>  $To^M Rh(CO)_2$  is a catalyst for the photoactivated decarbonylation of alcohols to alkane, CO, and  $H_2$ ,<sup>2</sup> however under homogeneous conditions,  $[HTo^M Rh(CO)_2]^+[PhSO_3]^-$  does not catalyze decarbonylation. In contrast  $To^M Ir(\eta^4-C_8H_{12})$  and  $Ph_2B(Ox^{Me_2})Ir(\eta^4-C_8H_{12})$  ( $Ox^{Me_2} = 4,4\text{-dimethyl-2-oxazoline}$ ) catalyze the thermal decarbonylation of primary alcohols to alkanes. In order to further enhance reactivity for carbonyl activation under photochemical or thermal conditions, we have synthesized new oxazolinyborate ligands. In particular, a new bis(oxazoliny) (carbene)phenylborate ligand  $[PhB(Ox^{Me_2})_2(Im^{Mes})]^-$  ( $Im^{Mes} = 1\text{-mesitylimidazole}$ ) is synthesized by the reaction of the borane  $[PhB(Ox^{Me_2})_2]_n$  and  $Im^{Mes}$ .<sup>3</sup> Metalation with rhodium gives  $\{PhB(Ox^{Me_2})_2(Im^{Mes})\}Rh(CO)_2$ . Although that compound is also not effective for photochemical or thermal decarbonylation of primary alcohols, it reacts with  $PhSiH_3$  under thermal conditions to give  $\{PhB(Ox^{Me_2})_2(Im^{Mes})\}RhH(SiH_2Ph)(CO)$  via oxidative addition of a silane Si-H bond. Notably, the tris(oxazoliny)borate analog is inert to silane oxidative addition.<sup>4</sup> The deoxygenation of esters to ethers is readily catalyzed by  $\{PhB(Ox^{Me_2})_2(Im^{Mes})\}RhH(SiH_2Ph)(CO)$  in combination with  $B(C_6F_5)_3$ . The mixed bis(oxazoline)(carbene)borate ligand also supports zinc alkyls and zinc alkyl peroxides (formed from reactions with  $O_2$ ). Thus,  $H[PhB(Ox^{Me_2})_2(Im^{Mes})]$  and  $ZnR_2$  ( $R = H, Me, Et$ ) react to give  $\{PhB(Ox^{Me_2})_2(Im^{Mes})\}ZnR$ . Reaction of  $\{PhB(Ox^{Me_2})_2(Im^{Mes})\}ZnEt$  and  $O_2$  provides crystallographically characterized  $\{PhB(Ox^{Me_2})_2(Im^{Mes})\}ZnOOEt$ , whereas  $\{PhB(Ox^{Me_2})_2(Im^{Mes})\}ZnMe$  and  $\{PhB(Ox^{Me_2})_2(Im^{Mes})\}ZnH$  are inert toward  $O_2$ . This reactivity follows the trend of our previous report of reactions between  $To^M ZnR$  and  $O_2$ .<sup>5</sup>

### References

1. Pawlikowski, A. V.; Gray, T. S.; Schoendorff, G.; Baird, B.; Ellern, A.; Windus, T. L.; Sadow, A. D., Structure, bonding, and ligand-based reactions of zwitterionic

- boratoiridium(I) complexes with oxazolanyl scorpionate ligands. *Inorganica Chimica Acta* **2009**, *362* (12), 4517-4525.
2. H.-A. Ho, K. Manna and A. D. Sadow, *Angewandte Chemie International Edition*, **2012**, **51**, 8607-8610.
  3. Xu, S.; Everett, W. C.; Ellern, A.; Windus, T. L.; Sadow, A. D., Oxygen Insertion Reactions of Mixed N-Heterocyclic Carbene-Oxazolanylborato Zinc Alkyl Complexes. *Dalton Transactions*, submitted.
  4. Ho, H.-A.; Dunne, J. F.; Ellern, A.; Sadow, A. D., Reactions of Tris(oxazolanyl)phenylborato Rhodium(I) with C–X (X = Cl, Br, OTf) Bonds: Stereoselective Intermolecular Oxidative Addition. *Organometallics* **2010**, *29* (18), 4105-4114.
  5. Mukherjee, D.; Ellern, A.; Sadow, A. D., Remarkably Robust Monomeric Alkylperoxyzinc Compounds from Tris(oxazolanyl)boratozinc Alkyls and O<sub>2</sub>. *Journal of the American Chemical Society* **2012**, *134* (31), 13018-13026.

**Elucidation of Heterogeneous Catalysis Mechanisms with Organic Oxygenates:  
Aldol Condensation on Cerium Oxide (111) and (100) Crystal Faces,  
and Benzylic Alcohol oxidation on Palladium Nanoparticles\***

Aditya (Ashi) Savara,<sup>1</sup> Florencia Calaza,<sup>1</sup> David R. Mullins,<sup>1</sup> Steven H. Overbury,<sup>1</sup>  
1. Oak Ridge National Laboratory, Chemical Sciences Division

Collaborators: Carine E.Chan-Thaw,<sup>2</sup> Ilenia Rossetti,<sup>2</sup> Alberto Villa,<sup>2</sup> Laura Prati<sup>2</sup>  
2. Dipartimento di Chimica, Università degli Studi di Milano, Milan, Italy

The chemistry of C-C coupling reactions catalyzed by metal oxides is still under study. One of the primary reactions for C-C coupling is aldol addition, in which two carbonyl compounds react to form a larger molecule. In the literature, several “bifunctional” catalysts, which contain both acid and base sites, have been reported to exhibit enhanced activity and/or selectivity towards aldol addition, but rational design of superior bifunctional catalysts is still not possible. Here, mechanistic insights on aldol addition catalysis are presented, based on recent results on aldol condensation of ethanal to form 2-butenal (ethanal + ethanal  $\rightarrow$  2-butenal + H<sub>2</sub>O). Ultrahigh vacuum experiments were performed with ethanal adsorption on oxidized and reduced CeO<sub>2</sub>(111) and CeO<sub>2</sub>(100) followed by temperature ramps. Aldol condensation was observed as a minor pathway on oxidized CeO<sub>2</sub>(100) at ~420 K. On partially reduced CeO<sub>x</sub>(111), stable enolates associated with Ce<sup>3+</sup> were detected prior to 420K, but aldol condensation was only observed as a minor pathway at the higher temperature of ~590K after a more complicated experimental procedure. Analysis of the mechanism in the context of the literature suggests that a) when a non-Brønsted acid site activates the carbonyl, the mechanism requires a reducible or partially reducible cation for the acid site (which Ce<sup>3+</sup> does not fulfill), and b) that in some cases, such as reduced sites on CeO<sub>x</sub>(111), enolates may bind “too strongly” to metal cations sites, preventing efficient aldol condensation.

Experiments were conducted on the liquid phase oxidation of benzyl alcohol to benzaldehyde and side products over Pd nanoparticles supported on activated carbon, with the aim of determining the operative chemical reaction network. From transient kinetic data, it was determined that there are two primary reaction paths: A) an alkoxy pathway leading to toluene, aldehyde, and benzyl ether, and B) a carbonyloxyl pathway (a radical species that is often called a “carboxylate” or “acetate”) leading to benzoic acid, benzene, and benzyl benzoate. From the mechanism elucidated, it is clear that site competition and the coverages of atomic hydrogen, atomic oxygen, and surface hydroxyls must be accounted for to achieve a complete description of the quantitative kinetics.

\*This research is part of FWP ERKCC96. For a full description of recent progress see the Abstract submitted by Steven H. Overbury.

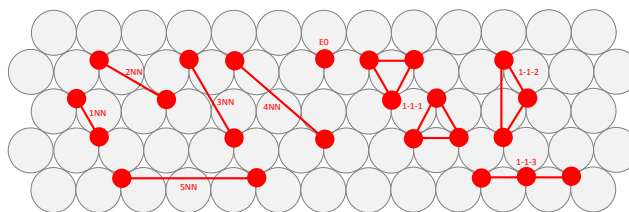
## Cluster Expansions in Catalysis

William F. Schneider

University of Notre Dame, Dept. of Chemical and Biomolecular Engineering

### Presentation Abstract

Often in computational catalysis we are confronted with describing systems in which the components interact in complicated, non-linear ways. For instance, interactions between the atoms in an alloy may favor certain alloy compositions and structures; interactions between atoms and vacancies at a surface may induce reconstructions; interactions between adsorbates can result in coverage-dependent adsorption. A cluster expansion (CE) is a useful formalism for representing the energy (or any scalar property) of a system in terms of the type, number, and arrangement of its components. CE's are conveniently fit to the results of DFT calculations and can be applied to any problem that can be mapped onto a lattice. In this work we describe our recent work to develop and apply CEs in the context of heterogeneous catalysis. First, we compare several common and one new approach to parameterizing two-dimensional CE's for surface adsorption. Second, we use the example of oxidation of a Pt surface to show how the process of fitting a CE can be helpful in discovering new, difficult to intuit surface features. Third, we show how the CE can be used to quantify coverage-dependent chemisorption on surfaces and how the CE can then be integrated into coverage-aware kinetic models. We use as example the catalytic oxidation of NO to NO<sub>2</sub> on the late transition metals.



### DE-FG02-06ER15839: Towards Realistic Models of Heterogeneous Catalysis: Simulations of Oxidation Catalysis from First Principles

Post-docs: Dr. Kurt Frey

Students: Laura Herder, Anshuman Bajpai

### RECENT PROGRESS

#### *Coverage-aware kinetic models*

In heterogeneous catalysis it is now well understood that the strength of the adsorbate-surface bond is correlated with the rates of surface reactions. In general, though, this bonding is a function not only of the surface and the adsorbate but also of the adsorbate coverage. This dependence emerges because, unlike the assumptions made in the simplest Langmuir-Hinshelwood kinetic models, adsorbates interact energetically with one another. The implications of adsorbate interactions on observed kinetics—like activation energies and rate

DE-FG02-06ER15839

orders—and on “optimal” catalytic materials, remain to be fully explored. We are examining these questions in the context of catalytic oxidations—reactions in which surfaces can accumulate high coverages of reactants. We combine density functional theory (DFT) calculations and cluster expansion techniques to develop and explore coverage-sensitive kinetic models.

Recently we have made progress on a number of fronts:

- (1) In work published in *PCCP*, we used DFT calculations to look carefully at O<sub>2</sub> dissociation pathways on Pt(111). This topic has generated a fair bit of confusion in the computational and experimental literature because of the presence of a number of competing reactions channels. We were able to combine these into a unified picture of the dissociation process at low coverage, and further showed that these competing channels all merge into a single one at higher coverages. Further, we developed a Brønsted-Evans-Polyani (BEP) correlation between dissociation barriers and adsorption energies as a function of local adsorbate coverage.
- (2) In work appearing in *Surf. Sci. Lett.* this year, we used the *PCCP* results in combination with our CE-based “reaction site” kinetic approach to predict the simplest of coverage-dependent reactions: the temperature-programmed desorption of O<sub>2</sub> from Pt(111). While this spectrum has been fit and modeled semi-empirically, this is the first fully first-principles, molecularly detailed model of the TPD. As shown in the Figure, the model predicts remarkably well the growth and temperature-dependence of the low and intermediate peaks observed experimentally. Further, by applying standard TPD analysis to the simulated spectrum, we are able to show how the underlying BEP relationships and presence of adsorbate ordering contribute to the fitted kinetic parameters.
- (3) We are interested extending the coverage modeling framework to lower-symmetry, more structured surfaces. In work appearing in *Topics in Catalysis* and in a contributed chapter to a *Computational Catalysis*, we describe a coverage-dependent adsorption model for oxygen on Pt(321). This surface exposes kinks and steps that present multiple competing sites for O and O<sub>2</sub> adsorption. With the aid of a five-site cluster expansion parameterized against 100’s of DFT calculations, we are able to predict the growth of ordered oxygen structures on the surface. The results agree with observed surface coverages and provide revised assignments of the surface vibrational spectroscopy (HREELS).

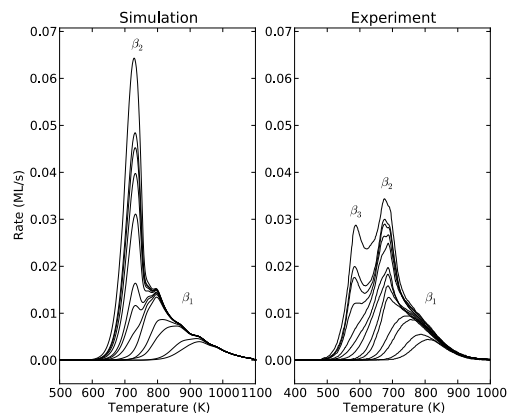


**Figure1:** Simulated (left) and observed<sup>1</sup> (right) O<sub>2</sub> TPD from Pt(111).

(4) In work reported in Jason Bray's 2013 dissertation and that we are preparing for publication, we have combined the Pt(321)-O CE results with an O<sub>2</sub> dissociation BEP to predict oxidation rates on this surface. We use the model to compare rates of NO oxidation to NO<sub>2</sub> on Pt(321) and Pt(111), two surfaces for which there is high-quality experimental results. As shown in the Figure to the right, we recover absolute rates, rate orders, and apparent activation energies that correspond well with experiment. Further, as with the TPD, we are able to identify the "site-averaged" activation energy as the key descriptor of surface reactivity and the leading contribution to both apparent activation energy and apparent rate order.

### Surface reconstructions

(5) As is evident from Figure 1, the descriptions of oxygen chemistry on Pt(111) that we have developed so far are not able to capture behavior at the very highest oxygen coverages. We understand the origins of these discrepancies: at sufficiently high oxygen coverages, the surface begins to reconstruct and oxidize. In this particular case, the reconstructions appear to be associated with adsorption of oxygen in sites so close to one another that metal atoms move out of the surface to "screen" the adsorbates from each other. As with the chemisorption problems above, this is a system that can be described (with greater effort) through a combination of DFT and CE models. To facilitate CE fitting, we have developed a new, "steepest descents" fitting algorithm that we describe in a paper under preparation for submission. With this tool in hand, we are proceeding to fit the reconstruction problem.

### Future Plans

In the systems studied to date only one species (oxygen) dominates the surface coverage problem. We are working to model more complicated multi-component systems in the same way, again with the aims (1) of properly describing coverage dependence and (2) shedding light on the manifestations of coverage on observed catalytic rates.

### Publications Acknowledging this Grant in 2011-2014

H. Wang and W. F. Schneider, "Adsorption and Reactions of NO<sub>x</sub> on RuO<sub>2</sub>(110)", *Catal. Today* **2011**, *165*, 49-55.

J. M. Bray and W. F. Schneider, "Potential Energy Surfaces for Oxygen Adsorption, Diffusion, and Dissociation at the Pt(321) Surface," *Langmuir* **2011**, *27*, 8177–8186.

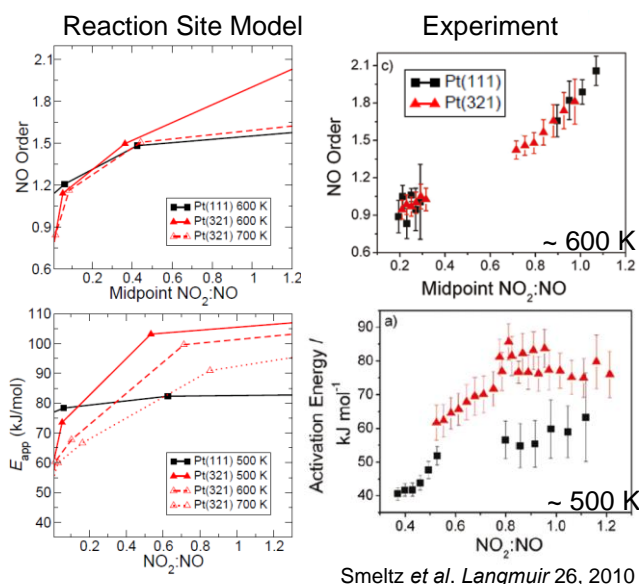


**Figure 2:** "Reaction site"-predicted and experimentally observed reaction orders (top) and apparent activation energies (bottom) for NO oxidation over Pt(111) and Pt(321).

- C. Wu, D. J. Schmidt, C. Wolverton, and W. F. Schneider, "Accurate coverage-dependence incorporated into first-principles kinetic models: Catalytic NO oxidation on Pt(111)," *J. Catal.* **2012**, 286, 88-94.
- H. Wang and W. F. Schneider, "Comparative chemistries of CO and NO oxidation over RuO<sub>2</sub>(110): Insights from first principles thermodynamics and kinetics," *Molec. Sim.* **2012**, 38, 615-630.
- J.-S. McEwen, J. Bray, C. Wu, and W. F. Schneider, "How low can you go? Minimum energy pathways for O<sub>2</sub> dissociation on Pt(111)," *Phys. Chem. Chem. Phys.*, **2012**, 14, 16677-16685.
- J. M. Bray and W. F. Schneider, "First-Principles Thermodynamic Models In Heterogeneous Catalysis," in *Computational Catalysis*, M. Janik and A. Asthagiri, eds., Royal Society of Chemistry:Cambridge (2013).
- J. M. Bray and W. F. Schneider, "Coverage-dependent adsorption at a low symmetry surface: DFT and statistical analysis of oxygen chemistry on kinked Pt(321)," *Topics Catal.* **2014**, 57, 89-105.
- J. M. Bray, I. Skavdahl, J.-S. McEwen, and W. F. Schneider, "First-principles Reaction Site Model for Coverage-Sensitive Surface Reactions: Pt(111)-O Temperature-Programmed Desorption," *Surf. Sci. Lett.*, **2014**, 622, L1-L6.

## Intrinsic heterogeneity in supported organometallic catalysts

Susannah L. Scott,<sup>1,2\*</sup> Baron Peters,<sup>1,2</sup> and Albert E. Stiegman<sup>3</sup>

<sup>1</sup> Department of Chemical Engineering, University of California, Santa Barbara

<sup>2</sup> Department of Chemistry & Biochemistry, University of California, Santa Barbara

<sup>3</sup> Department of Chemistry & Biochemistry, Florida State University

### Presentation abstract

Combining an organometallic precursor with a high surface-area oxide is frequently claimed to lead to a “well-defined” or single-site supported catalyst, although difficulties in characterizing and modeling such sites make such claims challenging to defend. Motivated to explore the relationships between surface organometallic fragments and self-initiating heterogeneous catalysts for olefin metathesis and polymerization, we aim to understand the origins and ramifications of active site heterogeneity both experimentally and computationally. The sites formed upon interaction of  $\text{CH}_3\text{ReO}_3$  with heavily chlorinated  $\gamma$ -alumina, which are active in olefin metathesis, reveal chlorine transfer from Al to Re which promotes tautomerization to the methylidene form, although such sites remain minor components according to active site counting. Similarly, grafting of  $\text{Cr}(\text{CHSi}(\text{CH}_3)_3)_3$  onto amorphous silica produces sites which are active in ethylene polymerization, but formation of large oligomers upon reaction with sub-stoichiometric amounts of ethylene suggests that few sites participate. A systematic computational method to explore the dependence of the activation barrier on small distortions in the local structure of the active site accounts for this behavior and attributes the origin of the heterogeneity to the active site-support interaction.

### DE-FG02-03ER15467: Hierarchical Design of Supported Organometallic Catalysts for Hydrocarbon Transformations

**Postdocs:** Alessandro Gallo, Zhenhuan Zhou

**Students:** Daniel Coller, Anthony Fong, Colin Gardner, Taeho Hwang, Daniel Ruiz, Stefan Seritan, Joshua Simmons, Youhong Wang, Ye Yuan

### RECENT PROGRESS

*Effect of support chlorination on an  $\text{MTO}/\text{Al}_2\text{O}_3$  olefin metathesis catalyst.* When supported onto alumina and silica-alumina, MTO becomes an active catalyst for olefin metathesis even at room temperature. The acidity of the support appears to be a key factor in MTO activation. Early literature reports suggested that Brønsted acidity was responsible, although our work showed that it is the Lewis acid sites that are directly involved in creating the active sites. In the past year, we explored chlorination of  $\gamma$ - $\text{Al}_2\text{O}_3$  followed by grafting of MTO as a means to increase the catalytic activity for olefin metathesis. It is well-known that chlorination leads to increased acidity of the support.

We observed a dramatic increase in reactivity for propylene homo-metathesis when MTO is grafted on Cl- $\gamma$ -Al<sub>2</sub>O<sub>3</sub> compared to  $\gamma$ -Al<sub>2</sub>O<sub>3</sub>, **Figure 1**. At 0 °C, equilibrium was established after 5 min over MTO/Cl- $\gamma$ -Al<sub>2</sub>O<sub>3</sub>, while MTO/  $\gamma$ -Al<sub>2</sub>O<sub>3</sub> required > 60 min. Interestingly, the increased activity is not directly correlated to the increase in the number of active sites for the chlorinated catalyst. In fact, active site counting showed that 12-16 % of the MTO is active on chlorinated alumina, while only 2 % is active when grafted on unmodified alumina. Despite the ca. 9-fold increase in the number of active sites, the catalytic activity for propylene homo-metathesis increased by a factor of 34. This implies that the active sites on Cl- $\gamma$ -

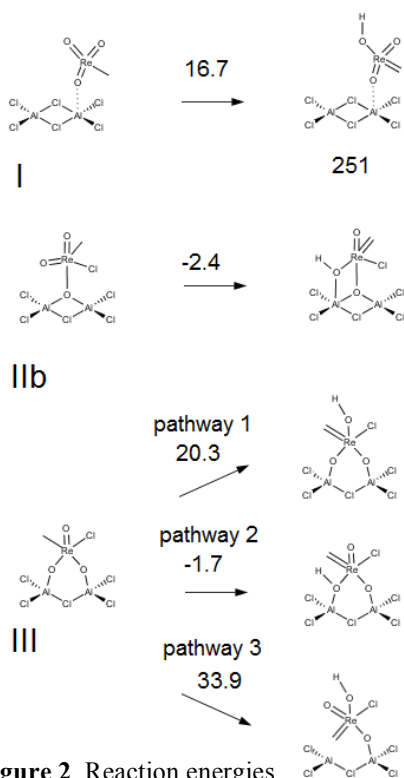


**Figure 2.** Reaction energies (kcal/mol) for carbene formation

#### *Understanding self-initiation in supported catalysts for ethylene polymerization.*

Grafting Cr[(CH(SiMe<sub>3</sub>)<sub>2</sub>)<sub>3</sub>] onto silica generates a high activity ethylene polymerization catalyst. Reaction with the surface hydroxyls was confirmed by IR. Elemental analysis (C, Cr) revealed the retention of one bis(trimethylsilyl)methyl ligand per grafted Cr site, i.e., [(≡SiO)<sub>2</sub>Cr(CH(SiMe<sub>3</sub>)<sub>2</sub>)]. The supported organochromium catalyst spontaneously initiates polymerization of gas phase ethylene at low pressure (ca. 125 Torr) with a rate law that is first-order in both P(C<sub>2</sub>H<sub>4</sub>) and moles of Cr. The specific activity and apparent activation energy of the model catalyst closely resemble that of the conventional Phillips catalyst, suggesting that they share a common polymerization mechanism.

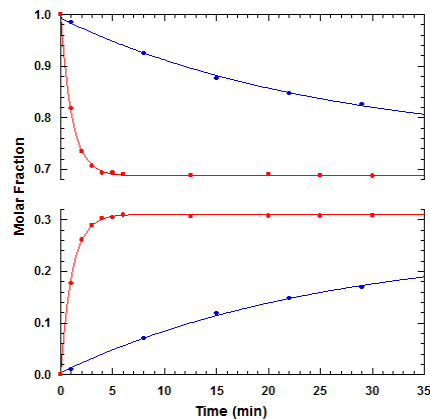


**Figure 1.** Kinetic profiles for propylene homo-metathesis at 0 °C: propylene consumption and product formation (ethene+butenes) for MTO on Cl- $\gamma$ -Al<sub>2</sub>O<sub>3</sub> (red dots: data; red line: fit) and on  $\gamma$ -Al<sub>2</sub>O<sub>3</sub> (blue dots: data; blue line: fit).

Al<sub>2</sub>O<sub>3</sub> differ from those previously reported for MTO/ $\gamma$ -Al<sub>2</sub>O<sub>3</sub>, as we also evidenced by <sup>13</sup>C solid-state NMR spectroscopy of MTO/Cl- $\gamma$ -Al<sub>2</sub>O<sub>3</sub>. The effect of chlorination on the nature and number of surface OH groups on  $\gamma$ -Al<sub>2</sub>O<sub>3</sub> was investigated using IR, <sup>1</sup>H and <sup>13</sup>C solid-state NMR, which revealed that OH groups are largely displaced by Cl. EXAFS analysis at the Re L<sub>III</sub> edge revealed the presence of a Re-Cl path.

The role of Cl in MTO activation was modeled using Al<sub>2</sub>Cl<sub>6</sub>. MTO can interact with this cluster in at least three ways: (1) via an oxo ligand binding to Al, (2) via exchange of a bridging Cl with an oxo ligand, or (3) via binding of an oxo ligand to Al with cleavage of a bridging Cl bond. All have similar energies, consistent with the observed heterogeneity of the active sites. However, transfer of Cl from Al to Re appears to promote tautomerization, leading to a Re carbene that is potentially active in metathesis, **Figure 2**.

Analysis of the products of super-low-pressure ethylene oligomerization ( $\text{Cr}/\text{C}_2\text{H}_4 = 8.3$ ) by Field Desorption (FD)-MS (**Figure 3**) revealed a mixture of hydrocarbons, most of which do not contain the initiating  $-\text{CH}(\text{SiMe}_3)_2$  ligand. The formation of long-chain oligomers suggests that few sites are highly active sites, as is found in the traditional Phillips catalyst. The heterogeneity may arise from the bonding of additional O-donor ligands derived from silica. Unexpectedly, the chains consist of not only integer but also half-integer numbers of ethylene subunits, with the former actually being more abundant. Presumably, both  $[(\equiv\text{SiO})_2\text{CrH}]$  and  $[(\equiv\text{SiO})_2\text{CrCH}_3]$  are formed by chain transfer/chain termination by both  $\beta\text{-H}$  and  $\beta\text{-CH}_3$  elimination.

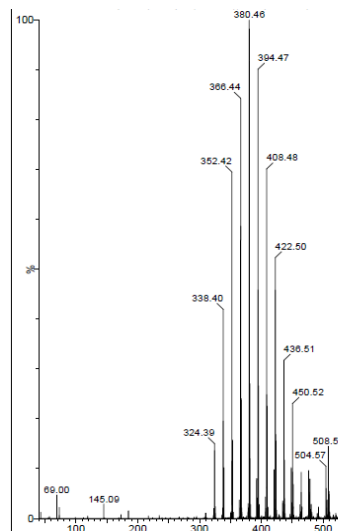


**Figure 3.** FD-MS analysis of oligomers produced in early-stage low-pressure ethylene polymerization by  $[(\equiv\text{SiO})_2\text{Cr}(\text{CH}(\text{SiMe}_3)_2)]$ .

***An algorithm for describing heterogeneity in catalyst sites on amorphous supports.*** For catalysts involving amorphous supports, the usual paradigm of predicting properties from catalyst structure is not viable because the molecular structure is unknown. Current computational methods for modeling catalysis on amorphous supports use isolated cluster models with arbitrary structural constraints, which is unsystematic and does not capture the inhomogeneous distribution of active sites present on the amorphous support.

We developed a sequential quadratic programming (SQP) algorithm that reverses the paradigm, and creates catalyst structures with specified catalytic activity, thus generating the most stable active and inactive sites for a given cluster topology. The SQP algorithm uses *ab initio* gradients and second derivatives of the energy to systematically generate low energy active sites with successively lower or higher activation energies. At each computed activation energy, the peripheral atoms are properly constrained to mimic the rigid environment around a solid active site. By comparing the structural differences between sites, important structure-property relationships can be uncovered, which can then be used to better understand catalytic activity on amorphous supports. In the past year, we have developed external plug-ins for use with the Gaussian 09 and Q-Chem computational chemistry software. The framework shows great promise as a useful tool for analysis of isolated sites on amorphous catalyst supports.

### **Publications Acknowledging this Grant in 2011-2014**

1. Xiao, P.; Davis, R. C.; Ouyang, X.; Li, J.; Thomas, A.; Scott, S. L.; Zhu, J. "Mechanism of NO reduction by CO over Pt/SBA-15", *Catal. Commun.*, **2014**, *50*, 69-72.
2. Ferrari, A.; Hunt, J.; Lita, A.; Ashley, B.; Stiegman, A. E. "Microwave-Specific Effects on the Equilibrium Constants and Thermodynamics of the Steam, Carbon and Related Reactions", *J. Phys. Chem. C*, **2014**, *118*, 9346-9356.
3. Hwang, T.; Goldsmith, B.; Peters, B.; Scott, S.L. "Water-Catalyzed Activation of  $\text{H}_2\text{O}_2$  by Methyltrioxorhenium: A Combined Computational-Experimental Study",

- Inorg. Chem.*, 2013, 52, 13904-13917.
4. Goldsmith, B. R.; Sanderson, E. D.; Bean, D.; Peters, B. "Isolated catalyst sites on amorphous supports: a systematic algorithm for understanding heterogeneities in structure and reactivity", *J. Chem. Phys.* **2013**, 138, 204105.
  5. Goldsmith, B. R.; Fong, A.; Peters, B. "Understanding reactivity with reduced potential energy landscapes: recent advances and new directions." In *Reaction Rate Constant Computations: Theories and Applications*, Eds Han, K.; Chu, T. Royal Society of Chemistry: Cambridge, U.K. **2013**, pp. 213-232.
  6. Tiozzo, C.; Bisio, C.; Carniato, F.; Gallo, A.; Scott, S. L.; Psaro R.; Guidotti, M. "Niobium-silica catalysts for the selective epoxidation of cyclic alkenes: the generation of the active site by grafting niobocene dichloride", *Phys. Chem. Chem. Phys.*, **2013**, 15, 13354-13362.
  7. Crosswhite, M.; Hunt, J.; Southworth, T.; Serniak, K.; Ferrari, A.; Stiegman, A. E. "Development of Magnetic Nanoparticles as Microwave-Specific Catalysts for the Rapid, Low-Temperature Synthesis of Formalin Solutions", *ACS Catal.*, **2013**, 3, 1318-1323.
  8. Dudley, G. B.; Stiegman, A. E.; Rosana, M. R. "Correspondence on Microwave Effects in Organic Synthesis", *Angew. Chem. Int. Ed.*, **2013**, 52, 7918-7923.
  9. Hunt, J.; Ferrari, A.; Lita, A.; Crosswhite, M.; Ashley, B.; Stiegman, A. E. "Microwave-Specific Enhancement of the Carbon-Carbon Dioxide (Boudouard) Reaction", *J. Phys. Chem. C*, **2013**, 117, 26871-26880.
  10. J. Zhu, X. Ouyang, M.-Y. Lee, R. C. Davis, S. L. Scott, A. Fischer, and A. Thomas, "Two-step synthesis of Fe<sub>2</sub>O<sub>3</sub> and Co<sub>3</sub>O<sub>4</sub> nanoparticles: towards a general method for synthesizing nanocrystalline metal oxides with high surface area and thermal stability", *RSC Adv.* **2012**, 2, 121-124.
  11. Peters, B. "Headspace diffusion limitations on heterogeneous catalysis in unstirred batch reactors", *Chem. Eng. Sci.*, **2012**, 71, 367-374.
  12. Tovar, T. M.; Stewart S. M.; Scott, S. L. "Origin of the ZnCl<sub>2</sub> Effect on CH<sub>3</sub>ReO<sub>3</sub>/γ-Al<sub>2</sub>O<sub>3</sub> in Olefin Metathesis", *Top. Catal.*, **2012**, 55, 530-537.
  13. Vicente, B. C.; Nelson, R. C.; Moses, A. W.; Chattopadhyay, S.; Scott, S. L. "Interactions Involving Lewis Acidic Aluminum Sites in Oxide-Supported Perrhenate Catalysts", *J. Phys. Chem. C* **2011**, 115, 9012-9024.
  14. Fleischman, S. D.; Scott, S. L. "Evidence for the Pairwise Disposition of Grafting Sites on Highly Dehydroxylated Silicas via Their Reactions with Ga(CH<sub>3</sub>)<sub>3</sub>", *J. Am. Chem. Soc.* **2011**, 133, 4847-4855.
  15. Shayib, R. M.; George, N.; Seshadri, R.; Burton, A. W.; Zones, S. I.; Chmelka, B. F. "Structure-Directing Roles and Interactions of Fluoride and Organocations with Siliceous Zeolite Frameworks", *J. Am. Chem. Soc.*, **2011**, 133, 18728-18741.
  16. Kurzman, J. A.; Li, J.; Schladt, T. D.; Parra, C. R.; Ouyang, X.; Davis, R. C.; Miller, J. T.; Scott, S. L.; Seshadri, R. "Pd<sup>2+</sup>/Pd<sup>0</sup> Redox Cycling in Hexagonal YMn<sub>0.5</sub>Fe<sub>0.5</sub>O<sub>3</sub>: Implications for Catalysis by PGM-Substituted Complex Oxides", *Inorg. Chem.* **2011**, 50, 8073-8084.
  17. Lee, M.-Y.; Scott, S. L. "Quantitative Investigation of a Hybrid Ziegler-Natta Catalyst Support Prepared by Grafting Di(n-butyl)magnesium onto Partially Dehydroxylated Silica", *Chem. Eur. J.* **2011**, 17, 4632-4639.

**Theoretical studies of water oxidation on titanium, cobalt, and nickel/iron oxides**

Annabella Selloni, Jia Chen, Ye-Fei Li  
Department of Chemistry, Princeton University, Princeton, N.J. 08544

**Abstract**

Water splitting on metal oxides has attracted a great deal of interest for more than forty years. While most of the work has focused on  $\text{TiO}_2$ , recently cobalt and mixed Ni-Fe oxides have also emerged as promising electrocatalysts for water oxidation due to their low cost and high activity. This talk reviews recent studies of our group on the oxidation of water on these materials. Using DFT+U calculations, we have compared the energetics of the oxygen evolution reaction (OER) on selected surfaces of  $\text{Co}_3\text{O}_4$ ,  $\text{CoOOH}$ ,  $\text{NiFe}_2\text{O}_4$ , pure and Fe-doped  $\text{NiOOH}$ . Based on the computed overpotentials, Fe-doped  $\beta$ - $\text{NiOOH}$  is predicted to be even more active than  $\text{RuO}_2$ , a well-established catalyst for the OER. By combining First Principles Molecular Dynamics simulations with hybrid functional calculations, we have studied the kinetics of the first proton-coupled-electron transfer at the water/ $\text{TiO}_2$  interface in the presence of a photoexcited hole. Our results provide evidence that the proton and electron transfers are not concerted but rather represent two sequential processes. Finally, we examined the OER activity of a  $\text{TiO}_2$  (001) film of anatase supported by a ferroelectric substrate. We find that the activity is directly related to the changes of the dynamically induced polarization in the supported  $\text{TiO}_2$  film during the reaction. Our results further show that by combining strain with polarization it is possible to generate a pathway with strongly reduced thermodynamic barriers relative to unsupported  $\text{TiO}_2$ .

**DE-FG02-12ER16286: Understanding Surfaces and Interfaces of Photocatalytic Oxide Materials with First Principles Theory and Simulations**

**Postdocs:** Jun Hee Lee<sup>(a)</sup>, Ye-Fei Li

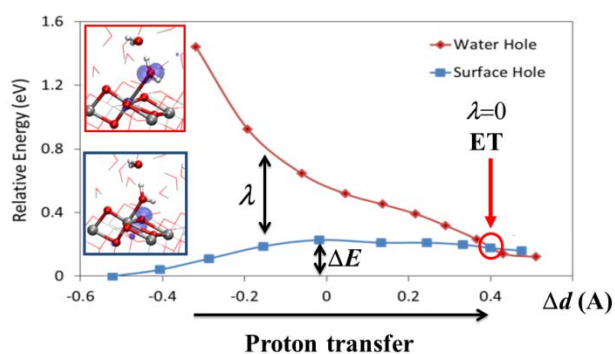
**Students:** Jia Chen<sup>(b)</sup>, Weiyi Hou, Sencer Selcuk

**Affiliations:** <sup>(a)</sup> Present address: Materials Science and Technology Division, Oak Ridge National Laboratory, Oak Ridge, TN 37831, USA; <sup>(b)</sup> Present address: Materials Science and Engineering, Columbia University, New York, NY 10027

**RECENT PROGRESS**

*Chemical Dynamics of the First Proton Coupled Electron Transfer of Water Oxidation on  $\text{TiO}_2$  Anatase* -  $\text{TiO}_2$  is one of the most widely used photoanode materials for photo-electrochemical water splitting, yet its performance is limited by the large overpotential for the oxygen evolution reaction (OER). To obtain insight into the origin of this limitation, we have carried out a theoretical study of the first proton coupled electron transfer (PCET), which is

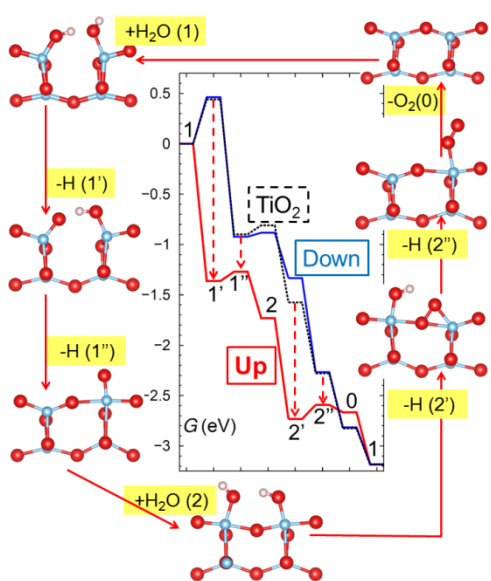
generally considered the rate-determining step of the OER on TiO<sub>2</sub>. We use a periodic model of



the TiO<sub>2</sub>/water interface that includes a slab of anatase TiO<sub>2</sub> and explicit water molecules, sample the solvent configurations by First Principles Molecular Dynamics, and determine the energy profiles of the two electronic states involved in the electron transfer (ET) by hybrid functional calculations. Our results indicate that the proton and electron transfer are not concerted but rather

sequential, with the proton transfer (PT) preceding the electron transfer (ET). The PT has a significant activation energy, in the range 0.2-0.5 eV, whereas the following ET is essentially barrierless and occurs via an inner sphere process, which is facilitated by a state in which one electronic hole is shared by the two oxygen ions involved in the transfer. Based on these results, the higher OER activity that is observed experimentally at high pH can also be explained.

**TiO<sub>2</sub>/Ferroelectric Heterostructures as Catalysts for Water Oxidation** – In the search for novel photocatalytic materials that are more efficient than TiO<sub>2</sub>, recent experimental studies have considered heterostructures composed of a TiO<sub>2</sub> thin film on a ferroelectric substrate. Despite

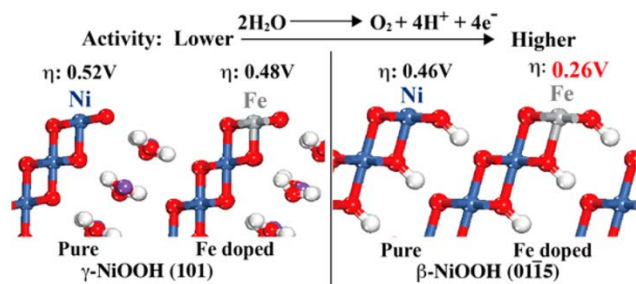


some encouraging results, understanding of the reactivity of these heterostructures is still limited.

Using DFT calculations, we have explored the chemical activity of epitaxial heterostructures of TiO<sub>2</sub> anatase on strained polar SrTiO<sub>3</sub>(STO) films focusing on the oxygen evolution reaction (OER), the bottleneck of water-splitting. Our results show that the reactivity of the TiO<sub>2</sub> surface is tuned by electric dipoles dynamically induced by the adsorbed species during the intermediate steps of the reaction while the initial and final steps remain unaffected. By varying the strain and thickness of the STO substrate, we further show that the strain and the induced dipole can be synergistically tuned to optimize the surface reactivity. Compared to the OER on unsupported TiO<sub>2</sub>, the combined

effects of the dynamically induced dipoles and epitaxial strain strongly reduce rate-limiting thermodynamic barriers and significantly improve the efficiency of the reaction.

**Mechanism and Activity of Water Oxidation on Pure and Fe-doped NiO<sub>x</sub>** - Mixed nickel-iron oxides have recently emerged as promising electrocatalysts for water oxidation due to their low cost and high activity, but the composition and structure of the catalyst's active phase under working conditions is not yet fully established. Using density functional theory calculations with



on-site Coulomb repulsion, we have studied the energetics of the OER on selected surfaces of pure and mixed Ni-Fe oxides that are possible candidates for the catalyst's active phase. The investigated surfaces are pure  $\beta\text{-NiOOH}(01\bar{1}5)$  and  $\gamma\text{-NiOOH}(101)$ , Fe-doped  $\beta\text{-NiOOH}(01\bar{1}5)$  and  $\gamma\text{-NiOOH}(101)$ ,  $\text{NiFe}_2\text{O}_4(001)$ , and  $\text{Fe}_3\text{O}_4(001)$ . We find that Fe-doped  $\beta\text{-NiOOH}(01\bar{1}5)$  has by far the lowest overpotential,  $\eta = 0.26$  V, followed by  $\text{NiFe}_2\text{O}_4(001)$ ,  $\eta = 0.42$  V. Based on the computed overpotential, Fe-doped  $\beta\text{-NiOOH}$  is even more active than  $\text{RuO}_2$ , a well-established catalyst for the OER.  $\text{NiFe}_2\text{O}_4$  is another efficient OER catalyst, but less active than Fe-doped  $\beta\text{-NiOOH}$ . Both Fe-doped  $\beta\text{-NiOOH}$  and  $\text{NiFe}_2\text{O}_4$  could contribute to the OER catalyst's active phase of Fe-doped  $\text{NiO}_x$ .

#### Publications Acknowledging this Grant in 2011-2014

1. Jun Hee Lee and A. Selloni,  $\text{TiO}_2/\text{Ferroelectric}$  Heterostructures as Dynamic Polarization-Promoted Catalysts for Photochemical and Electrochemical Oxidation of Water, *Phys. Rev. Letters* **2014**, *112*, in press.
2. Ye-Fei Li, Ulrich Aschauer, Jia Chen, and Annabella Selloni, Adsorption and Reactions of  $\text{O}_2$  with Anatase  $\text{TiO}_2$ , *Acc. Chem. Res.* **2014**, *47*, ASAP article.
3. Y. F. Li and A. Selloni, Mechanism and Activity of Water Oxidation on Selected Surfaces of Pure and Fe-doped  $\text{NiO}_x$ , *ACS Catal.* **2014**, *4*, 1148-1153.
4. J. Chen, Y.-F. Li, P. Sit, A. Selloni, Chemical Dynamics of the First Proton-Coupled Electron Transfer of Water Oxidation on  $\text{TiO}_2$  Anatase, *J. Am. Chem. Soc.*, **2013**, *135*, 18774 (Communication).
5. M. Setvín, U. Aschauer, P. Scheiber, Y.-F. Li, W. Hou, M. Schmid, A. Selloni, and U. Diebold, Reaction of  $\text{O}_2$  with Subsurface Oxygen Vacancies on  $\text{TiO}_2$  Anatase (101), *Science* **2013**, *341*, 988.
6. J. Chen, A. Selloni, First Principles Study of Cobalt (Hydr)Oxides under Electrochemical Conditions, *J. Phys. Chem. C* **2013**, *117*, 20002-20006.
7. T. Xia, Neng Li, Y. Zhang, M. B. Kruger, J. Murowchick, A. Selloni, and Xiaobo Chen, Directional Heat Dissipation across the Interface in Anatase–Rutile Nanocomposites, *ACS Appl. Mater. Interfaces*, **2013**, *5* (20), 9883–9890
8. Y.-F. Li, A. Selloni, Theoretical Study of Interfacial Electron Transfer from Reduced Anatase  $\text{TiO}_2(101)$  to Adsorbed  $\text{O}_2$ , *J. Am. Chem. Soc.*, **2013**, *135*, 9195.
9. R. Ciancio, A. Vittadini, A. Selloni, R. Arpaia, C. Aruta, F. M. Granozio, U. Scotti di Uccio, G. Rossi, E. Carlino, Evolution of nanostructures of anatase  $\text{TiO}_2$  thin films grown on (001)  $\text{LaAlO}_3$ , *J. Nanopart. Res.*, **2013**, *15*, 1735.
10. S. Selçuk, A. Selloni, Surface Structure and Reactivity of Anatase  $\text{TiO}_2$  Crystals with Dominant {001} Facets, *J. Phys. Chem.*, **2013**, *117*, 6358-6362.
11. F. Nunzi, E. Mosconi, L. Storchi, E. Ronca, A. Selloni, M. Graetzel, F. De Angelis, Inherent electronic trap states in  $\text{TiO}_2$  nanocrystals effect of saturation and sintering, *Energy & Environmental Science*, **2013**, *6*, 1221-1229.

12. P. Scheiber, M. Fidler, O. Dulub, M. Schmid, U. Diebold, W. Hou, U. Aschauer, A. Selloni, (Sub)surface mobility of oxygen vacancies at the TiO<sub>2</sub> anatase (101) surface, *Phys. Rev. Lett.* **2012**, *109*, 136193.
13. R. Ciancio, E. Carlino, G. Rossi, C. Aruta, U. Scotti di Uccio, A. Vittadini, A. Selloni, Magnéli-like phases in epitaxial anatase TiO<sub>2</sub> thin films, *Phys. Rev. B* **2012**, *86*, 104110.
14. J. Chen, A. Selloni, Water adsorption and oxidation at the Co<sub>3</sub>O<sub>4</sub>(110) surface, *J. Phys. Chem. Lett.* **2012**, *3*, 2808-2814.
15. U. Aschauer, A. Selloni, Hydrogen interaction with the anatase TiO<sub>2</sub>(101) surface, *Phys. Chem. Chem. Phys.* **2012**, *14*, 16595-16602.
16. J. Chen, A. Selloni, Electronic states and magnetic structure at the Co<sub>3</sub>O<sub>4</sub>(110) surface: A first-principles study, *Phys. Rev. B* **2012**, *85*, 085306.
17. A. Tilocca, A. Selloni, DFT-GGA and DFT+U simulations of thin water layers on reduced TiO<sub>2</sub> anatase, *J. Phys. Chem. C* **2012**, *116*, 9114-9121.
18. E. Mosconi, A. Selloni, F. De Angelis, Solvent Effects on the Adsorption Geometry and Electronic Structure of Dye-sensitized TiO<sub>2</sub>: a First Principles Investigation, *J. Phys. Chem. C* **2012**, *116*, 5932-5940.
19. Chenghua Sun, Yi Jia, Xiao-Hua Yang, Hua-Gui Yang, Xiangdong Yao, Gaoqing (Max) Lu, Annabella Selloni, Sean C. Smith, Hydrogen Incorporation and Storage in Well-defined Nanocrystals of Anatase Titanium Dioxide, *J. Phys. Chem. C* **2011**, *115*, 25590-25594.
20. C. Di Valentin, A. Selloni, Bulk and surface polarons in photoexcited anatase TiO<sub>2</sub>, *J. Phys. Chem. Letters* **2011**, *2*, 2223.
21. J. Chen, X. Wu, A. Selloni, Electronic structure and bonding properties of cobalt oxide in the spinel structure, *Phys. Rev. B* **2011**, *83*, 245204.
22. C.H. Sun, A. Selloni, A.J. Du, S.C. Smith, Interaction of Water with the Fluorine-Covered Anatase TiO<sub>2</sub>(001) Surface, *J. Phys. Chem. C* **2011**, *115*, 17092.
23. L.-M. Liu, S.-C. Li, H. Cheng, U. Diebold, A. Selloni, Growth and Organization of an Organic Molecular Monolayer on TiO<sub>2</sub>: Catechol on Anatase (101), *J. Am. Chem. Soc.* **2011**, *133*, 7816-7823
24. U. Aschauer, A. Selloni, Structure of the Rutile TiO<sub>2</sub>(011) Surface in an Aqueous Environment, *Phys. Rev. Lett.* **2011**, *106*, 166102

Wendy J. Shaw

**Enhancing the Performance of Hydrogenase Mimics with An Enzyme-Inspired Outer  
Coordination Sphere**

Wendy Shaw, Arnab Dutta, Sheri Lense, John Roberts, Bojana Ginovska-Pangovska  
Pacific Northwest National Laboratory

**Presentation Abstract**

We are designing an enzyme-inspired outer coordination sphere into redox active catalysts ( $\text{Ni}(\text{P}^{\text{R}}_2\text{N}^{\text{R}'_2})_2$ ) which oxidize and produce  $\text{H}_2$ , mimicking the hydrogenase enzyme, with the overall goal of using these well understood organometallics as a probe to understand how the protein scaffold contributes to catalysis. The incorporation of a single amino acid into the  $\text{P}_2\text{N}_2$  ring to make  $\text{H}_2$  oxidation catalysts,  $[\text{Ni}(\text{P}^{\text{Cy}}_2\text{N}^{\text{Amino acid}}_2)]^{2+}$ , results in water soluble complexes with rates up to 4 times faster than previously reported complexes, operating at 180 mV overpotential, close to the energy efficiency of the enzyme. We have demonstrated that the carboxylic acid groups facilitate rapid proton movement resulting in lower overpotentials, and that side chain functional groups can influence the structure of the active site, enhancing catalytic rates. Experiments at high temperature and high  $\text{H}_2$  pressure have resulted in unprecedented rates of  $\text{H}_2$  oxidation, as high as  $1.5 \times 10^6 \text{ s}^{-1}$ , at overpotentials below 300 mV. Despite these phenomenal results, there is still evidence of limiting proton and/or electron transfer, suggesting that even faster rates and lower overpotentials can be achieved. To realize or exceed the combination of enzyme-like rates and overpotentials, future studies will include investigating additional amino acids to understand contributions of other side chains in structural roles, as well as the role of the  $\text{pK}_a$  of the side chain in aiding proton movement. The addition of larger peptides to further enhance proton movement and control the positioning of functional groups to influence catalytic properties is also planned, building upon successes achieved attaching peptides to  $\text{H}_2$  production catalysts. Combining these approaches allows us to develop a mechanistic understanding of the role of the outer coordination sphere on molecular catalysts, and may also serve as a model system for understanding the protein scaffold in enzymes.

**DE-AC05-76RL0 1830: Early Career: Catalyst Biomimics: A novel approach in catalyst design**

**Postdocs and Junior Staff:** Arnab Dutta  
Sheri Lense

## RECENT PROGRESS

1) **Two-Relay Proton Channels.** Summary: We have synthesized and characterized two complexes ( $[\text{Ni}^{\text{II}}(\text{P}^{\text{Cy}}_2\text{N}^{(3\text{-pyridazyl)methyl}}_2)]^{2+}$ ,  $[\text{Ni}^{\text{II}}(\text{P}^{\text{Cy}}_2\text{N}^{\text{Glycine}}_2)]^{4+}$ ) with built-in proton channels. Both of these complexes provide significant improvements in rate and/or overpotential. This work resulted in publications in *Chemical Communications* and the *Journal of the American Chemical Society*.



**Figure 1.** Proton channels enhance catalytic properties. A) Parent complex ( $[\text{Ni}^{\text{II}}(\text{P}^{\text{Cy}}_2\text{N}^{\text{Benzyl}}_2)]^{2+}$ ) contains a single proton relay; B) the introduction of a second proton relay in the pyridazine group ( $[\text{Ni}^{\text{II}}(\text{P}^{\text{Cy}}_2\text{N}^{(3\text{-pyridazyl)methyl}}_2)]^{2+}$ ) facilitated proton transfer and reduced the overpotential of catalysis; C) the introduction of the carboxylic acid group in glycine as a second proton relay ( $[\text{Ni}^{\text{II}}(\text{P}^{\text{Cy}}_2\text{N}^{\text{Glycine}}_2)]^{4+}$ ) resulted in water solubility while maintaining the activity of the fastest parent complex and operating at a low (180 mV) overpotential under conditions relevant for fuel cells.

2) **Water soluble  $\text{H}_2$  oxidation complex with arginines enhances catalysis due to an enzyme-like stabilization.** Summary: We have designed, synthesized and characterized a hydrogen oxidation catalyst with the amino acid arginine. The pairing between guanidiniums results in a stabilization that enhances catalysis four times faster than the fastest reported catalyst. High

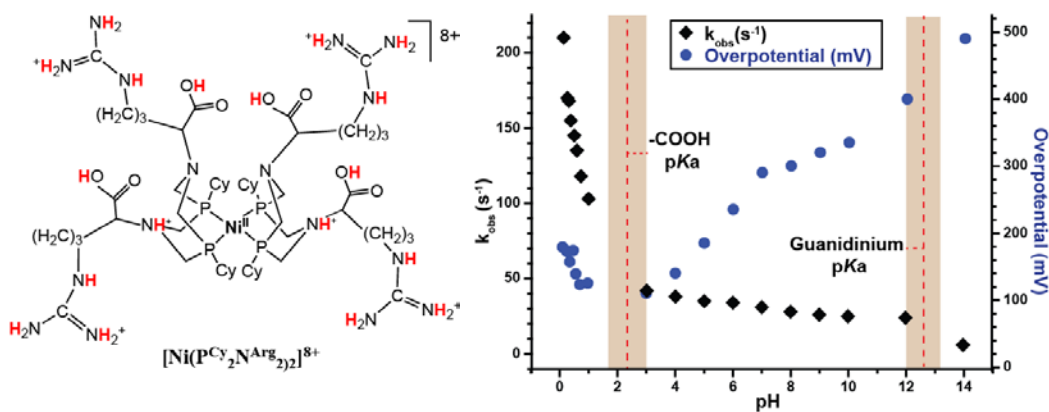


**Figure 2.**  $[\text{Ni}^{\text{II}}(\text{P}^{\text{Cy}}_2\text{N}^{\text{Arg}}_2)]^{8+}$  is an active  $\text{H}_2$  oxidation catalyst at all pH values, with enhanced rates at low pH, conditions most relevant for fuel cells. Overpotentials also vary as a function of pH, demonstrating a dependence on proton and/or electron transfer at high rates.

pressure results in rates of  $140,000\text{ s}^{-1}$  at an overpotential of 480 mV. This has been published in *Angewandte Chemie*.

3) **Computationally predicted mutations improve [FeFe]-hydrogenase activity.** Summary: investigations of the proton channel of [FeFe]-hydrogenase using molecular dynamics revealed a key residue at the mouth of the proton channel that was likely slowing activity due to the formation of a salt bridge. Our collaborators (Hegg, U. of Michigan) determined that our computations were correct: mutating the residue from arginine to Leucine enhanced enzymatic activity 3-fold. This suggests that there is a regulatory mechanism controlling proton transfer to the active site. This work is being prepared for submission to *Biochemistry*.

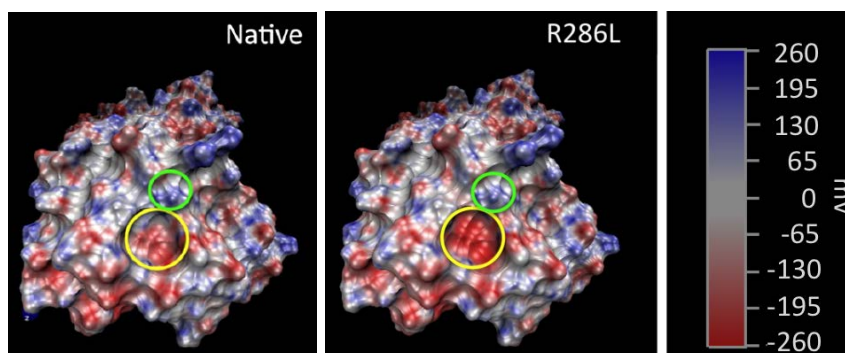


**Figure 5.** The mouth of the proton channel in the native enzyme has a less negative electrostatic potential than the mutant, and has a salt bridge created by the first member of the proton channel, providing an explanation for the enhanced rates observed for the mutant.

### Publications Acknowledging this Grant in 2011-2014

- 1 Dutta, A.; Roberts, J. A. S.; Shaw, W. J. Learning from Nature: Arg-Arg Pairing Enhances  $\text{H}_2$  Oxidation Catalyst Performance. *Angewandte Chemie* **2014**, *In Press*.
- 2 Lense, S.; Dutta, A.; Roberts, J. A. S.; Shaw, W. J. A Proton Channel Allows a Hydrogen Oxidation Catalyst to Operate at a Moderate Overpotential with Water Acting as a Base. *Chemical Communications* **2014**, *50*, 792-795.
- 3 Ginovska-Pangovska, B.; Ho, M. -H.; Linehan, J. C.; Cheng, Y.; Dupuis, M.; Raugei, S.; Shaw, W. J. Molecular dynamics study of the proposed proton transport pathways in [FeFe]-hydrogenase *Biochimica et Biophysica Acta (BBA) - Bioenergetics* **2014**, *1837*, 131-138.
- 4 Reback, M. L.; Buchko, G. W.; Kier, B. L.; Ginovska-Pangovska, B.; Xiong, Y.; Lense, S.; Hou, J.; Roberts, J. A. S.; Sorensen, C. M.; Raugei, S.; Squier, T. C.; Shaw, W. J. Enzyme design from the bottom up: an active nickel electrocatalyst with a peptide outer coordination sphere. *Chemistry: A European Journal* **2014**, *20*, 1510-1514.
- 5 Das, P.; Ho, M.-H.; O'Hagan, M.; Shaw, W. J.; Bullock, R. M.; Raugei, S.; Helm, M. L. Controlling proton movement: electrocatalytic oxidation of hydrogen by a nickel(II) complex containing proton relays in the second and outer coordination spheres. *Dalton Transactions* **2014**, *43*, 2744-2754.

- 6 Dutta, A., Lense, S., Hou, J., Engelhard, M., Roberts, J. A. S., Shaw, W. J. Minimal proton channel enables H<sub>2</sub> oxidation and production with a water soluble nickel-based catalyst. *J Am Chem Soc* **2013**, *135*, 18490-18496.
- 7 Reback, M. L.; Ginovska-Pangovska, B.; Ho, M.-H.; Jain, A.; Squier, T. C.; Raugei, S.; Roberts, J. A. S.; Shaw, W. J. The role of a dipeptide outer-coordination sphere on H<sub>2</sub>-production catalysts: influence on catalytic rates and electron transfer. *Chem. Eur. J.* **2013**, *19*, 1928-1941.
- 8 Shaw, W. J.; Helm, M. L.; DuBois, D. L. A modular, energy-based approach to the development of nickel containing molecular electrocatalysts for hydrogen production and oxidation. *Biochim. Biophys. Acta: Bioenergetics* **2013**, *1827*, 1123-1139.
- 9 Franz, J. A.; O'Hagan, M.; Ho, M.-H.; Liu, T.; Helm, M. L.; Lense, S.; DuBois, D. L.; Shaw, W. J.; Appel, A. M.; Raugei, S.; Bullock, R. M. Conformational dynamics and proton relay positioning in nickel catalysts for hydrogen production and oxidation. *Organometallics* **2013**, *32*, 7034-7042.
- 10 Galan, B. R.; Reback, M. L.; Jain, A.; Appel, A. M.; Shaw, W. J. Electrocatalytic oxidation of formate with nickel diphosphine dipeptide complexes: effect of ligands modified with amino acids. *European Journal of Inorganic Chemistry* **2013**, 5366-5371.
- 11 Buchko, G. W.; Jain, A.; Reback, M. L.; Shaw, W. J. Structural characterization of the model amphipathic peptide Ac-LKKLLKLLKLLKLL-NH<sub>2</sub> in aqueous solution and with 2,2,2-trifluoroethanol and 1,1,1,3,3,3-hexafluoroisopropanol. *Canadian Journal of Chemistry* **2013**, *91*, 406-413.
- 12 Jain, A.; Buchko, G. W.; Reback, M. L.; O'Hagan, M.; Ginovska-Pangovska, B.; Linehan, J. C.; Shaw, W. J. Active hydrogenation catalyst with a structured, peptide-based outer coordination sphere. *ACS Catalysis* **2012**, *2*, 2114-2118.
- 13 Jain, A.; Reback, M. L.; Lindstrom, M. L.; Thogerson, C. E.; Helm, M. L.; Appel, A. M.; Shaw, W. J. Investigating the role of the outer-coordination sphere in [Ni(P(Ph)<sub>2</sub>N(Ph)<sub>2</sub>)<sub>2</sub>]<sup>2+</sup> hydrogenase mimics. *Inorganic chemistry* **2012**, *51*, 6592-6602.
- 14 Shaw, W. J. The outer-coordination sphere: incorporating amino acids and peptides as ligands for homogeneous catalysts to mimic enzyme function. *Catalysis Reviews: Science and Engineering* **2012**, *54*, 489-550.
- 15 Lense, S.; Ho, M. H.; Chen, S. T.; Jain, A.; Raugei, S.; Linehan, J. C.; Roberts, J. A. S.; Appel, A. M.; Shaw, W. Incorporating amino acid esters into catalysts for hydrogen oxidation: steric and electronic effects and the role of water as a base. *Organometallics* **2012**, *31*, 6719-6731.
- 16 O'Hagan, M.; Ho, M. H.; Yang, J. Y.; Appel, A. M.; Rawkowski DuBois, M.; Raugei, S.; Shaw, W. J.; DuBois, D. L.; Bullock, R. M. Proton delivery and removal in [Ni(P<sup>R</sup><sub>2</sub>N<sup>R</sup><sub>2</sub>)<sub>2</sub>] hydrogen production and oxidation catalysts. *J Am Chem Soc* **2012**, *134*, 19409-19424.
- 17 Jain, A.; Lense, S.; Linehan, J. C.; Raugei, S.; Cho, H.; DuBois, D. L.; Shaw, W. J. Incorporating peptides in the outer-coordination sphere of bioinspired electrocatalysts for hydrogen production. *Inorganic chemistry* **2011**, *50*, 4073-85.

**Shaping the Catalytic Performance of Core@Shell Noble Metal Nanocatalysts**

Sara E. Skrabalak,\* Nathan E. Motl, Moitree Laskar, and Ethan Harak

Indiana University – Bloomington, Department of Chemistry

**Presentation Abstract**

Shape-controlled nanocrystals express facets with defined atomic arrangements, which can be selected to facilitate specific interactions between adsorbates and a surface and provide geometric control. Yet the strength of these symmetry-favored molecular interactions is predefined by metal selection and cannot be altered without changing the metal. Thus, the shape-controlled nanocrystals are being coupled with core@shell particle architectures to provide electronic control. This core@shell architecture can perturb the electronic structure of the shell metal on account of lattice strain and electron donation/withdraw from the bimetallic structure. Here, two shape-controlled core@shell nanocrystal systems will be described, with potential utility to hydrogenation and electrooxidation processes. The synthesis and structural characterization of shape-controlled Au@Pd and Rh@Pt nanocrystals will be provided. Preliminary catalysis results will also be presented which illustrate the potential of these nanostructures to offer independent geometric and electronic control in catalytic processes.

**Grant Number 205883:**

**Decoupling the Electronic and Geometric Parameters of Metal Nanocatalysts**

**Publications Acknowledging this Grant in 2013-2014**

1. Laskar, M.; Skrabalak, S. E.\* "Decoupling the Geometric Parameters of Pd Nanocatalysts" *ACS Catalysis*, **2014**, *4*, 1120-1128.

Igor I. Slowing

**Hybrid organic-inorganic catalysts for carbon-carbon coupling and redox reactions:  
characterization, catalytic activity and reaction mechanisms**

Andreja Bakac, Takeshi Kobayashi, Oleg Pestovsky, Marek Pruski, Aaron D. Sadow, Igor I. Slowing  
Ames Laboratory, U.S. DOE, Iowa State University, Ames, IA 50011-3111

**Presentation Abstract**

The overarching goal of this collaborative research project is to develop new catalytic principles for bringing together the best features of homogeneous and heterogeneous catalysis and ultimately enable the design of efficient catalysts with molecular-scale control of conversions, particularly those relevant to highly oxygenated compounds. The substantial challenges for rational design of catalysts for selective chemical conversions require understanding and control of the catalytic environment and reaction mechanisms. These requirements are addressed through the design of 3D, mesoporous interfacial catalysts. Doing so provides advantages in catalyst recovery, reaction control, sensitivity and efficiency. Our efforts combine expertise in mesoporous catalysis synthesis, transition metal chemistry, kinetics and mechanisms of catalytic reactions, photocatalysis, and solid-state (SS)NMR. Here, we specifically highlight the mechanistic studies of carbon-carbon coupling reactions catalyzed by amine-modified silica surfaces, the development of new heterogeneous catalysts for the conversion of alcohols to hydrocarbons, the studies of Fe<sup>2+</sup>-catalyzed oxidations of organic substrates by ozone in aqueous solvents, and the studies of catalytic materials utilizing the emerging SSNMR methodologies that employ dynamic nuclear polarization (DNP) and ultrafast magic angle spinning.

**AL-03-380-011: Homogeneous and Interfacial Catalysis in 3D Controlled Environment**

PI: Marek Pruski

Postdocs: Naftalie Opembe

Students: Hajem Baitenah, Andra Castle, Umesh Chaudhary, Jacob Fleckenstein, Melinda Reichert, Bradley Schmidt, Zachary Weinstein, Zhuoran Wang

**Recent Progress**

**(1) Rational design of mesoporous nanoparticle catalysts: from monofunctional to bifunctional multitasking nanostructures.** The mechanistic details of carbon-carbon coupling reactions catalyzed by amine-modified mesoporous silica nanoparticles (MSNs) were investigated using theoretical models, kinetic measurements and SSNMR spectroscopy.<sup>16,27,57</sup> These studies included the effects of structural properties of the support, catalytic amine groups, and solvent on the catalytic performance.<sup>16,27</sup> The mobility and conformation of amine groups was modeled with molecular mechanics and correlated with SSNMR measurements (Fig. 1a).<sup>57</sup> The limitations imposed by diffusion through narrow pores on activity were modeled with statistical mechanics, providing an explanation for the experimental results (Fig. 1b,c).<sup>27,57</sup> Catalyst poisoning was identified by kinetic analysis and the molecular structure of the deactivated intermediate was

elucidated by SSNMR (Fig. 1d).<sup>27</sup> The information gathered on the mechanism of the catalytic reaction was then employed to reactivate the catalyst and to modify the reaction conditions to achieve optimal conversion.<sup>16,27</sup> The in depth understanding of this catalytic process was used to assemble multicatalytic systems that performed tandem reactions for upgrading the molecular weight of alcohols (Fig. 1e).<sup>2,9</sup> The general strategy consisted in the assembly of two site-isolated catalysts: the first enabling low temperature oxidation of alcohols to aldehydes, and the second facilitating aldol condensation between the intermediate aldehydes. Site-isolation was achieved in these systems by immobilizing one catalyst inside of the pores of MSNs, while the other catalyst was bound to the external surface of the particles. This isolation prevented mutual poisoning of the catalysts.<sup>9,53</sup> The versatility of this method of assembly was proven by combining an organocatalyst with a second organocatalyst,<sup>53</sup> an enzyme,<sup>9</sup> or a metal nanoparticle.<sup>2</sup>

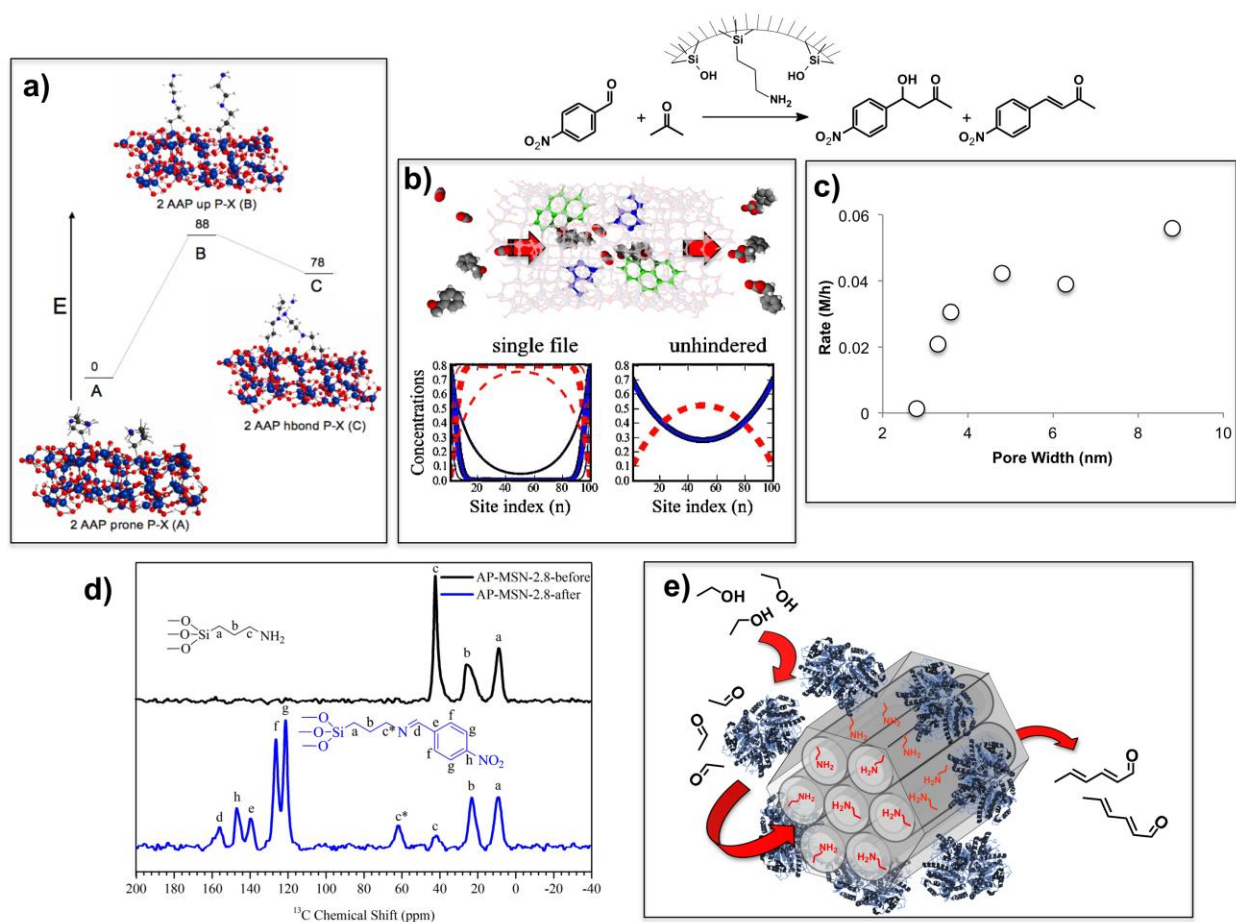


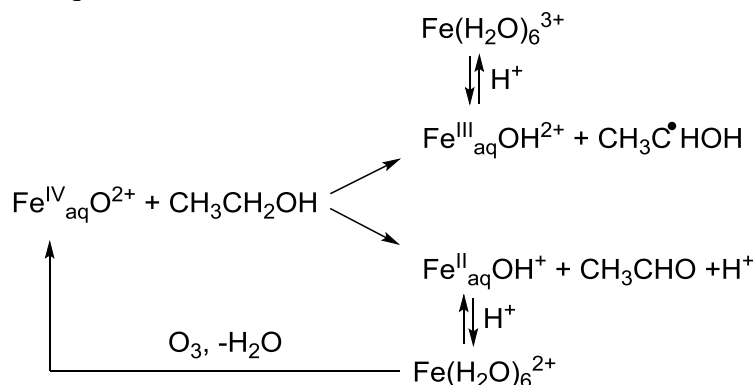
**Figure 1:** Rational design of multicatalytic system for tandem conversions. a) Molecular mechanics and SSNMR study of the conformation and mobility of catalytic groups; b) statistical mechanics modeling of diffusion through confined channels; c) effect of width of cylindrical pores on the catalytic activity of supported amines for the aldol condensation; d) detection of catalyst poisoning that reduces the effective pore width; e) optimized catalyst co-assembled with an enzyme within a single nanostructured support to give the tandem conversion of ethanol into hexadienal.

Hybrid multifunctional systems can be exploited to achieve other catalytic functions besides those offered by tandem catalysis. For example, secondary organic groups were explored as modulators of catalytic activity and as vehicles to selectively control the accessibility of reactants to the active

sites.<sup>6,54</sup> Co-immobilization of chiral modifiers along with Rh nanoparticles or Rh complexes in MSNs led to the development of highly enantioselective hydrogenation catalysts.<sup>54</sup> Incorporation of aminopropyl groups into the MSNs containing Ni nanoparticles produced a hydrotreatment catalyst capable of selectively sequestering free fatty acids from crude microalgal oil and selectively converting them into diesel-range liquid hydrocarbons with minimal cracking.<sup>6</sup> The concept of a bifunctional system in which the amine component is used to bind the fatty acids and the Ni metal to bind and activate H<sub>2</sub> was then extended to a monometallic system, in which two different phases of iron were produced within the pores of MSN: a metallic iron phase that bound and activated H<sub>2</sub>, and an oxidic iron phase that bound the fatty acids for catalytic hydrodeoxygenation.<sup>1</sup> The dynamic conversion between the two iron phases took place via a reverse Mars-Van Krevelen mechanism, and provide an inexpensive and sulfur-free alternative for the production of green diesel from biorenewable resources.

**(2) Oxygenate conversions with single-site catalysts.** We have been investigating the conversion of alcohols through photochemical decarbonylation catalysis which produces H<sub>2</sub> and CO in addition to the hydrocarbon. The preparation of MSN-surface-supported catalysts, and their relative reactivity toward alcohols and carbonyls, is discussed in a companion abstract. To prepare single site interfacial catalysts, we have targeted single-site zirconium amides on MSNs. In particular, Zr(NMe<sub>2</sub>)<sub>4</sub> has been grafted onto the MSN to give ≡Si-O-Zr(NMe<sub>2</sub>)<sub>3</sub>. The zirconium site's structure was assigned by a combination of SSNMR, elemental analysis, and reaction stoichiometry. Reactions of ≡Si-O-Zr(NMe<sub>2</sub>)<sub>3</sub> with reducing hydride transfer agents were explored toward early-metal systems for oxygenate conversions. Hydrogenolysis, silanolysis, and boranolysis reactions are under investigation toward catalytic hydrogenation, hydrosilylation, and hydroboration of oxygenates, as well as amination reactions. The characteristic features of homogenous catalytic conversions, such as isotope effects on selectivity,<sup>12</sup> provide key insight into the nature of the interfacial site.

**(3) Oxydations of organic substrates by ozone.** The reaction of aqueous Fe<sup>2+</sup> with ozone in acidic aqueous solutions generates an Fe(IV) species, Fe<sub>aq</sub>O<sup>2+</sup>, which oxidizes alcohols to aldehydes/ketones by a mixture of hydride and hydrogen atom transfers. Only the former path regenerates Fe<sup>2+</sup> which is critical for catalysis. As a result, the catalytic efficiency of Fe<sup>2+</sup>/O<sub>3</sub> combination is poor in aqueous solvents.



**Scheme 1**

The much higher reduction potential of the Fe(III)/Fe(II) couple in acetonitrile as compared to that in water suggests that preference for two-electron pathways of a hypothetical

iron(IV) species might be greater in acetonitrile, and might lead to greater catalytic efficiency. The most recent data show that Fe(II) is indeed a powerful catalyst for oxidations of organic substrates by ozone. Moreover, the reaction displays selectivity toward less oxidized products. For example, under a given set of conditions  $O_3$  oxidizes benzyl alcohol to a mixture of equimolar amounts of benzaldehyde and benzoic acid in 300 seconds. The same reaction in the presence of 20 micromolar Fe(II) takes only 20 seconds, producing mostly benzaldehyde ( $>>90\%$ ) and only traces of benzoic acid. Similar results were obtained with other alcohols, aldehydes and ethers.

**(4) Studies of catalytic surfaces by dynamic nuclear polarization NMR.** SSNMR characterizations of catalytic interfaces, such as those described in part (1) of the Progress Report, rely on new developments that afford quick studies ever smaller concentrations of molecules. We carried out exploratory studies involving two game-changing techniques, dynamic nuclear polarization (DNP) and ultrafast magic angle spinning (MAS) at 100 kHz, which offer dramatically improved sensitivity and resolution, respectively. The DNP studies, done in collaboration with G. Bodenhausen in Lausanne and O. Lafon in Lille, have shown that hyperpolarization of nuclear spins by the electrons offers  $>1000$  improvement in time performance, allowing for  $^{13}C$  and  $^{29}Si$  CPMAS measurements on silica surfaces to be completed within minutes (Figure 2).<sup>13,19</sup> Using DNP-enhanced  $^{15}N\{^1H\}$  CPMAS NMR, in concert with EXAFS and density-functional theory, we have concluded a study of the host-guest interactions between metal ions ( $Pt^{2+}$  and  $Cu^{2+}$ ) and a zirconium metal-organic framework (UiO-66-NH<sub>2</sub>) that was not possible with conventional NMR. The Ames Laboratory will soon install a BES-funded DNP instrument, enabling us to carry these measurements on a wide range of materials.

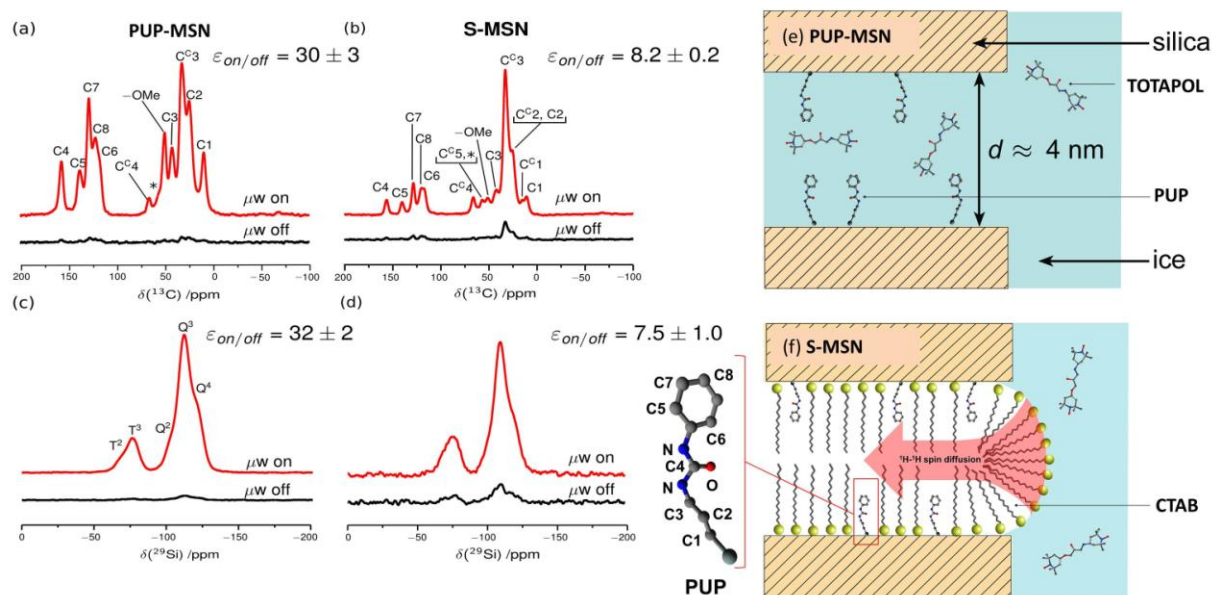


Figure 2: Natural abundance CPMAS spectra of (a, b)  $^{13}C$  and (c, d)  $^{29}Si$  in (a, c) extracted mesoporous silica nanoparticles, PUP-MSNs, and (b, d) surfactant-filled nanoparticles, S-MSNs, impregnated with a 12.5 mM TOTAPOL solution in  $H_2O$ . The PUP-MSN and S-MSN materials are shown schematically in (e) and (f). Both samples were functionalized with 3-(N-phenylureido)propyl (PUP) groups shown in the center of the figure. In (a) and (b), the peaks labeled with \* correspond to spinning sidebands. In each subfigure, the DNP-enhanced and standard spectra are labeled “on” and “off”, respectively. The spectra were acquired at a temperature of about 100 K using 3.2 mm sapphire rotors spinning at 10 kHz, using a Bruker BioSpin Avance III NMR spectrometer operating at 9.4 T and equipped with a 263 GHz gyrotron. The signal enhancements of  $\sim 30$  in (a) and (c) correspond to almost 1000-fold improvement in time performance.

Ultrafast MAS, which now can be performed at rates exceeding 100 kHz (6 million rpm), offers potential for new SSNMR capabilities with previously unachievable resolution and selectivity. Working in collaboration with JEOL Resonance Inc., which has developed the first 100-kHz MAS probehead, we have shown that the highly resolved 2D  $^1\text{H}$ - $^1\text{H}$  homonuclear correlation spectra acquired at such high MAS rate could be used to unravel the structure of a complex host-guest system.<sup>20</sup> Our most recent experiments demonstrated that this technology affords surprisingly high efficiency of heteronuclear polarization transfer (e.g.  $^1\text{H}$ - $^{13}\text{C}$ ) and endows SSNMR with spectral editing capabilities hitherto limited to solution NMR, essentially instituting the convergence of solid-state and solution NMR. For example, highly resolved 2D HMQC- and HSQC-type spectra of surface species can be acquired on natural abundance samples. These experiments will provide new insights about intermolecular correlations, which in turn are needed to unravel the conformations of surface species, characterize the distributions of multiple functionalities, and understand the cooperative catalytic phenomena.

### Publications (2011-present)

1. Kandel, K.; Anderegg, J.W.; Nelson, N.C.; Chaudhary, U.; Slowing, I.I., Supported iron nanoparticles for the hydrodeoxygenation of microalgal oil to green diesel. *J. Catal.* **2014**, *314*, 142-148. <http://dx.doi.org/10.1016/j.jcat.2014.04.009>
2. Nelson, N.C.; Chaudhary, U.; Kandel, K.; Slowing, I.I., Heterogeneous multicatalytic system for single-pot oxidation and C-C coupling reaction sequences. *Top. Catal.* **2014**, *57*, 1000-1006. <http://dx.doi.org/10.1007/s11244-014-0263-y>
3. Carraher, J. M.; Ellern, A.; Bakac, A., Preparation and reactivity of macrocyclic rhodium(III) alkyl complexes. *Inorg. Chim. Acta* **2014**, *409*, 254-258. <http://dx.doi.org/10.1016/j.ica.2013.09.022>
4. Althaus, S. M.; Mao, K. M.; Stringer, J. A.; Kobayashi, T.; Pruski, M., Indirectly detected heteronuclear correlation solid-state NMR spectroscopy of naturally abundant N-15 nuclei. *Solid State Nucl. Magn. Reson.* **2014**, *57-58*, 17-21. <http://dx.doi.org/10.1016/j.ssnmr.2013.11.001>
5. Alvarado, S. R.; Guo, Y. J.; Ruberu, T. P. A.; Tavasoli, E.; Vela, J., Inorganic chemistry solutions to semiconductor nanocrystal problems. *Coord. Chem. Rev.* **2014**, *263*, 182-196. <http://dx.doi.org/10.1016/j.ccr.2013.09.001>
6. Kandel, K.; Frederickson, C.; Smith, E. A.; Lee, Y. J.; Slowing, II, Bifunctional Adsorbent-Catalytic Nanoparticles for the Refining of Renewable Feedstocks. *ACS Catal.* **2013**, *3* (12), 2750-2758. <http://dx.doi.org/10.1021/cs4008039>
7. Fang, X. K.; Hansen, L.; Haso, F.; Yin, P. C.; Pandey, A.; Engelhardt, L.; Slowing, I.; Li, T.; Liu, T. B.; Luban, M.; Johnston, D. C., {Mo<sub>24</sub>Fe<sub>12</sub>} Macrocycles: Anion Templatation with Large Polyoxometalate Guests. *Angew. Chem.-Int. Edit.* **2013**, *52* (40), 10500-10504. <http://dx.doi.org/10.1002/anie.201304887>
8. Carraher, J. M.; Bakac, A., Alkyl group versus hydrogen atom transfer from metal alkyls to macrocyclic rhodium complexes. *Chem. Commun.* **2013**, *49* (54), 6099-6101. <http://dx.doi.org/10.1039/c3cc43472a>
9. Kandel, K.; Althaus, S. M.; Pruski, M.; Slowing, I. I., Supported Hybrid Enzyme-Organocatalysts for Upgrading the Carbon Content of Alcohols. In *Novel Materials for Catalysis and Fuels Processing*, BravoSuarez, J. J.; Kidder, M. K.; Schwartz, V., Eds. Amer Chemical Soc: Washington, **2013**; *1132*, pp 261-271.

- <http://dx.doi.org/10.1021/bk-2013-1132.ch011>
10. Bakac, A.; Pestovsky, O., Selective oxidation of organic substrates to partially oxidized products. US Patent 8507730, **2013**.
  11. Bakac, A.; Pestovsky, O.; Durfey, B. L.; Kristian, K. E., Kinetics and thermodynamics of nitric oxide binding to transition metal complexes. Relationship to dioxygen binding. *Chemical Science* **2013**, *4* (5), 2185-2192. <http://dx.doi.org/10.1039/c3sc50157d>
  12. Manna, K.; Everett, W. C.; Schoendorff, G.; Ellern, A.; Windus, T. L.; Sadow, A. D., Highly Enantioselective Zirconium-Catalyzed Cyclization of Aminoalkenes. *J. Am. Chem. Soc.* **2013**, *135* (19), 7235-7250. <http://dx.doi.org/10.1021/ja4000189>
  13. Kobayashi, T.; Lafon, O.; Thankamony, A. S. L.; Slowing, II; Kandel, K.; Carnevale, D.; Vitzthum, V.; Vezin, H.; Amoureux, J. P.; Bodenhausen, G.; Pruski, M., Analysis of sensitivity enhancement by dynamic nuclear polarization in solid-state NMR: a case study of functionalized mesoporous materials. *Physical Chemistry Chemical Physics* **2013**, *15* (15), 5553-5562. <http://dx.doi.org/10.1039/c3cp00039g>
  14. Tanabe, K. K.; Siladke, N. A.; Broderick, E. M.; Kobayashi, T.; Goldston, J. F.; Weston, M. H.; Farha, O. K.; Hupp, J. T.; Pruski, M.; Mader, E. A.; Johnson, M. J. A.; Nguyen, S. T., Stabilizing unstable species through single-site isolation: A catalytically active Ta-V trialkyl in a porous organic polymer. *Chemical Science* **2013**, *4* (6), 2483-2489. <http://dx.doi.org/10.1039/c3sc22268c>
  15. Wang, J.; Ackerman, D. M.; Lin, V. S. Y.; Pruski, M.; Evans, J. W., Controlling reactivity of nanoporous catalyst materials by tuning reaction product-pore interior interactions: Statistical mechanical modeling. *J. Chem. Phys.* **2013**, *138* (13), 134705. <http://dx.doi.org/10.1063/1.4798463>
  16. Kandel, K.; Althaus, S. M.; Peeraphatdit, C.; Kobayashi, T.; Trewyn, B. G.; Pruski, M.; Slowing, II, Solvent-Induced Reversal of Activities between Two Closely Related Heterogeneous Catalysts in the Aldol Reaction. *ACS Catalysis* **2013**, *3* (2), 265-271. <http://dx.doi.org/10.1021/cs300748g>
  17. Mao, K. M.; Kennedy, G. J.; Althaus, S. M.; Pruski, M., Determination of the Average Aromatic Cluster Size of Fossil Fuels by Solid-State NMR at High Magnetic Field. *Energy & Fuels* **2013**, *27* (2), 760-763. <http://dx.doi.org/10.1021/ef301804p>
  18. Vela, J., Molecular Chemistry to the Fore: New Insights into the Fascinating World of Photoactive Colloidal Semiconductor Nanocrystals. *J. Phys. Chem. Lett.* **2013**, *4* (4), 653-668. <http://dx.doi.org/10.1021/jz302100r>
  19. Lafon, O.; Thankamony, A. S. L.; Kobayashi, T.; Carnevale, D.; Vitzthum, V.; Slowing, II; Kandel, K.; Vezin, H.; Amoureux, J. P.; Bodenhausen, G.; Pruski, M., Mesoporous Silica Nanoparticles Loaded with Surfactant: Low Temperature Magic Angle Spinning C-13 and Si-29 NMR Enhanced by Dynamic Nuclear Polarization. *J. Phys. Chem. C* **2013**, *117* (3), 1375-1382. <http://dx.doi.org/10.1021/jp310109s>
  20. Kobayashi, T.; Mao, K.; Paluch, P.; Nowak-Krół, A.; Sniechowska, J.; Nishiyama, Y.; Gryko, D. T.; Potrzebowski, M. J.; Pruski, M., Study of Intermolecular Interactions in the Corrole Matrix by Solid-State NMR under 100 kHz MAS and Theoretical Calculations. *Angew. Chem.-Int. Edit.*, **2013**, *52*, 14108-14111. <http://dx.doi.org/10.1002/anie.201305475>
  21. Jana, B.; Hovey, M.; Ellern, A.; Pestovsky, O.; Sadow, A. D.; Bakac, A., Unusual structural motif in a zwitterionic Fe(II) complex of a tetradentate phosphine. *Dalton Trans.* **2012**, *41* (41), 12781-12785. <http://dx.doi.org/10.1039/c2dt31437a>
  22. Mao, K. M.; Kennedy, G. J.; Althaus, S. M.; Pruski, M., Spectral editing in C-13 solid-

- state NMR at high magnetic field using fast MAS and spin-echo dephasing. *Solid State Nucl. Magn. Reson.* **2012**, 47-48, 19-22.  
<http://dx.doi.org/10.1016/j.ssnmr.2012.07.003>
23. Ruberu, T. P. A.; Nelson, N. C.; Slowing, I. I.; Vela, J., Selective Alcohol Dehydrogenation and Hydrogenolysis with Semiconductor-Metal Photocatalysts: Toward Solar-to-Chemical Energy Conversion of Biomass-Relevant Substrates. *J. Phys. Chem. Lett.* **2012**, 3 (19), 2798-2802. <http://dx.doi.org/10.1021/jz301309d>
  24. Ho, H. A.; Manna, K.; Sadow, A. D., Acceptorless Photocatalytic Dehydrogenation for Alcohol Decarbonylation and Imine Synthesis. *Angew. Chem.-Int. Edit.* **2012**, 51 (34), 8607-8610. <http://dx.doi.org/10.1002/anie.201203556>
  25. Mukherjee, D.; Ellern, A.; Sadow, A. D., Remarkably Robust Monomeric Alkylperoxyzinc Compounds from Tris(oxazoliny)boratozinc Alkyls and O-2. *J. Am. Chem. Soc.* **2012**, 134 (31), 13018-13026. <http://dx.doi.org/10.1021/ja303440n>
  26. Althaus, S. M.; Mao, K. M.; Kennedy, G. J.; Pruski, M., Solid-State NMR Studies of Fossil Fuels using One- and Two-Dimensional Methods at High Magnetic Field. *Energy Fuels* **2012**, 26 (7), 4405-4412. <http://dx.doi.org/10.1021/ef3004637>
  27. Kandel, K.; Althaus, S. M.; Peeraphatdit, C.; Kobayashi, T.; Trewyn, B. G.; Pruski, M.; Slowing, II, Substrate inhibition in the heterogeneous catalyzed aldol condensation: A mechanistic study of supported organocatalysts. *J. Catal.* **2012**, 291, 63-68.  
<http://dx.doi.org/10.1016/j.jcat.2012.04.005>
  28. Ruberu, T. P. A.; Albright, H. R.; Callis, B.; Ward, B.; Cisneros, J.; Fan, H. J.; Vela, J., Molecular Control of the Nanoscale: Effect of Phosphine-Chalcogenide Reactivity on CdS-CdSe Nanocrystal Composition and Morphology. *ACS Nano* **2012**, 6 (6), 5348-5359. <http://dx.doi.org/10.1021/nn301182h>
  29. Carraher, J. M.; Pestovsky, O.; Bakac, A., Transition metal ion-assisted photochemical generation of alkyl halides and hydrocarbons from carboxylic acids. *Dalton Trans.* **2012**, 41 (19), 5974-5980. <http://dx.doi.org/10.1039/c2dt30210a>
  30. Alvarado, S. R.; Guo, Y. J.; Ruberu, T. P. A.; Bakac, A.; Vela, J., Photochemical versus Thermal Synthesis of Cobalt Oxyhydroxide Nanocrystals. *J. Phys. Chem. C* **2012**, 116 (18), 10382-10389. <http://dx.doi.org/10.1021/jp301459s>
  31. Bataineh, H.; Pestovsky, O.; Bakac, A., pH-induced mechanistic changeover from hydroxyl radicals to iron(IV) in the Fenton reaction. *Chem. Sci.* **2012**, 3 (5), 1594-1599. <http://dx.doi.org/10.1039/c2sc20099f>
  32. Fernandez, C.; Pruski, M., Probing Quadrupolar Nuclei by Solid-State NMR Spectroscopy: Recent Advances. In *Solid State NMR*, Chan, J. C. C., Ed. Springer-Verlag Berlin: Berlin, 2012; Vol. 306, pp 119-188.  
[http://dx.doi.org/10.1007/128\\_2011\\_141](http://dx.doi.org/10.1007/128_2011_141)
  33. Huang, Y. L.; Deng, W. H.; Guo, E. R.; Chung, P. W.; Chen, S.; Trewyn, B. G.; Brown, R. C.; Lin, V. S. Y., Mesoporous Silica Nanoparticle-Stabilized and Manganese-Modified Rhodium Nanoparticles as Catalysts for Highly Selective Synthesis of Ethanol and Acetaldehyde from Syngas. *ChemCatChem* **2012**, 4 (5), 674-680.  
<http://dx.doi.org/10.1002/cctc.201100460>
  34. Klobukowski, E. R.; Angelici, R. J.; Woo, L. K., Bulk Gold-Catalyzed Reactions of Isocyanides, Amines, and Amine N-Oxides. *Organometallics* **2012**, 31 (7), 2785-2792. <http://dx.doi.org/10.1021/om201068g>
  35. Marchuk, K.; Guo, Y. J.; Sun, W.; Vela, J.; Fang, N., High-Precision Tracking with Non-blinking Quantum Dots Resolves Nanoscale Vertical Displacement. *J. Am. Chem. Soc.*

- 2012**, *134* (14), 6108-6111. <http://dx.doi.org/10.1021/ja301332t>
36. Wang, C. J.; Liu, D. J.; Evans, J. W., Schloegl's second model for autocatalysis on hypercubic lattices: Dimension dependence of generic two-phase coexistence. *Phys. Rev. E* **2012**, *85* (4), 041109. <http://dx.doi.org/10.1103/PhysRevE.85.041109>
37. Hara, K.; Akahane, S.; Wiench, J. W.; Burgin, B. R.; Ishito, N.; Lin, V. S. Y.; Fukuoka, A.; Pruski, M., Selective and Efficient Silylation of Mesoporous Silica: A Quantitative Assessment of Synthetic Strategies by Solid-State NMR. *J. Phys. Chem. C* **2012**, *116* (12), 7083-7090. <http://dx.doi.org/10.1021/jp300580f>
38. Klobukowski, E. R.; Angelici, R. J.; Woo, L. K., Bulk Gold-Catalyzed Oxidations of Amines and Benzyl Alcohol Using Amine N-Oxides as Oxidants. *Catal. Lett.* **2012**, *142* (2), 161-167. <http://dx.doi.org/10.1007/s10562-011-0758-0>
39. Manna, K.; Kruse, M. L.; Sadow, A. D., Concerted C-N/C-H Bond Formation in Highly Enantioselective Yttrium(III)-Catalyzed Hydroamination. *ACS Catalysis* **2011**, *1* (11), 1637-1642. <http://dx.doi.org/10.1021/cs200511z>
40. Szajna-Fuller, E.; Bakac, A., Kinetics and mechanism of the reduction of a macrocyclic Rh(III) complex by chromium(II) ions: pH-controlled selectivity to rhodium(II) vs. rhodium(III) hydride. *Dalton Trans.* **2011**, *40* (40), 10598-10602. <http://dx.doi.org/10.1039/c1dt10747j>
41. Tsai, C. H.; Vivero-Escoto, J. L.; Slowing, I. I.; Fang, I. J.; Trewyn, B. G.; Lin, V. S. Y., Surfactant-assisted controlled release of hydrophobic drugs using anionic surfactant templated mesoporous silica nanoparticles. *Biomaterials* **2011**, *32* (26), 6234-6244. <http://dx.doi.org/10.1016/j.biomaterials.2011.04.077>
42. Alemseghed, M. G.; Ruberu, T. P. A.; Vela, J., Controlled Fabrication of Colloidal Semiconductor-Metal Hybrid Heterostructures: Site Selective Metal Photo Deposition. *Chemistry of Materials* **2011**, *23* (15), 3571-3579. <http://dx.doi.org/10.1021/cm201513a>
43. Klobukowski, E. R.; Mueller, M. L.; Angelici, R. J.; Woo, L. K., Conversions of Cyclic Amines to Nylon Precursor Lactams Using Bulk Gold and Fumed Silica Catalysts. *ACS Catalysis* **2011**, *1* (7), 703-708. <http://dx.doi.org/10.1021/cs200120c>
44. Mukherjee, D.; Thompson, R. R.; Ellern, A.; Sadow, A. D., Coordinatively Saturated Tris(oxazoliny)borato Zinc Hydride-Catalyzed Cross Dehydrocoupling of Silanes and Alcohols. *ACS Catalysis* **2011**, *1* (7), 698-702. <http://dx.doi.org/10.1021/cs2001016>
45. Pruski, M.; Woo, L. K.; Lin, W. B., Preface to Memorial Issue in Honor of Professor Victor S.-Y. Lin. *ACS Catalysis* **2011**, *1* (7), 734-735. <http://dx.doi.org/10.1021/cs200241q>
46. Ruberu, T. P. A.; Vela, J., Expanding the One-Dimensional CdS-CdSe Composition Landscape: Axially Anisotropic CdS(1-x)Se(x) Nanorods. *ACS Nano* **2011**, *5* (7), 5775-5784. <http://dx.doi.org/10.1021/nn201466b>
47. Tsai, C. H.; Chen, H. T.; Althaus, S. M.; Mao, K. M.; Kobayashi, T.; Pruski, M.; Lin, V. S. Y., Rational Catalyst Design: A Multifunctional Mesoporous Silica Catalyst for Shifting the Reaction Equilibrium by Removal of Byproduct. *ACS Catalysis* **2011**, *1* (7), 729-732. <http://dx.doi.org/10.1021/cs200222t>
48. Ho, H. A.; Gray, T. S.; Baird, B.; Ellern, A.; Sadow, A. D., Allylic C-H bond activation and functionalization mediated by tris(oxazoliny)borato rhodium(I) and iridium(I) compounds. *Dalton Trans.* **2011**, *40* (24), 6500-6514. <http://dx.doi.org/10.1039/c1dt10249d>
49. Kobayashi, T.; Mao, K.; Wang, S. G.; Lin, V. S. Y.; Pruski, M., Molecular ordering of

- mixed surfactants in mesoporous silicas: A solid-state NMR study. *Solid State Nuclear Magnetic Resonance* **2011**, *39* (3-4), 65-71.  
<http://dx.doi.org/10.1016/j.ssnmr.2011.02.001>
50. Jana, B.; Ellern, A.; Pestovsky, O.; Sadow, A.; Bakac, A., Synthesis of Monomeric Fe(II) and Ru(II) Complexes of Tetradentate Phosphines. *Inorg. Chem.* **2011**, *50* (7), 3010-3016.
51. Pestovsky, O.; Veysey, S. W.; Bakac, A., Kinetics and Mechanism of Hydrogen-Atom Abstraction from Rhodium Hydrides by Alkyl Radicals in Aqueous Solutions. *Chem.-Eur. J.* **2011**, *17* (16), 4518-4522. <http://dx.doi.org/10.1002/chem.201100094>
52. Manna, K.; Xu, S. C.; Sadow, A. D., A Highly Enantioselective Zirconium Catalyst for Intramolecular Alkene Hydroamination: Significant Isotope Effects on Rate and Stereoselectivity. *Angew. Chem.-Int. Edit.* **2011**, *50* (8), 1865-1868.  
<http://dx.doi.org/10.1002/anie.201006163>
53. Huang, Y. L.; Xu, S.; Lin, V. S. Y., Bifunctionalized Mesoporous Materials with Site-Separated Bronsted Acids and Bases: Catalyst for a Two-Step Reaction Sequence. *Angew. Chem.-Int. Edit.* **2011**, *50* (3), 661-664.  
<http://dx.doi.org/10.1002/anie.201004572>
54. Huang, Y.; Xu, S.; Lin, V. S. Y., Changing from Symmetric to Asymmetric Simply by Immobilizing the Catalyst on Mesoporous Silica Nanoparticle. *ChemCatChem* **2011**, *3* (1), 131-134. <http://dx.doi.org/10.1002/Cctc.201000294>
55. Kim, T. W.; Slowing, I. I.; Chung, P. W.; Lin, V. S. Y., Ordered Mesoporous Polymer-Silica Hybrid Nanoparticles as Vehicles for the Intracellular Controlled Release of Macromolecules. *ACS Nano* **2011**, *5* (1), 360-366.  
<http://dx.doi.org/10.1021/nn101740e>
56. Neal, S. R.; Ellern, A.; Sadow, A. D., Optically active, bulky tris(oxazolinyl)borato magnesium and calcium compounds for asymmetric hydroamination/cyclization. *J. Organomet. Chem.* **2011**, *696* (1), 228-234.  
<http://dx.doi.org/10.1016/j.jorganchem.2010.08.057>
57. Nedd, S.; Kobayashi, T.; Tsai, C-H.; Slowing, I.I.; Pruski, M.; Gordon, M.S. Using a reactive force field to correlate mobilities obtained from solid state <sup>13</sup>C NMR on mesoporous silica nanoparticle systems. *J. Phys. Chem. C* **2011**, *115*, 16333-16339.  
<http://pubs.acs.org/doi/abs/10.1021/jp204510m>
58. Liu, D-J.; Wang, J.; Ackerman, D.M.; Slowing, I.I.; Pruski, M.; Chen, H.; Lin, V.S.-Y.; Evans, J.W. Interplay between anomalous transport and catalytic reaction kinetics in single-file nanoporous systems. *ACS Catal.* **2011**, *1*, 751-763.  
<http://pubs.acs.org/doi/abs/10.1021/cs200115c>

Darío J. Stacchiola

**“Nanostructured oxide Catalysts: Studies from UHV to *In-situ* conditions”**

Darío J. Stacchiola, José A. Rodriguez, Mike White, Sanjaya Senanayake, Ping Liu

Department of Chemistry, Brookhaven National Laboratory, Upton, NY 11973

Low concentration of active sites in the oxide support of catalysts may be blocked by the anchoring of metal particles. By using a second oxide as a support (host), one can create a multifunctional configuration in with both metal and oxide active centers exposed to reactants.[1] The natural abundance of Cu and its catalytic performance for CO oxidation, water-gas shift (WGS) and methanol synthesis have made it a prime target for catalysis. The Achilles heel of Cu-based catalysts is its deactivation by complete oxidation to CuO or reduction to Cu,[2] in both cases losing active catalytic Cu<sup>+</sup> centers. They were the first reported to run CO oxidation ( $\text{CO} + 1/2\text{O}_2 \rightarrow \text{CO}_2$ ) at room temperature, but their lack of thermal stability at temperatures used on automobile catalytic converters leads to their deactivation. We show how the incorporation of Ti in a Cu<sub>2</sub>O film leads to the formation of a stable mixed-metal oxide, with a Cu<sup>+</sup> terminated surface active for CO oxidation.[3] The oxidation of CO during the WGS reaction ( $\text{CO} + \text{H}_2\text{O} \rightarrow \text{CO}_2 + \text{H}_2$ ) occurs in this case under an overall reducing environment. By using a combination of *in-situ* techniques combined with theory, we show how the formation of a multifunctional metal-oxide interface with ceria nanoparticles allows the stabilization of critical intermediates for an efficient associative reaction mechanism.[4] A similar metal-oxide interface can help to activate copper for the thermal reduction of CO<sub>2</sub>. Optimizing the oxide phase and metal-oxide interfaces in a catalyst can improve substantially their catalytic activity and selectivity.

- [1] D Stacchiola, SD Senanayake, P Liu, JA Rodriguez, Fundamental Studies of Well-Defined Surfaces of Mixed-Metal Oxides: Special Properties of MO<sub>x</sub>/TiO<sub>2</sub>(110) {M = V, Ru, Ce, or W}. *Chem. Rev.* **2013**, *113*, 4373–4390
- [2] AE Baber, F Xu, F Dvorak, K Mudiyansele, M Soldemo, J Weissenrieder, SD Senanayake, JT Sadowski, JA Rodriguez, V Matolín, MG White, DJ Stacchiola, *In-Situ* Imaging of Cu<sub>2</sub>O under Reducing Conditions: Formation of Metallic Fronts by Mass Transfer. *J. Am. Chem. Soc.* **2013**, *135*, 16781–16784
- [3] AE Baber, X Yang, HY Kim, K Mudiyansele, M Soldemo, J Weissenrieder, SD Senanayake, A Al-Mahboob, JT Sadowski, J Evans, JA Rodriguez, P Liu, FM Hoffmann, JG Chen, DJ Stacchiola, Stabilization of catalytically active Cu<sup>+</sup> surface sites on titanium-copper mixed oxide films. *Angew. Chem. Int. Ed.* **2014**, (DOI: 10.1002/anie.201402435)
- [4] K Mudiyansele, SD Senanayake, L Feria, S Kundu, AE Baber, J Graciani, AB Vidal, S Agnoli, J Evans, R Chang, S Axnanda, Z Liu, JF Sanz, P Liu, JA Rodriguez, DJ Stacchiola, Importance of the Metal-Oxide Interface in Catalysis: *In-situ* Studies by AP-XPS of the WGS Reaction. *Angew. Chem. Int. Ed.* **2013**, *52*, 5101–5105

**FWP: BNL CO-009 – CATALYSIS SCIENCE FOR ADVANCED FUELS**

**Postdocs:** Ashleigh Baber, Kumudu Mudiyansele

**Students:** Fang Xu

Albert E. Stiegman

## Elucidation of Active Site Formation in the Phillips Ethylene Polymerization Catalyst

Carole Brown,<sup>†</sup> Adrian Lita,<sup>†</sup> Mark Crosswhite,<sup>†</sup> Yuchuan Tao,<sup>†</sup> Melissa Mileham,<sup>†</sup> J. Krzystek,<sup>‡</sup> Randall Achey,<sup>†</sup> Riqiang Fu,<sup>‡</sup> Robert W. Meulenberg,<sup>¶</sup> Salvator Profeta,<sup>†</sup> Susannah L. Scott,<sup>§</sup> A. E. Stiegman<sup>\*,†</sup>

<sup>†</sup>Department of Chemistry and Biochemistry, Florida State University, Tallahassee, FL 32306 United States

<sup>‡</sup>National High Magnetic Field Laboratory, Tallahassee, FL 32310 United States

<sup>¶</sup>Lawrence Livermore National Laboratory, Materials Science & Technology Division, Livermore, CA 94550, United States

<sup>§</sup>Department of Chemical Engineering, University of California, Santa Barbara, CA 93106 United States

### Presentation Abstract

The Phillips catalyst is a single-site supported catalyst, initially made by the dispersion of Cr(VI) ions on silica. The active catalyst itself is formed by the reduction of the Cr(VI) at elevated temperatures. Industrially this is carried out using ethylene itself as the reductant, which gives rise to an induction period before polymerization begins. Using sol-gel chemistry we formed the Phillips catalyst as a microporous optically transparent monolith, which allows the reaction to be monitored spectroscopically. The microporous nature of the matrix allows only very slow diffusion of reaction, which slows down the process and allows intermediates to be formed stoichiometrically, isolated and studied. This approach for monitoring the reaction, coupled with the use of high-field/high-frequency electron paramagnetic resonance (HFEP) and solid-state nuclear magnetic resonance (NMR) spectroscopy ultimately facilitated the characterization of key intermediates in the process. With this matrix we were able to monitor, in-situ, the sequential reduction of the Cr(VI) to Cr(IV) and ultimately to Cr(II). The Cr(II) site, which has long been postulated as the endpoint of the reduction, was directly observed and characterized by HFEP spectroscopy. Under conditions of ethylene polymerization, the reductively generated Cr(II) was titrated with stoichiometric amounts of ethylene. The titration is nearly isobestic and at the endpoint, the C:Cr ratio was 1.75:1, consistent with approximately one ethylene per Cr ion. The oxidation state of the resulting complex is Cr(III) as determined by x-ray absorption near edge spectroscopy (XANES) and by HFEP which verified the disappearance of Cr(II) and the appearance of Cr(III). Characterization of the organometallic Cr(III) species was carried out by solid state NMR which showed two distinct resonances of approximately equal intensity at ~75 and 146 ppm consistent with an intact ethylene group. Further verification of this structural assignment was carried out by a dephasing study, which eliminated the possibility of methylene groups being present (i.e. an aliphatic Cr(III)-CH<sub>2</sub>CH<sub>3</sub>). As such, the active site is assigned, for the first time, to Cr(III) with a sigma-bound vinyl group: Cr(III)-CH=CH<sub>2</sub>.

**Grant # DE-FG02-03ER15467 Title: Hierarchical Design of Supported Organometallic Catalysts for Hydrocarbon Transformations**

**PI:** Susannah Scott, Albert E. Stiegman, Baron Peters

**Postdoc:** Matthew Polinski

**Students:** Anthony Ferrari

### RECENT PROGRESS

**Studies of the Active Site of the Phillips Catalyst.**

Recently, we completed a detailed study of the mechanism of ethylene polymerization on the Phillips ethylene polymerization catalyst ( $\text{Cr}/\text{SiO}_2$ ). Despite its use for more than 50 years in the production of high-density polyethylene, the active site responsible for the polymerization has not been elucidated. Like the olefin metathesis catalysts, prepared by dispersing Mo, W, and Re onto oxide supports, the Phillips catalyst is self-initiating. The results of our study, which utilized catalysts fabricated from Cr-doped, transparent sol-gel-derived silica, suggest that the active site is the Cr(III) vinyl species, shown in Figure 5.

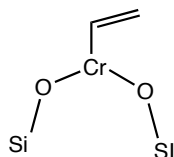
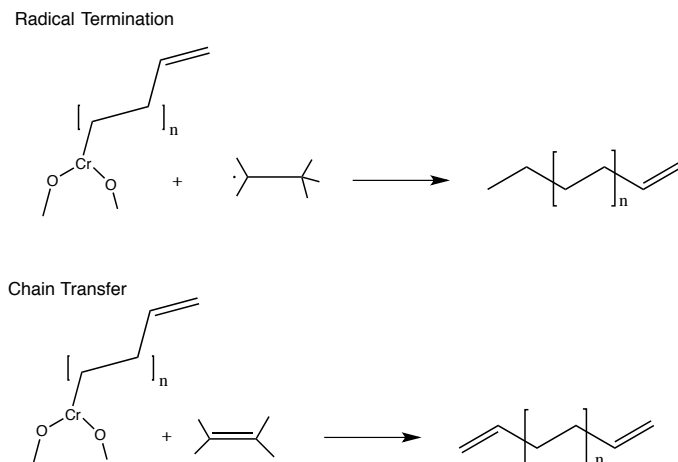


**Figure 1.** Proposed structure of the initiating site on the Phillips ethylene polymerization catalyst

If this hypothesis is correct, we can predict specific products that should be observed during the early stages of polymerization. In particular, the mechanism by which the  $\text{Cr}^{3+}\text{-CH=CH}_2$  species is proposed to form generates ethyl radicals (these have been detected), which in turn, couple to form n-butane as a byproduct (also detected). Since ethyl radicals can reductively cleave the metal-carbon bond of the  $\text{Cr-CH=CH}_2$  group, we also expect to see small, even-carbon number olefins such as 1-butene, 1-hexene, and others in Scheme 2. During the early-stage chain termination by  $\beta$ -H elimination, we expect dienes, such as 1,3-butadiene or 1,5-hexadiene to form.



**Scheme 2.** Predicted products of chain termination from a vinylchromium(III) initiating site

We have built a reaction system that will allow us to detect such products that form during the initial activation step and during the early stages of polymerization. The reaction cell consists of a temperature-controlled heating block, capable of programmed heating up to the reduction temperature. A glass reaction cell, situated in the block next to the thermocouple, holds the catalyst, which can be reduced by flowing CO or ethylene gas. With this system we can dose in incremental amount of ethylene and analyze the organic product by means of mass spectrometry and the formation of organometallic species (Figure 1 and 2) by means of Raman spectroscopy.

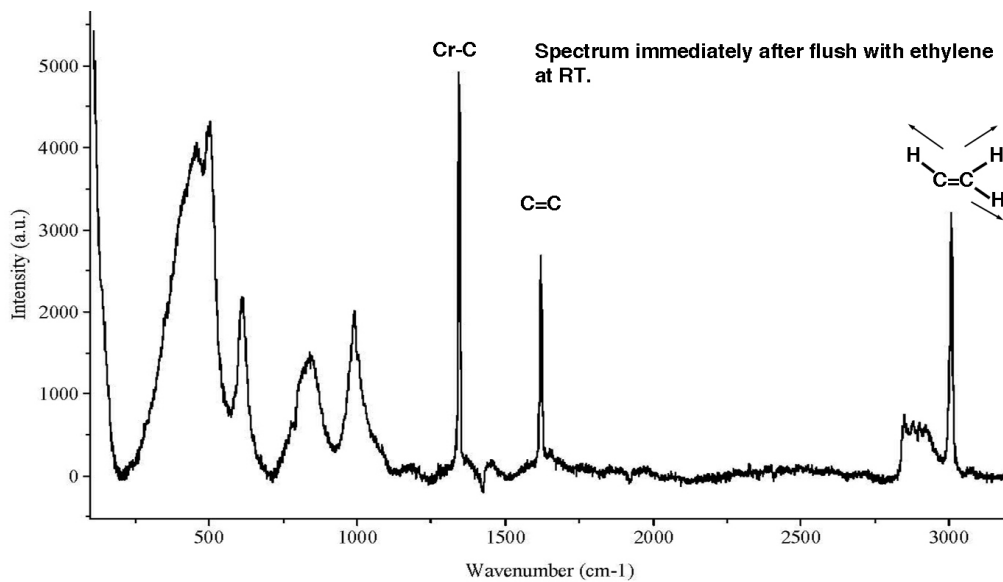


**Figure 3.** Raman spectrum of a Cr-silica monolith that has been reduced by CO to Cr(II), then flushed with ethylene at room temperature.

Among our first results in this controlled polymerization system was the Raman spectrum shown in Figure 3, which was achieved with a quick flush at room temperature of ethylene through a Cr-silica sol-gel monolith that had been reduced to Cr(II) under CO. The resulting Raman spectrum (Figure 3) gives confirmation of the terminal Cr-CH=CH<sub>2</sub> structure. Apparent in the spectrum are the symmetric C-H stretch (and, weaker and to lower energy the anti-symmetric C-H bands), the C=C stretch and the Cr-C stretch. The positions of these vibrational modes is consistent with the values determined theoretically from DFT calculations of model structures containing the Cr-CH=CH<sub>2</sub> unit.

#### Publications Acknowledging this Grant in 2011-2014

1. *Development of Magnetic Nanoparticles as Microwave-Specific Catalysts for the Rapid, Low-Temperature Synthesis of Formalin Solutions*, Mark Crosswhite, Jacob Hunt, Taylor Southworth, Kyle Serniak, Anthony Ferrari, and A. E. Stiegman, *ACS Catalysis*, 2013. **3**(6): p. 1318-1323.
2. *Correspondence on Microwave Effects in Organic Synthesis*, Gregory B. Dudley, Albert E. Stiegman, and Michael R. Rosana, *Angewandte Chemie-International Edition*, 2013. **52**(31): p. 7918-7923.
3. *Microwave-Specific Effects on the Equilibrium Constants and Thermodynamics of the Steam,  $\dot{A}$ iCarbon and Related Reactions*, Anthony Ferrari, Jacob Hunt, Adrian Lita, Bridgett Ashley, and A. E. Stiegman, *The Journal of Physical Chemistry C*, 2014.
4. *Microwave-Specific Enhancement of the Carbon-Carbon Dioxide (Boudouard) Reaction*, Jacob Hunt, Anthony Ferrari, Adrian Lita, Mark Crosswhite, Bridgett Ashley, and A. E. Stiegman, *Journal of Physical Chemistry C*, 2013. **117**(51): p. 26871-26880.

## **Redox-Active On-Surface Assembly of Metal-Organic Chains with Single-Site Pt(II)**

Daniel Skomski, Christopher D. Tempas, Kevin A. Smith, and Steven L. Tait  
Indiana University, Department of Chemistry

### **Presentation Abstract**

The formation and stabilization of well-defined transition metal single-sites at surfaces may open new routes to achieve higher selectivity in heterogeneous catalysts. Organic ligand coordination to produce a well-defined oxidation state in weakly reducing metal sites at surfaces, desirable for selective catalysis, has not been achieved. Here, we address this using metallic platinum interacting with a dipyriddy tetrazine ligand on a single crystal gold surface. X-ray photoelectron spectroscopy measurements demonstrate the metal-ligand redox activity and are paired with molecular-resolution scanning probe microscopy to elucidate the structure of the metal-organic network. Comparison to the redox-inactive diphenyl tetrazine ligand as a control experiment illustrates that the redox activity and molecular-level ordering at the surface rely on two key elements of the metal complexes: (i) bidentate binding sites providing a suitable square planar coordination geometry when paired around each Pt, and (ii) redox-active functional groups to enable charge transfer to a well-defined Pt(II) oxidation state. Ligand-mediated control over the oxidation state and structure of single-site metal centers that are in contact with a metal surface may enable advances in higher selectivity for next generation heterogeneous catalysts.

### **DE-FG02-12ER16351: Metal/Organic Surface Catalyst for Low-Temperature Methane Oxidation: Bi-Functional Union of Metal-Organic Complex and Chemically Complementary Surface**

PI: Steven L. Tait

Graduate student researchers: Daniel Skomski, Christopher D. Tempas, Benjamin Draper, Christopher Williams, Jennifer Sandahl

Undergraduate student researchers: Joseph McCann, Kevin A. Smith

Affiliations: Department of Chemistry, Indiana University

### **RECENT PROGRESS**

Stabilization and chemical control of transition metal centers is a critical problem in the advancement of heterogeneous catalysts to next-generation catalysts that exhibit high levels of selectivity, while maintaining strong activity and facile catalyst recycling. Supported metal nanoparticle catalysts typically suffer from having a wide range of metal sites with different coordination numbers and varying chemistry. This project is exploring new possibilities in catalysis by combining features of homogeneous catalysts with those of heterogeneous catalysts to develop new, bi-functional systems using molecular level control of catalyst structure and oxidation state. The systems are more complex than traditional heterogeneous catalysts in that they utilize sequential active sites to accomplish the desired overall reaction. The interaction of metal—organic catalysts with surface supports and their interactions with reactants to enable the catalysis of critical reactions at lower temperatures are at the focus of this study. While these are not likely to be stable in the high temperature environments ( $> 300\text{ }^{\circ}\text{C}$ ) typical of industrial heterogeneous catalysts, they could be applied in moderate temperature reactions ( $100\text{-}300\text{ }^{\circ}\text{C}$ ), made feasible by lowering reaction temperatures by better catalyst control.

We have experimented with different methods to achieve single-site metal center stabilization at the surface, specifically, multiple organic ligand coordination environments for Pt metal centers on a surface support. Characterization methods include high-resolution (atomic or molecular resolution) scanning tunneling microscopy (STM) and atomic force microscopy (AFM) as well as spectroscopic methods for chemical characterization, such as X-ray photoelectron spectroscopy (XPS) and high-resolution electron

energy loss spectroscopy (HREELS). We have also developed methodologies for stabilizing organic layers at a surface which will contribute to the development of the surface-supported metal-organic complexes and have developed the ability to characterize organic multilayers with molecular resolution.

### 1. Metal coordination using triazine species at Ag(111) surface

Initial experiments were conducted using tri-pyridyl triazine (TPTZ). This molecule provides multiple binding sites for the Pt centers and can achieve either two-fold or three-fold coordination, depending upon the conformational state of the pyridyl ring positions. A key goal in the study of this species is the question of whether Pt complexation with the organic ligand can be achieved in the 2D surface diffusion environment. The molecules are vapor deposited to the surface by sublimation from a Knudsen type evaporator. Pt atoms are subsequently vapor deposited from a solid Pt rod heated by an electron beam. The sample is annealed to accelerate diffusion of both the Pt and the TPTZ species. Experiments were conducted in an ultra-high vacuum system, allowing for precise control of the surface composition.

Scanning tunneling microscopy images are organized in Figure 1 to illustrate the progression of the system at multiple stages of the experiments on the Ag(111) surface. Here, we compare the deposition of metallic Pt with the combination of TPTZ and Pt, Pt-octaethylporphyrin (Pt-OEP), and the combination of Pt with dipyridyltetrazine (DPTZ). Upon deposition of TPTZ, some clusters or islands are observed at the silver surface. X-ray photoelectron spectroscopy (XPS) measurements of the N 1s core level reveal that the molecules are adsorbed in-tact. With the addition of Pt (Figure 1b), islands or clusters are observed on the surface that have dimensions consistent with just a few molecules and a few Pt atoms. Annealing treatments at 100 °C allow us to reach structures where sub-molecular resolution can be achieved. Annealing for an extending period of time at 250 °C leads to the formation of quasi-one-dimensional chains of the molecule across the surface. We are still investigating the nature of these structures and how effective they may be as surface catalysis systems. XPS measurement of the Pt 4f binding energy indicates that the metal in this system is in a metallic (charge 0) state.

The use of a metal-porphyrin complex to order transition metal centers on a surface is a logical approach to creating well-defined Pt centers at a surface (Figure 1c). There have been several research groups that have analyzed such structures previously. We have used a commercially available compound, platinum octaethylporphyrin (Pt-OEP), as a point of comparison for other complexes analyzed in this project. Scanning tunneling microscopy images and XPS are shown in Figure 1c after the sample has been annealed at 150 °C for 10 minutes. The annealing procedure has two effects on the sample. First, it provides additional thermal energy to achieve a highly ordered surface structure. Although this system orders upon deposition at room temperature, annealing allows for a reduction in the number of structural defects. The second effect of the annealing procedure is that excess layers of Pt-OEP are desorbed from the surface into the

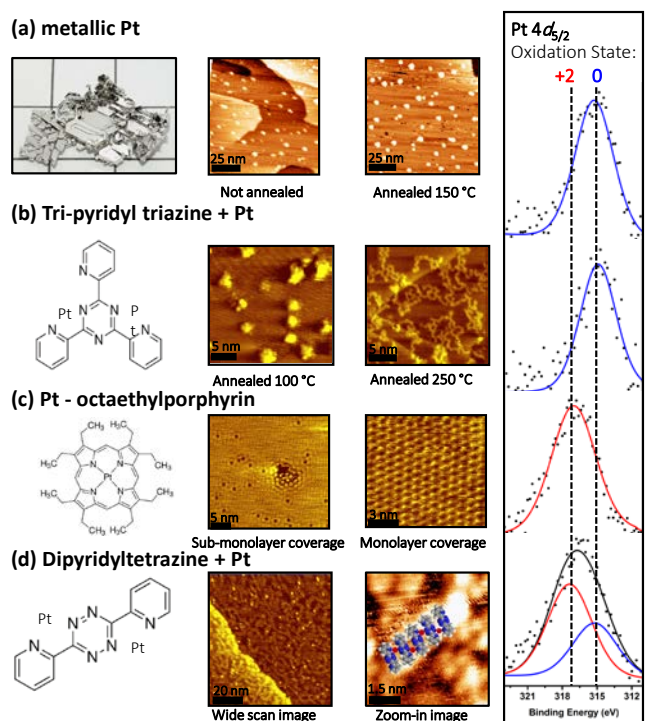


**Figure 1.** Compilation of STM and XPS results for (a) metallic Pt, (b) tri-pyridyl triazine + Pt, (c) Pt – octaethylporphyrin, and (d) dipyridyltetrazine + Pt on Ag(111). XPS of Pt 4f indicates metallic Pt in (a) and (b), but an oxidation state of +2 for (c) and (d).

gas phase. What remains on the surface is an extremely dense single layer of molecules. The molecules are packing in a (5x5) arrangement with respect to the unit cell basis vectors of the Ag(111) surface.

High-resolution electron energy loss spectroscopy (HREELS) was used to study the vibrational modes of the Pt-OEP on the Cu(100) surface under ultrahigh vacuum conditions (Fig. 2). HREELS provides vibrational data which are very valuable in understanding the interactions within the molecule and between the molecule and adsorbates or reactants. Here we have shown that the HREELS is sensitive to the modes of the molecule and, in future work, will study changes in the modes with different porphyrin substitutions, different metals, and upon adsorption of reactants.

## 2. Single-site metal centers with well-defined oxidation state on the Au(100) surface

We have recently studied the oxidation and structural ordering of weakly reducing metallic platinum on a gold surface by interaction with a dipyrindyl tetrazine ligand (**3**, Figure 3), yielding 1D surface coordination architectures. We find that the redox activity and molecular-level ordering rely on two key elements of the surface metal complexes: (1) metal binding pockets providing a quasi-square planar coordination geometry and (2) redox-active sub-units to enable charge transfer. Control experiments demonstrate that both elements are critical to produce well-defined and uniform metal center sites. The results demonstrate the importance of molecular design for achieving both redox activity as well as structural control in surface coordination architectures utilizing weakly oxidizing ligands and weakly reducing metals.

The redox character and bi-dentate binding pocket of the dipyrindyl tetrazine **3** facilitate Pt complexation, oxidation, and ordered 1D coordination chain formation on the reconstructed gold (100) surface in the sub-monolayer regime. XPS measurements demonstrate that Pt is not oxidized by the Au surface, but evidence ligand-mediated oxidation by a 2.2 eV chemical shift to higher platinum 4f electron binding energy as well as chemical changes in the tetrazine and pyridyl nitrogen atoms (N1s XPS). STM and NC-AFM imaging show that 2D Pt islands form on the surface in the absence of the ligand (Fig. 3f), but the pure Pt phase is dissolved in the formation of the strongly bonded, 1D metal-ligand coordination network (Fig. 3g) when ligands are present. Redox-active self-assembly into robust architectures is achieved with ligand **3** acting as a bi-dentate ligand (*via* the pyridyl/tetrazine binding pockets) as well as an oxidizing agent (*via* the electron-deficient tetrazine ring).

In addition to controlling the metal-ligand chemical

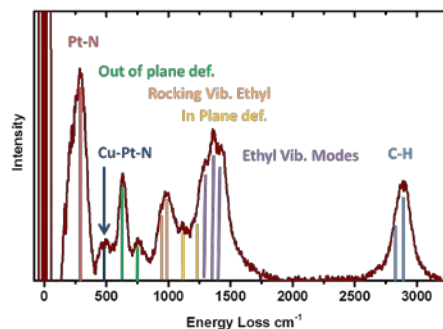


**Figure 2.** HREELS of Pt-OEP on the Cu(100) surface. Peak assignments are made based on prior studies of related systems.

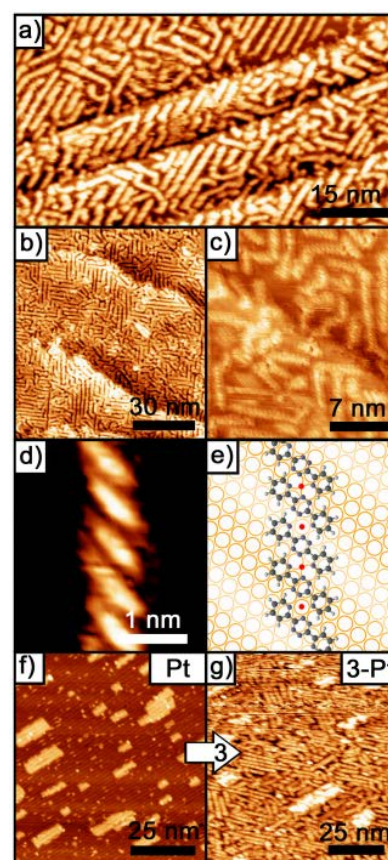


**Figure 3.** STM and AFM of **3**-Pt on Au(100). (a-d) **3**, then Pt deposited, then annealing at 170 °C for 14 hrs., yielding a **3**:Pt ratio of 1. (a) STM wide scan image. (b) AFM wide scan image. (c) AFM zoom-in image. (d) AFM molecular-resolution image of part of one chain. (e) Model of the chains. (f) Pure 2D Pt islands (without **3**) annealed at 170 °C for 15 min. (g) The surface in (f), after addition of **3** and then annealing again at 170 °C for 20 min, yielding a **3**:Pt ratio of 0.5.

state and achieving structural order, organic nanostructures must also be robust. Robust bonding affords resistance against interfacial diffusion as well as high thermal stability for potential uses in catalysis. High-temperature STM (150 °C) affords a means to probe the molecular-level stability of structures at elevated temperatures and in this case shows excellent stability at this temperature. Thermal stability of ionic 1D structures has not been demonstrated. The electrostatic interactions afforded by the use of metal di-cations, as well as coordinative transition metal bonding, seem to overcome weaker substrate-mediated interactions and yield 1D surface architectures with significant thermal stability.

### **3. Development of an interfacial organic layer for stable films**

A common problem in the development of organic interfaces with metal surfaces is that the contact of the first layer of organic material interacts strongly with the metal leading to structural disorder or even chemical decomposition. In this research program, we are attempting to provide an intimate contact between a metal-organic complex and a metal surface to create a sophisticated catalyst with multiple functional sites. However, we also want to maintain a uniform chemical character among the Pt sites available on the surface, which will require well-defined ligand fields from the organic components of the system.

Recent results in our group have demonstrated the ability to use an interfacial organic layer (IOL) to drive a highly ordered organic structure on a metal surface. Biphenyl tetracarboxylic acid (BTA) is an extremely mobile species on the surface studied, such that it does not form an ordered layer on the surface. However, growth of a terephthalic acid monolayer on the surface provides a stable interfacial layer that allows the BTA to form a highly ordered structure in the second layer. This illustrates a capability that may be useful in tuning the interaction of the Pt single site catalys complexes with the Ag surface in our studies of metal-organic catalyst complexes at surfaces. The IOL concept provides some control over the coupling between a functional organic layer and the underlying surface and may be useful in the development of this project.

### **4. Organic multilayer characterization with molecular resolution and high temperature scanning**

Multiple layers of a triazole ligand were deposited on the Ag(111) surface and imaged with high resolution by STM and NC-AFM. Analysis of each of several layers reveals the same surface packing as the monolayer. This illustrates two important points for this work. The first is the ability to correlate STM and AFM results, which may become important in our catalyst studies, especially if our modification of the metal surface leads to a decrease in surface conductivity that would necessitate AFM analysis. The other important point is the propagation of the two-dimensional molecular structure into multiple layers of the film. For analysis and design of complex surface catalysts this raises the point that it may be possible to achieve well defined organic complexes in various layers above the surface. This would allow more flexibility in probing the interfacial layer concept for the tuning of the catalytic behavior of the metal-organic complexes at the surface.

### **Publications Acknowledging this Grant in 2011-2014**

1. Skomski, D.; Tempas, C. D.; Smith, K.; Tait, S. L. Redox-active On-surface Assembly of Metal-organic Chains with Single-site Pt(II). *submitted 2014*.
2. Skomski, D.; Tait, S. L. Interfacial Organic Layers as Templates for Crystalline Organic Films with Carboxyl and Thiophene Functionalization. *J. Phys. Chem. C* **2014**, *118*, 1594-1601.
3. Skomski, D.; Jo, J.; Tempas, C. D.; Lee, D.; Tait, S. L. High-Fidelity Self-assembly of Crystalline and Parallel-oriented Organic Thin Films by  $\pi$ - $\pi$  Stacking from a Metal Surface. *submitted 2014*.
4. Sandahl, J.; Tait, S. L. Organic Coordination of Cr Metal Centers at Surfaces. *manuscript in preparation*.

## New Approaches for Activation of Substrates at a Metal Center

Miram Bowring, Allegra Liberman-Martin, Robert G. Bergman, Andy I. Nguyen and T. Don Tilley, Chemical Sciences Division, Lawrence Berkeley National Laboratory

### Presentation Abstract

Biological catalysts utilize steric and electronic modifications to attain a remarkable degree of substrate specificity. One mechanism by which enzymes finely tune reactivity is through allosteric regulation, in which the enzyme responds to the presence of a distant activator, which typically induces conformational changes that alter enzyme activity. Although tuning reactivity via chemical triggers is common in biological systems, there are currently few analogs in synthetic systems. We chose a strategy to vary electrophilicity using a remote chemical switch, in which second-sphere Lewis acid binding modulates electrophilicity in the first coordination sphere. Lewis acid coordination occurs at a remote ligand site, allowing for systematic studies of metal complexes with variable electrophilicity but conserved ligand structures. Platinum(II) complexes featuring remote nitrogen donor sites have been prepared, and binding of Lewis acidic boranes at these positions has been demonstrated. Biaryl reductive elimination is accelerated over 50,000-fold for the more electron-deficient, Lewis-acid-bound platinum complexes. A second topic concerns metal-mediated oxidation catalysis, and fundamental investigations on oxygen activation at cobalt. The approach described here is based on complexes with ligands designed to stabilize high oxidation states. These studies reveal rapid but selective activations of C–H bonds, and mechanistic studies have provided insight into the intermediates involved in oxygen cleavage.

### FWP Number CH030201: Catalysis and Chemical Transformations

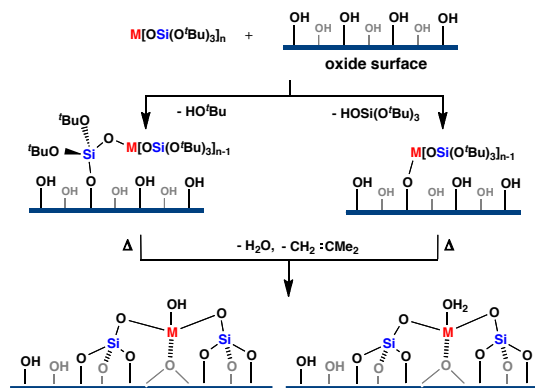
**Postdocs:** Pascal J. Guillo, Lorraine Raboin

**Students:** Paul J. Cordiero, Timothy C. Davenport, H. S. Ahn

### RECENT PROGRESS

#### *Well-defined, single-site catalysts for selective oxidations supported on synthetically modified metal oxide surfaces*

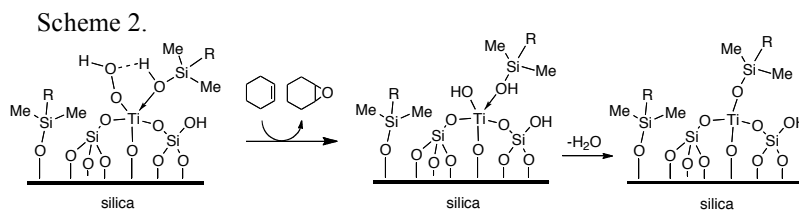
Research in this program has demonstrated that transition-metal and main-group element complexes of oxygen-rich ligands such as  $-\text{OSi}(\text{O}^t\text{Bu})_3$  and  $-\text{O}_2\text{P}(\text{O}^t\text{Bu})_2$  provide effective precursor routes to well-dispersed and site-isolated catalytic centers on an oxide support, as well as to support materials of controlled composition and structure. In the initial phase of this process, the precursor complexes react with acidic functionalities on the oxide surface, leading to a supported complex that is structurally similar to the molecular species. A mild calcination procedure ( $<150\text{ }^\circ\text{C}$ ) can then be used to eliminate the remaining hydrocarbon and add components to the



Scheme 1. The thermolytic molecular precursor (TMP) approach to single-site catalysts.

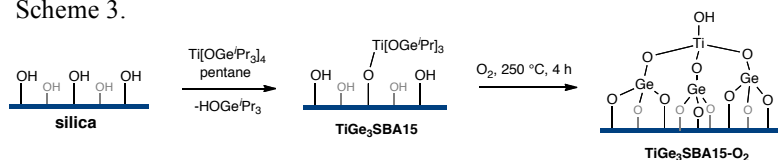
surface (such as additional silicon atoms) that help to stabilize and isolate the metal center (Scheme 1). This thermolytic molecular precursor (TMP) approach offers a number of synthetic advantages over more widely employed sol-gel or wet-impregnation routes, and provides good spectroscopic molecular models for the active site that is introduced onto the surface.

Previous research established the important role that "capping groups" can play in influencing reactivity at a catalytic site. Thus, Ti-OSiMe<sub>2</sub>R and Ta-OSiMe<sub>2</sub>R siloxy groups, introduced by reactions with isolated, surface-bound metal centers, dramatically increase selectivities in epoxidation catalysis, and this effect may involve hydrogen-bond interactions that activate a key hydroperoxy intermediate, as illustrated in Scheme 2. To further probe the influence of such interactions in O-atom transfers, Ti-OR capping groups of differing electronic properties (R = Ph, C<sub>6</sub>F<sub>5</sub>, COMe, COCF<sub>3</sub>) were introduced. This study identified the Ti-OPh group as providing the best performance among these Ti-based catalysts, perhaps due to an optimized activation of the hydroperoxy intermediate for O-atom transfer. Related investigations of Ta-based catalysts probed the influence of -OEMe<sub>3</sub> (E = Si, Ge, Sn) capping groups on catalysis, since Ti-O-Ge linkages have been associated with higher activities for epoxidation. Indeed, the Ta-OGeMe<sub>3</sub> species exhibit a significant increase in epoxidation rate and selectivity over comparable, uncapped centers.



Along with previously reported work on germanium-modified titanium catalysts, it appears that both Ti-O-Ge and Ta-O-Ge linkages in silica-supported catalysts significantly promote catalytic epoxidation activity. However, these results are based on catalysts obtained by treatment of the entire surface with a reagent containing germanium, and it would be more informative to interrogate well-defined catalytic centers derived from precursors that initially possess the hetero-linkage of interest. Thus, we succeeded in obtaining high yields of the new

Scheme 3.



germanium-containing molecular precursor Ti[OGe<sup>i</sup>Pr<sub>3</sub>]<sub>4</sub>, which was cleanly grafted onto SBA-15 to yield isolated Ti(IV) sites *via* the elimination of 1 equivalent of HOGe<sup>i</sup>Pr<sub>3</sub> (Scheme 3). The local environments of the supported materials, before and after calcination under O<sub>2</sub>, were studied by various spectroscopic methods, including XAS (in collaboration with Robert Rioux at Penn State). These materials, which possess -OTi(OGe)<sub>3</sub> coordination environments, are active catalysts for the epoxidation of cyclic and terminal olefins with alkyl hydroperoxides under anhydrous conditions. Compared to catalysts synthesized from siloxide-only precursors, the new catalysts produce two to three times more product after 9 h and under identical reaction conditions for the epoxidations of cyclohexene and 1-octene.

Considerable attention has focused on utilization of H<sub>2</sub>O<sub>2</sub> as an attractive, alternative oxidant for existing industrial processes, particularly given its high oxygen content and the release of only H<sub>2</sub>O as a byproduct. While activations of H<sub>2</sub>O<sub>2</sub> are considerably more facile than those associated with molecular oxygen, making it a kinetically attractive oxidant, this reagent originates from the partial reduction of molecular oxygen with valuable hydrogen. Thus, high H<sub>2</sub>O<sub>2</sub> efficiencies are required for economically viable

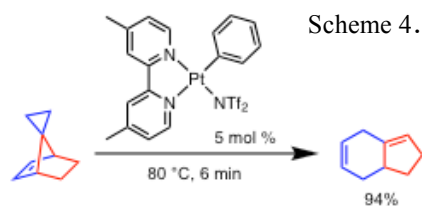
processes. To address this issue, we investigated the mechanisms for H<sub>2</sub>O<sub>2</sub> decomposition, and strategies for the inhibition of H<sub>2</sub>O<sub>2</sub> decomposition, for various Ti catalysts. The observed rates of H<sub>2</sub>O<sub>2</sub> decomposition at 65 °C follow the order **Bu<sub>cap</sub>TiSBA15** > **TiSBA15** and **TS-1** > **[Ti,Al]-MFI** and appear to be correlated with the availability of Brønsted sites on the surface. Significant retardation of the decomposition rates with the KH<sub>2</sub>PO<sub>4</sub> additive was found with **TiSBA15**, which suggests that the KH<sub>2</sub>PO<sub>4</sub> stabilizer may be useful for optimization of hydrogen peroxide efficiency in catalytic oxidations. DFT studies suggest that three Ti(IV)(OOH) intermediates are in equilibrium, and formation of Ti-O· and HOO· radical species are implicated in the H<sub>2</sub>O<sub>2</sub> decomposition. The potential role of KH<sub>2</sub>PO<sub>4</sub> in the H<sub>2</sub>O<sub>2</sub> decomposition process, as a proton acceptor in a [Ti(OO)(HOP(O)(OH)<sub>2</sub>)] complex, was suggested.

Initial investigations on the use of high surface area, mesoporous aluminum phosphate (AlPO) as a support for oxidation catalysts involved synthesis of Ti-AlPO materials by reaction of Ti alkoxide precursors with the AlPO surface. Spectroscopic and analytical methods demonstrate that the Ti centers are anchored onto the surface *via* bonding to both AlO<sup>-</sup> and PO<sup>-</sup> groups, and that isolated, tetrahedral centers as well as oligomerized titanium species may be obtained. These materials exhibit selectivities and activities for epoxidation of cyclohexene with TBHP that are similar to those of comparable Ti-silica materials.

Earlier success with use of precursor methods for the synthesis and study of single-site Pt centers on silica prompted a related study with Pd. The investigation of isolated, mononuclear Pd(II) sites on a solid support also offers the opportunity to compare stability and reactivity with related metallic nanoparticles and bulk metal. This was accomplished with precursors of the type (Bubpy)Pd[OSi(O<sup>t</sup>Bu)<sub>3</sub>](R), and the resulting materials were characterized by a range of methods including XAS. The supported Pd centers are robust in inert atmosphere up to the decomposition temperatures of the precursor complexes (150-200°C). The **PdSBA15** materials are catalysts for the semi-hydrogenation of 1-phenyl-1-propyne that are superior in stability and selectivity to the corresponding homogeneous catalysts.

### ***Metal complexes for bond activations in challenging substrates***

An important issue to resolve in mechanistic investigations of metal-catalyzed hydroarylations concerns the potential role of Brønsted acids, since such species lead to Friedel-Crafts catalysis and branched hydroarylation products, rather than the more desirable linear alkyl chains. In a mechanistic study of the hydroarylation of unactivated olefins with a (COD)Pt(OTf)<sub>2</sub> precatalyst, we showed that lanthanum-mediated proton generation leads to the observed catalysis by a Friedel-Crafts pathway. To develop a mechanistic probe for distinguishing between metal- and proton-catalyzed hydroarylations, a test substrate was designed. If a given hydroarylation is proton catalyzed, this substrate, the bridgehead-substituted norbornene derivative spiro[bicyclo[2.2.1]hept[2]ene-7,1'-cyclopropane], is expected to undergo protonation of the alkene to yield a non-classical carbocation intermediate that rearranges, leading to attack on the arene to give an aryl group α to the spiro cyclopropane group. This product would be chemically distinct from that produced by a metal-mediated insertion reaction, which should proceed without carbocation rearrangement. Unexpectedly, this substrate undergoes neither process when subjected to the hydroarylation catalyst (Bu<sub>2</sub>bipy)PtPh(NTf<sub>2</sub>), but is instead catalytically converted to 1,2,4,7,7a-pentahydroindene (Scheme 4). Mechanistic and computational studies showed

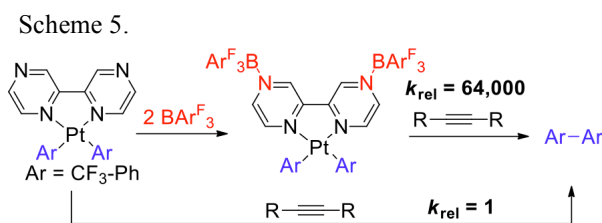


that the rearrangement involves initial C—H bond activation, followed by several C—C bond cleavage events.

Our study of electrophilic late metal center reactivity also includes the synthesis and characterization of well-behaved, dicationic platinum complexes that can be subjected to systematic reactivity and mechanistic studies in bond activations. Such complexes are potentially useful for selective activations of a number of challenging substrates, including non-functionalized hydrocarbons and olefins, and for the design of new catalytic cycles. With these goals in mind, the platinum dication  ${}^t\text{Bu}_2\text{bipyPt}(\text{NTf}_2)_2$  was prepared and characterized. The bistriflimide ligands of this complex are weakly coordinating, and can be easily displaced by solvent molecules. Preliminary work has shown that this complex activates the allylic C—H bond of cyclohexene, to produce a cationic allyl complex.

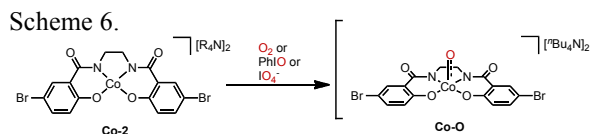
A new aspect to this program involves an additional challenge in catalysis science, which is the development of triggering mechanisms that might be used for the regulation of catalyst activity, in a manner analogous to allosteric regulations in enzymes for achieving a high degree of substrate specificity.

Although tuning reactivity *via* chemical triggers is common in biological systems, there are currently few analogs for synthetic catalysts. In particular, examples involving electronic triggers are rare. To develop a remote trigger that upon binding makes a Pt center more electrophilic,



we examined the binding of Lewis acids to bipyrazine (bpyz)-platinum complexes. The *para*-arrangement of nitrogen atoms featured in bpyz was envisioned to allow borane binding with formation of a zwitterionic complex having a major resonance contributor that may be described as an electrophilic platinum(IV) species. Because Lewis acid binding occurs at a remote ligand site, differences in the activity observed between borane-free and -bound complexes should enable us to evaluate the impact of increased electrophilicity on reactivity. Already, detailed mechanistic studies revealed that  $\text{B}(\text{C}_6\text{F}_5)_3$  binding resulted in a 64,000-fold increase in the rate of reductive elimination (Scheme 5).

New directions in fundamental bond activations employ earth-abundant first row metals, and extend initial results on the design and reactivity of metal-oxo species for C—H bond activations. One aspect of this work is based on our recent discovery of a dianionic cobalt(II) complex (**Co-2**, Scheme 6), supported by strongly electron-donating ligands, that rapidly activates  $\text{O}_2$  to produce a highly reactive intermediate (**Co-O**). The latter species, which may be independently generated with oxo-transfer agents ( $\text{PhIO}$ ,  $\text{IO}_4^-$ ), is believed to be a Co(IV)-oxo complex, as evidenced by mass-spectrometry and EPR (electron paramagnetic resonance) spectroscopy. This type of intermediate is often implicated for cobalt-catalyzed oxidations, and preliminary results indicate that C—H bonds in a range of hydrocarbons, including acetonitrile and phenylacetylene, are activated to cleanly produce Co-hydrocarbyl and Co-OH species. These transformations are especially promising as they employ a simple, atom-efficient oxidant ( $\text{O}_2$ ). The mechanism of this  $\text{O}_2$  cleavage is currently under investigation.



## Publications Acknowledging this Grant in 2011-2014

1. Bowring, M.; Bergman, R. G.; Tilley, T. D. Disambiguation of Metal and Bronsted Acid Catalyzed Pathways for Hydroarylation with a Platinum(II) Catalyst. *Organometallics* **2011**, *30*, 1295.
2. Cordiero, P. J.; Tilley, T. D. Enhancement of the Catalytic Activity of Titanium-Based Terminal Olefin Epoxidation Catalysts via Surface Modification with Functionalized Protic Molecules. *ACS Catal.* **2011**, *1*, 455.
3. Cordiero, P. J.; Tilley, T. D. Enhancement of Epoxidation Efficiencies for Ta-SBA15 Catalysts. The Influence of Modification with  $-EMe_3$  (E = Si, Ge, Sn) Groups. *Langmuir* **2011**, *27*, 6295.
4. Choi, Y. S.; Moschetta, E. G.; Miller, J. T.; Fasulo, M.; McMurdo, M. J.; Rioux, R. M.; Tilley, T. D. Highly Dispersed Pd-SBA15 Materials from Tris(*tert*-butoxy)siloxy Complexes of Pd(II). *ACS Catal.* **2011**, *1*, 1166.
5. Yoon, C. W.; Hirsekorn, K. F.; Neidig, M. L.; Yang, X.; Tilley, T. D. Mechanism of the Decomposition of Aqueous Hydrogen Peroxide over Heterogeneous TiSBA15 and TS-1 Selective Oxidation Catalysts: Insights from Spectroscopic and Density Functional Theory Studies. *ACS Catal.* **2011**, *1*, 1665.
6. Davenport, T. C.; Tilley, T. D. Dinucleating Naphthyridine-Based Ligand for Assembly of Bridged Dicopper(I) Centers: Three-Center Two-Electron Bonding Involving an Acetonitrile Donor. *Angew. Chem. Int. Ed.* **2011**, *50*, 12205.
7. Raboin, L.; Yano, J.; Tilley, T. D. Epoxidation catalysts derived from introduction of titanium centers onto the surface of mesoporous aluminophosphate: Comparisons with analogous catalysts based on mesoporous silica. *J. Catal.* **2012**, *285*, 168.
8. Guillo, P.; Fasulo, M. E.; Lipschutz, M. I.; Tilley, T. D. Synthesis and Characterization of Tantalum Silsesquioxane Complexes. *Dalton Trans.* **2013**, *42*, 1991.
9. Liberman-Martin, A.; Bergman, R. G.; Tilley, T. D. A Remote Lewis Acid Trigger Dramatically Accelerates Biaryl Reductive Elimination from a Platinum Complex. *J. Am. Chem. Soc.* **2013**, *135*, 9612.
10. Rumberger, E. M. W.; Ahn, H. S.; Bell, A. T.; Tilley, T. D. Water Oxidation Catalysis via Immobilization of the Dimanganese Complex  $[Mn_2(\mu-O)_2Cl(\mu-O_2CCH_3)(bpy)_2(H_2O)](NO_3)_2$  onto Silica. *Dalton Trans.* **2013**, *42*, 12238.
11. Bowring, M.; Bergman, R. G.; Tilley, T. D. Platinum-Catalyzed C-C Activation Induced by C-H Activation. *J. Am. Chem. Soc.* **2013**, *135*, 13121.
12. Cordiero, P. J.; Guillo, P.; Spanjiers, C. S.; Chang, J. W.; Fasulo, M. E.; Rioux, R. M.; Tilley, T. D. Titanium-Germoxo Precursor Route to Germanium-Modified Epoxidation Catalysts with Enhanced Activity. *ACS Catal.* **2013**, *3*, 2269.
13. Bowring, M.; Bergman, R. G.; Tilley, T. D. Isolation of a Dicationic Platinum Complex with Two Accessible Coordination Sites. *Organometallics* **2013**, *32*, 5266.
14. Ahn, H. S.; Davenport, T. C.; Tilley, T. D. Molecular cobalt electrocatalyst for proton reduction at low overpotential. *Chem. Comm.* **2014**, *50*, 3834.
15. Davenport, T. C.; Tilley, T. D. A Molecular Structural Analog of Proposed Dinuclear Active Sites in Cobalt-Based Water Oxidation Catalysts. *Chem. Comm.* **2014**, DOI: 10.1039/C3CC46865H.
16. Nguyen, A. I.; Hadt, R. G.; Solomon, E. I.; Tilley, T. D. Efficient C-H Bond Activations via  $O_2$  Cleavage by a Dianionic Cobalt(II) Complex. *Chem. Sci.* **2014**, DOI: 10.1039/C4SC00108G.

## ***In situ* SEIRAS Investigation of MOR on PtRu and FAOR on PtPb at Low Electrode Potential: a Re-visit of CO Poisoning and Bi-functional Mechanisms**

Dejun Chen<sup>1</sup>, Dianne O. Atienza<sup>1</sup>, Thomas C. Allison<sup>2</sup>, and YuYe J. Tong<sup>1</sup>

<sup>1</sup>*Department of Chemistry, Georgetown University, 37<sup>th</sup> & O Streets, NW, Washington DC 20057, USA;* <sup>2</sup>*Material Measurement Laboratory, National Institute of Standards and Technology, 100 Bureau Drive, Stop 8320, Gaithersburg, MD, 20899-8320, USA*

### **Presentation Abstract**

While Pt is widely observed to be the best monometallic anode material in electrocatalysis, it is easily poisoned by reaction-generated CO in both methanol and formic acid oxidation reactions (MOR and FAOR) due to relatively strong Pt-CO bonding and high water-activation potential, which renders it impractical for direct use in fuel cells and had led to the development of many bimetallic systems. For instance, alloying Ru to Pt substantially increases CO tolerance of the latter, leading to the best-performing electrocatalysts for MOR. This has been mainly attributed to the bi-functional mechanism in which the more oxophilic Ru adsorbs oxygen-containing species and enables oxidizing CO adsorbed on Pt at lower potential but to a lesser extent also to weakened Pt-CO bonding by alloyed Ru (the ligand effect). Similarly, under-potential deposition (upd) of Pb to a Pt surface substantially enhances FAOR. This has been interpreted as an electronic/ligand effect<sup>7</sup> as well as a third-body effect in which adsorbed Pb prevents dehydration of FA to CO by geometrically blocking certain surface sites. Although different in details, eliminating the poisonous CO is the key to both activity enhancement mechanisms that are the prevailing guiding principles in developing better electrocatalysts. However, our recent *in situ* surface enhanced IR reflection absorption spectroscopy (SEIRAS) studies of MOR on PtRu and FAOR on PtPb electrocatalysts show that the higher activity observed at low anodic electrode potential, i.e., < 0.5V vs RHE, has little to do with eliminating reaction-generated CO. Yet, it is such activity enhancement at low anodic potential that is most desirable to developing economically viable fuel cell applications. Our observations raise a critical question as to whether the aforementioned, though long-held, mechanisms are most appropriate for rationalizing the observed activity enhancements at low anodic potential, let alone for guiding the development of better anode electrocatalysts for DMFCs and DFAFCs. In this presentation, we will discuss ramifications of these observations and propose new mechanisms.

### **DE-FG02-07ER15895: In Situ NMR/IR/Raman and ab initial DFT Investigations of Unconventional Promoters of Catalytic Activity on Pt-Based: from Sulfur to Polymers to Iodine**

Postdocs: Eric Sorte, Dejun Chen  
Students: Dianne O. Atienzo (Ph. D), Yanyan Wang (Ph. D)

### **RECENT PROGRESS**

#### **1. <sup>195</sup>Pt – <sup>63</sup>Cu spin-echo-double-resonance (SEDOR):**

As a part of investigating why PtCu can have a much higher ORR activity as compared to pure Pt, we carried out the first SEDOR measurements. Figure 1 presents our recent <sup>195</sup>Pt–<sup>63</sup>Cu SEDOR (spin-echo double resonance) measurements carried out on ~7-nm Pt<sub>3</sub>Cu<sub>1</sub> alloy NPs that differentiate the <sup>195</sup>Pt atoms having from those not having <sup>63</sup>Cu as the next nearest neighbors. The black circles and red squares are the

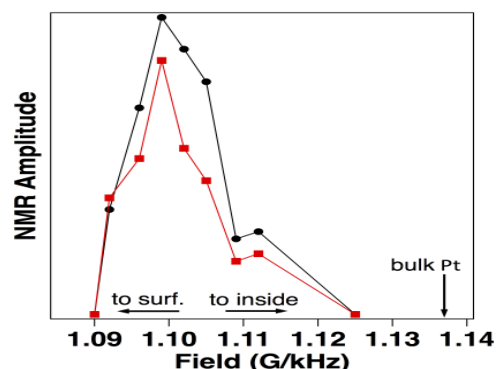


**Figure 1.** <sup>195</sup>Pt NMR spectra of ~7-nm Pt<sub>3</sub>Cu<sub>1</sub> alloy NPs w/o (black circles) w (red squares) <sup>63</sup>Cu SEDOR flipping.

$^{195}\text{Pt}$  spin-echo amplitudes without and with the  $^{63}\text{Cu}$  spins being flipped. If the  $^{195}\text{Pt}$  spins have  $^{63}\text{Cu}$  spins as their next-nearest neighbors, the  $^{63}\text{Cu}$  spin flipping de-phases the  $^{195}\text{Pt}$  spins during their spin echo formation thus leads to the decrease of the  $^{195}\text{Pt}$  spin-echo amplitude. As can be seen, the  $^{195}\text{Pt}$  spin-echo amplitude decreased dominantly at higher field (low frequencies) where the  $^{195}\text{Pt}$  inside the NPs resonates (the Pt bulk position indicated by the vertical arrow). This indicates that the  $\text{Pt}_3\text{Cu}_1$  NPs have an alloy core but a Pt shell structure that is in agreement with the EC results (not shown here). The uniqueness of such SEDOR spectroscopy is that it enables the local selectivity of pair-interaction and enhances both the chemical and spatial specificities of our investigative capability.

## 2. In situ SERS and SEIRAS Investigations of the Effect of Sulfide Adsorption on ORR.

Sulfide adsorption on surface of electrocatalysts is generally considered detrimental to the intended catalytic processes because of the frequently observed poisoning effect. However, our recent EC investigations have shown that at moderate coverages, the adsorbed sulfide can actually enhance the catalytic activity of the still uncovered Pt sites towards ORR. In order to understand better why such activity enhancement takes place, we carried out in situ SERS and SEIRAS, as show in Fig. 2.

Fig. 2a presents the in situ SERS band amplitude of PtO as function of the electrode potential for samples with different sulfide coverage.

As can be seen, the presence of adsorbed sulfide delayed the formation of Pt surface oxide, enabling the Pt surface have higher activity at high electrode potential. Figure 2b shows the in situ SEIRAS spectra between 950 to 1550  $\text{cm}^{-1}$  also for samples with different sulfide coverage. The ORR activity was highest at the coverage of 0.19 where the spectrum indicates the sample adsorbed largest amount of  $\text{O}_2$  and generated the highest amount of  $\text{HO}_2^-$  but no  $\text{HO}_2$ . These observations suggest that at the sulfide coverage of 0.19, electron and proton transfers were both operational on the surface. However, as the coverage of adsorbed sulfide increased, the surface became more poisoned. This led to the generation of  $\text{O}_2^-$  but  $\text{HO}_2^-$ , which implies that the proton transfer was blocked on the poisoned surface.

Careful electrochemical, including impedance spectroscopic, and *in situ* SEIRAS studies suggest the following. For MOR, the sulfide adsorption-induced more negatively charged Pt site caused delayed/suppressed adsorption of electrolyte anions and oxygen-containing species and increased amount of isolated free water monomers, which led to more available active sites, weakened bonding interaction between the Pt NPs and oxygen-containing species, and more active water species for enhancing MOR along the parallel reaction pathway. For CMOR, the enhanced activity was largely attributed to weakened bonding of oxygen-containing species with the adsorbed sulfide-modified Pt surface. Most recently, we have also observed such activity-enhancing effect on ORR as shown in Figure 2 where the results of rotating ring-disk bi-potential measurements are presented as the sulfide coverage changes. The currents on disk ( $i_d$ ) and ring ( $i_r$ ) electrodes were measured by varying the disk-electrode potentials between -0.25 to 0.71 V vs Ag/AgCl while holding the ring potential at 1.1 V in  $\text{O}_2$ -saturated electrolyte and at a constant rotation speed of 1600 rpm. The appearance of the ring current  $i_r$  indicates the production of  $\text{H}_2\text{O}_2$  which is the product of a 2-electron reduction of  $\text{O}_2$ . As can be seen, at the sulfide coverage of  $\theta_{\text{S,H}} = 0.16$ , the amount of  $\text{H}_2\text{O}_2$  produced was almost the same as that of pure Pt sample (40 wt% carbon-supported Pt) but the ORR activity was clearly enhanced. However, as the sulfide coverage increased, the production of  $\text{H}_2\text{O}_2$  also increased but the ORR activity

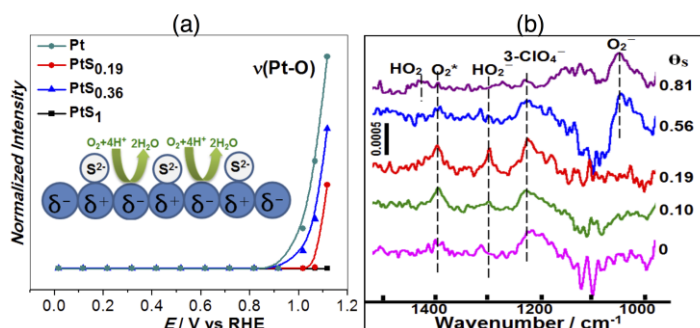


**Figure 2.** (a) *in situ* SERS band amplitude of PtO as function of potential for samples with different sulfide coverage. (b) *in situ* SEIRAS spectra @ 0.0 V (vs RHE) between 950 to 1550  $\text{cm}^{-1}$  for samples with different sulfide coverage.

decreased. It is still unclear at this moment what was the mechanistic reason for the observed ORR enhancement at  $\theta_{S,H} = 0.16$  but we hope that planed SEIRAS investigation will offer insightful information in this regard.

### 3. In Situ Investigation of MOR on Ru@Pt with Different Pt Loading.

Ru@Pt NPs offer more and better synthetic control of surface Pt composition of which the surface structures are complementary to those of the PtRu alloy NPs. Independent of Adzic's work on synthesizing Ru@Pt NPs, we have developed a polyol wet-chemistry based method to synthesize Ru@Pt NPs with different Pt packing densities. Very interesting preliminary SEIRAS results have been obtained on three Ru@Pt

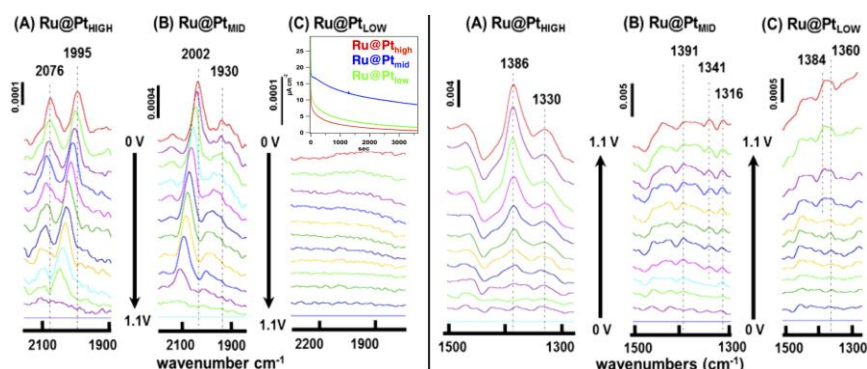


**Figure 3. Left Panel:** Potential dependent (stair-step) ATR-SEIRAS spectra of the  $\text{CO}_{\text{ads}}$  generated from MOR on the Ru@Pt NPs in 0.1M  $\text{HClO}_4$  + 0.5M MeOH with a potential step of 0.1V. **Right Panel:** from the same ATR-SEIRAS spectra as in the Left Panel but in the spectral window of 1300-1500 $\text{cm}^{-1}$  and potential change of 0.1V.

samples that were so synthesized with commercial Ru black as the starting material and with different Pt:Ru atomic ratios (1:1.7, 1:3.2, and 1:6.5 as determined by EDS and named as Ru@Pt<sub>HIGH</sub>, Ru@Pt<sub>MID</sub>, and Ru@Pt<sub>LOW</sub> respectively). Figure 3 (left panel) shows the potential-dependent *in situ* ATR-SEIRAS spectra of the  $\text{CO}_{\text{ads}}$  generated during the MOR on the Ru@Pt NPs with the inset showing the corresponding CA curves at 0.4V (vs. RHE).

In line with the previous observations, the peaks at 2076  $\text{cm}^{-1}$  and 1995  $\text{cm}^{-1}$  of the Ru@Pt<sub>HIGH</sub> NPs (Figure 3, Left Panel) were assigned to linear CO ( $\text{CO}_L$ ) adsorbed on the Pt-like and the PtRu-alloy-like or Pt-Ru boundary sites, respectively. No  $\text{CO}_{\text{ads}}$  on the Ru-like sites was observed, consistent with a high Pt coverage surface composition where few Ru-like sites exist. In the case of Ru@Pt<sub>MID</sub> (B, Left Panel), the peaks at 2002  $\text{cm}^{-1}$  and 1930  $\text{cm}^{-1}$  were assigned to  $\text{CO}_L$  adsorbed on the PtRu-alloy-like and on Ru sites. No  $\text{CO}_{\text{ads}}$  on the Pt-like sites was observed, indicating that the Pt islands formed at medium Pt coverage were small enough that few Pt-like sites exist. Interestingly, the formation of  $\text{CO}_L$  on the Ru-like sites was also observed during the MOR, notwithstanding the low amplitude. In view of the generally very low activity of Ru surfaces toward the MOR and that no  $\text{CO}_{\text{ads}}$  was observed on the Ru@Pt<sub>LOW</sub> sample during the MOR (C, Left Panel), the observed  $\text{CO}_L$ /Ru-like sites was likely a result of spill-over of  $\text{CO}_{\text{ads}}$  generated initially on the PtRu-alloy-like sites. However, the most interesting observation is that for the Ru@Pt<sub>LOW</sub> sample, no  $\text{CO}_{\text{ads}}$  on any of the types of surface sites was observed by the *in situ* SEIRAS during the stair-step MOR even though the MOR did take place and had a higher CA current than that of the Ru@Pt<sub>HIGH</sub> as shown in the inset. This observation was further confirmed by the preliminary time-dependent SEIRAS measurement at 0.4V (not shown here).

Two plausible causes could lead to the lack of observed  $\text{CO}_{\text{ads}}$  for the Ru@Pt<sub>LOW</sub> sample. The first is that the low Pt coverage led to the formation of Pt ensembles that were small enough to significantly suppress the indirect reaction pathway, which requires at least 3 to 4 neighboring sites leading to poisonous  $\text{CO}_{\text{ads}}$ . Consequently, no observable  $\text{CO}_{\text{ads}}$  was generated, but the MOR proceeded along the direct reaction pathway as discussed above. The second is that the surface was so active that the oxidation of the MOR-generated  $\text{CO}_{\text{ads}}$  was too quick to be detected by the SEIRAS. Since all three Ru@Pt samples showed almost the same onset potential for the gaseous CO oxidation (not shown here), the second cause seems unlikely. Therefore, it becomes very interesting to scrutinize the spectral

region in which the bands associated with formate species had been observed, as shown in Right Panel, Figure 3.

As can be seen in the right panel of Figure 3, two strong bands were observed at  $1386\text{ cm}^{-1}$  and  $1330\text{ cm}^{-1}$ , respectively, for the Ru@Pt<sub>HIGH</sub> sample (A). We tentatively assign the former to the C–H bending of the formic acid in the electrolyte vicinity to the surface (no dissociation of formic acid would be expected at the pH of the supporting electrolyte) and the latter to the symmetric O–C–O stretching mode,  $\nu(\text{O–C–O})$ , of formate with the two oxygen atoms bound to two Pt atoms: (Pt)O\*CHO\*(Pt), i.e., a bidentate conformation. That is, the MOR along the direct pathway generates bidentate-bound formate which could be dissolved into electrolyte and protonated instantaneously to form formic acid. For the Ru@Pt<sub>MID</sub> sample, three weak bands were observed at  $1391\text{ cm}^{-1}$ ,  $1341\text{ cm}^{-1}$ , and  $1316\text{ cm}^{-1}$ , respectively (B in Right Panel). We tentatively assign the former again to formic acid in the electrolyte and the latter two to bidentate-adsorbed formate on PtRu-alloy-like, i.e., (Pt)O\*CHO\*(Ru), and on Pt-like sites respectively. The much lower band intensity for all three species may be due to the much higher MOR activity observed in the Ru@Pt<sub>MID</sub> sample as shown in the inset and by the lower number of Pt-like sites.

For the Ru@Pt<sub>LOW</sub> sample, no bidentate-bound formate bands were observed (C in the right panel). Instead, a new band at  $1360\text{ cm}^{-1}$  was observed, which started appearing as early as 0.2V. We tentatively assign it to either monodentate-bound formate (Pt–O\*CHO) or the proposed COOH\*(Ru) species. We also note that the formic acid band does not appear until 0.8V.

Taken together, these preliminary results appear to be consistent with the proposed new mechanism, i.e., higher activity is associated with having more PtRu-alloy-like or Pt–Ru boundary sites and the possible observations of (Pt)O\*CHO\*(Ru) and COOH\*(Ru) species. We plan to carry out similar types of investigations to confirm these preliminary observations on Ru@Pt samples with a wider range of Pt loadings and a better IR spectrometer.

#### 4. Quantum Calculations of MOR on Pt and PtRu Surfaces.

Our recent work is focused on determining the mechanisms that govern the methanol oxidation reaction (MOR). To this end, we are studying the steps on the direct (leading to CO<sub>2</sub>) and indirect (leading to CO) pathways on 5 distinct surfaces: the pure Pt(111) surface, the core-shell Ru@Pt surface, and the alloy surfaces PtRu(1:1), PtRu(2:1), and PtRu(1:2). An example of this work is presented in Figure 4, where a methanol molecule is adsorbed on a Pt(111) surface (Figure 4a) and loses a methyl proton to form CH<sub>2</sub>OH (Figure 4b). The reaction profile for this process is depicted in Figure 4c. The full set of results involves 8 distinct reaction steps assessed on the five transition metal surfaces listed above. At present, the calculations are being performed at zero potential, but once these are complete, we will repeat the studies of the mechanism under potential control. When this phase of the work is completed, we will have a detailed energetic and mechanistic understanding of the MOR on a variety of surfaces.

We recently began exploring the formic acid oxidation reaction (FAOR) on Pt(111)Pb surfaces. This catalyst has shown enhanced activity in experiments, and we will work to identify the unique features of the catalyst mechanism in order to explain its superior activity.

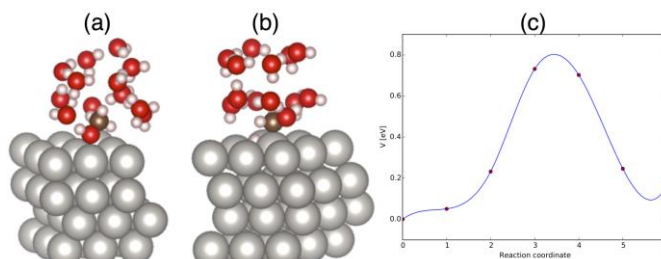


**Figure 4.** Atomistic models for before (a) and after (b) the dehydrogenation of the 1<sup>st</sup> methyl proton. (c) Calculated energy as a function as reaction coordinate.

## Publications Acknowledging this Grant in 2011-2014

1. Augusta M. Levendorf, De-Jun Chen, Christopher L. Rom<sup>†</sup>, Yangwei Liu, and **YuYe J. Tong**, "Electrochemical and in situ ATR-SEIRAS Investigation of Methanol and CO Electrooxidation on PVP-Free Cubic and Octahedral/Tetrahedral Pt Nanoparticles", *RSC Adv*, **2014**, *4*, 21284 - 21293.
2. Augusta M. Levendorf, Shi-Gang Sun and **YuYe J. Tong**, "*In situ* FT-IR Investigation of Methanol and CO Electro-oxidation on Cubic and Octahedral/ Tetrahedral Pt Nanoparticles Having Residual PVP", *Electrocatal.*, **2014**, DOI: 10.1007/s12678-014-0186-1.
3. **YuYe J. Tong**, "In situ Nuclear Magnetic Resonance Spectroscopy Applied to Understanding Chemical Processes for Electrochemical Energy Generation and Storage", **2013**, accepted; an invited book chapter for the Springer's *Handbook for Electrochemistry*.
4. Yuan Gao, Yangwei Liu, Ying Li, Oksana, Zaluzhna, **YuYe J. Tong**, "Mechanistic Insights into the Brust-Schiffrin Synthesis of Organochalcogenolate-Stabilized Metal Nanoparticles", **2013**, accepted; an invited book chapter for "Functional Nanometer-Sized Clusters of Transition Metals: Synthesis, Properties and Applications" by RSC in the RSC Smart Materials Series.
5. In-Su Park and **YuYe J. Tong**, "Sulfide-Adsorption-Enhanced Oxygen Reduction Reaction on Carbon-Supported Pt Electrocatalyst ", *Electrocatalysis*, **2013**, *4*, 117-122.
6. Thomas C. Allison, **YuYe J. Tong**, "Application of the Condensed Fukui Function to Predict Reactivity in Core-Shell Transition Metal Nanoparticles", *Electrochim. Acta*, **2013**, *101*, 334-340.
7. Georgeta C. Lica and **YuYe J. Tong**, "Electrochemical Impedance Spectroscopic Measurement of Potential of Zero Charge of Octanethiolate-Protected Au and Pd Nanoparticles", *J. Electroanal. Chem.*, **2013**, *688*, 349-353.
8. In-Su Park, De-Jun Chen, Dianne O. Atienza, **YuYe J. Tong**, "Electro-Oxidation of CO Monolayer on Sulfide-Adsorbed Pt Nanoparticles: A Combined Electrochemical and in situ ATR-IR Study", *Catal. Today*, **2013**, *202*, 175-182.
9. Dianne O. Atienza, Thomas C. Allison, **YuYe J. Tong**, "Spatially-Resolved Electronic Alterations as Seen by in situ <sup>195</sup>Pt and <sup>13</sup>C NMR in Ru@Pt and Au@Pt Core-Shell Nanoparticles", *J. Phys. Chem. C* **2012**, *116*, 26480-26486.
10. **YuYe J. Tong**, "Unconventional Promoters of Catalytic Activity in Fuel Cell Electrocatalysis", *Chem. Soc. Rev.*, **2012**, *41*, 8195-8209.
11. Oksana Zaluzhna, Ying Li, Thomas C. Allison, **YuYe J. Tong**, "Inverse-Micelle-Encapsulated Water-Enabled Bond Breaking of Dialkyl-Diselenide/Disulfide: a Critical Step for Synthesizing High-Quality Au Nanoparticles", *J. Am. Chem. Soc.*, **2012**, *134*, 17991-17996.
12. Oksana Zaluzhna, Chris Zangmeister, **YuYe J. Tong**, "Synthesis of Au and Ag nanoparticles with alkylselenocyanates", *RSC Adv.*, **2012**, *2*, 7396-7399.
13. Augusta M. Hofstead-Duffy, De-Jun Chen, **YuYe J. Tong**, "An in situ ATR-SEIRAS Study of Electrocatalytic Activity on Carbon-Supported Pt Nanoparticles Affected by PVP of Different Weight", *Electrochim. Acta*, **2012**, *82*, 543-549.
14. Augusta M. Hofstead-Duffy, De-Jun Chen, Shi-Gang Sun, **YuYe J. Tong**, "Origin of the current peak of negative scan in the cyclic voltammetry of methanol electro-oxidation on Pt-based electrocatalysts: a revisit to the current ratio criterion", *J. Mater. Chem.* **2012**, *22*, 5205-5208.
15. De-Jun Chen, Bolian Xu, Shi-Gang Sun, and **YuYe J. Tong**, "Electroless Deposition of Ultrathin Au film for Surface Enhanced in situ Spectroelectrochemistry and Reaction-Driven Surface Reconstruction for Oxygen Reduction Reaction", *Catal. Today*, **2012**, *182*, 46-53.
16. In-Su Park, Dianne O. Atienza, Augusta M. Hofstead-Duffy, De-Jun Chen, **YuYe J. Tong**, "Mechanistic insights on sulfide-adsorption enhanced activity of methanol electro-oxidation on Pt nanoparticles", *ACS Catalysis* **2012**, *2*, 168-174.
17. Thomas C. Allison and **YuYe J. Tong**, "Evaluation of Methods to Predict Reactivity of Gold Nanoclusters", *Phys. Chem. Chem. Phys.*, **2011**, *13*, 12858-12864.

18. Bingchen Du, Oksana Zaluzhna, **YuYe J. Tong**, "Electrocatalytic properties of Au@Pt nanoparticles: effects of Pt shell packing density and Au core size", *Phys. Chem. Chem. Phys.*, **2011**, *13*, 11568-11574.
19. De-Jun Chen, Augusta M. Hofstead-Duffy, In-Su Park, Dianne O. Atienza, Ceren Susut, Shi-Gang Sun, and **YuYe J. Tong**, "Identification of the most active sites and surface water species: A comparative study of CO and methanol oxidation reactions on core-shell M@Pt (M=Ru, Au) nanoparticles by in situ IR spectroscopy", *J. Phys. Chem. C*, **2011**, *115*, 8735-8743.
20. Ceren Susut, De-Jun Chen, Shi-Gang Sun, **YuYe J. Tong**, "Capping Polymer-Enhanced Electrocatalytic Activity on Pt Nanoparticles: A Combined Electrochemical and in situ IR Spectroelectrochemical Study", *Phys. Chem. Chem. Phys.*, **2011**, *13*, 7467-7474.
21. Ceren Susut, **YuYe J. Tong**, "Size Dependent Methanol Electro-oxidation Activity of Pt Nanoparticles with Different Shapes", *Electrocatalysis*, **2011**, *2*, 75-81.
22. Bolian Xu, In-Su Park, Ying Li, De-Jun Chen, **YuYe J. Tong**, "An in situ SERS Investigation of the Chemical States of Sulfur Species Adsorbed onto Pt from Different Sulfur Sources", *J. Electroanal. Chem.*, **2011**, *662*, 52-56.
23. Thomas Hsu-Yao, Kevin P. Browne, Nicole Honesty, **YuYe J. Tong**, "Polyoxometalate-Stabilized Pt Nanoparticles and Their Electrocatalytic Activities", *Phys. Chem. Chem. Phys.*, **2011**, *13*, 7433-7438.
24. In-Su Park, Bolian Xu, Dianne O. Atienza, Augusta M. Hofstead-Duffy, Thomas C. Allison, and **YuYe J. Tong**, "Chemical State of Adsorbed Sulfur on Pt Nanoparticles", *ChemPhysChem*, **2011**, *12*, 747-752.

David A. Vicić

**A Five-Coordinate Nickel(II) Fluoroalkyl Complex as a Precursor to a Spectroscopically Detectable Ni(III) Species**

ChengPan Zhang, Bo Chen, Peter Kaplan, Long Xu, and David A. Vicić\*

Department of Chemistry, Lehigh University, 6 E. Packer Ave., Bethlehem, PA 18015 USA

**Presentation Abstract**

Mechanistic proposals for nickel-catalyzed coupling reactions often invoke five-coordinate alkyl- or aryl-bound Ni(II) and/or high valent nickel(III) species, but due to their reactive nature, they have been difficult to study and fingerprint. Here, we invoke the stabilizing properties of fluoroalkyl ligands to access such nickel species bearing ligands that are commonplace in organic coupling reactions. We describe the synthesis of the unique precursors  $[(\text{MeCN})_2\text{Ni}(\text{CF}_3)_2]$  and  $[(\text{MeCN})_2\text{Ni}(\text{C}_2\text{F}_5)_2]$  that enables the synthesis of rare five-coordinate Ni(II) species bearing nickel carbon bonds similar to those that could be present in nickel-catalysed cross-coupling reactions. The complexes are stable enough to isolate, which permits the fingerprinting of the elusive organoNi(III) species proposed in terpyridyl nickel coupling reactions.

**DE-FG02-13ER16369: Development of Catalytic Alkylation and Fluoroalkylation Methods.**  
(Previous project number: DE-FG02-07ER15885)

**PI:** David A. Vicić

**Postdocs:** Cheng Pan Zhang, Huan Wang, and Bo Chen

**Students:** Peter T. Kaplan, Long Xu

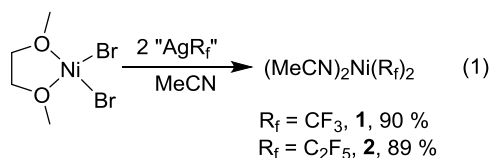
**Collaborators:** Axel Klein (Cologne, Germany) and Yulia Budnikova (Kazan, Russia)

## RECENT PROGRESS

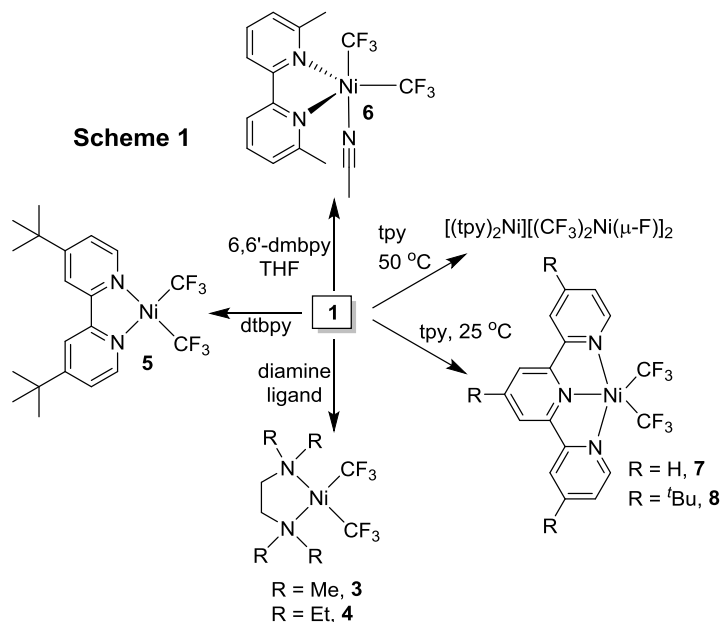
**Background and DOE Interest:** The DOE has had a long standing interest in the fundamental chemistry of fluorine ever since it was discovered that uranium hexafluoride exhibits a low vapor pressure and could be used to purify isotopically enriched uranium. Fluorination has become popular for other important reasons, like its known ability to increase the oxidative and thermal stability of new materials (examples: Teflon on a non-stick frying pan and seals that could withstand corrosive conditions), and its role in supporting new energy technologies is expected to grow. Moreover, fluorocarbons have shown great promise as oxidizers in metal-based pyrolant designs for the preparation of energetic materials, owing to the favorable enthalpy of formation of the metal-fluorine bond.<sup>1</sup> The development of new greener fluorination methods has also recently been listed as a priority research area by the ACS Green Chemistry Institute Pharmaceutical Roundtable.<sup>2</sup> One way to introduce fluorine into organic and organometallic molecules is through fluoroalkylation. Fluoroalkylation is synthetically challenging and requires protocols largely different from alkylation methods. Indeed, in an early quote from Emeléus underlining the differences between hydrocarbon and fluorocarbon chemistry: “progress may well be hindered by too great a dependence on analogy in considering future developments.”<sup>3</sup>

**Goal:** To develop new methods for alkyl and fluoroalkyl bond forming reactions based on a mechanistic understanding of the basic organometallic chemistry involved therein.

**Highlights:** One of the Specific Aims of this grant period was to prepare new perfluoroalkyl nickel complexes to understand the roles of geometry and oxidation states in reductive elimination reactions of perfluoroalkyl groups. In this way, we could better develop this first-row metal to perform catalytic perfluoroalkylation reactions. The synthesis of such a species first required access to a precursor bearing two perfluoroalkyl groups bound to nickel. The most versatile one we discovered was prepared by reacting “AgCF<sub>3</sub>” in acetonitrile with a Ni(II) source to give [(MeCN)<sub>2</sub>Ni(CF<sub>3</sub>)<sub>2</sub>] (**1**, eq 1). The reaction is not limited to trifluoromethyl groups as [(MeCN)<sub>2</sub>Ni(C<sub>2</sub>F<sub>5</sub>)<sub>2</sub>] (**2**) could also be prepared using a similar procedure. Complex **1** indeed proved to be a valuable synthetic precursor. A glimpse of its reactivity is described in Scheme 1. Access to **6**, **7**, and **8** is noteworthy. Four coordinate nickel(II) alkyl complexes can readily be



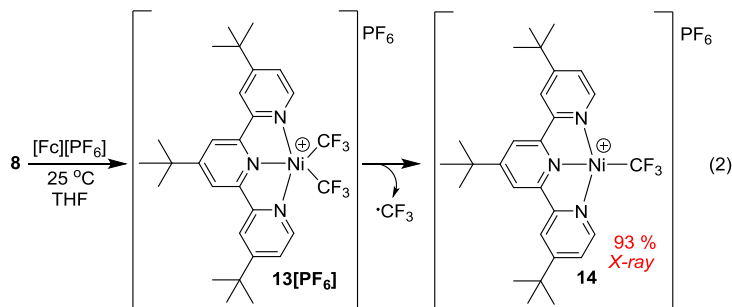
prepared, but decomposition to a reduced species typically occurs upon formation of higher-coordinate intermediates. It is anticipated that with precursor **1**, routes to a variety of new five coordinate perfluoroalkyl Ni(II) complexes will be readily available and will facilitate fundamental studies on this difficult-to-access geometry of organonickel.



Complex **8** cleanly reacts with

[ferrocenium][PF<sub>6</sub>] to initially produce what we speculate to be the targeted Ni(III) species **13** (eq 2). However, even upon rapid workup of the reaction, complex **14** was obtained. **14** is believed to arise from reductive homolysis of a trifluoromethyl radical from **13**. EPR spectroelectrochemistry was performed to spectroscopically characterize the one-electron oxidized and reduced forms of **8**.

Figure 1 shows EPR spectra at both temperatures for oxidized **8**. At 298 K an isotropic spectrum at  $g = 2.118$  is observed with no hyperfine splitting. The axial spectrum recorded at 110 K was



simulated with  $g_{\perp} = 2.154$  and  $g_{\parallel} = 2.013$ , which calculates to an averaged  $g_{av}$  value of 2.107, almost identical to the signal at 298 K. The relatively high values for both  $g_{av}$  and  $g$  anisotropy ( $\Delta g = g_{\perp} - g_{\parallel}$ ) of 0.141 and the axial character of the signal ( $g_{\perp} > g_{\parallel} > 2$ ) point to a marked contribution of Ni  $d$ -orbitals to the unpaired electron, consistent with calculated data (Figure 2).

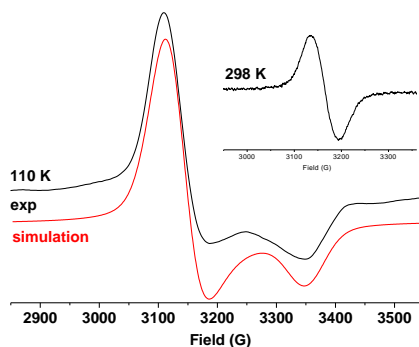


**Figure 1.** X-band EPR spectrum obtained during anodic electrolysis of **8** in THF/ $n\text{Bu}_4\text{N}[\text{PF}_6]$  at 110 K (glassy frozen solution) and at 298 K (insert top right).

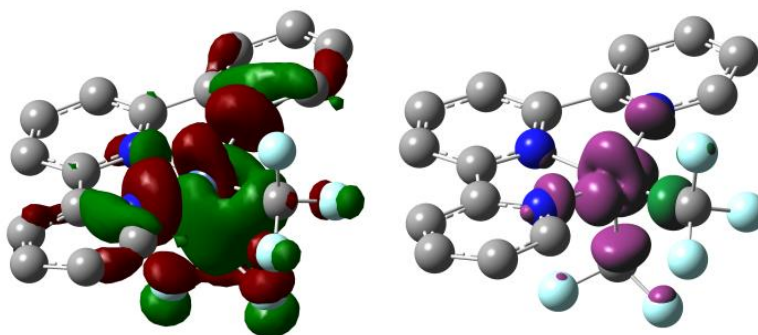


**Figure 2.** Calculated SOMO (left) and spin density (right) for the  $[(\text{tpy})\text{Ni}(\text{CF}_3)_2]$  cation in the gas phase.

In conclusion, for this Progress Report we describe the synthesis of a unique precursor that enables the synthesis of rare five-coordinate Ni(II) species bearing nickel carbon bonds similar to those that could be present in nickel-catalysed cross-coupling reactions. The complexes are stable enough to isolate, which permits the fingerprinting of the elusive organoNi(III) species proposed in terpyridyl nickel reactions.

#### References:

- (1) Miller, H. A.; Kusel, B. S.; Danielson, S. T.; Neat, J. W.; Avjian, E. K.; Pierson, S. N.; Budy, S. M.; Ball, D. W.; Iacono, S. T.; Kettwich, S. C. *J. Mater. Chem. A* **2013**, *1*, 7050.
- (2) Constable, D. J. C.; Dunn, P. J.; Hayler, J. D.; Humphrey, G. R.; Leazer, J. L., Jr.; Linderman, R. J.; Lorenz, K.; Manley, J.; Pearlman, B. A.; Wells, A.; Zaks, A.; Zhang, T. Y. *Green Chem.* **2007**, *9*, 411.
- (3) Emeleus, H. J. *Journal of the Chemical Society (Resumed)* **1954**, 2979.

### Publications Acknowledging this Grant in 2011-2014

1) "Improved Synthesis, Structure, and Reactivity of 1,4-Bis(trimethylsilyl)octafluorobutane" Chen, B.; Vivic, D. A. *J. Fluorine Chem.* **2014**, *in press*.

2) "Mild, Safe, and Versatile Reagents for (CF<sub>2</sub>)<sub>n</sub> Transfer and the Construction of Fluoroalkyl-Containing Rings" Kaplan, P. T.; Xu, L.; Chen, B.; McGarry, K. R.; Yu, S.; Wang, H.; Vivic, D. A. *Organometallics* **2013**, *32*, 7552-7558.

\*This article was highlighted in *C&E News* **2014**, *92*, 28-29.

3) "Organometallic Aspects of Fluoroalkylation Reactions with Copper and Nickel" Wang, H.; Vivic, D. A. *Synlett* **2013**, *24*, 1887-1898.\*

\*This article was a "Most Read" paper for the month of September for Synlett.

4) "A Five-Coordinate Nickel(II) Fluoroalkyl Complex as a Precursor to a Spectroscopically Detectable Ni(III) Species" Zhang, C. P.; Wang, H.; Klein, A.; Biewer, C.; Stirnat, K.; Yamaguchi, Y.; Gomez-Benitez, V.; Vivic, D. A. *J. Am. Chem. Soc.* **2013**, *135*, 8141-8144.

5) "Lithium Bromide-Induced Structural Changes in a Nickel Bis-Alkoxide Complex" Ichioka, H. and Vivic, D. A. *Acta Chim. Slov.* **2013**, *60*, 190-192.

6) "Oxidative Cleavage of CH<sub>3</sub> and CF<sub>3</sub> Radicals from BOXAM Nickel Complexes" Klein, A.; Vivic, D. A.; Biewer, C.; Kieltsch, I.; Stirnat, K.; Hamacher, C. *Organometallics* **2012**, *31*, 5334-5341.

7) "Synthesis and Structure of a Bis-Trifluoromethylthiolate Complex of Nickel" Zhang, C. P.; Vivic, D. A. *J. Fluorine Chem.* **2012**, *140*, 112-115.

8) "Oxidative Trifluoromethylthiolations of Aryl Boronic Acids Using a Copper/O<sub>2</sub>-Based Protocol" Zhang, C. P.; Vivic, D. A. *Chem. Asian J.* **2012**, *7*, 1756-1758.

9) "Oxygen-Bound Trifluoromethoxide Complexes of Copper and Gold" Zhang, C. P.; Vivic, D. A. *Organometallics* **2012**, *31*, 7812-7815.\*

\*invited contribution for the "Copper Organometallic Chemistry" issue. This work has also been listed as a "Most Read" (most downloaded) paper for the month of May by the ACS website.

10) "Synthesis and Electronic Properties of a Pentafluoroethyl-Derivatized Nickel Pincer Complex" Madhira, V. N.; Ren, P.; Vechorkin, O.; Hu, X., and Vicic, D. A. *Dalton Trans.* **2012**, *41*, 7915-7919.\*

\*invited contribution for the "New Talent Americas" issue

11) "Binuclear Arylnickel Complexes with Bis(arylimino)-1,4-Pyrazine Bridging Ligands" Klein, A.; Biewer, C.; Hamacher, C.; Hurkes, N.; Perez Outeiral, J.; Mora Paniagua, E.; Schmieder, A.-K.; Schuren, A. O.; Burma, P. R.; Ciszewski, J. T.; Vicic, D. A. *Eur J. Inorg. Chem.* **2012**, 2444-2455.

12) "Linear Bis-Perfluoroalkyl Complexes of Nickel Bipyridine" Yamaguchi, Y; Ichioka, I.; Klein, A.; Brennessel, W. W.; Vicic, D. A. *Organometallics* **2012**, *31*, 1477-1483.

\* invited contribution for the "Fluorine in Organometallic Chemistry" issue.

13) "Nickel-Catalyzed Synthesis of Aryl Trifluoromethyl Sulfides at Room Temperature" Zhang, C. P.; Vicic, D. A. *J. Am. Chem. Soc.* **2012**, *134*, 183-185.

14) "Electrochemical nickel-induced fluoroalkylation: synthetic, structural and mechanistical study" Mikhaylov, D. Y.; Budnikova, Y. H.; Gryaznova, T. V.; Dudkina, Y.; Khrizanphorov, M.; Kataeva, O.; Vicic, D. A. *Dalton Trans.* **2011**, *41*, 165-172.

15) "Redox Trends in Terpyridine Nickel Complexes" Ciszewski, J. T.; Mikhaylov, D. Y; Holin, K. V.; Kadirov, M. K.; Budnikova, Y. H.; Sinyahin, O. G.; Vicic, D. A. *Inorg. Chem.* **2011**, *50*, 196-198.

## Surface Science Studies of Nano-Crystalline TiO<sub>2</sub>

David Bennett and John M. Vohs,  
Department of Chemical and Biomolecular Engineering  
University of Pennsylvania

### Presentation Abstract

In this project we are bridging the materials gap between fundamental surface science studies of metal-oxide, single-crystal model catalysts, and high surface area catalysts that are used industrially by measuring structure-activity relationships for thin films of well-defined, metal oxide nanoparticles. We are currently using TiO<sub>2</sub> as a prototypical catalyst for selective- and photo-oxidation of organic oxygenates. Through wet synthesis techniques we are able to systematically vary the size and shape of TiO<sub>2</sub> nanocrystals and we are studying their reactivity as function of these parameters. We have developed methods to synthesize thin films of nanocrystalline TiO<sub>2</sub> on silicon single crystal supports and have demonstrated the thermal stability of these films. In this poster we present our initial studies of the partial oxidation of alcohols and the bimolecular ketonization of carboxylic acids as a function of particle size and shape. Preliminary studies of the photo-oxidation of alcohols as a function of TiO<sub>2</sub> particle size are also presented.

### Grant no. DE-FG02-04ER15605: Surface Science Studies of Nano-Crystalline Metal Oxide and Metal-Metal Oxide Core-Shell Catalysts

PI: J.M. Vohs  
Students: D. Bennett, P. Chen

### RECENT PROGRESS

#### *Background*

Recent advances in the nonmaterials synthesis provide for the exquisite control of the size and shape of metal oxide nanoparticles and allow one to systematically vary the amount and orientation of exposed crystal planes and the concentration of undercoordinated edge and corner sites. In this research program we are using thin films of well-defined metal oxide nanoparticles to extend surface science studies of structure-activity relationships for catalytically active metal oxides. The work aims to bridge the materials gap between surface science studies of model single crystal catalysts and high surface area catalysts that are used industrially. We are concentrating on catalytic systems that are of interest for complete-, selective- and photo-oxidation of organic oxygenates with the goal of determining the role

that highly undercoordinated cation and anion sites play in catalysis on oxides and then using this insight along with shape control to design highly active and selective catalysts for specific reactions.

### *Synthesis of nanocrystalline oxide thin film samples*

We are collaborating with the Murray group in Penn's chemistry department who are experts in the synthesis of well-defined nanomaterials. They have provided us with size- and shape-selected, anatase TiO<sub>2</sub> nanocrystals. As shown in Figure 1 these crystals have a truncated bi-pyramidal shape that predominantly expose {101} and {001} families of crystal planes. Variations in the synthesis conditions (e.g. solvent and surfactant compositions) allow the relative amounts of these two types of planes to be varied which in turn also allows for systematic variation in the number of edge and corner sites that are present at the vertices.

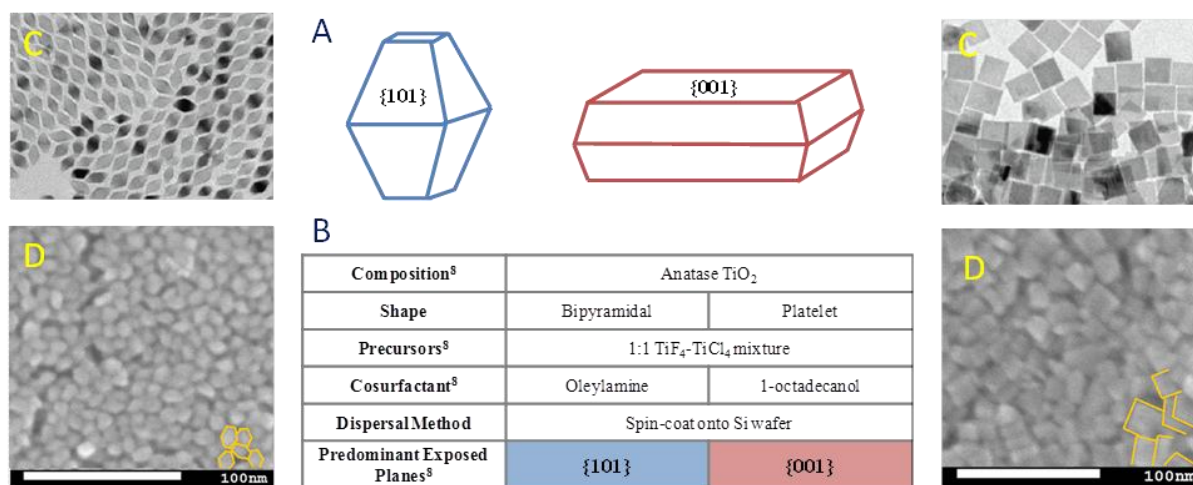


Figure 1. (A) Schematic showing the shape of the TiO<sub>2</sub> nanoparticles. (B) Synthesis conditions used to produce each shape. (C) SEM image of as-grown, bi-pyramidal nanocrystals showing the size uniformity. (D) SEM images of spin cast TiO<sub>2</sub> nanoparticle films supported on a Si(100) surface. These samples have been annealed in vacuum for extended periods at 800 K.

The SEM images for the as synthesized nanocrystals in Figure 1 demonstrate the high degree of size and shape uniformity of the nanocrystals and that we are able to produce bi-pyramidal samples with elongated and platelet morphologies. By varying synthesis conditions, such as reaction time and temperature, the size (5-30 nm) of the crystallites can be controlled. We have also demonstrated the growth of thin films (2-3 layers) of these TiO<sub>2</sub> nanocrystals on a Si(100) single crystal substrate using spin coating. Si(100) was chosen because it is electronically conductive (we use highly n-doped samples) which helps avoid charging when using electron spectroscopies such as XPS. It is also coated with a native oxide layer that has very low reactivity toward the alcohol and carboxylic acid reactants we are using as probe molecules. We have spent considerable time characterizing the structure of the TiO<sub>2</sub> nanoparticle films both after synthesis and more importantly after they had been annealed in vacuum at elevated temperatures, ~800 K, for extended periods of time. Since our goal is to investigate reactivity as a function of particle size and shape it was important to first establish that the particles do not sinter into larger crystals or agglomerates when heated in vacuum. As shown in Figure 1D, SEM analysis demonstrates that for these conditions the

annealed particles retain their initial size and shape. We are also in the process of doing extensive XPS analysis of the nanoparticle thin films as a function of temperature in order to determine the extent to which the particles undergo reduction upon heating in vacuum.

### Thermal Reactivity Studies

Previous studies of the reaction of small oxygenates on TiO<sub>2</sub> single crystal surfaces (mostly rutile, but there are also few for anatase) have identified undercoordinated Ti cations as active sites for the dissociative adsorption of alcohols and carboxylic acids. It has been shown that on Ti cations containing a single coordination vacancy, adsorbed acetate species react to form ketene at ~450 K, while on more defective surfaces with Ti cations having multiple coordination vacancies bimolecular ketonization of adsorbed acetates occurs to produce the coupling product acetone near 500 K. We are using these reactions to probe the types of sites exposed on nanocrystalline TiO<sub>2</sub> with the expectation that highly undercoordinated Ti sites will be present preferentially at the vertices between exposed crystal planes. Figure 2 displays TPD data for an acetic acid-dosed TiO<sub>2</sub> nanocrystal thin film sample (elongated bipyramidal, 15 nm) and shows the reactivity is similar to that reported for macroscopic single crystals with ketene being the major reaction product and a small amount of acetone also produced. We are currently in the process of

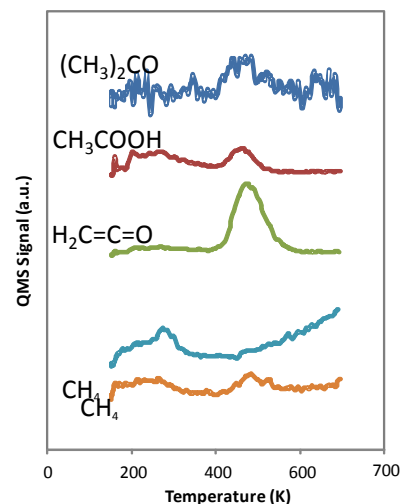


Figure 2. TPD spectra from acetic acid-dosed TiO<sub>2</sub> nanocrystals thin film sample (elongated bipyramidal 15 nm crystals)

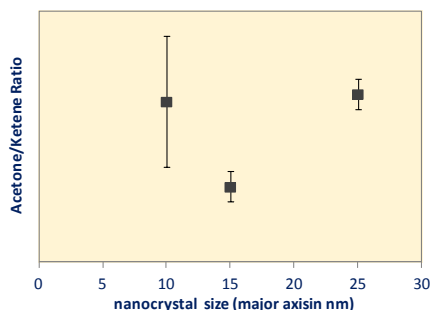


Figure 3. Acetone to ketene product ratio for acetic acid dosed TiO<sub>2</sub> nanocrystals thin films (elongated bipyramidal).

measuring the

product distributions as a function of the TiO<sub>2</sub> nanocrystallite size and aspect ratio. Preliminary data for the elongated bipyramidal-shaped particles (Figure 3) suggests a rather complex relationship between size and selectivity but we need to collect additional data to obtain any meaningful conclusions. We have also completed some studies of how the TiO<sub>2</sub> nanoparticle shape affects reactivity toward methanol. In this work significant variations in product yields were observed between the elongated and platelet nanocrystal morphologies.

### Photochemical Reactivity Studies

Since TiO<sub>2</sub> is a prototypical photocatalytic material we are also studying how the size and shape of nanocrystalline TiO<sub>2</sub> affects its activity for the photo-oxidation of small oxygenates. We have recently conducted preliminary studies of the photo-oxidation of methanol on one of our thin film TiO<sub>2</sub> nanocrystals samples. Previous studies by Henderson and others have shown that adsorbed methanol reacts to produce methyl formate on TiO<sub>2</sub> upon irradiation with photons with energies slightly greater than the band gap. Our first

experiments focused on determining if this reaction also occurs on our TiO<sub>2</sub> nanocrystals samples. Figure 4 shows TPD data from this work and displays the methylformate desorption signal as a function of the UV light exposure time for samples dosed with a saturation amount of methanol. Note that the expected chemistry is observed with the amount of methylformate produced increasing with increasing photon exposure.

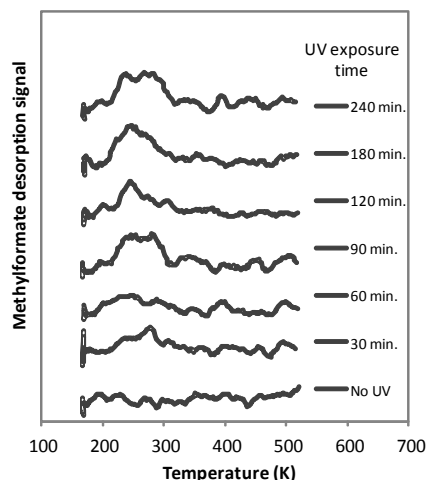


Figure 1. Methylformate product during TPD from methanol-dosed TiO<sub>2</sub> nanocrystal thin film sample (elongated bipyramidal 15 nm) as a function of UV radiation time.

#### ***Publications Acknowledging this Grant in 2013-2014***

1. Site Requirements for the Adsorption and Reaction of Oxygenates on Metal Oxide Surfaces, J.M. Vohs, *Chemical Reviews*, **113** (2013) 4136-4163. 268. Alloy
2. Formation and Chemisorption at Zn/Pt(111) Bimetallic Surfaces using Alkali ISS, XPD, and TPD, C.S. Ho, E. Martono, S. Banerjee, J. Roszell, J. Vohs, and B.E. Koel., *J. Phys. Chem. A*, **117** (2013) 11684-11694.
3. Reaction of CO, CH<sub>2</sub>O, CH<sub>3</sub>OH on Zn-Modified Pt(111) Surfaces, E. Martono and J.M. Vohs, *J. Phys. Chem. C*, **117** (2013) 6692-6701.

**Sub Nanometer Sized Clusters for Heterogeneous Catalysis**

Yong Wang<sup>1</sup> and Abhaya Datye<sup>2</sup>

<sup>1</sup> Voiland School of Chemical Engineering and Bioengineering, Washington State University

<sup>2</sup> Department of Chemical and Nuclear Engineering, University of New Mexico

**Presentation Abstract**

Precious metals can be atomically dispersed and stabilized on certain supports, leading to superior activity. Here, two examples are given in illustrating that improvements in our ability to stabilize transition metals in ionic form on high surface area supports can lead to superior catalytic behavior. In the first example, we have clear evidence of the trapping of ionic Pd on La-alumina, leading to weaker CO chemisorption, and hence lack of CO poisoning otherwise seen on metallic Pd at these low temperatures. The findings have important implication for the design of automotive exhaust catalysts for advanced combustion engines, the 150 °C challenge where DOE would like catalysts to achieve. In the second example, we found that when Ir and La halides are deposited on carbon, exposure to CO spontaneously generates a discrete molecular heterobimetallic structure. Such structure contains an Ir-La covalent bond that exhibits a very high productivity of ~1.5 mole acetyl/mole Ir/s for the carbonylation of methanol to produce acetic acid, similar to that of the commercial Ir-Ru homogeneous catalysts without need for Ru. The enhanced activity can be mechanistically rationalized by the presence of La within the ligand sphere of the discrete molecular Ir-La heterobimetallic structure which acts as a Lewis acid to accelerate the normally rate-limiting CO insertion in Ir catalyzed carbonylation. Similar approaches can potentially help expand the applicability of single atom catalysts to a broader class of heterogeneously catalyzed reactions.

## DE-FG02-05ER15712: Nanostructured Catalysts for Hydrogen Generation from Renewable Feedstocks

**PI:** Abhaya Datye, University of New Mexico (UNM)  
**Co-PI:** Yong Wang, Washington State University (WSU)  
**Post-docs:** Barr Halevi (UNM, 2008 - 2012), He Zhang (WSU) commenced in 2010.  
**Graduate Students:** Eric Petersen, Patrick Burton – graduated 2011, Jonathan Paiz, graduated 2013 (UNM), Stephen Davidson (WSU).  
**Undergrad Students:** Jay McCabe, Monique Cordova  
**Collaborators:** Robert Schlögl, Fritz Haber Institute, Berlin, Germany.  
Larry Allard, Oak Ridge National Laboratories  
Hua Guo, University of New Mexico  
Franklin Tao, University of Notre Dame  
Shenqiang Ren, University of Kansas  
Donghai Mei, Pacific Northwest National Laboratories  
Jean-Sabin McEwen, Washington State University

### RECENT PROGRESS

#### *Stabilization Of Pd<sup>2+</sup> on Alumina Doped with La<sup>3+</sup>*

In recent work on CO oxidation of 2.5 wt% Pd/alumina and La-alumina, we noticed that the catalysts prepared using lanthana-stabilized alumina were more reactive (Fig. 1). Closer

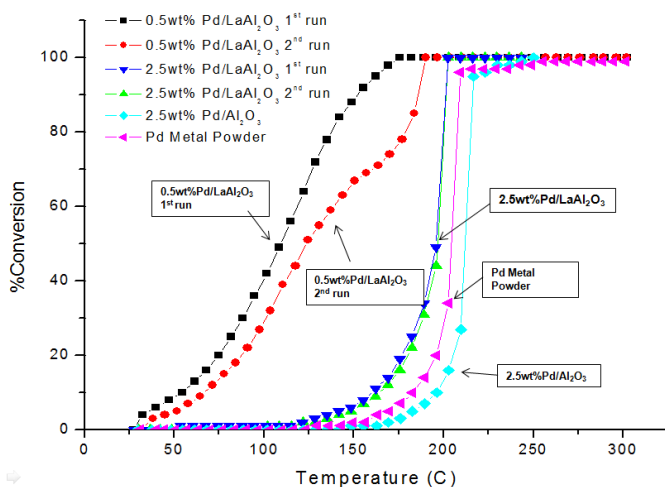


**Figure 1.** CO oxidation reactivity of 0.5 wt% Pd/La-alumina (100 mg) compared with 2.5 wt% Pd/La-alumina (20 mg), 2.5 wt% Pd/alumina (20 mg) and metallic Pd powder (20 mg).

examination of the Pd/La-alumina revealed that the La<sup>3+</sup> is atomically dispersed on the alumina (Fig. 2), which is key to its ability to stabilize gamma alumina by preventing the alumina phase transformation to alpha-alumina. La is added to automotive catalyst supports to prevent loss of surface area during use at elevated temperatures. FTIR spectroscopy coupled with EXAFS suggested that the La-containing catalysts allowed O<sub>2</sub> to compete more effectively with adsorbed CO on Pd leading to improved low temperature reactivity. Detailed analysis of the AC-STEM images showed that atomically dispersed Pd species were present along with the La, as shown in Figure 2 on the next page. In order to separate the contributions of the metallic phase and the atomically dispersed phase, we prepared catalysts with 0.5 wt% of Pd. Figure 1 shows the performance of the 0.5 wt% Pd/La-alumina, compared with the other catalysts. The 0.5 wt% Pd/alumina is not shown because its behavior is similar to that of 2.5 wt% Pd/Al<sub>2</sub>O<sub>3</sub>. In the experiments reported in Fig. 1, we varied the amount of catalyst to ensure that supported Pd catalysts had the same amount of Pd loaded into the reactor. The metal powder also had the same number of surface sites as the

2.5 wt% Pd samples. The 0.5 wt% Pd/La-alumina catalysts show improved low temperature light-off and overall TOF ( $1.9 \times 10^{-3} \text{ s}^{-1}$ ) at 70 °C, over an order of magnitude greater than metallic Pd ( $1.3 \times 10^{-4} \text{ s}^{-1}$ ) (extrapolated from higher temperatures due to the low reactivity on metallic Pd at this temperature). We confirmed that the data at 70 °C were in the kinetic regime by performing repeated runs at low temperature where the conversion is low and we used the Mears criterion to ensure we were not subject to heat and mass transfer limitations. We performed operando EXAFS/XANES and CO oxidation to probe further into the origins of this low temperature reactivity. The results show that the La-alumina is more effective at stabilizing  $\text{Pd}^{2+}$  on the surface. During reaction, the Pd transforms to an intermediate oxidation state ( $\sim\text{Pd}^{\delta+}$ ). A reaction mechanism was developed based on DFT analysis which suggests that the bridging oxygen bound to the Pd site plays a key role in the reaction mechanism, which changes from a Langmuir-Hinshelwood on metallic Pd to a Mars van Krevelen type of reaction on the single atom sites. EXAFS of the initial calcined sample shows that  $\text{Pd}^{2+}$  has 4 nearest oxygen neighbors at 2.04 Å, very similar to bulk PdO. But XANES analysis during CO oxidation shows oxidation state changes. These isolated  $\text{Pd}^{2+}$  sites on alumina differ from those in PdO because the oxygens are now bridging with  $\text{Al}^{3+}$  or  $\text{La}^{3+}$  sites. The role of  $\text{La}^{3+}$  is apparent in the stability

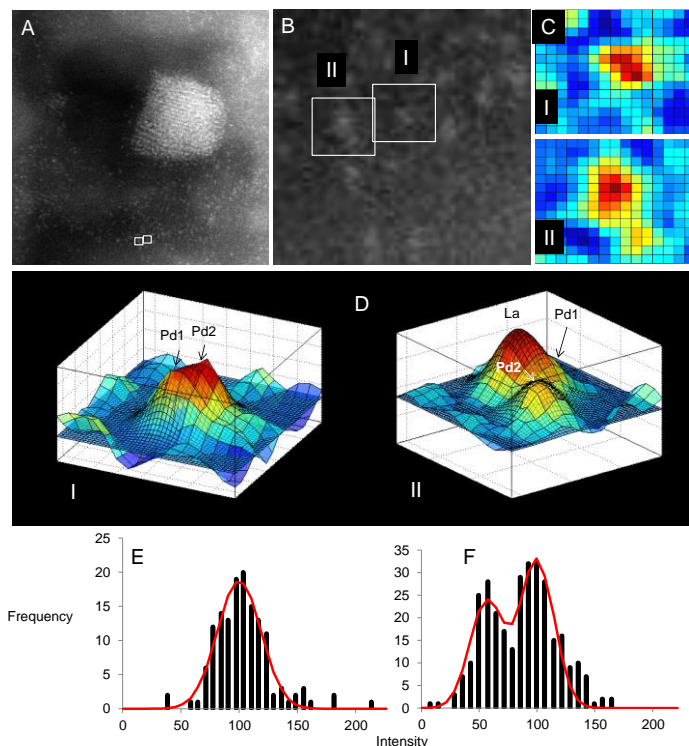


**Figure 4.** Intensity analysis of ACEM images obtained from a La-stabilized  $\gamma$ -alumina support sample with a 2.5 wt.% Pd-loading. (A) Pd-metal particle surrounded by isolated single atom species. (B) An enlarged region from (A), showing a higher magnification view. (C) Colorized intensity maps from regions I and II. (D) 2-D Gaussian-function fits to the intensity maps in (C). (E) and (F) Normalized intensity distributions, obtained from 2-D Gaussian-function fits of images (not shown) obtained from alumina (E) showing a single peak and from Pd/La-alumina (F) showing two peaks corresponding to Pd and La electron backscatter intensity (which is consistent with the atomic numbers of Pd and La).

of these dispersed species. Figure 1 shows the second run on the 0.5 wt% catalyst, which is still significantly more active than metallic Pd, but the 0.5 wt% Pd/alumina is not able to retain the ionic form of Pd which transforms to metallic clusters. A similar observation was reported by Paredis et al.<sup>1</sup> during the reaction of NO with  $\text{H}_2$  on alumina, where a  $\text{Pd}^{\delta+}$  state on alumina was suggested as a transient species.

In our experiments, the metallic clusters formed during reaction can, however, be redispersed on the support and we are able to reversibly create the high activity state of the Pd/La-alumina catalyst. In summary, we have clear evidence by XAS, AC-STEM and FTIR of the trapping of ionic Pd on La-alumina, leading to weaker CO chemisorption and hence lack of CO poisoning otherwise seen on metallic Pd at these low temperatures. The findings have important implication for the design of automotive exhaust catalysts for advanced

combustion engines, the 150 °C challenge where DOE<sup>2</sup> would like catalysts to achieve light-off below 150 °C.

There is evidence in the literature on automotive catalysts from researchers at Ford who identified both a dispersed as well as a particulate phase for noble metals such as Pd and Pt<sup>3,4,5</sup>. This dispersed phase is what we are seeing here in Fig. 2. Similar low temperature reactivity is also seen on Pd/CeO<sub>2</sub> for CO oxidation and has also been linked to an ionic form of Pd<sup>6</sup>. In Fig. 1 only at low loadings of Pd do we see the enhanced reactivity of this ionic form of Pd. The reason is that the larger metal particles act as sinks for the mobile species emitted during Ostwald ripening. This is why the 2.5 wt% Pd catalyst does not show low temperature light-off since it does not have a high enough concentration of the ionic Pd. We do see a few of the Pd single atoms, as evident from the image in Figure 2. In summary, our preliminary work shows that ionic Pd can be trapped not only on reducible supports like CeO<sub>2</sub><sup>6</sup>, but also on non-reducible supports like alumina. On the latter, however, we see only a limited numbers of trapping sites, except on the alumina that has atomically dispersed La<sup>3+</sup> acting as trapping sites for Pd<sup>2+</sup>. Based on this work, we can now propose a strategy for increasing the number of such trapping sites on alumina surfaces.

### ***Ir-La/C Catalysts for Carbonylation***

The carbonylation of methanol to acetic acid is widely practiced among homogeneous catalytic processes, with > 6 x 10<sup>9</sup> kg of acetic acid produced each year<sup>7</sup>(the only other homogeneous process practiced on a large scale is the hydroformylation of propylene to n-butylaldehyde on a scale of 4 x 10<sup>9</sup> to 5 x 10<sup>9</sup> kg/year<sup>8</sup>. There are two homogeneous catalytic processes currently applied at commercial scale: Celanese employs an Rh-Li catalyst, BP an Ir – Ru catalyst, and the mechanisms of each process are well understood<sup>9</sup>. Transforming either of these processes to a heterogeneous vapor phase reaction has been challenging.

Our recent work<sup>10</sup> showed that Ir-La/C catalysts exhibited a very high activity for the carbonylation of methanol to acetyls, achieving a productivity of ~1.5 mole acetyl/mol Ir•s with >99% selectivity to acetyl (acetic acid and methyl acetate). In addition, the La-promoted Ir on carbon catalyst is very stable and has been operated continuously for more than one month with no detectable loss in activity or selectivity. However, in the absence of La, the Ir/C catalyst showed a significantly lower productivity of ~0.5 mole acetyl/mol Ir•s under the same reaction conditions, and catalyst deactivated within several hours time-on-stream (TOS). A productivity of ~1.5 mole acetyl/mol Ir•s for the Ir-La/C catalyst is similar to the commercial homogeneous Ir/Ru catalyst (1/2 molar ratio), where ~1 mole acetyl/Ir•s was observed using a batch autoclave reactor<sup>11</sup>. It is worth noting that such a high activity for the Ir-La/C catalysts was achieved without need for a second precious metal Ru.

More importantly, we found that the Ir-La/C catalyst appears to function like its homogenous analogue. We used a combination of different chemical and physical characterization (XPS, CO-TPD, HRTEM etc) to confirm that the superior catalyst activity may be due to the spontaneous generation of the discrete

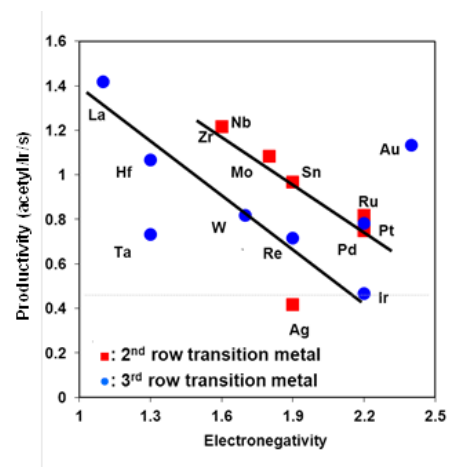


**Figure 3. Methanol carbonylation productivity (acetyl/Ir/s) as a function of electronegativity of promoter of Ir-M/C (M = transition metal).**

molecular structure of  $[\text{Ir}(\text{CO})_2\text{I}_2]^-$  by exposure catalyst to CO, and the excellent catalyst stability is attributed to the stabilization of Ir dispersion and  $\text{Ir}^{1+}$  oxidation state by La. Furthermore, from the activity measurements using transition metals with different electronegativities (La, Hf, W, Re, Zr, Nb, Mo, Sn), we found that the high activity of Ir-La/C is likely due to the Lewis acid assisted CO insertion by La on a molecular structure of  $\text{Cl}(\text{CO})_2\text{Ir-LaCl}_2(\text{s})_3$  (Figure 3). Although the Ir-La/C catalyst is extremely stable under ordinary operating conditions (e.g., 240°C), rapid deactivation occurred at temperatures exceeding >300°C (~50% reduction in activity within 10 hours TOS). XPS examination of the deactivated catalyst indicated that the Ir was reduced to zero valent Ir. Sintering of Ir species to form ~10 nm Ir particles was also observed by TEM characterization. In addition, it was found that rapid deactivation of the Ir/C catalyst within several hours TOS at 240°C was due to the reduction of Ir to zero valent Ir. Apparently, catalyst deactivation is due to both the reduction of  $\text{Ir}^{1+}$  to  $\text{Ir}^0$  and sintering of Ir species, and the presence of La inhibits the deactivation of Ir catalysts. This example illustrates the roles of  $\text{Ir}^{1+}$ , its stabilization, and manipulation of its surrounding ligands in achieving superior catalytic performances. However, the following scientific questions still remain unaddressed, which limit further advancement of this catalytic system and the application of a similar strategy to a broader class of reactions: 1) by what mechanisms does La stabilize the dispersion of Ir and its +1 oxidation state? 2) what is the stoichiometry of Ir/La in the molecular structure containing Ir-La covalent bonds and its relationship with the methanol carbonylation activity? 3) by what mechanisms does the support or ligand (e.g., C) stabilize the molecular structure of  $\text{Cl}(\text{CO})_2\text{Ir-LaCl}_2(\text{s})_3$ .

## References

- 1 K. Paredis, L.K. Ono, F. Behafarid, Z.F. Zhang, J.C. Yang, A.I. Frenkel, and B.R. Cuenya, *Evolution of the Structure and Chemical State of Pd Nanoparticles during the in Situ Catalytic Reduction of NO with H<sub>2</sub>*. Journal of the American Chemical Society, 2011. **133**(34): p. 13455-13464.
- 2 USDRIVE Advanced Combustion and Emission Control Roadmap. 2013; Available from: [http://www1.eere.energy.gov/vehiclesandfuels/pdfs/program/acec\\_roadmap\\_june2013.pdf](http://www1.eere.energy.gov/vehiclesandfuels/pdfs/program/acec_roadmap_june2013.pdf).
- 3 J.Z. Shyu, K. Otto, W.L.H. Watkins, G.W. Graham, R.K. Belitz, and H.S. Gandhi, *Characterization of pd/gamma-alumina catalysts containing ceria*. Journal of Catalysis, 1988. **114**(1): p. 23-33.
- 4 J.Z. Shyu and K. Otto, *Identification of platinum phases on gamma-alumina by XPS*. Applied Surface Science, 1988. **32**(1-2): p. 246-252.
- 5 K. Otto, W.H. Weber, G.W. Graham, and J.Z. Shyu, *Identification of dispersed platinum on gamma-alumina by laser-Raman spectroscopy*. Applied Surface Science, 1989. **37**(2): p. 250-257.
- 6 E.M. Slavinskaya, R.V. Gulyaev, O.A. Stonkus, A.V. Zadesenets, P.E. Plyusnin, Y.V. Shubin, S.V. Korenev, A.S. Ivanova, V.I. Zaikovskii, I.G. Danilova, and A.I. Boronin, *Low-temperature oxidation of carbon monoxide on Pd(Pt)/CeO<sub>2</sub> catalysts prepared from complex salts*. Kinetics and Catalysis, 2011. **52**(2): p. 282-295.
- 7 H.J. Arpe, *Industrial Organic Chemistry*. 5th edition ed. 2010, Weinheim: Wiley-VCH.
- 8 D.J. Cole-Hamilton, *Homogeneous Catalysis--New Approaches to Catalyst Separation, Recovery, and Recycling*. Science, 2003. **299**(5613): p. 1702-1706.
- 9 A. Haynes, *Acetic Acid Synthesis by Catalytic Carbonylation of Methanol*, in *Catalytic Carbonylation Reactions*, M. Beller, Editor. 2006, Springer Berlin Heidelberg. p. 179-205.
- 10 J.H. Kwak, R. Dagle, G.C. Tustin, J.R. Zoeller, L.F. Allard, and Y. Wang, *Molecular Active Sites in Heterogeneous Ir-La/C-Catalyzed Carbonylation of Methanol to Acetates*. The Journal of Physical Chemistry Letters, 2014. **5**(3): p. 566-572.
- 11 A. Haynes, P.M. Maitlis, G.E. Morris, G.J. Sunley, H. Adams, P.W. Badger, C.M. Bowers, D.B. Cook, P.I.P. Elliott, T. Ghaffar, H. Green, T.R. Griffin, M. Payne, J.M. Pearson, M.J. Taylor, P.W. Vickers, and R.J. Watt, *Promotion of Iridium-Catalyzed Methanol Carbonylation: Mechanistic Studies of the Cativa Process*. Journal of the American Chemical Society, 2004. **126**(9): p. 2847-2861.

---

## Publications Acknowledge this Grant in 2011-2014

1. Zhang, H.; Lebarbier, V.; Karim, A. M.; Sun, J.; Halevi, B.; DeLariva, A.; Datye, A.; Wang, Y. The influence of ZnO facets on Pd/ZnO catalysts for methanol steam reforming. (revisions submitted to *ACS Catalysis*)
2. Liu, C.; Wang, H.; Karim, A.; Sun, J.; Wang, Y. Advances in catalytic pyrolysis of lignocellulosic biomass. *Chem.Soc.Rev.* **2014**, DOI:10.1039/c3cs60414d (invited review)
3. Kwak, J.; Dagle, R.; Tustin, G.; Zoeller, J.; Allard, L.; Wang, Y. Molecular active sites in heterogeneous Ir-La/C catalyzed carbonylation of methanol to acetates. *J.Phy.Chem.Lett.* **2014**, dx.doi.org/10.1021/jz402728e
4. Sun, J.; Wang, Y. Review of ethanol conversion to chemicals and fuels. *ACS Catalysis* **2014**, dx.doi.org/10.1021/cs4011343. (cover art for the No.4 issue of 2014).
5. Davison, S.; Sun, J.; Zhang, H.; Wang, Y. Supported metal catalysts for alcohol/sugar alcohol steam reforming. *Dalton Transactions* **2014**, DOI:10.1039/c4dt00521j (invited perspective, cover of the issue 31 of 2014).
6. Davidson S.; Sun, J.; Wang, Y. The effect of ZnO addition on Co/C catalyst for vapor and aqueous phase reforming of ethanol. *Catal.Today* **2014**, dx.doi.org/10.1016/j.cattod.2013.12.044.
7. Davidson, S.; Sun, J.; Wang, Y. Ethanol steam reforming on Co/CeO<sub>2</sub>: the effect of ZnO promoter. *Topics in Catalysis* **2013**, doi: 10.1007/s11244-013-0103-5.
8. Gaudet, J. R.; de la Riva, A.; Peterson, E. J.; Bolin, T.; Datye, A. K. Improved Low-Temperature CO Oxidation Performance of Pd Supported on La-Stabilized Alumina. *ACS Catalysis* **2013**, p. 846-855.
9. Halevi, B.; Peterson, E. J.; Roy, A.; Delariva, A.; Jeroro, E.; Gao, F.; Wang, Y.; Vohs, J. M.; Kiefer, B.; Kunkes, E.; Hävecker, M.; Behrens, M.; Schlögl, R.; Datye, A. K. Catalytic reactivity of face centered cubic PdZn  $\alpha$  for the steam reforming of methanol. *Journal of Catalysis* **2012**, 291: p. 44-54.
10. Hensley, A. J.; Zhang, R.; Wang, Y.; McEwen, J. S. Energetic and electronic interactions between benzene and PdFe surfaces: a density functional theory study. *J.Phy.Chem.C.* **2013**, 117, 24317-24328.
11. Liu, C. J.; Sun, J.; Smith, C.; Wang, Y. A study of Zn<sub>x</sub>Zr<sub>y</sub>O<sub>z</sub> mixed oxides for direct conversion of ethanol to isobutene. *Appl.Catal.A: General* **2013**, doi:10.1016/j.apcata.2013.07.011.
12. Sun, J.; Karim, A. M.; Zhang, H.; Kovarik, L.; Li, X.; McEwen, J. S.; Hensley, A. J.; Wang, Y. Vapor phase hydrodeoxygenation of guaiacol on carbon supported metal catalysts. *Journal of Catalysis* **2013**, doi:10.1016/j.jcat.2013.05.020.
13. Johnson, R. S.; DeLaRiva, A.; Ashbacher, V.; Halevi, B.; Villanueva, C. J.; Smith, G. K.; Lin, S.; Datye, A. K.; Guo, H. The CO oxidation mechanism and reactivity on PdZn alloys. *Physical Chemistry Chemical Physics* **2013**, 15: p. 7768-7776.

- 
14. DeLaRiva, A. T.; Hansen, T. W.; Challa, S. R.; Datye, A. K. In situ Transmission Electron Microscopy of catalyst sintering. *Journal of Catalysis* **2013**, 308: p. 291-305, invited review for the 50<sup>th</sup> anniversary special edition of Journal of Catalysis.
  15. Halevi, B.; Lin, S.; Roy, A.; Zhang, H.; Jeroro, E.; Vohs, J.; Wang, Y.; Guo, H.; Datye, A. K. High CO<sub>2</sub> Selectivity of ZnO Powder Catalysts for Methanol Steam Reforming. *The Journal of Physical Chemistry C* **2013** 117(13): p. 6493-6503.
  16. Sun, J.; Mei, D.; Karim, A.; Datye, A.; Wang, Y. Minimizing the formation of coke and methane on Co nanoparticles in steam reforming of biomass-derived oxygenates. *ChemCatChem*. **2013**, DOI:10.1002/cctc.201300041.(cover page featured in the June issue).
  17. Wei, A.; Sun, J.; Zhang, H.; Li, Y.; Datye, A.; Wang, Y. Bimetallic nanocatalysts hydrogen generation. *Chem.Soc.Review* **2012**, DOI:10.1039/C2CS35201J – invited review
  18. Benavidez, A. D.; Kovarik, L.; Genc, A.; Agrawal, N.; Larsson, E. M.; Hansen, T. W.; Karim, A. M.; Datye, A. K. Environmental transmission electron microscopy study of the origins of anomalous particle size distributions in supported metal catalysts. *ACS Catalysis* **2012** 2(11): p. 2349-2356.
  19. Roy, B.; Martinez, U.; Loganathan, K.; Datye, A. K.; Leclerc, C. A. Effect of preparation methods on the performance of Ni/Al<sub>2</sub>O<sub>3</sub> catalysts for aqueous-phase reforming of ethanol: Part I-catalytic activity. *International Journal of Hydrogen Energy* **2012**, 37(10): p. 8143-8153.
  20. Roy, B.; Artyushkova, K.; Pham, H. N.; Li, L.; Datye, A. K.; Leclerc, C. A. Effect of preparation method on the performance of the Ni/Al<sub>2</sub>O<sub>3</sub> catalysts for aqueous-phase reforming of ethanol: Part II-characterization. *International Journal of Hydrogen Energy* **2012**, 37(24): p. 18815-18826.
  21. Peterson, E. J.; Halevi, B.; Kiefer, B.; Spilde, M. N.; Datye, A. K.; Peterson, J.; Daemen, L.; Llobet, A.; Nakotte, H. Aerosol synthesis and Rietveld analysis of tetragonal (beta(1)) PdZn. *Journal of Alloys and Compounds* 2011, 509(5): p. 1463-1470.
  22. Burton, PD.; Boyle, T. J.; Datye, A. K. Facile, surfactant-free synthesis of Pd nanoparticles for heterogeneous catalysts. *Journal of Catalysis* **2011**, 280(2): p. 145-149.
  23. Karim, A. M.; Su, Y.; Engelhard, M. H.; King, D. L.; Wang, Y. Catalytic roles of Co<sup>0</sup> and Co<sup>2+</sup> during steam reforming of ethanol on Co/MgO catalysts. *ACS Catalysis* **2011**, dx.doi.org/10.1021/cs200014j.
  24. Smith, G. K.; Lin, S.; Lai, W. Z.; Datye, A.; Xie, D. Q.; Guo, H. Initial steps in methanol steam reforming on PdZn and ZnO surfaces: Density functional theory studies. *Surface Science* **2011**, 605(7-8): p. 750-759.
  25. Lebarbier, V. M.; Karim, A. M.; Engelhard, M. H.; Wu, Y.; Xu, B-Q.; Petersen, E.; Datye, A. K.; Wang, Y. The effect of Zn addition on oxidation state of cobalt for Co/ZrO<sub>2</sub> catalysts. *ChemSusChem*. **2011**, 4(11) pp1679-1684. Doi:10.1002/cssc.201100240.
  26. Sun, J.; Zhu, K.; Gao, F.; Wang, C.; Liu, J.; Peden, C. H. F.; Wang, Y. Direct conversion of bio-ethanol to isobutene on nanosized Zn<sub>x</sub>Zr<sub>x</sub>O<sub>z</sub> mixed oxides with balanced acid-base sites. *J.Am.Chem.Soc.* **2011**, 133(29) pp11096-11099, DOI: 10.102/ja204235v

Michael G. White

**Role of Charge Transfer and Stoichiometry in Promoting Water Dissociation on Supported Metal Oxide Clusters**

M. Nakayama,<sup>1</sup> Y. Yang,<sup>2</sup> P. Liu<sup>1</sup> and M. G. White<sup>1,2</sup>

<sup>1</sup>Chemistry Department, Brookhaven National Laboratory, Upton NY 11973

<sup>2</sup>Department of Chemistry, Stony Brook University, Stony Brook, NY 11794

**Abstract**

The unique catalytic activity of supported nanoparticles versus their bulk counterparts is often attributed to electronic interactions with the support that result in charge transfer, structural changes or creation of new active sites at the particle-support interface. For oxide supported Cu catalysts, which are of interest for promoting the water-gas-shift (WGS) reaction and methanol synthesis, the metal oxide-Cu electronic interactions are known to strongly influence activity. In this work, we are using size-selected deposition to explore the interfacial electronic structure of a number of small metal oxide clusters (Mo, W, Ti, Nb) on Cu(111) and Cu<sub>2</sub>O/Cu(111) surfaces as model “inverse” catalysts. Such inverse systems are useful for investigating the chemical role of the oxide, and in some cases, can be even more active than the conventional catalysts. The extent and direction of charge transfer at the interface are extracted from coverage dependent work function measurements using two-photon photoemission (2PPE) and theoretical DFT calculations. The trends observed for charge transfer are correlated with their ability to dissociate adsorbed water molecules, which is an important step in the WGS reaction. As O-vacancies can play an important role for adsorbate binding and water dissociation on oxide surfaces, both stoichiometric and sub-stoichiometric oxide clusters are being studied. These studies highlight the unique ability of cluster deposition to prepare well-defined “reduced” surface oxides by controlling the stoichiometry of the clusters rather than by post-deposition heating or chemical treatments.

**FWP CO-009: Catalysis Science for Advanced Fuels**

**Subtask 2: Nanostructured Materials for Catalysis**

PIs: Ping Liu, Jose Rodriguez, Dario Stacchiola

Postdocs: Ashleigh Baber, Wei An

Graduate Students: Shizhong Liu, Danielle O’Connor, Yixiong Yang (Ph.D. 2013), Fang Xu

**RECENT PROGRESS**

***Atomic structure Cu<sub>2</sub>O oxide thin films on Cu(111)***

We have shown that when exposing Cu(111) surfaces to oxygen, in addition to the previously reported oxygen-chemisorbed and reconstructed 29- and 44-Cu<sub>2</sub>O phases,<sup>1-7</sup> a set of intermediate surface oxide structures are formed. By increasing the oxygen chemical potential, formation of hexagonal and pentagonal-heptagonal (5-7) Cu<sub>2</sub>O rings is observed

(see Figure 1). Similar phases are observed in the reverse process, when reducing the  $\text{Cu}_2\text{O}$  film to metallic  $\text{Cu}(111)$ . Topological defects, called Stone-Wales (S-W) defects, formed by the introduction of pentagonal and heptagonal rings into a hexagonal network (i.e., 5-7 defects) are well-known in carbon materials and a few other  $\text{sp}^2$  bonded materials. We show that an S-W-type transformation and 5-7 defects can also occur at the surface of non- $\text{sp}^2$  bonded materials, such as a copper oxide surface, where the bonds between atoms have a strong ionic character. The 5-7  $\text{Cu}_2\text{O}$  structure can alter the adsorption properties of the substrate by introducing sub-nanometer confined sites on the  $\text{Cu}(111)$  surface. It is observed that the heptagonal, hexagonal and pentagonal rings of  $\text{Cu}_2\text{O}$  have different electronic structures.

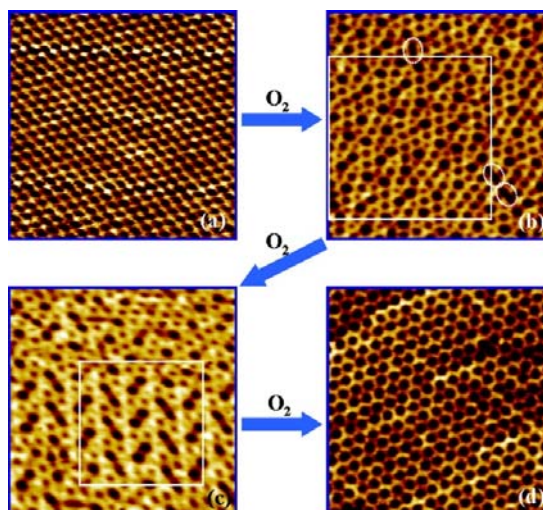


Fig. 1: STM images of (a)  $\text{Cu}(111)$ ; (b)  $\text{Cu}_2\text{O}$  surface oxide with local order (100 L  $\text{O}_2$ ); (c) showing regions with long-range order (180 L  $\text{O}_2$ ); (d) crystalline hexagonal  $\text{Cu}_2\text{O}$  surface oxide.

The adsorption of  $\text{CO}$  on the 5-7 structure shows two peaks in the IRRAS spectrum at 2100 and 2038  $\text{cm}^{-1}$ , which can be assigned to the atop adsorption on  $\text{Cu}^{\delta+}$  and  $\text{Cu}$  sites inside the 7-ring, respectively, based on the DFT results. An oxygen covered surface was previously suggested as the active  $\text{Cu-O}$  system for the selective oxidation of methanol to formaldehyde. We have now identified the 5-7 structure as the selective active phase that produces the maximum formaldehyde yield from the partial oxidation of methanol. Since the 5-7 structure was obtained by oxidizing the  $\text{Cu}(111)$  surface at 550 K or reducing the  $\text{Cu}_2\text{O}/\text{Cu}(111)$  film with  $\text{CO}$  at 800 K, it is expected to be stable under reactions requiring lower temperatures such as  $\text{CO}$  oxidation and methanol partial oxidation. These results demonstrate that the formation of specific sites on oxide layers formed on top of metal surfaces can significantly alter the activity and selectivity of catalysts, and that the atomic determination of these active sites can be achieved by the study of well-defined systems.

### ***In Situ and Theoretical Studies of $\text{Cu}_2\text{O}$ Reduction***

The reduction of a  $\text{Cu}_2\text{O}/\text{Cu}(111)$  film by  $\text{CO}$  was studied *in situ*. LEEM imaging shows the propagation of metallic fronts as the reduction progresses. AP-XPS and AP-IRRAS show that the reduction of  $\text{Cu}_2\text{O}$  proceeds in the presence of only adsorbed  $\text{CO}$  molecules. Using AP-STM, the reaction was monitored at the nanoscale, observing the structural transformation from the  $\text{Cu}_2\text{O}(111)$  film to glass-like hex/5-7 ring structures, to metallic  $\text{Cu}$ . The hex/5-7 intermediate

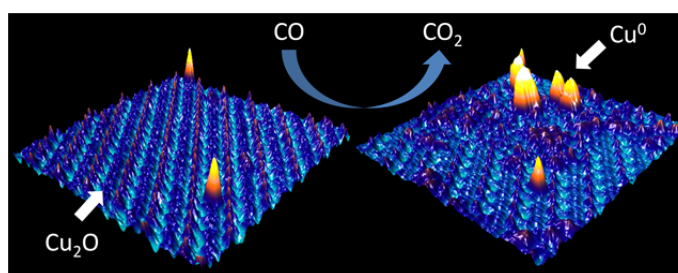


Fig. 2: In-situ STM imaging during the reduction of a  $\text{Cu}_2\text{O}$  film.

propagated across the surface as a front and precursor to the metallic phase. *In situ* measurements show that the reduction begins at defects in the  $\text{Cu}_2\text{O}(111)$  film terraces and step edges. At terrace defects, the oxide buckles during reduction, appearing as bright protrusions before converting into the ring structure (Figure 2). Most of the Cu atoms released by reduction of  $\text{Cu}_2\text{O}$  in the presence of CO undergo mass transfer to step edges, causing a massive reconstruction and phase separation between the oxide and metal. The AP *in situ* experiments presented here show the dynamic nature of catalytic surfaces, including oxidation state changes and morphological restructuring. Highly resolved images under ambient pressures provide an unprecedented look into the dynamic nature of active sites generated in the presence of the reactants

Density functional theory (DFT) was also used to study the CO titration of  $\text{Cu}_x\text{O}$  thin films in order to gain a better understanding of the roles that the Cu(111) support and surface defects play in tuning catalytic performances. As noted above, different conformations are observed during CO reduction, namely, the 44 structure and a recently identified (5-7-7-5) Stone-Wales defect (5-7 structure).

The DFT calculations show that the Cu(111) support is important to the reducibility of supported  $\text{Cu}_x\text{O}$  thin films. Compared to the  $\text{Cu}_2\text{O}(111)$  bulk surface, at the initial stage CO titration is less favorable for both the 44 and 5-7 structures (Figure 3). The strong  $\text{Cu}_x\text{O} \leftrightarrow \text{Cu}$  interaction results in charge transfer from Cu to  $\text{Cu}_x\text{O}$  which is able to stabilize the oxide film and hinder the removal of oxygen. However, with the formation of more oxygen vacancies, the

binding between  $\text{Cu}_x\text{O}$  and Cu(111) is weakened and the oxide film is destabilized, while  $\text{Cu}_2\text{O}(111)$  is likely to become the most stable system under the reaction conditions (Figure 3). In addition, surface defects also play an essential role. While the CO titration reaction proceeds, the 5-7 structure displays the highest activity among all three systems. Compared to the 44 structure and  $\text{Cu}_2\text{O}(111)$ , the Stone-Wales defects on the surface of the 5-7 structure exhibit significant differences in CO binding energy, stability of lattice oxygen, and therefore, reduction activity. The DFT results agree well with the experimental measurements, showing that by adopting the unique conformation, the 5-7 structure is the

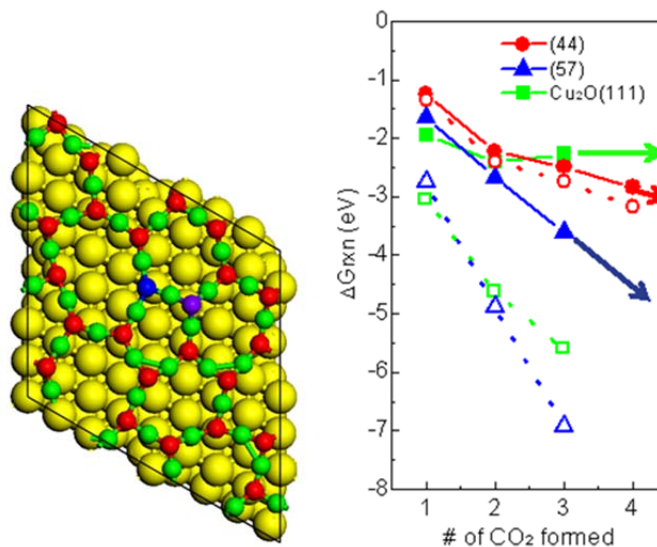


Fig. 3: Left Structure of 5-7 structure. . Yellow:  $\text{Cu}^{1+}$  in the sub-surface of  $\text{Cu}_2\text{O}(111)$  and  $\text{Cu}^0$  in Cu(111) substrate; green:  $\text{Cu}^{\delta+}$  in the surface layer; red: unlabeled O; purple: O for 3-coordinated  $\text{O}_{3C}$  (or  $\text{O}_U$ ); blue : O for 4-coordinated  $\text{O}_{4C}$  (or  $\text{O}_L$ ). Right: Gibbs reaction energy for CO titration under relatively low CO pressure at 298K (solid) and 800K (open, dotted line). The arrows indicate the projected energy variation for further reduction.

active phase of  $\text{Cu}_x\text{O}$ , being able to facilitate the redox reaction and the  $\text{Cu}_2\text{O}/\text{Cu}(111) \leftrightarrow \text{Cu}$  transition.

#### ***Mixed Metal Oxide Thin Films: $\text{TiCuO}_x/\text{Cu}(111)$***

Historically, the complexity and lack of stability of mixed Cu oxide materials under reaction conditions has prevented their widespread use, despite the promise for CO oxidation due to their low cost and physicochemical properties. We have synthesized stable  $\text{TiCuO}_x$  films, which are very active for CO oxidation, and by combining microscopic and spectroscopic experimental studies with theoretical simulations we have been able to describe their complex structure at the atomic level (see Figure 4). The presence of Ti prevents the oxidation and reduction of the  $\text{Cu}_2\text{O}$  films under reaction conditions, thereby enhancing the robustness of the catalyst. Furthermore, the presence of Ti stabilizes  $\text{Cu}^+$  ions on the surface locally coordinated to three oxygen atoms, which act as better adsorption sites for CO than sites on pure  $\text{TiO}_2$  or  $\text{Cu}_2\text{O}$ . This discovery and the description of its origin can help to develop Cu-based oxidation catalysts.

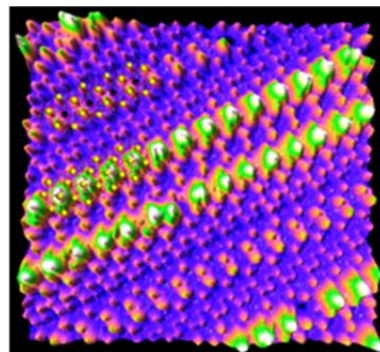


Fig. 4: STM image and DFT-based structure of a  $\text{CuTiO}_x$  film, where  $\text{Cu}^+$  sites are stabilized at the surface.

#### ***Metal Oxide/Cu(111) Surfaces as “Inverse” Catalysts***

##### ***$\text{CeO}_2/\text{Cu}_2\text{O}/\text{Cu}(111)$***

Copper and cerium oxides are both cost-effective materials widely used in catalytic applications. These two materials individually are not good catalysts for reactions such as CO oxidation or the WGS. When ceria NPs are supported on  $\text{Cu}(111)$ , this inverse model catalyst becomes very active for CO oxidation and the water-gas-shift reaction. We developed a new methodology that leads to the growth of ceria NPs which expose exclusively the (111) or (100) surface planes. Ceria NPs exposing the highly stable (111) surface plane were synthesized via the evaporation of Ce atoms onto the  $\text{Cu}(111)$  surface (650 K) in a background pressure of  $\text{O}_2$ . When the surface of  $\text{Cu}(111)$  is pre-oxidized with  $\text{O}_2$  or  $\text{NO}_2$ , rectangular  $\text{CeO}_2(100)$  structures (see Figure 5) are observed to grow rather than hexagonal  $\text{CeO}_2(111)$ . For bulk surfaces,  $\text{CeO}_2(100)$  is less stable but more reactive than  $\text{CeO}_2(111)$ . According to our DFT calculations, the formation of  $\text{CeO}_2(100)$  is associated with a rectangular copper oxide phase formed during the process. The latter is presumably  $\text{Cu}_4\text{O}_3(001)$ , and the Ce atoms are constrained in a square configuration and forced to adopt a geometry which is not a stable termination for bulk ceria. The formation energy of  $\text{CeO}_2(111)$  on  $\text{Cu}(111)$  is slightly lower than that of  $\text{CeO}_2(100)$  on  $\text{Cu}_4\text{O}_3(001)$ . This opens the door for enhanced chemical activity and applications in important

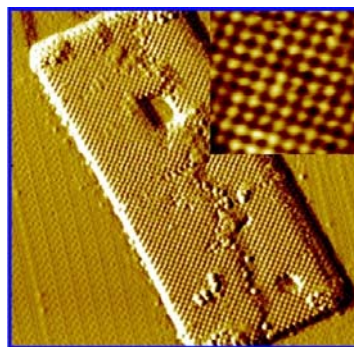


Fig 5: STM images of  $\text{CeO}_2(100)$  particles prepared on an oxidized  $\text{Cu}(111)$  surface.

processes for CO oxidation as well as PROX, WGS, synthesis of alcohols from CO/CO<sub>2</sub> hydrogenation, and NO reduction.

It was observed experimentally that the inverse CeO<sub>x</sub>/Cu(111) model catalyst is 20–60 times more active for CO oxidation than Cu(111). Calculations using DFT+U was employed to understand the promoting effect of CeO<sub>x</sub>, where triangular CeO<sub>x</sub> particles on Cu(111) (Figure 6) were constructed to simulate the small particles observed in STM. Our calculations show that there is a charge transfer of 3.96e from the Cu slab to the particle, leading to an oxidation of the Cu surface and a reduction of the oxide particle. As a result, the reduction in CO and the reversibility of the reduction/oxidation cycles are both energetically favorable, in accordance with the experiments. The stabilized Ce<sup>3+</sup> is believed to be the O<sub>2</sub> dissociation bottleneck on Cu(111) and promote the formation of active Cu oxides, while still allowing the efficient removal of O via CO oxidation.

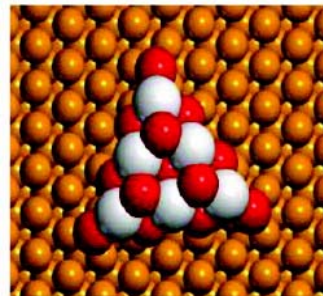


Fig. 6: Top view of the DFT optimized structure of a Ce<sub>6</sub>O<sub>13</sub> cluster on Cu(111).

#### *Size-Selected Metal Oxide Clusters on Cu(111)*

It is well established that electron transfer at the particle-support interface can play an important role in determining catalytic activity for a specific reaction. In the case of CeO<sub>x</sub> nanoparticles on Cu(111) discussed above, electron transfer effectively reduces the CeO<sub>x</sub> particles by stabilizing Ce<sup>3+</sup> cations and oxidizes the Cu atoms in close proximity. The combination enhances the catalytic activity of the CeO<sub>x</sub>/Cu(111) surface for CO oxidation and the WGS reaction. Recent DFT studies by Liu and coworkers for small oxide clusters (MoO<sub>3</sub>, ZrO<sub>2</sub>, ZnO, TiO<sub>2</sub>) on Cu(111) have also correlated interfacial electron transfer with reactivity of the oxide for water dissociation, which is a key step in the WGS reaction. Our recent work has focused on correlating the reactivity of small metal oxide clusters deposited by size-selected deposition onto Cu(111) and Cu<sub>2</sub>O/Cu(111) surfaces with measurements of the surface dipole, which in many cases can be directly correlated with interfacial electron transfer. The latter was probed by coverage dependent work function measurements using two-photon photoemission (2PPE). The ability of mass-selection to control the metal to oxygen ratio also allowed both fully “oxidized” (stoichiometric) and “reduced” cluster to be investigated. In general, we

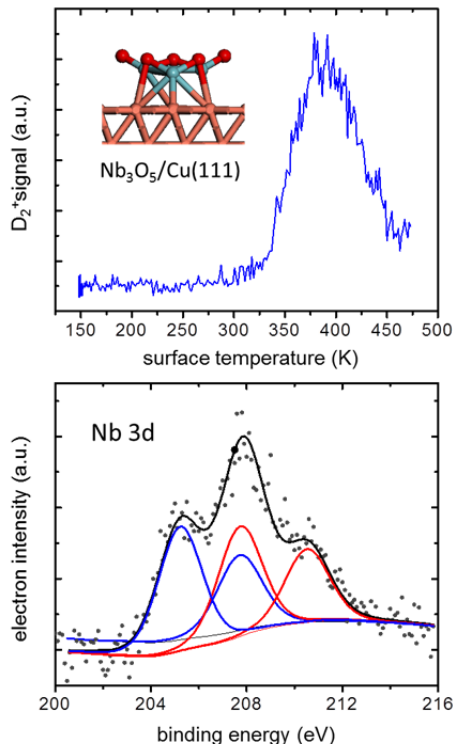


Fig. 7: TPR (top) and XPS (bottom) spectra of “reduced” Nb<sub>3</sub>O<sub>5</sub> clusters deposited on Cu(111). The TPR spectrum shows D<sub>2</sub> formation following D<sub>2</sub>O adsorption at 110 K. The Nb 3d XPS spectra indicate the presence of Nb<sup>5+</sup> and reduced Nb<sup>4+</sup>/Nb<sup>3+</sup> cations before and after water dissociation.

find that clusters exhibiting the largest surface dipoles, e.g.,  $\text{Mo}_3\text{O}_x$  and  $\text{W}_3\text{O}_x$  ( $x = 6, 9$ ), do not dissociate water, whereas, those clusters with small surface dipoles, e.g.,  $\text{Ti}_3\text{O}_6$  and  $\text{Nb}_3\text{O}_5$ , resulted in water dissociation as evidenced by  $\text{D}_2$  formation in TPR experiments. (see Figure 7). Interestingly, both oxidized and reduced  $\text{Nb}_x\text{O}_y$  clusters ( $x/y = 3/5, 3/7, 4/7, 4/10$ ) are able to promote water dissociation on  $\text{Cu}(111)$  whereas only the reduced  $\text{Nb}_x\text{O}_y$  ( $x/y = 3/5, 4/7$ ) clusters led to water dissociation on the oxidized  $\text{Cu}_2\text{O}/\text{Cu}(111)$  surface. These experiments demonstrate the importance of cluster stoichiometry and specific electronic interactions with the support surface in determining surface reactivity.

#### *Inverse $\text{SnO}_x/\text{Pt}(111)$ Catalysts for the Electrooxidation of Simple Alcohols*

A newly constructed instrument with combined surface science and electrochemical capabilities is currently being used for fundamental investigations of mixed metal-metal oxide catalysts for the electrooxidation of methanol and ethanol (MOR) and ethanol (EOR). This work is motivated by the development of ternary  $\text{Rh}/\text{SnO}_x/\text{Pt}$  electrocatalysts by Adzic and co-workers at BNL that were found to promote the complete oxidation of ethanol at reasonable potentials and kinetic currents. The ternary catalysts were prepared and tested as powders, and it has been a challenge to understand the role of each

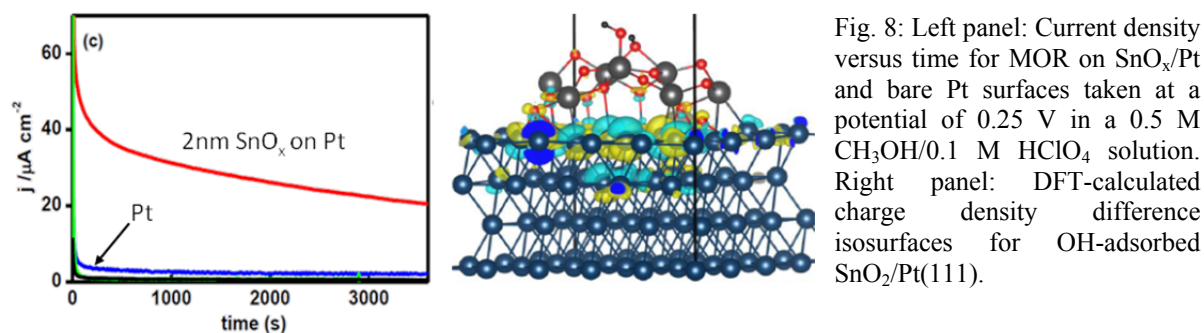


Fig. 8: Left panel: Current density versus time for MOR on  $\text{SnO}_x/\text{Pt}$  and bare Pt surfaces taken at a potential of 0.25 V in a 0.5 M  $\text{CH}_3\text{OH}/0.1$  M  $\text{HClO}_4$  solution. Right panel: DFT-calculated charge density difference isosurfaces for OH-adsorbed  $\text{SnO}_2/\text{Pt}(111)$ .

component in promoting the EOR. In an effort to identify the role of the  $\text{SnO}_x$  co-catalyst we have focused on the analogous “inverse catalyst” of  $\text{SnO}_x$  deposited on a  $\text{Pt}(111)$  surface (or electrode). For these studies  $\text{SnO}_x$  nanoislands on  $\text{Pt}(111)$  were prepared in UHV and characterized by XPS and ISS before and after ambient electrochemical activity testing in acidic electrolyte solutions containing methanol or ethanol. The results showed that small ( $\leq 2\text{nm}$ )  $\text{SnO}_x$  particles resulted in a 40-50x increase in EOR activity which could be correlated with the presence of reduced  $\text{Sn(II)}$  species (see Figure 8). The latter promote the dissociation of water and the eventual oxidation of CO absorbed on Pt sites by -OH groups formed at the  $\text{Pt}-\text{SnO}_x$  interface. DFT studies show that the unique chemical properties of small, Pt-supported  $\text{SnO}_2$  NPs are attributed to the interaction between  $\text{SnO}_2$  and  $\text{Pt}(111)$  and the unique structural flexibility. Future studies will more fully explore the  $\text{SnO}_x$  size-dependent activity by using a size-selected cluster deposition source, which is an integral component of the new electrochemistry instrument. The cluster source will allow us to deposit clusters in the 1-5 nm range onto the Pt substrate, which can be transferred to the UHV chamber for surface science characterization and moved to the electrochemical cell for MOR/EOR activity testing.

## Publications Acknowledging this Grant in 2011-2014

### 2014

1. Baber, A. E.; Yang, X.; Kim, H. Y.; Mudiyansele, K.; Soldemo, M.; Weissenrieder, J.; Senanayake, S. D.; Al-Mahboob, A.; Sadowski, J. T.; Evans, J.; Rodriguez, J. A.; Liu, P.; Hoffmann, F. M.; Chen, J. G.; Stacchiola, D. J., Stabilization of Catalytically Active Cu<sup>+</sup> Surface Sites on Titanium-Copper Mixed-oxide Films. *Angew. Chem. Int. Ed. Engl.* **2014**, *53* (21), 5336-40.
2. An, W.; Baber, A.E.; Xu, F.; Soldemo, M.; Weissenrieder, J.; Stacchiola, D.; Liu, P., Mechanistic Study of CO Titration on Cu<sub>x</sub>O/Cu(111) (x≤2) Surfaces. *ChemCatChem*. DOI: 10.1002/cctc.201402177.
3. Magee, J. W.; Zhou, W-P.; White, M. G.; Promotion of Pt Surfaces for Ethanol Electro-Oxidation by the Addition of Small SnO<sub>2</sub> Nanoparticles: Activity and Mechanism. *Appl. Catal. B: Environ.* **2014**, *152–153*, 397–402.
4. Yang, Y.; Zhou, J.; Nakayama, M.; Nie, L.; Liu, P.; White, M.G., Surface Dipoles and Electron transfer at the Metal Oxide-Metal Interface: a 2PPE Study of Size-Selected Metal Oxide Clusters Supported on Cu(111). *J. Phys. Chem.C*, accepted for publication.

### 2013

5. An, W.; Liu, P., Size and Shape Effects of Pd@Pt Core–Shell Nanoparticles: Unique Role of Surface Contraction and Local Structural Flexibility. *J. Phys. Chem. C* **2013**, *117* (31), 16144-16149.
6. Baber, A. E.; Mudiyansele, K.; Senanayake, S. D.; Beatriz-Vidal, A.; Luck, K. A.; Sykes, E. C.; Liu, P.; Rodriguez, J. A.; Stacchiola, D. J., Assisted Deprotonation of Formic Acid on Cu(111) and Self-assembly of 1D chains. *PCCP* **2013**, *15* (29), 12291-8.
7. Baber, A. E.; Xu, F.; Dvorak, F.; Mudiyansele, K.; Soldemo, M.; Weissenrieder, J.; Senanayake, S. D.; Sadowski, J. T.; Rodriguez, J. A.; Matolin, V.; White, M. G.; Stacchiola, D. J., In situ imaging of Cu<sub>2</sub>O under reducing conditions: formation of metallic fronts by mass transfer. *J. Am. Chem. Soc.* **2013**, *135* (45), 16781-4.
8. Liu, P.; Yang, Y.; White, M. G., Theoretical perspective of alcohol decomposition and synthesis from CO<sub>2</sub> activation. *Surf. Sci. Rep.* **2013**, *68*, 233-272.
9. Mudiyansele, K.; An, W.; Yang, F.; Liu, P.; Stacchiola, D. J., Selective molecular adsorption in sub-nanometer cages of a Cu<sub>2</sub>O surface oxide. *PCCP* **2013**, *15* (26), 10726-31.
10. Mudiyansele, K.; Kim, H. Y.; Senanayake, S. D.; Baber, A. E.; Liu, P.; Stacchiola, D., Probing adsorption sites for CO on Ceria. *PCCP* **2013**, *15* (38), 15856-62.
11. Mudiyansele, K.; Yang, Y.; Hoffmann, F. M.; Furlong, O. J.; Hrbek, J.; White, M. G.; Liu, P.; Stacchiola, D. J., Adsorption of Hydrogen on the surface and sub-surface of Cu(111). *J. Chem. Phys.* **2013**, *139* (4), 044712.
12. Nerko, D.; Axnanda, S.; Zhou, W.-P.; Lofaro, J.; White, M. G., Synthesis and Characterization of surface oxide films on CoGa (100). *Surf. Sci.* **2013**, *616*, 192-197.

### 2012

13. Liu, P., Understanding the Behavior of TiO<sub>2</sub>(110)-Supported Pd<sub>7</sub> Cluster: A Density Functional Study. *J. Phys. Chem. C* **2012**, *116* (48), 25337-25343.

14. Baber, A. E.; Torres, D.; Muller, K.; Nazzarro, M.; Liu, P.; Starr, D. E.; Stacchiola, D. J., Reactivity and Morphology of Oxygen-Modified Au Surfaces. *J. Phys. Chem. C* **2012**, *116* (34), 18292-18299.
15. Rajasekaran, S.; Kaya, S.; Abild-Pedersen, F.; Anniyev, T.; Yang, F.; Stacchiola, D.; Ogasawara, H.; Nilsson, A., Reversible graphene-metal contact through hydrogenation. *Phys.Rev. B* **2012**, *86* (7), 075417.
16. Zhou, W.-P.; An, W.; Su, D.; Palomino, R.; Liu, P.; White, M. G.; Adzic, R. R., Electrooxidation of Methanol at SnO<sub>x</sub>-Pt Interface: A Tunable Activity of Tin Oxide Nanoparticles. *J. Phys. Chem. Lett.* **2012**, *3* (22), 3286-3290.
17. Hoffmann, F. M.; Hoo, Y. S.; Cai, T. H.; White, M. G.; Hrbek, J., Infrared study of Triruthenium Dodecacarbonyl interactions with Gold. *Surf. Sci.* **2012**, *606* (23-24), 1906-1913.
18. Axnanda, S.; Zhou, W. P.; White, M. G., CO oxidation on nanostructured SnO<sub>x</sub>/Pt(111) surfaces: Unique properties of reduced SnO<sub>x</sub>. *PCCP* **2012**, *14* (29), 10207-10214.
19. Zhou, J.; Zhou, J.; Camillone, N.; White, M. G., Electronic charging of non-metallic clusters: size-selected Mo<sub>x</sub>S<sub>y</sub> clusters supported on an ultrathin Alumina film on NiAl(110). *PCCP* **2012**, *14* (22), 8105-8110.
20. Yang, Y.; White, M. G.; Liu, P., A Theoretical Study of Methanol Synthesis from CO<sub>2</sub> Hydrogenation on Metal-Doped Cu(111) Surfaces. *J. Phys. Chem. C* **2012**, *116* (1), 248-256.
21. Liu, M. F.; Choi, Y. M.; Yang, L.; Blinn, K.; Qin, W. T.; Liu, P.; Liu, M. L., Direct Octane fuel cells: A promising power for transportation. *Nano Energy* **2012**, *1* (3), 448-455.
- 2011**
22. Choi, Y.; Liu, P., Understanding of ethanol decomposition on Rh(111) from density functional theory and kinetic Monte Carlo simulations. *Catal. Today* **2011**, *165* (1), 64-70.
23. Yang, F.; Graciani, J.; Evans, J.; Liu, P.; Hrbek, J.; Sanz, J. F.; Rodriguez, J. A., CO Oxidation on Inverse CeO<sub>x</sub>/Cu(111) Catalysts: High Catalytic Activity and Ceria-Promoted Dissociation of O<sub>2</sub>. *J. Am. Chem. Soc.* **2011**, *133* (10), 3444-3451.
24. Yang, F.; Choi, Y.; Liu, P.; Stacchiola, D.; Hrbek, J.; Rodriguez, J. A., Identification of 5-7 defects in a copper oxide surface. *J. Am. Chem. Soc.* **2011**, *133* (30), 11474-7.
25. Yang, F.; Choi, Y.; Agnoli, S.; Liu, P.; Stacchiola, D.; Hrbek, J.; Rodriguez, J. A., CeO<sub>2</sub> ↔ CuO<sub>x</sub> Interactions and the Controlled Assembly of CeO<sub>2</sub>(111) and CeO<sub>2</sub>(100) Nanoparticles on an Oxidized Cu(111) Substrate. *J. Phys. Chem. C* **2011**, *115* (46), 23062-23066.
26. Zhou, W.-P.; Axnanda, S.; White, M. G.; Adzic, R. R.; Hrbek, J., Enhancement in Ethanol Electrooxidation by SnO<sub>x</sub> Nanoislands Grown on Pt(111): Effect of Metal Oxide-Metal Interface Sites. *J. Phys. Chem. C* **2011**, *115* (33), 16467-16473.
27. Yang, L.; Choi, Y.; Qin, W.; Chen, H.; Blinn, K.; Liu, M.; Liu, P.; Bai, J.; Tyson, T. A.; Liu, M., Promotion of water-mediated carbon removal by nanostructured Barium Oxide/Nickel interfaces in Solid Oxide Fuel Cells. *Nat. Commun.* **2011**, *2*, 357.

Judith C. Yang

### Noncrystalline-to-crystalline Transformations in Pt Nanoparticles

C.S. Bonifacio,<sup>1</sup> L. Li,<sup>1</sup> Z. Zhang,<sup>1</sup> J.C. Yang,<sup>1</sup> Q. Wang,<sup>2</sup> A.I. Frenkel,<sup>2</sup> S.I. Sanchez,<sup>3</sup>  
J.H. Kang,<sup>3</sup> R.G. Nuzzo,<sup>3</sup> F.D. Vila,<sup>4</sup> J. J. Kas,<sup>4</sup> J.J. Rehr,<sup>4</sup> E.A. Stach,<sup>5</sup> J. Ciston,<sup>5</sup> L.  
Wang,<sup>6</sup> D.J. Johnson,<sup>6,7</sup>

<sup>1</sup>Dept. of Chem. and Petrol. Eng.; Mech. and Mater. Sci. Eng., Univ. of Pittsburgh, Pittsburgh, <sup>2</sup>Dept. of Physics, Yeshiva Univ., New York, <sup>3</sup>Dept. of Chemistry, Univ. of Illinois Urbana-Champaign, Urbana, <sup>4</sup>Dept. of Physics, Univ. of Washington, Seattle, <sup>5</sup>Center for Functional Nanomater., Brookhaven Natl. Lab. <sup>6</sup>The Ames Lab., Ames <sup>7</sup>Mat. Sci. and Eng., and Chem. and Bio. Eng., Iowa State Univ.

#### Presentation Abstract

Supported sub-nanometer to nanometer size Pt nanoparticles (NPs) were shown to have the noncrystalline-to-crystalline transition in the size range between 1 and 4 nm. Through high-resolution transmission electron microscopy (HRTEM), extended X-ray absorption fine structure spectroscopy (EXAFS) and first-principle simulations, the nanostructural behaviors of the NPs were found to be strongly affected by particle size, support and adsorbates such as H<sub>2</sub>. A nonabrupt noncrystalline-to-crystalline transition zone was observed where a size regime for disordered and ordered NPs coexists. This NP size dependent transition was shown to be dependent on both the adsorbate and the support. Here, the results were obtained from more than 3000 NPs acquired by HRTEM and analyzed via a statistical description of particle-support-adsorbate interactions. Noncrystalline particles are characterized by enhanced bond length disorder that originates from both heterogeneous binding sites on the support and strongly non-vibrational dynamics of particles in this size range.

Grant Number: DE FG02-03ER15476

**Grant Title: The Reactivity and Structural Dynamics of Supported Metal Nanoclusters Using Electron Microscopy, *in situ* X-Ray Spectroscopy, Electronic Structure Theories, and Molecular Dynamics Simulations.**

**PIs:** Ralph G. Nuzzo, Anatoly I. Frenkel, Judith C. Yang, John J. Rehr

**Postdocs:** C. Bonifacio, U. Jung, A. Elsen, S. Zhao, J. Kas, Y. Li, F. Vila

#### RECENT PROGRESS

##### 1. Shape determination from “atom-counting” of nanoparticles

The characterization of the structure and chemistry of catalytic materials on support is important for the heterogeneous catalytic reactions. The surface interaction of the catalysts on the support determines the shape, i.e., 3D information. (S)TEM characterization provides a 2D projection of the sample and 3D information can only be obtained through quantitative analysis. To obtain the 3D shape of the nanoparticles, the relationship of number of atoms in a cluster and nanoparticle diameter is necessary. In this case, the group of **J. Yang** has developed a quantitative scanning transmission electron microscopy (QSTEM) where the absolute intensity of the Z-contrast images gives the number of atoms in nanoparticles (NPs) using a non-aberration corrected TEM/STEM, a modern JEOL 2100F. Results (Fig. 5) showed an average number of atoms of  $12.9 \pm 10.0$  Au atoms and average size of  $0.8 \pm 0.2$  nm for Au NPs/carbon while  $17.2 \pm 11.0$  Au atoms and average size of  $0.9 \pm 0.2$  nm for Au NPs/ $\gamma$ -Al<sub>2</sub>O<sub>3</sub>. Our previous work has shown the feasibility of the technique for Au nanoparticles on C and  $\gamma$ -Al<sub>2</sub>O<sub>3</sub> supports. Further analysis of the data for shape determination was based on a 2D or 3D shape by fitting of the function (size vs. number of atoms/nanoparticle) in terms of  $r^2$  or  $r^3$  dependence, respectively. In this case, Au on carbon has three shapes: raft, cuboctahedral or truncated

cuboctahedral, while Au on  $\gamma$ -Al<sub>2</sub>O<sub>3</sub> is cuboctahedral or truncated cuboctahedral (Fig. 1). Such technique is straight-forward yet provides atomic-scale 3D information from which the nanoparticle and support interaction can be derived. In collaboration with **E. Stach** the QSTEM technique was applied with angstrom spatial resolution and 0.2 eV energy resolution. Currently work with the microscope manufacturer (Hitachi) is undergoing to obtain the optimal detector conditions for QSTEM.

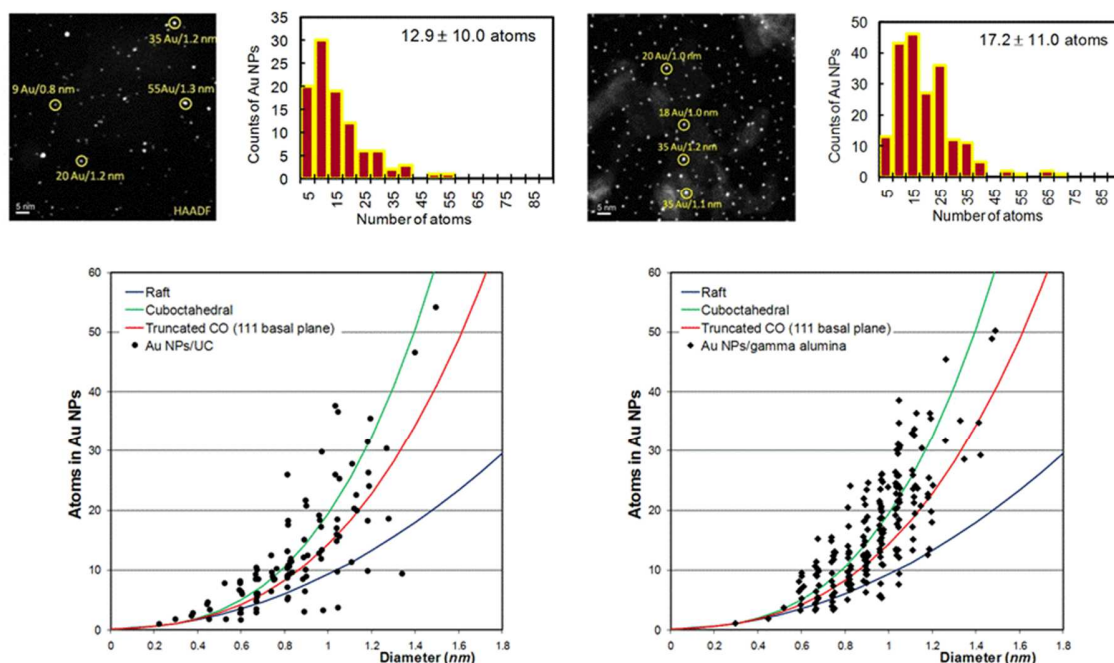


**Figure 1.** Z-contrast images of Au on carbon and  $\gamma$ -Al<sub>2</sub>O<sub>3</sub> used to quantify the number of atoms per nanoparticle. The shape of the Au nanoparticles was determined by fitting the measured number of atoms versus the size of particles.

## 2. Characterization of multimetallic catalyst systems

Ni-Co core-shell nanoparticles were characterized as a model system for CO<sub>2</sub> reduction reactions, i.e., CO<sub>2</sub>-based Fischer-Tropsch synthesis. We studied the structural stability of Ni-Co core-shell nanoparticles in high temperature exposures and reducing environments through *in situ* TEM heating revealing reconfiguration of the core-shell structure at T>600°C. ETEM experiments with the Ni-Co NPs exposed to O<sub>2</sub> and H<sub>2</sub> gases simulating the oxidation and reduction reactions revealed Ni diffusion to the surface of the nanoparticle after 2 cycles of oxidation and reduction.

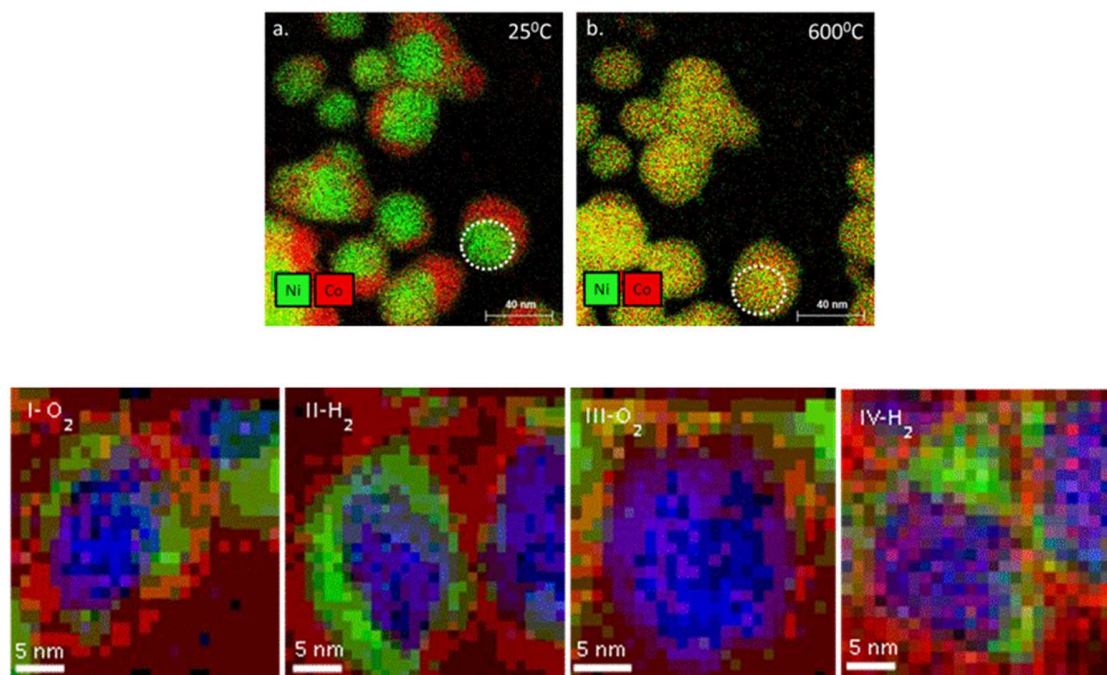


**Figure 2.** (top) EDS maps of Ni (green)-Co (red) core-shell NPs showing the reconfiguration of the core-shell structure after in situ TEM annealing at 600 °C. (bottom) EELS spectrum images (Ni-blue, Co-green and O-red) of the core-shell NPs after two cycles of oxidation and reduction in the ETEM resulting to Ni diffusing from the core to the surface of the NPs (marked area of IV-H<sub>2</sub>).

#### Publications Acknowledging this Grant in 2011-2014

1. Erickson, E.M.; Oruc, M.E.; Small, M.W.; Wetzel, D.J.; Cason, M.W.; Hoang, T.T.H.; Li, D.; Marinkovic, N.S.; Frenkel, A.I.; Gewirth, A.A.; Nuzzo, R.G. A Comparison of Atomistic and Continuum Approaches to the Study of Bonding Dynamics in Electrocatalysis: Microcantilever Stress and In-Situ EXAFS Observations of Platinum Bond Expansion Due to Oxygen Adsorption During the Oxygen Reduction Reaction, *Anal. Chemistry*, **submitted**.
2. Frenkel, A.I.; van Bokhoven, J.A. X-Ray Spectroscopy for Chemical and Energy Sciences (invited) *J. Sync. Rad.*, **submitted**.
3. Shan, J.; Zhang, S.; Choksi, T.; Zhu, W.; Zhang, Y.; Li, Y.; Nguyen, L.; Chafe, A.; Greeley, J.; Frenkel, A.I.; Tao, F. Tuning catalytic performance through a single or sequential post-synthesis reaction in a gas phase. *Nature Comm.*, **submitted**.
4. Huang, W.; Shan, J.; Nguyen, L.; Li, Y.; Zhang, S.; Frenkel, A.I.; Tao, F. Catalytic conversion of methane to methanol and formic acid on singly dispersed palladium oxide species on internal surface of ZSM5. *Angew. Chem. Int. Ed.*, **submitted**.
5. Shan, J.; Huang, W.; Nguyen, L.; Yu, Y.; Zhang, S.; Li, Y.; Frenkel, A.I.; Tao, F. Conversion of methane to methanol in gas phase on a bent mono( $\mu$ -oxo)nickel anchored on internal surface of micro-pores. *Langmuir*, **submitted**.
6. Zhang, S.; Nguyen, L.; Liang, J.; Li, J.; Shan, J.; Frenkel, A.I.; Patlolla, A.; Liu, J.; Huang, W.; Tao, F. Catalysis on an isolated bimetallic site. *Nature Chem.*, **submitted**.
7. Zhang, L.; Yang, C.; Frenkel, A.I.; Wang, S.; Xiao, G.; Brinkman, K.; Chen, F. Co-generation of electricity and chemicals from propane fuel in solid oxide fuel cells with anode containing nano-bimetallic catalyst. *J. Power Sources*, **2014**, 262, 421-428
8. Rehr, J.J.; Vila, F.D. Dynamic Structural Disorder in Supported Nanoscale Catalysts. *J. Chem. Phys.* **2014**, 140, 134701.
9. Small, M.W.; Kas, J.; Kvashnina, K.O.; Rehr, J.J.; Nuzzo, R.G.; Tromp, M.; Frenkel, A.I. Effects of adsorbate coverage and bond length disorder on the d-band center in carbon-supported Pt catalysts. *Chem. Phys. Chem.* **2014**, DOI: 10.1002/cphc.201400055
10. Frenkel, A.I.; Cason, M.; Elsen, A.; Jung, U.; Small, M.W.; Nuzzo, R.G.; Vila, F.D.; Rehr, J.J.; Stach, E.A.; Yang, J.C. Effects of complex interactions on structure and dynamics of supported metal catalysts. *J. Vac. Sci. Tech.* (Invited Critical Review) **2014**, 32, 020801-0208017.

11. Frenkel, A.I.; Small, M.W.; Smith, J.G.; Nuzzo, R.G.; Kvashnina, K.O.; Tromp, M. An In-Situ Study of Bond Strains in 1 nm Pt Catalysts and Their Sensitivities to Cluster-Support and Cluster-Adsorbate Interactions. *J. Phys. Chem. C* **2013**, *117*, 23286-23294.
12. Frenkel, A.I.; Wang, Q.; Sanchez, S.I.; Small, M.W.; Nuzzo, R.G. Short range order in bimetallic nanoalloys: An extended X-ray absorption fine structure study. *J. Chem. Phys.* **2013**, *138*, 064202.
13. Zhang, Z.; Li, L.; Yang, J.C. Adhesion of Pt nanoparticles supported on  $\gamma$ -Al<sub>2</sub>O<sub>3</sub> single crystal. *J. Phys. Chem. C* **2013**, *117*, 21407-21412.
14. Li, L.; Wang, L.-L.; Johnson, D.D.; Zhang, Z.; Sanchez, S.I.; Kang, J.H.; Nuzzo, R.G.; Wang, Q.; Frenkel, A.I.; Ciston, J.; Stach, E.A.; Yang, J.C. Noncrystalline-to-crystalline transformations in Pt nanoparticles. *J. Am. Chem. Soc.* **2013**, *135*, 13062-13072.
15. Stach, E.A.; Zakharov, D.; Akatay, M.C.; Baumann, P.; Ribeiro, F.; Zvienevich, Y.; Li, Y.; Frenkel, A.I. Developments in environmental transmission electron microscopy for catalysis research *Microsc. Microanal.* **2013**, *19*, Suppl. 2, 1174-1175.
16. Zhang, S.; Tao, F.; Frenkel, A.I.; Takeda, S. Singly anchored Pt and Pd atoms on Co<sub>3</sub>O<sub>4</sub> and their catalytic performance. *Microsc. Microanal.* **2013**, *19*, Suppl. 2, 1620-1621.
17. Stach, E.A.; Baumann, P.; Li, Y.; Zakharov, D.; Frenkel, A.I. Using operando methods to characterize working catalysts with TEM, XAS, EXAFS and Raman Spectroscopy. *Microsc. Microanal.* **2013**, *19*, Suppl. 2, 1674-1675.
18. Zhang, S.; Shan, J.-J.; Zhu, Y.; Frenkel, A.I.; Patlolla, A.; Huang, W.; Yoon, S.; Wang, L.; Yoshida, H.; Takeda, S.; Tao, F. WGS Catalysis and in-situ studies of CoO(1-x)PtCo(n)/Co<sub>3</sub>O<sub>4</sub> and Pt(m)Co(m')/CoO(1-x) nanorod catalysts. *J. Am. Chem. Soc.* **2013**, *135*, 8283-8293.
19. Merte, L.R.; Ahmadi, M.; Behafarid, F.; Ono, L.K.; Lira, E.; Matos, J.; Li, L.; Yang, J.C.; Cuenya, B.R. Correlatign Catalytic Methanol Oxidation with the Structure and Oxidation State of Size-Selected Pt Nanoparticles. *ACS Catal.* **2013**, *3*, 1460-1468.
20. Korobko, R.; Lerner, A.; Li, Y.; Frenkel, A.I.; Lubomirsky, I. Electric field increases local symmetry in Gd-doped ceria. *Nature Mater.*, **submitted**.
21. Wu, L.-b.; Wu, L.-h.; Yang, W.-m.; Frenkel, A.I. Study of the local structure and oxidation state of iron in complex oxide catalysts for propylene ammoxidation. *Cat. Sci. & Technol.*, 2014, **in press**.
22. He, L.; Liu, F.; Hautier, G.; Oliveira, M.J.T.; Marques, M.A.L.; Vila, F.D.; Rehr, J.J.; Rignanes, G.-M.; Zhou, A. Accuracy of generalized gradient approximation functionals for density-functional perturbation theory calculations. *Phys. Rev. B* **2014**, *89*, 064305.
23. Frenkel, A.I.; Khalid, S.; Hanson, J.C.; Nachtegaal, M. QEXAFS in Catalysis Research: Principles, Data Analysis and Applications. In *In-situ Characterization of Heterogeneous Catalysts*, Chupas, P.; Hanson, J.; Rodriguez, J.A., Eds., John Wiley and Sons **2013**.
24. Frenkel, A.I.; Hanson, J.C. Combined XAFS-XRD methods in Catalysis Research. In *In-situ Characterization of Heterogeneous Catalysts*, Chupas, P.; Hanson, J.; Rodriguez, J. A., Eds., John Wiley and Sons **2013**.
25. Kossoy, A.; Wang, Q.; Korobko, R.; Grover, V.; Feldman, Y.; Wachtel, E.; Tyagi, A.K.; Frenkel, A.I.; Lubomirsky, I. Evolution of the local structure at the phase transition in CeO<sub>2</sub>-Gd<sub>2</sub>O<sub>3</sub> solid solutions. *Phys. Rev. B* **2013**, *87*, 054101.
26. Perelshtein, I.; Ruderman, E.; Perkash, N.; Tzanov, T.; Beddow, J.; Joyce, E.; Mason, T.; Blanes, M.; Molla, K.; Patlolla, A.; Frenkel, A.I.; Gedanken, A., Chitosan and chitosan-ZnO-based complex nanoparticles: formation, characterization, and antibacterial activity. *J. Mater. Chem. B* **2013**, *1*, 1968-1976.
27. Sanchez, S.I.; Small, M.W.; Bozin, E.S.; Wen, J.-G.; Zuo, J.-M.; Nuzzo, R.G., Metastability and Structural Polymorphism in Noble Metals: the Role of Composition and Metal Atom Coordination in Mono- and Bimetallic Nanoclusters. *ACS Nano* **2013**, *7*, 1542-1557.
28. Amit, Y.; Eshet, H.; Faust, A.; Patlolla, A.; Rabani, E.; Banin, U.; Frenkel, A.I. Unraveling the Impurity Location and Binding in Heavily Doped Semiconductor Nanocrystals: The Case of Cu in InAs Nanocrystals. *J. Phys. Chem. C* **2013**, *117*, 13688-13696.
29. Amit, Y.; Eshet, H.; Milo, O.; Rabani, E.; Frenkel, A.I.; Banin, U. How to dope a semiconductor nanocrystal. *ECS Trans.* **2013**, *58*, 127-133.
30. Yancey, D.F.; Chill, S.T.; Zhang, L.; Frenkel, A.I.; Henkelman, G.; Crooks, R.M. A theoretical and experimental examination of systematic ligand-induced disorder in Au dendrimer-encapsulated nanoparticles. *Chem. Science* **2013**, *4*, 2912-2921.
31. Wang, L.; Zhang, S.; Zhu, Y.; Patlolla, A.; Shan, J.-J.; Yoshida, H.; Takeda, S.; Frenkel, A.I.; Tao, F. Catalysis and In-situ Studies of Rh/Co<sub>3</sub>O<sub>4</sub> Nanorods in Reduction of NO with H<sub>2</sub>. *ACS Catalysis* **2013**, *3*, 1011-1019.
32. Patlolla, A.; Baumann, P.; Xu, W.; Senanayake, S.; Rodriguez, J.A.; Frenkel, A.I. Characterization of Metal-Oxide Catalysts in Operando Conditions by Combining X-Ray Absorption and Raman Spectroscopies in the Same Experiment. *Top. Catal.* **2013**, *56*, 896-904.

33. Amakawa, K.; Sun, L.; Guo, C.; Havecker, M.; Kube, P.; Wachs, I.E.; Lwin, S.; Frenkel, A.I.; Patlolla, A.; Hermann, K.; Schlogl, R.; Trunschke, A. *How strain affects the reactivity of surface metal oxide catalysts. Angew. Chem. Int. Ed.* **2013**, *52*, 13553-13557.
34. Frenkel, A.I., Applications of extended X-ray absorption fine-structure spectroscopy to studies of bimetallic nanoparticle catalysts. *Chem. Soc. Rev.* **2012**, *41*, 8163-8178.
35. Yang, J.C.; Small, M.W.; Grieshaber, R.V.; Nuzzo, R.G., Recent Developments and Applications of Electron Microscopy to Heterogeneous Catalysis. *Chem. Soc. Rev.* **2012**, *41*, 8179-8194.
36. Zhang, Z.; Gleeson, B.; Jung, K.; Li, L.; Yang, J.C., A Diffusion Analysis of Transient Subsurface gamma-Ni<sub>3</sub>Al Formation During beta-NiAl Oxidation, *Acta. Mater.* **2012**, *60*, 5273-5283.
37. Zhang, Z.; Jung, K.; Li, L.; Yang, J.C., Kinetic Aspects of Initial Stage Thin gamma-Al<sub>2</sub>O<sub>3</sub> Film Formation on Single Crystalline beta-NiAl (110). *J. Appl. Phys.* **2012**, *111*, 34312.
38. Erickson, E. M.; Thorum, M. S.; Vasic, R.; Marinkovic, N.; Frenkel, A. I.; Gewirth, A. A.; Nuzzo, R. G., In-Situ Electrochemical X-ray Absorbance Spectroscopy Oxygen Reduction Catalysis with High Oxygen Flux. *J. Am. Chem. Soc.* **2012**, *134*, 197-200.
39. Small, M. W.; Sanchez, S. I.; Marinkovic, N. S.; Frenkel, A. I.; Nuzzo, R. G., Influence of Adsorbates on the Electronic Structure, Bond Strain, and Thermal Properties of an Alumina-Supported Pt Catalyst. *ACS Nano*, **2012**, *6*, 5583-5595.
40. Yan, W.; Vasic, R.; Frenkel, A. I.; Koel, B. E., Intra-particle reduction of arsenite (As(III)) by nanoscale zerovalent iron (nZVI) investigated with *in-situ* X-ray absorption spectroscopy. *Environ. Sci. & Technology* **2012**, *46*, 7018-7026.
41. Patlolla, A.; Zunino III, J.; Frenkel, A. I.; Iqbal, Z., Thermochromism in Polydiacetylene-metal oxide nanocomposites *J. Mater. Chem.* **2012**, *22*, 7028-7035.
42. Myers, S. V.; Frenkel, A. I.; Crooks, R. M., In Situ Structural Characterization of Platinum Dendrimer-Encapsulated Oxygen Reduction Electrocatalysts. *Langmuir* **2012**, *28*(2), 1596-1603.
43. Ryu, H.; Lei, H.; Frenkel, A. I.; Petrovic, C., Local structural disorder-induced superconductivity in K(x)Fe(2-y)Se(2) materials *Phys. Rev. Lett.* **2012**, *85*, 224515.
44. Chen, W.-F.; Sasaki, K.; Ma, C.; Frenkel, A. I.; Marinkovic, N.; Muckerman, J. T.; Zhu, Y.; Adzic, R. R., Noble metal-free hydrogen-evolution catalysts based on NiMo nitride nanosheets. *Angew. Chemie Int. Ed.* **2012**, *51*, 6131-6135.
45. Yadgarov, L.; Rosentsveig, R.; Leitun, G.; Albu-Yaron, A.; Moshkovitz, A.; Perfiliev, V.; Vasic, R.; Frenkel, A. I.; Enyashin, A. N.; Seifert, G.; Rapoport, L.; Tenne, R., Controlled doping of MS<sub>2</sub> (M=W, Mo) nanotubes and fullerene-like nanoparticles *Ang. Chemie, Int. Ed.* **2012**, *51*, 1148-1151.
46. Yih, K.; Hamdemir, I.K.; Mondoch, J.E.; Bayrem, E.; Ozkar, S.; Vasic, R.; Frenkel, A.I.; Anderson, O.P.; Finke, R.G., Synthesis and Characterization of [Ir(1,5-Cyclooctadiene)(μ-H)]<sub>4</sub>: A Tetrametallic Ir<sub>4</sub>H<sub>4</sub>-core, Coordinatively Unsaturated Cluster. *Inorg. Chem.* **2012**, *51*, 3186-3193.
47. Frenkel, A.I.; Vasic, R.; Dukesz, B.; Li, D.; Chen, M.; Zhang, L.; Fujita, T.; Thermal Properties of Nanoporous Gold. *Phys. Rev. B* **2012**, *85*, 195419.
48. Landon, J.; Demeter, E.; Inoglu, N.; Keturakis, C.; Wachs, I.E.; Vasic R.; Frenkel, A.I.; Kitchin, J.R., Spectroscopic Characterization of Mixed Fe-Ni Oxide Electrocatalysts for the Oxygen Evolution Reaction in Alkaline Electrolytes. *ACS Catalysis* **2012**, *2*, 1793-1801.
49. Korobko, R.; Patlolla, A.; Kossoy, A.; Wachtel, E.; Tuller, H.L.; Frenkel, A.I.; Lubomirsky, I., Giant Electrostriction in Gd-doped Ceria. *Adv. Mater.* **2012**, *24*, 5857-5861.
50. Lyahovitskaya, V.; Feldman, Y.; Zon, I.; Yoffe, A.; Frenkel, A.I., Strain-arranged structure in amorphous films. *J. Mater. Res.* **2012**, *27*, 2819-2828.
51. Coppage, R.; Slocik, J. M.; Briggs, B. D.; Frenkel, A. I.; Naik, R. R.; Knecht, M. R., Determining peptide sequence effects that control the size, structure and function of nanoparticles. *ACS Nano* **2012**, *6*, 1625-1636.
52. Patlolla, A.; Carino, E.V.; Ehrlich, S.N.; Stavitski, E.; Frenkel, A.I., Application of Operando XAS, XRD, and Raman Spectroscopy for Phase Speciation in Water Gas Shift Reaction Catalysts. *ACS Catalysis* **2012**, *2*, 2216-2223.
53. Lei, H.; Ryu, H.; Ivanovski, V.; Warren, J.B.; Frenkel, A.I.; Cekic, B.; Yin, W.-G.; Petrovic, C., Structure and physical properties of the layered iron oxychalcogenide BaFe<sub>2</sub>Se<sub>2</sub>O. *Phys. Rev. B* **2012**, *86*, 195133.
54. M. W. Small, S. I. Sanchez, L. D. Menard, J. H. Kang, A. I. Frenkel and R. G. Nuzzo, The Atomic Structural Dynamics of γ-Al<sub>2</sub>O<sub>3</sub> Supported Ir-Pt Nanocluster Catalysts Prepared From a Bimetallic Molecular Precursor: A Study Using Aberration-Corrected Electron Microscopy and X-ray Absorption Spectroscopy, *Journal of the American Chemical Society*, **2011**, *133*, 3582-3591.
55. W. Du, D. Su, Q. Wang, A. I. Frenkel, X. Teng, Promotional effects of Bismuth on the formation of Platinum-Bismuth nanowires and the electrocatalytic activity toward ethanol oxidation, *Crystal Growth & Design*, **2011**, *11*, 594-599.
56. A. Piovano, G. Agostini, A. I. Frenkel, T. Bertier, C. Prestipino, M. Ceretti, W. Paulus, C. Lamberti, Time-resolved in situ XAFS study of the electrochemical oxygen intercalation in SrFeO<sub>2.5</sub> Brownmillertite structure: comparison with the homologous SrCoO<sub>2.5</sub> system, *J. Phys. Chem. C* **2011**, *115*, 1311-1322.

57. Alley, W. M.; Hamdemir, I. K.; Wang, Q.; Frenkel, A. I.; Li, L.; Yang, J. C.; Menard, L. D.; Nuzzo, R. G.; Ozkar, S.; Yih, K.; Johnson, K. A.; Finke, R. G., Industrial Ziegler-Type Hydrogenation Catalysts Made from Co(neodecanoate)(2) or Ni(2-ethylhexanoate)(2) and AlEt<sub>3</sub>: Evidence for Nanoclusters and Sub-Nanocluster or Larger Ziegler-Nanocluster Based Catalysis. *Langmuir* **2011**, *27*, 6279-6294.
58. Danh, N.-T.; Frenkel, A. I.; Wang, J.; O'Brien, S.; Akins, D. L., Cobalt-polypyrrole-carbon black (Co-PPY-CB) electrocatalysts for the oxygen reduction reaction (ORR) in fuel cells: Composition and kinetic activity. *Applied Catalysis B-Environmental* **2011**, *105*, 50-60.
59. Du, W.; Su, D.; Wang, Q.; Frenkel, A. I.; Teng, X., Promotional Effects of Bismuth on the Formation of Platinum-Bismuth Nanowires Network and the Electrocatalytic Activity toward Ethanol Oxidation. *Cryst. Growth Des.* **2011**, *11*, 594-599.
60. Du, W.; Wang, Q.; LaScala, C. A.; Zhang, L.; Su, D.; Frenkel, A. I.; Mathur, V. K.; Teng, X., Ternary PtSnRh-SnO<sub>2</sub> nanoclusters: synthesis and electroactivity for ethanol oxidation fuel cell reaction. *J. Mater. Chem.* **2011**, *21*, 8887-8892.
61. Du, W.; Wang, Q.; Saxner, D.; Deskins, N. A.; Su, D.; Krzanowski, J. E.; Frenkel, A. I.; Teng, X., Highly Active Iridium/Iridium-Tin/Tin Oxide Heterogeneous Nanoparticles as Alternative Electrocatalysts for the Ethanol Oxidation Reaction. *J. Am. Chem. Soc.* **2011**, *133*, 15172-15183.
62. Frenkel, A. I.; Wang, Q.; Marinkovic, N.; Chen, J. G.; Barrio, L.; Si, R.; Lopez Camara, A.; Estrella, A. M.; Rodriguez, J. A.; Hanson, J. C., Combining X-ray Absorption and X-ray Diffraction Techniques for *in-situ* Studies of Chemical Transformations in Heterogeneous Catalysis: Advantages and Limitations. *J. Phys. Chem. C* **2011**, *115*, 17884-17890.
63. Frenkel, A. I.; Yevick, A.; Cooper, C.; Vasic, R., Modeling the Structure and Composition of Nanoparticles by Extended X-Ray Absorption Fine-Structure Spectroscopy. *Annual Review Of Analytical Chemistry, Vol 4* **2011**, *4*, 23-39.
64. Li, L.; Zhang, Z.; Ciston, J.; Stach, E. A.; Wang, L.-l.; Johnson, D. D.; Wang, Q.; Frenkel, A. I.; Sanchez, S. I.; Small, M. W.; Nuzzo, R. G.; Yang, J. C., H<sub>2</sub>-driven crystallization of supported Pt nanoparticles observed with aberration-corrected Environmental TEM. *Microsc. Microanal.* **2011**, *17*, 1604-1605.
65. Marinkovic, N. S.; Wang, Q.; Barrio, L.; Ehrlich, S. N.; Khalid, S.; Cooper, C.; Frenkel, A. I., Combined *in-situ* X-ray absorption and diffuse reflectance infrared spectroscopy: An attractive tool for catalytic investigations. *Nuclear Instruments & Methods In Physics Research Section A-* **2011**, *649*, 204-206.
66. Marinkovic, N. S.; Wang, Q.; Frenkel, A. I., *In-situ* diffuse reflectance IR spectroscopy and X-ray absorption spectroscopy for fast catalytic processes. *Journal Of Synchrotron Radiation* **2011**, *18*, 447-455.
67. Paredis, K.; Ono, L. K.; Behafarid, F.; Zhang, Z.; Yang, J. C.; Frenkel, A. I.; Cuenya, B. R., Evolution of the Structure and Chemical State of Pd Nanoparticles during the *in-situ* Catalytic Reduction of NO with H<sub>2</sub>. *J. Am. Chem. Soc.* **2011**, *133*, 13455-13464.
68. Paredis, K.; Ono, L. K.; Mostafa, S.; Li, L.; Zhang, Z.; Yang, J. C.; Barrio, L.; Frenkel, A. I.; Cuenya, B. R., Structure, chemical composition, and reactivity correlations during the *in-situ* oxidation of 2-propanol. *J. Am. Chem. Soc.* **2011**, *133*, 6728-6735.
69. Sasaki, K.; Kuttiyil, K. A.; Barrio, L.; Su, D.; Frenkel, A. I.; Marinkovic, N.; Mahajan, D.; Adzic, R. R., Carbon-Supported IrNi Core-Shell Nanoparticles: Synthesis, Characterization, and Catalytic Activity. *J. Phys. Chem. C* **2011**, *115*, 9894-9902.
70. Zhang, Z.; Li, L.; Wang, L.-l.; Sanchez, S. I.; Wang, Q.; Johnson, D. D.; Frenkel, A. I.; Nuzzo, R. G.; Yang, J. C., The Role of  $\beta$ -Al<sub>2</sub>O<sub>3</sub> Single Crystal Support to Pt Nanoparticles Construction. *Microsc. Microanal.* **2011**, *17*, 1324-1325.
71. Zhang, Z.; Li, L.; Yang, J. C.,  $\gamma$ -Al<sub>2</sub>O<sub>3</sub> thin film formation via oxidation of  $\beta$ -NiAl(1 1 0). *Acta Mater.* **2011**, *59*, 5905-5916.
72. Lei, H.; Ryu, H.; Frenkel, A. I.; Petrovic, C., Anisotropy in BaFe<sub>2</sub>Se<sub>3</sub> single crystals with double chains of FeSe tetrahedra *Physical Review B* **2011**, *84*, 214511.
73. Shen, X.-F.; Morey, A.; Liu, J.; Ding, Y.-S.; Durand, J.; Wang, Q.; Wen, W.; Hines, W. A.; Hanson, J. C.; Bai, J.; Frenkel, A. I.; Reiff, W.; Aindow, M.; Suib, S. L.; Cai, J., Characterization of the Fe-doped mixed-valent tunnel structure manganese oxide KOMS-2 *J. Phys. Chem. C* **2011**, *115*, 21610-21619.
74. Coppage, R.; Slocik, J. M.; Briggs, B. D.; Frenkel, A. I.; Heinz, H.; Naik, R. R.; Knecht, M. R., Crystallographic Recognition Controls Peptide Binding for Bio-Based Nanomaterials. *J. Am. Chem. Soc.* **2011**, *133*, 12346-12349.

**Au/TiO<sub>2</sub> in Thermal and Photoassisted Catalysis**

Ji Bong Joo, Robert Dillon, Ilkeun Lee, Yadong Yin, Christopher J. Bardeen  
and Francisco Zaera\*

Department of Chemistry, University of California, Riverside, California 92521, USA

Email: zaera@ucr.edu

**Presentation Abstract**

The synthesis of Au@Void@TiO<sub>2</sub> yolk-shell nanostructures has been developed and tuned to control specific properties, including metal nanoparticle size and shell diameter, thickness, porosity, and crystallinity. These new nanostructures have provided us with the control needed to characterize the general properties and performance of Au/titania catalysts. In terms of the production of hydrogen from water with semiconductor photocatalysts, it is well known that such photocatalysis can be promoted by adding small amounts of metals to their surfaces. This catalytic enhancement is commonly attributed to a fast transfer of the excited electrons generated by photon absorption from the semiconductor to the metal, a step that prevents de-excitation back to the ground electronic state. However, we have obtained experimental evidence that suggests an alternative pathway that does not involve electron transfer to the metal but requires it to act as a catalyst for the recombination of the hydrogen atoms made via the reduction of protons on the surface of the semiconductor instead. In terms of the ease with which catalysts made out of gold nanoparticles dispersed on titania supports oxidize carbon monoxide to carbon dioxide around room temperature, we report on a unique gold/titania-based catalyst that, in addition to such room-temperature catalysis, displays a second active regime at much lower temperatures, as low as 120 K. We show that this new catalytic regime follows a mechanism different to that operative at room temperature, and involves at least three titania-adsorbed CO species and a synergy between the CO and O<sub>2</sub> uptakes on the surface. New titanate sites, formed upon treatment of regular Au/TiO<sub>2</sub> catalysts with NaOH, appear to be responsible for the opening of this new reaction channel.

**DE-FG02-09ER16096: SISGR - Design and Characterization of Novel  
Photocatalysts With Core-Shell Nanostructures**

PIs: Francisco Zaera (PI), Christopher J. Bardeen (Co-PI), Yadong Yin (Co-PI)  
Post-docs: Ilkeun Lee, Ji Bong Joo  
Graduate Students: Robert Dillon, Qiao Zhang, Michael Dahl, Zhenda Lu, James Goebel

**RECENT PROGRESS**

Our project involves both the development of synthetic strategies for the making of new nanostructures, including metal-supporting nanorods and core-shell and yolk-shell nanoarchitectures, and the use of those, together with more conventional samples, to probe their photophysical behavior and their catalytic and photocatalytic performance.

*1. Synthesis.*

We continue to improve on our synthesis of metal/TiO<sub>2</sub> core-shell and yolk-shell composite nanostructures. A controlled sol-gel process has been recently developed to directly coat gold nanoparticles with a thin layer of TiO<sub>2</sub> to produce Au@TiO<sub>2</sub> core-shell nanoparticles, which can be rendered crystalline via calcination at high temperatures. The Au weight percent can be controlled by repeating the coating process while decreasing the water content and core concentration, making it possible to systematically tune the shell thickness over a large range without the need for an excessive number of coating steps. Catalysts with varying Au weight percents and corresponding shell thicknesses, as well as various calcination temperatures, were tested for their efficacy in the UV-driven reforming of ethanol to produce hydrogen.

We have also developed a photocatalytic strategy for the synthesis of colloidal Ag-TiO<sub>2</sub> nanorod composites in which each TiO<sub>2</sub> nanorod contains a single Ag nanoparticle on its surface. The size of the Ag nanoparticles can be precisely controlled by varying the irradiation time and the amount of alcohol additive. The Ag-TiO<sub>2</sub> nanorod composites were used as electron transport

layers in the fabrication of organic solar cells, and were shown to show notable enhancement in power conversion efficiency (6.92%) compared with pure TiO<sub>2</sub> nanorods (5.81%) as well as higher external quantum efficiency due to improved charge separation and transfer.

Finally, we are developing a method for incorporating carbon materials into TiO<sub>2</sub> hollow shells in order to improve the absorption of the visible light of the catalysts and to replace noble metals for enhanced charge separation. Our method includes coating resorcinol–formaldehyde resin on colloidal objects with controllable thickness and then converting the crosslinked polymer into carbon through a simple calcination process. We are currently studying the effect of doped carbon to the catalytic activity of TiO<sub>2</sub> photocatalysts.

## 2. Catalytic Characterization.

It is well known that the addition of metals such as platinum or gold to semiconductors enhances their activity as photocatalysts, in particular for water splitting to produce H<sub>2</sub>. This effect is currently explained by a mechanism where the excited electrons produced by absorption of light are transferred from the semiconductor to the metal before they have the opportunity to recombine with their corresponding holes and return to the ground electronic state. In this scheme (left panel of Figure 1), the protons from water are reduced on the surface of the metal, in sites physically separated from those on the semiconductor, where oxygen production takes place. However, several pieces of evidence argue against this mechanism, and in favor of an

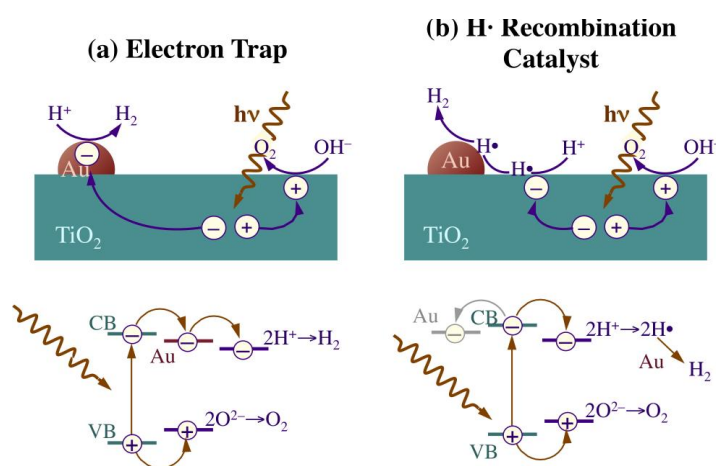


**Figure 1**

alternative where the reduced atomic hydrogen then migrates to the metal and recombines to yield the final molecular hydrogen product (Figure 1, right panel). The new information from our study include time-dependent fluorescence measurements indicating no changes upon addition of the metal to the titania, evidence of O<sub>2</sub> production

with titania alone, without any metal, if reducible ions such as  $\text{Ce}^{4+}$ ,  $\text{Ag}^+$ , or  $\text{IO}_3^-$  are added to the water phase, data indicating the photocatalytic activity of NiO/titania catalysts but not of C/titania samples, even if electron transfer is not viable with the first pair but it should be easy with the second, and additional photocatalytic activity evidence with catalysts where the gold nanoparticles have been electrically isolated using a thin silica shell.

In terms of thermal oxidation reactions with catalysts based on gold nanoparticles, those have received much attention lately. However, as far as we know, all reported conversions require thermal activation, and show significant catalytic activity starting only at moderate (~room) temperatures. Here we report on a unique case where the steady-state catalytic rate of oxidation of carbon monoxide increases again at lower temperatures, all the way down to

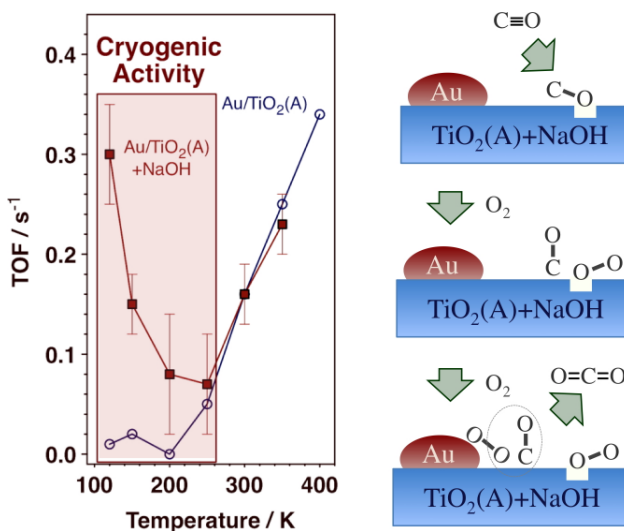


**Figure 2**

120 K, the lowest temperature we were able to achieve with our experimental setup (Figure 2, left). We argue that the behavior observed here is the consequence of a change in the mechanism of the reaction: the way this cryogenic-temperature reaction proceeds is different than in the other reported cases. Three different adsorbed CO states on the titania surface were identified as participants in the mechanism of the reaction (Figure 2, right), and amorphous and titanate-type surface states were determined to be required for the cryogenic activity.

## Publications Acknowledging this Grant in 2013-2014<sup>1-19</sup>

- (1) Joo, J. B.; Dillon, R.; Lee, I.; Yin, Y.; Bardeen, C. J.; Zaera, F. Promoter of Atomic Hydrogen Recombination as an Alternative Mechanism to Electron Trap for the Role of Metals in the Photocatalytic Production of H<sub>2</sub>. *Proc. Natl. Acad. Sci. U. S. A.* **2014**, in press.
- (2) Zaera, F. New Advances in the Use of Infrared Absorption Spectroscopy for the Characterization of Heterogeneous Catalytic Reactions. *Chem. Soc. Rev.* **2014**, DOI: 10.1039/C1033CS60374A.
- (3) Wang, W.; Ye, M.; He, L.; Yin, Y. Nanocrystalline TiO<sub>2</sub>-Catalyzed Photoreversible Color Switching. *Nano Lett.* **2014**, *14*, 1681-1686.
- (4) Shang, L.; Bian, T.; Zhang, B.; Zhang, D.; Wu, L.-Z.; Tung, C.-H.; Yin, Y.; Zhang, T. Graphene-Supported Ultrafine Metal Nanoparticles Encapsulated by Mesoporous Silica: Robust Catalysts for Oxidation and Reduction Reactions. *Angew. Chem., Int. Ed.* **2014**, *53*, 250-254.
- (5) Goebel, J.; Joo, J. B.; Dahl, M.; Yin, Y. Synthesis of Tailored Au@TiO<sub>2</sub> Core-Shell Nanoparticles for Photocatalytic Reforming of Ethanol. *Catal. Today* **2014**, *225*, 90-95.
- (6) Zaera, F. Shape-Controlled Nanostructures in Heterogeneous Catalysis. *ChemSusChem* **2013**, *6*, 1797-1820.
- (7) Zaera, F. Nanostructured Materials for Applications in Heterogeneous Catalysis. *Chem. Soc. Rev.* **2013**, *42*, 2746-2762.
- (8) Li, J.; Liang, X.; Joo, J. B.; Lee, I.; Yin, Y.; Zaera, F. Mass Transport across the Porous Oxide Shells of Core-Shell and Yolk-Shell Nanostructures in Liquid Phase. *J. Phys. Chem. C* **2013**, *117*, 20043-20053.
- (9) Joo, J. B.; Zhang, Q.; Dahl, M.; Zaera, F.; Yin, Y. Synthesis, Crystallinity Control, and Photocatalysis of Nanostructured Titanium Dioxide Shells. *J. Mater. Res.* **2013**, *28*, 362-368.
- (10) Joo, J. B.; Vu, A.; Zhang, Q.; Dahl, M.; Gu, M.; Zaera, F.; Yin, Y. A Sulfated ZrO<sub>2</sub> Hollow Nanostructure as an Acid Catalyst in the Dehydration of Fructose to 5-Hydroxymethylfurfural. *ChemSusChem* **2013**, *6*, 2001-2008.

- (11) Joo, J. B.; Lee, I.; Dahl, M.; Moon, G. D.; Zaera, F.; Yin, Y. Controllable Synthesis of Mesoporous TiO<sub>2</sub> Hollow Shells: Toward an Efficient Photocatalyst. *Adv. Funct. Mater.* **2013**, *23*, 4246-4254.
- (12) Joo, J. B.; Dahl, M.; Li, N.; Zaera, F.; Yin, Y. Tailored Synthesis of Mesoporous TiO<sub>2</sub> Hollow Nanostructures for Catalytic Applications. *Energy Environm. Sci.* **2013**, *6*, 2082-2092.
- (13) Dillon, R. J.; Joo, J.-B.; Zaera, F.; Yin, Y.; Bardeen, C. J. Correlating the Excited State Relaxation Dynamics as Measured by Photoluminescence and Transient Absorption with the Photocatalytic Activity of Au@TiO<sub>2</sub> Core-Shell Nanostructures. *Phys. Chem. Chem. Phys.* **2013**, *15*, 1488-1496.
- (14) Lu, Q.; Lu, Z.; Lu, Y.; Lv, L.; Ning, Y.; Yu, H.; Hou, Y.; Yin, Y. Photocatalytic Synthesis and Photovoltaic Application of Ag-TiO<sub>2</sub> Nanorod Composites. *Nano Lett.* **2013**, *13*, 5698-5702.
- (15) Gao, C.; Goebel, J.; Yin, Y. Seeded Growth Route to Noble Metal Nanostructures. *Journal of Materials Chemistry C* **2013**, *1*, 3898-3909.
- (16) Li, N.; Zhang, Q.; Liu, J.; Joo, J.; Lee, A.; Gan, Y.; Yin, Y. Sol-Gel Coating of Inorganic Nanostructures with Resorcinol-Formaldehyde Resin. *Chem. Commun.* **2013**, *49*, 5135-5137.
- (17) Ye, M.; Lu, Z.; Hu, Y.; Zhang, Q.; Yin, Y. Mesoporous Titanate-Based Cation Exchanger for Efficient Removal of Metal Cations. *Journal of Materials Chemistry A* **2013**, *1*, 5097-5104.
- (18) Wang, W.; Dahl, M.; Yin, Y. Hollow Nanocrystals through the Nanoscale Kirkendall Effect. *Chem. Mater.* **2013**, *25*, 1179-1189.
- (19) Liu, Y.; Goebel, J.; Yin, Y. Templated Synthesis of Nanostructured Materials. *Chem. Soc. Rev.* **2013**, *42*, 2610-2653.

This page is intentionally blank.

# Participant List

This page is intentionally blank.

## Catalysis Research Meeting

July 20–23, 2014

### Participant List

Frank Abild-Pedersen  
SLAC National Accelerator Laboratory  
abild@slac.stanford.edu

Mahdi Abu-Omar  
Purdue University  
mabuomar@purdue.edu

Eric Altman  
Yale University  
eric.altman@yale.edu

Perla Balbuena  
Texas A&M University  
balbuena@tamu.edu

Ludwig Bartels  
University of California - Riverside  
bartels@ucr.edu

Bart Bartlett  
University of Michigan  
bartmb@umich.edu

Ali Belkacem  
Lawrence Berkeley National Laboratory  
abelkacem@lbl.gov

Alexis Bell  
University of California - Berkeley  
bell@cchem.berkeley.edu

John Berry  
University of Wisconsin - Madison  
berry@chem.wisc.edu

Aditya Bhan  
University of Minnesota  
abhan@umn.edu

Thomas Bligaard  
SLAC National Accelerator Laboratory  
bligaard@slac.stanford.edu

Suzanne Blum  
University of California - Irvine  
blums@uci.edu

Phillip Britt  
Oak Ridge National Laboratory  
brittpf@ornl.gov

Emilio Bunel  
Argonne National Laboratory  
ebunel@anl.gov

Charles Campbell  
University of Washington  
charliec@uw.edu

Peng Chen  
Cornell University  
pc252@cornell.edu

Geoffrey Coates  
Cornell University  
gc39@cornell.edu

David Cox  
Virginia Tech  
dfcox@vt.edu

Paul Dauenhauer  
University of Massachusetts  
dauenhauer@ecs.umass.edu

William Delgass  
Purdue University  
delgass@purdue.edu

David Dixon  
University of Alabama  
dadixon@bama.ua.edu

Zdenek Dohnálek  
Pacific Northwest National Laboratory  
zdenek.dohnalek@pnnl.gov

James Dumesic  
University of Wisconsin  
dumesic@engr.wisc.edu

Joshua Figueroa  
University of California - San Diego  
jsfig@ucsd.edu

Richard Finke  
Colorado State University  
rfinke@lamar.colostate.edu

Anatoly Frenkel  
Yeshiva University  
anatoly.frenkel@yu.edu

Cynthia Friend  
Harvard University  
cfriend@seas.harvard.edu

Bruce Garrett  
Pacific Northwest National Laboratory  
bruce.garrett@pnnl.gov

Bruce Gates  
University of California - Davis  
bcgates@ucdavis.edu

Andrew Gellman  
Carnegie Mellon University  
gellman@cmu.edu

Alexander Harris  
Brookhaven National Laboratory  
alexh@bnl.gov

Michael Henderson  
Pacific Northwest National Laboratory  
ma.henderson@pnnl.gov

Andreas Heyden  
University of South Carolina  
heyden@cec.sc.edu

Adam Hock  
Illinois Inst. of Tech. - Argonne National Laboratory  
ahock@iit.edu

Thomas Jaramillo  
Stanford University  
jaramillo@stanford.edu

Cynthia Jenks  
Ames Laboratory  
cjenks@ameslab.gov

Nørskov Jens  
SUNCAT  
norskov@stanford.edu

William Jones  
University of Rochester  
jones@chem.rochester.edu

Christopher Jones  
Georgia Technical Institute  
christopher.jones@chbe.gatech.edu

Alexander Katz  
University of California - Berkeley  
askatz@berkeley.edu

John Kitchin  
Carnegie Mellon University  
jkitchin@andrew.cmu.edu

Harold Kung  
Northwestern University  
hkung@northwestern.edu

Johannes Lercher  
Pacific Northwest National Laboratory  
johannes.lercher@pnnl.gov

Ping Liu  
Brookhaven National Laboratory  
pingliu3@bnl.gov

Diane Marceau  
U.S. Dept. of Energy - Basic Energy Sciences  
diane.marceau@science.doe.gov

Tobin Marks  
Northwestern University  
t-marks@northwestern.edu

Paul Maupin  
U.S. Dept. of Energy - Basic Energy Sciences  
paul.maupin@science.doe.gov

Eric McFarland  
University of California - Santa Barbara  
ewmcfar@engineering.ucsb.edu

Horia Metiu  
University of California - Santa Barbara  
metiu@chem.ucsb.edu

John Miller  
U.S. Dept. of Energy - Basic Energy Sciences  
john.miller@science.doe.gov

Daniel Mindiola  
University of Pennsylvania  
mindiola@sas.upenn.edu

Raul Miranda  
U.S. Dept. of Energy - Basic Energy Sciences  
raul.miranda@science.doe.gov

Liviu Mirica  
Washington University - St. Louis  
mirica@wustl.edu

Charles Mullins  
University of Texas - Austin  
mullins@che.utexas.edu

David Mullins  
Oak Ridge National Laboratory  
mullinsdr@ornl.gov

SonBinh Nguyen  
Argonne National Lab/Northwestern University  
stn@northwestern.edu

Jack Norton  
Columbia University  
jrn11@columbia.edu

Justin Notestein  
Northwestern University  
j-notestein@northwestern.edu

Colin Nuckolls  
Columbia University  
cn37@columbia.edu

Ralph Nuzzo  
University Of Illinois  
r-nuzzo@illinois.edu

Steven Overbury  
Oak Ridge National Laboratory  
overburysh@ornl.gov

Umit Ozkan  
Ohio State University  
ozkan.1@osu.edu

Gerard Parkin  
Columbia University  
parkin@columbia.edu

Talat Rahman  
University of Central Florida  
talat.rahman@ucf.edu

Ashwin Ramasubramaniam  
University of Massachusetts - Amherst  
ashwin@umass.edu

Fabio Ribeiro  
Purdue University  
fabio@purdue.edu

Robert Rioux  
Pennsylvania State University  
rioux@enr.psu.edu

José Rodriguez  
Brookhaven National Laboratory  
rodriguez@bnl.gov

Yuriy Roman  
Massachusetts Institute of Technology  
yroman@mit.edu

Aaron Sadow  
Ames Laboratory  
sadow@iastate.edu

Melanie Sanford  
University of Michigan  
mssanfor@umich.edu

Aditya Ashi Savara  
Oak Ridge National Laboratory  
savaraa@ornl.gov

William Schneider  
University of Notre Dame  
wschneider@nd.edu

Richard Schrock  
Massachusetts Institute of Technology  
rrs@mit.edu

Susannah Scott  
University of California - Santa Barbara  
sscott@engineering.ucsb.edu

Annabella Selloni  
Princeton University  
aselloni@princeton.edu

Wendy Shaw  
Pacific Northwest National Laboratory  
wendy.shaw@pnnl.gov

Sara Skrabalak  
Indiana University - Bloomington  
sskrabal@indiana.edu

Igor Slowing  
Ames Laboratory  
islowing@ameslab.gov

Dario Stacchiola  
Brookhaven National Laboratory  
djs@bnl.gov

Shannon Stahl  
University of Wisconsin - Madison  
stahl@chem.wisc.edu

Albert Stiegman  
Florida State University  
stiegman@chem.fsu.edu

Steven Tait  
Indiana University  
tait@indiana.edu

Franklin (Feng) Tao  
University of Notre Dame  
franklin.tao.2011@gmail.com

Don Tilley  
Lawrence Berkeley National Laboratory  
tdtilley@berkeley.edu

YuYe Tong  
Georgetown University  
yyt@georgetown.edu

David Vicić  
Lehigh University  
vici@lehigh.edu

John Vohs  
University of Pennsylvania  
vohs@seas.upenn.edu

Christine Wade  
Brandeis University  
thomasc@brandeis.edu

Casey Wade  
Brandeis University  
cwade@brandeis.edu

Yong Wang  
Washington State University/PNNL  
yongwang@pnl.gov

Robert Waymouth  
Stanford University  
waymouth@stanford.edu

Michael White  
Brookhaven National Lab/Stony Brook University  
mgwhite@bnl.gov

Judith Yang  
University of Pittsburgh  
judyyang@pitt.edu

John T. Yates, Jr.  
University of Virginia  
johnt@virginia.edu

Francisco Zaera  
University of California  
zaera@ucr.edu

## Functionalization of metal-organic frameworks for heterogeneous catalysis and selective aqueous cation capture

Casey R. Wade\*, Sarah Baranowski, S. Olivia Gunther  
Brandeis University, Dept. of Chemistry

Metal-organic frameworks (MOFs) have emerged as a new class of tunable, porous materials with potential applications in a number of areas, including heterogeneous catalysis and molecular/ion sensing and separation. We are currently focusing on the design of new MOF materials with chelating secondary metal binding sites for 1) the incorporation of low-valent metal centers as active sites for heterogeneous catalysis and 2) selective capture of metal ions for detection/separation applications. Apart from heterogenization, we seek to take advantage of the potential benefits MOF-supported catalysts may offer with respect to substrate or product size/shape selectivity and increased activity versus homogeneous catalysts. Our approach in this area involves the incorporation of phosphine, N-heterocyclic carbene, and other soft donor groups into organic linkers as secondary metal binding sites to host site-isolated, low-valent metal centers. This presentation will highlight our recent work with MOFs containing linkers based on POCOP-type pincer ligands (Figure 1).

In addition to heterogeneous catalysis, we seek to design water-stable MOF supports containing secondary metal binding sites for selective capture of aqueous metal ions. Specifically, we are targeting materials capable of toxic metal ion ( $\text{Hg}^{2+}$ ,  $\text{Cd}^{2+}$ ,  $\text{Pb}^{2+}$ ) remediation and lanthanide/actinide separations. Our approach involves the use of amine-functionalized organic linkers and postsynthetic modification strategies to vary the nature of secondary metal binding sites and tune factors such as pore size and hydrophilicity (Figure 2).

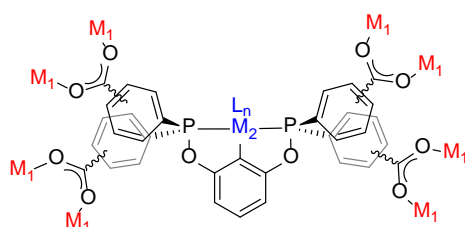


Figure 1

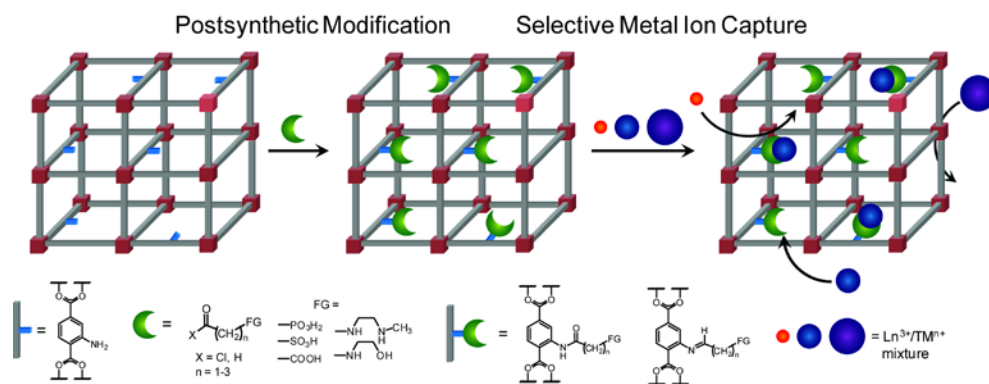


Figure 2

Ralph G. Nuzzo

**A Comparative *In Operando* Study of the Atomic and Electronic Properties of the Hydrogenation of Ethylene over Supported Pd and Pt Catalysts**

A. Elsen<sup>1</sup>, U. Jung<sup>1</sup>, S. Zhao<sup>1</sup>, R. G. Nuzzo<sup>1</sup>, Y. Li<sup>2</sup>, A. I. Frenkel<sup>2</sup>, C. Fittz<sup>3</sup>, J. C. Yang<sup>3</sup>, J. Kas<sup>4</sup>, F. Vila<sup>4</sup>, J. J. Rehr<sup>4</sup>, E. A. Stach<sup>5</sup>.

<sup>1</sup>Department of Chemistry, University of Illinois, Urbana, <sup>2</sup>Department of Physics, Yeshiva University, New York, <sup>3</sup>Department of Material Science and Engineering and Department of Chemical Engineering, University of Pittsburgh, <sup>4</sup>Department of Physics, University of Washington, Seattle, <sup>5</sup>Center for Functional Nanomaterials, Brookhaven National Laboratory, New York

**Presentation Abstract**

The results of a comparative *in operando* study of the hydrogenation of ethylene over supported Pd and Pt catalysts are described. The structural dynamics evidenced in this exemplary C-H bond forming reaction were characterized in mixed atmospheres ranging between pure hydrogen and ethylene by in situ X-ray absorption spectroscopy (XAS) and scanning transmission electron microscopy (STEM). Pronounced changes in the atomic and electronic structures of the catalysts (e.g., defined transitions between hydrogen- and hydrocarbon-covered surfaces, size changes, and gas-phase composition-dependent hydrogen de-/intercalation) are found to occur during the reaction, but have only little impact on the largely reversible mass-action kinetics observed for both catalysts. The data demonstrate significant structural and dynamical complexity within what is generally accepted to be a structure-insensitive reaction.

**Grant Number: DE FG02-03ER15476**

**Grant Title: The Reactivity and Structural Dynamics of Supported Metal Nanoclusters Using Electron Microscopy, *in situ* X-Ray Spectroscopy, Electronic Structure Theories, and Molecular Dynamics Simulations.**

**PIs:** Ralph G. Nuzzo, Anatoly I. Frenkel, Judith C. Yang, John J. Rehr

**Postdocs:** A. Elsen, C. Bonifacio, U. Jung, S. Zhao, J. Kas, Y. Li, F. Vila

**RECENT PROGRESS**

Although numerous studies on catalytic reactions have provided comprehensive information on reaction rates and kinetics, knowledge about the interplay of the structural and electronic properties of the catalysts during reaction is still scarce. In this respect, the hydrogenation of unsaturated hydrocarbons over supported nanoparticles is of particular interest because of its industrial importance.

We present a comparative *in operando* X-ray absorption spectroscopy (XAS, i.e., both X-ray absorption near edge structure, XANES and extended X-ray absorption fine structure, EXAFS) and residual gas analysis (RGA) study, complemented by *ex situ* scanning transmission electron microscopy (STEM) of the hydrogenation of ethylene, the simplest unsaturated hydrocarbon, over nanoscale Pd and Pt catalysts supported on silica. The hydrogenation was carried out as an isothermal process under ambient conditions and continuous gas flow. The reactivity was controlled by varying the hydrogen-to-ethylene ratio in the feed gas from pure hydrogen to ethylene and back to hydrogen.

Analysis of the STEM images yield for both Pd/SiO<sub>2</sub> and Pt/SiO<sub>2</sub> samples well-defined and narrow particle size distributions. The average particle sizes are  $1.31 \pm 0.43$  Å for Pd/SiO<sub>2</sub> and  $1.11 \pm 0.34$  Å for Pt/SiO<sub>2</sub>. After the XAS

measurements, the Pd/SiO<sub>2</sub> particles exhibit a much broader size distribution with a considerably increased average size of  $2.21 \pm 1.00$  Å, whereas for the Pt/SiO<sub>2</sub> particles the size distribution with a size of  $1.00 \pm 0.31$  Å is virtually the same as before the XAS experiments.

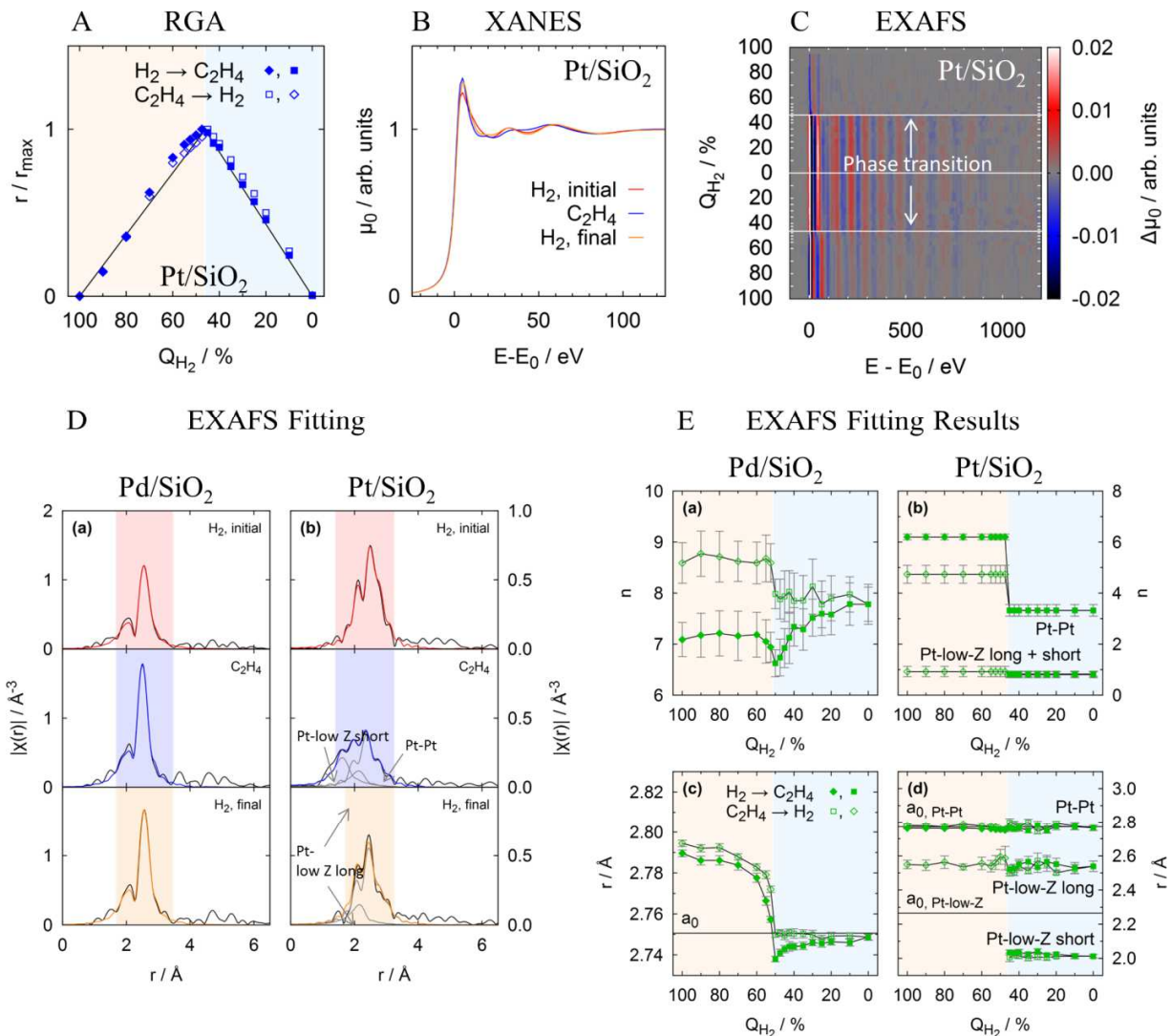
The RGA spectra recorded during the XAS measurements (Figure 1A) show for both catalysts that the ethane production rates increase in the hydrogen-rich atmospheres and decrease in the ethylene-rich atmospheres with a pronounced maximum at intermediate gas ratios. The rates change approximately linearly with the gas ratio, corresponding to an overall first-order rate dependence on the hydrogen partial pressure and a zero-order dependence on the ethylene pressure, as it is commonly accepted for this reaction under the applied experimental conditions.

The XAS spectra (K edge for Pd/SiO<sub>2</sub>, L<sub>3</sub> edge for Pt/SiO<sub>2</sub>) are distinctively different in hydrogen- and ethylene-rich atmospheres (Figure 1B) with a pronounced, mostly reversible, transition at the gas ratios corresponding to the maximum ethane production rates (Figure 1C), similar for both catalysts. This transition can be attributed to the fact that in the hydrogen-rich atmospheres, atomic hydrogen is present at the surface, whereas in the ethylene-rich atmospheres a carbonaceous species, i.e., ethylidyne according to earlier literature, is the dominant surface species.

EXAFS fitting results (Figure 1D and E) confirm that the Pd/SiO<sub>2</sub> nanoparticles grow during the reaction sequence, in particular in the ethylene-rich atmospheres in the forward sequence from pure hydrogen to ethylene and in the backward sequence upon the transition from ethylene- to hydrogen-rich atmospheres (Figure 1E). The results are in particular in very good agreement with those of the pre- and post-experimental STEM particle size analysis. Considering both outcomes (and assuming truncated cuboctahedral particle shapes), it can be concluded that the particles grow during the reaction by a factor of 4. For Pt/SiO<sub>2</sub>, in addition to the metal-metal contribution identified for Pd/SiO<sub>2</sub>, two Pt-low-Z contributions can occur depending on the experimental conditions (Figure 1D), the so-called long- and short bond (the Pd K edge EXAFS is significantly less sensitive in this respect than Pt L<sub>3</sub> edge EXAFS). Both Pt-low-Z contributions are formed upon the transition from hydrogen- to ethylene-rich atmospheres. Upon reverse transition from ethylene- to hydrogen-rich atmospheres, the long-bond contribution persists, whereas the short-bond contribution vanishes completely. Therefore, the short-bond contribution can be attributed to ethylidyne reversibly adsorbed on the Pt particles in the ethylene-rich atmospheres; the long-bond contribution is presumably due to irreversible carbide formation. Nevertheless, also for Pt/SiO<sub>2</sub> the results of the EXAFS fitting are in good agreement with the STEM particle size analysis.

In addition, for the Pd/SiO<sub>2</sub> particles in the hydrogen-rich atmospheres the deintercalation and intercalation of hydrogen during the forward and backward sequence, respectively, can be directly followed by the changes of the metal-metal bond length (Figure 1D). From these changes a maximum hydrogen content in the pure hydrogen atmosphere of  $n = 0.17 \pm 0.03$  can be determined, indicative of a mixed  $\alpha$ - and  $\beta$ -palladium hydride phase. In contrast, Pt/SiO<sub>2</sub> only adsorbs hydrogen at the surface and the bond length stays constant during the reaction sequence.

Despite these pronounced and, in parts, adverse changes in the atomic and electronic structures of the Pd/SiO<sub>2</sub> and Pt/SiO<sub>2</sub> catalysts (e.g., defined transitions between hydrogen- and hydrocarbon-covered surfaces, size changes, and gas-phase composition-dependent hydrogen de-/intercalation), the virtually unaffected hydrogenation reactivity demonstrates the significant structural and dynamical complexity within this reaction, which is generally accepted to be structure-insensitive. This suggests an interesting point to address by theoretical calculations (e.g. by modelling the changes in the d-band occupancy), which are currently underway.



A. Normalized ethane production rates over Pt/SiO<sub>2</sub> during an XAS experiment.  
 B. L<sub>3</sub>-edge XANES spectra for Pt/SiO<sub>2</sub> in pure H<sub>2</sub> and C<sub>2</sub>H<sub>4</sub> atmospheres, respectively, showing distinct changes in the white line intensity.  
 C. Series of L<sub>3</sub>-edge EXAFS spectra for Pt/SiO<sub>2</sub> for the whole measurement sequence from pure H<sub>2</sub> to C<sub>2</sub>H<sub>4</sub> and back to H<sub>2</sub>, showing pronounced transitions. The measurement sequence is displayed from top to bottom.  
 D. Fourier-transform EXAFS magnitude  $|\chi(r)|$  and best-fit results for Pd/SiO<sub>2</sub> and Pt/SiO<sub>2</sub> in pure H<sub>2</sub> and C<sub>2</sub>H<sub>4</sub>, respectively.  
 E. EXAFS fitting results (coordination numbers  $n$  and interatomic distances  $r$ ) for Pd/SiO<sub>2</sub> and Pt/SiO<sub>2</sub> in different mixed H<sub>2</sub> and C<sub>2</sub>H<sub>4</sub> atmospheres.

### Publications Acknowledging this Grant in 2011-2014

1. Erickson, E.M.; Oruc, M.E.; Small, M.W.; Wetzel, D.J.; Cason, M.W.; Hoang, T.T.H.; Li, D.; Marinkovic, N.S.; Frenkel, A.I.; Gewirth, A.A.; Nuzzo, R.G. A Comparison of Atomistic and Continuum Approaches to the Study of Bonding Dynamics in Electrocatalysis: Microcantilever Stress and In-Situ EXAFS Observations of Platinum Bond Expansion Due to Oxygen Adsorption During the Oxygen Reduction Reaction, *Anal. Chemistry*, **submitted**.
2. Frenkel, A.I.; van Bokhoven, J.A. X-Ray Spectroscopy for Chemical and Energy Sciences (invited) *J. Sync. Rad.*, **submitted**.
3. Shan, J.; Zhang, S.; Choksi, T.; Zhu, W.; Zhang, Y.; Li, Y.; Nguyen, L.; Chafe, A.; Greeley, J.; Frenkel, A.I.; Tao, F. Tuning catalytic performance through a single or sequential post-synthesis reaction in a gas phase. *Nature Comm.*, **submitted**.
4. Huang, W.; Shan, J.; Nguyen, L.; Li, Y.; Zhang, S.; Frenkel, A.I.; Tao, F. Catalytic conversion of methane to methanol and formic acid on singly dispersed palladium oxide species on internal surface of ZSM5. *Angew. Chem. Int. Ed.*, **submitted**.
5. Shan, J.; Huang, W.; Nguyen, L.; Yu, Y.; Zhang, S.; Li, Y.; Frenkel, A.I.; Tao, F. Conversion of methane to methanol in gas phase on a bent mono( $\mu$ -oxo)dinickel anchored on internal surface of micro-pores. *Langmuir*, **submitted**.
6. Zhang, S.; Nguyen, L.; Liang, J.; Li, J.; Shan, J.; Frenkel, A.I.; Patlolla, A.; Liu, J.; Huang, W.; Tao, F. Catalysis on an isolated bimetallic site. *Nature Chem.*, **submitted**.
7. Zhang, L.; Yang, C.; Frenkel, A.I.; Wang, S.; Xiao, G.; Brinkman, K.; Chen, F. Co-generation of electricity and chemicals from propane fuel in solid oxide fuel cells with anode containing nano-bimetallic catalyst. *J. Power Sources*, **2014**, 262, 421-428
8. Rehr, J.J.; Vila, F.D. Dynamic Structural Disorder in Supported Nanoscale Catalysts. *J. Chem. Phys.* **2014**, 140, 134701.
9. Small, M.W.; Kas, J.; Kvashnina, K.O.; Rehr, J.J.; Nuzzo, R.G.; Tromp, M.; Frenkel, A.I. Effects of adsorbate coverage and bond length disorder on the d-band center in carbon-supported Pt catalysts. *Chem. Phys. Chem.* **2014**, DOI: 10.1002/cphc.201400055
10. Frenkel, A.I.; Cason, M.; Elsen, A.; Jung, U.; Small, M.W.; Nuzzo, R.G.; Vila, F.D.; Rehr, J.J.; Stach, E.A.; Yang, J.C. Effects of complex interactions on structure and dynamics of supported metal catalysts. *J. Vac. Sci. Tech.* (Invited Critical Review) **2014**, 32, 020801-0208017.
11. Frenkel, A.I.; Small, M.W.; Smith, J.G.; Nuzzo, R.G.; Kvashnina, K.O.; Tromp, M. An In-Situ Study of Bond Strains in 1 nm Pt Catalysts and Their Sensitivities to Cluster-Support and Cluster-Adsorbate Interactions. *J. Phys. Chem. C* **2013**, 117, 23286-23294.
12. Frenkel, A.I.; Wang, Q.; Sanchez, S.I.; Small, M.W.; Nuzzo, R.G. Short range order in bimetallic nanoalloys: An extended X-ray absorption fine structure study. *J. Chem. Phys.* **2013**, 138, 064202.
13. Zhang, Z.; Li, L.; Yang, J.C. Adhesion of Pt nanoparticles supported on  $\gamma$ -Al<sub>2</sub>O<sub>3</sub> single crystal. *J. Phys. Chem. C* **2013**, 117, 21407-21412.
14. Li, L.; Wang, L.-L.; Johnson, D.D.; Zhang, Z.; Sanchez, S.I.; Kang, J.H.; Nuzzo, R.G.; Wang, Q.; Frenkel, A.I.; Ciston, J.; Stach, E.A.; Yang, J.C. Noncrystalline-to-crystalline transformations in Pt nanoparticles. *J. Am. Chem. Soc.* **2013**, 135, 13062-13072.
15. Stach, E.A.; Zakharov, D.; Akatay, M.C.; Baumann, P.; Ribeiro, F.; Zvienevich, Y.; Li, Y.; Frenkel, A.I. Developments in environmental transmission electron microscopy for catalysis research *Microsc. Microanal.* **2013**, 19, Suppl. 2, 1174-1175.
16. Zhang, S.; Tao, F.; Frenkel, A.I.; Takeda, S. Singly anchored Pt and Pd atoms on Co<sub>3</sub>O<sub>4</sub> and their catalytic performance. *Microsc. Microanal.* **2013**, 19, Suppl. 2, 1620-1621.
17. Stach, E.A.; Baumann, P.; Li, Y.; Zakharov, D.; Frenkel, A.I. Using operando methods to characterize working catalysts with TEM, XAS, EXAFS and Raman Spectroscopy. *Microsc. Microanal.* **2013**, 19, Suppl. 2, 1674-1675.
18. Zhang, S.; Shan, J.-J.; Zhu, Y.; Frenkel, A.I.; Patlolla, A.; Huang, W.; Yoon, S.; Wang, L.; Yoshida, H.; Takeda, S.; Tao, F. WGS Catalysis and in-situ studies of CoO(1-x)PtCo(n)/Co<sub>3</sub>O<sub>4</sub> and Pt(m)Co(m')/CoO(1-x) nanorod catalysts. *J. Am. Chem. Soc.* **2013**, 135, 8283-8293.
19. Merte, L.R.; Ahmadi, M.; Behafarid, F.; Ono, L.K.; Lira, E.; Matos, J.; Li, L.; Yang, J.C.; Cuenya, B.R. Correlating Catalytic Methanol Oxidation with the Structure and Oxidation State of Size-Selected Pt Nanoparticles. *ACS Catal.* **2013**, 3, 1460-1468.
20. Korobko, R.; Lerner, A.; Li, Y.; Frenkel, A.I.; Lubomirsky, I. Electric field increases local symmetry in Gd-doped ceria. *Nature Mater.*, **submitted**.

21. Wu, L.-b.; Wu, L.-h.; Yang, W.-m.; Frenkel, A.I. Study of the local structure and oxidation state of iron in complex oxide catalysts for propylene ammoxidation. *Cat. Sci. & Technol.*, 2014, **in press**.
22. He, L.; Liu, F.; Hautier, G.; Oliveira, M.J.T.; Marques, M.A.L.; Vila, F.D.; Rehr, J.J.; Rignanese, G.-M.; Zhou, A. Accuracy of generalized gradient approximation functionals for density-functional perturbation theory calculations. *Phys. Rev. B* **2014**, *89*, 064305.
23. Frenkel, A.I.; Khalid, S.; Hanson, J.C.; Nachtegaal, M. QEXAFS in Catalysis Research: Principles, Data Analysis and Applications. In *In-situ Characterization of Heterogeneous Catalysts*, Chupas, P.; Hanson, J.; Rodriguez, J.A., Eds., John Wiley and Sons **2013**.
24. Frenkel, A.I.; Hanson, J.C. Combined XAFS-XRD methods in Catalysis Research. In *In-situ Characterization of Heterogeneous Catalysts*, Chupas, P.; Hanson, J.; Rodriguez, J. A., Eds., John Wiley and Sons **2013**.
25. Kossoy, A.; Wang, Q.; Korobko, R.; Grover, V.; Feldman, Y.; Wachtel, E.; Tyagi, A.K.; Frenkel, A.I.; Lubomirsky, I. Evolution of the local structure at the phase transition in CeO<sub>2</sub>-Gd<sub>2</sub>O<sub>3</sub> solid solutions. *Phys. Rev. B* **2013**, *87*, 054101.
26. Perelshtein, I.; Ruderman, E.; Perkas, N.; Tzanov, T.; Beddow, J.; Joyce, E.; Mason, T.; Blanes, M.; Molla, K.; Patlolla, A.; Frenkel, A.I.; Gedanken, A., Chitosan and chitosan-ZnO-based complex nanoparticles: formation, characterization, and antibacterial activity. *J. Mater. Chem. B* **2013**, *1*, 1968-1976.
27. Sanchez, S.I.; Small, M.W.; Bozin, E.S.; Wen, J.-G.; Zuo, J.-M.; Nuzzo, R.G., Metastability and Structural Polymorphism in Noble Metals: the Role of Composition and Metal Atom Coordination in Mono- and Bimetallic Nanoclusters. *ACS Nano* **2013**, *7*, 1542-1557.
28. Amit, Y.; Eshet, H; Faust, A.; Patlolla, A.; Rabani, E.; Banin, U.; Frenkel, A.I. Unraveling the Impurity Location and Binding in Heavily Doped Semiconductor Nanocrystals: The Case of Cu in InAs Nanocrystals. *J. Phys. Chem. C* **2013**, *117*, 13688-13696.
29. Amit, Y.; Eshet, H; Milo, O.; Rabani, E.; Frenkel, A.I.; Banin, U. How to dope a semiconductor nanocrystal. *ECS Trans.* **2013**, *58*, 127-133.
30. Yancey, D.F.; Chill, S.T.; Zhang, L.; Frenkel, A.I.; Henkelman, G.; Crooks, R.M. A theoretical and experimental examination of systematic ligand-induced disorder in Au dendrimer-encapsulated nanoparticles. *Chem. Science* **2013**, *4*, 2912-2921.
31. Wang, L.; Zhang, S.; Zhu, Y.; Patlolla, A.; Shan, J.-J.; Yoshida, H.; Takeda, S.; Frenkel, A.I.; Tao, F. Catalysis and In-situ Studies of Rh/Co<sub>3</sub>O<sub>4</sub> Nanorods in Reduction of NO with H<sub>2</sub>. *ACS Catalysis* **2013**, *3*, 1011-1019.
32. Patlolla, A.; Baumann, P.; Xu, W.; Senanayake, S.; Rodriguez, J.A.; Frenkel, A.I. Characterization of Metal-Oxide Catalysts in Operando Conditions by Combining X-Ray Absorption and Raman Spectroscopies in the Same Experiment. *Top. Catal.* **2013**, *56*, 896-904.
33. Amakawa, K.; Sun, L.; Guo, C.; Havecker, M.; Kube, P.; Wachs, I.E.; Lwin, S.; Frenkel, A.I.; Patlolla, A.; Hermann, K.; Schlögl, R.; Trunschke A. How strain affects the reactivity of surface metal oxide catalysts. *Angew. Chem. Int. Ed.* **2013**, *52*, 13553-13557.
34. Frenkel, A.I., Applications of extended X-ray absorption fine-structure spectroscopy to studies of bimetallic nanoparticle catalysts. *Chem. Soc. Rev.* **2012**, *41*, 8163-8178.
35. Yang, J.C.; Small, M.W.; Grieshaber, R.V.; Nuzzo, R.G., Recent Developments and Applications of Electron Microscopy to Heterogeneous Catalysis. *Chem. Soc. Rev.* **2012**, *41*, 8179-8194.
36. Zhang, Z.; Gleeson, B.; Jung, K.; Li, L.; Yang, J.C., A Diffusion Analysis of Transient Subsurface gamma-Ni<sub>3</sub>Al Formation During beta-NiAl Oxidation, *Acta. Mater.* **2012**, *60*, 5273-5283.
37. Zhang, Z.; Jung, K.; Li, L.; Yang, J.C., Kinetic Aspects of Initial Stage Thin gamma-Al<sub>2</sub>O<sub>3</sub> Film Formation on Single Crystalline beta-NiAl (110). *J. Appl. Phys.* **2012**, *111*, 34312.
38. Erickson, E. M.; Thorum, M. S.; Vasic, R.; Marinkovic, N.; Frenkel, A. I.; Gewirth, A. A.; Nuzzo, R. G., In-Situ Electrochemical X-ray Absorbance Spectroscopy Oxygen Reduction Catalysis with High Oxygen Flux. *J. Am. Chem. Soc.* **2012**, *134*, 197-200.
39. Small, M. W.; Sanchez, S. I.; Marinkovic, N. S.; Frenkel, A. I.; Nuzzo, R. G., Influence of Adsorbates on the Electronic Structure, Bond Strain, and Thermal Properties of an Alumina-Supported Pt Catalyst. *ACS Nano*, **2012**, *6*, 5583-5595.
40. Yan, W.; Vasic, R.; Frenkel, A. I.; Koel, B. E., Intra-particle reduction of arsenite (As(III)) by nanoscale zerovalent iron (nZVI) investigated with *in-situ* X-ray absorption spectroscopy. *Environ. Sci. & Technology* **2012**, *46*, 7018-7026.
41. Patlolla, A.; Zunino III, J.; Frenkel, A. I.; Iqbal, Z., Thermochromism in Polydiacetylene-metal oxide nanocomposites *J. Mater. Chem.* **2012**, *22*, 7028-7035.
42. Myers, S. V.; Frenkel, A. I.; Crooks, R. M., In Situ Structural Characterization of Platinum Dendrimer-Encapsulated Oxygen Reduction Electrocatalysts. *Langmuir* **2012**, *28*(2), 1596-1603.

43. Ryu, H.; Lei, H.; Frenkel, A. I.; Petrovic, C., Local structural disorder-induced superconductivity in  $K(x)Fe(2-y)Se(2)$  materials *Phys. Rev. Lett.* **2012**, *85*, 224515.
44. Chen, W.-F.; Sasaki, K.; Ma, C.; Frenkel, A. I.; Marinkovic, N.; Muckerman, J. T.; Zhu, Y.; Adzic, R. R., Noble metal-free hydrogen-evolution catalysts based on NiMo nitride nanosheets. *Angew. Chemie Int. Ed.* **2012**, *51*, 6131-6135.
45. Yadgarov, L.; Rosentsveig, R.; Leitus, G.; Albu-Yaron, A.; Moshkovitz, A.; Perfiliev, V.; Vasic, R.; Frenkel, A. I.; Enyashin, A. N.; Seifert, G.; Rapoport, L.; Tenne, R., Controlled doping of MS<sub>2</sub> (M=W, Mo) nanotubes and fullerene-like nanoparticles *Ang. Chemie, Int. Ed.* **2012**, *51*, 1148-1151.
46. Yih, K.; Hamdemir, I.K.; Mondocho, J.E.; Bayrem, E.; Ozkar, S.; Vasic, R.; Frenkel, A.I.; Anderson, O.P.; Finke, R.G., Synthesis and Characterization of [Ir(1,5-Cyclooctadiene)( $\mu$ -H)]<sub>4</sub>: A Tetrametallic Ir<sub>4</sub>H<sub>4</sub>-core, Coordinatively Unsaturated Cluster. *Inorg. Chem.* **2012**, *51*, 3186-3193.
47. Frenkel, A.I.; Vasic, R.; Dukesz, B.; Li, D.; Chen, M.; Zhang, L.; Fujita, T.; Thermal Properties of Nanoporous Gold. *Phys. Rev. B* **2012**, *85*, 195419.
48. Landon, J.; Demeter, E.; Inoglu, N.; Keturakis, C.; Wachs, I.E.; Vasic R.; Frenkel, A.I.; Kitchin, J.R., Spectroscopic Characterization of Mixed Fe-Ni Oxide Electrocatalysts for the Oxygen Evolution Reaction in Alkaline Electrolytes. *ACS Catalysis* **2012**, *2*, 1793-1801.
49. Korobko, R.; Patlolla, A.; Kossoy, A.; Wachtel, E.; Tuller, H.L.; Frenkel, A.I.; Lubomirsky, I., Giant Electrostriction in Gd-doped Ceria. *Adv. Mater.* **2012**, *24*, 5857-5861.
50. Lyahovitskaya, V.; Feldman, Y.; Zon, I.; Yoffe, A.; Frenkel, A.I., Strain-arranged structure in amorphous films. *J. Mater. Res.* **2012**, *27*, 2819-2828.
51. Coppage, R.; Slocik, J. M.; Briggs, B. D.; Frenkel, A. I.; Naik, R. R.; Knecht, M. R., Determining peptide sequence effects that control the size, structure and function of nanoparticles. *ACS Nano* **2012**, *6*, 1625-1636.
52. Patlolla, A.; Carino, E.V.; Ehrlich, S.N.; Stavitski, E.; Frenkel, A.I., Application of Operando XAS, XRD, and Raman Spectroscopy for Phase Speciation in Water Gas Shift Reaction Catalysts. *ACS Catalysis* **2012**, *2*, 2216-2223.
53. Lei, H.; Ryu, H.; Ivanovski, V.; Warren, J.B.; Frenkel, A.I.; Cekic, B.; Yin, W.-G.; Petrovic, C., Structure and physical properties of the layered iron oxychalcogenide BaFe<sub>2</sub>Se<sub>2</sub>O. *Phys. Rev. B* **2012**, *86*, 195133.
54. M. W. Small, S. I. Sanchez, L. D. Menard, J. H. Kang, A. I. Frenkel and R. G. Nuzzo, The Atomic Structural Dynamics of  $\gamma$ -Al<sub>2</sub>O<sub>3</sub> Supported Ir-Pt Nanocluster Catalysts Prepared From a Bimetallic Molecular Precursor: A Study Using Aberration-Corrected Electron Microscopy and X-ray Absorption Spectroscopy, *Journal of the American Chemical Society*, **2011**, *133*, 3582-3591.
55. W. Du, D. Su, Q. Wang, A. I. Frenkel, X. Teng, Promotional effects of Bismuth on the formation of Platinum-Bismuth nanowires and the electrocatalytic activity toward ethanol oxidation, *Crystal Growth & Design*, **2011**, *11*, 594-599.
56. A. Piovano, G. Agostini, A. I. Frenkel, T. Bertier, C. Prestipino, M. Ceretti, W. Paulus, C. Lamberti, Time-resolved in situ XAFS study of the electrochemical oxygen intercalation in SrFeO<sub>2.5</sub> Brownmillertite structure: comparison with the homologous SrCoO<sub>2.5</sub> system, *J. Phys. Chem. C* **2011**, *115*, 1311-1322.
57. Alley, W. M.; Hamdemir, I. K.; Wang, Q.; Frenkel, A. I.; Li, L.; Yang, J. C.; Menard, L. D.; Nuzzo, R. G.; Ozkar, S.; Yih, K.; Johnson, K. A.; Finke, R. G., Industrial Ziegler-Type Hydrogenation Catalysts Made from Co(neodecanoate)<sub>2</sub> or Ni(2-ethylhexanoate)<sub>2</sub> and AlEt<sub>3</sub>: Evidence for Nanoclusters and Sub-Nanocluster or Larger Ziegler-Nanocluster Based Catalysis. *Langmuir* **2011**, *27*, 6279-6294.
58. Danh, N.-T.; Frenkel, A. I.; Wang, J.; O'Brien, S.; Akins, D. L., Cobalt-polypyrrole-carbon black (Co-PPY-CB) electrocatalysts for the oxygen reduction reaction (ORR) in fuel cells: Composition and kinetic activity. *Applied Catalysis B-Environmental* **2011**, *105*, 50-60.
59. Du, W.; Su, D.; Wang, Q.; Frenkel, A. I.; Teng, X., Promotional Effects of Bismuth on the Formation of Platinum-Bismuth Nanowires Network and the Electrocatalytic Activity toward Ethanol Oxidation. *Cryst. Growth Des.* **2011**, *11*, 594-599.
60. Du, W.; Wang, Q.; LaScala, C. A.; Zhang, L.; Su, D.; Frenkel, A. I.; Mathur, V. K.; Teng, X., Ternary PtSnRh-SnO<sub>2</sub> nanoclusters: synthesis and electroactivity for ethanol oxidation fuel cell reaction. *J. Mater. Chem.* **2011**, *21*, 8887-8892.
61. Du, W.; Wang, Q.; Saxner, D.; Deskins, N. A.; Su, D.; Krzanowski, J. E.; Frenkel, A. I.; Teng, X., Highly Active Iridium/Iridium-Tin/Tin Oxide Heterogeneous Nanoparticles as Alternative Electrocatalysts for the Ethanol Oxidation Reaction. *J. Am. Chem. Soc.* **2011**, *133*, 15172-15183.
62. Frenkel, A. I.; Wang, Q.; Marinkovic, N.; Chen, J. G.; Barrio, L.; Si, R.; Lopez Camara, A.; Estrella, A. M.; Rodriguez, J. A.; Hanson, J. C., Combining X-ray Absorption and X-ray Diffraction Techniques for *in-situ* Studies

- of Chemical Transformations in Heterogeneous Catalysis: Advantages and Limitations. *J. Phys. Chem. C* **2011**,*115*, 17884-17890.
63. Frenkel, A. I.; Yevick, A.; Cooper, C.; Vasic, R., Modeling the Structure and Composition of Nanoparticles by Extended X-Ray Absorption Fine-Structure Spectroscopy. *Annual Review Of Analytical Chemistry, Vol 4* **2011**,*4*, 23-39.
64. Li, L.; Zhang, Z.; Ciston, J.; Stach, E. A.; Wang, L.-l.; Johnson, D. D.; Wang, Q.; Frenkel, A. I.; Sanchez, S. I.; Small, M. W.; Nuzzo, R. G.; Yang, J. C., H<sub>2</sub>-driven crystallization of supported Pt nanoparticles observed with aberration-corrected Environmental TEM. *Microsc. Microanal.* **2011**,*17*, 1604-1605.
65. Marinkovic, N. S.; Wang, Q.; Barrio, L.; Ehrlich, S. N.; Khalid, S.; Cooper, C.; Frenkel, A. I., Combined *in-situ* X-ray absorption and diffuse reflectance infrared spectroscopy: An attractive tool for catalytic investigations. *Nuclear Instruments & Methods In Physics Research Section A-* **2011**,*649*, 204-206.
66. Marinkovic, N. S.; Wang, Q.; Frenkel, A. I., *In-situ* diffuse reflectance IR spectroscopy and X-ray absorption spectroscopy for fast catalytic processes. *Journal Of Synchrotron Radiation* **2011**,*18*, 447-455.
67. Paredis, K.; Ono, L. K.; Behafarid, F.; Zhang, Z.; Yang, J. C.; Frenkel, A. I.; Cuenya, B. R., Evolution of the Structure and Chemical State of Pd Nanoparticles during the *in-situ* Catalytic Reduction of NO with H<sub>2</sub>. *J. Am. Chem. Soc.* **2011**,*133*, 13455-13464.
68. Paredis, K.; Ono, L. K.; Mostafa, S.; Li, L.; Zhang, Z.; Yang, J. C.; Barrio, L.; Frenkel, A. I.; Cuenya, B. R., Structure, chemical composition, and reactivity correlations during the *in-situ* oxidation of 2-propanol. *J. Am. Chem. Soc.* **2011**,*133*, 6728-6735.
69. Sasaki, K.; Kuttiyiel, K. A.; Barrio, L.; Su, D.; Frenkel, A. I.; Marinkovic, N.; Mahajan, D.; Adzic, R. R., Carbon-Supported IrNi Core-Shell Nanoparticles: Synthesis, Characterization, and Catalytic Activity. *J. Phys. Chem. C* **2011**,*115*, 9894-9902.
70. Zhang, Z.; Li, L.; Wang, L.-l.; Sanchez, S. I.; Wang, Q.; Johnson, D. D.; Frenkel, A. I.; Nuzzo, R. G.; Yang, J. C., The Role of  $\alpha$ -Al<sub>2</sub>O<sub>3</sub> Single Crystal Support to Pt Nanoparticles Construction. *Microsc. Microanal.* **2011**,*17*, 1324-1325.
71. Zhang, Z.; Li, L.; Yang, J. C.,  $\gamma$ -Al<sub>2</sub>O<sub>3</sub> thin film formation via oxidation of  $\beta$ -NiAl(1 1 0). *Acta Mater.* **2011**,*59*, 5905-5916.
72. Lei, H.; Ryu, H.; Frenkel, A. I.; Petrovic, C., Anisotropy in BaFe<sub>2</sub>Se<sub>3</sub> single crystals with double chains of FeSe tetrahedra *Physical Review B* **2011**, *84*, 214511.
73. Shen, X.-F.; Morey, A.; Liu, J.; Ding, Y.-S.; Durand, J.; Wang, Q.; Wen, W.; Hines, W. A.; Hanson, J. C.; Bai, J.; Frenkel, A. I.; Reiff, W.; Aindow, M.; Suib, S. L.; Cai, J., Characterization of the Fe-doped mixed-valent tunnel structure manganese oxide KOMS-2 *J. Phys. Chem. C* **2011**, *115*, 21610-21619.
74. Coppage, R.; Slocik, J. M.; Briggs, B. D.; Frenkel, A. I.; Heinz, H.; Naik, R. R.; Knecht, M. R., Crystallographic Recognition Controls Peptide Binding for Bio-Based Nanomaterials. *J. Am. Chem. Soc.* **2011**,*133*, 12346-12349.